Università degli Studi di Napoli *Federico II*

Dottorato di Ricerca in Fisica

Ciclo 37°

Coordinatore: Prof. Vincenzo Canale

Non-perturbative results for Quantum Chromodynamics: from charged sectors to near conformal dynamics

Settore Scientifico Disciplinare: FIS/02

Dottoranda

Alessandra D'Alise

Tutor

Francesco Sannino

Anni: 2021/2024

Dedicated to my family. I truly and deeply love you.

Dedicata alla mia famiglia. Pienamente, profondamente vi amo.

List of Papers

Papers discussed in this thesis

- J. Bersini, **A. D'Alise**, F. Sannino and M. Torres, "The θ-angle and axion physics of two-color QCD at fixed baryon charge," JHEP **11** (2022), 080 [arXiv:2208.09226 [hep-th]].
- J. Bersini, **A. D'Alise**, F. Sannino and M. Torres, "Charging the conformal window at nonzero θ angle," Phys. Rev. D **107** (2023) no.12, 12 [arXiv:2208.09227 [hep-th]].
- J. Bersini, **A. D'Alise**, C. Gambardella and F. Sannino, "Scaling results for charged sectors of near conformal QCD," Phys. Rev. D **109** (2024) no.12, 125015. [arXiv:2401.08457 [hep-th]].
- J. Bersini, **A. D'Alise**, M. Torres and F. Sannino, "The Dilatonic Dynamics of Baryonic Crystals, Branes and Spheres," Phys. Rev. D **110** (2024) no.9, 094008 [arXiv:2310.04083 [hep-ph]].

Other Papers written during the PhD

- **A. D'Alise**, G. De Nardo, M. G. Di Luca, G. Fabiano, D. Frattulillo, G. Gaudino, D. Iacobacci, M. Merola, F. Sannino and P. Santorelli, *et al.* "Standard model anomalies: lepton flavour non-universality, g − 2 and W-mass," JHEP **08** (2022), 125 [arXiv:2204.03686 [hep-ph]].
- **A. D'Alise**, G. Fabiano, D. Frattulillo, S. Hohenegger, D. Iacobacci, F. Pezzella and F. Sannino, "Positivity conditions for generalized Schwarzschild space-times," Phys. Rev. D **108** (2023) no.8, 084042 [arXiv:2305.12965 [gr-qc]].

- M. Arzano, **A. D'Alise** and D. Frattulillo, "Entanglement entropy in conformal quantum mechanics," JHEP **10** (2023), 165 [arXiv:2306.12291 [hep-th]].
- L. Ciambelli, **A. D'Alise**, V. D'Esposito, D. Đorđevic, D. Fernández-Silvestre and L. Varrin, PoS **QG-MMSchools** (2024), 010 [arXiv:2307.08460 [hep-th]].
- **A. D'Alise**, G. Fabiano, D. Frattulillo, D. Iacobacci, F. Sannino, P. Santorelli and N. Vignaroli, "New Physics Pathways from B Processes," Nucl. Phys. B **1006** (2024), 116631 doi:10.1016/j.nuclphysb.2024.116631 [arXiv:2403.17614 [hep-ph]].
- M. Arzano, **A. D'Alise** and D. Frattulillo, "Entanglement entropy and horizon temperature in conformal quantum mechanics," PoS **CORFU2023** (2024), 276 doi:10.22323/1.463.0276 [arXiv:2405.02623 [hep-th]].
- B. Buonomo, **A. D'Alise**, R. Della Marca and F. Sannino, "Information index augmented eRG to model vaccination behaviour: A case study of COVID-19 in the US," [arXiv:2407.20711v1 [q-bio.PE]]
  (under Review for publication in Physica A: Statistical Mechanics and its Applications)
- **A. D'Alise**, D. Iacobacci and F. Sannino, "A Temporal Playbook for Multiple Wave Dengue Pandemic from Latin America and Asia to Italy," [arXiv:2411.03837 [q-bio.PE]]

Foreword

The material of the thesis is schematically organised as follows.

- chapter 1 is dedicated to introducing preliminary concepts about conformal field theories and the notion of conformal and scale invariance.
- chapter 2 reviews the large charge expansion and discusses examples of conformal field theories invariant under general symmetry groups.
- chapter 3 illustrates background notions about the phase diagram at zero temperature for two-colour QCD and three-colour QCD and is partly based on unpublished material.
- chapter 4 is based on [1].
- chapter 5 reviews the concept of the conformal window and the construction of the dilaton effective field theory.
- chapter 6 is based on [2].
- chapter 7 is based on [3].
- chapter 8 introduces preliminary concepts for solitonic dynamics.
- chapter 9 is based on [4].

Abstract

This thesis delves into the near conformal dynamics of Quantum Chromodynamics (QCD) and QCD-like theories, with a particular focus on the role of large charge sectors, solitonic objects, and the dilaton in the context of conformal and near conformal phases. It emphasises the importance of exploring near conformal field theories due to the deep connections between conformal symmetry, quantum phase transitions, and non-perturbative effects in strongly interacting systems. These topics are intricately tied to QCD and its extensions, where both theoretical challenges and phenomenological implications are at stake. The work not only contributes to the understanding of fundamental quantum phase transitions but also has profound implications for the study of nuclear matter in extreme environments. Through its multifaceted approach, this research pushes the boundaries of theoretical and phenomenological investigations in strongly coupled systems.

Contents

Introduction

By homely gifts and hindered words
The human heart is told
Of nothing -
"Nothing" is the force
That renovates the World
— Emily Dickinson

Understanding the complex forces that govern Nature is an ongoing endeavour. The dynamics of strongly coupled theories represents one of the most intriguing challenges in theoretical physics. Although significant progress has been made in recent decades due to a diverse array of analytical and numerical techniques, numerous puzzles persist. At the forefront of these challenges stands Quantum Chromodynamics (QCD), the crown jewel of the Standard Model of particle interactions, which remains fraught with mysteries. QCD's complex physical spectrum, chiral symmetry breaking and confinement, and phase structure concerning light matter fields, temperature, and density, pose substantial analytical challenges.

Phase diagrams are a crucial tool for mapping how matter evolves under different conditions. They depict the preferred phase of matter at thermodynamic equilibrium, with phase transitions marking the boundaries between different states. These transitions are often linked to symmetry changes within the system. Even though phase diagrams are commonly introduced in basic science education with examples like water's temperature-pressure diagram amongst others, they extend far beyond everyday materials and explore extreme states like plasma and other QCD matter.

Visualising the full QCD phase diagram is challenging, but certain regions have garnered more attention because of their scientific relevance. One such area is the Quark-Gluon Plasma (QGP), a nearly perfect fluid of quarks and gluons believed to have existed just after the Big Bang. The transition from confined quarks to QGP is known as the deconfinement transition, while the chiral transition marks the restoration of broken symmetries as the chiral condensate melts. These transitions are central to understanding QCD at high temperatures.

Despite extensive research, the QCD phase diagram continues to captivate scientists, especially its temperature-baryon density plane, which has significant astrophysical applications. In fact, QCD challenges are not limited to high temperatures. Investigations also extend to ultrahigh-density regimes found in neutron stars, the remnants of massive stars. Studying their cores offers insight into QCD under extreme densities, where temperature plays a lesser role. The properties of matter in neutron star cores remain elusive, and exploring them could fill critical gaps in the QCD phase diagram.

Theoretical studies of QCD face significant obstacles, particularly in first-principles approaches, due to the complexity of the theory. Lattice QCD simulations have become a key method for exploring QCD, especially at zero and finite temperature. However, lattice studies at finite baryon density encounter a “sign problem", where the fermion determinant becomes complex, preventing standard importance sampling techniques. Ongoing research aims to overcome this issue, but for now, QCD at finite baryon density remains a formidable theoretical challenge.

This work is mainly based on investigating sectors of strongly interacting theories at zero temperature, focussing on the dynamics of the lightest particles that emerge in these realms. A key aim is to explore the theoretical phase diagrams within the mathematical framework determined by the relevant physical parameters. Specifically, a significant area of research involves exploring the non-perturbative dynamics of strongly interacting theories. The analysis of sectors of quantum field theory provides critical contributions to understanding the QCD and QCD-like phase diagrams. In this context, effective field theories (EFTs) have been instrumental in representing strong theories at lower energy scales, offering valuable insight into QCD. Indeed, QCD at finite and large densities presents a formidable theoretical task, since it poses challenges for numerical methods. However, reducing the number of colours allows for a rigorous description of the QCD vacuum properties at high baryon density, as well as interesting finite density phenomena, including phase transitions. This thesis presents the investigation of the phase diagram of two-colour QCD by exploring innovative sectors of the theory, especially those with finite baryon charge density and the inclusion of the topological term responsible for strong CP violation. This work presents an original finding that demonstrates the influence of both the θ-angle and axion dynamics on two-colour QCD, and, more generally, on $Sp(2N)$ QCD, especially when there exists a non-zero baryon charge and varying numbers of matter fields. It thoroughly examines the impact of these factors on the vacuum properties, the breaking of chiral symmetry, and the spectrum. A significant contribution of this study is its detailed analysis of the phase diagram in the presence of a topological term as the number of matter fields changes. Incorporating a CP-violating topological operator adds complexity to the vacuum structure, thus revealing new phases. The study delves into phase transitions, noting the importance of whether the number of flavours is odd or even. Specifically, the main and notable result is that the spontaneous CP symmetry breaking at $\theta = \pi$, known as Dashen's phenomenon, is absent in the superfluid phase when the number of flavours is odd while new phase transitions appear at $\theta = \pi/2$ and $\theta = 3\pi/2$.

Generally, theories manifest scale-invariant behaviour in the proximity of phase transitions. In physics, scale invariance embodies the idea that a system appears unchanged regardless of how much one zooms in or out. Generally, while scale invariance is relatively intuitive, the concept of conformal invariance is not. In fact, the latter preserves the shapes of objects and ensures that the angles between curves remain constant, even as their sizes change. Importantly, while a system exhibiting scale invariance does not necessarily have to be conformally invariant, the two concepts frequently overlap in various physical scenarios. Since exploring the mathematical foundations of conformal transformations is crucial in modern theoretical physics, a central question that this thesis aims to address is to clarify when and why scale invariance is promoted to conformal invariance. Understanding this complex network of ideas is crucial to distinguish between the two concepts.

Therefore, conformal field theory (CFT) plays a crucial role in modelling critical systems within condensed matter physics, demonstrating its broad applicability in everyday phenomena. In fact, Nature's beauty is closely tied to its underlying symmetries, where a phenomenon evolves from one equilibrium state to another, reflecting a recursive behaviour. For instance, the epidemic renormalization group approach is gaining traction in the literature, shedding light on the endemic states of pandemics and thereby demonstrating the real-world applications of these theoretical constructs.

In strongly interacting theories, the coupling constant, which measures the interaction strength, varies greatly across different energy scales. This phenomenon, often referred to as "running", involves changes in the interaction strength depending also on the conditions of the underlying theory such as the presence of matter content.

In fact, the fluctuation in the coupling constant results from the interplay of two opposing effects: an "anti-screening" contribution strengthening interactions as distances decrease caused by charged gauge bosons and a "screening" effect coming from matter fields, at the same distances. Thus, the coupling constant represents a delicate balance between these opposing forces.

The dynamics of these theories are further complicated by chiral symmetry breaking. When this phenomenon occurs below a certain energy scale, fermions acquire mass, leading to significant alterations in both the dynamics and behaviour of the coupling constant.

Under specific conditions, particularly when there is a sufficiently large number of matter fields, the coupling constant can converge to a fixed value at low energies before chiral symmetry breaking occurs. This behaviour indicates the emergence of a "conformal phase", in which the theory exhibits scale-invariant characteristics.

Moreover, when the number of distinct matter particles is just below the threshold for entering this conformal phase, the coupling constant shows minimal variation as the energy scale changes, behaving as though it is "walking" rather than "running". Thus, the behaviour of the coupling constant in strongly interacting theories reflects a delicate balance among various forces and energy scales, leading to phenomena like running, walking, and the emergence of conformal phases.

This intricate regime of the theory can be traced back to the pioneering work of Banks and Zaks, who discovered a perturbative infrared fixed point in massless QCD as the number of quark flavours approaches, but stays below, the critical point at which asymptotic freedom is lost. The range of quark flavours and colours that permit conformality is referred to as the conformal window. As the number of flavours decreases, the theory approaches the aforementioned quantum phase transition, delineating a boundary below which confinement and chiral symmetry breaking occur. This transition region is characterised by walking dynamics, where the running of the gauge coupling slows across a significant energy range.

In this context, the underlying theory appears close to achieving scale invariance but has yet to attain it fully. This precise regime of the theory can be seen as a departure from conformality, and hence the term “near conformality". Therefore, completing the framework for the low-energy description of QCD and QCD-like theories when the number of flavours allows for near conformal dynamics is crucial. This research delves deeper into conformal field theory, yielding a rich set of insights, particularly in understanding critical condensed matter systems and strongly coupled theories like QCD. CFT serves as a powerful tool in analysing QCD’s behaviour, especially near critical points, where understanding the dynamics of confinement and chiral symmetry breaking becomes essential. Here, the interplay between CFT and QCD comes to the forefront: CFT provides a robust framework for studying the critical phenomena associated with QCD, particularly in regimes where the theory approaches conformal symmetry.

Hence, knowledge about the low-energy description of QCD and QCD-like theories in sectors of fixed charge is enriched in this work within the near conformality regime. The infrared dynamics of the near conformal theory can be modelled by augmenting the standard chiral Lagrangian through the introduction of a new light scalar degree of freedom, commonly referred to as the dilaton, which possesses the same quantum numbers as the vacuum. In this scenario, the dilaton serves as the Goldstone boson resulting from the spontaneous breaking of scale invariance, while sources of explicit conformal breaking leading to the near conformal phase can be encoded in the effective dilaton potential. These phenomenological applications have spurred several investigations into the resulting dilaton effective field theory.

Understanding the intricacies of this behaviour necessitates an exploration of quantities that define the underlying conformal field theory, known as CFT data. Consequently, a primary focus of this work is the examination of the dimensions of operators, which describe how various quantities within a system scale. This investigation is particularly pertinent in the context of QCD, where understanding the scaling dimensions of operators provides essential insights into the dynamics of confinement and the nature of the phase transitions. Furthermore, the dimensions of operators can be translated into energy levels using a powerful technique: transitioning from the flat geometry of a plane to the curved geometry of a cylinder. This mapping is particularly advantageous because time translations are always a symmetry on the cylinder, allowing for effective problem-solving even in systems that do not strictly adhere to scale invariance. By shifting our perspective to the cylinder, one unlocks additional symmetries that guide toward consistent solutions, even in more complex or regulated systems where exact scale invariance may not hold.

Another cornerstone of this work is the study of large charge sectors of QCD-like theories, which provides a novel analytical tool for investigating strongly coupled systems. The state-operator correspondence allows one to compute the scaling dimensions of charged operators, which map onto the ground state energies of charged states on a curved background. This connection has been used to perform semiclassical calculations of scaling dimensions, particularly in the large charge limit. In fact, physical systems characterised by a large quantum number are amenable to be treated semiclassically, and this property is valid for relativistic scalar quantum field theories (QFTs) invariant under global symmetries at large internal charge. One of the most exciting aspects of this framework is that it permits analytical control over theories that are otherwise difficult to tackle using traditional methods. The large charge methodology has been validated via lattice simulations and is extended in this thesis to include topological sectors, such as the θ-angle dependence in two- and three-colour QCD.

In particular, the analysis is performed for both two-colour QCD with fixed baryon charge and three-colour QCD with fixed isospin charge. This extension introduces new scaling corrections due to explicit conformal symmetry breaking from quark mass terms and the dilaton potential. The θ-angle dependence is encoded within these corrections, revealing novel insights into the interplay between topological effects and near conformal dynamics. Furthermore, the thesis explores how the dilaton is coupled to fixed-charge operators, incorporating novel corrections to the scaling dimensions that arise from deformations away from the conformal fixed point. Specifically, this thesis demonstrates how the large charge limit significantly simplifies the dilaton potential, enabling model-independent predictions regarding the Q-scaling of near conformal corrections to observables within the large charge sector of the theory. These corrections are represented in terms of powers of the dilaton and pion masses, with the θ-angle dependence entering into the pion mass. The charge-dependent novel scalings of the near conformal corrections are proportional to the anomalous dimension of the quark mass operator and the one defining the dilaton potential which are the two parameters responsible for driving the theory away from conformality.

The non-perturbative nature of QCD at low- to intermediate-energy and density regimes makes calculating nuclear matter properties from first principles extremely difficult. Around six decades ago, a new avenue in quantum field theory arose, focussing on non-linear classical field equations, with solutions interpreted as new kinds of particles, distinct from the elementary particles described by quantised field excitations. These new solutions possess a topological structure. Therefore, Skyrme's concept of baryons as topological solitons, the Skyrmions, has also found traction in other theoretical models which help study the non-perturbative aspects of QCD-like theories. In fact, Skyrmions, originally introduced as topological solitons in chiral Lagrangians, represent baryons in the large colour limit of QCD.

Additionally, over the last two decades, generalised nuclear effective theories have evolved to include the field content and topological structures of the Skyrme model at low energies. These theories are designed to gradually evolve toward compatibility with QCD symmetries at higher energies, achieved by coupling the Skyrme field with the dilaton and vector mesons using hidden local symmetry. The transition from low- to high-energy involves fields moving from a spontaneously broken phase to an unbroken one. These nuclear effective theories preserve some topological aspects of the Skyrme model, although their dynamics are more complex.

Moving beyond local operator scaling, this thesis also investigates solitonic solutions, such as Skyrmions, in the low-energy effective description of QCD-like theories, focussing on how these objects behave in near conformal regimes. The addition of the dilaton to the chiral Lagrangian not only augments the effective theory but also provides new avenues for modelling dense nuclear matter, such as the core of neutron stars.

Therefore, here it is explored how the dilaton modifies the properties of Skyrmions, impacting their mass, size, and energy profiles. These solitons are studied numerically using the hedgehog ansatz, revealing, for the first time to our knowledge, how their physical properties are influenced by key parameters such as the anomalous dimension of the quark mass operator, the dilaton mass, and the scaling dimension of the operator responsible for breaking conformality.

The study also extends to more exotic solitonic structures, such as Skyrmion crystals and brane-like configurations, which are of interest for understanding the non-perturbative phase structure of dense QCD-like matter. Analytical novel solutions for Skyrmion crystals are presented, highlighting how the dilaton influences the baryon number distributions in these extended objects.

Plan of the thesis

- chapter 1 seeks to deepen the current understanding of the relationship between scale invariance and conformal invariance, focussing on the renormalization group flow and its implications for physical systems. To this aim, the discussion begins with preliminary notions about the conformal algebra and the conformal group, the non-linear realisation of the conformal symmetry and the introduction of the dilaton field.

- chapter 2 sets the stage for discussing how to compute conformal field theory data for operators carrying large internal quantum numbers in theories with global symmetries. Through the lens of the state-operator correspondence, this approach can also be interpreted as studying conformal field theory in states with fixed charge density, suggesting a fresh angle to tackle analytically strongly coupled theories.

- chapter 3 is a comprehensive review of two-colour QCD at non-zero baryon and isospin charge and on three-colour QCD at non-zero isospin chemical potential.

- chapter 4 is the first chapter showing innovative results in the research field on the QCD phase diagram. It encompasses the phase diagram of two-colour QCD, delving into previously uncharted sectors of the theory, particularly those with finite baryon charge density and the inclusion of the topological term responsible for strong CP violation, whose physical implications range from models of dark matter to composite Higgs dynamics. This study has yielded discoveries regarding the theory's phase transitions. The chapter begins by introducing the phases of QCD for different colours and flavours. Then the two-colour effective pion Lagrangian at non-zero baryon charge is introduced, including both the θ-angle term as well as the axion field. The stage is set by the determination of the vacuum structure of the theory both in the normal and superfluid phases as a function of the different number of matter fields. Here, it is shown how new phases emerge due to the interplay of the θ-angle term, quark masses, and baryon chemical potential. In particular, the study is on the dynamics of $N_f = 2, 3, 6, 7, 8$ flavours and general properties depending on the even versus odd number of flavours are unveiled. The work stops at eight flavours since around and above this number one expects the dynamics to either become near conformal or conformal. Notably, one of the main discoveries is that in the case of even flavours one observes a first order CP phase transition for $\theta = \pi$ both in the normal and superfluid phase, except for the case of $N_f = 2$ for which in the superfluid case the transition disappears as also discussed in the literature. Furthermore, for the odd case, the normal phase still supports CP breaking at $\theta = \pi$ while in the superfluid phase, the $\theta = \pi$ is replaced by novel first-order phase transitions for $\theta = \frac{\pi}{2}$ and $\theta = \frac{3\pi}{2}$. Lastly, there is a detailed analysis of the patterns of chiral symmetry breaking in the normal and superfluid phases and the determination of the spectrum and associated dispersion relations.

- chapter 5 goes down the rabbit hole of the concept of the conformal window and near conformality as well as the corresponding effective field theory description, stressing the motivations to include the presence of the dilaton field.

- chapter 6 shines a light on the impact of the θ-angle and axion dynamics for two-colour QCD at non-zero baryon charge and as a function of the number of matter fields on the vacuum properties, the pattern of chiral symmetry breaking as well as the spectrum of the theory. Precisely, it shows how the vacuum acquires a rich structure when the underlying CP violating topological operator is added to the theory. The chapter opens with a novel introduction of the dilaton for the two-colour low energy effective theory at non-zero baryon chemical potential including the θ-angle operator and axion field. Preparing for the state-operator correspondence the theory is coupled to a non-trivial gravitational background with cylindrical topology. The classical vacuum structure on the cylinder is then determined in an expansion in inverse powers of the baryon charge. This allows us to determine one of the main results of the work, namely the θ-dependence of the near conformal scaling dimensions of the baryon-charged operators, including the interplay on the quark and dilaton masses and potential. Conformal breakings due to the dynamics of the dilaton, to the chiral and conformal lagrangian order that is considered, are universally proportional to the dilaton squared mass and the coefficient of proportionality depends on the precise choice of the dilaton potential. The near conformal corrections coming from the presence of the pion mass are independent of the value of the dilaton potential operator and are universally proportional to the fourth power of the pion mass (i.e. quadratic in the underlying fermion masses). Furthermore, the chapter unveils a subtle dependence of the dynamics of the superfluid phase on the anomalous dimension of the fermion condensate. The corrections to the near conformal scaling dimensions stemming from the quantum fluctuations arising from the spectrum of the theory are also evaluated.

- chapter 7 uncovers the near conformal properties of finite isospin density QCD on a non-trivial gravitational background. The first result presented is the classical ground state energy computed through the semiclassical large charge expansion. In the conformal limit this energy maps, via state-operator correspondence, into the scaling dimension of the lowest-lying operator of fixed isospin charge Q. Precisely, the chapter shows its leading near conformal corrections at the lower boundary of the QCD conformal window. The characteristic Q-scalings arising from these near conformal corrections are driven by the quark mass operator anomalous dimension, as well as the conformal dimension of the operator responsible for dynamically shifting QCD away from the conformal window. This work presents the characteristic scalings as an original and innovative result. Furthermore, the pattern of symmetry breaking, the associated physical spectrum, and their dispersion relations are elucidated. Lastly, the chapter also discusses the $\mu - \theta$ QCD phase diagram, with μ the isospin chemical potential.

- chapter 8 aims to introduce topological solitons and the Skyrme model, laying the table for subsequent discussion on solitons' dynamics.
- chapter 9 investigates the novel influence of dilatonic dynamics on Skyrme spheres, crystals, and branes. Precisely, it focuses on how variations in the dilatonic model parameters, that reflect different underlying near conformal dynamics, affect the macroscopic properties of Skyrmions. Additionally, inspired by the possible emergent scale symmetry in dense Skyrmion matter, it also presents the original impact of the dilaton on the analytic brane solutions. The innovative findings presented here are expected to have broad implications, from advancing our understanding of near conformal dynamics in QCD-like theories to offering insights for phenomenological studies of nuclear matter in extreme conditions.

Part I

PRELIMINARIES I: CONFORMAL INVARIANCE AND LARGE CHARGE

Introduction to Part I

This thesis works opens with a review of the mathematical framework of conformality. The journey begins with an introduction to the intuitive idea behind the properties of conformal transformations. The latter constitute the bones of, perhaps, one of the most revolutionary ideas in physics: the renormalization group. However, the idea of conformal symmetry is strictly bound with the idea of scale invariance. The deep connection between these two invariances has made resonance in the last decades and it is still a debated argument nowadays. In fact, *mathematically* represent distinct concepts, but *may coincide physically* [5].

. Clearly, since they are denoted with two different names, they mathematically refer to two distinct properties. In fact, scale invariance refers to the property of a system to look exactly the same whether one stands closer or far to it. Nevertheless, whether or not this repetitive structure is the organizing principle of Nature remains of a philosophical matter.

The triumph of the application of scale invariance in theoretical physics is based on the renormalization group idea. In layman terms, it is just a recursive application of scale transformation and the concept of “coarse graining". Conformal invariance, on the other hand, takes its nomenclature from latin and refers to objects having the same shape. Precisely, it is the property of preserving the angles between the curves of a system. Our human perception easily approximately recognize invariance under scale transformation and not that under conformal transformations [5]. Therefore, there is no fundamental reason why a system that is scale invariant must also be conformally invariant.

However, it is important to understand why in modern theoretical physics there is often no clear distinction between these concepts in research. This could be due to the overlap in the behaviour of such systems or the practical challenges in distinguishing them in many physical contexts.

The first chapter of this thesis aims to better clarify the distinction and the physical enhancement from scale invariance to conformal invariance. The answer to the latter enhancement likely lies in the renormalization group flow. In particular, the concepts of irreversibility in the renormalization group flow and the counting of degrees of freedom will be crucial in the discussions. The irreversibility of the renormalization group flow can be understood intuitively: as previously mentioned, the flow involves a coarse-graining, leading to a loss of information. It would be highly counter-intuitive if the renormalization group flow exhibited cyclic or chaotic behaviour.

The theoretical foundation for this coarse-graining is provided by the "c-theorem", which states that there exists a function (known as the "c-function") that decreases monotonically along the renormalization group flow. This function essentially counts the degrees of freedom at a given energy scale. If such a function exists, it precludes the possibility of cyclic or chaotic behaviour in the renormalization group flow. In the context of relativistic quantum field theories in 2 dimensions ($d = 2$), there is proof that such a function exists, ensuring that the renormalization group flow is irreversible [5].

Actually, scale-invariant but non-conformal field theories are closely linked to the potential for cyclic or chaotic behaviour in the renormalization group flow, creating a tension between these concepts. The proof of irreversibility of the renormalization group flow in $d = 2$ dimensions implies that in this case, scale invariance must enhance to conformal invariance.

The first chapter of this thesis work opens with the introduction of the conformal group and the state-operator correspondence. By virtue of this, dilations on the plane can be understood as stretching or compressing the plane uniformly, and these are related to scaling transformations. When considering the cylinder, these dilations correspond to time translations. This means that changing the scale on the plane is analogous to moving forward or backward in time on the cylinder.

In the context of operator dimensions, the dilation charge on the plane represents the scaling dimensions of operators, which can be thought of as the "weights" assigned to different operators under scaling transformations. These scaling dimensions translate to energy levels when mapped to the cylinder, where the Hamiltonian H_{cyl} determines the energy spectrum.

Thus, the task of finding the dimension of a particular operator on the plane translates to finding the energy of the corresponding state on the cylinder. This mapping is powerful because time translations on the cylinder are always a symmetry, even when the system is not at a fixed point (i.e., not scale invariant).

This offers a significant advantage: while dilations on the plane require the system to be at a critical point where scale invariance holds, time translations on the cylinder do not have this restriction. Consequently, semiclassical computations mapped to the cylinder benefit from an additional symmetry that guides the classical solution, even away from criticality [6].

In more detail, in a regulated theory (one that includes some cut-off to avoid infinities), simple scaling solutions on the plane may not be consistent due to the lack of exact scale invariance. However, on the cylinder, one can consistently look for solutions that are stationary in time. This involves identifying a solution that remains constant over time, taking advantage of the symmetry of time translations on the cylinder.

Hence, chapter 1 aims to elucidate the following points:

1. Mapping dilations to time translations: dilations (scaling transformations) on the plane correspond to time translations on the cylinder.

2. Spectrum correspondence: the scaling dimensions of operators on the plane correspond to energy levels on the cylinder.

3. Advantage of cylinder symmetry: time translations on the cylinder remain a symmetry even away from critical points, unlike dilations on the plane.

4. Consistent solutions: on the cylinder, it is possible to find solutions that are stationary in time.

This approach simplifies the problem and provides additional tools to find consistent solutions, even in theories that are not perfectly scale-invariant. In chapter 2, point 4 starts the ball rolling for discussion about computing conformal field theory data relative to operators carrying a large value of some (internal) quantum number in theories with global symmetries. Via the state-operator correspondence, this can also be seen as the study of conformal field theory in states of fixed charge density.

Conformal Invariance and Conformal Field Theories

1

CHAPTER

§ 1.1 An invitation

1.1.1 Statistical Mechanics: critical phenomena and phase transitions

Let us begin with the following thought experiment. Take a large piece of material and measure some of its macroscopic properties, such as density, compressibility, or magnetisation. Then divide it into two halves and measure these properties again on each part, under the same external conditions. In both cases, one will find the same results obtained for the initial piece as a whole, so divide both pieces into other two halves and repeat the experiment on each piece again and again. After many iterations, this no longer holds true, as at the length scale of atoms and molecules, our paradigms must change, in order to explain their quite different individual nature. This length scale is of the order of a few interatomic spacings and gives us an idea of what is termed the correlation length: the distance over which the fluctuations of the microscopic degrees of freedom are significantly correlated with each other. Therefore, fluctuations in two parts of the material that are much further apart than the correlation length, such as those obtained in this experiment, do not make any appreciable difference to the macroscopic properties and can be neglected [7, 8].

This holistic precept, that *the whole is not necessarily equal to the sum of its parts*, finds in statistical physics one of its most important realisations. This branch of physics has become an essential tool for understanding and making quantitative predictions on diverse phenomena involving a large number of interacting degrees of freedom.

In 1869 the observation of the critical opalescence phenomenon by the Irish chemist Thomas Andrews paved the way for the study of the most important subjects of interest in statistical physics: critical phenomena and phase transitions. Subsequently, around 1895, Pierre Curie observed a similarity between the critical behaviours of a liquid-gas phase transition and that of the ferromagnetic transition in iron, highlighting the concept of universality of critical phenomena [9]. The need to formulate a theory that could explain these observations led to the introduction of the renormalization group.

Generally, a phase is a state of matter in which the macroscopic physical properties of the material are uniform on the macroscopic length scale; it is described by a thermodynamic function that depends on certain macroscopic variables called *control parameters*. This dependence is represented in a phase diagram, where a certain number of boundaries separate the different phases in which the material can be found. A change in the control parameters across a phase boundary causes a phase transition, and at a critical point these boundaries disappear: two phases become indistinguishable and the material shows anomalous behaviour. A phase can also be characterised by a certain degree of order quantified by an order parameter: if in the system under consideration it is possible to identify a symmetry at the microscopic level, one can say that the system itself is in a non-ordered phase, for which the order parameter is zero. When a phase transition occurs, there could be a symmetry breaking that creates some type of order quantified by a non-zero order parameter.

Phase transitions manifest themselves through the emergence of singularities in functions that represent physical quantities, such as jumps, cusps, and divergences. According to Paul Ehrenfest classification, phase transitions are labelled by the lowest-order derivative of the free energy that shows a singularity at the transition: hence, one can deal with first-, second-, third-order transitions and so on. In the modern scheme, one can divide them into two categories:

- First-order or discontinuous phase transitions: in passing from one stable phase to another, there is a discontinuous change in entropy (the first derivative of the free energy) at the transition temperature, corresponding to latent heat and generally to a finite correlation length.

- Continuous phase transitions: they are characterised by a continuous change in entropy, and so no latent heat, and an infinite correlation length. In this case, the fluctuations are correlated over all distance scales, which thereby forces the system to be in a unique, critical, phase.

Commonly speaking, continuous phase transitions are generally identified with critical phenomena occurring at the critical point where two or more phases become indistinguishable; meanwhile, from the symmetry point of view, one can link first-order transitions to the breaking of a symmetry. Several other ones are known as infinite-order phase transitions, they are typical of systems with a few spatial dimensions, they are continuous but break no symmetries; the most famous example is the Kosterlitz - Thouless transition in the two-dimensional XY model. Many quantum phase transitions, e.g. in two-dimensional electron gases, belong to this class.

A material can show both first-order and continuous phase transitions, depending on the conditions. One may mention, as an example, the uniaxial ferromagnet [8]: in this case, two interesting external control parameters can be varied, the temperature T and the applied magnetic field H; the phase diagram is very simple and shown in Figure 1.1. To describe how magnetisation M behaves with respect to the applied field H for different temperature regimes, one obtains Figure 1.2.

In the case where the temperature is lower than a critical value T_c, called Curie temperature, the magnetisation, which is calculated as the first derivative of the free

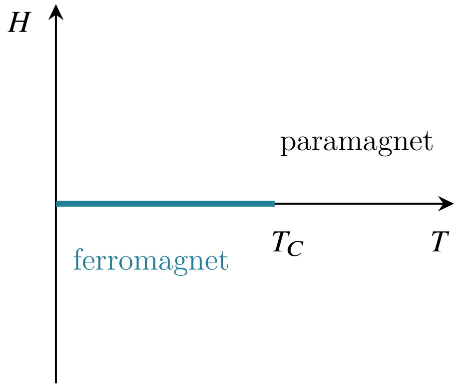

Figure 1.1.: Phase diagram of a uniaxial ferromagnet.

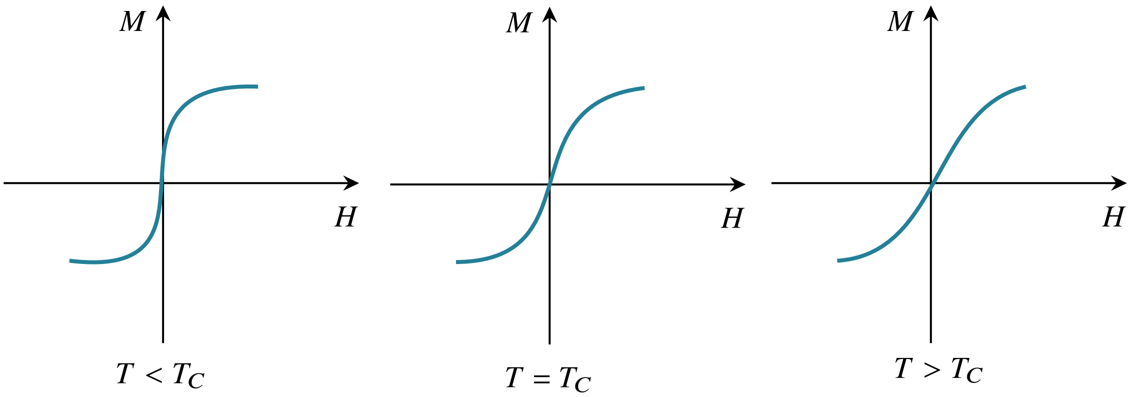

Figure 1.2.: Magnetisation versus applied field, for various temperatures.

energy with respect to the field H, shows a discontinuity, so one is dealing with a first-order transition.

In fact, the two different limits $H \to 0^+$ and $H \to 0^-$ give opposite finite values for the (spontaneous) magnetisation, and the precise value actually assumed, say, chosen by the system, depends only on its previous history: one has a spontaneous symmetry breaking (SSB). What happens in this example is that, although the Hamiltonian describing the system is invariant under simultaneous reversal of all the magnetic degrees of freedom, this discrete symmetry is not shared by the state assumed by the system itself. The magnetisation, which represents the degree of alignment of the microscopic spins in the material, corresponds to the order parameter that is established with the breaking of the symmetry.

To give also an immediate example of a continuous broken symmetry, just simply consider, more generally, the same ferromagnet in three dimensions for which the broken symmetry is the rotational invariance of spins. As T approaches the critical value, such a jump goes to zero and the transition becomes continuous. Additionally, the point given by $H = 0$ and $T = T_c$ is a critical end-point. From this value of T on, the material shows paramagnetic properties as the magnetisation varies with H continuously. If now one observes the behaviour of the magnetisation versus the temperature, keeping H fixed near 0^+, in lowering T and crossing T_c, M goes from 0 to a finite positive value in a continuous way: one is dealing with a continuous and, in particular, a second-order transition. In fact, analysing the behaviour of the susceptibility reveals interesting dynamics. This susceptibility is the second derivative of the free energy with respect to the external field and consequently the first derivative of the magnetisation with respect to the same external field. As $H \to 0^+$, one finds a divergence at the critical point. See Figures. 1.3 and 1.4.

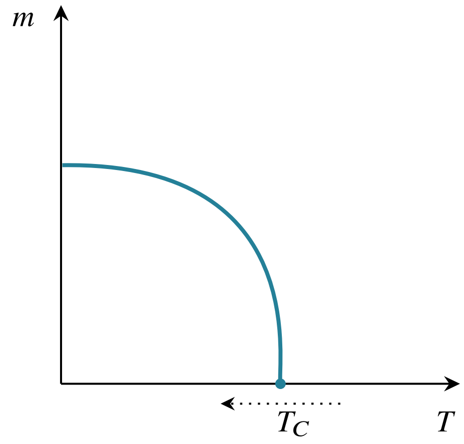

Figure 1.3.: Example of a second-order transition.

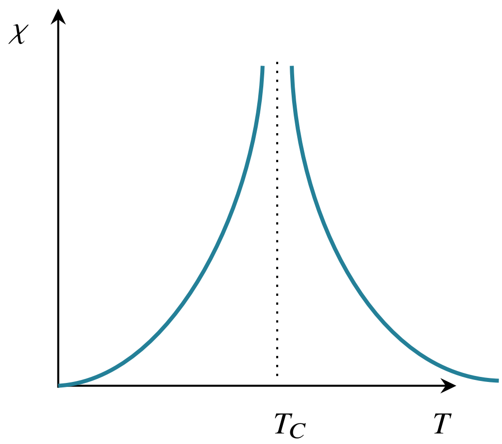

Figure 1.4.: The magnetic susceptibility diverges at the critical point.

To complete this section let us return to the previously mentioned concept of universality, bringing up the important following fact: near the critical point the physical quantities, including the correlation length, exhibit a power-law behaviour with respect to adimensional quantities corresponding to the relative distance of the control parameters from their critical value, e.g. $t = (T - T_c)/T_c$. The exponents that characterise these laws are called *critical exponents*. In particular, the correlation function $G(r)$ decays exponentially as a function of the distance r, if r is greater than the correlation length and if the temperature is not at its critical value:

$$G(r) \propto r^{-\frac{d-1}{2}} e^{-\frac{r}{\xi}} \quad (r \gg \xi, \quad T \neq T_c)\,. \tag{1.1}$$

As the value of the correlation length increases rapidly, and eventually diverges, the system approaches the critical point with the following law

$$\xi \propto |t|^{-\nu} \quad (T \neq T_c)\,. \tag{1.2}$$

When the temperature is tuned to be exactly at the critical value, the correlation function decays slowly in a still power-law manner but characterised by a new (anomalous) exponent η

$$G(r) \propto r^{-d+2-\eta} \quad (T = T_c)\,. \tag{1.3}$$

The origin of the anomalous exponent can be explained through a heuristic argument [8]. Most physical problems have more than one characteristic scale, and so, in general, the physical quantities depend on the adimensional ratios of these multiple scales. However, it is possible to have simplifications when there is a large difference between them. To give an example, in the planetary motion problem it is possible to neglect the planet's radius length when compared to the huge distances under consideration. However, the same does not hold true when considering a system near the critical point. In fact, let us think of a system characterised by an interatomic distance a and a correlation length ξ. Following the same reasoning, one would be tempted to neglect a when it is much smaller than ξ, but this would lead to a wrong result for the behaviour of the correlation function. The motivation lies in the fact that, at the critical point, all fluctuations at all length scales are important and a cannot be neglected. These considerations affect the power-law describing the correlation function near the critical point, in a way that an anomalous dimension appears.

Precisely, these fluctuations on all length scales appear simultaneously, causing a non-analytic behaviour in the physical quantities and the presence of these singularities made the usual theoretical perturbative approach inappropriate. Despite these difficulties, there are some simplifications in the study of these phenomena, the most important being precisely the universality property: many features of systems near a continuous phase transition are independent of microscopic details. These systems, which share properties such as the symmetries of the Hamiltonian, the number of spatial dimensions, and the range of interactions, can be classified into a relatively small number of equivalence classes, called *universality classes*. In this way, apparently different systems described by different theories are arranged together by similar behaviour near criticality, described in terms of the same set of critical exponents [9].

The calculation of the critical exponents is one of the most important points in the study of critical phenomena. It is important to recognise them as the scaling dimensions of operators in the formalism that will be developed in this chapter and to stress that they will play a fundamental role due to the state-operator correspondence. The development of an analytical method was necessary and that of the renormalization group has been the most important tool. Let us introduce it in a systematic way.

1.1.2 **The Renormalization Group flow**

As one could understand from this brief introductory summary of critical phenomena, the renormalization group plays a crucial role in providing a comprehensive view capable of explaining the origins of power-law behaviours and universality. The basic idea, suggested by Kadanoff (1966) and then developed by Wilson (1971), is to follow the change of physical quantities when the distance or the energy scale is varied. This is accomplished through a combined operation of coarse graining and a successive re-scaling of the degrees of freedom of the system. After changing the scale of the system, the coarse graining process consists of choosing a rule that groups the various degrees of freedom in sub-groups and assigning to each one a single "effective" degree of freedom representing its overall content at this new scale. In this way, the shorter-length fluctuations are eliminated. An example regarding the case of the Ising model is the "block-spin" operation that, following a majority rule, assigns to every 3×3 spin cell a single spin in the way represented in Figure 1.5.

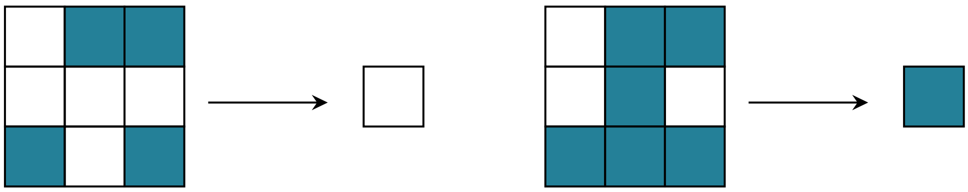

Figure 1.5.: Block-spin transformation in which we apply the majority rule to replace $3 \times 3 = 9$ Ising spins by a single spin.

The operation of re-scaling is just to expand again the system restoring the original scale. In doing this, one ends up with a less detailed description of the same system in terms of a smaller number of degrees of freedom. Hence, the attention is shifted from the shorter- to longer-length behaviour of the system. An unbounded repetition of these "lossy" scale transformations creates a succession of models that all describe the same physics at large distances. However, in these models, the structure of small distance is gradually eliminated, and the total information decreases. As these scale transformations do not have an inverse, their set (the renormalization group) is, formally speaking, only a semi-group. If this sequence of operations reaches a limit, it exhausts all length scales and leads to a macroscopic system invariant under these transformations. In this case, universality is explained: the system reveals critical behaviour, and all the statistical models described by the same set of critical exponents belong to the same universality class.

Wilson was the first to recognise the many similarities between the theory of critical phenomena and the quantum field theory describing the fundamental interactions at the microscopic scale. In QFT the parameters involved, like the masses of particles and the coupling constants quantifying the intensity of their interactions, are also dependent on the energy scale. For example, it is well known that the charge of the electron at very small distances (high energies) is different with respect to the one "dressed" measured at large distances (low energies) and this change, called "*running*" of the coupling constant, is determined by the renormalization group equation (RGE). Calling μ the energy scale corresponding to the generic length scale λ, the β-function defined by

$$\beta = \beta(g^R) = \mu \, \frac{\partial g^R}{\partial \mu} \tag{1.4}$$

measures the rate of change of the renormalized coupling constant g^R with respect to the energy scale. Let us recall here that, in fact, the corresponding "bare" quantity g^0 is scale invariant, $\frac{\partial g^0}{\partial \mu} = 0$, that is why from this point on, the superscript "R" is automatically implied in all formulas below, unless otherwise stated.

In this regard, it is also worth noting that the presence of the derivative $\mu \frac{\partial}{\partial \mu} = \frac{\partial}{\partial \ln \mu}$ reflects the multiplicative behaviour of these scale changes also known as dilations. In fact, if $\mu \frac{\partial}{\partial \mu}$ is their associated operator, one can linearise the definition of the β-function obtaining an eigenvalue equation that reads

$$\mu \frac{\partial g}{\partial \mu} = d_g \, g \,, \tag{1.5}$$

where the eigenvalue d_g is the scaling dimension of g. It can then be solved obtaining

$$g(\mu) = \mu^{d_g} \, g(1) \,, \tag{1.6}$$

an equation that describes how the coupling constant "scales" with respect to the renormalization scale μ, starting from the initial value $\mu = 1$. It can be further emphasised that if $t = \ln \mu$ the equation (1.5) defines a dynamical process in "time" t. In fact, this energy dependence of interaction strengths in physical systems can be reflected in the trends observed in pandemics [10, 11], for example[1].

The β-function defined depends on both the value of μ and g, while the coupling constant changes with μ according to (1.6). If one plots the latter behaviour of the coupling constant with respect to μ, the outcome is the so-called renormalization group flow: by varying the energy scale one moves in the parameters' space of a theory, which in turn defines the space of theories themselves. To visualise it, let us imagine studying a theory with two coupling constants g_1 and g_2, whose flow is represented in Figure 1.6.

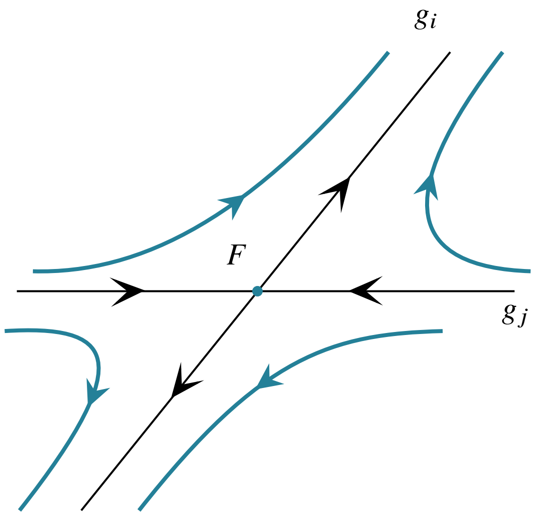

Figure 1.6.: Schematic illustration of the parameter flow when one of the exponents is positive and the other negative.

As previously stated, in doing successive scale transformations, the theory may exhibit

[1] Exactly, a pandemic progression can be described by a flow in time of a function of the total number of infected individuals where the effect of a virus on it is the same in spirit of a source of explicit conformal symmetry breaking term (further details about the latter are discussed in chapter 5). In fact, the latter drives the pandemic dynamics from an unstable equilibrium to a stable one. These fixed points can be interpreted as the beginning of the global outbreak and its endemic state, respectively.

scale invariance. This means that the system described is characterised by the same values of parameters regardless of the distance or the energy. The values (g_1^*, g_2^*) for which this happens define a *fixed point* (FP). By definition, they are the values for which the β-function is zero

$$\beta_i(g_i^*) = \mu \frac{\partial g_i}{\partial \mu}\bigg|_{g_i = g_i^*} = 0 \qquad i = 1, 2\,. \tag{1.7}$$

Expanding to the first order around them one can infer their local stability properties [12]:

$$\beta_i(g_i) = \beta_i(g_i^*) + \frac{\partial \beta_i}{\partial g_j}\bigg|_{g_j = g_j^*} (g_j - g_j^*)\,;$$

the first derivative term is an auto-perturbation quantifying how much one departs from the scale invariance and it is proportional to the scale dimension of g, namely

$$\frac{\partial \beta_i}{\partial g_j}\bigg|_{g_j = g_j^*} = \frac{\partial}{\partial g_j}\Big(\mu \frac{\partial g_i}{\partial \mu}\Big)\bigg|_{g_j = g_j^*} = \frac{\partial}{\partial g_j}\Big(d_{g_i}\, g_i(\mu)\Big)\bigg|_{g_j = g_j^*} = d_{g_i}\delta_{ij} = d_{g_j}\,,$$

hence

$$\beta_i(g_i) = \beta_i(g_i^*) + d_{g_i}(g_i - g_i^*)\,. \tag{1.8}$$

If these eigenvalues are positive the corresponding terms in the Lagrangian of the theory, are called *relevant* for which they grows when μ grows, making us depart from the fixed values (g_1^*, g_2^*). This FP is thus unstable and the arrows in the RG flow departs from it: it is an ultraviolet unstable fixed point. When these eigenvalues are negative, the corresponding Lagrangian terms are called *irrelevant*. They “decay” at large scales, making us move in the flow towards the fixed point. It is referred to as an infrared stable fixed point.
In the limit case in which all the eigenvalues are zero, the corresponding operators are called *marginal*. Then, to solve the RGE and to determine the behaviour of these quantities one has to go to the second order

$$\mu \frac{\partial g_i(\mu)}{\partial \mu} \sim B g_i^2 \quad \longrightarrow \quad g_i(\mu) = \frac{g_i(1)}{1 - B\, g_i(1) \ln \mu}\,; \tag{1.9}$$

if $g_i(1) \sim 1$ when μ is large then

$$g_i(\mu) = -\frac{1}{B \ln \mu}\,, \tag{1.10}$$

so, when $\mu \to \infty$, the solution for the perturbation goes to 0 and one has logarithmic (so very slow and marginal) convergence to the FP.

These introductory concepts orbit around the notion of *scale invariance*. Throughout this chapter, similarities and differences between this concept and the more general one associated with *conformal invariance* will be discussed at length. In fact, conformal transformations, defined by their preservation of angles, are more general than translations, rotations, or Lorentz transformations, which preserve lengths or their relativistic equivalent, the spacetime interval [13][2]

In the modern context, quantum field theories at renormalization group fixed points define CFTs.

In the following sections, it will be shown that in Lorentz-invariant quantum field theories in d dimensions, the trace of the energy-momentum tensor is a linear combination of scalar operators of dimension d, with coefficients being the RG β-functions, along with contributions involving lower-dimensional operators with derivatives and mass terms if present. At RG fixed points, the β-functions vanish, and if this results in a zero trace for the energy-momentum tensor, the fixed point defines a CFT. In this chapter, the conformal group is the first argument introduced, and it is demonstrated how CFTs can be analysed using the basic requirements of conformal symmetry, along with the locality and unitarity conditions satisfied by quantum field theories, to significantly constrain the spectrum of operators and their scaling dimensions (mainly following [5, 19–21]). Additionally, the concept of symmetry will be examined with particular attention to the spontaneous symmetry breaking of conformal symmetry down to Poincaré one. Furthermore, the non-linear realisation of the conformal invariance will be explored [22–27]. These ideas are pivotal for the rest of this thesis work.

§ 1.2 The conformal group in $d \geq 3$ dimensions

This first chapter begins with the introduction of the conformal group in a generic dimension d of the spacetime. To begin with, consider a d-dimensional manifold $\mathcal{M}$ which can be Riemannian or pseudo-Riemannian. In the first case, the metric will be the Lorentzian one $\eta_{\mu\nu}$[3] while in the latter the euclidean metric, namely the Kronecker delta $\delta_{\mu\nu}$ [28].

A d-dimensional manifold is said to be conformally flat if the invariant line element can be written as

$$\mathrm{d}s^2 = \underbrace{e^{2\omega(x)}}_{\triangleq\, \Omega(x)}\ \mathrm{d}x^\mu\ \mathrm{d}x^\nu \begin{cases} \eta_{\mu\nu} & \text{lorentzian signature} \\ \delta_{\mu\nu} & \text{euclidean signature} \end{cases} \tag{1.11}$$

where $\Omega(x)$ is called the conformal factor, allowed to be x-dependent.

Generally, a metric that satisfies this definition is called *conformally flat*. As a result:

[2] They were considered in the 19th century (for a historical overview, see [14]), and they were first applied in a fundamental physics context by Bateman [15], who demonstrated the invariance of the four-dimensional scalar wave equation under conformal transformations. Bateman [16] and Cunningham [17] later extended this to Maxwell's equations for the electromagnetic field. However, conformal transformations do not play a significant role in classical electrodynamics [18], since they do not remain symmetrical when coupled with matter, and problems arise with causality.

[3] Throughout this chapter the signature of the metric will be diag$(-1, 1, 1, 1, \dots)$.

Definition 1.2.1

> *The conformal group is a sub-group of the group of general coordinate transformations, in general diffeomorphisms, preserving the conformal flatness of the metric.*

The conformal transformations have the property of preserving angles between vectors while distorting the lengths. Therefore, under a change of coordinates $x^\mu \mapsto x'^\mu \equiv y^\mu = x^\mu + \epsilon^\mu$, said $g_{\mu\nu}$ the metric tensor of a given d-dimensional manifold:

$$g'_{\mu\nu}(x') = \Omega(x)\ g_{\mu\nu}(x) \iff g_{\mu\nu}(x^\mu + \epsilon^\mu)\frac{\partial y^\mu}{\partial x^\alpha}\frac{\partial y^\nu}{\partial x^\beta} = \Omega(x)\ g_{\alpha\beta}(x)\ . \tag{1.12}$$

To find the generators of the infinitesimal conformal transformations ϵ^μ let us follow [28] and consider

$$\left(g_{\mu\nu}(x) + \epsilon^\rho\partial_\rho g_{\mu\nu}(x)\right)\left(\delta^\mu{}_\alpha + \partial_\alpha\epsilon^\mu\right)\left(\delta^\nu{}_\beta + \partial_\beta\epsilon^\nu\right) = \Omega(x)\ g_{\alpha\beta}(x) \tag{1.13}$$

$$\xrightarrow{O(\epsilon^2)} \underbrace{\epsilon^\rho\partial_\rho g_{\alpha\beta}(x) + g_{\alpha\nu}(x)\partial_\beta\epsilon^\nu + g_{\mu\beta}(x)\partial_\alpha\epsilon^\mu}_{\mathcal{L}_{\epsilon^\rho\partial_\rho}\ g_{\alpha\beta}(x) \quad \text{Lie derivative of} \quad g_{\alpha\beta}(x)} = (\Omega(x) - 1)\ g_{\alpha\beta}(x) \tag{1.14}$$

then, recalling the definition of affine connection $\boldsymbol{\nabla}$ and said $\Gamma^\alpha_{\beta\gamma}$ its coefficients [28], one arrives at

$$\boldsymbol{\nabla}: \quad \mathfrak{X}(\mathcal{M}) \times \mathfrak{X}(\mathcal{M}) \to \mathfrak{X}(\mathcal{M}) \implies \left(\boldsymbol{\nabla}_\mu\epsilon\right)_\lambda = \partial_\mu\epsilon_\lambda - \Gamma^\sigma_{\mu\lambda}\epsilon_\sigma\ , \tag{1.15}$$

so equation (1.14) becomes

$$\boldsymbol{\nabla}_\alpha\epsilon_\beta + \boldsymbol{\nabla}_\beta\epsilon_\alpha = (\Omega(x) - 1)\ g_{\alpha\beta}(x)\ . \tag{1.16}$$

Now, considering a constant metric $\boldsymbol{\nabla} \equiv \partial$, by contracting (1.16) with $g^{\alpha\beta}$ one ends up with

$$\partial_\alpha\epsilon_\beta + \partial_\beta\epsilon_\alpha = \frac{2}{D}\boldsymbol{\nabla}\cdot\epsilon\ g_{\alpha\beta} \implies \left(g_{\sigma\beta}\,\Box + (D-2)\partial_\sigma\partial_\beta\right)\boldsymbol{\nabla}\cdot\epsilon = 0\ . \tag{1.17}$$

Therefore, depending on the dimensionality of $\mathcal{M}$ the cases to study are two: $d = 2$ or $d > 2$. Considering the latter case, from equation (1.17) ϵ^μ can be at most quadratic in x[4]. Hence, the conformal group contains the following transformations:

1. Translations

$$\epsilon^\mu = a^\mu \triangleq P^\mu \quad \text{whose infinitesimal generators are} \quad a^\mu\partial_\mu \quad \text{in number} \quad d \tag{1.18}$$

2. Lorentz transformations

$$\epsilon^\mu = \omega^\mu{}_\nu\, x^\nu \triangleq J^\mu_\nu \quad \text{whose infinitesimal generators are} \quad \omega^\mu{}_\nu\, x^\nu\partial_\mu \quad \text{in number} \quad \frac{d(d-1)}{2} \tag{1.19}$$

[4] Actually, from (1.17) it does not immediately follow that ϵ has to be at most quadratic in x. However, for $d > 2$ one can show the stronger relation $\partial_\mu\partial_\nu\partial_\rho\epsilon_\lambda = 0$ for any indices μ, ν, λ, ρ, which then implies that ϵ is at most bilinear in x.

3. Dilations

$$\epsilon^\mu = \lambda x^\mu \triangleq D \quad \text{whose infinitesimal generators are} \quad \lambda x^\mu \partial_\mu \quad \text{in number} \quad 1 \tag{1.20}$$

4. Special conformal transformations:
   they are a sequence of transformations, inversion→translation→inversion, therefore

$$\epsilon^\mu = b^\mu x^2 - 2x^\mu b \cdot x \triangleq K^\mu \quad \text{whose infinitesimal generators are} \quad \left(b^\mu x^2 - 2x^\mu b \cdot x\right) \partial_\mu \quad \text{in number} \quad d\ . \tag{1.21}$$

To summarise, the following infinitesimal transformations are conformal transformations

$$\delta x^\mu = a^\mu + \omega^\mu{}_\nu x^\nu + \lambda x^\mu + b^\mu x^2 - 2x^\mu b \cdot x \tag{1.22}$$

and the general form of the generators of the conformal group is

$$P_\mu = -i\partial_\mu \tag{1.23}$$
$$J_{\mu\nu} = i\left(x_\mu \partial_\nu - x_\nu \partial_\mu\right) \tag{1.24}$$
$$D = -ix^\mu \partial_\mu \tag{1.25}$$
$$K_\mu = -i\left(2x_\mu x^\nu \partial_\nu - x^2 \partial_\mu\right) \tag{1.26}$$

where the total number of generators is $\frac{(d+2)(d+1)}{2}$. These generators satisfy the following $SO(2,d)$ algebra

$$\left[J_{\mu\nu}, J_{\rho\sigma}\right] = i\eta_{\mu\rho} J_{\nu\sigma} + \quad \text{permutation} \tag{1.27}$$
$$\left[J_{\mu\nu}, P_\rho\right] = i\left(\eta_{\mu\rho} P_\nu - \eta_{\nu\rho} P_\mu\right) \tag{1.28}$$
$$\left[J_{\mu\nu}, K_\rho\right] = i\left(\eta_{\mu\rho} K_\nu - \eta_{\nu\rho} K_\mu\right) \tag{1.29}$$
$$\left[J_{\mu\nu}, D\right] = 0 \tag{1.30}$$
$$\left[D, P_\mu\right] = iP_\mu \tag{1.31}$$
$$\left[D, K_\mu\right] = -iK_\mu \tag{1.32}$$
$$\left[K_\mu, P_\nu\right] = -2iJ_{\mu\nu} - 2i\eta_{\mu\nu} D\ . \tag{1.33}$$

It is important to stress that a given sub-algebra made with the Poincaré and dilation operators can render a theory Poincaré and scale invariant *without* being invariant under the full conformal group. Moreover, the question of whether or not scale invariance automatically implies invariance under special conformal transformations has been the subject of much debate in literature and will be discussed throughout this chapter. While there have been several counterexamples found in which scale symmetry was preserved alone, these examples are limited and have so far been constrained to the case $d = 2$ (see [5, 29, 30] and references therein).

1.2.1 Representation of the conformal group

Let us now turn the gaze on how the conformal generators act on classical fields [20]. Generally, conformal invariance at the classical level does not also guarantee conformal invariance at the quantum level. Quantum field theories may rely on parameters depending on the scale of energy. This means that conformal symmetry may be broken by the introduction of a scale needed for regularization prescriptions. Nevertheless, these concepts will be discussed throughout this thesis. For the moment, let T_a denote a matrix representation such that under an infinitesimal conformal transformation a given field $\phi(x)$ transforms as

$$\phi'(x') = (1 - \epsilon^a T_a)\ \phi(x)\ . \tag{1.34}$$

To obtain the general form of these generators, consider the sub-group of the full conformal group leaving the origin invariant. Let us denote the values at $x = 0$ of these generators of rotations, dilations and special conformal transformations with $s_{\mu\nu}$, $\tilde{\Delta}$ and κ_μ, respectively. They must form a matrix representation of the following reduced algebra [20]

$$\left[\tilde{\Delta}, s_{\mu\nu}\right] = 0 \tag{1.35}$$
$$\left[\tilde{\Delta}, \kappa_\mu\right] = -i\kappa_\mu \tag{1.36}$$
$$\left[\kappa_\mu, \kappa_\nu\right] = 0 \tag{1.37}$$
$$\left[\kappa_\rho, s_{\mu\nu}\right] = i\left(\eta_{\rho\nu}\kappa_\nu - \eta_{\rho\nu}\kappa_\mu\right) \tag{1.38}$$
$$\left[s_{\mu\nu}, s_{\rho\sigma}\right] = i\left(\eta_{\nu\rho}s_{\mu\sigma} + \eta_{\mu\sigma}s_{\nu\rho} - \nu \leftrightarrow \mu\right)\ . \tag{1.39}$$

Now, consider the scenario where the field ϕ transforms according to an irreducible representation of the Lorentz group. Schur's lemma ensures that any matrix commuting with $s_{\mu\nu}$ must be a multiple of the identity. Therefore, from (1.35) $\tilde{\Delta}$ needs to be a number and because dilations generate non-compact transformations, their finite-dimensional representations are necessarily non-unitary and $\tilde{\Delta}$ is necessarily non-Hermitian. Specifically, $\tilde{\Delta} = -i\Delta$ with Δ is the scaling dimension of the field ϕ, where generally, the scaling dimension of a generic field is defined by the action of a scale transformation on the field

$$\phi(\lambda x) = \lambda^{-\Delta}\ \phi(x)\ . \tag{1.40}$$

Additionally, since $\tilde{\Delta}$ is proportional to the identity, (1.36) automatically shows that κ_μ vanish. Hence, the overall transformation rules for the field ϕ are

$$P_\mu\phi(x) = -i\partial_\mu\phi(x) \tag{1.41}$$
$$J_{\mu\nu}\phi(x) = i\left(x_\mu\partial_\nu - x_\nu\partial_\mu\right)\phi(x) + s_{\mu\nu}\phi(x) \tag{1.42}$$
$$D\phi(x) = -i\left(x^\mu\partial_\mu + \Delta\right)\phi(x) \tag{1.43}$$
$$K_\mu\phi(x) = \left(-2i\Delta x_\mu - x^\nu s_{\mu\nu} - 2ix_\mu x^\nu\partial_\nu + ix^2\partial_\mu\right)\phi(x)\ . \tag{1.44}$$

§ 1.3 Radial quantization, unitarity and state-operator correspondence

In CFT the observables of the theory that are the quantities of interest are the n-point correlation functions of *fields*. With *field*, one means any local quantity with coordinate dependence. Let us consider the two-point function

$$\langle \phi_1(x_1)\phi_2(x_2)\rangle = \frac{1}{\mathcal{Z}} \int \mathcal{D}\Phi_i \; \phi(x_1)\phi_2(x_2) \; e^{-S[\Phi_i]} \tag{1.45}$$

where Φ_i is the set of all fields in the theory while S is the conformally invariant action and ϕ_1 and ϕ_2 under a scale transformation transform as in (1.34). Under a scale transformation $x' = \lambda x$, the two-point function transforms as [20, 21]

$$\langle \phi_1(\lambda x_1)\phi_2(\lambda x_2)\rangle = \lambda^{-\Delta_1-\Delta_2} \langle \phi_1(x_1)\phi_2(x_2)\rangle \tag{1.46}$$

and because the invariance under Poincaré symmetry implies causality (specifically that information cannot travel faster than the speed of light), then

$$\langle \phi_1(x_1)\phi_2(x_2)\rangle = f\left(|x_1 - x_2|\right) \qquad \Longrightarrow \qquad f(\lambda x) = \lambda^{-\Delta_1-\Delta_2} \, f(x) \tag{1.47}$$

which implies that the two-point function is constrained to be of the form

$$\langle \phi_1(x_1)\phi_2(x_2)\rangle = \frac{d_{12}}{|x_1 - x_2|^{\Delta_1+\Delta_2}} \; . \tag{1.48}$$

It is not required that $\Delta_1 = \Delta_2$. Instead, the consequence of the special conformal transformation

$$x'^{\mu} = \frac{x^{\mu} - (x\cdot x)b^{\mu}}{1 - 2(b\cdot x) + (b\cdot b)(x\cdot x)} \tag{1.49}$$

implies that the distance between two points transforms as

$$\left|x'_i - x'_j\right| = \frac{|x_i - x_j|}{\gamma_i^{1/2}\gamma_j^{1/2}} \quad \text{with} \quad \gamma_i = 1 - 2(b\cdot x_i) + b^2 x_i^2 \tag{1.50}$$

thus

$$\frac{d_{12}}{|x_1 - x_2|^{\Delta_1+\Delta_2}} = \frac{d_{12}}{\gamma_1^{\Delta_1}\gamma_2^{\Delta_2}} \, \frac{(\gamma_1\gamma_2)^{(\Delta_1\Delta_2)/2}}{|x_1 - x_2|^{\Delta_1+\Delta_2}} \tag{1.51}$$

is satisfied only if $\Delta_1 = \Delta_2$. Hence, the two-point function in a conformally invariant theory is constrained to be:

$$\langle \phi_1(x_1)\phi_2(x_2)\rangle = \frac{d_{12}}{|x_1 - x_2|^{2\Delta_1}} \; . \tag{1.52}$$

The time has come to discuss the state-operator correspondence. To this end, let us discuss the foliation of the spacetime, namely the division of the d-dimensional spacetime into $d-1$-dimensional regions where each one has its own Hilbert space [21]. Two Hilbert spaces associated with two different surfaces related by a symmetry transformation are the same Hilbert space. Let us define the states of these regions. Generally, the "in" states $|in\rangle$ are those obtained by inserting operators in the past of a given surface, while the "out" states those obtained by inserting operators in the future. Two in and out states living on different surfaces are connected by some unitary operator U if there exist no other states in between them [21] (see Figure 1.7).

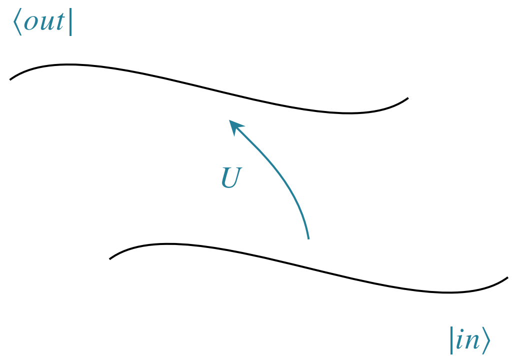

Figure 1.7.: States living on different surfaces and the evolution operator U connecting them.

The correlation function is $\langle out|U|in\rangle$. This concept is not significantly distant from the approaches commonly employed in Poincaré-invariant theories. To better appreciate this argument, in Poincaré-invariant theories the foliated surfaces are of equal time and to move from one surface to another, the Hamiltonian H is employed via the unitary evolution operator $U = \exp\{iHt\}$. Instead, in conformally invariant theories, spacetime is opportunely divided using spheres S^{d-1} having different radii R_i centred at the origin. To move from one foliation to another, the dilation operator D is used instead of the Hamiltonian. Since D commutes with the Lorentz generator $J_{\mu\nu}$ (1.30), the states can be classified according to their scaling dimension Δ and spin l [20, 21]:

$$D\,|\Delta\rangle = i\Delta\,|\Delta\rangle \tag{1.53}$$

$$J_{\mu\nu}\,|\Delta, l\rangle = s_{\mu\nu}\,|\Delta, l\rangle \ . \tag{1.54}$$

The following change of coordinates

$$\tau \equiv R\log\frac{r}{R} \implies ds^2 = e^{2\frac{\tau}{R}}\left(d\tau^2 + R^2\, d\Omega_{d-1}^2\right) , \tag{1.55}$$

maps $\mathbb{R}^d$ to $\mathbb{R}\times S^{d-1}$ (in fact (1.55) is conformally equivalent to the metric of a cylinder). Hence, τ acts as the natural time coordinate for the evolution from one sphere to another. The evolution operator is

$$U = e^{iD\tau/R} \tag{1.56}$$

thus

$$U\,|\Delta\rangle = e^{-\frac{\Delta}{R}\tau} = \left(\frac{r}{R}\right)^{-\Delta}|\Delta\rangle \ . \tag{1.57}$$

These observations constitute the heart of the so-called *radial quantization*. Moreover, moving to the origin $r \to 0$ in this radial quantization is equivalent to moving to the infinite past $\tau \to -\infty$. Similarly, moving to infinity $r \to \infty$ corresponds to approaching the infinite future $\tau \to \infty$. In terms of states, the creation of a state at a given radius R is obtained by placing an object inside the sphere having that radius and the state is created at a given time by placing an object in the infinite past. Consequently, in the absence of any objects being placed, one deals with the vacuum state of the theory $|0\rangle$, namely that state which by definition is invariant under the action of the full conformal group. The dilation eigenvalue, the *radial quantization energy*, is zero for this state. If an operator is placed at the origin, the action on this state would create another state with a given scaling dimension

$$|\Delta\rangle = \mathcal{O}_\Delta(x=0)\,|0\rangle \ , \tag{1.58}$$

while inserting an operator at $x \neq 0$ creates a state that is not an eigenstate of the dilation operator because dilations move the insertion point. In fact

$$|\Psi\rangle = \mathcal{O}_\Delta(x)\,|0\rangle = e^{iPx}\mathcal{O}_\Delta(0)\ e^{-iPx}\,|0\rangle = e^{iPx}\ \ |\Delta\rangle = \sum_n \frac{(iPx)^n}{n!}\ \ |\Delta\rangle \tag{1.59}$$

the state $|\Psi\rangle$ is a superposition of states having different eigenvalues. Now, since $\left[D, P_\mu\right] = iP_\mu$, it is understood that the operator P_μ when acting on $|\Delta\rangle$ raises its energy by one unit

$$|\Delta\rangle \xrightarrow{P_\mu} |\Delta+1\rangle \ , \tag{1.60}$$

hence the generator of translations acts as a raising operator for the states $|\Delta\rangle$. Naturally, if on the one hand, there is a raising operator on the other there must be a lowering operator. To introduce the corresponding lowering operator, a crucial key point is the notion of *unitarity*. Therefore, let us go back to the metric on the cylinder [5]

$$ds^2_{cyl} = d\tau^2 + R^2 d\Omega^2_{d-1} = \left(\frac{R}{r}\right)^2 \left(dr^2 + r^2 d\Omega^2_{d-1}\right) \tag{1.61}$$

according to which, a field in Euclidean space and a field on the cylinder are related by

$$\phi(\tau, \Omega_{d-1})_{cyl} = \left(\frac{r}{R}\right)^\Delta \phi(x)_{\mathbb{R}^d} \tag{1.62}$$

namely, on the cylinder one essentially works with the same field as in flat spacetime. Then, let us better explore the connection between flat fields and fields on the cylinder to have a notion of hermitian conjugation on the cylinder [5] (and references therein). Unitarity on the cylinder is related to the notion of reflection positivity in Euclidean space. Indeed, after performing the Wick rotation to get Euclidean signature $x_0 = i\tau$, reflection positivity states that

$$\langle \mathcal{O}(x)\mathcal{T}\,[\mathcal{O}(x)]\rangle \geq 0 \quad \text{with} \quad \mathcal{T}\,[\mathcal{O}(x_1,\ldots,\tau)] = \mathcal{O}^\dagger(x_1,\ldots,-\tau) \tag{1.63}$$

meaning that any two-point function with operators inserted with property $\mathcal{T}[\mathcal{O}] = \mathcal{O}^\dagger$ has to be positive. The reflection operator corresponds to the inversion operator. Time-reversal in Euclidean signature corresponds to a coordinate inversion on the flat space $\mathbb{R}^d$, since for a Hermitian field the following

$$\phi(\tau,\Omega_{d-1})^\dagger_{cyl} = \left(e^{\tau H_{cyl}}\phi(0)e^{-\tau H_{cyl}}\right)^\dagger = e^{-\tau H_{cyl}}\phi(0)^\dagger e^{\tau H_{cyl}} = \phi(-\tau,\Omega_{d-1})_{cyl} \tag{1.64}$$

holds. Precisely, Hermitian conjugation in unitary theory requires taking $x_0 = i\tau$ to $x_0^* = -i\tau$, i.e. it corresponds to a reflection across the surface of $\tau = 0$. In radial quantization, when performing the change of coordinates $\tau = R\log(r/R)$, this time-reversal transformation corresponds to a coordinate inversion $\mathscr{R} : r \to r^{-1}$ [5]. Correlation functions measure the overlap between states corresponding to a path integral inside the unit sphere and those outside it. In Minkowski spacetime, the smearing of states is replaced by the limit as r approaches infinity, necessary for defining conjugate states using local operators. Taking this limit into account facilitates deriving unitarity bounds through the interaction of generators P_μ and K_μ, which are effectively conjugate to each other under inversion:

$$P_\mu^\dagger = \mathscr{R}P_\mu\mathscr{R} = K_\mu \tag{1.65}$$

and act as ladder operators for dilation eigenvalues.

Therefore, the translation generator and the special conformal transformation generator act as raising and lowering operators for the states $|\Delta\rangle$, respectively. It is natural to use their actions to define the notion of *primary operator*.

Definition 1.3.1

A primary operator is an operator that is annihilated by the action of K_μ while those obtained by successive application of P_μ are said descendants.

Given this definition, one might question whether there exists a minimum value for the scaling dimension of a primary operator.

Unitarity bounds are a consequence of the positivity of the two-point functions: the scaling dimension of a primary operator is bounded from below $\Delta \geq \Delta_{min}$ [33–35]

$$\Delta_{min} = l + D - 2,\ l > 0 \quad \text{for} \quad Spin - l \quad \text{traceless symmetric representations of} \quad SO(p,q).$$
$$\Delta_{min} = \frac{D-2}{2}, \quad l = 0 \quad \text{for scalar representations.}$$

Generally, when a primary operator is inserted at the origin, one obtains a state with scaling dimension Δ that is annihilated by the lowering operator K_μ. Conversely, given a state with scaling dimension Δ being annihilated by K_μ, one can obtain an associated local primary operator. To sum up:

$$|\Delta\rangle \xrightarrow{P_\mu} |\Delta+1\rangle \xrightarrow{P_\mu} |\Delta+2\rangle \ldots \tag{1.66}$$

$$|0\rangle \xleftarrow{K_\mu} |\Delta\rangle \xleftarrow{K_\mu} |\Delta+1\rangle \ldots . \tag{1.67}$$

This one-to-one correspondence in conformal field theory between the states on a given time slice and local operators defined by their scaling dimensions and representations

[5] Nevertheless, invariance under the conformal algebra does not imply invariance under the inversion (see e.g. [31, 32]).

under the Lorentz group is known as the *state-operator correspondence* [13, 36, 37].

This section concludes with a crucial observation for this work. In radial-quantization, given the state-operator correspondence, the action of an operator O at $\tau = -\infty$ creates a state on the cylinder with the same quantum numbers and with energy given by (see (1.57)) [36]

$$E = \frac{\Delta}{R} \ . \tag{1.68}$$

Due to the above relation, the goal of chapter 6 and chapter 7 will be to compute scaling dimensions of fixed charge operators which will turn to the computation of the energy spectrum on the cylinder.

The spectrum of operator dimensions on the plane corresponds to the energy spectrum on the cylinder. Dilations in the plane represent time translations on the cylinder. Therefore, the eigenvalues of the dilation operator D correspond to the eigenvalues of H_{cyl} [6]. Thus, the computation of the dimension of a given operator on the plane translates to the determination of the energy of the corresponding state on the cylinder.

This viewpoint offers an advantage since time translations on the cylinder, unlike dilations on the plane, remain a symmetry even away from the fixed point [6, 21]. Therefore, as will be further developed in chapter 2, mapping semiclassical computations to the cylinder introduces an additional symmetry that controls the classical solution, even when not at criticality. In contrast, in the regulated theory, a simple scaling ansatz for the radial dependence of the solution is inconsistent because scale invariance is absent. However, on the cylinder, it is possible to consistently find a solution that remains stationary over time [6].

§ 1.4 **Conserved currents and the energy-momentum tensor**

In any quantum field theory, one postulates that the symmetries of the system are realised by local conserved currents [5]. When such a current exist, j_μ, and it is conserved, $\partial^\mu j_\mu = 0$, the conserved charge is defined as

$$Q = \int d^{d-1}x \ j_0 \ . \tag{1.69}$$

Such assumption that the existence of the current instead of that of the charge is necessary for a symmetry to exist is known as the “Noether assumption" [38]. According to it, because of the translational invariance, the theory possesses a conserved energy-momentum tensor

$$\partial^\mu T_{\mu\nu} = 0 \tag{1.70}$$

while invariance under Lorentz transformation imposes the Belinfante prescription [39], namely that the energy-momentum tensor can be adapted to be symmetric [5]

$$T_{\mu\nu} = T_{\nu\mu} \ . \tag{1.71}$$

The current associated to a scale transformation $x^\mu \to \lambda x^\mu$ is defined as

$$j^D_\mu = x^\rho T_{\mu\rho} - J_\mu \tag{1.72}$$

where J_μ is the *virial* current [40] and counts the internal degrees of freedom responsible for a scale transformation. It generates the additional scaling of fields, preserving the total scale invariance of the theory, since $x^\rho T_{\mu\rho}$ generates spacetime dilation only. From the previous expression, it is easy to notice that the dilation charge is conserved if one requires

$$T^\mu_\mu = \partial^\mu J_\mu \ , \tag{1.73}$$

whereas special conformal transformations require

$$T^\mu_\mu = 0 \ . \tag{1.74}$$

Therefore, under the Noether assumption, a given relativistic quantum field theory is scale-invariant if and only if the divergence of the local virial current gives the trace of the energy-momentum tensor. The theory is conformal invariant if, in addition, the latter can be improved to be traceless. Hence, the theory is generally enhanced to be conformally invariant if the trace of the energy-momentum tensor can be written as the divergence of the virial current[6]. It is important to emphasise that the energy-momentum tensor in interacting quantum field theories incorporates the effects of the renormalization group. The trace of the energy-momentum tensor captures how the system responds to scale transformations, showing quantum effects that emerge when the renormalization scale changes. These effects, which remain unseen at the classical level, are crucial in understanding scaling transformations in quantum field theories.

1.4.1 An example: interacting theories

A formal argument can be developed to establish a connection between the trace of the energy-momentum tensor and the flow of the renormalization group.

Quantum field theories exhibit renormalization group invariance, meaning that changing the renormalization scale (or cut-off, in the Wilsonian framework) leaves physical quantities unchanged if the coupling constant is simultaneously modified and operators are redefined[7]. Studying the renormalization group invariance is equivalent to analysing how the theory responds to scale transformations [5]. Assuming no dimensionful coupling constants g^I, denoting with O the operator of the theory, with $J^\mu_a(x)$ vector operators whose corresponding background sources are $a^a_\mu(x)$, it can be demonstrated that in a massless theory, one has [5]

$$T^\mu_\mu \propto \beta^I O_I + \left(\rho^a_I D_\mu g^I\right) J^\mu_a + D_\mu \left(v^a J^\mu_a\right) \ . \tag{1.75}$$

This expression of the trace of the energy-momentum tensor proportional to quantum

[6] Then, the enhancement from scale invariance to conformal invariance is achieved by removing the virial current through the available improvements of the energy-momentum tensor specific for the theory considered [5].

[7] This procedure is referred to as renormalization group transformation.

corrections is known as the *trace identity*. The renormalization of the coupling constants introduces a running of the coupling constants under the change of the local scale transformation: β^I is the scalar β-function for the corresponding operator O_I which is necessary to cancel the divergence appearing in the coupling constant renormalization for g^I. In parallel, the terms ρ_I^a and v^a are related to the renormalization group running for the vector background source a_μ^a. In addition, when J_a^μ is conserved, there is no contribution to (1.75).

To give an example, let us consider interacting field theories. In this scenario, (1.75) reads

$$T_\mu^\mu = \beta^I O_I + v^a \left(\partial_\mu J_a^\mu\right) \ . \tag{1.76}$$

Let us consider the case of an $SU(N)$ gauge theory with N_f pairs of Dirac fermion transforming under the fundamental representation. Since there is no parity-even non-conserved gauge invariant vector operator having dimension 3, then $v^a = 0$. Therefore

$$T_\mu^\mu \propto \frac{\beta(g)}{4g^2} \ \mathrm{Tr}\left\{F^{\mu\nu}F_{\mu\nu}\right\} \ , \tag{1.77}$$

and because there is no candidate for the virial current, (1.77) cannot be expressed as its divergence as in (1.73). Moreover, since requiring scale invariance means requiring $\beta(g) = 0$, (1.77) automatically implies conformal invariance [5].

§ 1.5 Spontaneous symmetry breaking of conformal invariance

In relativistic quantum field theories spontaneous symmetry breaking is described by the Goldstone theorem [41, 42] (for more details see appendix A). The latter states, in its naive formulation, that for a physical system having global internal symmetry group G spontaneously broken down to a sub-group H, there is a massless mode, i.e. a Goldstone boson, corresponding to each broken generator. The number of Goldstone bosons is given by the dimension of the coset space G/H, namely $\dim(G/H) = \dim(G) - \dim(H)$. However, when it comes to spacetime symmetries, there is no *naive* generalization of the theorem. A notorious example is the spontaneous symmetry breaking of conformal symmetry down to Poincaré symmetry [22–24, 43–45].

Let us explore it further. The discussion in this section is only at the classical level and serves as a first bridge in unveiling the connection between scale and conformal invariance. A deeper analysis will be performed in section 1.7.

Let us consider a local field $\sigma(x)$ and let us re-write the generators of the conformal group in terms of the energy-momentum tensor. To each conformal transformation corresponds a conserved charge which in turn is the generator of that conformal transformation. Using (1.41),(1.42), (1.43) and (1.44) the commutation relations of the generators with $\sigma(x)$ are [46]

$$\left[P_\mu, \sigma(x)\right] = -i\partial_\mu\sigma(x) \tag{1.78}$$

$$\left[J_{\mu\nu}, \sigma(x)\right] = i\left(x_\mu\partial_\nu - x_\nu\partial_\mu\right)\sigma(x) + s_{\mu\nu}\sigma(x) \tag{1.79}$$

$$[D,\sigma(x)] = -i\left(x^\mu\partial_\mu + \Delta\right)\sigma(x) \tag{1.80}$$

$$\left[K_\mu,\sigma(x)\right] = \left(-2i\Delta x_\mu - x^\nu s_{\mu\nu} - 2ix_\mu x^\nu\partial_\nu + ix^2\partial_\mu\right)\sigma(x)\ . \tag{1.81}$$

Due to conformal invariance, each generator of the conformal group can be expressed in terms of the conserved charges which in turn are written in terms of the energy-momentum tensor. Precisely

$$P^\mu = \int d^3x\, T^{0\mu} \tag{1.82}$$

$$J^{\mu\nu} = \int d^3x\, \left(x^\mu T^{0\nu} - x^\nu T^{0\mu}\right) \tag{1.83}$$

$$D = \int d^3x\, x_\mu T^{0\mu} \tag{1.84}$$

$$K^\mu = \int d^3x\, \left(2x_\nu x^\mu - \delta^\mu_\nu x^2\right)T^{0\nu}\ . \tag{1.85}$$

Since Poincaré symmetry is not spontaneously broken, one needs to assume that the *vev* of the commutation relations (1.78) and (1.79) vanish. It is natural to suppose $\sigma(x)$ to be a scalar local field and to set $s_{\mu\nu}$ to zero. The central key-point [47] is to derive the Kallen-Lehmann spectral representation [48] of the two-point function between $\sigma(x)$ and $T^{\mu\nu}$. To this aim, let us insert a complete set of states $\int\frac{d^3p}{(2\pi)^3}|p,\lambda\rangle\langle p,\lambda|$ to obtain

$$\begin{aligned}\langle 0|[T^{\mu\nu}(x),\sigma(y)]|0\rangle = \sum_\lambda\int\frac{d^3p}{(2\pi)^3}\frac{1}{2E_p(\lambda)}\Big(&\langle 0\,|T^{\mu\nu}(0)|\,p,\lambda\rangle\,\langle p,\lambda|\sigma(0)|0\rangle e^{-ip(x-y)}\\ &-\langle 0|\sigma(0)|p,\lambda\rangle\,\langle p,\lambda\,|T^{\mu\nu}(0)|\,0\rangle\, e^{ip(x-y)}\Big)\end{aligned} \tag{1.86}$$

where the above is based on the observation that the vacuum remains invariant under the action of P_μ. The demonstration that follows is mainly based on the work [47] and leads to important concepts for this thesis work. Therefore, following [47], let us define two invariant functions

$$\Delta^\pm\left(x-y;m_\lambda^2\right) = i\int\frac{d^3p}{(2\pi)^3 2E_p(\lambda)}e^{\mp ip(x-y)} \tag{1.87}$$

having the properties

$$\left(\Box + m^2\right)\Delta^\pm\left(x-y;m^2\right) = 0 \tag{1.88}$$

$$\partial_0\Delta^\pm\left(x-y;m^2\right)\Big|_{x^0} = y^0 = \pm i\frac{1}{2}\delta^3(x-y)\ , \tag{1.89}$$

in terms of which one arrives at

$$\begin{aligned}\langle 0|[T^{\mu\nu}(x),\sigma(y)]|0\rangle = \textstyle\sum_\lambda \Delta^+\left(x-y;m_\lambda^2\right)\langle 0\,|T^{\mu\nu}(0)|\,p,\lambda\rangle\,\langle p,\lambda|\sigma(0)|0\rangle -\\ \Delta^-\left(x-y;m_\lambda^2\right)\langle 0|\sigma(0)|p,\lambda\rangle\,\langle p,\lambda\,|T^{\mu\nu}(0)|\,0\rangle\ .\end{aligned} \tag{1.90}$$

Then, assuming the spectral condition, the spectral representation of the two-point function can be written [47]

$$\langle 0|[T^{\mu\nu}(x),\sigma(y)]|0\rangle = \int_0^\infty dm^2\left(\partial^\mu\partial^\nu+\eta^{\mu\nu}\Box\right)\left[\rho_+\left(m^2\right)\Delta^+\left(x-y;m^2\right)- \rho_-\left(m^2\right)\Delta^-\left(x-y;m^2\right)\right]\ . \tag{1.91}$$

Since the theory is conformally invariant, the energy-momentum tensor is traceless and so

$$\langle 0|\left[\eta_{\mu\nu}T^{\mu\nu}(x),\sigma(y)\right]|0\rangle = -3\int_0^\infty dm^2\left[\rho_+\left(m^2\right)\Box\Delta^+\left(x-y;m^2\right)- \right. \tag{1.92}$$

$$\left.\rho_-\left(m^2\right)\Box\Delta^-\left(x-y;m^2\right)\right] \tag{1.93}$$

$$= 3\int_0^\infty dm^2 m^2\left[\rho_+\left(m^2\right)\Delta^+\left(x-y;m^2\right)- \right. \tag{1.94}$$

$$\left.\rho_-\left(m^2\right)\Delta^-\left(x-y;m^2\right)\right] = 0 \tag{1.95}$$

which in turn needs to be zero for every x and y. This implies that $m^2\rho_\pm\left(m^2\right)=0$, satisfied for

$$\rho_\pm\left(m^2\right) = c_\pm\delta\left(m^2\right) \tag{1.96}$$

where $c_+ \neq -c_-$ except $c_\pm = 0$ since $\rho\left(m^2\right)\geq 0$. Therefore, making use of the Dirac delta one arrives at

$$\langle 0|[T^{\mu\nu}(x),\sigma(y)]|0\rangle = i\frac{1}{2}\left(c_+ + c_-\right)\partial^\mu\partial^\nu D(x-y) \tag{1.97}$$

where $D(x-y)$ stands for the massless propagator. Until now, $c_{(\pm)}$ has been undefined. However, its value can be obtained by comparing this expression with the equal time commutation relations in (1.78),(1.79),(1.80) and (1.81). Hence, evaluating all possible equal time forms of the two-point function using the properties (1.88) and (1.89), one has

$$\langle 0|\left[T^{0\nu}(x),\sigma(y)\right]|0\rangle = 0 \quad \text{and} \tag{1.98}$$

$$\langle 0|\left[T^{0i}(x),\sigma(y)\right]|0\rangle = \frac{1}{2}\left(c_+ + c_-\right)\partial_i\delta^3(x-y)\ . \tag{1.99}$$

The evaluation of the vacuum expectation values of the conformal generators with the scalar field is obtained from expressions (1.82)-(1.85)

$$i\langle 0|[P^\mu,\sigma(y)]|0\rangle = i\int d^3x\,\langle 0|\left[T^{0\mu}(x),\sigma(y)\right]|0\rangle = 0 \tag{1.100}$$

$$i\langle 0|[J^{\mu\nu},\sigma(y)]|0\rangle = i\int d^3x\,\langle 0|\left[x^\mu T^{0\nu}(x)-x^\nu T^{0\mu}(x),\sigma(y)\right]|0\rangle = 0 \tag{1.101}$$

$$i\langle 0|[D,\sigma(y)]|0\rangle = i\int d^3x\,\langle 0|\left[x_\mu T^{0\mu}(x),\sigma(y)\right]|0\rangle = 3\frac{1}{2}\left(c_+ + c_-\right) \tag{1.102}$$

$$i\langle 0|[K^\mu,\sigma(y)]|0\rangle = i\int d^3x\left(2x^\mu x_\nu-\delta^\mu_\nu x^2\right)\langle 0|\left[T^{0\nu}(x),\sigma(y)\right]|0\rangle = 6\frac{1}{2}\left(c_+ + c_-\right)y^\mu \tag{1.103}$$

from which it is clear that the vacuum expectation value for the Poincaré group vanishes while the scale and special conformal generators get a vacuum expectation value when

$c_{(\pm)} \neq 0$. Hence, the latter are spontaneously broken symmetries. Moreover, using (1.80) and (1.81)

$$i \langle 0|[D, \sigma(y)]|0\rangle = \Delta \langle 0|\sigma(y)|0\rangle \tag{1.104}$$

$$i \langle 0|[K^\mu, \sigma(y)]|0\rangle = 2y^\mu \Delta \langle 0|\sigma(y)|0\rangle \tag{1.105}$$

implies the following relation [47]

$$\frac{1}{2}(c_+ + c_-) = \frac{\Delta}{3} \langle 0|\sigma(0)|0\rangle \tag{1.106}$$

where the y-dependence is dropped due to translational invariance. The previous relation can be used to find the expression for the two-point function (1.97)

$$i \langle 0|[T^{\mu\nu}(x), \sigma(y)]|0\rangle = -\frac{\Delta}{3} \langle 0|\sigma(0)|0\rangle \, \partial^\mu \partial^\nu D(x-y) \ . \tag{1.107}$$

Therefore, once the scalar field acquires a non-zero vacuum expectation value, conformal invariance undergoes spontaneous breaking. According to the Goldstone theorem, this leads to the emergence of a massless Goldstone boson, denoted as σ.

With the spontaneous breaking of conformal invariance, both the dilation generator and the special conformal generators are broken. One might argue for the appearance of five Goldstone bosons for each broken generator. However, in equation (1.107), polarisation vectors do not appear on the right-hand side as one would expect due to the broken special conformal generators [47]. Consequently, only a single Goldstone boson is present. This particular boson is commonly known as the *dilaton*.

§ 1.6 Non Linear realisation of Conformal Invariance

Let us pause for a moment to make the following important digression [25, 27]. The concept of symmetry holds a paramount position in modern physics. Within field theory, symmetry is essential for defining fundamental concepts such as particles and charges, since it imposes stringent constraints on the properties, interactions, and correlations of fields and particles. In QFT, Wigner's theorem states that symmetry transformations act as either unitary or anti-unitary operators on the Hilbert space. These transformations arrange states in the Hilbert space into representations (or more precisely, projective representations) of the symmetry group G. As nicely summarised in [25, 27], symmetry realisation in Hilbert space manifests in two principal forms:

- The Wigner-Weyl realisation, where the vacuum state remains invariant under all symmetry transformations.
- The Nambu-Goldstone realisation, which involves degenerate vacua capable of transforming into each other under specific symmetry transformations.

In the Wigner-Weyl realisation, excited states above the vacuum in the Hilbert space are organised into linear representations of the symmetry group. Consequently, the field operators associated with these states lie in the same linear representations. Thus, symmetry is linearly realised in the Wigner-Weyl realisation.

Conversely, in the Nambu-Goldstone realisation, vacua are invariant only under a sub-group H of the full symmetry group G. When a group element outside H acts on a vacuum state, it transitions to another vacuum. Intuitively, the local application of such actions across different spacetime points generates a unique massless excitation known as the Goldstone mode, as established by the Nambu-Goldstone theorem. Although other particle states may coexist within this framework, their masses can vary within the same representation of the full symmetry group G. Thus, the spectrum of the Nambu-Goldstone realisation is different from that of the Wigner-Weyl realisation.

Furthermore, the field operators corresponding to states in the Nambu-Goldstone realisation, including Goldstone modes and other particles, do not form linear representations of G. Consequently, the symmetry is non-linearly realised in the Nambu-Goldstone realisation [25, 27].

In the language of the Lagrangian formulation of field theory, symmetry is reflected in the invariance of the action S under the action of the group G, regardless of whether it is realised linearly or non-linearly. In the case of linear realisation, constructing such action is relatively straightforward: a G-invariant Lagrangian L with covariant field operators can be easily developed. However, in the context of non-linear realisation, the construction process becomes significantly more complex. This section discusses how to construct low-energy effective theories with non-linearly realised symmetries.

The standard method for writing down a G-invariant Lagrangian with non-linear realisation is known as the *coset construction*. In this framework, the Goldstone modes can be identified as points in the coset space G/H, where again H denotes the linearly realised sub-group of the full symmetry group G.

1.6.1 The coset construction: general formulation

The discussion that will follow is specialised to global internal symmetries and strictly follows and reviews the discussion carried out in [27]. Hence, consider a general theory whose symmetry is described by a semi-simple and simply connected Lie group G. In particular, suppose that H is a sub-group of G being linearly realised. The Lagrangian of the theory is formulated using both Goldstone fields and additional fields that linearly represent H. In this scenario, the Goldstone fields are characterised as bosonic functions defined over spacetime points, that take values in the coset space G/H. For our purpose, let us focus on the corresponding Lie algebras [27, 28]. Therefore, let the Lie algebra associated with G and H be denoted as $\mathfrak{g}$ and $\mathfrak{h}$, respectively. As a next step, consider an arbitrary symmetry-breaking pattern of the form $G \rightsquigarrow H$. Generally, the generators of G can be grouped into two categories:

1. The generators of all other unbroken symmetries: V^a with $a = 1, \cdots, \dim(\mathfrak{h})$.
2. The generators of broken symmetries: A^i where $\alpha = 1, \cdots \dim(\mathfrak{g}) - \dim(\mathfrak{h})$.

The basis can always be chosen to be orthonormal and such that the structure constants are totally antisymmetric: $\mathrm{Tr}\left\{V^a V^b\right\} = \delta^{ab}$, $\mathrm{Tr}\left\{A^i A^j\right\} = \delta^{ij}$, and $\mathrm{Tr}\left\{V^a A^i\right\} = 0$. Furthermore, $\left[V^a, V^b\right] = \mathrm{i} f^{abc} V^c$, $\left[A^i, A^j\right] = \mathrm{i} f^{ijk} A^k + \mathrm{i} f^{ija} V^a$ and $\left[V^a, A^i\right] = \mathrm{i} f^{aij} A^j$.

Since the Goldstone fields $\pi^i = \pi^i(x)$ parameterise the coset space, a representative element $U(\pi)$ in G/H can be represented as

$$U(\pi) = e^{\mathrm{i}\pi\cdot A} \ . \tag{1.108}$$

If $g \in G$ and $h \in H$, a general transformation of $U(\pi)$ preserving (1.108) is of the form

$$g : U(\pi) \to U(\pi') = gU(\pi)h^\dagger(g,\pi) \tag{1.109}$$

and since $\pi = \pi(x)$ is a function of spacetime, also $h(g,\pi)$ is. To be a group realisation, the following properties are required

$$\begin{aligned} h(g_2 g_1,\pi) &= h(g_2,\pi'(g_1,\pi))h(g_2 g_1,\pi) \\ h(1,\pi) &= 1 \\ h(h,\pi) = h \implies h : U(\pi) &= hU(\pi)h^\dagger \\ &\implies h : \pi^i A^i \to \pi^i hA^i h^\dagger = \pi^i D^{ij}(h)A^j \ . \end{aligned} \tag{1.110}$$

The construction of non-trivial G-invariant quantities that transform covariantly, i.e. $\mathrm{D}U \to g\mathrm{D}Uh^\dagger$, consists in considering the Maurer-Cartan form:

$$\omega = -i\ U^\dagger(\pi)\mathrm{d}U(\pi) \implies \omega \to h\omega h^\dagger - i\ h\mathrm{d}h^\dagger \tag{1.111}$$

that can be further decomposed in terms of the generators of $\mathfrak{g}$ as

$$\begin{aligned} \omega &= \omega_V + \omega_A = \omega_V^a V^a + \omega_A^i A^i \\ \omega_V &\to h\omega_V h^\dagger - i\ h\mathrm{d}h^\dagger \\ \omega_A &\to h\omega_A h^\dagger \ . \end{aligned} \tag{1.112}$$

This means that ω_V acts as 1-form connection while ω_A is the covariant differential of $U(\pi)$. The components corresponding to unbroken generators transform like gauge connections while the components corresponding to broken ones transform covariantly. Therefore [27], on a given field ϕ transforming linearly under H, the action of G can be non-linearly manifested via $h = h(g,\pi)$, resulting in ϕ undergoing the transformation $\phi \to D(h(g,\pi))\phi$, which is a covariant transformation. Consequently, the initial global symmetry transformation h is promoted to a local one, with the associated gauge connection simply represented by ω_V.

The generalisation of non-linearly realised spacetime symmetries is quite straightforward. The first thing to account for is the non-linear transformation of spacetime coordinates x^μ under the action of spacetime translation P^μ, since a coordinate shift resembles that of Goldstone bosons under broken symmetry transformation. Hence, since the P^μ are treated as broken generators, the spacetime itself is viewed as the coset space: Poincaré/Lorentz. Following the discussion above, the coset space can be parametrised by

$$U(\pi,x) = e^{ix_\mu P^\mu}\ e^{i\pi^i(x)A^i} \tag{1.113}$$

while (1.109) is generalised as follows

$$g: \quad U(\pi(x),x) = gU(\pi'(x'),x')\ h^{-1}(g,\pi(x)) \ , \tag{1.114}$$

where h^{-1} is used instead of $h^\dagger$ since Lorentz group is non-compact and $g \in G$ and $h \in H$ may not be unitary, as a consequence. In this scenario, the Maurer-Cartan form is given by

$$\begin{aligned}\omega &= -i\, U(\pi, x)\mathrm{d}U(\pi, x) = \omega_P + \omega_J + \omega_V + \omega_A \\ &= \omega_P^\mu P_\mu + \frac{1}{2}\omega_J^{\mu\nu} J_{\mu\nu} + \omega_V^a V^a + \omega_A^i A^i\end{aligned} \tag{1.115}$$

and since P and A are the broken generators, the components ω_P and ω_A transform covariantly while ω_J and ω_V like gauge connections. Additionally, for any field ϕ transforming linearly under the unbroken symmetry H, the covariant derivative acts on it as

$$\mathrm{D}\phi = \left[\mathrm{d} + \omega_V^i D(V_i) + \frac{1}{2}\omega_J^{\mu\nu} D(J_{\mu\nu})\right] \phi\ . \tag{1.116}$$

A phenomenon specific to broken spacetime symmetries deserves discussion. In this context, the count of independent Goldstone fields may not correspond to the number of broken generators. The conventional counting rule for Goldstone modes fails when the theory does not satisfy the conditions outlined by the Goldstone theorem. Fundamentally, the original Goldstone theorem applies exclusively to global internal symmetry breaking accompanied by a manifest Poincaré symmetry. Deviation from any of these conditions could impact the assertion of the theorem.

In cases of local symmetry breaking, the emergence of massive gauge bosons instead of massless Goldstone modes illustrates the well-known Higgs mechanism. Notable examples in non-relativistic scenarios include phonons resulting from broken translation and rotational symmetry. In such scenarios, the clear differentiation between spacetime symmetry and internal symmetry becomes less distinct.

Moreover, examples such as the dilaton for broken conformal symmetry highlight instances of broken spacetime symmetry [25, 27]. Consequently, a comprehensive extension of the Goldstone theorem requires careful examination in each of these cases.

The coset construction captures this mismatch between Goldstones and broken generators by imposing additional constraints to preserve all the symmetries. These constraints, known as the *inverse Higgs constraints*, lead to the expression of some Goldstones in terms of the others. When two broken generators are related by a commutation relation with P^μ as $[P^\mu, A_1] \propto A_2$ the ω_{A_2} component of the Maurer-Cartan form can be set to zero to solve for redundant Goldstone parameters [25–27, 49].

The spontaneous symmetry breaking of the conformal group down to the Poincaré one is a master example. Precisely, the commutation relation (1.33) leads to the introduction of the inverse Higgs constraint $\omega_D = 0$ which in turn manifests that even though there are five broken generators (four corresponding to boosts and one to dilations), some modes are redundant.

Specifically, in this scenario, the unbroken sub-algebra is the Poincaré algebra and one parameterises the coset space by

$$U(\sigma, \xi, x) = e^{ix^\mu P_\mu}\ e^{i\sigma(x)D}\ e^{i\xi^\mu(x)K_\mu} \tag{1.117}$$

while the Maurer-Cartan form is

$$\omega = -i\, U^{-1}\, \mathrm{d}U = \omega_P^\mu P_\mu + \frac{1}{2}\omega_J^{\mu\nu} J_{\mu\nu} + \omega_D D + \omega_K^\mu K_\mu \tag{1.118}$$

with

$$\begin{aligned} \omega_P^\mu &= e^\sigma \mathrm{d}x^\mu \\ \omega_J^{\mu\nu} &= -2e^\sigma \left(\xi^\mu \mathrm{d}x^\nu - \xi^\nu \mathrm{d}x^\mu\right), \\ \omega_D &= \mathrm{d}\sigma + 2e^\sigma \xi^\mu \mathrm{d}x_\mu, \\ \omega_K^\mu &= \mathrm{d}\xi^\mu + \xi^\mu \mathrm{d}\sigma + e^\sigma \left(2\xi^\mu \xi_\lambda - \xi^2 \delta_\lambda^\mu\right) \mathrm{d}x^\lambda. \end{aligned} \tag{1.119}$$

Therefore $\omega_D = 0$ leads to

$$\xi^\mu = -\frac{1}{2} e^{-\sigma} \partial^\mu \sigma\ . \tag{1.120}$$

Then one can use this constraint to eliminate ξ^μ from the Maurer-Cartan form so that the resulting low energy theory contains only one Goldstone mode, namely the dilaton field σ. Furthermore, for any other Lorentz tensor ϕ lying in the representation D of the Lorentz group, the covariant derivative is given by

$$\omega_P^\mu \mathrm{D}_\mu \phi = \left[\mathrm{d} + \frac{\mathrm{i}}{2}\omega_J^{\mu\nu} D\left(J_{\mu\nu}\right)\right]\phi. \tag{1.121}$$

Let us now construct the conformal-invariant low-energy Lagrangian. At the lowest order in dilaton derivative, one has

$$S_0 = \int \omega_P^0 \wedge \omega_P^1 \wedge \omega_P^2 \wedge \omega_P^3 = \int \mathrm{d}^4 x e^{4\sigma}\ . \tag{1.122}$$

To construct the kinetic term, one arrives at the second order in $\partial_\mu \sigma$ and makes use of ω_K^μ

$$S_2 = \int \omega_K^0 \wedge \omega_P^1 \wedge \omega_P^2 \wedge \omega_P^3 = \frac{1}{2}\int \mathrm{d}^4 x e^{2\sigma} \left(\partial_\mu \sigma\right)^2\ . \tag{1.123}$$

Generally, any Lagrangian exhibiting a symmetry group $H \subset G$ can be rendered invariant under G by introducing Goldstone bosons, thus suggesting the spontaneous breaking of the symmetry G. In the context where G represents the conformal group and H represents the Poincaré group, although the generators that undergo breakdown are the dilation and special conformal transformations, the inclusion of a single massless mode, the dilaton, is adequate and necessary to confer conformal invariance to the Lagrangian [22, 23, 50]. This phenomenon is intricately linked to the observation that a scale-invariant theory also possesses conformal invariance under certain conditions, a characteristic shared by a broad spectrum of theories, as will be discussed in the last section of the chapter (section 1.7).

1.6.2 Dilaton dressing: conferring conformal invariance

This section concludes with the discussion of the *dilaton dressing* which, in turn, is pivotal for chapter 6, chapter 7 and chapter 9. Consider a theory in which conformal invariance is spontaneously broken. The dilaton field is the Goldstone associated with the spontaneous symmetry breaking of the dilations while the additional four (Nambu-)Goldstone bosons ((N)GBs) associated with the breaking of the special conformal symmetry can be identified with the derivatives of the dilaton, rather than independent propagating fields. Below the breaking scale that will henceforth be denoted with f, having the dimension of length, the symmetry is realised non-linearly. Precisely, under a scale transformation

$$x \longrightarrow e^{\alpha} x \tag{1.124}$$

the dilaton field transforms non-linearly, i.e. it undergoes a shift [22, 23, 51]

$$\sigma(x) \rightarrow \sigma(e^{\alpha} x) - \frac{\alpha}{f} \ , \tag{1.125}$$

it works as a *conformal compensator* [52] and is introduced to restore conformal invariance at the action level to provide a mechanism for breaking conformality in a controllable manner. Therefore, the Lagrangian density is scale-invariant if one assigns the following transformation property to any operator O_k with mass dimension k [52,53]

$$O_k(x) \mapsto e^{(k-4)\sigma \ f} O_k(e^{\alpha} x) \ . \tag{1.126}$$

A heuristic way of understanding the effects of scale transformations on the theory can be obtained by observing that

$$\begin{aligned} \mathcal{L} = \sum_i g_i(\mu)\, O_{k_i}(x) \quad \text{with} \quad & \begin{cases} O_k(x) & \mapsto e^{k_i \alpha} O_k(e^{\alpha} x) \\ \mu & \mapsto e^{-\alpha} \mu \end{cases} \\ \implies \delta \mathcal{L} = \sum_i g_i(\mu) \left(k_i + x^{\mu} \partial_{\mu}\right) O_{k_i}(x) + & \sum_i \beta_i(g) \frac{\partial \mathcal{L}}{\partial g^i} \end{aligned} \tag{1.127}$$

which in turn leads to the divergence of the scale current to be

$$j^{D\ \mu} = T^{\mu}_{\nu} x^{\nu} \implies \partial_{\mu} j^{D\ \mu} = T^{\mu}_{\mu} = \sum_i g_i(\mu)\, (k_i - 4)\, O_{k_i}(x) + \sum_i \beta_i(g) \frac{\partial \mathcal{L}}{\partial g^i} \tag{1.128}$$

which is zero, i.e. the theory is scale-invariant, if $k_i = 4$ and $\beta_i = 0$.

Up to this point, the notions of conformal invariance, scale invariance and their spontaneous breakings have been introduced with particular attention, stressing the role of the dilaton field. The latter has been presented as the Goldstone boson emerging from spontaneous symmetry breaking of dilation symmetry and can consequently be considered as the Goldstone boson of spontaneous breaking of conformal invariance. Armed with these notions, the following section will examine the connection between conformal and scale invariance.

§ 1.7 Conformal Invariance vs Scale Invariance and the a-theorem

This section serves to better explore the connection between scale invariance and conformal invariance. In fact, under precise assumptions, the former can be enhanced to the latter. The first proof was given by Zamolodchikov in $d = 2$ dimensions. Under the hypothesis of unitarity, Poincaré invariance (namely causality), discrete spectrum, existence of the scale current and unbroken scale invariance [26, 54] two-dimensional quantum field theories satisfy *Zamolodchikov's c-theorem* [54]. In the next subsection, the theorem is discussed following an introduction to the conformal group in two dimensions.

1.7.1 The conformal group in two dimensions and the c-theorem

At the beginning of section 1.2, it was observed that (1.17) has two different solutions depending on the dimensionality of the manifold. In this subsection, let us consider the remaining scenario $d = 2$. Here, equation (1.17) becomes the Cauchy-Riemann equation

$$\partial_1\epsilon_1 = \partial_2\epsilon_2 \tag{1.129}$$

$$\partial_1\epsilon_2 = -\partial_2\epsilon_1 \tag{1.130}$$

therefore, writing $\epsilon(z) = \epsilon^1 + i\epsilon^2$ and $\bar{\epsilon}(\bar{z}) = \epsilon^1 - i\epsilon^2$ in terms of the complex coordinates $z, \bar{z} = x^1 \pm ix^2$, it is clear that conformal transformations coincide with the analytic coordinate transformations

$$z \longrightarrow f(z) \qquad \bar{z} \longrightarrow \bar{f}(\bar{z}) \tag{1.131}$$

whose local algebra is infinite-dimensional. Thus, the group of infinitesimal conformal transformations in two dimensions is generated by all the meromorphic functions $\epsilon = \epsilon(z)$ and $\bar{\epsilon} = \bar{\epsilon}(\bar{z})$. These can be expanded in their Laurent series, hence

$$\epsilon(z) = \sum_{n\in\mathbb{Z}} \epsilon_n z^{n+1} \quad \text{and} \quad \bar{\epsilon}(\bar{z}) = \sum_{n\in\mathbb{Z}} \epsilon_n \bar{z}^{n+1} \ . \tag{1.132}$$

Introducing the notation $\partial_z = \partial/\partial z$ and $\bar{\partial}_{\bar{z}} = \partial/\partial\bar{z}$, then a basis of generators is given by

$$l_n = z^{n+1}\partial_z \ , \quad \bar{l}_n = \bar{z}^{n+1}\bar{\partial}_{\bar{z}} \tag{1.133}$$

and the algebra satisfied by l_n and $\bar{l}_n$ is the *Witt algebra* [55]

$$\begin{cases} l_n &= z^{n+1}\partial_z \\ \bar{l}_n &= \bar{z}^{n+1}\bar{\partial}_{\bar{z}} \end{cases} \Longleftrightarrow \quad \text{Witt algebra} \quad [l_m, l_n] = (m-n)l_{m+n}, \left[\bar{l}_m, \bar{l}_n\right] = (m-n)\bar{l}_{m+n}$$
$$\text{and} \quad \left[l_m, \bar{l}_n\right] = 0 \ , \tag{1.134}$$

where these generators are related to those defining conformal transformations since one can define a *restricted conformal group* formed by

$$l_{-1} : z \to z + \epsilon \quad \text{translations} \tag{1.135}$$
$$l_0 : z \to z + \epsilon z \quad l_0 + \bar{l}_0 \quad \text{scalings}, \quad i(l_0 - \bar{l}_0) \quad \text{rotations} \tag{1.136}$$
$$l_1 : z \to z + \epsilon z^2 \qquad \text{special conformal transformations.} \tag{1.137}$$

The Witt algebra admits a central extension called the *Virasoro algebra*

$$[L_m, L_n] = (m-n)L_{m+n} + \frac{c}{12}\,(m^3 - m)\delta_{m+n,0} \tag{1.138}$$
$$\left[\bar{L}_m, \bar{L}_n\right] = (m-n)\bar{L}_{m+n} + \frac{\bar{c}}{12}\,(m^3 - m)\delta_{m+n,0} \tag{1.139}$$
$$\left[L_m, \bar{L}_n\right] = 0 \tag{1.140}$$

where c is called the *central charge*. Denoting the energy-momentum tensor with $T = T_{zz}$ and labelling $T = T^{\mu}_{\mu}$, the conservation of the energy-momentum tensor reads

$$\bar{\partial}_{\bar{z}} T + 4\partial_z T = 0\ . \tag{1.141}$$

In his work [54] the author introduces

$$F(|z|^2) = (2\pi)^2\ z^4\,\langle T(z,\bar{z})T(0)\rangle \tag{1.142}$$
$$G(|z|^2) = (2\pi)^2\ z^3\bar{z}\,\langle T(z,\bar{z})T(0)\rangle \tag{1.143}$$
$$H(|z|^2) = (2\pi)^2\ z^2\bar{z}^2\,\langle T(z,\bar{z})T(0)\rangle \tag{1.144}$$

together with the c-function

$$C = 2\left(F - \frac{1}{2}G - \frac{3}{16}H\right) \tag{1.145}$$

and shows that along the renormalization group flow, the c-function decreases. It agrees with the central charge at the fixed point, demonstrating that $\langle T(z,\bar{z})T(0)\rangle = 0$. This conclusion holds since, at a scale-invariant fixed point, $T_{\mu\nu}$ is assumed to scale canonically with the scale dimension $\Delta = 2$ [56].

Ultimately, for a CFT, the function C in (1.145) is equal to the central charge c. This discussion is the heart of Zamolodchikov's c-theorem: along a renormalization flow connecting two different CFTs, the function C decreases from the ultraviolet to the infrared and assumes the value c at the fixed point. Since $\langle T(z,\bar{z})T(0)\rangle = 0$ then from unitarity and causality (in line with the Reeh-Schlieder theorem [57]), $T(z,\bar{z}) = 0$ holds as an operator identity. Hence, scale invariance implies conformal invariance.

Furthermore, the same theorem can be recast alternatively. Precisely, consider to expand T with respect to the operators in the theory [5]

$$T = \mathcal{B}^I O_I \quad \text{with} \quad \mathcal{B} \quad \text{related to the} \quad \beta\text{-functions} \tag{1.146}$$

then the c-theorem can be formulated as[8]

$$\frac{\mathrm{d}c}{\mathrm{d}\log\mu} = \mathcal{B}^I \chi_{IJ}\, \mathcal{B}^J \geq 0 \tag{1.147}$$

$$\chi_{IJ} = \frac{3}{2}\, |z|^4 \, \langle O_I(z,\bar{z}) O_J(0)\rangle \Big|_{|z|=\mu^{-1}} \tag{1.148}$$

where χ_{IJ} is a positive definite metric called the Zamolodchikov metric. Since it is positive definite, the C-function stays constant along the renormalization group flow if and only if the $\mathcal{B}^I$'s vanish so that the theory is conformally invariant.

A concluding remark for this section refers to the property of c to count the degrees of freedom of the system [5]. If the theory is quantised on a cylinder via radial quantisation, the scaling dimension of an operator on the flat space is identified with the energy spectrum on the cylinder. Then the Cardy formula [7]

$$\rho(E) \sim \exp\left\{4\pi\sqrt{\frac{Ec}{6}}\right\} \tag{1.149}$$

expresses the asymptotic density of states with a given radial energy E to be proportional to the central charge. Hence, the latter dictates the effective degrees of freedom of the CFT. For this reason, since the renormalization group flow represents a coarse graining with the effective reduction of the degrees of freedom, it is reasonable that the central charge decreases along the RG flow, as stated by the c-theorem [9].

1.7.2 The trace anomaly and the a-theorem

Up to this point, the focus has been on the spacetime symmetry of flat Minkowski (or Euclidean) spacetime. However, the properties of the energy-momentum tensor are more effectively derived when a curved background is considered. With this in mind, let us discuss the energy-momentum tensor within a curved background and its relationship with the distinction between scale invariance and conformal invariance [5].

In general relativity, one of the fundamental principles is that the energy-momentum tensor acts as a source of gravity by coupling to the metric $g_{\mu\nu}$. Imagine being able to couple a Poincaré-invariant quantum field theory to a general covariant gravitational theory (which may not be done uniquely). The energy-momentum tensor is thus conventionally defined as

$$T_{\mu\nu} = \frac{2}{\sqrt{|g|}}\frac{\delta S}{\delta g^{\mu\nu}} \quad \text{where} \quad S = \int d^d x \sqrt{|g|}\mathcal{L}(\phi, g_{\mu\nu}) \,. \tag{1.150}$$

The conservation of the energy-momentum tensor as well as the symmetry property $T_{\mu\nu} =$

[8] To be precise, the fact that the C-function relies on the running coupling constants and does not explicitly depend on the energy scale μ may not be readily apparent. However, a local renormalization group analysis confirms this assertion.

[9] In conclusion, it is important to stress that the c-theorem used the hypothesis that a theory needs to be unitary (to ensure $H \geq 0$ so that C is decreasing) and Poincaré invariant (conservation of $T_{\mu\nu}$ and application of the Reeh-Schlieder theorem), which admits the existence of a scale current and unbroken scale invariance, as well as a discrete spectrum in scaling dimension.

$T_{\nu\mu}$ is automatically given by the diffeomorphism invariance of the action S [58].

If the action exhibits scale invariance or constant Weyl invariance, $g_{\mu\nu} \to e^{2\omega} g_{\mu\nu}$, where ω is a spacetime-independent constant, then the action density retains scale invariance modulo a total derivative term [58]. Consequently, the trace of the energy-momentum tensor arises from the divergence of the virial current, reflecting the characteristics of the curved background (as anticipated in section 1.4).

On the other hand, if the action is *Weyl invariant*, $g_{\mu\nu} \to e^{2\omega(x)} g_{\mu\nu}$, where $\omega(x)$ is an arbitrary scalar function dependent on spacetime, then the action density itself must remain invariant under the Weyl rescaling. Consequently, the energy-momentum tensor is traceless [58].

It is important to recall that conformal killing vectors of the d-dimensional Minkowski spacetime (where $d > 2$) are generated by the conformal algebra $SO(2,d)$ including translations, Lorentz rotations, dilations, and special conformal transformations. Again, these vectors induce a diffeomorphism that preserves the metric up to an overall Weyl factor. In the context of Weyl invariance, on Minkowski spacetime, a theory automatically attains conformal invariance. However, the converse may not hold: coupling a conformal field theory to gravity may not preserve Weyl invariance [5, 58].

In particular, on a curved background with various background sources, the conformal field theory breaks the Weyl invariance due to the so-called Weyl anomaly [59]. Weyl anomaly plays a central role in discussing scale invariance vs. conformal invariance from the viewpoint of the Schwinger functional. The trace of the energy-momentum tensor T^μ_μ is supposed to be zero in conformal field theories, but in general, it is not on the curved background due to the Weyl anomaly. Considering the complete quantum theory, in $d = 2$ dimensions, the quantity $\langle T^\mu_\mu \rangle$ may not vanish. Actually

$$\langle T^\mu_\mu \rangle = -\frac{c}{12}\,\mathcal{R} \tag{1.151}$$

is a trace anomaly called Weyl anomaly and it is proportional to the scalar curvature $\mathcal{R}$.

Moving to $d = 4$ dimensions, from dimensional grounds, the most generic possibility for the form of the Weyl anomaly is

$$\begin{aligned}
\langle T^\mu_\mu \rangle &= c\,(\text{Weyl})^2 - a\ \text{Euler} + b\mathcal{R}^2 + \tilde{b}\Box\mathcal{R} + d\ \epsilon^{\mu\nu\rho\sigma}\ \mathcal{R}_{\mu\nu}^{\ \ \alpha\beta}\mathcal{R}_{\alpha\beta\rho\sigma} \\
\text{Weyl}^2 &= \mathcal{R}^2_{\mu\nu\rho\sigma} - 2\mathcal{R}^2_{\mu\nu} + \frac{1}{3}\,\mathcal{R}^2 \\
\text{Euler} &= \mathcal{R}^2_{\mu\nu\rho\sigma} - 4\mathcal{R}^2_{\mu\nu} + \mathcal{R}^2\ .
\end{aligned} \tag{1.152}$$

Nevertheless, it is possible to show [59] that the Weyl anomaly is indeed of the form

$$\langle T^\mu_\mu \rangle = c\,(\text{Weyl})^2 - a\ \text{Euler} \tag{1.153}$$

where [59, 60]

$$c = \frac{1}{90(8\pi)^2}, \qquad a = \frac{1}{90(8\pi)^2} \quad \text{for a real scalar,} \tag{1.154}$$

$$c = \frac{6}{90(8\pi)^2}, \qquad a = \frac{11}{90(8\pi)^2} \quad \text{for a Dirac fermion,} \tag{1.155}$$

$$c = \frac{12}{90(8\pi)^2}, \qquad a = \frac{62}{90(8\pi)^2} \quad \text{for a real vector.} \tag{1.156}$$

In literature, there are examples [61] where c does not show monotonicity along the RG flow. Therefore, a naive guess for the analogue of the c-theorem in $d = 4$ dimensions cannot be supported by a similar discussion to the $d = 2$ case. Hence, a remains the only candidate to suit the pivotal role in Zamolodchikovs c-theorem in $d = 4$ dimensions. The *Cardy's conjecture* consists in postulating that

$$a = -\frac{1}{64\pi^2} \int_{S^4} d^4x \sqrt{|g|} \langle T^\mu_\mu \rangle \tag{1.157}$$

behaves as the central charge in $d = 2$ dimensions. This conjecture can be formulated in different versions:

- Weak version: $a_{\mathrm{UV}} \geq a_{\mathrm{IR}}$ along the flow between two CFTs [62, 63].
- Strong version: $\frac{\mathrm{d}a(g(\mu))}{\mathrm{d}\log\mu} \geq 0$ along the RG flow.
- Gradient formula (strongest version): $\mathcal{B}^I = \chi^{IJ}\partial_J a$ hence $\frac{\mathrm{d}a(g(\mu))}{\mathrm{d}\log\mu}\mathcal{B}^I\chi_{IJ}\mathcal{B}^J$.

All of these formulations are indeed supported by perturbative proofs [64, 65] and state that the coefficient in front of the Euler density in the Weyl anomaly (1.153) must be monotonically decreasing along the RG flow. It is worth mentioning that for $d > 4$ dimensions, scale invariance does not automatically imply conformal invariance, or at least not yet supported by full proofs.

In fact, in four dimensions, the most that can be proved so far is the so-called weak *a-theorem* [62, 66]. This theorem, unlike the c-theorem, does not provide information about the behaviour of a between these fixed points. The goal now is to present a brief overview, nicely done in [67], of a proof for the weak a-theorem, based on the discussion found in [5]. The focus is on the RG flow from the UV fixed point to the IR fixed point. For such a flow to exist, the conformal field theory must be perturbed. This modification is assumed to occur by adding an operator O. Under a Weyl transformation, $g_{\mu\nu} \to e^{2\omega}g_{\mu\nu}$, the operator O transforms as $O \to e^{-\Delta\omega}O$, where Δ represents the dimension of O. To ensure that the theory remains classically Weyl invariant, O is replaced by $e^{-(4-\Delta)\sigma}O$, where σ being the dilaton.

So, consider the RG flow from the UV fixed point to the IR fixed point [67]. Let us stress an important step here. For there to be flow at all, the CFT must be perturbed, i.e. modified. Hence, the flow is induced by adding to the UV CFT a relevant operator O that, since it is relevant, its scaling dimension Δ satisfies $\Delta < 4$. The dilaton field is considered to compensate for this violation due to the relevant transformation. Hence, dressing the operator, the overall action in the UV reads

$$S_{\mathrm{UV}} = S_{\mathrm{CFT,\,UV}} + \lambda \int \sqrt{g}\, d^4x\, O(x)\, e^{-(4-\Delta)f\sigma} + \frac{1}{2f^2} \int \left(f^2(\partial\sigma)^2 - \frac{\mathcal{R}}{6} \right) e^{-2f\sigma} \sqrt{g}\, d^4x \,. \tag{1.158}$$

To cross over from the UV to the IR it suffices to require that the energy scale of spontaneous conformal symmetry breaking is much larger than other scales of the theory. Hence, since f has the dimension of length, it suffices to send $f \to 0$. Stated differently, the dilaton can be assumed to decouple. Hence the effective action in the infrared reads [67]

$$S_{\text{eff}} = S_{\text{CFT, IR}} + \frac{1}{2f^2} \int \left(f^2 (\partial\sigma)^2 - \frac{\mathcal{R}}{6} \right) e^{-2f\sigma} \sqrt{g}\, d^4x + S_{WZ} \tag{1.159}$$

with S_{WZ} the Wess-Zumino term. It can be argued that the Weyl anomaly remains the same for both the original UV theory and the effective IR theory, despite the differences in their actions (for example, while the dilaton is decoupled in the IR action, it is not in the UV action). To maintain the Weyl anomaly unchanged, the Wess-Zumino term is introduced. Since the anomaly in $S_{\text{CFT, IR}}$ is different from that of the original theory, it works as a compensator for these variations. Additionally, it is constructed in such a way that the Weyl anomaly is cancelled at the conformal fixed point. The overall expression then reads

$$S_{\text{eff}} = S_{\text{CFT, IR}} + \frac{1}{2} \int d^4x \left((\partial\sigma)^2 e^{-2f\sigma} - 2(a_{UV} - a_{IR}) f^4 (\partial\sigma)^4 \right) \tag{1.160}$$

and the weak version of the a-theorem is proven as a consequence of causality and unitarity.

$a_{UV} - a_{IR} \geq 0$ must hold to prevent the dilaton from travelling faster than light.

This last discussion ends the first chapter and completes the introductory framework needed for the subsequent chapters.

Quantum Field Theories at fixed charge and large quantum numbers

Chapter 2

§ 2.1 An invitation

Throughout the preceding chapter, the significant role of symmetries in physics has been highlighted. Specifically, for the focus of this thesis, the dynamics of Goldstone bosons play a central role. Indeed, their low-energy dynamics are predominantly governed by symmetry. Therefore, conducting experimental studies on the dynamics of Goldstone bosons at low energies and long distances allows strong insights into fundamental symmetries and the patterns of their spontaneous breaking [6]. In a typical Lorentz-invariant framework, the number of Goldstones corresponds to the number of broken generators and are massless and travelling at the speed of light. However, in Nature, various systems exhibit spontaneous breaking of spacetime symmetries, leading to a broader range of possibilities permitted by the Goldstone theorem [6, 68–71]. In this chapter, let us delve into systems characterised by finite density for a specific spontaneously broken charge.

Imagine studying how certain systems behave under specific conditions, like when they are at finite density. Of course, these systems evolve according to the Hamiltonian. Now, when one wants to find the most stable state of these systems, one looks for the state with the lowest energy.

Precisely, the protagonists of this chapter are relativistic systems at finite density with a specific charge Q, whose temporal evolution is established by a Hamiltonian H. In such scenarios, the system's ground state can be identified as the state having the lowest eigenvalue relative to a modified Hamiltonian, denoted as $\bar{H}$

$$\bar{H} = H + \mu Q \ , \tag{2.1}$$

where μ represents the chemical potential.

The focus lies on systems of this type that break boost invariance, time translations governed by H, intrinsic charge Q, and an additional set of internal charges Q_i. Importantly, the modified Hamiltonian $\bar{H}$ remains intact by design. This symmetry-breaking scheme defines a zero-temperature superfluid phase [72, 73].

In the following, a review of the general properties of the spectrum stemming from the spontaneous breaking of symmetries in finite-density states will be conducted mainly following [6, 74, 75].

The dynamics of Goldstone modes at low energies can effectively be described in terms of symmetries and through a systematic expansion involving derivatives [76, 77] (for more, see chapter 3). However, the presence of a mass gap (namely that $\omega(\mathbf{k}=0) \propto \mu$) for the gapped Goldstones presents both conceptual and technical challenges. In fact, on the one hand, these modes are crucial for constructing an effective field theory that remains invariant under the complete symmetry group. On the other hand, in various significant cases, such as QCD at high isospin density [78–81] and the large charge sector of conformal field theories with non-abelian symmetries [82], the chemical potential itself acts as the cut-off of the EFT. This fact paradoxically suggests that gapped Goldstones may not be included in the latter[1].

The superfluid scenario discussed here is relevant in various contexts, such as elucidating the low energy physics of certain condensed matter systems [84] or understanding QCD (as well as QCD-like theories) at finite density [85]. This thesis partly delves into the analysis of conformal field theory data concerning operators with significantly high values of an internal quantum number within theories possessing global symmetries.

Generally, starting from (1.69), an operator O is said to carry a value $\bar{Q}$ of the charge Q if

$$[Q, O] = \bar{Q}\, O \,. \tag{2.2}$$

In terms of the state-operator correspondence, this can also be viewed as an exploration of CFTs with states characterised by fixed charge density. In this chapter, the main ideas behind CFT analysis at large charge will be introduced. It will be argued that the spectrum of operators bearing a substantial large charge tends to exhibit classical behaviour, thus lending itself to analysis through a semiclassical expansion, which corresponds to expanding in inverse powers of the charge. To set the stage, a straightforward quantum mechanical example will be presented in section 2.2.

This example suggests that physical systems characterised by large quantum numbers are amenable to semiclassical treatment. Furthermore, it will be seen that this conclusion also applies to relativistic scalar quantum field theories with global symmetries when there is a large internal charge.

Since this thesis is devoted to the study of low-energy dynamics of strongly interacting field theories, it should be remembered that for these theories there is no small coupling parameter, which would enable a systematic perturbative expansion of observables. However, even in such scenarios, a weakly coupled description can effectively emerge within certain sectors of the theory [6] (for more details see the appendix B). QCD is an example of this phenomenon, where at energies E much smaller than the hadron scale of

[1] However, in [83], taking the case of a $SU(2)$ symmetry template, it is shown that such an effective field theory can be formulated by focussing on both gapless and gapped Goldstone modes at small 3-momentum. In this framework, the EFT obeys certain rules: the gapless Goldstones exhibit soft behaviour, while the gapped ones move slowly. These rules are analogous to those found in standard non-relativistic EFTs, such as the one used to describe positronium.

$\Lambda_{QCD} = 4\pi F_\pi \sim 1$ GeV[2], the theory can be studied using the chiral Lagrangian, focussing on Goldstone degrees of freedom (see chapter 3). The feasibility of a perturbative description is associated with a significant separation between relevant mass scales, where the ratio E/Λ_{QCD} serves as the small expansion parameter, as will be reviewed in chapter 3. Despite lacking an intrinsic mass scale, a phenomenon similar to the low-energy QCD arises within CFTs when analysing operators characterised by large quantum numbers under an internal symmetry group G [6].

Initially highlighted in [82], this concept is based on the following premise: as a consequence of the state-operator correspondence, a scalar operator with charge Q under a specific generator of the group G, corresponds to a state having charge density $\rho \sim Q/R^{d-1}$ within the theory compactified on a cylinder $\mathbb{R} \times S^{d-1}$ with radius R. For large Q values, the mass scale associated with the charge density $\rho^{1/(d-1)} \sim Q^{1/(d-1)}/R$ significantly exceeds the compactification scale of $1/R$. Within this scale regime, the CFT state and its excitations are associated with a condensed matter finite-density phase, with the simplest possibility being a generalised superfluid phase [6]. Assuming the theory to be in a superfluid phase, the charged states can be associated with excitations of the corresponding Goldstone modes, whose properties are predominantly governed by the symmetry, irrespective of other details of the theory.

Finally, similar to the chiral Lagrangian framework in QCD, there will be a review of how precise predictions are obtained through an effective field theory description, where the derivative and loop expansions are regulated by the ratio between the infrared and ultraviolet scales, $1/R$ and $\rho^{1/(d-1)}$, respectively.

§ 2.2 Quantum Field Theories at large charge: the Hydrogen atom test-bed

To set the stage, consider the case of the quantum mechanical Hydrogen atom in the limit of the infinite mass of the proton [74, 75]. Denoting J the angular momentum, its eigenvalues are labelled by the azimuthal quantum number l while those corresponding to its projection on the z-axis, J_z, by the magnetic quantum number m. Throughout this section, the system will be considered at large magnetic quantum number, in a sense that will be clarified soon.

Denoting with $\mathbf{q}$ and m_e the momentum and the mass of the electron respectively, the Hamiltonian governing the system is

$$H = \frac{\mathbf{q}^2}{2m_e} - \frac{\alpha}{r} \tag{2.3}$$

where α/r is the notorious Coulomb potential and $\alpha = 1/137$ is the fine structure constant. For the discussion ahead, let us introduce the Lagrangian expressed in spherical coordinates

$$L = \frac{m_e}{2}\left(\dot{r}^2 + r^2\dot{\theta}^2 + r^2\sin^2\theta\dot{\phi}^2\right) + \frac{\alpha}{r}\ , \tag{2.4}$$

[2] F_π is the pion decay constant.

where the dot stands for the time derivative. The resolution of the Schrödinger equation furnishes the following eigenvalues

$$E_n = -\frac{m_e \alpha^2}{2n^2} \tag{2.5}$$

where $n \geq 1$ is the integer quantum number, the principal quantum number, labelling the different energy levels. The latter constrains the values of l and m to be $1 \leq l \leq n-1$ and $-l \leq m \leq l$. The ground state energy of the system is achieved for

$$E^{\text{qm}}_{\text{ground}}(m) = -\frac{m_e \alpha^2}{2(m+1)^2} \tag{2.6}$$

corresponding to have $l = m = n-1$. Additionally, the previous result can be recast as

$$E^{\text{qm}}_{\text{ground}}(m) = -\frac{m_e \alpha^2}{2m^2}\left(1 - \frac{2}{m} + \frac{3}{m^2} + \dots\right) \equiv E^{\text{qm (0)}}_{\text{ground}}\left(1 + \sum_{j=1}^{\infty} a_j m^{-j}\right) . \tag{2.7}$$

The classical counterpart of the problem at fixed angular momentum $l = m$ is governed by the following effective potential made by the contributions of a centrifugal and Coulomb term

$$V_{\text{eff}} = \frac{m^2}{2m_e r^2} - \frac{\alpha}{r} . \tag{2.8}$$

Minimising it leads to solving the motion of the electron. Specifically, the electron moves around a circle with radius $r_* = m^2/(m_e \alpha)$. This solution, after substitution into the Hamiltonian, yields the expression for the ground state energy of the system which reads

$$E^{\text{cl}}_{\text{ground}} = -\frac{m_e \alpha^2}{2m^2} . \tag{2.9}$$

Hence, a first look at (2.5) and (2.9) shows that for very large angular momenta, $m \to \infty$, $m+1 \sim m$ and

$$\frac{E^{\text{qm}}_{\text{ground}} - E^{\text{cl}}_{\text{ground}}}{E^{\text{qm}}_{\text{ground}}} \sim \frac{2}{m} \xrightarrow{m\to\infty} 0 . \tag{2.10}$$

The emergence of classical physics at large angular momentum is a phenomenon worth exploring. Focussing on the radial wave function provides a concrete perspective. According to the standard WKB procedure [35](and references therein), the quasi-classical treatment becomes valid for $d\lambda_r = dr \ll 1$, where the radial wavelength is defined as $\lambda_r = 2\pi\hbar/|\mathbf{p}| \sim r/m$, thus implying $m \gg 1$. Physically, the centrifugal force keeps r localised on the classical trajectory for $m \gg 1$; it can be observed that the spread of the exact expression of the wave function scales as $\Delta r^2/r_*^2 \propto 1/m$. Consequently, the exact result can be computed by expanding the corresponding path integral around the classical trajectory. This is explicit in (2.7) where the leading order $E^{\text{qm (0)}}_{\text{ground}}$ matches the classical result $E^{\text{cl}}_{\text{ground}}$ while the corrections leading to the exact quantum result are expressed in powers of $1/m$. The systematic calculation of $1/m$ corrections to the classical result will be discussed in detail in the following.

It will also be clear that, when considering the scenario of a quantum field theory at large quantum numbers, the situation becomes more intricate due to the presence of an infinite number of degrees of freedom. Although the fundamental picture remains similar, the complexity increases. In general, the semiclassical description in the context of a field theory takes the form of an effective field theory for certain light degrees of freedom. The existence of such light modes is typically guaranteed by the fact that a state with high charge density unavoidably breaks certain symmetries, both in spacetime and often internally. Consequently, the long-distance dynamics of the system is governed by the associated Goldstone modes [41, 86].

This brief introduction motivates the bridge between the quantum framework at large quantum numbers and the classical result. The time has come to discuss how this result can be obtained semiclassically for large angular momentum. It will be shown throughout this section that this semiclassical expansion is a large quantum number expansion in $1/m$. The starting point consists of expanding the path integral around a configuration with fixed angular momentum J_z.

The following discussion, mainly based on [6], may be lengthy and involve mathematical details, but will clearly explain how the methodology works and why it is worth exploring. Specifically, let us consider the matrix element of the Euclidean evolution operator e^{-TH} between two states possessing angular momentum $J_z = m$, along with fixed arbitrary values for r and θ [6,35]. First of all, when performing the limit $T \to \infty$, the system will be projected onto the state having the lowest energy. Precisely, if Ψ_0 denotes such lowest-energy state, performing the limit T towards infinity while keeping the angular momentum m constant, will result in

$$\left\langle r_f, \theta_f, m \left| e^{-TH} \right| r_i, \theta_i, m \right\rangle \xrightarrow{T\to\infty} \left\langle r_f, \theta_f, m \mid \Psi_0, m \right\rangle \left\langle \Psi_0, m \mid r_i, \theta_i, m \right\rangle e^{-E^{\mathrm{qm}}_{\mathrm{ground}}(m)T} \tag{2.11}$$

where subleading corrections are exponentially suppressed in T [6]. Since ϕ and m are conjugate variables, the previous matrix element can indeed be re-written as

$$\left\langle r_f, \theta_f, m \left| e^{-TH} \right| r_i, \theta_i, m \right\rangle = \iint \frac{d\phi_i d\phi_f}{2\pi} e^{-im(\phi_f - \phi_i)} \int_{(r_i,\theta_i,\phi_i)}^{(r_f,\theta_f,\phi_f)} \mathcal{D}r\mathcal{D}\theta\mathcal{D}\phi \; e^{-\int_{-T/2}^{T/2} d\tau L_E}, \tag{2.12}$$

where τ is the Euclidean time and L_E is the Euclidean version of (2.4)

$$L_E = \frac{m_e}{2}\left(\dot r^2 + r^2\dot\theta^2 + r^2\sin^2\theta\dot\phi^2\right) - \frac{\alpha}{r}. \tag{2.13}$$

In particular, the presence of the wave functions $e^{im\phi_i}$ and $e^{-im\phi_f}$ in (2.12) ensure the right value for the angular momentum J_z for the initial and final states, respectively. The key point is that (2.12) can be computed systematically in a saddle-point approximation when $m \gg 1$. Therefore, assuming this, let us continue with the computations. Incorporating the variation of the boundary terms, let us observe that the stationarity conditions arising from (2.12) can be expressed as:

$$\ddot r = r\dot\theta^2 + r\sin^2\theta\dot\phi^2 + \frac{\alpha}{m_e r^2}, \quad \ddot\theta = \sin\theta\cos\theta\dot\phi^2, \quad m_e r^2\sin^2\theta\dot\phi = -im. \tag{2.14}$$

Without losing generality, to simplify the computations, one is free to choose convenient boundary conditions. Precisely, let us choose $r_i = r_f = \frac{m^2}{m_e\alpha}$ and $\theta_i = \theta_f = \pi/2$, which in turn imply

$$r_s = \frac{m^2}{m_e\alpha} \equiv r_*, \quad \theta_s = \frac{\pi}{2}, \quad \phi_s = -i\frac{m}{m_e r_*^2}\tau + \phi_*, \tag{2.15}$$

where ϕ_* is an integration constant.

It is worth taking a moment to acknowledge that the Lagrangian (2.4) is invariant under a $SO(4)$ symmetry and that the solution (2.15) breaks spontaneously time translations along with the $SO(4)$ symmetry to the sub-group generated by $\bar{H} = H - \mu J_z$. In fact, coming back to Lorentzian time $\tau \to it$, the third solution in (2.15) can be written as

$$\phi_s = \phi_* + \frac{m}{m_e r_*^2}t \equiv \phi_* + \mu(m)\ t \quad \text{where} \quad \mu(m) = \frac{m}{m_e r_*^2}\ . \tag{2.16}$$

At this stage, all the necessary ingredients are in place to compute the ground state energy of the system. Let us evaluate the classical action on the solution (2.15). The outcome reads

$$\int_{-T/2}^{T/2} d\tau L_E + im\left(\phi_f - \phi_i\right) = \frac{m_e\alpha}{2m^2}T = -E_{\text{ground}}^{\text{qm (0)}}T, \tag{2.17}$$

which is exactly the leading order value for the energy at large m in (2.7). Furthermore, by elucidating the relationship between m and ϕ as conjugate variables, it becomes evident that the latter works as a chemical potential, quantifying the system's response to changes in m. Specifically

$$\frac{\partial E_{\text{ground}}^{\text{qm (0)}}}{\partial m} = \frac{m}{m_e r_*^2} = \mu\ . \tag{2.18}$$

Let us take a moment to review the key results obtained thus far. The analysis began with the standard Euclidean representation of the path integral, where the matrix element between two eigenstates of angular momentum $J_z = m$ was computed. In the limit $T \to \infty$, the amplitude (2.11) projects onto the state with the lowest energy for a fixed angular momentum $J_z = m$. The structure of the resulting path integral indicates that it can be effectively solved in the limit $m \gg 1$ using the saddle-point approximation. Based on this assumption, an expression for the ground state energy was derived, which corresponds exactly to the first term in (2.7). It is now possible to show that (2.7) can be seen as a series expansion in powers of $1/m$, and that the quantum corrections to the path integral calculation correspond to these $1/m$ terms. Let us proceed with the computation of these corrections.

To compute now the leading quantum correction to the classical result, let us parameterise the quantum (dimensionless) fluctuations as

$$r = r_s + r\mathfrak{r} \implies \mathfrak{r} = \frac{r - r_*}{r} \tag{2.19}$$

$$\theta = \theta_s + \vartheta \implies \vartheta = \theta - \frac{\pi}{2} \tag{2.20}$$

$$\phi = \phi_s + \varphi \implies \varphi = \phi + i\frac{m}{m_e r_*^2}\tau - \phi_0. \tag{2.21}$$

In terms of these fluctuations, the path integral in (2.12) becomes

$$\left\langle r_f, \theta_f, m \left| e^{-TH} \right| r_i, \theta_i, m \right\rangle = e^{-\frac{m_e \alpha}{2m^2} T} \int \mathcal{D}\mathfrak{r}\; \mathcal{D}\vartheta\; \mathcal{D}\varphi\; e^{-\int_{-T/2}^{T/2} d\tau L_E'} , \tag{2.22}$$

where L_E' is the Euclidean Lagrangian in terms of $\mathfrak{r}, \vartheta$ and φ and reads

$$L_E' = \frac{m_e r_*^2}{2} \left[\dot{\mathfrak{r}}^2 + \frac{m^2}{m_e^2 r_*^4} \mathfrak{r}^2 + \dot{\vartheta}^2 + \frac{m^2}{m_e^2 r_*^4} \vartheta^2 + \left(\dot{\varphi} - \frac{2im}{m_e r_*^2} \mathfrak{r} \right)^2 \right] + \dots . \tag{2.23}$$

To make manifest that the corrections come in powers of $1/m$, it is convenient to re-scale the time as

$$\tau = \tilde{\tau}\, \frac{m_e r_*^2}{m} \quad \text{such that} \quad \int d\tau\; L_E' = m \int d\tilde{\tau}\; \tilde{L}_E' , \quad \text{where} \quad \tilde{L}_E' \equiv L_E' \left(\frac{m}{m_e r_*^2} = 1 \right) . \tag{2.24}$$

From this identification, it is self-evident the significance attributed to $1/m$: is indeed the loop counting parameter in the path integral. Precisely, (2.7) coincides with a loop expansion. The lowest-order correction to $E^{\text{qm }(0)}_{\text{ground}}$ comes from $\tilde{L}_E'$ and it is given by the corresponding one-loop fluctuation determinant which is

$$\frac{1}{2} \int d\omega \left[2 \log \left(\omega^2 + \frac{m^2}{m_e^2 r_*^4} \right) + \log \omega^2 \right] = \Lambda_{UV} + \frac{m_e \alpha}{m^3} , \tag{2.25}$$

where Λ_{UV} is a regularization scheme-dependent divergent term [6, 35]. The (2.25) coincides with the second term in (2.7).

In summary, this section used the example of the Hydrogen atom to illustrate how the semiclassical approach can be employed to describe a system in a sector with a large charge, in this case represented by the angular momentum.

§ 2.3 Quantum Field Theories at fixed charge

The discussion carried out in the previous section has demonstrated that physical systems characterised by a large quantum number are amenable to being treated semiclassically. This property is valid for relativistic scalar QFTs invariant under global symmetries at large internal charges. Moreover, the leading trajectory upon which the semiclassical approximation is built breaks both spacetime and internal symmetries. For clarity and organisation, let us begin with the initial concepts.

Equation (1.69) defines a conserved charge associated with a given Noether current. Fixing the charge of a given system means imposing a certain constant value on this charge $\bar{Q}$. At the Hamiltonian level, the charge constraint equals the introduction of a chemical potential that works as a Lagrange multiplier for the Hamiltonian H. In formulæ

$$H \xrightarrow{\text{fixing the charge}} \bar{H} = H + \mu Q \ . \tag{2.26}$$

The immediate consequence of this fixing is the breaking of spacetime symmetries since it is the time component of the conserved Noether current that has been fixed, by definition. The ground state is defined as that state minimising $\bar{H}$, namely [3]

$$\bar{H}\,|0\rangle = 0\ . \tag{2.27}$$

This condition can be realised in two scenarios. The first scenario involves the ground state being an eigenstate of both H and Q simultaneously, thus preserving both symmetries [35]. This scenario manifests in nature within Fermi liquids [49, 87], where the internal symmetry group is $U(1)$, corresponding to particle number in the non-relativistic limit. The second case contemplates $|0\rangle$ breaking spontaneously both H and Q but being an eigenstate of the diagonalised $\bar{H}$. If the charge fixing generates a non-zero *vev*, the ground state cannot be an eigenstate of $\bar{Q}$ and one cannot classify the states with the eigenvalues of H, which means that the non-relativistic $\bar{H}$ needs to be diagonalised. However, it is not worth proceeding in this direction. This is because employing the non-relativistic Hamiltonian $\bar{H}$ to describe the system is merely a mathematical choice [35].

The true nature of the system is relativistic and it is H that governs the microscopic time evolution of the operators. Conversely, within its fixed charge sectors, the ground state spontaneously breaks Lorentz invariance through the interaction of the charge with μ, which can thus be interpreted as the zeroth component of an external gauge field (a full discussion is in chapter 3). This viewpoint is indeed the one adopted to describe condensed matter systems [73].

The bridge between systems characterised by large charge and QFTs at fixed charge is given in the following discussion. Firstly, let us explore the phase where these theories live. Hence, consider for simplicity the case of a system having an internal $U(1)$ symmetry that consequently is generated by Q, namely

$$[Q, H] = 0, \quad \text{with} \quad H \quad \text{the Hamiltonian of the system.} \tag{2.28}$$

Supposing that the theory is invariant under the Poincaré group means that the symmetries generated by

$$P_0 \equiv H \quad \text{time translation} \tag{2.29}$$
$$P_i \quad \text{space translations} \tag{2.30}$$
$$J_i \quad \text{rotations} \tag{2.31}$$
$$K_i \quad \text{boosts} \tag{2.32}$$

are preserved. However, fixing the charge Q to the $\bar{Q}$ value breaks the Poincaré group to the one made by

$$\bar{P}_0 \equiv H + \mu Q\ , \qquad P_i\ , \qquad J_i\ . \tag{2.33}$$

This symmetry-breaking pattern defines a *superfluid phase*. Hence, QFTs at large charge are a natural playground for superfluid phases to arise.

[3] Generally, note that the ground state satisfies $\bar{H}\,|0\rangle = \lambda\,|0\rangle$, where the minimum is λ. However, a cosmological constant term can always be added to the Hamiltonian to set $\lambda = 0$, with no physical consequences if there is no dynamic gravity.

Consider, as an illustrative example, a CFT incorporating an additional global $U(1)$ symmetry [35]. This discussion will show how the charge fixing explicitly breaks boosts and time translations while the ground state additionally breaks the global symmetry spontaneously. Hence, a $U(1)$ scalar field theory is described by the following Lagrangian density

$$\mathcal{L} = \partial_\mu\phi^*\partial^\mu\phi - V(\phi^*\phi) = \partial_\mu\phi^*\partial^\mu\phi - \frac{\lambda}{4}(\phi^*\phi)^2\,, \tag{2.34}$$

where $\Pi = \partial_0\phi^*$ and $\Pi^* = \partial_0\phi$ are the momentum densities conjugate to ϕ and ϕ^*, respectively, while

$$j^\mu = i(\partial^\mu\phi^*\phi - \phi^*\partial^\mu\phi) \tag{2.35}$$

is the corresponding $U(1)$ Noether current. As already anticipated, its temporal component is fixed by fixing the charge Q. Additionally, the relativistic Hamiltonian density is given by

$$\mathcal{H} = \Pi\Pi^* + \partial_i\phi^*\partial^i\phi + V(\phi^*\phi) \tag{2.36}$$

and the corresponding non-relativistic quantity to minimise is

$$\bar{\mathcal{H}} = \mathcal{H} - \mu j^0 = |\Pi^* - i\mu\phi|^2 + \partial_i\phi^*\partial^i\phi + V_{\text{eff}}(\phi^*\phi) \quad \text{with} \quad V_{\text{eff}}(\phi^*\phi) = V(\phi^*\phi) - \mu^2\phi^*\phi\,. \tag{2.37}$$

From this final expression, it can be concluded that the time dependence of ϕ is determined by the first term $|\Pi^* - i\mu\phi|^2$. Setting it to zero implies that

$$\Pi^* = i\mu\phi \quad \rightarrow \quad \phi(t) = \phi(0)e^{i\mu t}\,. \tag{2.38}$$

Fixing the charge produces a centrifugal barrier resulting in the effective potential

$$V_{\text{eff}}(\phi^*\phi) = V(\phi^*\phi) - \mu^2\phi^*\phi = \frac{\lambda}{4}(\phi^*\phi)^2 - \mu^2\phi^*\phi\,. \tag{2.39}$$

Therefore, the ground state of the theory constitutes a spatially homogeneous field configuration that minimises the above effective potential V_{eff}. Expanding the complex scalar field ϕ as

$$\phi = \frac{1}{\sqrt{2}}\rho\, e^{i\chi} \quad \rightarrow \quad \phi^*\phi = \frac{1}{2}\rho^2 \tag{2.40}$$

the effective potential becomes a double-wall effective potential for the radial mode ρ

$$V_{\text{eff}}(\rho) = \frac{\lambda}{16}\rho^4 - \frac{1}{2}\mu^2\rho^2\,. \tag{2.41}$$

Its first order derivative consists in a third order polynomial in ρ, whose zeros correspond to a maximum for V_{eff} in $\rho = 0$ and to the minima $\rho = \pm 2\mu/\sqrt{\lambda}$.

Therefore, the massless angular mode χ corresponds to the Goldstone boson expected from the spontaneous breaking of the global symmetry $U(1)$ in this global superfluid transition. In condensed matter language, this mode is the superfluid phonon.

The next section will explore symmetry breaking in this theory, combining the foundational concepts from chapter 1 with discussions from the previous sections.

§ 2.4 Unveiling $U(1)$ invariance: a study of Large Charge Expansion in CFTs

The overall goal of this section is to elucidate the methodology delineated in the preceding chapter. It also aims to apply this methodology to the foregoing sections to embrace d-dimensional CFTs invariant under an internal symmetry group G [6, 75, 88]. Therefore, let us examine the correlation functions in the Euclidean space $\mathbb{R}^d$. Let $O_{\vec{Q}}(x)$ denote the operator having the minimal scaling dimension for fixed values of the charges $\vec{Q} = (Q_1, \ldots, Q_N)$ associated with the Cartan generators $\bar{Q}_I$ of the group. Generally, these correlation functions take the form

$$\left\langle O^{\dagger}_{\vec{Q}}\left(x_{\text{out}}\right) O_m\left(x_m\right) \ldots O_1\left(x_1\right) O_{\vec{Q}}\left(x_{in}\right)\right\rangle, \tag{2.42}$$

where $O^{\dagger}_{\vec{Q}}(x)$ denotes the conjugate operator of $O_{\vec{Q}}(x)$, carrying charge $-\vec{Q}$ while the operators O_i here represent additional operators carrying finite quantum numbers.

As explained in chapter 1, the state-operator correspondence in the limit $x_{in} \to 0$ and $x_{\text{out}} \to \infty$ maps the action of $O_{\vec{Q}}$ and $O^{\dagger}_{\vec{Q}}$ in the vacuum to the creation of a primary state $|\vec{Q}\rangle$ for the theory on $\mathbb{R} \times S^{d-1}$, with sphere radius R [6]. Consequently, by the underlying Weyl invariance of the theory, the theory quantized on the cylinder the vacuum correlator in (2.42) is equivalent to the matrix element below for

$$\left\langle \vec{Q}, \tau_{\text{out}}\left| O_m\left(\tau_m, \tilde{n}_m\right) \ldots O_1\left(\tau_1, \tilde{n}_1\right)\right| \vec{Q}, \tau_{\text{in}}\right\rangle, \tag{2.43}$$

where $\tau = R\log(|x|/R)$ represents Euclidean time on the cylinder[4], $\tilde{n}^{\mu} = x^{\mu}/|x|$ specifies the coordinates on the sphere, and the states are defined in the Schrödinger picture

$$|\vec{Q}, \tau_{\text{in}}\rangle \equiv e^{H\tau_{\text{in}}}\,|\vec{Q}\rangle = e^{E_{\vec{Q}}\tau_{\text{in}}}\,|\vec{Q}\rangle\,, \quad \langle\vec{Q}, \tau_{\text{out}}| \equiv \langle\vec{Q}|\, e^{-H\tau_{\text{out}}} = \langle\vec{Q}|\, e^{-E_{\vec{Q}}\tau_{\text{out}}}\,. \tag{2.44}$$

Let us recall that the energy of the state on the cylinder is related to the scaling dimension $\Delta_{\vec{Q}}$ of the corresponding operator as (see section 1.3 in chapter 1)

$$E_{\vec{Q}} = \frac{\Delta_{\vec{Q}}}{R}\,. \tag{2.45}$$

Here (2.43) mirrors the setup explored for the Hydrogen atom in section 2.2. It suggests that, for sufficiently large Q_I values, the path integral corresponding to the matrix element in equation (2.43) will predominantly follow a semiclassical trajectory outlining a specific symmetry-breaking pattern [6].

Precisely, operator insertions and states with higher energy will be interpreted as excitations over the classical configuration associated with the ground state $|\vec{Q}\rangle$. The symmetries of the leading trajectory can be inferred by considering the insertion of the operator $O_{\vec{Q}}$ at $x_{in} = 0$ and $x_{\text{out}} = \infty$, which defines the boundary conditions for the path

[4] Note that in chapter 1 this map was introduced in radial coordinates.

integral.

These conditions break translations P_μ and special conformal transformations K_μ. The rotation group $SO(d)$ may or may not be broken if the operator $O_{\vec{Q}}$ carries or does not carry spin. Assuming the simplest and most plausible scenario where $O_{\vec{Q}}$ is a scalar, the case under study in the previous section implies that $|\vec{Q}\rangle$ describes a state with homogeneous charge density.

The behaviour of the dilation generator D, corresponding to the Hamiltonian on the cylinder, and the internal group G, remains to be determined. Since the origin and the point at infinity remain stable under dilations, the generator D may or may not be broken. As already explained, the most natural scenario is a superfluid phase, wherein both the dilation generator and G are broken, leaving unbroken a linear combination of D and the Cartan generators (see (2.29) to (2.32) and (2.33) along with discussion in section 1.3)

$$\bar{D} = D + \mu_I \bar{Q}_I \; . \tag{2.46}$$

This indeed aligns with the test-bed scenario of the Hydrogen atom.

In conclusion, the expected symmetry-breaking pattern characterising the leading semiclassical trajectory typically reads as

$$SO(d+1,1) \times G \longrightarrow SO(d) \times \bar{D} \times G', \tag{2.47}$$

where $G' \subset G$ denotes the internal unbroken sub-group. Consequently, the Goldstone excitations corresponding to the pattern in (2.47) characterise the properties of the ground state and its fluctuations. Therefore, the path integral (2.43) can be effectively computed using a low-energy action for the Goldstones, whose most general form is largely constrained by the non-linear realisation of the symmetry.

Thus, re-visiting the example in the previous section, the quartic structure due to the presence of $\mu^2 > 0$ implies that the radial mode ρ acquires a $vev \neq 0$. This means that the $U(1)$ symmetry is spontaneously broken. In particular, the second-order derivative of V_{eff} for the physical radial field ρ gives a mass $m_\rho \propto \mu$, while the angular field χ results to be massless. The symmetry-breaking pattern induced by the charge fixing in a $3+1$ dimensional theory is thus the following

$$SO(4,2) \times U(1) \to SO(4) \times D \times U(1) \rightsquigarrow SO(4) \times D' \tag{2.48}$$

where $D' = D + \mu Q$.

2.4.1 Path Integral and spectrum

To illustrate that the path integral (2.43) can be effectively computed using a low-energy action for the Goldstones, consider the path integral corresponding to the free evolution in Euclidean time of the ground state under fixed charges Q_I. This is described by equation (2.43) without insertions.Let us turn the attention to the most general action for the Goldstones compatible with the symmetry-breaking pattern (2.47). In the following, this action is denoted with $S[\chi, \pi]$, where χ^I represents the Goldstone fields associated with the Cartan charges. The matrix element then reads as

$$\left\langle \vec{Q} \left| e^{-HT} \right| \vec{Q} \right\rangle = \int d^N \chi_i d^N \chi_f \int_{\chi_i,\pi_i}^{\chi_f,\pi_f} \mathcal{D}\chi \mathcal{D}\pi \exp\left\{ -S[\chi,\pi] - \frac{i}{\Omega_{d-1}} \int_{-T/2}^{T/2} d\tau \int d\Omega_{d-1} \dot{\chi}^I Q_I \right\} , \tag{2.49}$$

where $\Omega_{d-1} = \frac{2\pi^{d/2}}{\Gamma(d/2)}$ represents the volume of the $d-1$-dimensional sphere [6, 35]. Similar to the Hydrogen atom scenario, the last term in the action serves as a boundary term, determining the charge of the initial and final state (see (2.12))[5].

The characterisation of the leading trajectory in the path integral in terms of the symmetry-breaking pattern in (2.47) does not necessarily imply that the state $|\vec{Q}\rangle$ truly breaks the symmetry. In reality, the latter is an eigenstate of both the operators $\bar{Q}^I$ and the dilation D. However, it is worth mentioning that it is indeed the existence of such a semiclassical trajectory dominating the path integral that leads to the description of the system in terms of a low-energy action for the Goldstone fields associated with the corresponding breaking pattern [6][6].

Usually, the most general action that non-linearly realises the symmetry in equation (2.47) can be systematically constructed using the CCWZ approach [76, 77] for broken spacetime symmetries [89] (see section 1.6). Even though this method offers a systematic approach to deriving all terms up to a specified order in the derivative expansion, in the subsequent discussion a more intuitive construction is presented.

2.4.2 Semiclassical analysis

Given that the theory under examination is a CFT, a key assumption moving forward will be the invariance under Weyl rescaling of the metric. This is crucial because Weyl invariance allows one to map the theory to the cylinder [7]. For the discussion that will follow, it suffices to consider a single shift-invariant superfluid Goldstone associated with the breaking of the $U(1)$ symmetry to realise the symmetry-breaking pattern (2.47). Specifically, the superfluid Goldstone is denoted as

$$\chi(x) = \pi(x) - i\mu\tau \ . \tag{2.50}$$

Furthermore, the chemical potential μ in (2.50) will ultimately be determined by the charge Q. Additionally, $\pi(x)$ appearing in (2.50) represents the massless excitation having a linear dispersion relation that has been called the superfluid phonon [91]. A natural objection to this discussion may regard the use of a unique Goldstone boson and the absence of additional Goldstones emerging from boosts. However, the most general Poincaré-invariant action can only involve contributions constrained by Lorentz

[5] Furthermore, the precise specification of the boundary conditions for the additional Goldstones π_i becomes irrelevant in the $T \to \infty$ limit, similar to those for r and θ in the Hydrogen atom scenario. For large Q_I, this integral can be evaluated using the saddle-point method, as highlighted in [6].

[6] Additionally, one shall contemplate the possibility that the leading trajectory in the path integral does not break the dilation operator. Nevertheless, commenting on this eventuality is far from the scope of this thesis.

[7] It is widely believed that all unitary CFTs exhibit Weyl invariance (allowing for anomalies) [90].

invariance.

Therefore, denoting with $g_{\mu\nu}$ the metric on the cylinder $\mathbb{R}\times S^{d-1}$ and introducing [6]

$$\tilde{g}_{\mu\nu} \equiv g_{\mu\nu}\,(\partial\chi)^2 \quad \text{where} \quad (\partial\chi) = \left(-\partial_\mu\chi g^{\mu\nu}\partial_\nu\chi\right)^{1/2} \tag{2.51}$$

which is manifestly invariant under Weyl transformations, the most general action for χ reads

$$\begin{aligned} S[\chi] &= -\int d^d x\sqrt{\tilde{g}}\left\{c_1 - c_2\tilde{\mathcal{R}} + c_3\tilde{\mathcal{R}}^{\mu\nu}\partial_\mu\chi\partial_\nu\chi + O\left(\tilde{\nabla}^4\right)\right\} \\ &= -c_1\int d^d x\sqrt{g}(\partial\chi)^d \\ &+ c_2\int d^d x\sqrt{g}(\partial\chi)^d\left\{\frac{\mathcal{R}}{(\partial\chi)^2} + (d-1)(d-2)\frac{\left[\nabla_\mu(\partial\chi)\right]^2}{(\partial\chi)^4}\right\} \\ &- c_3\int d^d x\sqrt{g}(\partial\chi)^d\left\{\mathcal{R}_{\mu\nu}\frac{\partial^\mu\chi\partial^\nu\chi}{(\partial\chi)^4} + (d-1)(d-2)\frac{\left[\partial^\mu\chi\nabla_\mu(\partial\chi)\right]^2}{(\partial\chi)^6}\right. \\ &\left. +(d-2)\nabla_\mu\left[\frac{\partial^\mu\chi\partial^\nu\chi}{(\partial\chi)^2}\right]\frac{\nabla_\nu(\partial\chi)}{(\partial\chi)^3}\right\} + O\left((\partial\chi)^d\frac{\nabla^4}{(\partial\chi)^4}\right) \end{aligned} \tag{2.52}$$

where $\mathcal{R}^\rho_{\mu\sigma\nu}$ and $\tilde{\mathcal{R}}^\rho_{\mu\sigma\nu}$ are the Riemann tensors derived from g_μ and $\tilde{g}_{\mu\nu}$, respectively while $\mathcal{R}$ and $\tilde{\mathcal{R}}$ their corresponding Ricci scalars. The underlying CFT determines the values of the Wilson coefficients c_1, c_2 and c_3 appearing in (2.52). The latter control the derivative expansion[8] along with the chemical potential $\mu = \langle(\partial\chi)\rangle$.

Equation (2.49) using (2.52) becomes

$$\left\langle Q\left|e^{-HT}\right|Q\right\rangle = \int \mathcal{D}\chi\,\exp\left\{-\int_{-T/2}^{T/2} d\tau\int d^{d-1}x\sqrt{g}\left[\mathcal{L} + i\frac{Q}{R^{d-1}\Omega_{d-1}}\dot{\chi}\right]\right\}, \tag{2.53}$$

that can thus be computed semiclassically around the saddle-point solution

$$\chi_s = \pi_* - i\mu\tau\ . \tag{2.54}$$

It is worth noting that on the solution, the term proportional to c_3 in the action (2.52) vanishes since $\mathcal{R}_{00} = 0$ on $\mathbb{R}\times S^{d-1}$. Considering that rotations on $\mathbb{R}\times S^{d-1}$ play a role similar to translations in flat space, one can verify that the solution (2.54) precisely realises the symmetry breaking pattern in (2.47) in terms of a single field, as anticipated. Similar to the case of the Hydrogen atom in (2.15), π_* stands as an integration constant.

Consistent with prior anticipations, the charge Q is obtained via the chemical potential as

$$\frac{Q}{R^{d-1}\Omega_{d-1}} = j_0 = i\frac{\partial\mathcal{L}}{\partial\dot{\chi}} = c_1 d\mu^{d-1} - c_2(d-2)\mu^{d-3}\mathcal{R} + O\left(\mu^{d-5}\right)\ , \tag{2.55}$$

with j_μ being the $U(1)$ Noether current. On a cylinder, the Ricci scalar is equal to $\mathcal{R} = (d-1)(d-2)/R^2$ so equation (2.55) can be solved perturbatively for large Q, leading to

$$R\mu = \left(\frac{Q}{c_1 d\Omega_{d-1}}\right)^{\frac{1}{d-1}}\left[1 + \frac{c_2(d-2)^2}{c_1 d}\left(\frac{Q}{c_1 d\Omega_{d-1}}\right)^{-\frac{2}{d-1}} + O\left(\left(\frac{Q}{c_1 d\Omega_{d-1}}\right)^{-\frac{4}{d-1}}\right)\right]\ . \tag{2.56}$$

[8] To give an example, for strongly coupled theory they are written in inverse powers of 4π's [92].

It is important to mention that in the limit $Q \gg 1$ the chemical potential scales as

$$\mu \propto Q^{\frac{1}{d-1}} + O\left(Q^{-2/(d-1)}\right) \tag{2.57}$$

and that the action evaluated on (2.56) leads to the following expression of the energy on the cylinder

$$E_Q \xrightarrow[\text{in } Q\gg 1]{\text{leading order}} \tilde{E}_Q = \frac{\alpha_1}{R}\, Q^{\frac{d}{d-1}} + \frac{\alpha_2}{R}\, Q^{\frac{d-2}{d-1}} + O\left(Q^{\frac{d-4}{d-1}}\right), \tag{2.58}$$

where the α_is are written in terms of the Wilson coefficients:

$$\alpha_1 = \frac{c_1(d-1)\Omega_{d-1}}{(c_1 d\Omega_{d-1})^{\frac{d}{d-1}}}, \quad \alpha_2 = \frac{c_2(d-1)(d-2)\Omega_{d-1}}{(c_1 d\Omega_{d-1})^{\frac{d-2}{d-1}}}\,. \tag{2.59}$$

By the state-operator correspondence and making use of (2.45), the scaling dimension of the lightest operator with fixed charge $Q \gg 1$ results in[9]

$$\Delta_Q = E_Q\, R \xrightarrow[\text{in } Q\gg 1]{\text{leading order}} \tilde{\Delta}_Q = \tilde{E}_Q\, R = \alpha_1\, Q^{\frac{d}{d-1}} + \alpha_2\, Q^{\frac{d-2}{d-1}} + O\left(Q^{\frac{d-4}{d-1}}\right)\,. \tag{2.60}$$

Additionally, one-loop corrections to (2.58) are obtained from the fluctuation determinant coming from Gaussian integration of the fluctuations action.

Precisely, following the example for the Hydrogen atom, using (2.50) and expanding the leading low-energy action (second line in (2.52)) to quadratic order in the fluctuations, i.e.

$$S^{(2)} \simeq \frac{d(d-1)}{2} c_1 \mu^{d-2} \int d^d x \sqrt{g} \left[\dot{\pi}^2 + \frac{1}{d-1}(\partial_i \pi)^2 + O\left(\nabla^4/\mu^2\right)\right] \tag{2.61}$$

leads to the following one-loop contribution to the energy

$$\begin{aligned} T E^{(1)} &= \frac{1}{2} \log\det\left[-\partial_\tau^2 - \frac{1}{d-1}\Delta^{\left(S^{(d-1)}\right)} + O\left(\nabla^4/\mu^2\right)\right] \\ &= \frac{T}{R}\left[\beta_0 + \beta_1 Q^{-\frac{2}{d-1}} + O\left(Q^{-\frac{4}{d-1}}\right)\right] \end{aligned} \tag{2.62}$$

with $\left|g^{ij}\right| \nabla_i \nabla_j = \Delta^{\left(S^{(d-1)}\right)}$ being the Laplacian on the $d-1$-dimensional sphere.

Several comments are now in order. Firstly, (2.61) is the action describing the superfluid phonon having speed of sound

$$v_G = \frac{1}{\sqrt{d-1}}\,. \tag{2.63}$$

This property arises directly from the traceless nature of the energy-momentum tensor and since it only depends on the number of dimensions d, the dimensionless coefficient

[9] Note that the scaling with Q of the leading term in (2.60) could have been inferred on dimensional grounds [82]. Indeed, for a scale-invariant theory in the semiclassical regime, the charge density j_0 and the energy density $\mathcal{E}$ are expected to obey a local relation of the form $\mathcal{E} \propto j_0^{\frac{d}{d-1}}$, as will be shown in the subsequent section.

β_0 appearing in the large Q expansion result in (2.62) cannot depend on the Wilson coefficients c_is. The overall result for the lowest scaling dimension thus reads as

$$Q^{\frac{d}{d-1}}\left[\alpha_1+\alpha_2 Q^{-\frac{2}{d-1}}+\alpha_3 Q^{-\frac{4}{d-1}}+\dots\right]+Q^0\left[\beta_0+\beta_1 Q^{-\frac{2}{d-1}}+\dots\right]. \tag{2.64}$$

Furthermore, a deeper look at (2.58) shows that when d is odd no term scaling as Q^0 ever emerges. Therefore, in odd spacetime dimensions, the one-loop correction of order $O(Q^0)$ cannot be renormalized by any local counterterm and it is hence calculable. This implies that it remains independent of the microscopic details of the CFT, being solely determined by symmetry considerations and the spatial dimension. The Q^0-contribution exhibits a universal value across all three-dimensional $U(1)$-invariant CFTs characterised by a superfluid phase in their large charge sector [82, 88, 93].

With this milestone achieved, which will be crucial for discussions in chapter 6 and in chapter 7, let us better dive into the theory defined by the Lagrangian density in (2.34). Precisely, in the following subsections it is shown how the radial mode (or more precisely its vev) plays the role of the RG-flow parameter. In this sense, it plays the role of a dilaton since the RG transformation is a local scale transformation [82, 93].

2.4.3 Zooming in: consequences of fixing the charge on the RG flow

Returning to Lagrangian density (2.34) and expressing it using the polar coordinates of the complex field ϕ, as presented in (2.40), yields:

$$\mathcal{L}=\frac{1}{2}(\partial\rho)^2+\frac{1}{2}\rho^2(\partial\chi)^2-\frac{\lambda}{16}\rho^4\,. \tag{2.65}$$

This theory is specifically considered to be defined in dimensions $d<4$ to ensure the existence of an infrared Wilson-Fisher fixed point.

The goal of this subsection is to show how the low-energy physics of a fixed charge sector can be effectively described by an action that exhibits approximate scale invariance.

The central idea to achieve this conclusion is to use the radial mode of the field to identify the energy scale of the renormalization group flow as one approaches the fixed point. By focussing on the behaviour of the radial mode, it becomes possible to effectively characterise how the energy scale influences the RG flow. This approach not only provides insight into the scaling properties of the theory but also aids in identifying the relevant physical parameters that govern the behaviour of the system in the low-energy regime [35, 93]. Therefore, let us examine the RG flow.

The exact Wilsonian RG flow is truncated to that of the quartic coupling only, not considering renormalizations of other operators. By integrating out modes and lowering the cut-off Λ, the RG evolution of the quartic coupling $\lambda(\Lambda)$ is induced. As the progression towards the infrared continues [10], the first scale encountered is determined by λ as

$$\Lambda_\lambda=\lambda^{\frac{1}{d-4}} \tag{2.66}$$

[10] We assume that the theory flows to an attractive FP in the infrared.

and hence [35, 93]:

- When $\Lambda = \Lambda_\lambda$ the corrections to the coupling are of the same order as the coupling itself.
- Since it is assumed that the theory converges towards an attractive fixed point in the infrared regime, when $\Lambda \ll \Lambda_\lambda$, the coupling assumes its fixed point value λ^*:

$$\lambda^* = \frac{\lambda(\Lambda)}{\Lambda^{4-d}} \ . \tag{2.67}$$

As seen in section 2.3, fixing the charge results in an effective potential for ρ which in turn develops a *vev*. Additionally, in section 2.4.2, it is shown how $\partial\chi$ acquires a *vev* that is nothing else than the chemical potential, as a consequence of the charge-fixing constraint. Moreover, since χ is the superfluid phonon, $\partial\chi$ remains free and massless in the infrared regime. However, looking at (2.65) suggests that the fluctuation of the radial mode may indeed be gapped. This is the case. In fact, studying the fluctuations ϱ of the radial mode

$$\rho = \langle\rho\rangle + \varrho \tag{2.68}$$

the squared mass associated to ϱ is

$$m_\varrho^2 = \frac{3}{8}\,\lambda\,\langle\rho\rangle^2 \tag{2.69}$$

which represents the second scale encountered during the flow towards the IR. Consequently, below m_ϱ the field ϱ decouples and its contributions to the running of the quartic coupling are suppressed by positive powers Λ/m_ϱ. As a result, the quartic coupling itself freezes at the value (i.e. (2.67) evaluated at the scale $\Lambda = m_\varrho$) [35]

$$\lambda(m_\varrho) = \lambda^*\, m_\varrho^{4-d} = \left[\left(\frac{3}{8}\ \langle\rho\rangle^2\right)^{4-d} \lambda^{*\,2}\right]^{\frac{1}{d-2}} \tag{2.70}$$

and the Lagrangian density (2.65) at this scale is

$$\mathcal{L}_\Lambda = \frac{\langle\rho\rangle^2}{2}(\partial\chi)^2 - \left[\left(\frac{3}{8}\right)^{4-d} \lambda^{*\,2}\right]^{\frac{1}{d-2}} \langle\rho\rangle^{\frac{2d}{d-2}} + O\left(\frac{\Lambda}{\langle\rho\rangle^{\frac{2}{d-2}}}\right) \tag{2.71}$$

which is approximately scale-invariant up to corrections of order $O\left(\Lambda/\langle\rho\rangle^{\frac{2}{d-2}}\right)$ [93]. It is worth noting that the underlying theory is still conformally invariant *but* it is in its charged sector that conformal invariance is spontaneously broken by $\langle\rho\rangle$. At this scale, the fluctuations of ρ are frozen, and hence it only remains to study the dynamics of $\partial\chi$. In particular, its *vev* is the chemical potential, which is given by the constraint on the EOM. Specifically, the chemical potential in terms of $\langle\rho\rangle$ is

$$\mu^2 = \frac{2d}{d-2}\left[\left(\frac{3}{8}\right)^{4-d} \lambda^{*\,2}\right]^{\frac{1}{d-2}} \langle\rho\rangle^{\frac{4}{d-2}} \tag{2.72}$$

and additionally

$$\langle\rho\rangle = 6^{\frac{d-4}{4(d-1)}} \left(\frac{d-2}{d}\right)^{\frac{d-2}{4(d-1)}} (2\lambda^*)^{-\frac{1}{2(d-1)}} (q)^{\frac{d-2}{2(d-1)}} \quad \text{with} \quad q = \frac{Q}{R^{d-1}\Omega_{d-1}}, \tag{2.73}$$

$$\mu = 6^{\frac{4-d}{2(d-1)}} \left(\frac{d}{d-2}\right)^{\frac{d-2}{2(d-1)}} (2\lambda^* \, q)^{\frac{1}{d-1}} \ . \tag{2.74}$$

The pivotal insight lies in the observation that the radial mode ρ does not contribute to the IR dynamics, thus it can be integrated out. Consequently, the physics at energy Λ is governed by the newly introduced scale arising from charge fixing, which is proportionate to the charge density. To elucidate this concept, the following Figure 2.1 provides a concise summary of the hierarchical structure elucidated in this subsection.

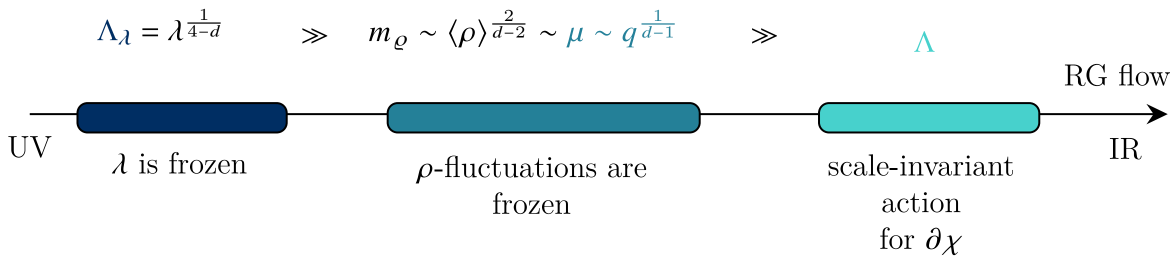

Figure 2.1.: Schematic summary of the energies involved during the RG flow analysed in the text.

Hence, on the cylinder (and generally on any compact curved manifold characterised by a length scale R), the EFT remains well-defined on length scales much smaller than R, with the latter serving as an infrared cut-off. This, in consequence, implies the following chain of inequalities

$$\underbrace{\Lambda_\lambda}_{\text{UV cutoff}} \gg \left(\frac{Q}{R^{d-1}\Omega_{d-1}}\right)^{\frac{1}{d-1}} \gg \Lambda \gg \underbrace{\frac{1}{R}}_{\text{IR cutoff}} \ . \tag{2.75}$$

This discussion highlighted the role of the radial mode, particularly its *vev*, in serving as a parameter for the RG flow [93]. This establishes a crucial connection, as the radial mode functions similarly to a dilaton, since the RG transformation can be understood as a local scale transformation. By recognising this analogy, one can appreciate how variations in the radial mode can influence the energy scale of the system.

Having this in mind, let us provide in the following subsection a more precise understanding of this connection by developing the effective field theory for the infrared physics of the $U(1)$ model within a sector of fixed charge. This will involve the analysis of the dynamics of the system directly at the IR fixed point. By focussing on this methodology, the discussion aims to deepen the understanding of the role played by the radial mode in shaping the physical properties of the model in the IR regime. This foundational understanding will pave the way for understanding the approaches employed in chapter 6 and chapter 7. This involves highlighting both the motivations behind these methods and the methodologies themselves that guide the subsequent analyses.

2.4.4 Zooming in: consequences of fixing the charge on the IR theory

As is known, when the global symmetry undergoes spontaneous breaking, the system can be naturally described in terms of a free massless (Goldstone) field [93]. However, armed with the concept introduced in chapter 1, to achieve the anticipated conformal symmetry at the fixed point, this Goldstone field must be complemented by another field, the dilaton [53]. It will become evident that this corresponds precisely to the radial mode of the EFT [93, 94].

To come to this conclusion, let us consider a two-derivative EFT for the Goldstone field of the form

$$\mathcal{L} = \frac{f_\pi^2}{2}(\partial\chi)^2 - C^d \tag{2.76}$$

with f_π and C being constant of the underlying theory. Following the discussion in section 1.6.2, to non-linearly realise conformal invariance of the action, one needs to *dress* the Lagrangian density with the dilaton. In this case, the outcome reads

$$\mathcal{L}_{\text{CFT}} = \frac{f_\pi^2}{2}(\partial\chi)^2\, e^{-2f\sigma} - C^{d+1}\, e^{-2\left(\frac{d+1}{d-1}\right)f\sigma} + \frac{1}{2}(\partial\sigma)^2\, e^{-2f\sigma} - \frac{\mathcal{R}}{12f^2}\, e^{-2f\sigma} + O\!\left(\mathcal{R}^2\right) \tag{2.77}$$

which is an effective action for the two Goldstones, χ and σ, emerging from the breaking of the internal and conformal symmetry, respectively. Recasting these two fields as follows

$$\Sigma = \sigma + i f_\pi \chi \quad \text{and introducing} \quad \phi = \frac{1}{\sqrt{2}f}\, e^{-f\Sigma} \tag{2.78}$$

(2.77) becomes

$$\mathcal{L} = \partial\phi^*\partial\phi - \frac{\mathcal{R}}{6}\,\phi^*\phi - u\,(\phi^*\,\phi)^{\frac{d}{d-2}} + \dots\,. \tag{2.79}$$

Therefore, the dilaton field acts as the radial mode of ϕ and $u = 2^{\frac{d}{d-2}}(Cf)^d$ is a dimensionless quantity, consistent with the fact that (2.79) describes a CFT, which by definition has no dimensionful parameters.

Let us also stress that, when $C = 0$, the above lagrangian simply reads

$$\mathcal{L} = \partial\phi^*\partial\phi - \frac{\mathcal{R}}{6}\,\phi^*\phi \tag{2.80}$$

and the lowest-lying operator with $U(1)$ charge Q is, of course, ϕ^Q whose scaling dimension is $\Delta = Q$. This linear scaling of the dimension to the value of the charge in the large charge limit $Q \gg 1$ signals the presence of a *moduli space* as outlined in [95].

The condition of the presence of a moduli space is essential for a given CFT to feature spontaneous breaking of conformal symmetry. However, in the course of the present chapter, it has been shown that the scaling dimension displays the characteristic leading-order behaviour of (2.60) at $Q \gg 1$, that is, $\tilde{\Delta}_Q = \tilde{E}_Q\, R \sim \alpha_1\, Q^{\frac{d}{d-1}}$, which instead holds in generic interacting CFTs *without* a moduli space.

Nevertheless, the existence of an at most approximate moduli space can be guaranteed by the presence of the C-term. To be more precise, an approximate moduli space can be ensured by introducing sources of explicit breaking of scale invariance that generate a non-trivial dilaton potential, as will be better explained in chapter 5. For this purpose, a C-term can be added to the model since it represents the simplest relevant coupling that remains consistent with conformal invariance.

As shown in [75, 82] (and reviewed in appendix B) and better described in chapter 6 and chapter 7, the large charge sector of the theory in (2.79) can be studied semiclassically within the following double scaling limit

$$Q \to \infty \,, \qquad u \to 0 \,, \qquad Qu = \text{fixed} \tag{2.81}$$

which leads to the characteristic form of the scaling dimension of the lowest-lying charged operator

$$\Delta_Q = \sum_{j=-1} \frac{\Delta_j(uQ)}{Q^j} \,. \tag{2.82}$$

It was shown in [75] that depending on the value of the *'t Hooft coupling Qu* the leading order Δ_{-1} actually reads

$$\begin{cases} \tilde{\Delta}_{-1} &= Q + \frac{Q^2 u}{8\pi^2} - \frac{Q^3 u^2}{32\pi^4} + O\big((uQ)^4\big) \quad \text{for small} \quad Qu \\ \tilde{\Delta}_{-1} &= \frac{3}{2}\frac{Q^{4/3}u^{1/3}}{4\pi^{2/3}} + \frac{\pi^{2/3}Q^{2/3}}{2^{2/3}u^{1/3}} - \frac{\pi^2}{6u} + O\big((uQ)^{-1/3}\big) \quad \text{for large} \quad Qu \end{cases} \tag{2.83}$$

and the two results can be interpolated by varying the product Qu. In fact, in doing so, Δ_Q interpolates between the first (linear) regime typical of theories having moduli space with the second result characteristic of generic bosonic CFTs without moduli space [95].

In a theory where scale invariance remains explicitly unbroken, spontaneous breaking of this symmetry can occur only if the C-term is zero. This will be further explored in chapter 5 by introducing deformations to the conformal field theory by incorporating sources of conformal breaking. The discussion will then review the general structure of the dilaton potential and the common approximations found in the literature. This approach sets the stage for understanding how small deformations in the theory affect symmetry breaking.

This section is concluded by stressing that the description that employs the dilaton to characterise the radial mode thus offers a pathway to introduce a slight mass term for σ, which explicitly breaks conformal invariance. This concept has been used to investigate near conformal dynamics at large charge [94] and this idea forms the core of the current thesis [2–4].

To fix the ideas, in the following Figure 2.2 there is a summary of the concepts outlined in this chapter.

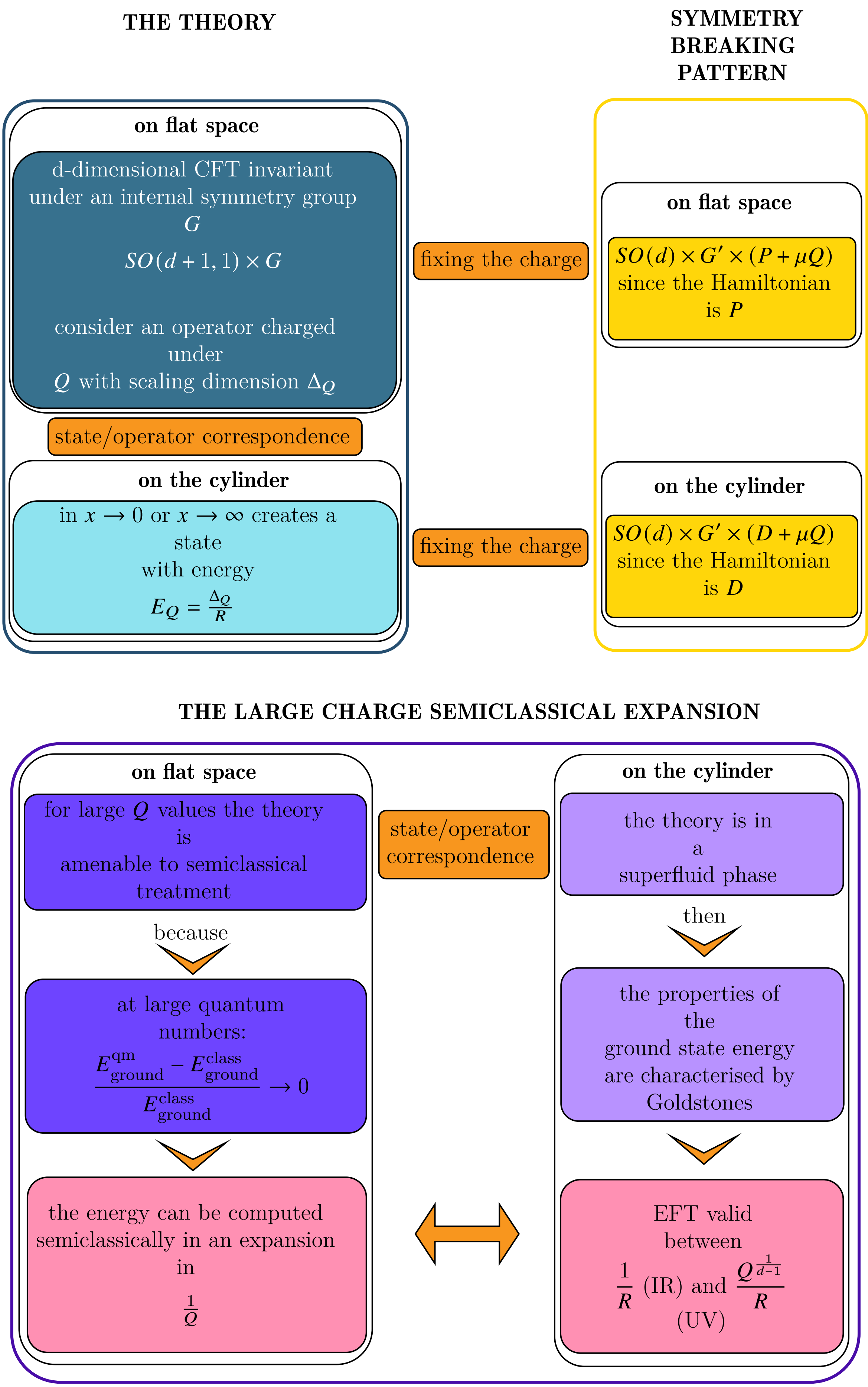

Figure 2.2.: Conceptual diagram containing the main concepts outlined in this chapter.

Part II

QCD AND QCD-LIKE THEORIES AT NON-ZERO ISOSPIN AND BARYON DENSITY

Introduction to Part II

Understanding the dynamics of strongly coupled theories remains an open challenge, making it one of the most fascinating topics in theoretical physics. Partial progress has been made both analytically and numerically via a number of tools developed in the past decades. Quantum Chromodynamics, featuring three colours and several light flavours, has been chosen by Nature as one of the pillars of the Standard Model of particle interactions. QCD therefore stands out within the landscape of strongly coupled theories. However, several relevant questions remain unanswered about its dynamics, from the QCD physical spectrum to the interplay between chiral symmetry breaking and confinement, to its phase structure as a function of light matter fields (conformal window), temperature, and matter density. For example, knowledge about the phase diagram informs a number of physical applications ranging from the inner structure of Neutron stars [96] to the thermal history of the early Universe [97] and last but not least to applications beyond standard model physics and cosmology (see [98, 99] and references therein). Another unsolved puzzle is the absence or unexplained strong suppression [100, 101] of the otherwise legitimate presence in the theory of the topological term responsible for strong CP violation. Its possible resolutions in terms of either the axion physics [102–107] or its alternatives such as the ones in which CP is broken spontaneously [108–110] or models in which the emergent Goldstone boson is not an axion (which would have a non-zero mass) [111] (see also [112]) are under active experimental and theoretical investigation.

Reducing the number of colours from three to two provides a number of theoretical advantages and increases potential phenomenological applications beyond the QCD template. This is due, in a nutshell, to the symplectic nature of the matter representation that enhances the quantum global symmetries for the light flavours from $SU(N_f) \times SU(N_f) \times U(1)_B$ to $SU(2N_f)$. The enhancement of the quantum global symmetries (demonstrated on the lattice in [113, 114]) has far-reaching consequences [115, 116], such as the possibility of the minimal construction of composite Goldstone Higgs theories [117] to the natural introduction of number changing operators (stemming from the Wess-Zumino term) crucial to models in which dark matter genesis occurs within the dark sector itself [118–121]. When discussing non-zero baryon charge, the model allows for well defined lattice simulations because the action remains real, differently from ordinary QCD. For a review of the various applications of the theory beyond the ones mentioned here, see [98, 99]. Last but not least this model together with ordinary QCD has been one of the most studied theories on the lattice as function of light flavours in the hunt for the predicted lower edge of the conformal window [122–125] and its dynamical properties [113, 114, 126, 126–136], finite baryon density [137–157] and last but not least the investigation of gravity-free asymptotic safety at large number of matter fields (proven rigorously in [158, 159] for gauge-Yukawa theories) and suggested for gauge-fermion theories in [160] investigated on the lattice in [161, 162].

The goal of chapter 4 is to go beyond the state-of-the-art by providing an in-depth analysis of the θ-angle and axion physics at non-zero baryon chemical potential of two-colour QCD whose earlier studies appeared in [163]. To appreciate the contents of the chapter, in chapter 3 a full review of the necessary notions will be provided.

Phase diagram of dense QCD and QCD-like theories

3

CHAPTER

§ 3.1 Overview

Strong interactions among fundamental particles constitute the driving force behind the energy production in stars which constitutes the predominant mass within the luminous universe. The theoretical framework governing these interactions, Quantum Chromodynamics, provides a comprehensive description. However, the intricate and non-linear nature of these interactions presents formidable challenges to complete understanding. Exploring the mechanisms behind the generation of particle masses and the confinement phenomenon is imperative. Additionally, understanding the diverse phases of QCD under extreme conditions of temperature or density and the transitions between these phases represents some of the most pressing inquiries in the realm of physics [164].

Phase diagrams represent our understanding of how matter and its characteristics evolve under varying conditions. They illustrate the preferred phase of matter at thermodynamic equilibrium based on selected macroscopic thermodynamic variables. Within these diagrams, phase transitions delineate the boundaries between different phases, typically categorised as first-order, second-order, or crossovers. The Ehrenfest classification distinguishes between these transitions by identifying divergences in the derivatives of the free energy concerning thermodynamic variables (see section 1.1.1). Symmetry alterations can be quantified using an associated order parameter, finite in one phase but not in another, signifying symmetry breaking or restoration.

In *elementary* schools, the most common phase diagram that students learn is the temperature-pressure diagram for water [164]. However, phase diagrams extend beyond compounds and materials and are not limited solely to solid, liquid, or gaseous states. Under specific conditions, the electromagnetic forces that typically govern the interactions among molecules and atoms in our everyday world can be surpassed. At high temperatures, plasma forms as electrons gain enough kinetic energy from thermal collisions to escape the electromagnetic forces of nuclei.

Generally, visualising the full QCD phase diagram in its entirety is impractical due to its complexity. The comprehensive diagram holds significance, as QCD represents a fundamental theory of Nature. However, attention is primarily directed towards parameters and planes relevant to specific scientific inquiries.

For instance, the Quark-Gluon Plasma phase, believed to have been the primordial state of matter shortly after the Big Bang, is a focal point of investigation. This phase existed during a period of extremely high temperatures and densities. Research into this form of matter is a key motivation behind Heavy Ion Collision (HIC) experiments, which involve the study of matter under extreme conditions characterised by large magnetic fields, angular momenta, and high-energy collisions. The QGP phase is often described as a nearly perfect fluid composed of quarks and gluons, yet it remains strongly coupled. These experiments replicate the extreme conditions thought to have existed microseconds after the Big Bang, making them highly relevant to cosmology. However, studying this phase of QCD matter is exceptionally challenging in such experiments because the QGP formed in heavy-ion collisions is far from equilibrium and only exists for a fleeting moment. As a result, much of the current understanding of hot QCD matter at zero baryon chemical potential comes from lattice QCD simulations. The transition from the hadronic (confined) phase to the QGP is known as the *deconfinement transition*, which is believed to be a crossover between these two phases. This occurs at a temperature where the typical momentum transfer scale is on the order of the characteristic QCD scale corresponding to $T \sim 10^{12}\,\mathrm{K}$. When strong-interaction matter becomes deconfined, quarks and gluons are no longer bound into colour-neutral states, and the chiral condensate “melts", leading to the restoration of spontaneously broken chiral symmetry, i.e. *chiral transition* [165].

Chiral symmetry is an approximate global symmetry of QCD, $SU(N_f)_L \times SU(N_f)_R$ with N_f being the number of flavours of the theory. When quarks are massive, this group is explicitly broken down to the diagonal sub-group $SU(N_f)_V$. For $N_f = 2$, the flavours that come into play are the up and the down and since both have small masses at the Gev scale, they can be considered to be massless. Then, the chiral symmetry becomes exact *but* it is spontaneously broken by the QCD vacuum. This symmetry-breaking pattern is the chiral symmetry breaking and the order parameter associated with it is the chiral condensate $\langle\bar{\psi}\psi\rangle$.

Chiral symmetry breaking gives rise to the presence of pseudo-scalar mesons (such as pions) and contributes to significantly higher masses of baryons compared to the sum of their constituent quarks' bare masses. Quarks within hadrons can be conceptualised as possessing an effective mass much greater than their bare mass because of chiral symmetry breaking. Moving to higher energies, the vacuum responsible for spontaneously breaking the symmetry becomes less relevant, leading to the restoration of chiral symmetry. As a result, quarks return to their intrinsic masses and may even become nearly massless. This transition, characterised by the chiral condensate approaching zero, serves as an indicator, though it is only an approximate order parameter. In the physical scenario, where chiral symmetry is not exact, the condensate does not precisely reach zero at the transition. $\langle\bar{\psi}\psi\rangle$ functions as an order parameter only in the massless quark or chiral limit. Chiral symmetry can also be broken through diquark condensates $\langle\psi\psi\rangle$ in certain colour superconductors.

Confinement forces quarks to be the constituents of hadrons at low energies. At such energy levels, chiral symmetry breaking governs the masses of these hadrons. There is a temptation to posit a relationship between deconfinement and chiral restoration, perhaps implying that one necessarily accompanies the other [165].

It is also believed that deconfinement and chiral symmetry restoration can occur at much lower temperatures if the density is sufficiently high. At extremely large densities, the strong interaction weakens because of asymptotic freedom, allowing the study of QCD at finite density perturbatively. In this regime, calculations indicate that at sufficiently low temperatures, quark matter exhibits a Cooper pair instability, where quark pairs form a condensate, becoming the ground state. Since quark pairs cannot form a colour-neutral (singlet) state, their condensation spontaneously breaks the local $SU(3)$ colour gauge symmetry, much like how gauge symmetry in electromagnetism is broken in conventional superconductivity, leading to a type of "Meissner effect" for gluons. This new phase of QCD matter is known as the *colour-superconducting* phase. Additionally, unlike electrons, the quarks involved in the Cooper pair condensate have colour, flavour, and spin degrees of freedom. As a result, quarks can pair in various configurations, giving rise to different colour-superconducting phases, each associated with the distinct colour, flavour, and spin structures of the quark pairs.

Additionally, as reviewed in [165], the investigation of matter also extends to those regimes where the temperature has less impact than others. The study of matter at ultra-high densities only occurs in the cores of extremely compact stars, the neutron stars, namely the remnants of massive stars. These stars also possess magnetic fields up to 10^8 to 10^{15} times stronger than the Earth's. With typical radii of 10 to 14 km and masses around 1.4 times that of the Sun, neutron stars are among the densest objects in the universe, with densities exceeding five times that of nuclear matter, surpassed only by black holes.

Moreover [165], the ground state of matter at the core of neutron stars remains elusive. Conditions such as high baryon densities, magnetic fields, and angular motion are prevalent in compact stars. Along with elevated temperatures resulting from mergers, these factors prompt the exploration of matter under extreme circumstances, which are represented on the QCD phase diagram.

Consequently, the parameters most commonly considered in these studies include temperature (T), particle density represented by baryon chemical potential (μ_B) and isospin chemical potential (μ_I), among others. Figure 3.1 schematically represents the phases summarised above [166].

Despite decades of dedicated research, the QCD phase diagram continues to captivate the interest of numerous theoretical and experimental groups. The phase diagram, plotted in the temperature-baryon density plane, is intriguing and holds significant relevance for various astrophysical applications. The Facility for Antiproton and Ion Research (FAIR) and the Nuclotron-Based Ion Collider Facility (NICA) aim to concentrate on regimes featuring high baryon density and low-temperature [167].

Generally, QCD poses significant challenges for first-principles theoretical studies, which remain unattainable at present. Although various theoretical approaches employ simplifying approximations, these often introduce uncontrolled systematic uncertainties. Consequently, lattice simulation has emerged as the most promising avenue for investigating QCD. Grounded in the principles of quantum field theory, lattice simulation offers a means to control and systematically diminish uncertainties [167–174].

Due to the substantial contributions of lattice simulation, there exists a fairly comprehensive understanding of QCD properties at both zero and finite temperatures. However, lattice studies of QCD at finite baryon density encounter a significant obstacle known as the *sign problem*. This issue arises from the fermion determinant, responsible for dynamical quarks, becoming complex, rendering the direct application of importance sampling infeasible within this region of the phase diagram. However, there are ongoing efforts to devise strategies to circumvent the sign problem.

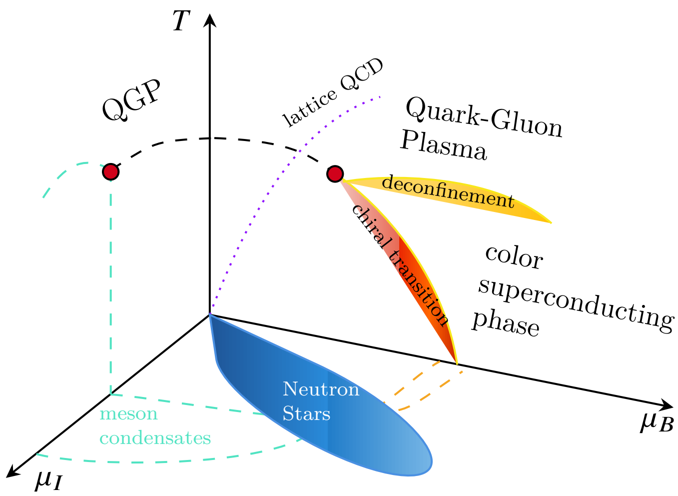

Figure 3.1.: Cartoon schematically representing the QCD phase diagram as a function of the temperature T, the baryon chemical potential μ_B and the isospin chemical potential μ_I.

Various methods have been explored to address the sign problem in QCD lattice simulations at finite baryon density, including lattice simulation with imaginary chemical potential [175], complex Langevin dynamics [176], the Lefschetz thimble method [177] and the density of states approach [178]. Although some of these techniques enable the study of QCD at low baryon densities, they often fall short when dealing with higher densities, and reliability remains a concern. Consequently, a comprehension of QCD properties at moderate and large baryon densities is still lacking.

Given the current impossibility of directly simulating QCD at finite baryon density on the lattice, alternative avenues involve investigating QCD-like theories devoid of the sign problem. Examples include QCD with finite isospin density [80, 179], two-colour QCD with fundamental quarks [140, 180], QCD with an arbitrary number of colours but adjoint quarks, and QCD with the G_2 gauge group [181]. This chapter opens by presenting two-colour QCD with fundamental quarks at finite baryon and isospin density. Here, the pseudo-reality of quark fields ensures a positive fermion determinant for an even number of flavours, eliminating the sign problem.

It is important to stress that two-colour QCD and three-colour QCD exhibit notable disparities. Notably, their chiral symmetry groups differ, suggesting the likelihood of distinct phases and phase transitions. Additionally, in two-colour QCD, baryons behave as bosons, whereas in three-colour QCD, they are fermions. However, despite these distinctions, both theories share many common properties. For this reason, lattice simulations of two-colour QCD provide valuable insights into the properties of dense three-colour QCD. In both theories, confinement and chiral symmetry breaking occur at low temperatures, transitioning to deconfinement and restoration of chiral symmetry at higher temperatures. Moreover, several physical observables, including the meson spectrum [182], exhibit close agreement between the two theories, implying similar characteristic scales.

In addition to measuring various observables, lattice simulations of dense two-colour QCD offer insights into phenomena expected to occur in dense three-colour scenarios. Take, for instance, the condensation of diquarks in dense matter. In both contexts, as densities increase, a Fermi sphere of quarks emerges, which tends to become unstable leading to diquark condensation [183]. However, while this condensate in three-colour QCD lacks colour-singlet properties, in two-colour QCD it does not.

In this chapter, the basic properties of the QCD Lagrangian are first summarised. At the cost of being a little bit pedantic, the stage is set with the introduction of the concept of effective field theories. Then, chiral perturbation theory is discussed as an effective field theory for QCD. The transformation properties of the degrees of freedom in χPT are subsequently examined. The discussion continues with a full review of two-colour QCD at fixed baryon and isospin charge. The latter prepares the table for the three-colour QCD case. Hence, two-flavours and three-flavours QCD at non-zero chemical potentials are discussed, demonstrating how the isospin chemical potential is incorporated into the chiral Lagrangian. Finally, the chapter ends with the corresponding analysis of the phase diagram.

§ 3.2 Review of fundamentals of Quantum Chromodynamics

Let us review the fundamentals of Quantum Chromodynamics [184]. QCD is the non-abelian gauge theory that governs the strong interaction in Nature, with $SU(3)$ acting as the underlying gauge group. This theory includes eight gauge bosons, one corresponding to each generator of the gauge group, commonly referred to as gluons. The matter constituents of QCD consist of colour-carrying spin-$1/2$ fermions known as quarks. There exist six distinct types of quarks distinguished by a quantum property termed flavour. Although these six flavours of quarks possess varying masses, they exhibit similar behaviour to gluon fields. The QCD Lagrangian density, derived from the gauge principle, is formulated as follows [184]

$$
\begin{aligned}
\mathcal{L}_{\text{QCD}} &= \sum_f \bar{\psi}_f \left(i\not{\mathcal{D}} - m_f\right) \psi_f - \frac{1}{4} F^a_{\mu\nu}\, F^{a\ \mu\nu} \\
\not{\mathcal{D}} &\equiv \gamma^\mu \mathcal{D}_\mu \\
\mathcal{D}_\mu &= \partial_\mu + i g \lambda_a A^a_\mu \\
F^a_{\mu\nu} &= \partial_\mu A^a_\nu - \partial_\nu A^a_\mu - g f_{abc}\, A^b_\mu A^c_\nu
\end{aligned}
\tag{3.1}
$$

with λ_a the Gell-Mann matrices, A_a is the a's gluon field whereas g is the QCD coupling constant. For each quark flavour, the quark field consists of a colour triplet (subscripts r, g, and b standing for “red", “green" and “blue", respectively)

$$\psi_f = \begin{pmatrix} \psi_{f,r} \\ \psi_{f,g} \\ \psi_{f,b} \end{pmatrix}.$$

The latter transforms in the fundamental representation **3** of the gauge group, while the antiquarks transform in the antifundamental representation $\overline{\mathbf{3}}$ of the gauge group. Instead, gluons transform in the adjoint representation **8**.

The six quarks are commonly divided into three light flavours up, down, and strange (u, t and s), and three heavy flavours charm, bottom, and top (c, b and t) [184]

$$\begin{pmatrix} m_u = 0.005\text{GeV} \\ m_d = 0.009\text{GeV} \\ m_s = 0.175\text{GeV} \end{pmatrix} \ll 1\text{GeV} < \begin{pmatrix} m_c = (1.15 - 1.35)\text{GeV} \\ m_b = (4.0 - 4.4)\text{GeV} \\ m_t = 174\text{GeV} \end{pmatrix}.$$

In this context, the scale of 1 Gev corresponds to the masses of the lightest hadrons containing light quarks. If the six-quark masses had been identical, the QCD Lagrangian would have exhibited $SU(6)$-flavour symmetry. However, because of the significant mass gap exceeding 1 GeV between the two sets of quarks, an approximate symmetry is anticipated to persist among the three, or more prominently, the two lightest quark flavours.

Due to asymptotic freedom, the coupling constant g is large at low-energy scales, making it impossible to analytically calculate low-energy strong processes using standard perturbative QCD, where g is used as an expansion parameter. Therefore, effective theories or models are necessary to study low-energy strong interaction processes. This chapter is devoted to the study of effective theories to explore the phase diagram of QCD in the high-density regime. Additionally, the discussion will be further developed in chapter 9 where it is introduced another such effective model for baryons: the Skyrme model [185]. The advantage of the Skyrme model, as will be shown, is its ability to describe meson and baryon dynamics in free space, baryonic matter, and medium-modified hadron properties in a unified manner.

3.2.1 The chiral Lagrangian

Many theoretical physicists aspire to find a theory of everything, a framework that unifies fundamental interactions and explains all phenomena through the dynamics of Nature’s basic elements. Yet, even with such a theory, detailed analysis may not fully capture Nature’s complexity across scales. Some theories cover vast energy scales, allowing focus on low-energy dynamics without complete knowledge of higher-energy dynamics. The basic concept stands in identifying parameters that are larger or smaller than the pertinent energy scale, allowing them to approach infinity or zero, as appropriate. Effective field theory serves as a valuable tool in describing low-energy physics through the relevant degrees-of-freedom characteristic of that energy scale.

EFTs can be devised using matching calculations. This process begins at a high-energy scale, where physics is governed by a collection of heavy fields denoted by Φ with a mass M, along with a set of light particle fields ϕ. The Lagrangian is then expressed in the general form:

$$\mathcal{L}(\Phi,\phi)_{\text{heavy}} + \mathcal{L}(\phi) \tag{3.2}$$

where $\mathcal{L}(\phi)$ comprises terms independent of the heavy fields, and $\mathcal{L}(\Phi,\phi)_{\text{heavy}}$ includes the remaining components. As the energy scale Λ becomes greater than M, the evolution of the theory from one energy scale to another is delineated by the renormalisation group. However, once Λ decreases below the scale M, the effective theory transitions to one without heavy fields. This distinguishes effective theories from Wilsonian renormalisation, in which the theory remains unaltered. In the EFT approach, a series of operators constructed using the light fields are manually introduced to formulate the Lagrangian for the new EFT, expressed as

$$\mathcal{L}(\phi) + \delta\mathcal{L}(\phi)\ . \tag{3.3}$$

At scale $\Lambda = M$, alignment between high-energy and low-energy theories sets the new field interaction coefficients, reflecting heavy-field dynamics. Coefficients in $\mathcal{L}(\phi)$ differ due to matching conditions. In the context of low-energy QCD, perturbative matching is not feasible. This scenario is typical for EFTs in which the transition to the new theory occurs through a phase transition induced by spontaneous symmetry breaking. Consequently, the matching procedure cannot be employed to construct a low-energy effective field theory for hadronic QCD.

Nevertheless, predictive low-energy effective field theories can also be constructed for non-perturbative theories. Chiral perturbation theory (χPT) for QCD at low energies began with the idea that spontaneously broken chiral symmetry's Goldstone bosons are suitable degrees of freedom. This idea aligns with what Weinberg termed a "folk theorem":

Folk Theorem

If one formulates the most comprehensive Lagrangian feasible, encompassing all terms consistent with the presumed symmetry principles, and then computes matrix elements using this Lagrangian to any given order of perturbation theory, the outcome will correspond to the most comprehensive possible S-matrix. This S-matrix is consistent with analyticity, perturbative unitarity, cluster decomposition, and the assumed symmetry properties.

In χPT, Weinberg's theorem allows an infinite number of terms leading to many couplings, requiring a system to organise and limit these couplings for practical phenomenology. Transforming Weinberg's theorem into a practical tool for phenomenological purposes necessitates two components:

1. A framework for organising the terms within the effective Lagrangian.

2. A systematic approach to assessing the significance of diagrams arising from the interaction terms of the effective Lagrangian when computing physical processes.

In χPT, the terms in the Lagrangian are structured via a derivative expansion, or equivalently by powers of momentum.

χPT aims to model physics below the confinement scale Λ_{QCD} using a momentum expansion of derivatives. This expansion allows the effective Lagrangian to be handled in a perturbative fashion. Imposing $SU(2)_L \times SU(2)_R$ invariance, the theory in terms of Goldstone bosons is constructed as

$$\begin{aligned}\mathcal{L} &= \mathcal{L}_2 + \mathcal{L}_4 + \mathcal{L}_6 + \mathcal{L}_8 + \ldots \\ &= \frac{1}{4}F_\pi^2 \mathrm{Tr}\{\partial_\mu U \partial^\mu U^\dagger\} + \alpha_4 \mathrm{Tr}^2\{(\partial_\mu U \partial^\mu U^\dagger)\} + \tilde{\alpha}_4 \mathrm{Tr}\{\partial_\mu U \partial_\nu U^\dagger\} \cdot \mathrm{Tr}\{\partial^\mu U \partial^\nu U^\dagger\} + \ldots\ .\end{aligned} \tag{3.4}$$

Due to a dimensional analysis (in mass dimension):

$$\dim(d^4x\, \alpha_n \mathrm{Tr}\{\partial^n\}) = -4 + \dim(\alpha_n) + n = 0 \quad \Rightarrow \quad \dim(\alpha_n) = 4 - n\,.$$

Considering only one expansion parameter in the theory, identified as the cut-off scale $\Lambda = \Lambda_{\text{QCD}}$, then

$$\alpha_n \sim \frac{1}{\Lambda^{n-4}} \sim \Lambda^{4-n}\,. \tag{3.5}$$

Considering theories with a single scale, an organised expansion is made in terms of

$$\frac{\partial^n}{\Lambda^n} \sim \frac{q^n}{\Lambda^n}\,, \tag{3.6}$$

an expansion analogous to a Taylor series in terms of momentum. Lorentz invariance requires that the expansion is made up of even powers of momenta, but, at non-zero baryon or isospin chemical potential, Lorentz symmetry is broken and odd powers in derivatives may appear. The coefficients of the Lagrangian are not generally known and must be determined on a case-by-case phenomenological basis or via lattice first-principles simulations.

§ 3.3 Universal aspects of QCD-like theories

Two-colour QCD ($\mathrm{QC_2D}$) offers the advantage of being more cost-effective to simulate compared to QCD, as it has fewer degrees of freedom of colour. However, despite this simplification, two-colour QCD shares numerous qualitative features with its full-colour counterpart: it exhibits strong coupling, infrared confinement, and asymptotic freedom at high energies. Moreover, two-colour QCD displays a chiral symmetry-breaking pattern similar to QCD. In particular, unlike QCD with adjoint matter, the chiral and deconfinement crossovers coincide at a vanishing chemical potential [186, 187].

However, significant differences persist. For instance, in the pure gauge theory of two-colour QCD, the deconfinement transition is a second-order phase transition, contrasting with the first-order transition in QCD. Perhaps the most notable distinction lies in the resolution of the sign problem. Consequently, two-colour QCD provides an excellent platform for investigating the finite-density phase diagram of QCD-like theories from first principles.

In two-colour QCD, differently from three-colour QCD, baryons (diquarks) appear as pseudo-Goldstone bosons. An implication of this phenomenon is the Bose-Einstein condensation of diquarks at an intermediate chemical potential, similar to the nuclear liquid-gas transition in QCD [188].

Thus, two-colour QCD is an ideal testing ground for effective theories probing the QCD phase diagram. These theories can be thoroughly evaluated by comparing them with first-principle lattice calculations throughout the phase diagram.

3.3.1 Introducing QC_2D: the global symmetry $U(2N_f)$

The low-energy behaviour of quantum field theory is governed by its lightest degrees of freedom. In three-colour QCD, these degrees-of-freedom manifest as Goldstone bosons, which find description through χPT [189–191]. This effective framework is independent of specific models and is rooted in the symmetry properties of the quark action.

However, in three-colour QCD, the description of baryons within χPT becomes problematic, as the mass of the lightest baryon is comparable to the scale of chiral symmetry breaking. This limitation does not apply to two-colour QCD. In $\mathrm{QC_2D}$, owing to the pseudo-reality of quark fields, the chiral group encompasses a larger set of generators compared to the three-colour scenario. This enlarged group includes the generator associated with baryon charge, rendering the lightest baryons as Goldstone bosons. Consequently, it becomes feasible to investigate low-density $\mathrm{QC_2D}$ using a model-independent, symmetry-based effective theory [139, 188]. In the following, there will be a review of this effective theory and its ensuing predictions.

First of all, chapter 2 showed how the fixing of a charge affects the dynamics of a theory breaking the relativistic invariance and how the additional SSB of the "fixed" symmetry can lead the system into a superfluid phase. Let us introduce the proper Lagrangian density with N_f massless Dirac fermions

$$\mathcal{L} = -\frac{1}{4g^2} F^a_{\mu\nu} F^{\mu\nu}_a + \sum_f^{N_f} i\,\bar{\psi}_f \gamma^\mu \mathcal{D}_\mu \psi_f \tag{3.7}$$

where $F^a_{\mu\nu}$ is the gluon field strength, F^a_μ is the gluon field itself, τ^a are the Pauli matrices for the $SU(2)$ (colour) gauge group and a is the gauge algebra index, $a = 1, 2, 3$. The covariant derivative is defined, as customary, as a Lie algebra-valued 1-form built with the gauge field F^a_μ

$$\mathcal{D}_\mu = \partial_\mu - iF^a_\mu \frac{\tau_a}{2} \,. \tag{3.8}$$

Henceforth, the fermion fields transform in the fundamental (vectorial) representation of the gauge group $SU(N)$, which is complex in the general case $N > 2$. It is easy to recognize that, when quarks are massless, the classical global symmetry group of the theory is

$$U(N_f)_L \times U(N_f)_R \sim SU(N_f)_L \times SU(N_f)_R \times U(1)_L \times U(1)_R \,.$$

The $N = 2$ case is an exceptional one since the fundamental representation is pseudo-real, hence the global symmetry group is enlarged to $U(2N_f)$ [180]. To better appreciate this, consider the simple case of a Dirac Lagrangian for a single massless quark $\psi = (\psi_L, \psi_R)$, which is $U(1)_L \times U(1)_R$ invariant

$$\mathcal{L}_D = i\bar{\psi}\gamma^\mu \mathcal{D}_\mu \psi = i\psi_L^\dagger \bar{\sigma}^\mu \mathcal{D}_\mu \psi_L + i\psi_R^\dagger \sigma^\mu \mathcal{D}_\mu \psi_R \,, \tag{3.9}$$

where $\sigma^\mu = (\mathbb{1}, \vec{\sigma})$ and $\bar{\sigma}^\mu = (\mathbb{1}, -\vec{\sigma})$.

It is very easy to prove that the quantity

$$\tilde{\psi} = i\sigma_2 \tau_2 \psi_R^* \,, \tag{3.10}$$

where σ_2 is the Pauli generator of the $SU(2)$ spin group, transforms as a left quark. Renaming $\psi_L \to \psi$ and substituting $\psi_R \to i\tau_2\sigma_2\tilde{\psi}^*$ one obtains

$$\mathcal{L}_D = i\psi^\dagger \bar{\sigma}^\mu \mathcal{D}_\mu \psi + i\tilde{\psi}^T \sigma_2 \tau_2 \sigma^\mu \mathcal{D}_\mu \tau_2 \sigma_2 \tilde{\psi}^* \,.$$

The pseudo-reality of the fundamental representation determines the properties:

$$\tau_a^* = \tau_a^T = -\tau_2 \tau_a \tau_2 \quad \to \quad \mathcal{D}_\mu^T = -\tau_2 \mathcal{D}_\mu \tau_2 \,, \tag{3.11}$$

that, together with the fact that $\sigma_2 \sigma^\mu \sigma_2 = \bar{\sigma}^{\mu T}$, leads to

$$\mathcal{L} = i\psi^\dagger \bar{\sigma}^\mu \mathcal{D}_\mu \psi - i\tilde{\psi}^T \mathcal{D}_\mu^T \bar{\sigma}^{\mu T} \tilde{\psi}^* \,.$$

Doing the transpose ^{T} on the second term, remembering that it makes appear an extra minus sign due to the exchange of fermion fields, the final Lagrangian density reads

$$\mathcal{L} = i\psi^\dagger \bar{\sigma}^\mu \mathcal{D}_\mu \psi + i\tilde{\psi}^\dagger \bar{\sigma}^\mu \mathcal{D}_\mu \tilde{\psi} = iQ^\dagger \bar{\sigma}^\mu \mathcal{D}_\mu Q \,, \tag{3.12}$$

where

$$Q = \begin{pmatrix} \psi \\ \tilde{\psi} \end{pmatrix} = \begin{pmatrix} \psi_L \\ i\sigma_2\tau_2\psi_R^* \end{pmatrix} . \tag{3.13}$$

In this way, as both ψ and $\tilde{\psi}$ transform as left quarks, the starting symmetry $U(1)_L \times U(1)_R$ is thus enlarged to $U(2)$.

One can easily generalise this result to the case of N_f Dirac fermions. Therefore, QC$_2$D with N_f massless Dirac fermion fields has an enhanced classical symmetry group

$$U(2N_f) \sim SU(2N_f) \times U(1)_A$$

where the $U(1)_A$ symmetry is an axial symmetry that will not survive quantum corrections. These are quantum anomalies, and, in particular, this one related to $U(1)_A$ is known as the Adler-Bell-Jackiw anomaly (ABJ anomaly). The enhanced quantum global symmetry group for QC_2D is thus $SU(2N_f)$.

Additionally, the development of a non-zero expectation value of the quark bilinear (the chiral condensate)

$$\bar{\psi}\psi = q_R^\dagger q_L + q_L^\dagger q_R = \frac{1}{2} Q^T \sigma_2 \tau_2 \begin{pmatrix} 0 & 1 \\ -1 & 0 \end{pmatrix} Q + h.c. \tag{3.14}$$

spontaneously breaks $SU(2N_f)$ down to $Sp(2N_f)$, producing $2N_f^2 - N_f - 1$ massless Goldstone bosons.

3.3.2 Charging QC_2D: adding non zero baryon and isospin chemical potentials

The chemical potential appears as a Lagrange multiplier when constraining the dynamics of a system fixing a charge. The baryon and isospin charges generate the symmetry groups $U(1)_B$ and $U(1)_I$ and both are sub-groups of the residual global symmetry group $Sp(2N_f)$, in this case. The generators of $Sp(2N_f)$ can be written in $N_f \times N_f$ blocks as [48, 192]

$$T_k = \begin{pmatrix} A_k & B_k \\ B_k^\dagger & -A_k^T \end{pmatrix} \tag{3.15}$$

where A is hermitian, B is symmetric and $k = 1, ..., 2N_f^2 + N_f = \dim(Sp(2N_f))$. A common choice for these matrices is the following

$$B = \frac{1}{2}\begin{pmatrix} 1 & 0 \\ 0 & -1 \end{pmatrix} \otimes \mathbb{1}_{N_f} \qquad\qquad I = \frac{1}{2}\begin{pmatrix} \sigma^3 & 0 \\ 0 & -\sigma^3 \end{pmatrix} \otimes \mathbb{1}_{N_f}\,. \tag{3.16}$$

Fixing them implies adding terms of the type $-\mu Q$ to the fundamental Lagrangian. The charge densities Q coincide with the temporal components of the usual 4-currents associated with the $U(1)_B$ and a $U(1)_I$ symmetries in a fermion theory. They can be built as quark bilinears

$$\bar{\psi}\gamma_0\psi = \psi_L^\dagger\psi_L + \psi_R^\dagger\psi_R = Q^\dagger \begin{pmatrix} 1 & 0 \\ 0 & -1 \end{pmatrix} Q + h.c. = 2Q^\dagger B Q + h.c. \tag{3.17}$$

$$\bar{\psi}\gamma_0\sigma_3\psi = \psi_L^\dagger\psi_L + \psi_R^\dagger\psi_R = Q^\dagger \begin{pmatrix} \sigma^3 & 0 \\ 0 & -\sigma^3 \end{pmatrix} Q + h.c. = 2Q^\dagger I Q + h.c. \tag{3.18}$$

Adding these terms is actually equivalent to introduce new "gauge" background time-like fields which minimally couple to the covariant derivative $\mathcal{D}_\mu$

$$\mathcal{D}_\mu \;\to\; \mathcal{D}_\mu - i\mu_B B_\mu - i\mu_I I_\mu\,, \quad B_\mu = \delta_\mu^0 B\,, \quad I_\mu = \delta_\mu^0 I\,. \tag{3.19}$$

The introduction of both these chemical potentials explicitly breaks the symmetry $Sp(2N_f)$. Precisely, if $U \in Sp(2N_f)$, asking for the invariance equals to require that

$$2Q^\dagger BQ \to 2Q^\dagger U^\dagger BUQ = 2Q^\dagger BQ \Rightarrow U^\dagger BU = B \to [B, U] = 0\,,$$

$$2Q^\dagger IQ \to 2Q^\dagger U^\dagger IUQ = 2Q^\dagger IQ \Rightarrow U^\dagger IU = I \to [I, U] = 0\,.$$

Therefore, the residual symmetry group is generated by those generators of $Sp(2N_f)$ that commute with B and I.

Furthermore, the introduction of chemical potentials at the Lagrangian level implies newly added terms which, in turn, also affect the configuration of the ground state. Consequently, the latter must minimise the enlarged Hamiltonian. The new configurations for the vacuum can, in principle, spontaneously break the fixed symmetries belonging to the residual symmetry group, leading to superfluid transitions.

Central to this section is to analysis of the vacuum structure and the superfluid transitions occurring when the $U(1)_B$ and $U(1)_I$ symmetries spontaneously break. Creating a phase diagram for the case of a generic number of flavours N_f is complicated. However, it suffices to consider the minimal case $N_f = 2$.

3.3.3 QC_2D phase diagram

The theory will be constructed in a non-linear way using an exponential parameterisation. This approach reveals itself to be very simple even in analysing the vacuum structure.

Building the Lagrangian

The effective chiral Lagrangian describing the Goldstones dynamics resulting from this breaking pattern is the following

$$\mathcal{L}_{\text{eff}} = v^2 \mathrm{Tr}\{\partial_\mu \Sigma \partial^\mu \Sigma^\dagger\} + m_\pi^2 v^2 \mathrm{Tr}\{M\Sigma + M^\dagger \Sigma^\dagger\}\,, \tag{3.20}$$

where $4\pi v$ is the energy scale of the chiral symmetry breaking. Here, the theory is realised through an exponential parameterisation and Σ labels the matrix field. The field Σ transforms in the two-index antisymmetric representation of $SU(2N_f)$

$$\Sigma \to U\Sigma U^T, \qquad U \in SU(2N_f)\,, \tag{3.21}$$

the mass term preserving the transformations $U \in Sp(2N_f) \subset SU(2N_f)$, such that $U^T M U = M$, is given by

$$M = -i\sigma_2 \otimes \mathbb{1}_{N_f} = \begin{pmatrix} 0 & -1 \\ 1 & 0 \end{pmatrix} \otimes \mathbb{1}_{N_f}\,. \tag{3.22}$$

The value of the condensate in the underlying microscopic theory is represented by $v \propto F_\pi$ through the Gell-Mann-Oakes-Renner relations, while m_π is the degenerate masses of the pseudo-Goldstones.

At the effective level, one can charge the theory by adding μ_B and μ_I through a covariant derivative

$$\partial_\mu \Sigma \to \mathcal{D}_\mu \Sigma = \partial_\mu \Sigma - i[(\mu_B B_\mu + \mu_I I_\mu)\Sigma + \Sigma(\mu_B B_\mu + \mu_I I_\mu)^T] \tag{3.23}$$

$$\partial_\mu \Sigma^\dagger \to \mathcal{D}_\mu \Sigma^\dagger = \partial_\mu \Sigma^\dagger + i[\Sigma^\dagger(\mu_B B_\mu + \mu_I I_\mu) + (\mu_B B_\mu + \mu_I I_\mu)^T \Sigma^\dagger] \tag{3.24}$$

where $B_\mu = \delta^0_\mu B$ and $I_\mu = \delta^0_\mu I$. The resulting Lagrangian is thus

$$\begin{aligned}\mathcal{L}_{\text{eff}} = {} & v^2 \mathrm{Tr}\{\partial_\mu \Sigma \partial^\mu \Sigma^\dagger\} + 4iv^2 \mathrm{Tr}\{(\mu_B B + \mu_I I)\Sigma^\dagger \partial_0 \Sigma\} + m_\pi^2 v^2 \mathrm{Tr}\{M\Sigma + M^\dagger \Sigma^\dagger\} \\ & + 2v^2 \mathrm{Tr}\{\Sigma(\mu_B B + \mu_I I)\Sigma^\dagger(\mu_B B + \mu_I I) + (\mu_B B + \mu_I I)^2\}\,. \end{aligned} \tag{3.25}$$

Let Σ_c denote the full vacuum configuration. When setting to zero the chemical potentials, the vacuum is uniquely determined by the chiral condensation phenomenon

$$\Sigma_c = \Sigma_M \tag{3.26}$$

where Σ_M is the chiral condensate. In this case, the spectrum of the theory consists of $2N_f^2 - N_f - 1$ GBs and when $N_f = 2$ corresponds to a degenerate 5-plet: 3 pions $\pi_0, \pi^\pm$ $(B = 0, I = 0, \pm1)$, a baryon and an anti-baryon named diquark and anti-diquark $(B = \pm1, I = 0)$.

The inclusion of a chemical potential results in competition with the chiral condensate (or the mass term) in determining the vacuum configuration. This contribution can be thought of as the introduction of a new direction along which the vacuum can "rotate". In the scenario where $\mu_B \neq 0$ and $\mu_I = 0$, this compelling behaviour can be described as a rotation defined in terms of a tilt angle φ as

$$\Sigma_c = \Sigma_M \cos\varphi + i\Sigma_B \sin\varphi \tag{3.27}$$

where Σ_B is the quantity which independently minimises the corresponding term in the Lagrangian [193]. Adding a second chemical potential means introducing another rotation described in terms of a second tilt angle η. Thus, when $\mu_B \neq 0$ and $\mu_I \neq 0$, the vacuum ansatz becomes

$$\Sigma_c = \Sigma_M \cos\varphi + i(\Sigma_B \cos\eta + \Sigma_I \sin\eta)\sin\varphi\,. \tag{3.28}$$

This will be taken as the ansatz for the ground state configuration; the tilt angles will be determined via the EOMs.

It is interesting to notice that (2.38) suggests another way to introduce a generic chemical potential μ. The ansatz for the vacuum can be modified by introducing a "time-dependence" as

$$\Sigma_c(t) = e^{i\tilde{\mathscr{M}}t}\Sigma_c(0) \quad \leftrightarrow \quad \partial_\nu \to \partial_\nu + i\mu\,\delta^0_\nu \mathscr{M} \tag{3.29}$$

where $\tilde{\mathscr{M}} = \mu\mathscr{M}$, with $\mathscr{M}$ being the generator of the fixed symmetry $U(1)_{\mathscr{M}}$. It is very easy to prove that this dependence only affects the explicit breaking pattern

$$Sp(2N_f) \to C(\mathscr{M})$$

where $C(\mathscr{M})$ is the sub-group generated by all those generators of $Sp(2N_f)$ which commute with $\mathscr{M}$. The spontaneous breaking pattern remains determined by the alignment of Σ_c.

As the mechanism of chiral condensation is related to the term Σ_M, the other two mechanisms of condensation are related to the additional terms Σ_B and Σ_I, which spontaneously break the symmetries $U(1)_B$ and $U(1)_I$, causing the system to live in a superfluid phase. The condensates inducing these transitions can be calculated by introducing a diquark and pion sources j_B and j_I. Being $\mathcal{L}_{\text{eff}}(\Sigma_c)$ the effective phenomenological Lagrangian describing the GBs dynamics one has

$$\langle\bar{\psi}\psi\rangle = -\frac{\partial\mathcal{L}_{\text{eff}}(\Sigma_c)}{\partial m_q} = 4G\cos\varphi \quad \text{Chiral Condensate} \tag{3.30}$$

$$\langle\psi\psi\rangle = -\frac{\partial\mathcal{L}_{\text{eff}}(\Sigma_c)}{\partial j_B} = 4G\sin\varphi\cos\eta \quad \text{Diquark Condensate} \tag{3.31}$$

$$\langle\pi\rangle = -\frac{\partial\mathcal{L}_{\text{eff}}(\Sigma_c)}{\partial j_I} = 4G\sin\varphi\sin\eta \quad \text{Pion Condensate} \tag{3.32}$$

$$n_B = -\frac{\partial\mathcal{L}_{\text{eff}}(\Sigma_c)}{\partial\mu_B} = 2F_\pi^2\mu_B(1+\cos(2\eta))\sin^2\varphi \quad \text{Baryon Number Density} \tag{3.33}$$

$$n_I = -\frac{\partial\mathcal{L}_{\text{eff}}(\Sigma_c)}{\partial\mu_I} = 2F_\pi^2\mu_I(1-\cos(2\eta))\sin^2\varphi \quad \text{Isospin Number Density} \tag{3.34}$$

where F_π is the scale of spontaneous symmetry breaking that determines the pions' mass, while G is the chiral condensate in the chiral limit which can be traded for the vacuum pion mass using the Gell-Mann-Oakes-Renner relation:

$$m_\pi^2 = 2mG\,, \quad G = \frac{\langle\bar{\psi}\psi\rangle_0}{N_f F_\pi^2}\,. \tag{3.35}$$

The angle η is constrained to have a value $\eta = 0$ or $\eta = \pi/2$, which leads the system exclusively into a baryon or an isospin superfluid phase. The positivity requirement for the quantity $\sin\varphi$ will constrain the values of μ_B and μ_I for the formation of the corresponding condensates.

As a last notable digression, let us spend a few words on the phase diagram, referring to [193]. The resulting $\mu_B - \mu_I$ phase diagram for QC_2D with $N_f = 2$ quarks is represented in Figure 1 in [193]. On the horizontal axis, $\mu_I = 0$, there is a phase transition corresponding to the diquark (baryon) condensation for values of μ_B greater than m_π. Similarly, at $\mu_B = 0$, there is a transition corresponding to the condensation of pions if $\mu_I > m_\pi$. This can also be concluded from the fact that there is a simple discrete symmetry in the microscopic theory when, at the same time, $d \leftrightarrow \tilde{d}$ and $\mu_B \leftrightarrow \mu_I$. This is the reason why the phase diagram is symmetric under the reflection around the $\mu_B = \mu_I$ line. The two different diquark and pion condensations compete on this line and thus the transition along the line itself is of first order. When both chemical potentials are below the critical threshold established by m_π, neither the baryon nor the isospin condensate is non-zero, and the chiral condensate determines alone the vacuum alignment. The system is in the normal phase.

As a function of μ_B the mass of the pion is constant as long as $\mu_B < m_\pi$, for which the transition occurring at $\mu_I = m_\pi$ happens at all values of μ_B. This justifies the horizontal line on which the pions condense. Due to the discrete symmetry of the whole diagram, this automatically also justifies the vertical line $\mu_B = m_\pi$ on which the diquarks condense.

3.3.4 **Equations of motion and Ground State Energy**

Vacuum determination in this charged theory considers the already mentioned competitive behaviour of mass and both baryon and isospin chemical potentials. The starting point is the following ansatz:

$$\Sigma_c = \Sigma_M\cos\varphi + i(\Sigma_B\cos\eta + \Sigma_I\sin\eta)\sin\varphi \tag{3.36}$$

representing the "superposition" matrix which takes into account the two contributions led by the mass and the chemical potentials' sectors. When the chemical potentials are set to zero, the vacuum aligns with the chiral condensate Σ_M. When they are turned on, the vacuum is considered as the result of two different rotations associated with two tilt angles φ and η, which in turn are determined by the EOMs. In the following expressions, there are the quantities that independently minimise the corresponding terms in the Lagrangian:

$$\Sigma_M = \begin{pmatrix} 0 & 1 \\ -1 & 0 \end{pmatrix} \otimes \mathbb{1}_{N_f} = -M \tag{3.37}$$

$$\Sigma_B = \begin{pmatrix} J & 0 \\ 0 & J \end{pmatrix} \otimes \mathbb{1}_{N_f}, \qquad J = -i\sigma^2 = \begin{pmatrix} 0 & -1 \\ 1 & 0 \end{pmatrix} \tag{3.38}$$

$$\Sigma_I = \begin{pmatrix} 0 & \sigma^1 \\ -\sigma^1 & 0 \end{pmatrix} \otimes \mathbb{1}_{N_f}. \tag{3.39}$$

To determine the ground state energy density (GSE), the Lagrangian (3.25) is evaluated on this ansatz obtaining

$$\mathcal{L}[\Sigma_0] = 4N_f v^2 m_\pi^2 \cos\varphi + N_f v^2(\mu_B^2 + \mu_I^2)\sin^2\varphi + N_f v^2(\mu_B^2 - \mu_I^2)\cos(2\eta)\sin^2\varphi\ . \tag{3.40}$$

Using the full expression $\mathcal{L}[\Sigma_0]$ the EOMs read

$$\begin{aligned} \varphi:&\quad \sin\varphi(2m_\pi^2 - (\mu_B^2 + \mu_I^2)\cos\varphi - (\mu_B^2 - \mu_I^2)\cos(2\eta)\cos\varphi) = 0 \\ \eta:&\quad 2(\mu_B^2 - \mu_I^2)\sin^2\varphi\sin(2\eta) = 0 = -\frac{\partial\mathcal{L}[\Sigma_0]}{\partial\eta}\ . \end{aligned} \tag{3.41}$$

From the former one obtains

$$\cos\varphi = \frac{2m_\pi^2}{(\mu_B^2 + \mu_I^2) + (\mu_B^2 - \mu_I^2)\cos(2\eta)} \tag{3.42}$$

while from the latter

$$2\eta = k\pi \quad\rightarrow\quad \eta = k\frac{\pi}{2}\ . \tag{3.43}$$

If $2\eta \in [0,\pi]$, for which $2\eta \in [\pi, 2\pi]$ are the corresponding negative rotations, one can just take $\eta \in [0,\pi/2]$. The values that extremize $\mathcal{L}$, being zeros of its first derivative, are $\eta = 0$ and $\eta = \frac{\pi}{2}$, associated to $k = 0$ and $k = 1$.

To find the vacuum energy density $\mathcal{E} = -\mathcal{L}[\Sigma_0]$ one needs to consider the two cases that maximise $\mathcal{L}$, minimising $\mathcal{E}$:

1. $$\eta = 0 \quad \text{when} \quad \mu_B > \mu_I \quad\rightarrow\quad \Sigma_c = \Sigma_M\cos\varphi + i\Sigma_B\sin\varphi \tag{3.44}$$

   which forces the system to be in a superfluid baryon phase.

2. $$\eta = \frac{\pi}{2} \quad \text{when} \quad \mu_I > \mu_B \quad\rightarrow\quad \Sigma_c = \Sigma_M\cos\varphi + i\Sigma_I\sin\varphi \tag{3.45}$$

   is the "specular" case named superfluid isospin phase.

In these two cases, $\cos\varphi$ can assume the following two values

$$\cos\varphi\Big|_{\eta=0} = \frac{m_\pi^2}{\mu_B^2} \qquad\qquad \cos\varphi\Big|_{\eta=\frac{\pi}{2}} = \frac{m_\pi^2}{\mu_I^2}\,, \tag{3.46}$$

substituting in $\mathcal{L}[\Sigma_0]$ yields the GSEs below

$$\mathcal{E} = -N_f\nu^2\Big[2\,\frac{m_\pi^4+\mu_B^4}{\mu_B^2}\Big] \quad \text{Superfluid Baryon Phase}\,, \tag{3.47}$$

$$\mathcal{E} = -N_f\nu^2\Big[2\,\frac{m_\pi^4+\mu_I^4}{\mu_I^2}\Big] \quad \text{Superfluid Isospin Phase.} \tag{3.48}$$

A superfluid transition occurs when the corresponding chemical potential is greater than a critical value, which here is m_π. When the chemical potentials are below the critical value the vacuum alignment is determined uniquely by the mass term:

$$\varphi = 0 \quad \text{when} \quad \mu_B, \mu_I < m_\pi \quad \rightarrow \quad \Sigma_c = \Sigma_M \tag{3.49}$$

and the system is in the normal phase. To recap:

$$\mathcal{E} = -\frac{2\nu^2N_f}{\mu_B^2}(m_\pi^4+\mu_B^4) \quad \text{Superfluid Baryon Phase,} \tag{3.50}$$

$$\mathcal{E} = -\frac{2\nu^2N_f}{\mu_I^2}(m_\pi^4+\mu_I^4) \quad \text{Superfluid Isospin Phase,} \tag{3.51}$$

$$\mathcal{E} = -4\nu^2N_f m_\pi^2 \quad \text{Normal Phase.} \tag{3.52}$$

3.3.5 Symmetry-Breaking Pattern

Let us recall that, in addition to gauge symmetry, the theory at zero chemical potentials is characterised by a precise global symmetry group, spontaneously broken by the chiral condensate. Subsequently, with the fixing of the charges at the Lagrangian level, this residual symmetry is explicitly broken, and then this symmetry is again spontaneously broken by the formation of diquark or pion condensates. In this section, the complete symmetry-breaking pattern in all the possible cases is obtained by varying those parameters characterising the dynamics: the quark mass m and the two chemical potentials μ_B and μ_I.

The unbroken sub-group is determined by finding those matrices of the broken symmetry group. These matrices are left invariant by the explicit terms introduced at the Lagrangian level, or by the vacuum in cases of spontaneous symmetry breaking.

- $m = 0,\ \mu_B = \mu_I = 0$

The theory is classically invariant under the enhanced global symmetry group $U(2N_f)$, broken at the quantum level by the ABJ anomaly to $SU(2N_f)$. The quark condensate is responsible for the spontaneous chiral symmetry breaking, which breaks the global symmetry to $Sp(2N_f)$. This is easily confirmed by imposing that

$$U\Sigma_M U^T = \Sigma_M, \quad U \in SU(2N_f) \Leftrightarrow T_i\Sigma_M = -\Sigma_M T_i^T, \quad T_i \in \mathfrak{su}(2N_f)$$

and remembering that the symplectic residual symmetry is implied by the symplectic structure of Σ_M. Therefore, the symmetry-breaking pattern is

$$SU(2N_f) \rightsquigarrow Sp(2N_f)$$

where $\rightsquigarrow$ stems for spontaneous breaking. The low-energy spectrum consists of $\dim(SU(2N_f)) - \dim(Sp(2N_f)) = 2N_f^2 - N_f - 1$ massless Goldstone bosons transforming under the antisymmetric representation of $Sp(2N_f)$.

- $m \neq 0,\ \mu_B = \mu_I = 0$

The presence of the mass term $M = -\Sigma_M$ at the Lagrangian level explicitly breaks the global symmetry to the same residual symplectic sub-group:

$$SU(2N_f) \longrightarrow Sp(2N_f)$$

In this case the same $2N_f^2 - N_f - 1$ d.o.f. acquire a mass.

- $m = 0,\ \mu_B \neq 0,\ \mu_I = 0$

The introduction of the baryon chemical potential at the Lagrangian fundamental level implies adding the following term

$$\mathcal{L}_B = 2\mu_B Q^\dagger B Q = \mu_B Q^\dagger \begin{pmatrix} 1 & 0 \\ 0 & -1 \end{pmatrix} Q\,. \tag{3.53}$$

Therefore

$$Q \longrightarrow UQ, \quad Q^\dagger \longrightarrow Q^\dagger U^\dagger, \quad U \in Sp(2N_f) \tag{3.54}$$

dictates the condition for the invariance

$$U^\dagger \begin{pmatrix} 1 & 0 \\ 0 & -1 \end{pmatrix} U = \begin{pmatrix} 1 & 0 \\ 0 & -1 \end{pmatrix} \quad \Leftrightarrow \quad [U, B] = 0\,, \tag{3.55}$$

which, in turn, determines the explicit symmetry breaking in $SU(N_f)_L \times SU(N_f)_R \times U(1)_B$, easily individuated because of the block decomposition of B. μ_B contributes to determining the vacuum of the theory: when its value is greater than m_π a diquark condensate is formed, spontaneously breaking the symmetry. Being Σ_B the vacuum configuration that minimises the $\mathcal{L}_B$ at the effective level, the complete vacuum is given by

$$\Sigma_c = \Sigma_M \cos\varphi + i\Sigma_B \sin\varphi, \quad \Sigma_B = \begin{pmatrix} J & 0 \\ 0 & J \end{pmatrix}, \tag{3.56}$$

where J is a symplectic matrix. Hence, the condition

$$U\Sigma_B U^T = \Sigma_B, \quad U \in SU(N_f)_L \times SU(N_f)_R \times U(1)_B \tag{3.57}$$

implies that the vacuum preserves the sub-group $Sp(N_f)_L \times Sp(N_f)_R$. It is easy to verify that the same condition, seen from the generators' point of view

$$T_i \Sigma_B = -\Sigma_B T_i^T, \quad T_i \in \mathfrak{su}(N_f)_L \times \mathfrak{su}(N_f)_R \times \mathfrak{u}(1)_B$$

is not verified by the generator B of $U(1)_B$, for which this symmetry is spontaneously broken (superfluid baryon transition). Collecting these results, the symmetry-breaking pattern is

$$SU(2N_f) \rightsquigarrow Sp(2N_f) \to SU(N_f)_L \times SU(N_f)_R \times U(1)_B \rightsquigarrow Sp(N_f)_L \times Sp(N_f)_R.$$

The final spectrum is made up of $N_f^2 - N_f - 1$ massless Goldstone bosons, and N_f^2 modes with mass proportional to μ_B. The sum of all these corresponds to the total number of $2N_f^2 - N_f - 1$ d.o.f.

- $m \neq 0,\ \mu_B \neq 0,\ \mu_I = 0$

The presence of an explicit mass term breaks the chiral symmetry group into its diagonal (vectorial) sub-group. Considering the usual Dirac mass term

$$m(\psi_L^\dagger \psi_R + \psi_R^\dagger \psi_L) \tag{3.58}$$

if the fields transform under the chiral group $SU(N_f)_L \times SU(N_f)_R$ as

$$\begin{aligned} \psi_L &\to g_L \psi_L, \quad g_L \in SU(N_f)_L \\ \psi_R &\to g_R \psi_R, \quad g_R \in SU(N_f)_R \end{aligned} \tag{3.59}$$

the mass term is invariant if $g_L^\dagger g_R = 1$, so if $g_L = g_R = g_V$, say left and right quarks transform in the same way under a vectorial sub-group $SU(N_f)_V$.

Considering both contributions of the mass and baryon chemical potential will result in a final symmetry sub-group $Sp(N_f)_V$, as summarised in Figure 3.2.

$$\begin{tikzcd} SU(2N_f) \arrow[r, "m\,\neq 0"'] & Sp(2N_f) \arrow[r, "\mu_B\,\neq 0"'] & SU(N_f)_L \times SU(N_f)_R \times U(1)_B \arrow[r, rightsquigarrow] \arrow[d, "m \neq 0"'] & Sp(N_f)_L \times Sp(N_f)_R \arrow[d, "m \neq 0"'] \\ & & SU(N_f)_V \times U(1)_B \arrow[r, rightsquigarrow, "\Sigma_B"] & Sp(N_f)_V \end{tikzcd}$$

Figure 3.2.: Symmetry-breaking pattern in the baryon case.

The last spontaneous branch of the diagram will be of great relevance when investigating the conformal window (see chapter 5) in chapter 6: the superfluid (baryon) transition creates $\frac{N_f^2 - N_f}{2}$ true massless Goldstone bosons transforming according to the antisymmetric representation of $Sp(N_f)_V$ plus a singlet. The remaining d.o.f. acquire mass due to both μ_B and m. It is important to underline that this naive counting of Goldstone bosons is correct since one is dealing with type I GBs only, since the dimension of their representation corresponds to the number of broken generators.

- $m = 0,\ \mu_B = 0,\ \mu_I \neq 0$

As in the baryon case, adding the isospin means adding a term at the Lagrangian level:

$$\mathcal{L}_I = 2\mu_I Q^\dagger I Q = \mu_I Q^\dagger \begin{pmatrix} \sigma^3 & 0 \\ 0 & -\sigma^3 \end{pmatrix} Q, \tag{3.60}$$

and the condition of invariance corresponds to

$$U^\dagger \begin{pmatrix} \sigma^3 & 0 \\ 0 & -\sigma^3 \end{pmatrix} U = \begin{pmatrix} \sigma^3 & 0 \\ 0 & -\sigma^3 \end{pmatrix} \quad \Leftrightarrow \quad [U, I] = 0\,. \tag{3.61}$$

The above can equivalently be written as follows

$$U^\dagger \begin{pmatrix} B & 0 \\ 0 & -B \end{pmatrix} U = \begin{pmatrix} B & 0 \\ 0 & -B \end{pmatrix} \tag{3.62}$$

and the outcome leads to the same symmetry pattern of the baryon case but with "halved" groups:

$$SU(2N_f) \rightsquigarrow Sp(2N_f) \to SU\Big(\frac{N_f}{2}\Big)_u \times SU\Big(\frac{N_f}{2}\Big)_d \times SU\Big(\frac{N_f}{2}\Big)_{\tilde{u}} \times SU\Big(\frac{N_f}{2}\Big)_{\tilde{d}} \times U(1)_I\ .$$

The $U(1)_I$ symmetry also verifies the condition of invariance. As μ_B introduces an asymmetry between left and right quarks, μ_I also introduces an unbalance between the u and d quarks. However, expanding σ^3 in the expression of I it is possible to realise that the rotations between the components $u = u_L$ and $\tilde{d} = d_R$, and between $d = d_L$ and $\tilde{u} = u_R$, are preserved. Hence, the residual invariant sub-group is isomorphic to $SU(N_f)_{u\tilde{d}} \times SU(N_f)_{d\tilde{u}} \times U(1)_I$.

Again, a spontaneous symmetry breaking by the vacuum is expected: the proper configuration is given by

$$\Sigma_c = \Sigma_M \cos\varphi + i\Sigma_I \sin\varphi \tag{3.63}$$

where the structure of Σ_I influences the invariant sub-group through the condition

$$U\Sigma_I U^T = \Sigma_I\,, \quad U \in SU(N_f)_{u\tilde{d}} \times SU(N_f)_{d\tilde{u}} \times U(1)_I\,, \tag{3.64}$$

explicitly

$$U \begin{pmatrix} 0 & \sigma^1 \\ -\sigma^1 & 0 \end{pmatrix} U^T = \begin{pmatrix} 0 & \sigma^1 \\ -\sigma^1 & 0 \end{pmatrix}. \tag{3.65}$$

Since this group acts separately on the two just mentioned couples of quarks, the elements in the previous condition can be rearranged to write

$$U_{u\tilde{d}} \begin{pmatrix} 0 & 1 \\ -1 & 0 \end{pmatrix} U^T_{u\tilde{d}} = \begin{pmatrix} 0 & 1 \\ -1 & 0 \end{pmatrix} \tag{3.66}$$

and

$$U_{d\tilde{u}} \begin{pmatrix} 0 & 1 \\ -1 & 0 \end{pmatrix} U^T_{d\tilde{u}} = \begin{pmatrix} 0 & 1 \\ -1 & 0 \end{pmatrix}. \tag{3.67}$$

From the symplectic structure of matrices, one deduces that the residual group symmetry is $Sp(N_f)_{u\tilde{d}} \times Sp(N_f)_{d\tilde{u}}$. Moreover, as expected, the symmetry $U(1)_I$ is spontaneously broken by the formation of the pion condensate, leading the system to the superfluid (isospin) phase. The pattern is the following

$$SU(2N_f) \rightsquigarrow Sp(2N_f) \to SU(N_f)_{u\tilde{d}} \times SU(N_f)_{d\tilde{u}} \times U(1)_I \rightsquigarrow Sp(N_f)_{u\tilde{d}} \times Sp(N_f)_{d\tilde{u}} \ .$$

- $m \neq 0, \mu_B = 0, \mu_I \neq 0$

As in the previous case, an explicit mass term breaks the chiral symmetry in a vectorial symmetry. For this reason, it is easy to understand that, the invariant sub-group found in this isospin case, $SU(\frac{N_f}{2})_u \times SU(\frac{N_f}{2})_d \times SU(\frac{N_f}{2})_{\tilde{u}} \times SU(\frac{N_f}{2})_{\tilde{d}} \times U(1)_I$, is explicitly broken in $SU(\frac{N_f}{2})_{uV} \times SU(\frac{N_f}{2})_{dV} \times U(1)_I$.

The vacuum then breaks this group to the corresponding symplectic without the $U(1)_I$: $Sp(\frac{N_f}{2})_{uV} \times Sp(\frac{N_f}{2})_{dV}$. Since there is still the possibility to simultaneously rotate u and $\tilde{d}$ and d and $\tilde{u}$, this sub-group is promoted to the enlarged symmetry $Sp(N_f)_{udV}$. In addition, the same result can be obtained repeating the same reasoning starting from the group $SU(N_f)_{u\tilde{d}} \times SU(N_f)_{d\tilde{u}} \times U(1)_I$ and arriving at the group $SU(N_f)_{udV}$ before the superfluid transition is triggered.

Due to this consideration, the massless Goldstone bosons' counting yields the same number obtained in the baryon case: $\frac{N_f^2 - N_f}{2}$.

The symmetry-breaking pattern for the isospin case is shown in Figure 3.3:

$$\begin{tikzcd}
SU(2N_f) \arrow[r, "m \neq 0"'] & Sp(2N_f) \arrow[r, "\mu_I \neq 0"'] & SU(N_f)_{u\bar{d}} \times SU(N_f)_{d\bar{u}} \times U(1)_I \arrow[dl, "m \neq 0"] \arrow[dr, rightsquigarrow, "\Sigma_I"] & \\
& SU(N_f)_{ud\ V} \times U(1)_I \arrow[dr, rightsquigarrow] & & Sp(N_f)_{u\bar{d}} \times Sp(N_f)_{d\bar{u}} \arrow[dl, "m \neq 0"] \\
& & Sp(N_f)_{ud\ V} &
\end{tikzcd}$$

Figure 3.3.: Symmetry-breaking pattern in the isospin case.

- $m \neq 0,\ \mu_B \neq 0,\ \mu_I \neq 0$

There are both chemical potentials and the vacuum (and consequently the pattern) depends on the internal hierarchy between them: if $\mu_B > \mu_I$ there is a superfluid baryon phase transition while if $\mu_B < \mu_I$ there is a superfluid isospin phase transition.

Therefore, by collecting all the considerations and all the partial schemes of the previous cases, one can build the following:

$$
\begin{tikzcd}
SU(2N_f) \arrow[r, "m\neq 0"'] & Sp(2N_f) \arrow[r, "\mu_B \neq 0"'] \arrow[dd, "\mu_I \neq 0"'] & SU(N_f)_L \times SU(N_f)_R \times U(1)_B \arrow[r, squiggly] \arrow[d, "m \neq 0"'] & Sp(N_f)_L \times Sp(N_f)_R \times U(1)_I \arrow[d, "m \neq 0"'] \\
 & & SU(N_f)_V \times\ U(1)_B \times U(1)_I \arrow[r, squiggly, "\Sigma_B"] & Sp(N_f)_{ud\ V} \times U(1)_I \\
 & SU(N_f)_{u\overline{d}} \times SU(N_f)_{d\overline{u}} \times U(1)_B \times U(1)_I \arrow[dl, "m\neq 0"'] \arrow[dr, squiggly, "\Sigma_I"] & & \\
SU(N_f)_{ud\ V} \times U(1)_B \times\ U(1)_I \arrow[dr, squiggly] & & Sp(N_f)_{u\overline{d}} \times\ Sp(N_f)_{d\overline{u}} \times U(1)_B \arrow[dl, "m\neq 0"'] & \\
 & Sp(N_f)_{ud\ V} \times U(1)_B & &
\end{tikzcd}
$$

Figure 3.4.: The full symmetry-breaking pattern.

Here the subscript udV is equivalent to V, while the L/R could be also written as $L = ud$ and $R = \tilde{u}\tilde{d}$.

According to this scheme, it is clear that the simultaneous presence of both chemical potentials necessarily leads to the group $SU(N_f)_{udV} \times U(1)_B \times U(1)_I$. As a consequence, the internal hierarchy between μ_B and μ_I establishes what kind of superfluid transition occurs. Due to this observation, the number of true Goldstones is $\frac{N_f^2 - N_f}{2}$.

It is evident, especially from Figure 3.4, that between the baryon and isospin cases, there is a sort of "*duality*". If in the former case, quarks are coupled according to helicity, in the latter they are coupled if being different both in helicity and flavour.

3.3.6 **Dispersion Relations**

The mechanism of SSB implies the appearance of a non-zero vacuum expectation value. When studying the underlying theory in this spontaneously broken phase, the true field operators associated with the creation and annihilation of real particles are the fluctuations to that *vev*: $\psi = \langle\psi\rangle + \tilde{\psi}$. The effective theory for the Goldstone modes can be written in terms of the fluctuations of the vacuum configuration. As counted in the previous paragraph, the chiral condensate caused $2N_f^2 - N_f - 1$ Goldstone bosons to appear. However, many of these acquire a mass because of the explicit symmetry breakings due to the non-zero quark masses and chemical potentials [180]. Only $\frac{N_f^2 - N_f}{2}$ are true massless Goldstone bosons and they correspond to those appearing in a superfluid transition.

In this section, attention is shifted to the determination of the dispersion relations for all massive and massless d.o.f. in the special case of 2 flavours. When approaching the conformal window (see chapter 5) in chapter 6 the focus will be only on the true massless ones.

The $2N_f^2 - N_f - 1$ Goldstone bosons, appearing in the chiral symmetry breaking, can be collected in the matrix Σ which represents the fluctuations with respect to the chiral condensate Σ_M:

$$\Sigma = U\Sigma_M U^T \,. \tag{3.68}$$

Σ is a $2N_f \times 2N_f$ antisymmetric matrix with $\det\Sigma = 1$, for which it has exactly $2N_f^2 - N_f - 1$ independent components. The Goldstone manifold is given by the coset $SU(2N_f)/Sp(2N_f)$, whose generators are denoted as X_a, with $a = 1, \ldots, 2N_f^2 - N_f - 1$. According to the latter statement, the parameterisation reads

$$U = e^{i\Pi} \,, \quad \Pi = \pi_a \frac{X_a}{\sqrt{2N_f}} \,, \tag{3.69}$$

the fields π_a correspond to the Goldstone modes, while the quantity $\sqrt{2N_f}$ is a normalisation factor.

The $(2N_f)^2 - 1$ generators of $SU(2N_f)$ can be divided into two groups indicated by T_k and X_a [194]. The T_k generators leave Σ_M invariant

$$e^{i\phi_k T_k}\Sigma_M e^{(i\phi_k T_k)^T} = \Sigma_M \quad \to \quad T_k\Sigma_M = -\Sigma_M T_k^T \,, \tag{3.70}$$

and they correspond to the generators of $Sp(2N_f)$.

The remaining generators X_a form the coset $SU(2N_f)/Sp(2N_f)$ and they satisfy:

$$X_a\Sigma_M = \Sigma_M X_a^T \quad \to \quad \Sigma = U\Sigma_M U^T = U^2\Sigma_M \,. \tag{3.71}$$

It is worth observing that these defining relations are left unaltered if one performs a simultaneous rotation $V \in SU(2N_f)$ of both Σ_M and the generators X_a as

$$\Sigma_M \to V\Sigma_M V^T \,, \qquad\qquad X_a \to VX_aV^\dagger \,. \tag{3.72}$$

This partition in T_k and X_a depends on the matrix around which fluctuations are studied: if Σ_M is changed, also X_a needs to be changed [180].

The generators of $SU(2N_f)$ can be written in $N_f \times N_f$ blocks as [194]

$$T_k = \begin{pmatrix} A_k & B_k \\ B_k^\dagger & -A_k^T \end{pmatrix} \qquad\qquad X_a = \begin{pmatrix} C_a & D_a \\ D_a^\dagger & C_a^T \end{pmatrix} \tag{3.73}$$

where A is hermitian, B is symmetric, C is hermitian and traceless, D is antisymmetric. To be precise, $a = 1, ..., 2N_f^2 - N_f - 1 = \dim(SU(2N_f)/Sp(2N_f))$ and $k = 1, ..., 2N_f^2 + N_f = \dim(Sp(2N_f))$.

Consequently, this block decomposition can be applied to the fluctuations too leading to

$$\Pi = \begin{pmatrix} P & Q \\ Q^\dagger & P^T \end{pmatrix} \,. \tag{3.74}$$

According to the properties of the matrices C and D, the number of independent components of each block is given by

$$N_P = N_f^2 - 1 \qquad\qquad N_Q = N_f(N_f - 1) \,. \tag{3.75}$$

To determine the dispersion relations for the π_a fields, the effective Lagrangian is expanded up to the second order in the fluctuations Π. Doing this for arbitrary N_f determines a complicated phase diagram. However, the simplest case $N_f = 2$ is enough to capture the physical essence of the problem.

So, let us proceed in this direction. To build the Π matrix, an explicit realisation of the $SU(4)$ algebra is required to have a corresponding realisation for the broken generators X_a. This can be found in the appendix of [195] and shown below. The 10 T_k generators of $Sp(4)$ are divided into two subsets:

$$T_i = \begin{pmatrix} A_i & 0 \\ 0 & -A_i^T \end{pmatrix} \qquad\qquad T_j = \begin{pmatrix} 0 & B_j \\ B_j^\dagger & 0 \end{pmatrix}, \tag{3.76}$$

the $A_i = \tau_i$ with $i = 1, 2, 3$ are the Pauli matrices, $A_4 = \tau_4 = \mathbb{1}$ while the indices $j = 5, ..., 10$ refer to $B_5 = \mathbb{1}$, $B_6 = i\mathbb{1}$, $B_7 = \tau_3$, $B_8 = i\tau_3$, $B_9 = \tau_1$ and $B_{10} = i\tau_1$.
The 5 generators of the coset $SU(4)/Sp(4)$ are instead:

$$X_i = \begin{pmatrix} C_i & 0 \\ 0 & C_i^T \end{pmatrix} \qquad\qquad X_j = \begin{pmatrix} 0 & D_j \\ D_j^\dagger & 0 \end{pmatrix} \tag{3.77}$$

where $C_i = \tau_i$ with $i = 1, 2, 3$ give the Pauli matrices again while $j = 4, 5$ gives $D_4 = \tau_2$ and $D_5 = i\sigma_2$.

From this explicit realisation of the broken generators X_a the Goldstone matrix can be built as

$$\Pi = \sum_a \pi_a \frac{X_a}{\sqrt{2N_f}} = \begin{pmatrix} \pi_3 & \pi_1 - i\pi_2 & 0 & \pi_5 - i\pi_4 \\ \pi_1 + i\pi_2 & -\pi_3 & -\pi_5 + i\pi_4 & 0 \\ 0 & -\pi_5 - i\pi_4 & \pi_3 & \pi_1 + i\pi_2 \\ \pi_5 + i\pi_4 & 0 & \pi_1 - i\pi_2 & -\pi_3 \end{pmatrix},$$

where the P block contains 3 independent components while the Q one contains the remaining 2, as expected. These combinations of fields can be renamed to match the corresponding 5-plet of particles that characterise the spectrum of the theory in the case $N_f = 2$:

- $\pi_3 \to \pi_0$ is the neutral pion
- $\pi_1 + i\pi_2 \to \pi^+$ is the positive charged pion
- $\pi_1 - i\pi_2 \to \pi^-$ is the negative charged pion
- $\pi_5 - i\pi_4 \to q$ is the diquark
- $\pi_5 + i\pi_4 \to q^*$ is the anti-diquark

As a consequence:

$$\Pi = \sum_a \pi_a \frac{X_a}{\sqrt{2N_f}} = \begin{pmatrix} \pi_0 & \pi^- & 0 & q \\ \pi^+ & -\pi_0 & -q & 0 \\ 0 & -q^* & \pi_0 & \pi^+ \\ q^* & 0 & \pi^- & -\pi_0 \end{pmatrix}. \tag{3.78}$$

This matrix allows for determining the dispersion relations and the phase diagram.

Normal Phase

In this situation, both chemical potentials are below the critical threshold established by m_π, for which the vacuum is aligned with the chiral condensate. Expanding the fluctuations to the second order leads to

$$\Sigma = U\Sigma_M U^T = U^2\Sigma_M = (1 + 2i\Pi - 2\Pi^2 + ...)\Sigma_M \tag{3.79}$$

and substituting into the effective Lagrangian (3.25) the result is

$$\begin{aligned}\mathcal{L} = 16\nu^2[(-m_\pi^2 + \mu_B^2)qq^* - m_\pi^2\pi_0^2 + (-m_\pi^2 + \mu_I^2)\pi^-\pi^+ + \partial_\mu\pi_0\partial^\mu\pi_0 + \\ \partial_\mu\pi^-\partial^\mu\pi^+ + \partial_\mu q\partial^\mu q^* + i\mu_B q^*\partial_t q - i\mu_B q\partial_t q^* + i\mu_I\pi^+\partial_t\pi^- - i\mu_I\pi^-\partial_t\pi^+]\ .\end{aligned} \tag{3.80}$$

Then after integration by parts neglecting the total derivatives and performing a Fourier transform

$$\partial_t \rightarrow -i\omega\,,\ \partial_j \rightarrow -ik_j \quad \Rightarrow \quad -\partial_\mu\partial^\mu \rightarrow \omega^2 - k^2\,, \tag{3.81}$$

the Lagrangian can be written as

$$\frac{\mathcal{L}}{16\nu^2} = \begin{pmatrix} \pi_0 & \pi^+ & \pi^- & q & q* \end{pmatrix} D^{-1} \begin{pmatrix} \pi_0 \\ \pi^+ \\ \pi^- \\ q \\ q* \end{pmatrix}, \tag{3.82}$$

where D^{-1} is the inverse propagator:

$$\begin{pmatrix} -k^2-m_\pi^2+\omega^2 & 0 & 0 & 0 & 0 \\ 0 & 0 & -k^2-m_\pi^2+(\mu_I-\omega)^2 & 0 & 0 \\ 0 & -k^2-m_\pi^2+(\mu_I+\omega)^2 & 0 & 0 & 0 \\ 0 & 0 & 0 & 0 & -k^2-m_\pi^2+(\mu_B+\omega)^2 \\ 0 & 0 & 0 & -k^2-m_\pi^2+(\mu_B-\omega)^2 & 0 \end{pmatrix}.$$

Solving the equation $\det D^{-1} = 0$ for ω, one obtains the dispersion relations for the Goldstone fields that are

$$\pi_0 : \quad \omega = \sqrt{k^2 + m_\pi^2} \tag{3.83}$$

$$\pi^+ : \quad \omega = \sqrt{k^2 + m_\pi^2} + \mu_I \tag{3.84}$$

$$\pi^- : \quad \omega = \sqrt{k^2 + m_\pi^2} - \mu_I \tag{3.85}$$

$$q : \quad \omega = \sqrt{k^2 + m_\pi^2} + \mu_B \tag{3.86}$$

$$q^* : \quad \omega = \sqrt{k^2 + m_\pi^2} - \mu_B\ . \tag{3.87}$$

The contribution given by the chemical potentials consists of a shift in the rest energies, according to the charges of the corresponding modes [163]. The charged pions have isospin but not baryon number, the diquark and the anti-diquark are baryons but they do not have isospin.

Superfluid Baryon Phase

In this phase, the vacuum of the theory is not simply Σ_M but the result of its compelling behaviour with the baryon term, so

$$\Sigma_c = \Sigma_M \cos\varphi + i\,\Sigma_B \sin\varphi\,. \tag{3.88}$$

The tilt angle φ expresses the rotation of the chiral condensate along the direction of Σ_B, leading to the vacuum configuration Σ_c. This rotation can be highlighted as [180]

$$\Sigma_c = V_\varphi \Sigma_M V_\varphi^T = V_\varphi^2\,\Sigma_M\,, \quad V_\varphi^2 = e^{i\varphi X_2} \tag{3.89}$$

being X_2 the generator which rotates Σ_M into Σ_B

$$X_2 = \Sigma_B \Sigma_M^{-1} = \begin{pmatrix} 0 & J \\ -J & 0 \end{pmatrix}. \tag{3.90}$$

The fluctuations of Σ around Σ_c can be parameterised as

$$\Sigma = U_\varphi \Sigma_M U_\varphi^T \tag{3.91}$$

where U_φ are unitary matrices generated by rotated generators $V_\varphi X_a V_\varphi^\dagger$. However, the meson mass matrix is diagonal in the basis given by the parameterisation

$$\Sigma = V_\varphi U \Sigma_M U^T V_\varphi^T \tag{3.92}$$

where the coset generators X_a have been rotated back to their value assumed in the normal phase. The price paid is the loss of φ-dependence for the U. Keep the rotation V_φ unspecified turns to be very useful in doing these calculations. For instance, one can consider the following rotated matrix

$$V_\varphi^\dagger B V_\varphi = B\cos\varphi + iX_1 \sin\varphi \tag{3.93}$$

where X_1, similarly to X_2, belongs to the coset of broken generators with respect to Σ_M and corresponds to the generator into which B is rotated while Σ_M is rotated into Σ_B, namely

$$X_1 = BX_2 = \begin{pmatrix} 0 & J \\ J & 0 \end{pmatrix}. \tag{3.94}$$

One can perform the same calculations done in the normal phase, expanding up to second order in the fluctuations Π. For the block decomposition of Π, it is convenient to consider, instead of the P and Q blocks, the following projections [180]

$$P_S = \frac{1}{2}(P + JP^T J) \qquad Q_R = \frac{1}{2}(Q + JQ^\dagger J) \qquad Q_I = \frac{1}{2}(Q - JQ^\dagger J)\,, \tag{3.95}$$

and the associated degeneracies, in the case $N_f = 2$, are

$$N_{P_S} = N_P = 3 \qquad\qquad N_{Q_R} = N_{Q_I} = \frac{N_Q}{2} = 1\,. \tag{3.96}$$

It is important to note that Q_R and Q_I are mixed by the linear derivative term. For all φ there is a solution for which the rest energy $\mathcal{E}(0) = 0$: it is the true massless Goldstone boson branch denoted by $\tilde{Q}$, which is a combination of Q_R and Q_I. In the simple case $N_f = 2$ there is only one such massless Goldstone boson in $\tilde{Q}$ and let us denote it with $\tilde{q}$. The linear combination $\tilde{Q}^\dagger$ orthogonal to $\tilde{Q}$ contains the d.o.f. denoted as $\tilde{q}^*$.

The final results for the dispersion relations in the superfluid baryon case are the following [163]

$$\pi_0 : \quad \omega = \sqrt{k^2 + \mu_B^2} \tag{3.97}$$

$$\pi^+ : \quad \omega = \sqrt{k^2 + \mu_B^2} + \mu_I \tag{3.98}$$

$$\pi^- : \quad \omega = \sqrt{k^2 + \mu_B^2} - \mu_I \tag{3.99}$$

$$\tilde{q}^* : \quad \omega^2 = k^2 + 2\mu_B^2(1 + 3\cos^2\varphi) + 2\mu_B\sqrt{4k^2\cos^2\varphi + \mu_B^2(1 + 3\cos^2\varphi)^2} \tag{3.100}$$

$$\tilde{q} : \quad \omega^2 = k^2 + 2\mu_B^2(1 + 3\cos^2\varphi) - 2\mu_B\sqrt{4k^2\cos^2\varphi + \mu_B^2(1 + 3\cos^2\varphi)^2} \tag{3.101}$$

The rest energy of the last mode is zero: this is the 1 massless Goldstone boson expected to appear in the superfluid transition. When generalised to $N_f \neq 2$, the $\frac{N_f^2 - N_f}{2}$ GBs produced in this transition are the modes that will be the protagonists when studying the large charge limit approaching the conformal window since they dominate the large charge dynamics (see chapter 6).

Superfluid Isospin Phase

In this phase the vacuum results from the compelling behaviour of the chiral condensate and the isospin term

$$\Sigma_c = \Sigma_M \cos\varphi + i\,\Sigma_I \sin\varphi\,. \tag{3.102}$$

This scenario mirrors the previous one. Precisely, the dispersion relations are found by exchanging $\mu_B \leftrightarrow \mu_I$ and the charged pions with the charged diquark/anti-diquark.

After this extensive rundown of calculations and the detailed study of two-colour QCD, it is now time to proceed to a case of greater physical interest,which will be more intuitive due to the established groundwork.

§ 3.4 QCD at finite isospin chemical potential

The time has come to review the results of three-colour QCD. Let us recall that usually, one invokes numerical methods to tackle this study since there are no reliable analytic tools to approach the theory in the strongly coupled regime. It is generally accepted that QCD at finite baryon density differs from finite-temperature QCD because the transition to quark degrees-of-freedom is driven by high conserved charge density (like baryon number), not temperature. This motivates studying QCD at finite isospin chemical potential μ_I, whose symmetry is *conserved* in strong interactions. Building on the emphasis at the beginning of this chapter, the regime of finite isospin chemical potential significantly impacts the real world, as exemplified by non-zero μ_I systems like neutron stars.

3.4.1 Two-flavour QCD

Let us review the two-flavour scenario mainly following [80]. To set the stage, as a first toy model one can ignore the baryon chemical potential and consider two light quarks having the same value of isospin chemical potential but different in sign [80, 179][1]. This approach results in a non-trivial model, suitable for Monte Carlo methods, that shares characteristics with two-colour QCD and represents a physically relevant theory: QCD with three colours.

Let us start with some mathematically important considerations that will have consequences on the pattern of spontaneous symmetry breaking.

In vacuum QCD one knows that the Euclidean Dirac operator $\mathcal{D} = \gamma(\partial + iA) + m$ satisfies $\det D \geq 0$ because of

$$\gamma_5 \mathcal{D} \gamma_5 = \mathcal{D}^\dagger \, . \tag{3.103}$$

Moreover, if $M = \bar{\psi}\Gamma\psi$ is a generic meson, pseudo-scalar correlation functions ($\langle \bar{\psi}(x) i\gamma_5 \tau_i \psi(x) \psi(0)(-i)\tau_i \gamma_5 \bar{\psi}^\dagger(0) \rangle$) always majorate $I = 1$ meson correlation functions and saturate the so-called Buniakowski-Schwartz inequality. This implies that the symmetry-breaking pattern is restricted, it cannot be driven by a condensate of $\langle \bar{\psi}\gamma_5\psi \rangle$ for example.

If one now switches on the baryon chemical potential, in three-colour QCD one would not have $\det \mathcal{D} \geq 0$ anymore but if it is the isospin chemical potential to be turned on, the positivity constraint would still be valid [80]. In fact now $\mathcal{D} = \gamma(\partial + iA) + \frac{\mu_I}{2}\gamma_0\tau_3 + m$ and

$$\tau_{1(2)} \gamma_5 \mathcal{D} \gamma_5 \tau_{1(2)} = \mathcal{D}^\dagger \, . \tag{3.104}$$

The Buniakowski-Schwartz inequality now implies that the lightest meson or equivalently the condensate must be of the form $\bar{\psi} i\gamma_5 \tau_{1,2} \psi$ which means that it has to be a linear combination of $\pi^- \sim \bar{u}\gamma_5 d$ and $\pi^+ \sim \bar{d}\gamma_5 u$.

Chiral Lagrangian and phase diagram

Let us suppose to deal with a small isospin chemical potential so that chiral perturbation theory can be used. To account for such a theory, one requires that no particles other than pions are excited due to the chemical potential [80, 179]. This gives $\mu_I \simeq m_\rho$ as an upper limit on the applicability of chiral perturbation theory. When $\mu_I = 0$ the chiral Lagrangian exhibits the familiar global symmetry of $SU(2)_L \times SU(2)_R$ subsequently broken explicitly to $SU(2)_V$ if all masses are equal. In this scenario, the chiral Lagrangian is characterised by only two phenomenological parameters: the pion decay constant F_π

[1] There is a need to outline here that such a model is unstable for weak decays and as a result does not conserve isospin. Focusing on the strong regime, one can disregard insignificant electromagnetic and weak effects.

and its vacuum mass m_π. Introducing an isospin chemical potential leads to further spontaneous breaking of the global symmetry to $U(1)_V$. Notably, the effects of the isospin chemical potential can be incorporated without additional phenomenological parameters.

The finite μ_I chiral Lagrangian is obtained by promoting the global $SU(2)_L \times SU(2)_R$ symmetry to a local gauge symmetry, with the covariant derivative being

$$\mathcal{D}_0\Sigma = \partial_0\Sigma - \underbrace{\frac{\mu_I}{2}(\tau_3\Sigma - \Sigma\tau_3)}_{\text{isospin generator } \frac{\tau_3}{2}} \quad \text{and} \quad \mathcal{D}_i\Sigma = \partial_i\Sigma \,, \tag{3.105}$$

which leads to

$$\mathcal{L} = \frac{F_\pi^2}{4}\mathrm{Tr}\{\partial\Sigma\partial\Sigma^\dagger\} + \boxed{\frac{F_\pi^2}{8}\mu_I^2\mathrm{Tr}\{\tau_3\Sigma\tau_3\Sigma^\dagger - \mathbb{1}\}} - \boxed{\frac{F_\pi^2 m_\pi^2}{2}\mathrm{Re}\{\mathrm{Tr}\{\Sigma\}\}} \,. \tag{3.106}$$

The violet term favours the directions of Σ that anti-commute with τ_3 (that is, τ_1 and τ_2), while the magenta term prefers the vacuum direction $\Sigma = \mathbb{1}$. Therefore, the ansatz for the vacuum is

$$\bar{\Sigma} = \boxed{\mathbb{1}\cos\varphi} + i\,\boxed{(\tau_1\cos\eta + \tau_2\sin\eta)\sin\varphi} \,. \tag{3.107}$$

The tilt angle φ is determined by minimising the vacuum energy. The energy is degenerate for the angle η, corresponding to the spontaneous breaking of the $U(1)_V$ symmetry generated by τ_3 in the Lagrangian. The ground state is a pion superfluid, with one massless Goldstone mode. Additionally, there are also two massive modes in the superfluid (the π^0 and a combination of π^+ and π^-). The system behaves similarly as for the baryon two-colour QCD:

- $|\mu_I| < m_\pi$: the vacuum is $\bar{\Sigma} = \mathbb{1}$ and $\varphi = 0$.
- $|\mu_I| > m_\pi$: the minimum occurs at $\cos\varphi = \frac{m_\pi^2}{\mu_I^2}$ and the necessary energy apt to excite a π^- quantum, $m_\pi - |\mu_I|$, is negative. As a result, it is energetically favourable to excite a large number of these quanta. Since the pions are bosons, the system is in a Bose-Einstein condensation of π^- (this is the case if a negative isospin chemical potential is present; otherwise it would be a Bose-Einstein condensation of π^+).

The spectrum of the theory is easily computed by expanding the Lagrangian (3.106) around the minimum (3.107).

Let us end this brief subsection with a final remark. As more pions are forced into the condensate, the pions are packed closer, and their interaction becomes stronger. When $|\mu_I| \sim m_\rho$, the chiral perturbation theory fails, and one has to call for full QCD [80].

§ 3.5 QCD at finite isospin and strangeness chemical potential

3.5.1 Three flavours QCD

For the rest of this chapter, the focus is on the QCD phase diagram for small chemical potentials associated with each quark flavour. The theory with three light-quark flavours, for which this effective theory approach can be used, will be presented. A non-trivial phase diagram emerges since there are three distinct phases: a normal phase, a pion condensation phase and a kaon condensation phase [196].

3.5.2 Symmetries of the fundamental Lagrangian and symmetry-breaking patterns

Let us look at the microscopic Lagrangian in detail, that, for the sake of clarity, it is here re-written

$$\mathcal{L}_{QCD} = \bar{\psi}\left(i\not{\mathcal{D}} - M\right)\psi - \frac{1}{4}F_{\mu\nu}F^{\mu\nu} \quad \text{with} \quad \psi^T = (u, d, s) \quad \text{and} \quad M = diag(m, m, m_s), \tag{3.108}$$

with the up and down quarks considered to be degenerate in mass and $\mathcal{D} = \partial + igA_\mu - iv_\mu$

$$v_\mu = \mu\delta_{\mu 0} \quad \text{with} \quad \mu = diag(\mu_u, \mu_d, \mu_s) = \frac{\mu_B - \mu_s}{3}\mathbb{1} + \frac{1}{2}\mu_I T_3 + \frac{1}{\sqrt{3}}\mu_s T_8 \; . \tag{3.109}$$

where μ_s is the strangeness chemical potential and T_3 and T_8 are the two generators of the Cartan sub-algebra of $SU(3)$, namely

$$T_3 = \begin{pmatrix} 1 & 0 & 0 \\ 0 & -1 & 0 \\ 0 & 0 & 0 \end{pmatrix} \quad \text{and} \quad T_8 = \begin{pmatrix} \frac{1}{2} & 0 & 0 \\ 0 & \frac{1}{2} & 0 \\ 0 & 0 & -1 \end{pmatrix} \; . \tag{3.110}$$

The discussion will review the work [196] and, of course, references therein. The generators of the algebra will be denoted with T_a with $a = 1, \ldots, 8$ and they are proportional to the Gell-Mann matrices. For the considerations that will follow, let us introduce the three $\mathfrak{su}(2)$ sub-algebras of $SU(3)$. These are the ones generated by the following three sets of generators

- $T_3, \qquad T_+ = T_1 + iT_2, \qquad T_- = T_1 - iT_2$ with weight $Y = \frac{2}{\sqrt{3}}T_8$
- $V_3, \qquad V_+ = T_4 + iT_5, \qquad V_- = T_4 - iT_5$ with weight $K = T_3 - \frac{1}{\sqrt{3}}T_8$
- $U_3, \qquad U_+ = T_6 + iT_7, \qquad U_- = T_6 - iT_7$ with weight $Q = T_3 + \frac{1}{\sqrt{3}}T_8$.

Let us analyse step by step the explicit symmetry-breaking pattern that characterises (3.108).

A summary of the complete symmetry-breaking pattern of the theory is shown in Figure 3.5. The first row describes the invariance of massless QCD with respect to the left- and right-handed rotations of the quark fields. The group $U(1)_Q$ is a sub-group of the chiral symmetry one. These left- and right-handed rotations are locked together when the chiral condensate forms in vacuum: the above global symmetry group is then broken down to the one leaving the vacuum invariant $SU(3)_V \times U(1)_B$.

According to the Goldstone theorem, this symmetry-breaking pattern gives rise to eight NGBs corresponding to the broken generators. However, the bare quark masses explicitly break the chiral symmetry, meaning these modes are not true NGBs but rather massive pseudo-NGBs, which are identified with the pseudo-scalar meson octet. Assuming that the light quark masses are degenerate implies that the isospin symmetry is not broken. This leads to the global symmetry group illustrated in the second row of Figure 3.5 where $SU(2)_I$ is the isospin symmetry group, while $U(1)_Y$ is the one generated by T_8. Since the isospin symmetry is preserved, the pions are all degenerate in mass, that is, m_π. The same is true for the kaons: they are grouped in iso-doublets with degenerate masses m_K. The differences in the value of the masses between pions and kaons hold because of the strange quark. Lastly, the η field has mass $\sqrt{(4m_K^2 - m_\pi^2)/3}$ as will be better shown later.

Moreover, the chemical potentials in the theory are responsible for both explicit and spontaneous symmetry breakings. The former is at the Lagrangian level, while the latter causes the meson condensations. The explicit breaking happens since Lorentz boost invariance is not preserved while space rotations and translations are unaffected. This results in an isotropic and homogeneous medium. Since the presence of the chemical potential fixes the isospin charge, they also break the charge symmetry: the charged conjugated states now have different masses.

Precisely, the only generators commuting with the Hamiltonian of the theory are the ones corresponding to the Cartan sub-algebra, namely T_3 and T_8. This means that the presence of the chemical potential induces the explicit symmetry-breaking pattern shown in the third row of Figure 3.5, where $U(1)_I$ and $U(1)_Y$ are the groups generated by T_3 and T_8, respectively. This leftover symmetry group is the one characterising the normal phase, namely where no meson condensates form. This symmetry group is made up of three independent phase rotations of the flavour fields. A superfluid phase occurs if one of the three remaining $U(1)$ groups is spontaneously broken. The corresponding meson condensate that forms thus depends on the broken generator.

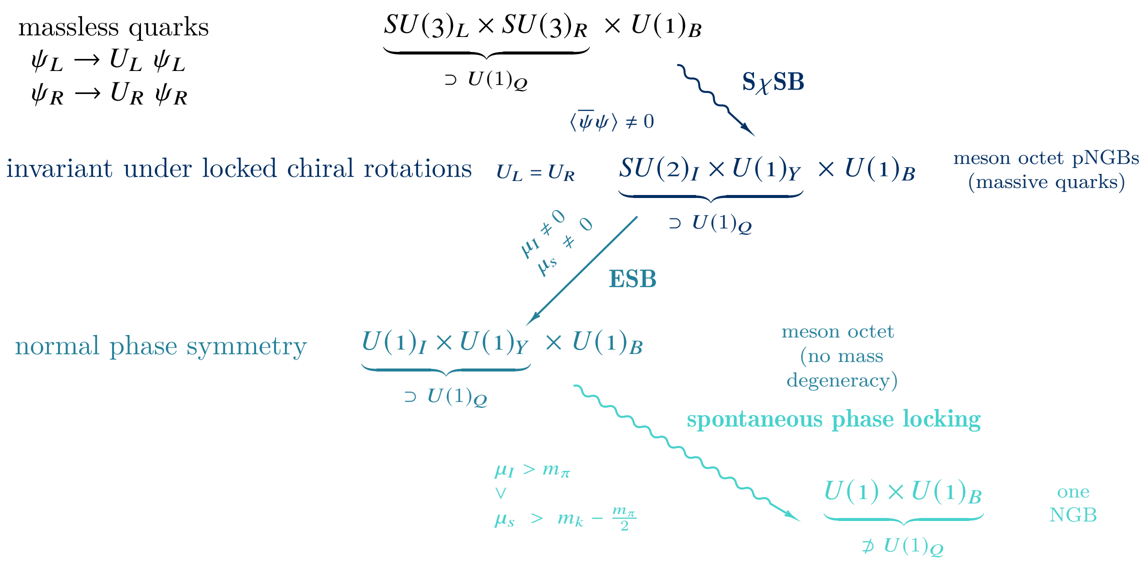

Figure 3.5.: The full symmetry-breaking pattern.

Before delving into the details of the superfluid phases let us focus more on the normal phase. Firstly, since

$$[H, T_3] = 0 \quad \text{and} \quad [H, T_8] = 0 \tag{3.111}$$

the eigenstates of the Hamiltonian can be grouped in isospin multiplets.

Exactly, these multiplets are labelled by the values $|T^2 = T_1^2 + T_2^2 + T_3^2, T_3\rangle$, $|V^2 = T_4^2 + T_5^2 + V_3^2, V_3\rangle$ and $|U^2 = T_6^2 + T_7^2 + U_3^2, U_3\rangle$ since T^2, V^2 and U^2 commute with T_3 and T_8. Each multiplet is characterised by states that have differences in mass proportional to the chemical potentials. To be precise, there is a mass splitting in the isospin multiplets due to the presence of the isospin chemical potential and, in addition, mass splitting between states having different hypercharges proportional to the strangeness chemical potential μ_s. Those states having zero isospin and strangeness, π_0 and η, are not affected. Therefore, in the normal phase, one has (see Figure 3.6):

$$\begin{aligned}
m_{\pi_0} &= m_\pi \\
m_{\boxed{\pi_+}} &= m_\pi - \mu_I \\
m_{\boxed{\pi_-}} &= m_\pi + \mu_I \\
m_{\boxed{K_+}} &= m_K - \frac{1}{2}\mu_I - \mu_s \\
m_{\boxed{K_-}} &= m_K + \frac{1}{2}\mu_I + \mu_s \\
m_{\boxed{K_0}} &= m_K + \frac{1}{2}\mu_I - \mu_s \\
m_{\boxed{\bar{K}_0}} &= m_K - \frac{1}{2}\mu_I + \mu_s \\
m_\eta &= \sqrt{\frac{4m_K^2 - m_\pi^2}{3}}\,.
\end{aligned} \tag{3.112}$$

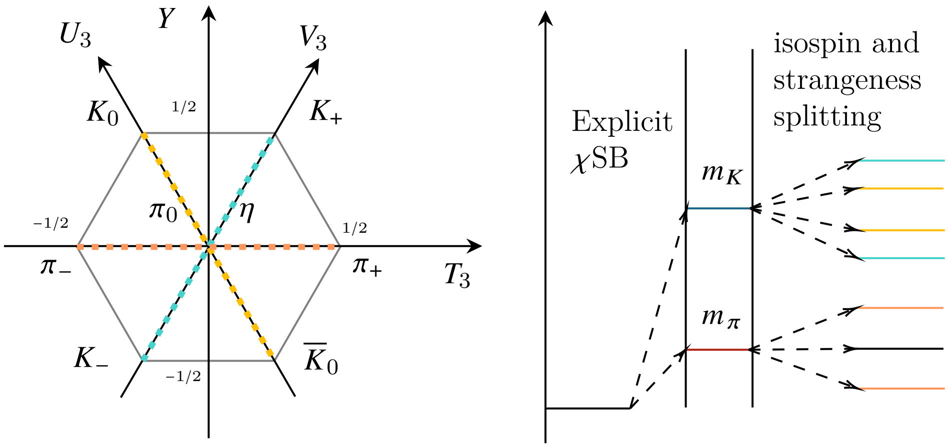

Figure 3.6.: Left: a sketch of the weight diagram of the mesonic octet. The dotted coloured lines indicate the three isospin multiplets: (π_+, π_-) having T=1 , (K_+, K_-) having V=1 and $(K_0, \bar{K}_0)$ with U=1 . Right: mass levels in the normal phase due to explicit chiral symmetry breaking and the corresponding splitting for the presence of the isospin and strangeness potentials. The former is taken to be smaller than the latter.

By inspecting the masses in the normal phase, one immediately realises that when tuning the values of the chemical potentials one of them can become zero. When this happens a phase transition occurs: one moves from the normal to a superfluid phase. The nature of this superfluid phase depends on whether it is a pion or a kaon that condenses. For instance, when $\mu_I = m_\pi$ the π_+ becomes massless[2].

At this point, let us analyse the last row of the symmetry-breaking pattern in Figure 3.5. Firstly, the normal phase will persist until no mode is massless, namely, when conditions for the last symmetry pattern are not satisfied. The superfluid phases can happen when one of the ladder generators associated with the $\mathfrak{su}(2)$ sub-algebras is spontaneously broken:

- T_+ leads π^+ to condense.
- V_+ leads K^+ to condense.
- U_+ leads K^0 to condense.

At the level of the symmetry-breaking pattern, the situation is depicted in Figure 3.7.

Important considerations are now in order. Firstly, the two mechanisms of chiral spontaneous symmetry breaking and meson condensation are independent: this means that the chiral condensate and the meson condensate can coexist. On the other hand, pion and kaon condensation cannot coexist because the respective broken ladder operators do not commute [197].

[2] This happens when $\mu_I > 0$, as already stated previously in the chapter.

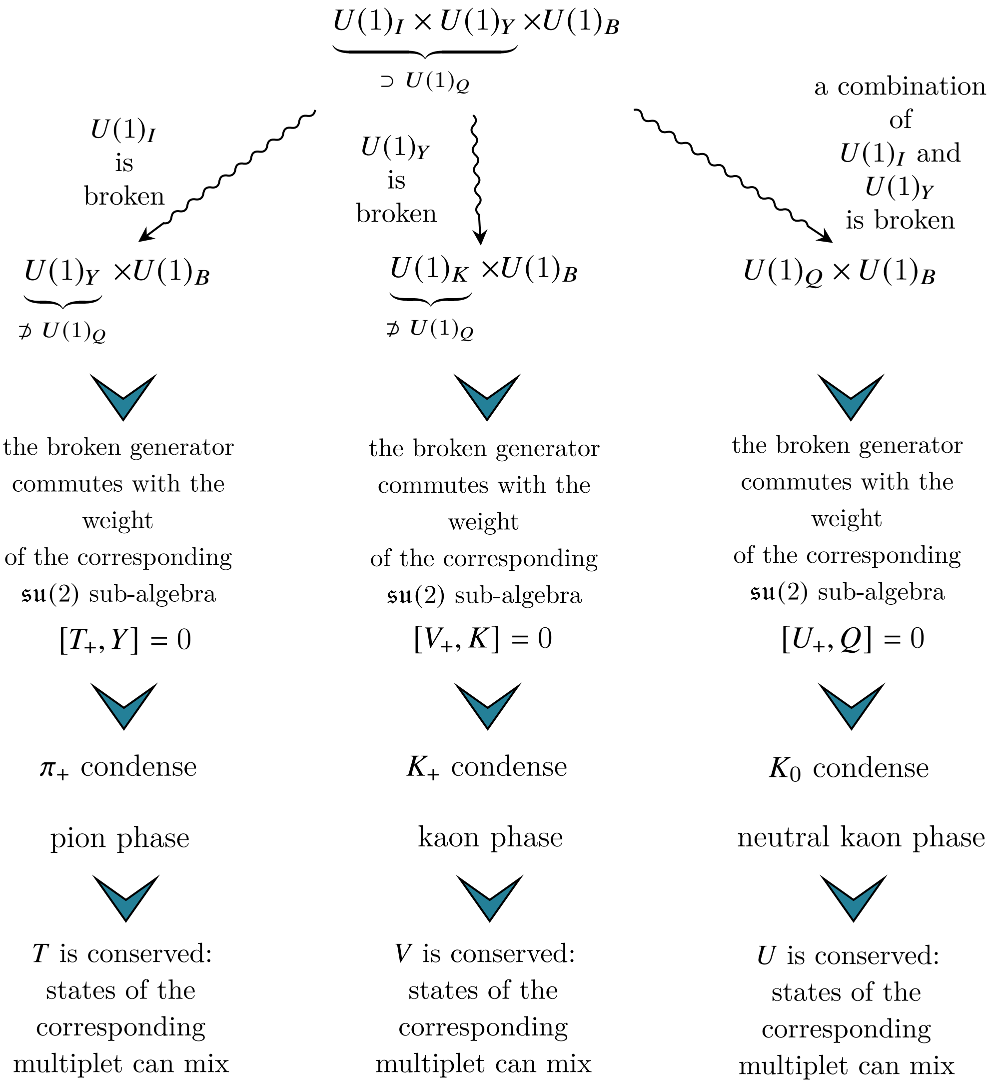

Figure 3.7.: Mind map summarising the superfluid phases conditions and the corresponding symmetry-breaking patterns.

3.5.3 Chiral perturbation theory

Let Σ be the field collecting the meson fields transforming as

$$\Sigma \longrightarrow L\Sigma R^{\dagger} \tag{3.113}$$

where $L, R \in SU(N_f)_{L,R}$. The leading $O(q^2)$ chiral perturbative Lagrangian describing the in-medium pseudo-scalar mesons reads

$$\mathcal{L} = \frac{F_\pi^2}{4} Tr\left\{\mathcal{D}_\mu \Sigma \mathcal{D}^\mu \Sigma^\dagger\right\} + \frac{F_\pi^2}{4} Tr\left\{X\Sigma^\dagger + \Sigma X^\dagger\right\} \quad \text{with} \quad \mathcal{D}_\mu \Sigma = \partial_\mu \Sigma + \frac{i}{2}\left[v_\mu, \Sigma\right] , \tag{3.114}$$

and $\langle X \rangle = 2BM$. By expanding the covariant derivative one obtains the following Lagrangian

$$\mathcal{L} = \frac{F_\pi^2}{4} Tr\left\{\partial_\mu \Sigma \partial^\mu \Sigma^\dagger\right\} - i\frac{F_\pi^2}{2} Tr\left\{B\left[\Sigma^\dagger, \partial_t \Sigma\right]\right\} + \frac{F_\pi^2 G}{2} Tr\left\{M(\Sigma + \Sigma^\dagger)\right\} - \frac{F_\pi^2}{2} Tr\left\{B\Sigma B\Sigma^\dagger - B^2\right\} \tag{3.115}$$

and the most general $SU(3)$ homogeneous vacuum expectation value can be written as

$$\bar{\Sigma} = e^{i\varphi \mathbf{n}\cdot\lambda} \,. \tag{3.116}$$

One expects that in each different meson condensed phase the vacuum is aligned in a specific way, depending on the meson condensing. In fact, this will result in the ground state having vanishing projection along the isospin and strangeness directions, respectively, while the other rotations around the direction of the chemical potential leave the vacuum invariant [196].

Therefore, in the pion condensed phase the non-vanishing components should be (n_1, n_2), in the kaon one (n_4, n_5) while in the neutral condensed phase (n_6, n_7). So

$$\bar{\Sigma}_\pi = e^{i\varphi\lambda_2} = \begin{pmatrix} \cos\varphi & \sin\varphi & 0 \\ -\sin\varphi & \cos\varphi & 0 \\ 0 & 0 & 1 \end{pmatrix} \tag{3.117}$$

$$\bar{\Sigma}_K = e^{i\varphi\lambda_5} = \begin{pmatrix} \cos\varphi & 0 & \sin\varphi \\ 0 & 1 & 0 \\ -\sin\varphi & 0 & \cos\varphi \end{pmatrix} \tag{3.118}$$

$$\bar{\Sigma}_{K_0} = e^{i\varphi\lambda_7} = \begin{pmatrix} 1 & 0 & 0 \\ 0 & \cos\varphi & \sin\varphi \\ 0 & -\sin\varphi & \cos\varphi \end{pmatrix} \,. \tag{3.119}$$

One can actually set up a more general ansatz as follows

$$\bar{\Sigma} = e^{-i\zeta\lambda_2}\, e^{-i\beta\lambda_7}\, e^{-i\varphi\lambda_2}\, e^{i\beta\lambda_7}\, e^{+i\zeta\lambda_2} \tag{3.120}$$

with $\zeta, \beta, \varphi \in \left[0, \frac{\pi}{2}\right]$. The normal phase corresponds to $\varphi = 0$ and is independent of any value of the other two angles. In contrast, the pion condensed phase corresponds to $\beta = 0, \zeta = 0$ while the kaon condensed one occurs at $\beta = \frac{\pi}{2}, \zeta = 0$. Instead, when $\zeta = \frac{\pi}{2}, \beta = \frac{\pi}{2}$ the K^0 condensed phase happens. The ansatz (3.120) can be further simplified to study the pion and kaon condensed phase by setting $\zeta = 0$. Henceforth $\zeta = 0$ so that the only kaon condensation phase that will be handled is the one associated with the condensation of K_+.

The two different phases are summarised below. Let us recall that at zero chemical potential, the masses of the pNGBs are given by the Gell-Mann-Oakes-Renner relation where

$$m_\pi^2 = 2Gm \tag{3.121}$$

$$m_K^2 = G(m + m_s) \tag{3.122}$$

$$m_\eta^2 = 2G\frac{m + 2m_s}{3} = \frac{4m_K^2 - m_\pi^2}{3} \,, \tag{3.123}$$

hence

- β=0 : the static part of (3.115) becomes

$$\mathcal{L} = -2Gm\cos\varphi - Gm_s - \frac{f_\pi^2}{2}\mu_I^2\sin^2\varphi \tag{3.124}$$

  with

$$\begin{cases}\cos\varphi = 1 & \text{for } \mu_I < m_\pi \\ \cos\varphi = \frac{m_\pi^2}{\mu_I^2} & \text{for } \mu_I > m_\pi\end{cases} \quad \text{and} \quad \bar{\Sigma} = \begin{pmatrix}\cos\varphi & \sin\varphi & 0\\ -\sin\varphi & \cos\varphi & 0\\ 0 & 0 & 1\end{pmatrix} \tag{3.125}$$

- β=$\frac{\pi}{2}$: the static part of (3.115) is

$$\mathcal{L} = -Gm - G(m+m_s)\cos\varphi - \frac{f_\pi^2}{2}\left(\frac{\mu_I}{2}+\mu_s\right)^2\sin^2\varphi \tag{3.126}$$

  with

$$\begin{cases}\cos\varphi = 1 & \text{for } \frac{\mu_I}{2}+\mu_s < m_K \\ \cos\varphi = \frac{m_K^2}{\left(\frac{\mu_I}{2}+\mu_s\right)^2} & \text{for } \frac{\mu_I}{2}+\mu_s > m_K\end{cases} \quad \text{and} \quad \bar{\Sigma} = \begin{pmatrix}\cos\varphi & 0 & \sin\varphi\\ 0 & 1 & 0\\ -\sin\varphi & 0 & \cos\varphi\end{pmatrix}. \tag{3.127}$$

The minimum of the static part of the Lagrangian determines the vacuum alignment. The three phases are thus defined as follows

1. Normal phase $\mu_I < m_\pi$ & $\mu_s < m_K - \frac{\mu_I}{2}$:

$$\cos\varphi = 1 \quad \text{for any} \quad \beta \in \left(0, \frac{\pi}{2}\right). \tag{3.128}$$

2. Pion condensation phase $\mu_I > m_\pi$ & $\mu_s < \frac{-m_\pi^2+\sqrt{(m_\pi^2-\mu_I^2)^2+4m_K^2\mu_I^2}}{2\mu_I}$:

$$\cos\varphi = \frac{m_\pi^2}{\mu_I^2} \quad \text{and} \quad \beta = 0\,. \tag{3.129}$$

3. Kaon condensation phase $\mu_I > m_\pi$ & $\mu_s > \frac{-m_\pi^2+\sqrt{(m_\pi^2-\mu_I^2)^2+4m_K^2\mu_I^2}}{2\mu_I}$:

$$\cos\varphi = \frac{m_K^2}{\left(\frac{\mu_I}{2}+\mu_s\right)^2} \quad \text{and} \quad \beta = \frac{\pi}{2}\,. \tag{3.130}$$

It is important to note here that in the plane (μ_I, μ_s) the curve $\mu_s > \frac{-m_\pi^2+\sqrt{(m_\pi^2-\mu_I^2)^2+4m_K^2\mu_I^2}}{2\mu_I}$ is a first-order line curve where the pion and kaon condensation phases compete. Additionally, the two condensed phases are separated by the normal one by a second-order transition curve.

Lastly, for each phase, by expanding the effective lagrangian (3.114) to the second order in the Goldstone fields, the masses of the excitations can be easily computed.

3.5.4 Spectrum

It is important to remember that in the superfluid phases, the original fields are mixed because the Goldstone manifold changes as the normal phase is left. Moreover, the all-spectrum is cumbersome to compute; it suffices to study simpler cases only. So, (3.114) is expanded up to the second order in the excitations with the following ansatz

$$\Sigma = e^{i\frac{\Phi}{\sqrt{2}F_\pi}}\bar{\Sigma}e^{i\frac{\Phi}{\sqrt{2}F_\pi}} \quad \text{where} \quad \Phi = \begin{pmatrix} \frac{\pi_0}{\sqrt{2}} + \frac{\eta}{\sqrt{6}} & \pi_+ & K_+ \\ \pi_- & -\frac{\pi_0}{\sqrt{2}} + \frac{\eta}{\sqrt{6}} & K_0 \\ K_- & \bar{K}_0 & -\frac{2}{\sqrt{6}}\eta \end{pmatrix}, \tag{3.131}$$

where $\bar{\Sigma}$ is the vacuum ansatz of the corresponding phase. To simplify the computations, it is convenient to re-write the matrix Φ in the following way

$$\Phi = \sum_{i=1}^{8} \pi_i \lambda_i = \begin{pmatrix} \frac{\pi_3}{\sqrt{2}} + \frac{\pi_8}{\sqrt{6}} & \frac{\pi_1 - i\pi_2}{\sqrt{2}} & \frac{\pi_4 - i\pi_5}{\sqrt{2}} \\ \frac{\pi_1 + i\pi_2}{\sqrt{2}} & -\frac{\pi_3}{\sqrt{2}} + \frac{\pi_8}{\sqrt{6}} & \frac{\pi_6 - i\pi_7}{\sqrt{2}} \\ \frac{\pi_4 + i\pi_5}{\sqrt{2}} & \frac{\pi_6 + i\pi_7}{\sqrt{2}} & -\sqrt{\frac{2}{3}}\pi_8 \end{pmatrix} \tag{3.132}$$

and then re-write the spectrum in terms of the previous basis.

- Normal phase

Let us notice that the overall Lagrangian can be written in block diagonal form

$$\mathcal{L} = \Pi D^{-1}\, \Pi^T \tag{3.133}$$

where $\Pi = \{\pi_1, \pi_2, \pi_3, \pi_4, \pi_5, \pi_6, \pi_7, \pi_8\}$ while the inverse propagator reads

$$D^{-1} = \left(\begin{array}{c|c} \begin{matrix} D_{12} & \begin{matrix}0\\ \vdots\end{matrix} \\ 0\cdots\cdots & D_{33}\end{matrix} & \mathbf{0} \\ \hline \mathbf{0} & \begin{matrix} D_{45} & \mathbf{0} & \begin{matrix}0\\ \vdots\end{matrix}\\ \mathbf{0} & D_{67} & \begin{matrix}\vdots\\ 0\end{matrix} \\ 0\cdots\cdots & \cdots 0 & D_{88}\end{matrix}\end{array}\right) \tag{3.134}$$

where

$$D_{12} = \begin{pmatrix} \frac{1}{2}\left(\omega^2 - k^2 - m_\pi^2 + \mu_I^2\right) & -i\omega\mu_I \\ i\omega\mu_I & \frac{1}{2}\left(\omega^2 - k^2 - m_\pi^2 + \mu_I^2\right) \end{pmatrix} \tag{3.135}$$

$$D_{33} = \frac{1}{2}\left(\omega^2 - k^2 - m_\pi^2\right) \tag{3.136}$$

$$D_{45} = \begin{pmatrix} \frac{1}{2}\left(\omega^2 - k^2 - m_K^2 + \left(\frac{1}{2}\mu_I + \mu_s\right)^2\right) & -i\omega(\frac{1}{2}\mu_I + \mu_s) \\ i\omega(\frac{1}{2}\mu_I + \mu_s) & \frac{1}{2}\left(\omega^2 - k^2 - m_K^2 + \left(\frac{1}{2}\mu_I + \mu_s\right)^2\right) \end{pmatrix} \tag{3.137}$$

$$D_{67} = \begin{pmatrix} \frac{1}{2}\left(\omega^2 - k^2 - m_K^2 + \left(\frac{1}{2}\mu_I - \mu_s\right)^2\right) & -i\omega(\frac{1}{2}\mu_I - \mu_s) \\ i\omega(\frac{1}{2}\mu_I - \mu_s) & \frac{1}{2}\left(\omega^2 - k^2 - m_K^2 + \left(\frac{1}{2}\mu_I - \mu_s\right)^2\right) \end{pmatrix} \tag{3.138}$$

$$D_{88} = \frac{1}{2}\left(\omega^2 - k^2 - \frac{1}{3}m_\pi^2 - \frac{4}{3}m_K^2\right) . \tag{3.139}$$

At this point, solving the equation $\det\{D^{-1}\} = 0$ and then setting $k = 0$ leads to the set of masses spoilt in (3.112).

- Pion condensation phase

In the superfluid phases, the original Goldstone fields are mixed. As the normal phase is left, the Goldstone manifold changes, rendering the original octet of Goldstone bosons unsuitable as coordinates for the new Goldstone manifold. The new appropriate fields will be denoted with a tilde and will be those ensuring that the kinetic term in the Lagrangian is canonical, namely [197]

$$\tilde{\pi}_{1,3} = \pi_{1,3}\cos\varphi \tag{3.140}$$

$$\tilde{\pi}_{4,5,6,7} = \pi_{4,5,6,7}\cos\left(\frac{\varphi}{2}\right) . \tag{3.141}$$

In this scenario, using $\bar{\Sigma} = \bar{\Sigma}_\pi$, one obtains

$$\mathcal{L} = \tilde{\Pi} D^{-1}\, \tilde{\Pi}^T \tag{3.142}$$

where $\tilde{\Pi} = \{\tilde{\pi}_1, \tilde{\pi}_2, \tilde{\pi}_3, \tilde{\pi}_4, \tilde{\pi}_5, \tilde{\pi}_6, \tilde{\pi}_7, \tilde{\pi}_8\}$ is the vector of all the Goldstone fields while

$$D^{-1} = \left(\begin{array}{cc|ccc} D_{12} & \begin{matrix}0\\ \vdots\end{matrix} & & \mathbf{0} & \\ 0 \cdots & D_{33} & & & \\ \hline & & D_{45} & \mathbf{0} & \begin{matrix}0\\ \vdots\end{matrix} \\ & \mathbf{0} & \mathbf{0} & D_{67} & \begin{matrix}\vdots\\ 0\end{matrix} \\ & & 0 \cdots & \cdots 0 & D_{88} \end{array}\right) \tag{3.143}$$

$$D_{12} = \begin{pmatrix} \omega^2 - k^2 - \frac{m_\pi^2}{\cos\varphi} + \mu_I^2 & -2i\omega\mu_I\cos\varphi \\ 2i\omega\mu_I\cos\varphi & \omega^2 - k^2 - m_\pi^2\cos\varphi + \mu_I^2\cos(2\varphi) \end{pmatrix} \tag{3.144}$$

$$D_{33} = \omega^2 - k^2 - \frac{m_\pi^2}{\cos\varphi} \tag{3.145}$$

$$D_{45} = \begin{pmatrix} \omega^2 - k^2 - m_K^2 + \frac{1}{2}\mu_I(\mu_I + 2\mu_s)\cos\varphi - \frac{\mu_I^2}{4} + \mu_s^2 & -i\omega(\mu_I\cos\varphi + 2\mu_s) \\ i\omega(\mu_I\cos\varphi + 2\mu_s) & \omega^2 - k^2 - m_K^2 + \frac{1}{2}\mu_I(\mu_I + 2\mu_s)\cos\varphi - \frac{\mu_I^2}{4} + \mu_s^2 \end{pmatrix} \tag{3.146}$$

$$D_{67} = \begin{pmatrix} \omega^2 - k^2 - m_K^2 + \frac{1}{2}\mu_I(\mu_I - 2\mu_s)\cos\varphi - \frac{\mu_I^2}{4} + \mu_s^2 & -i\omega(\mu_I\cos\varphi - 2\mu_s) \\ i\omega(\mu_I\cos\varphi - 2\mu_s) & \omega^2 - k^2 - m_K^2 + \frac{1}{2}\mu_I(\mu_I - 2\mu_s)\cos\varphi - \frac{\mu_I^2}{4} + \mu_s^2 \end{pmatrix} \tag{3.147}$$

$$D_{88} = \omega^2 - k^2 - \frac{1}{3}m_\pi^2(2-\cos\varphi) - \frac{4}{3}m_K^2 \,. \tag{3.148}$$

Again, solving the equation $\det\{D^{-1}\} = 0$ and then setting $k = 0$, yields a set of masses that read:

$$\begin{aligned}
m_{\tilde{\pi}_0} &= \mu_I \\
m_{\tilde{\pi}_+} &= 0 \\
m_{\tilde{\pi}_-} &= \frac{\sqrt{3m_\pi^4 + \mu_I^4}}{\mu_I} \\
m_{\tilde{K}_+} &= \frac{\sqrt{-2\mu_I^2\left(m_\pi^2 - 2m_K^2\right) + \mu_I^4 + m_\pi^4} - 2\mu_I\mu_s - m_\pi^2}{2\mu_I} \\
m_{\tilde{K}_-} &= \frac{\sqrt{-2\mu_I^2\left(m_\pi^2 - 2m_K^2\right) + \mu_I^4 + m_\pi^4} + 2\mu_I\mu_s + m_\pi^2}{2\mu_I} \\
m_{\tilde{K}_0} &= \frac{\sqrt{-2\mu_I^2\left(m_\pi^2 - 2m_K^2\right) + \mu_I^4 + m_\pi^4} - 2\mu_I\mu_s + m_\pi^2}{2\mu_I} \\
m_{\tilde{\bar{K}}_0} &= \frac{\sqrt{-2\mu_I^2\left(m_\pi^2 - 2m_K^2\right) + \mu_I^4 + m_\pi^4} + 2\mu_I\mu_s - m_\pi^2}{2\mu_I} \\
m_{\tilde{\eta}} &= \frac{\sqrt{m_\pi^4 - 2(m_\pi^2 - 2m_K^2)\mu_I^2}}{\sqrt{3}\mu_I} \,.
\end{aligned} \tag{3.149}$$

- Kaon condensation phase

The new appropriate fields are labelled with a tilde and are those ensuring the canonical form of the kinetic term in the Lagrangian. In the kaon phase, these fields are defined as [197]

$$\tilde{\pi}_{1,2,6,7} = \pi_{1,2,6,7}\cos\left(\frac{\varphi}{2}\right) \tag{3.150}$$

$$\tilde{\pi}_4 = \pi_4\cos\varphi \quad \text{and} \tag{3.151}$$

$$\begin{pmatrix}\tilde{\pi}_3 \\ \tilde{\pi}_8\end{pmatrix} = \begin{pmatrix} -\frac{\sqrt{3}}{2} & \frac{1}{2} \\ \frac{1}{2}\cos\varphi & \frac{\sqrt{3}}{2}\cos\varphi \end{pmatrix}\begin{pmatrix}\pi_3 \\ \pi_8\end{pmatrix} \,. \tag{3.152}$$

Therefore, using $\bar{\Sigma} = \bar{\Sigma}_K$, one obtains

$$\mathcal{L} = \tilde{\Pi} D^{-1}\,\tilde{\Pi}^T \tag{3.153}$$

where now $\tilde{\Pi} = \{\tilde{\pi}_1, \tilde{\pi}_2, \tilde{\pi}_4, \tilde{\pi}_5, \tilde{\pi}_6, \tilde{\pi}_7, \tilde{\pi}_3, \tilde{\pi}_8\}$ is the vector of all the Goldstone fields while

$$D^{-1} = \left(\begin{array}{cc|cc} D_{12} & \mathbf{0} & \multicolumn{2}{c}{\multirow{2}{*}{$\mathbf{0}$}} \\ \mathbf{0} & D_{45} & & \\ \hline \multicolumn{2}{c|}{\multirow{2}{*}{$\mathbf{0}$}} & D_{67} & \mathbf{0} \\ & & \mathbf{0} & D_{38} \end{array}\right) \tag{3.154}$$

$$D_{12} = \begin{pmatrix} \omega^2 - k^2 + \frac{1}{2}(\mu_I^2 - 2m_\pi^2 - 2\mu_I\mu_s + \mu_I(\mu_I + 2\mu_s)\cos\varphi) & -\frac{1}{2}i\omega(3\mu_I - 2\mu_s + (\mu_I + 2\mu_s)\cos\varphi) \\ \frac{1}{2}i\omega(3\mu_I - 2\mu_s + (\mu_I + 2\mu_s)\cos\varphi) & \omega^2 - k^2 + \frac{1}{2}(\mu_I^2 - 2m_\pi^2 - 2\mu_I\mu_s + \mu_I(\mu_I + 2\mu_s)\cos\varphi) \end{pmatrix} \tag{3.155}$$

$$D_{45} = \begin{pmatrix} \omega^2 - k^2 - \frac{m_K^2}{\cos\varphi} + \frac{1}{4}(\mu_I + 2\mu_s)^2 & -i\omega(\mu_I + 2\mu_s)\cos\varphi \\ i\omega(\mu_I + 2\mu_s)\cos\varphi & \omega^2 - k^2 - m_K^2\cos\varphi + \frac{1}{4}(\mu_I + 2\mu_s)^2\cos(2\varphi) \end{pmatrix} \tag{3.156}$$

$$D_{67} = \begin{pmatrix} \omega^2 - k^2 - m_K^2 + \frac{1}{2}\mu_I(\mu_I - 2\mu_s) + (-\frac{1}{4}\mu_I^2 + \mu_s^2)\cos\varphi & -\frac{1}{2}i\omega(-3\mu_I + 2\mu_s + (\mu_I + 2\mu_s)\cos\varphi) \\ \frac{1}{2}i\omega(-3\mu_I + 2\mu_s + (\mu_I + 2\mu_s)\cos\varphi) & \omega^2 - k^2 - m_K^2 + \frac{1}{2}\mu_I(\mu_I - 2\mu_s) + (-\frac{1}{4}\mu_I^2 + \mu_s^2)\cos\varphi \end{pmatrix} \tag{3.157}$$

$$D_{38} = \begin{pmatrix} \omega^2 - k^2 - \frac{m_K^2}{\cos\varphi} & \frac{m_\pi^2 - m_K^2}{\sqrt{3}} \\ \frac{m_\pi^2 - m_K^2}{\sqrt{3}} & \omega^2 - k^2 - \frac{2}{3}m_\pi^2 - \frac{1}{3}m_K^2\cos\varphi \end{pmatrix}. \tag{3.158}$$

In the kaon phase, the equation $\det\{D^{-1}\} = 0$ with $k = 0$ leads to the following masses

$$\begin{aligned} m_{\tilde{\pi}_0}^2 &= \frac{1}{6}\left(\frac{4m_K^4}{(\mu_I + 2\mu_s)^2} - M_{38} + \frac{3\mu_I^2}{4} + 3\mu_I\mu_s + 2m_\pi^2 + 3\mu_s^2\right) \\ m_{\tilde{\pi}_+}^2 &= \frac{8m_K^2\left(\mu_I^2 - 4\mu_s^2\right) - \left|4m_K^2 + (3\mu_I - 2\mu_s)(\mu_I + 2\mu_s)\right| M_{12} + (\mu_I + 2\mu_s)^2\left(5\mu_I^2 - 4\mu_I\mu_s + 8m_\pi^2 + 4\mu_s^2\right) + 16m_K^4}{8(\mu_I + 2\mu_s)^2} \\ m_{\tilde{\pi}_-}^2 &= \frac{8m_K^2\left(\mu_I^2 - 4\mu_s^2\right) + \left|4m_K^2 + (3\mu_I - 2\mu_s)(\mu_I + 2\mu_s)\right| M_{12} + (\mu_I + 2\mu_s)^2\left(5\mu_I^2 - 4\mu_I\mu_s + 8m_\pi^2 + 4\mu_s^2\right) + 16m_K^4}{8(\mu_I + 2\mu_s)^2} \\ m_{\tilde{K}_+}^2 &= 0 \\ m_{\tilde{K}_-}^2 &= \frac{(\mu_I + 2\mu_s)^4 + 48m_K^4}{4(\mu_I + 2\mu_s)^2} \\ m_{\tilde{K}_0}^2 &= \mu_I^2 \\ m_{\tilde{\bar{K}}_0}^2 &= \frac{\left(\mu_I^2 - 4m_K^2 - 4\mu_s^2\right)^2}{4(\mu_I + 2\mu_s)^2} \\ m_{\tilde{\eta}}^2 &= \frac{1}{6}\left(\frac{4m_K^4}{(\mu_I + 2\mu_s)^2} + M_{38} + \frac{3\mu_I^2}{4} + 3\mu_I\mu_s + 2m_\pi^2 + 3\mu_s^2\right) \end{aligned} \tag{3.159}$$

where

$$M_{38} = \sqrt{\left(\frac{3(\mu_I + 2\mu_s)^4 + 16m_K^4}{4(\mu_I + 2\mu_s)^2} + 2m_\pi^2\right)^2 - 6m_\pi^2\left((\mu_I + 2\mu_s)^2 + 4m_K^2 - 2m_\pi^2\right)} \tag{3.160}$$

$$M_{12} = \sqrt{-8m_K^2(\mu_I + 2\mu_s)^2 + 16m_\pi^2(\mu_I + 2\mu_s)^2 + (\mu_I + 2\mu_s)^4 + 16m_K^4}\,. \tag{3.161}$$

The total masses are shown in Figure3.8 for the values $m_\pi = 140$ MeV and $m_K = 495$ MeV. Of course, to display the different phases, the numerical values of the chemical potential μ_s change from plot to plot. In Figure3.8.(a) the values are $\mu_s = 200$ MeV, in Figure3.8.(b) $\mu_s = 550$ MeV while in Figure 3.8.(c) the chosen value is $\mu_s = 460$ MeV.

After this in-depth exploration of two-colour and three-colour QCD, where the baryon and isospin charges are fixed in the former and only the isospin charge in the latter, the chapter comes to an end. The concepts and frameworks introduced here establish a necessary foundation for understanding the material presented in chapter 4, chapter 6 and in chapter 7. These ideas guide the exploration of advanced topics and methods in the previously mentioned chapters.

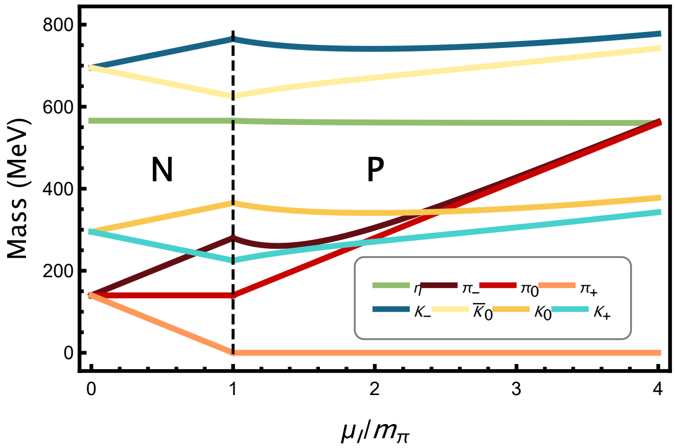

(a) Normal and pion phase for $\mu_s = 200$ MeV.

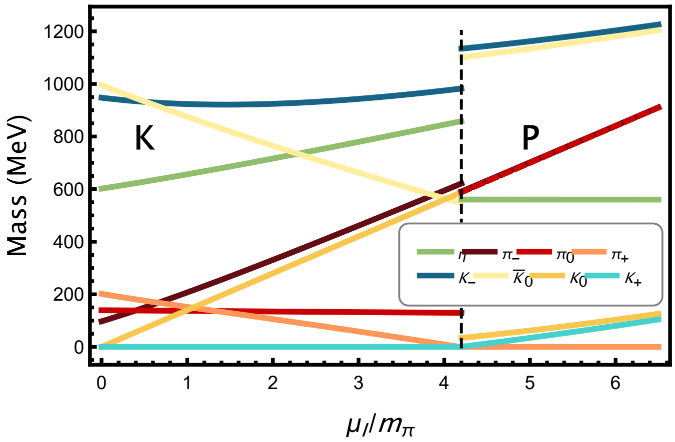

(b) Kaon and pion phase for $\mu_s = 550$ MeV.

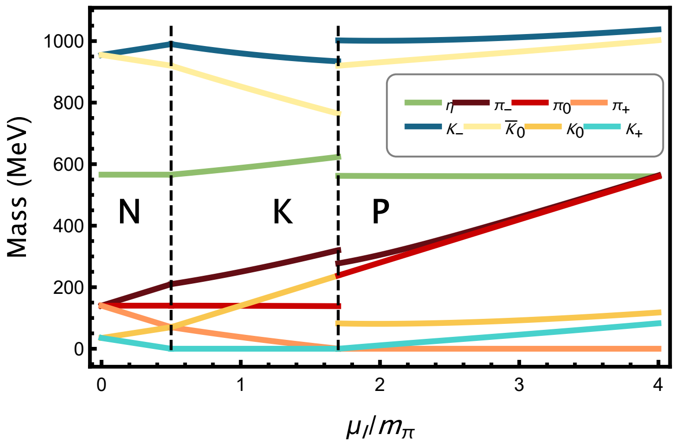

(c) Normal, kaon and pion phase for $\mu_s = 460$ MeV.

Figure 3.8.: Masses of the meson octet obtained for $m_\pi = 140$ MeV and $m_K = 495$ MeV.

4 Chapter

The θ-angle and axion physics of QCD-like theories at non-zero baryon density

With key concepts established in earlier chapters, new findings obtained in [1] are here presented. Precisely, this chapter discusses how the θ-angle and axion dynamics influence two-colour QCD (and more generally any $Sp(2N)$ QCD) when there is a non-zero baryon charge and varying numbers of matter fields. It explores how these factors affect the vacuum properties, chiral symmetry breaking, and the spectrum of the theory. When a CP-violating topological operator is introduced, the vacuum structure becomes more complex, leading to the discovery of new phases. Additionally, the following discussion examines the transitions between these phases, especially concerning whether there are odd or even numbers of flavours. Finally, it identifies the critical chemical potential, depending on the θ-angle, that marks the shift from the normal phase to the superfluid phase of the theory. In support of the discussion, the appendix C provides more details on the θ-angle physics.

§ 4.1 Two-colour chiral Lagrangian

Let us open this chapter with a recollection of useful formulæ introduced in chapter 3. Therefore, following discussion in section 3.3.1 (using the same notation), section 3.3.2 and section 3.3.3, the Lagrangian of N_f Dirac fermions transforming according to the fundamental representation of two-colour QCD reads

$$\mathcal{L} = -\frac{1}{4g^2}F_{\mu\nu}\cdot F^{\mu\nu} + i\bar{Q}\bar{\sigma}^{\nu}\left[\partial_\nu - iF_\nu\cdot\frac{\tau}{2}\right]Q - \frac{1}{2}m_q Q^T\tau_2 EQ + \text{h.c.}\,. \tag{4.1}$$

At zero fermion mass (i.e. $m = 0$) the theory exhibits the classical $U(2N_f)$ symmetry broken at the quantum level by the ABJ anomaly to $SU(2N_f)$. The Dirac mass term breaks explicitly the symmetry to $Sp(2N_f)$ and the $2N_f \times 2N_f$ matrix E reads:

$$E = \begin{pmatrix} 0 & 1 \\ -1 & 0 \end{pmatrix} \otimes \mathbb{1}_{N_f}\,. \tag{4.2}$$

At small number of flavours the dynamics is expected to be strong enough for a fermion condensate to form breaking the $SU(2N_f)$ global symmetry spontaneously to a smaller sub-group expected to be the maximal diagonal one. However, only recently, first-principle lattice simulations have been able to demonstrate this pattern of chiral symmetry breaking in [113] which has been further confirmed in [114] for two Dirac flavours. Increasing the number of flavours the dynamics can change and one expects the existence of a critical number of flavours N_f^{II} above which an IR interacting conformal fixed point emerges (these concepts will be better developed in chapter 5)[1].

For any $2 < N_f < N_f^{II}$ it is therefore natural to expect the pattern of spontaneous symmetry breaking to be $SU(2N_f) \to Sp(2N_f)$. Generalising this theory to arbitrary N while keeping the same global symmetries requires considering $Sp(2N)$ gauge groups[2]. The associated chiral Lagrangian that embodies the previous pattern of symmetry breaking reads [98, 115]

$$\mathcal{L}_{\text{eff}} = \nu^2 Tr\{\partial_\mu \Sigma \partial^\mu \Sigma^\dagger\} + m_\pi^2 \nu^2 Tr\{M\Sigma + M^\dagger \Sigma^\dagger\} \ , \tag{4.3}$$

with Σ transforming linearly under a chiral rotation as

$$\Sigma \to u \Sigma u^T \ , \qquad u \in SU(2N_f) \ , \tag{4.4}$$

and the mass matrix M being

$$M = -i\sigma_2 \otimes \mathbb{1}_{N_f} = \begin{pmatrix} 0 & -1 \\ 1 & 0 \end{pmatrix} \otimes \mathbb{1}_{N_f} \ . \tag{4.5}$$

To take into account a non-vanishing baryon charge, it thus suffices to couple it to a chemical potential μ[3] that can be introduced as the zero component of a background gauge field via the covariant derivative

$$\partial_\mu \mapsto \mathcal{D}_\mu = \partial_\mu - i\mu\delta_\mu^0 B \, , \qquad B \equiv \begin{pmatrix} 1/2 & 0 \\ 0 & -1/2 \end{pmatrix} \otimes \mathbb{1}_{N_f} \ . \tag{4.6}$$

As explained at length in chapter 3, for non-zero μ the Lagrangian is no longer invariant under $SU(2N_f)$ transformations. When the mass term is zero the $SU(2N_f)$ symmetry is explicitly broken as

$$SU(2N_f) \xrightarrow{m=0,\ \mu\neq 0} SU(N_f)_L \times SU(N_f)_R \times U(1)_B \ , \tag{4.7}$$

conversely, for $m \neq 0$ one has

$$SU(2N_f) \xrightarrow{m\neq 0,\ \mu\neq 0} SU(N_f)_V \times U(1)_B \ . \tag{4.8}$$

By using the covariant derivative (4.6) into eq.(4.3), the effective Lagrangian describing

[1] This dynamics has been investigated theoretically [125] and via first-principle lattice simulations [382]. A recent up-to-date review can be found in [99]. It is also being investigated on the lattice [161] searching for the existence of an interacting non-perturbative UV fixed point [160] similar to the one shown to exist in [158, 159] for gauge-Yukawa theories.

[2] The study of these theories and the associated conformal window has been discussed in [125].

[3] Since this chapter focuses on baryon chemical potential only, the μ_B introduced in chapter 3 is here replaced with μ.

the theory at non-zero baryon charge is thus obtained

$$\mathcal{L}_B = v^2 Tr\{\partial_\mu \Sigma \partial^\mu \Sigma^\dagger\} + 4\mu v^2 Tr\{B\Sigma^\dagger \partial_0 \Sigma\} + m_\pi^2 v^2 Tr\{M\Sigma + M^\dagger \Sigma^\dagger\} \\ + 2\mu^2 v^2 \left[Tr\{\Sigma B^T \Sigma^\dagger B\} + Tr\{BB\}\right] \; . \tag{4.9}$$

4.1.1 The θ-angle and the $\mathrm{U}(1)$ problem

To discuss the physics of the θ-angle and of the axial anomaly [?, 268, 269], the topological charge density is introduced (for further details see appendix C)

$$q(x) = \frac{g^2}{64\pi^2}\epsilon^{\mu\nu\rho\sigma} F^a_{\mu\nu} F^a_{\rho\sigma} \; , \tag{4.10}$$

which is incorporated in the effective Lagrangian as

$$\mathcal{L}_{q(x)} = \frac{i}{4} q(x) \mathrm{Tr}\{\log\Sigma - \log\Sigma^\dagger\} - \theta q(x) + \frac{q(x)^2}{4av^2} \; . \tag{4.11}$$

Here the new Σ is related to the old one that transforms only under $SU(2N_f)$ via [266]

$$\Sigma \to \Sigma e^{i\frac{S}{\sqrt{2N_f}}\mathbb{1}_{2N_f}} \; , \tag{4.12}$$

with the S-field a singlet of $SU(2N_f)$ transforming under the anomalous $U(1)_A$, and it is parent to the η' particle in ordinary QCD.

The minimal choice to neglect orders higher than $q^2(x)$ is justified at large number of colours [4]. Here, to keep the same pattern of chiral symmetry breaking the $SU(2)$ of colour generalises to $Sp(2N)$ and not $SU(N)$. The linear term allows accommodating for the $U(1)_A$ anomaly. The coefficient of the quadratic term in $q(x)$ is known as the topological susceptibility of the Yang-Mills theory. The coefficients of these terms are coherently chosen such that the axial anomaly $\partial_\mu J_5^\mu = 4N_f q(x)$ is reproduced in two-colour QCD with quarks in the fundamental representation [266].

Notice that $q(x)$ is a background auxiliary field introduced to implement the anomalous transformation at the action level in a linear fashion. It can, therefore, be integrated out via its equations of motion, yielding the following effective Lagrangian

$$\mathcal{L}_\theta = v^2 Tr\{\partial_\mu \Sigma \partial^\mu \Sigma^\dagger\} + 4\mu v^2 Tr\{B\Sigma^\dagger \partial_0 \Sigma\} + m_\pi^2 v^2 Tr\{M\Sigma + M^\dagger \Sigma^\dagger\} \\ + 2\mu^2 v^2 \left[Tr\{\Sigma B^T \Sigma^\dagger B\} + Tr\{BB\}\right] - av^2 \left(\theta - \frac{i}{4} Tr\{\log\Sigma - \log\Sigma^\dagger\}\right)^2 \; . \tag{4.13}$$

The action of the symmetry groups is summarised in Table 4.1 where the axial generator A in this notation is

$$A = \frac{1}{2}\begin{pmatrix} 1 & 0 \\ 0 & 1 \end{pmatrix} \otimes \mathbb{1}_{N_f} \; . \tag{4.14}$$

[4] See discussion in [266, 402].

	$[SU(2)]$	$SU(N_f)_L$	$\times$	$SU(N_f)_R$	$\times$	$U(1)_V$	$\times$	$U(1)_A$
q_L	$\square$	$\square$		$\mathbf{1}$		$+1$		$+1$
$i\sigma_2\tau_2 q_R^*$	$\square$	$\mathbf{1}$		$\bar{\square}$		-1		$+1$

	$[SU(2)]$	$SU(2N_f)$	$\times$	$U(1)_A$
Q	$\square$	$\square$		$+1$

Table 4.1.: Transformation properties of q_L, $i\sigma_2\tau_2 q_R^*$ and Q under the action of the symmetry groups.

4.1.2 The axion and the baryon charge

For the Standard Model three-colours QCD there is no experimental evidence of strong CP violation. This constrains the associated value of the effective theta angle $\bar{\theta} = \theta + \arg\det(M)$, with M the physical quark mass matrix, to be $\bar{\theta} < 10^{-10}$. The limit comes from the bound on the neutron electric dipole moment $|d_n| = C_{\rm EDM} e\,\bar{\theta} < 1.8 \times 10^{-26} e$ cm [100, 101], where $C_{\rm EDM} = 2.4(1.0) \times 10^{-16}$ cm [403] is related to the effective nucleon interactions with the axion explained in the appendix of [266].

From a theoretical viewpoint, a tiny value of a physical parameter unprotected by any symmetry requires an explanation. One solution for the so-called strong CP problem was proposed in the 70s by R. Peccei and H. Quinn [367,368] (see appendix C). The proposal makes use of an additional $U(1)_{PQ}$ symmetry which is quantum mechanically anomalous and spontaneously broken leading to the axion as an extra (pseudo-)Goldstone boson. Axion physics has led to a great deal of both theoretical and phenomenological work including active experimental searches beyond the original QCD axion [404]. An alternative solution to the strong CP problem featuring new composite dynamics and heavier (if not completely absent) axions was proposed in [111] and reconsidered in [112] and applied extensively in model building in [419–421].

Of course, when discussing the θ-angle physics here, depending on the physical application of the model, one can allow for new sources of CP breaking, perhaps relevant for some models of dark matter or Standard Model secluded sectors [404]. Nevertheless, it is interesting to entertain the possibility that an axion is present in the theory and therefore explore its finite chemical potential dynamics and impact. Here, v_{PQ} denotes the scale of $U(1)_{PQ}$ spontaneous symmetry breaking and a_{PQ} denotes the coefficient of the $U(1)_{PQ}$ anomalous term. To include the axion in this theory, (4.13) is extended to the following effective Lagrangian

$$\mathcal{L}_{\hat{a}} = v^2 Tr\{\partial_\mu\Sigma\partial^\mu\Sigma^\dagger\} + v_{PQ}^2\partial_\mu\mathcal{N}\partial^\mu\mathcal{N}^\dagger + 4\mu v^2 Tr\{B\Sigma^\dagger\partial_0\Sigma\} + m_\pi^2 v^2 Tr\{M\Sigma + M^\dagger\Sigma^\dagger\}$$
$$+ 2\mu^2 v^2\left[Tr\{\Sigma B^T\Sigma^\dagger B\} + Tr\{BB\}\right] - a v^2\left(\theta - \frac{i}{4}Tr\{\log\Sigma - \log\Sigma^\dagger\} - \frac{i}{4}a_{PQ}(\log\mathcal{N} - \log\mathcal{N}^\dagger)\right)^2 . \tag{4.15}$$

The details on how to construct the extended effective theory can be found in [266] and are reviewed in appendix C.

§ 4.2 Determining the Vacuum

The focus of this section is on the vacuum structure of theory (4.13) in the presence of the θ-angle and finite baryon charge. In particular, there will first be the study of the general conditions that determine the classical vacuum solution as a function of θ and μ. Armed with these results, there will be a careful analysis of the properties of the vacuum in the concrete cases $N_f = 2, 3, 6, 7, 8$ and N_f arbitrary. To begin with, first notice that for vanishing θ the vacuum is determined by the competition of mass and baryon chemical potential, as previously explained in chapter 3 at length. In other words, the ground state can be written as [180]

$$\Sigma_c = \begin{pmatrix} 0 & \mathbb{1}_{N_f} \\ -\mathbb{1}_{N_f} & 0 \end{pmatrix} \cos\varphi + i \begin{pmatrix} J & 0 \\ 0 & J \end{pmatrix} \sin\varphi \qquad \text{where} \qquad J = \begin{pmatrix} 0 & -\mathbb{1}_{N_f/2} \\ \mathbb{1}_{N_f/2} & 0 \end{pmatrix}, \tag{4.16}$$

where the angle φ is determined by the equations of motion.

To study the effect of θ on the vacuum solutions it is convenient to introduce the Witten variables α_i as [260]

$$\Sigma_0 = U(\alpha_i)\Sigma_c\,, \qquad U(\alpha_i) \equiv \mathrm{diag}\{e^{-i\alpha_1}, \ldots, e^{-i\alpha_{N_f}}, e^{-i\alpha_1}, \ldots, e^{-i\alpha_{N_f}}\}\,. \tag{4.17}$$

These variables reflect the possibility to generalise the mass matrix in (4.5) by replacing the $\mathbb{1}_{N_f}$ with $\mathrm{diag}\{e^{-i\alpha_1}, \ldots, e^{-i\alpha_{N_f}}\}$. Each phase is the overall axial transformation for each left-right quark pair. The reason why one cannot consider a single (odd number of) Weyl fermion(s) at the time (as is the case for real gauge representations) is that one cannot write a mass term in this case and the theory overall suffers from a topological anomaly [394].

The above is taken to be the general ansatz for the vacuum. The Lagrangian evaluated on this ansatz reads

$$\mathcal{L}_\theta[\Sigma_0] = \nu^2 \left[4m_\pi^2 X \cos\varphi + 2\mu^2 N_f \sin^2\varphi - a\bar{\theta}^2\right] \tag{4.18}$$

where for later convenience, the following quantities have been introduced

$$\bar{\theta} = \theta - \sum_i^{N_f} \alpha_i\,, \qquad X = \sum_i^{N_f} \cos\alpha_i \tag{4.19}$$

where $\bar{\theta}$ is the effective theta angle that enters physical observables.

The equations of motion read

$$\sin\varphi \left(N_f \cos\varphi - \frac{m_\pi^2}{\mu^2} X\right) = 0 \tag{4.20}$$

$$2m_\pi^2 \sin\alpha_i \cos\varphi = a\bar{\theta}\,, \quad i = 1, .., N_f \tag{4.21}$$

and the energy density of the system is

$$\mathcal{E} = -v^2 \left[4m_\pi^2 X - a\bar{\theta}^2\right] , \qquad \text{normal phase } (\varphi = 0) \tag{4.22}$$

$$\mathcal{E} = -v^2 \left[2\frac{N_f^2\mu^4 + m_\pi^4 X^2}{N_f\mu^2} - a\bar{\theta}^2\right] , \qquad \text{superfluid phase } \left(\cos\varphi = \frac{m_\pi^2}{N_f\mu^2}X\right) . \tag{4.23}$$

Note that when $a \gg m_\pi$ all the θ-dependence is contained in an effective pion mass $m_\pi^2(\theta) \equiv \frac{m_\pi^2 X}{N_f}$. For $\theta = 0$ (i.e. $U(\alpha_i) = \mathbb{1}$) one has $X = N_f$ and $\bar{\theta} = 0$, and one recovers the results in [180], reviewed in chapter 3. In this case, a normal to superfluid phase transition occurs when $\mu = m_\pi$, i.e. when $\cos\varphi = 1$. For $\theta \neq 0$ the θ-dependence of the energy may be different in the two phases.

Therefore, to find the conditions for the onset of the superfluid phase, one first needs to determine the θ vacuum in both phases. To this end, first observe that in the normal (superfluid) phase the energy density is minimised when X (X^2) is minimised.

In the former case, the Witten variables are related to θ by the well-known equation

$$2m_\pi^2 \sin\alpha_i = a\bar{\theta} = a\left(\theta - \sum_i^{N_f} \alpha_i\right) . \tag{4.24}$$

For the general solution there must be for any $\bar{\theta}$ fixed $\sin\alpha_i = \sin\alpha_j$. To solve for the α_i, the expansion in the parameter $\frac{m_\pi^2}{a}$ is considered and taken to be small. Concretely, at the leading order one needs to solve for $\bar{\theta} = 0$ and the angles α_i satisfy

$$\alpha_i = \begin{cases} \pi - \alpha, & i = 1, \ldots, n \\ \alpha, & i = n+1, \ldots, N_f \end{cases} \tag{4.25}$$

where α is the solution of the following modular equation

$$n(\pi - \alpha) + (N_f - n)\alpha = \theta \text{ Mod } 2\pi . \tag{4.26}$$

The modulo comes from the fact that if a solution $\{\alpha_i\}$ of eq.(4.24) is found, then it is possible to build another solution as follows

$$\alpha_1(\theta + 2\pi) = \alpha_1(\theta) + 2\pi , \qquad \alpha_i(\theta + 2\pi) = \alpha_i(\theta) , \quad i = 2, \ldots, N_f . \tag{4.27}$$

However, since the physics depends only on $e^{-i\alpha_i}$, the dynamics is invariant under $\theta \to \theta + 2\pi$. The solution of eq.(4.26) can be written as

$$\alpha = \frac{\theta + (2k - n)\pi}{(N_f - 2n)}, \quad k = 0, \ldots, N_f - 2n - 1 , \quad n = 0, ..., \left[\frac{N_f - 1}{2}\right] . \tag{4.28}$$

The range for k above emerges because for $k \geq N_f - 2n$, the solution for a given n is repeated. Additionally, when $n \neq 0$, the vacuum spontaneously breaks $Sp(2N_f)$ because of the different phases for each quark flavour.

It is well-known that CP is preserved when $\bar{\theta} = 0$. For equal mass quarks as considered here, this happens when $m_\pi = 0$ or $\theta = 0$. On the other hand, for $\theta = \pi$ the Lagrangian (4.13) possesses CP symmetry but in the normal phase the latter is spontaneously broken by the vacuum [262, 265, 266, 362] [5], leading to a strong θ-dependence near $\theta = \pi$. In fact, assuming that the ground state does not break $Sp(2N_f)$ spontaneously (i.e. $n = 0$), the vacua lie at [262]

$$U(\alpha_i) = e^{i\frac{\theta+2\pi k}{N_f}}\, \mathbb{1}_{2N_f} \,. \tag{4.29}$$

For $\theta = \pi$ one has $X = \cos\left(\frac{(2k+1)\pi}{N_f}\right)$, which is minimised when $k = 0$ and $k = N_f - 1$, that is

$$U(\alpha_i) = e^{\frac{i\pi}{N_f}}\, \mathbb{1}_{2N_f} \,, \qquad U(\alpha_i) = e^{-\frac{i\pi}{N_f}}\, \mathbb{1}_{2N_f} \,. \tag{4.30}$$

The two solutions are related by a CP transformation $U \to U^\dagger$ and thus CP is spontaneously broken. For $N_f > 2$ the minima are separated by an energy barrier while for $N_f = 2$ the leading order quark-mass induced potential vanishes[6], apparently leading to a paradoxical situation according to which one has massless pions and no explicit breaking of chiral symmetry.

The paradox is simply resolved by going to higher orders in the mass for the chiral Lagrangian. Once these corrections are taken into account they lift, as expected, the vacuum degeneracy yielding two minima separated by a barrier [263, 264].

The spontaneous breaking of CP at $\theta = \pi$ is known as Dashen's phenomenon [265] and has been thoroughly studied in the literature [260, 262–264, 362, 393, 422]. As will be later shown, in the superfluid phase CP may be violated or not at $\theta = \pi$ depending on the value of N_f. Once determined the α_i to the leading order in $\frac{a}{m_\pi^2}$, subleading corrections can be more easily computed.

Note that in the superfluid phase the equation of motion (4.21) becomes

$$\frac{2m_\pi^4}{N_f \mu^2} X \sin\alpha_i = a\bar{\theta} \,, \qquad i = 1, .., N_f. \tag{4.31}$$

Hence, in this case, the natural expansion parameter is $\frac{m_\pi^4}{a\mu^2}$ leading to an enhanced suppression compared to the normal phase.

This section is concluded by considering specific values of N_f to cover most of the phase diagram for which chiral symmetry is expected to break spontaneously.

4.2.1 $N_f = 2$

The starting scenario is that of $N_f = 2$ which has been previously considered in [163] at the leading order in $\frac{m_\pi^2}{a}$. In this limit, the two angles $\{\alpha_1, \alpha_2\}$ satisfy $\alpha_1 + \alpha_2 = \theta + 2k\pi$. Additionally, because $\sin\alpha_1 = \sin\alpha_2$:

$$\sin\alpha_1 = \sin\left(\theta + 2k\pi - \alpha_1\right) \tag{4.32}$$

[5] See also the discussion about the impact on the $\theta = \pi$ solution due to quark masses ordering provided in the appendix of [266].

[6] As well explained in the work by Smilga [263] this phenomenon occurs because the trace of $SU(2)$ matrices are real.

yielding the solutions

$$\sin\alpha_1 = \sin\alpha_2 = \sin\left(\frac{\theta}{2} + k\pi\right). \tag{4.33}$$

Only $k = 0$ and $k = 1$ are independent solutions of the equations of motion and agree with the general result in equation (4.28) for the α_i for $N_f = 2$ that has the two solutions corresponding to $n = 0$ and $k = 0, 1$ (i.e. $\{\alpha_1, \alpha_2\} = \{\frac{\theta}{2}, \frac{\theta}{2}\}$ and $\{\alpha_1, \alpha_2\} = \{\frac{\theta+2\pi}{2}, \frac{\theta+2\pi}{2}\}$).

To determine the solution corresponding to the ground state for any value of θ one needs to consider the ground state energy. In the normal phase, the energy is linear in X and therefore the original equation of motion's solutions cross at $\theta = \pi$ where Dashen's phenomenon occurs stemming from spontaneous CP symmetry breaking. Because in the superfluid phase the ground state energy is proportional to X^2, the two solutions are identical yielding a degenerate ground state. Interestingly, this degeneracy is not lifted by higher-order corrections in $\frac{m_\pi^2}{a}$. The θ-dependence in the two phases is shown in Figure 4.1.

Additionally, when $\theta = \pi$ the effective mass $m_\pi^2(\theta) \sim m_\pi^2\left|\cos\left(\frac{\theta}{2}\right)\right|$ vanishes up to the correction of order $O\left(\frac{m_\pi^2}{a}\right)$. Therefore, the mass term disappears from the Lagrangian and the global flavour symmetry is again $SU(4)$ consequently leading to massless Goldstones when it spontaneously breaks to $Sp(4)$ [163]. Nevertheless, there is no chiral symmetry restoration in the fundamental Lagrangian. As mentioned, this apparent paradox is solved by realising that $SU(4)$ is still broken by higher-order mass terms in the effective Lagrangian also for $a \to \infty$ [163, 262, 263].

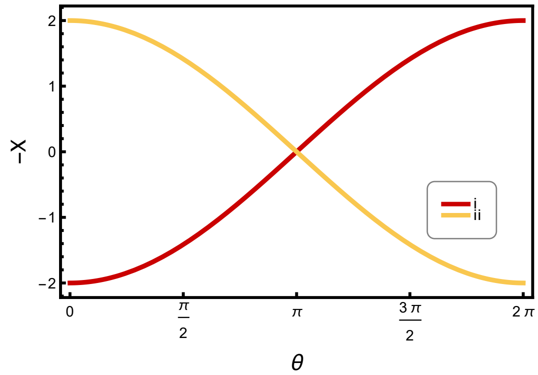

(a) θ-dependence of the energy in the normal phase for $N_f = 2$.

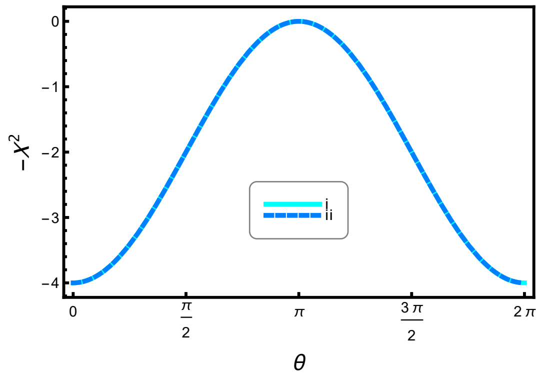

(b) θ-dependence of the energy in the superfluid phase for $N_f = 2$.

Figure 4.1.: θ-dependence of the energy for $N_f = 2$.

By including the first two subleading corrections in $\frac{m_\pi^2}{a}$, the energy density in the two phases reads

$$\mathcal{E}(\theta) = -8m_\pi^2\nu^2\left(\left|\cos\frac{\theta}{2}\right| + \frac{1}{2}\frac{m_\pi^2}{a}\sin^2\frac{\theta}{2} - \frac{1}{4}\frac{m_\pi^4}{a^2}\left|\sin\frac{\theta}{2}\sin\theta\right|\right), \quad \text{normal phase} \tag{4.34}$$

$$\mathcal{E}(\theta) = -\nu^2\left(\frac{4\left(m_\pi^4\cos^2\frac{\theta}{2} + \mu^4\right)}{\mu^2} + \frac{m_\pi^8\sin^2\theta}{a\mu^4} - \frac{m_\pi^{12}\sin^2\theta\cos\theta}{a^2\mu^6}\right), \quad \text{superfluid phase}\,. \tag{4.35}$$

At fixed quark masses, the superfluid phase transition occurs at a critical value of the chemical potential given by

$$\mu_c = m_\pi(\theta) = m_\pi \left[\sqrt{\left| \cos\frac{\theta}{2} \right|} + O\left(\frac{m_\pi^2}{a}\right) \right], \tag{4.36}$$

implying that it can be realised for tiny values of the chemical potential when $\theta \sim \pi$. To estimate μ_c in the region $\theta \sim \pi$, $\phi \equiv \theta - \pi$ is introduced and the leading correction in $\frac{m_\pi^2}{a}$ is taken into account. As a result, for small $|\phi|$ the critical chemical potential in the region $\theta \sim \pi$ reads

$$\mu_c \sim m_\pi \sqrt{\frac{m_\pi^2}{a} + \frac{|\phi|}{2}}, \tag{4.37}$$

and vanishes for $a \to \infty$ and $\phi \to 0$.

Still, in the superfluid phase the energy is an analytic function of θ. This can be better appreciated by analysing the CP order parameter $\langle F\tilde{F}\rangle \propto -\frac{\partial E}{\partial \theta}$ shown in Figure 4.2 for the two phases. The normal phase is characterised by a discontinuous CP order parameter at $\theta = \pi$ while it is clear from Figure 4.2.(b) that the superfluid phase displays a smooth behaviour for any value of the θ-angle and vanishes for $\theta = \pi$.

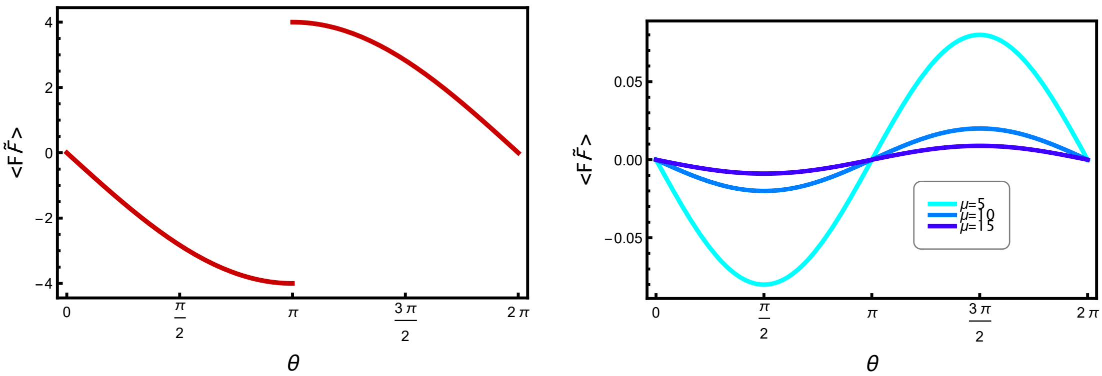

(a) CP order parameter for $N_f = 2$ in the normal phase.

(b) CP order parameter for $N_f = 2$ in the superfluid phase.

Figure 4.2.: CP order parameter as a function of θ both in the normal and superfluid phase for $N_f = 2$.

The discontinuity of the CP order parameter in the normal phase translates into a divergent topological susceptibility $\chi = \dfrac{\partial^2 E}{\partial \theta^2}$ at $\theta = \pi$. Note that the presence of the baryon chemical potential suppresses CP violation for every value of θ as can be seen from Figure 4.2.(b).

Finally, the effective $\bar{\theta}$ angle for $\theta = \pi$ is now studied at higher-orders in $\frac{m_\pi^2}{a}$ for the solutions of the equations of motion. The overall result is

$$\bar{\theta} = \frac{2m_\pi^2}{a} \sin\frac{\theta}{2} \underset{\theta=\pi}{=} \frac{2m_\pi^2}{a} + O\left(\frac{m_\pi^6}{a^3}\right), \qquad \text{normal phase} \tag{4.38}$$

$$\bar{\theta} = \frac{m_\pi^4}{a\mu^2} \sin\theta \underset{\theta=\pi}{=} 0, \qquad \text{superfluid phase}. \tag{4.39}$$

Note that eq.(4.39) is exact to all orders in $\frac{m_\pi^4}{a\mu^2}$ since the equation of motion (4.31) becomes

$$\frac{m_\pi^4}{a\mu^2}\sin(2\alpha) = \pi - 2\alpha\,, \tag{4.40}$$

and has the solution $\alpha = \pi/2$ (equivalent to $\alpha = 3\pi/2$ under a shift $\theta \to \theta + 2\pi$). Therefore to the present order in the chiral expansion, there is no spontaneous CP symmetry breaking in the superfluid phase for $\theta = \pi$.

4.2.2 $N_f = 3$

Compared to the previous subsection, the $N_f = 3$ case leads to a richer vacuum structure as has been first pointed out in [263], who studied the physics in the normal phase. In fact, the followings are the four solutions for the set $\{\alpha_i\} = \{\alpha_1\,, \alpha_2\,, \alpha_3\}$

$$\textbf{i.}\left\{\frac{\theta}{3}, \frac{\theta}{3}, \frac{\theta}{3}\right\}, \quad \textbf{ii.}\left\{\frac{\theta+2\pi}{3}, \frac{\theta+2\pi}{3}, \frac{\theta+2\pi}{3}\right\}, \quad \textbf{iii.}\left\{\frac{\theta+4\pi}{3}, \frac{\theta+4\pi}{3}, \frac{\theta+4\pi}{3}\right\}, \quad \textbf{iv.}\left\{\theta-\pi\,, \theta-\pi\,, 2\pi-\theta\right\}. \tag{4.41}$$

In Figure 4.3.(a) is shown the value of the variable $-X$ as a function of θ. Recalling that in the normal phase, the energy is minimised when X is maximised, the physical vacuum is ruled by the solutions **i.** and **iii.** which cross at $\theta = \pi$ where Dashen's phenomenon occurs [263].

In the superfluid phase, the story changes since now the minimum of energy is achieved when X^2 is maximised. The situation is depicted in Figure 4.3.(b): here the relevant solutions are **i.**, **ii.**, **iii.**. Solutions **i.** and **ii.** cross at $\theta = \frac{\pi}{2}$ whereas **ii.** and **iii.** cross at $\theta = \frac{3\pi}{2}$. Therefore, at $\theta = \pi$ there is a unique minimum and CP is conserved. In other words, Dashen's phenomenon at $\theta = \pi$ is again absent in the superfluid region. However, two new non-analytic points occur, one at $\theta = \frac{\pi}{2}$ and the other at $\theta = \frac{3\pi}{2}$. These are indications of two novel first-order phase transitions because the derivative of the free energy (corresponding to the CP order parameter $\left\langle F\widetilde{F}\right\rangle$) jumps at these two values of θ.

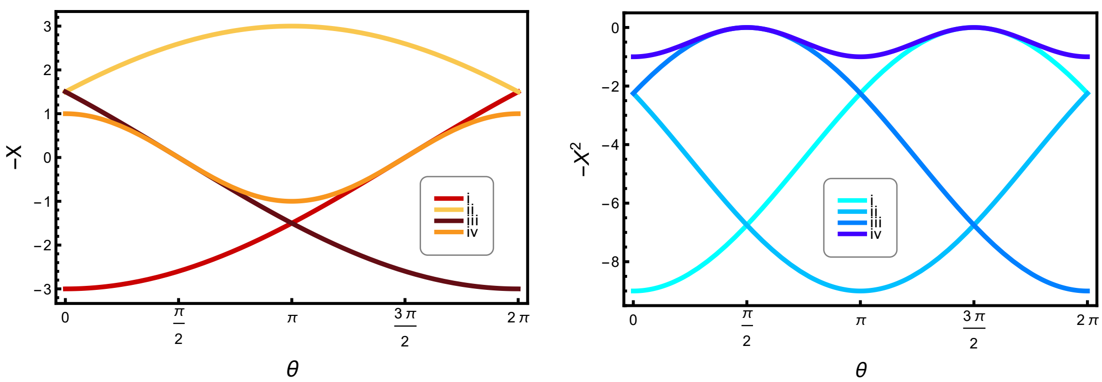

(a) θ-dependence of the energy in the normal phase for $N_f = 3$.

(b) θ-dependence of the energy in the superfluid phase for $N_f = 3$.

Figure 4.3.: θ-dependence of the energy for $N_f = 3$.

Having determined the θ-vacuum in the two regions, the gaze is now turned to study the transition between the normal and superfluid phases. Since the $U(\alpha_i)$ that minimises the energy depends on θ and differs in the two phases, one should determine the critical μ by comparing the energies (4.22) and (4.23) in the given intervals of θ. Specifically, when the superfluid solution exists (i.e. $\cos\varphi \leq 1$) it is always realised. In turn, the critical chemical potential is $\mu_c = m_\pi(\theta)$, which is displayed in Figure 4.4. Differently from the $N_f = 2$ case, μ_c exhibits a mild dependence on θ and oscillates near the value $\mu_c = m_\pi$.

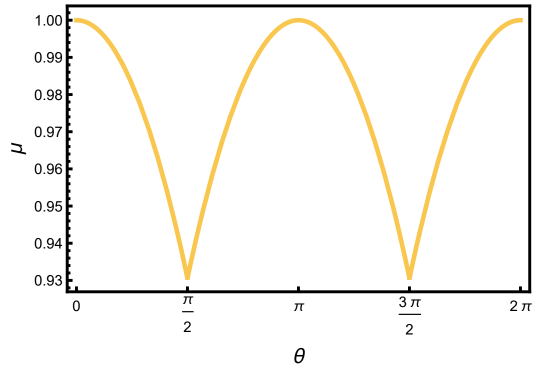

Figure 4.4.: Normalized critical chemical potential ($m_\pi = \nu = 1$) above which the superfluid phase is realised as a function of θ for $N_f = 3$.

The CP order parameter is plotted for the normal and superfluid phases in Figure 4.5 (a) and Figure 4.5 (b), respectively.

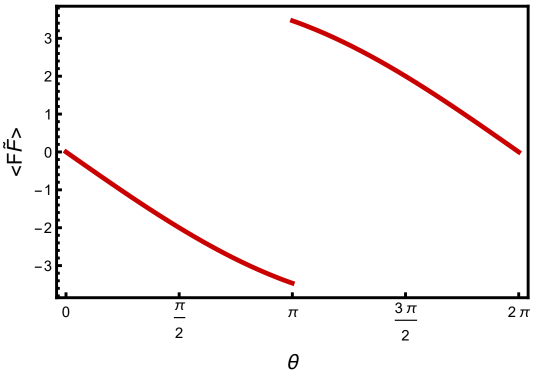

(a) The CP order parameter $\langle F\tilde{F}\rangle$ as a function of θ in the normal phase. Here $m_\pi = \nu = 1$.

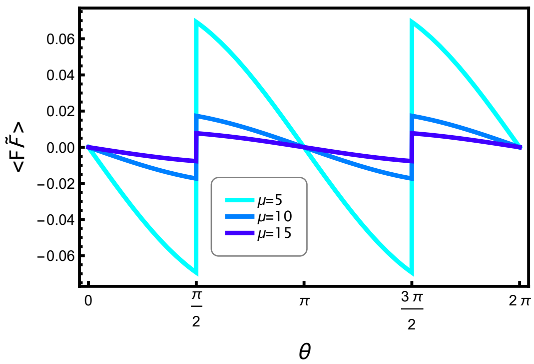

(b) The CP order parameter $\langle F\tilde{F}\rangle$ as a function of θ in the superfluid phase for different values of the chemical potential: $\mu = 5, 10, 15$. Here $m_\pi = \nu = 1$.

Figure 4.5.: θ-dependence of the CP order parameter for $N_f = 3$.

Finally, the value of $\bar{\theta}$ at $\theta = \pi$ for the ground state energy is shown. Precisely, the expression in the $\frac{m_\pi^2}{a}$ expansion is

$$\bar{\theta} = \frac{\sqrt{3}m_\pi^2}{a} - \frac{m_\pi^4}{\sqrt{3}a^2} - \frac{m_\pi^6}{6\sqrt{3}a^3} + \mathcal{O}\left(\frac{m_\pi^8}{a^4}\right), \qquad \text{normal phase} \tag{4.42}$$

$$\bar{\theta} = 0, \qquad \text{superfluid phase}\,. \tag{4.43}$$

4.2.3 $N_f = 6$

For the case of $N_f = 6$ let us, at first, assume that chiral symmetry breaking occurs away from a potential nearby (as a function of flavours) conformal phase (as it will discussed in chapter 5 and in chapter 7). The full set of solutions is given by

$$\begin{aligned}
&\text{Solutions i-vi}: \alpha_1 = \alpha_2, \cdots = \alpha_6 = \frac{\theta + 2\pi k}{6}, && && k = 0, \dots, 5 \\
&\text{Solutions vii-ix}: \alpha_1 = \alpha_2 = \cdots = \alpha_5 = \frac{\theta - \pi + 2\pi k}{4}, && \alpha_6 = \pi - \alpha_1, && k = 0, \dots, 3 \\
&\text{Solutions x-xii}: \alpha_1 = \alpha_2 = \cdots = \alpha_4 = \frac{\theta - 2\pi + 2\pi k}{2}, && \alpha_5 = \alpha_6 = \pi - \alpha_1, && k = 0, 1 .
\end{aligned} \tag{4.44}$$

Here the relevant solutions for $U(\alpha_i)$ have $\alpha_1 = \alpha_2 = \cdots = \alpha_6 = \alpha$. Moreover, all the solutions appear in pairs of degenerate energy in the superfluid phase as already observed in the $N_f = 2$ case.
This can be understood by noting that when N_f is even, then from a given solution α of eq.(4.28) it is possible to build another solution as $\alpha + \pi$ that will lead to the same $-X^2$.

As displayed in Figure 4.6.(a), in the normal phase the minimum of the energy is achieved for $\alpha = \frac{\theta}{6}$ (defined as solution i) and $\alpha = \frac{\theta + 10\pi}{6}$ (solution iii) with the two solutions crossing at $\theta = \pi$. This occurs also in the superfluid phase but now solution i and iii are degenerate for every value of θ with $\alpha = \frac{\theta}{6} + \pi$ and $\alpha = \frac{\theta + 4\pi}{6}$, respectively. In Figure 4.6.(b) the phase diagram of the theory as a function of θ and μ is shown. Differently from $N_f = 2$, there is still a Dashen phenomenon at $\theta = \pi$ and therefore CP breaks spontaneously for this value.

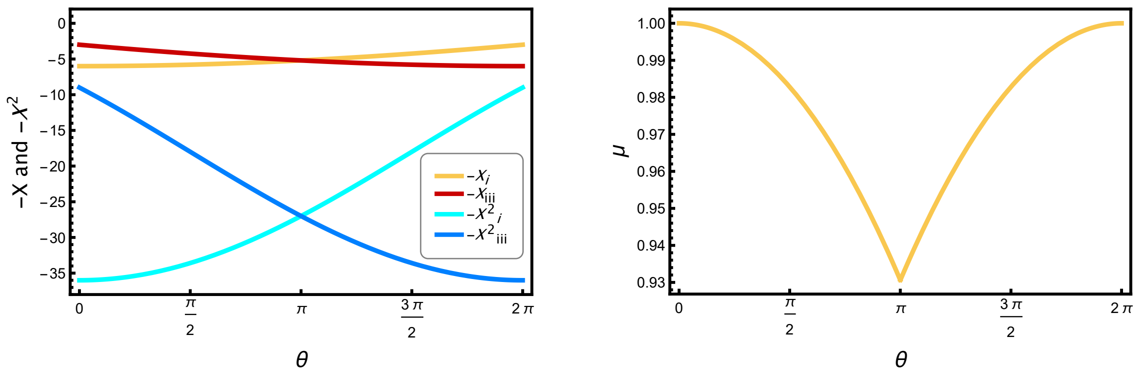

(a) θ-dependence of the energy for $N_f = 6$ both in the normal and superfluid phase.

(b) Normalized critical chemical potential ($m_\pi = \nu = 1$) above which the superfluid phase is realised as a function of θ.

Figure 4.6.: θ-dependence of the energy and of the critical chemical potential for $N_f = 6$.

Therefore, in the $N_f = 6$ case there is spontaneous breaking of CP at $\theta = \pi$ in both phases as can be seen considering the CP order parameter represented in Figure 4.7.(a) and Figure 4.7.(b).

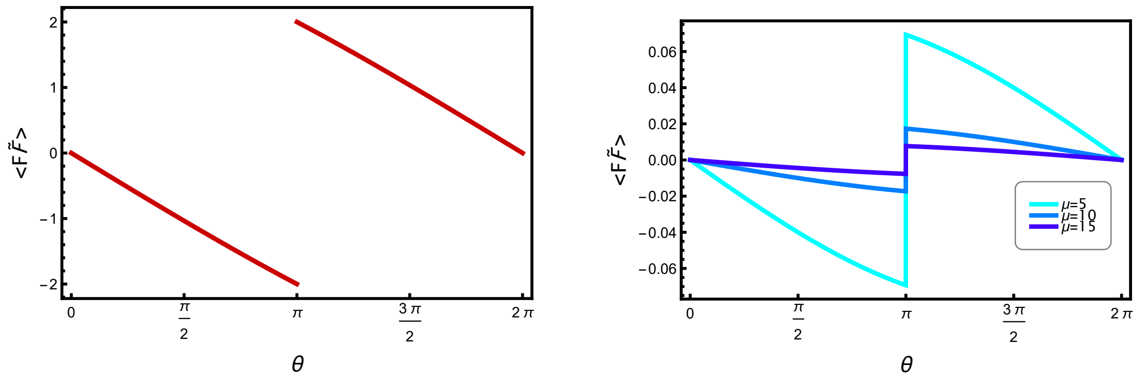

(a) The CP order parameter $\langle F\tilde{F}\rangle$ as a function of θ in the normal phase. Here $m_\pi = \nu = 1$.

(b) The CP order parameter $\langle F\tilde{F}\rangle$ as a function of θ in the superfluid phase for different values of the chemical potential: $\mu = 5, 10, 15$. Here $m_\pi = \nu = 1$.

Figure 4.7.: θ-dependence of the CP order parameter for $N_f = 6$.

Finally, the value of $\bar{\theta}$ at $\theta = \pi$ expanded in $\frac{m_\pi^2}{a}$ reads

$$\bar{\theta} = \frac{m_\pi^2}{a} - \frac{m_\pi^4}{2\sqrt{3}a^2} + \frac{5m_\pi^6}{72a^3} + \mathcal{O}\left(\frac{m_\pi^8}{a^4}\right), \qquad \text{normal phase} \tag{4.45}$$

$$\bar{\theta} = -\frac{\sqrt{3}m_\pi^4}{2a\mu^2} + \frac{m_\pi^8}{4\sqrt{3}a^2\mu^4} + \frac{m_\pi^{12}}{48\sqrt{3}a^3\mu^6} + \mathcal{O}\left(\frac{m_\pi^{16}}{a^4\mu^8}\right), \qquad \text{superfluid phase .} \tag{4.46}$$

4.2.4 $N_f = 7$

For the $N_f = 7$ case, there are 16 solutions of eq.(4.28) which are given by

$$\begin{aligned}
\text{Solutions i-vii}: &\ \alpha_1 = \alpha_2, \cdots = \alpha_7 = \frac{\theta + 2\pi k}{7}, && k = 0, \ldots, 6\\
\text{Solutions viii-xii}: &\ \alpha_1 = \alpha_2 = \cdots = \alpha_5 = \frac{\theta - \pi + 2\pi k}{5}, \quad \alpha_6 = \alpha_7 = \pi - \alpha_1\,, && k = 0, \ldots, 4\\
\text{Solutions xiii-xv}: &\ \alpha_1 = \alpha_2 = \alpha_3 = \frac{\theta - 2\pi + 2\pi k}{3}, \quad \alpha_4 = \alpha_5 = \alpha_6 = \alpha_7 = \pi - \alpha_1, && k = 0, \ldots, 2\\
\text{Solution xvi}: &\ \alpha_1 = \theta - 3\pi, \quad \alpha_2 = \alpha_3 = \cdots = \alpha_7 = \pi - \alpha_1\ .
\end{aligned} \tag{4.47}$$

The solution that minimises the energy and their corresponding θ-dependence in the two phases is shown in Figure 4.8. As in the previous cases, the solutions that minimise the energy have all equal angles, corresponding here to the first set of solutions in (4.47). In particular, in the normal phase the minimum of the energy is achieved for $\alpha = \frac{\theta}{7}$ and $\alpha = \frac{\theta+12\pi}{7}$ with the two solutions crossing at $\theta = \pi$ (in Figure 4.8.(a)).
The θ-dependence in the superfluid phase is analogous to the $N_f = 3$ case. In fact, the relevant solutions are $\alpha = \frac{\theta}{7}$, $\alpha = \frac{\theta+6\pi}{7}$, and $\alpha = \frac{\theta+12\pi}{7}$ with the first two crossing at $\theta = \frac{\pi}{2}$ while the second and the third at $\theta = \frac{3\pi}{2}$. As already described in the $N_f = 3$ subsection, the energy is characterised by a unique minimum and CP intact symmetry at $\theta = \pi$.

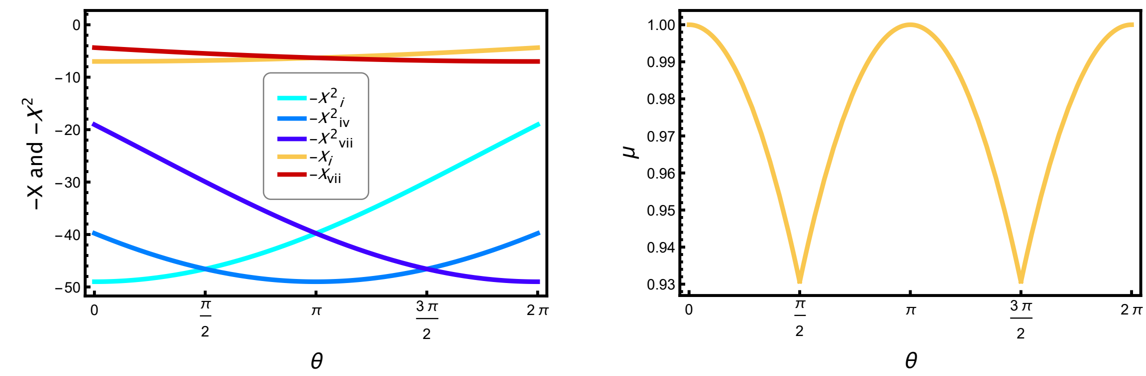

(a) θ-dependence of the energy for $N_f = 7$ both in the normal and superfluid phase.

(b) Normalized critical chemical potential ($m_\pi = \nu = 1$) above which the superfluid phase is realised as a function of θ.

Figure 4.8.: θ-dependence of the energy and of the critical chemical potential for $N_f = 7$.

The critical chemical potential is shown in Figure 4.8.(b). It oscillates with period 2π between the values $\mu_c = m_\pi$ and $\mu_c = m_\pi(\theta)$. Figure 4.8 leads to further investigate the physical meaning of the $\theta = \frac{\pi}{2}$ and $\theta = \frac{3\pi}{2}$ points. As a consequence, the CP order parameter is analysed and shown in Figure 4.9 as a function of θ. As can be seen in the figure, the aforementioned points are actually points of discontinuity of the CP order parameter. Therefore, it signals the occurrence of a first-order phase transition.

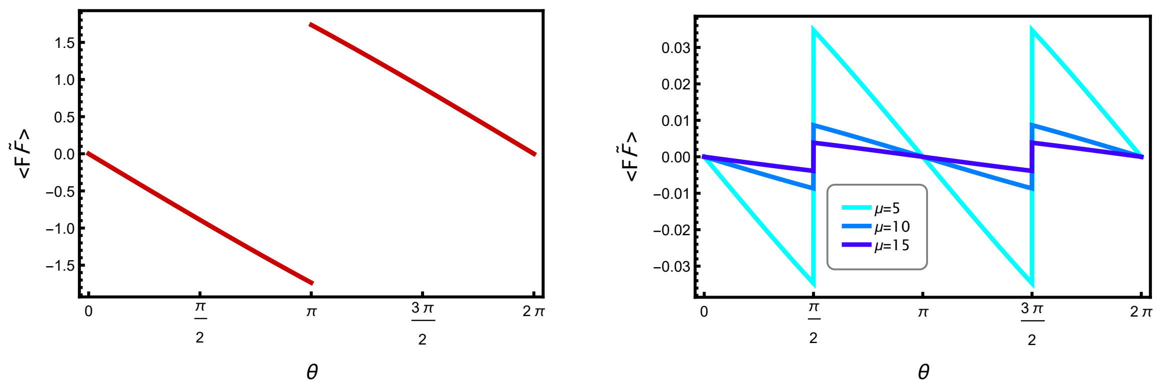

(a) The CP order parameter $\langle F\tilde{F}\rangle$ as a function of θ in the normal phase. Here $m_\pi = \nu = 1$.

(b) The CP order parameter $\langle F\tilde{F}\rangle$ as a function of θ in the superfluid phase for different values of the chemical potential: $\mu = 5, 10, 15$. Here $m_\pi = \nu = 1$.

Figure 4.9.: θ-dependence of the CP order parameter for $N_f = 7$.

Finally, the values of $\bar{\theta}$ at $\theta = \pi$ in the $\frac{m_\pi^2}{a}$ expansion are

$$\bar{\theta} = \frac{2m_\pi^2 \sin\frac{\pi}{7}}{a} - \frac{2m_\pi^4 \cos\frac{3\pi}{14}}{7a^2} + \frac{2m_\pi^6 \sin\frac{\pi}{7}\left(1 + 3\sin\frac{3\pi}{14}\right)}{49a^3} + O\left(\frac{m_\pi^8}{a^4}\right), \qquad \text{normal phase} \tag{4.48}$$

$$\bar{\theta} = 0, \qquad \text{superfluid phase}\,. \tag{4.49}$$

4.2.5 $N_f = 8$

The general expression for the solutions of (4.28) for the $N_f = 8$ case read

$$
\begin{aligned}
\text{Solutions i-viii} : \alpha_1 = \cdots = \alpha_8 &= \frac{\theta + 2\pi k}{8}, & & k = 0, \ldots, 7 \\
\text{Solutions ix-xiv} : \alpha_1 = \cdots = \alpha_6 &= \frac{\theta - \pi + 2\pi k}{6}, & \alpha_7 = \alpha_8 = \pi - \alpha_1, & k = 0, \ldots, 5 \\
\text{Solutions xv-xviii} : \alpha_1 = \cdots = \alpha_4 &= \frac{\theta - 2\pi + 2\pi k}{4}, & \alpha_5 = \cdots = \alpha_8 = \pi - \alpha_1, & k = 0, \ldots, 3 \\
\text{Solutions xix-xx} : \alpha_1 = \alpha_2 &= \frac{\theta - 3\pi + 2\pi k}{2}, & \alpha_3 = \cdots = \alpha_8 = \pi - \alpha_1, & k = 0, 1\ .
\end{aligned} \tag{4.50}
$$

In line with previous analyses, the θ-dependence of the energy is minimised by the solutions with all equal angles. Figure 4.10 displays the behaviour of this minimum in the range $\theta \in [0, 2\pi]$ as well as the phase diagram of the theory. The θ-dependence is analogous to $N_f = 6$ case as it can be further deduced by studying the CP order parameter with its behaviour shown in Figure 4.11.

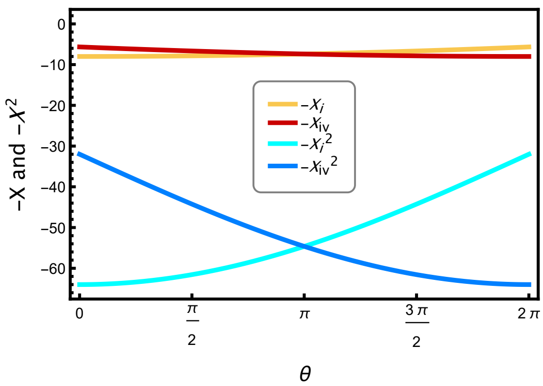

(a) θ-dependence of the energy for $N_f = 8$ both in the normal and superfluid phase.

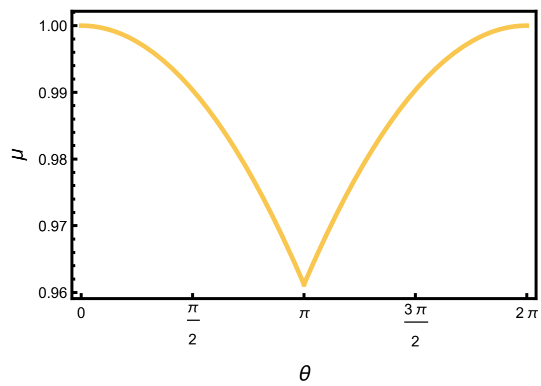

(b) Normalized critical chemical potential $(m_\pi = \nu = 1)$ above which the superfluid phase is realised as a function of θ.

Figure 4.10.: θ-dependence of the energy and of the critical chemical potential for $N_f = 8$.

The value of $\bar{\theta}$ at $\theta = \pi$ in an $\frac{m_\pi^2}{a}$ expansion reads

$$
\bar{\theta} = \frac{2m_\pi^2 \sin\frac{\pi}{8}}{a} - \frac{m_\pi^4}{4\sqrt{2}a^2} + \frac{\left(1 + \frac{3}{\sqrt{2}}\right) m_\pi^6 \sin\frac{\pi}{8}}{32a^3} + O\left(\frac{m_\pi^8}{a^4}\right), \qquad \text{normal phase} \tag{4.51}
$$

$$
\bar{\theta} = \frac{m_\pi^4}{\sqrt{2}a\mu^2} - \frac{m_\pi^8}{8a^2\mu^4} + \frac{m_\pi^{12}}{64\sqrt{2}a^3\mu^6} + O\left(\frac{m_\pi^{16}}{a^4\mu^8}\right), \qquad \text{superfluid phase}\ . \tag{4.52}
$$

4.2.6 **Considerations for general** $\mathrm{N_f}$

Having analysed in detail the physics for different values of N_f away from the conformal window, let us take a step back and consider the emerging structure hinting at structural differences between the even/odd N_f cases in the superfluid phase. Firstly, note that

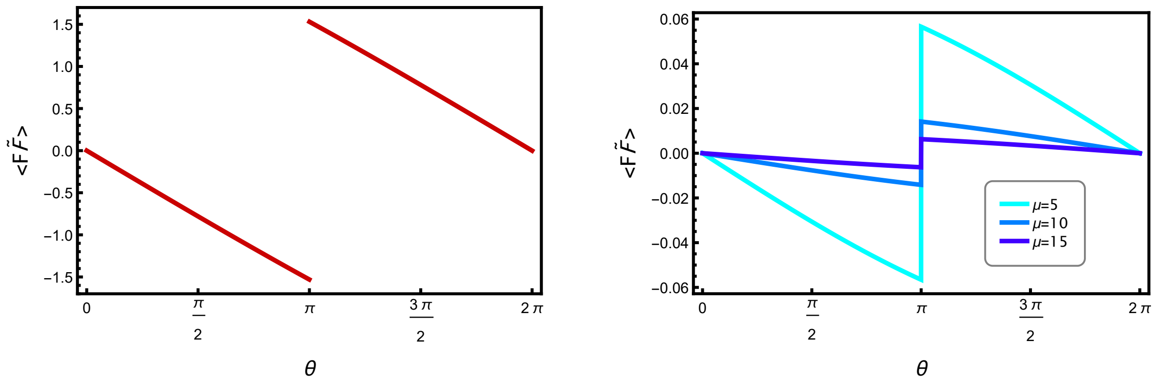

(a) The CP order parameter $\langle F\tilde{F}\rangle$ as a function of θ in the normal phase. Here $m_\pi = \nu = 1$.

(b) The CP order parameter $\langle F\tilde{F}\rangle$ as a function of θ in the superfluid phase for different values of the chemical potential: $\mu = 5, 10, 15$. Here $m_\pi = \nu = 1$.

Figure 4.11.: θ-dependence of the CP order parameter for $N_f = 8$.

solutions of the EOM are generally not periodic of 2π for θ. In fact, the periodicity condition can be satisfied only if at least two solutions cross in the interval $\theta \in [0, 2\pi]$. Taking $U = e^{-i\alpha}\mathbb{1}_{2N_f}$, one can ask when two different solutions of the equation of motion can have the same energy. This corresponds to requiring

$$\cos\left(\frac{\theta + 2\pi k_1}{N_f}\right) = \cos\left(\frac{\theta + 2\pi k_2}{N_f}\right) , \qquad \text{normal phase} \tag{4.53}$$

$$\cos^2\left(\frac{\theta + 2\pi k_1}{N_f}\right) = \cos^2\left(\frac{\theta + 2\pi k_2}{N_f}\right) , \qquad \text{superfluid phase .} \tag{4.54}$$

Both conditions are satisfied when $k_1 = -\frac{\theta}{\pi} - k_2 + N_f$. Since k_1, k_2 are integers, it follows that the energy can only be non-trivially equal for $\theta = \pi$. Therefore, to find the two different solutions, in the normal phase, covering the full $[0, 2\pi]$ interval for θ it is sufficient to consider the case $k_1 = 0$ that for $[0, \pi]$ interval corresponds to the ground state energy, furthermore at $\theta = \pi$ it forces the second solution to be $k_2 = N_f - 1$. This result is in agreement with the findings for the specific cases above for the normal phase.

In the superfluid phase, there are two additional solutions to the second condition (4.54):

- When N_f is even one has the solution $k_1 = k_2 + \frac{N_f}{2}$ which does not depend on θ. This corresponds to the observation that the solutions for even N_f organise themselves in pairs (α and $\alpha + \pi$) with the same energy for every θ. Additionally, of course, one still has the normal phase solution $k_1 = 0$ and $k_2 = N_f - 1$ together with their superfluid degenerate partners. These two classes of solutions cross at $\theta = \pi$ except for the special $N_f = 2$ case for which the crossing disappears. Note that the pairs of completely degenerate solutions remain such to all orders in $\frac{m_\pi^2}{a}$. In fact, given the EOM for a certain α
$$\frac{m_\pi^4}{a\mu^2}\sin(2\alpha) = \theta - N_f\alpha\,, \tag{4.55}$$
then it follows the same EOM for $\alpha + \pi$, upon shifting the θ-angle as $\theta \longrightarrow \theta + N_f\pi$. Being N_f even, this corresponds to a shift by an integer multiple of 2π.

- When N_f is odd there is the solution $k_1 = -k_2 + \frac{N_f}{2} - \frac{\theta}{\pi}$ which can be realised for $\theta = \frac{\pi}{2}$ and $\theta = \frac{3\pi}{2}$. Since the solution that minimises the energy near $\theta = 0$ is $\alpha = \frac{\theta}{N_f}$, then it will cross at $\theta = \frac{\pi}{2}$ with the solution for $\theta > \frac{\pi}{2}$ that becomes $\alpha = \frac{\theta+2\pi k_2}{N_f} = \frac{\theta-\pi}{N_f} + \pi$. The latter solution represents the minimum till $\theta = \frac{3\pi}{2}$ where its energy crosses with $\alpha = \frac{\theta-2\pi}{N_f}$. As a consequence, the vacuum is always non degenerate at $\theta = \pi$ where CP is conserved. In particular, for $\theta = \pi$, $\bar{\theta}$ vanishes to all orders in $\frac{m_\pi^4}{a\mu^2}$ since the equation of motion (4.31) admits the minimum energy solution $\alpha = \theta = \pi$. On the other hand, there are two novel first-order phase transitions at $\theta = \frac{\pi}{2}, \frac{3\pi}{2}$ due to a jump of the physical vacuum between the two minima and characterised by a discontinuous CP order parameter.

Finally, it is worth to estimate the tension of the domain wall between the two degenerate vacua at $\theta = \pi$ for even N_f in the superfluid phase. To this end, consider the Lagrangian (4.13) and look for solutions $\alpha_i = \alpha_i(x)$ that interpolate between the two degenerate ground states(4.30) at $\theta = \pi$ with x the coordinate orthogonal to the domain wall. By considering the ansatz (4.17), the tension of the wall is thus obtained

$$T = 2\nu^2 \int_{-\infty}^{\infty} dx \left[\sum_{i=1}^{N_f} \alpha_i'(x)^2 - \frac{m_\pi^4}{\mu^2 N_f} \left(\sum_{i=1}^{N_f} \cos\left(\frac{\pi}{N_f} + \alpha_i(x) \right) \right)^2 \right] \tag{4.56}$$

where α_i is shifted as $\alpha_i \to \alpha_i + \frac{\pi}{N_f}$ such that the boundary conditions are $\alpha(-\infty) = 0$ and $\alpha(\infty) = \pi$. As discussed in [262], the boundary condition fixes $\alpha_i = \alpha$ for $i = 1, \ldots, N_f - 1$ and $\alpha_{N_f} = -(N_f - 1)\alpha$, leading to

$$T = 2\nu^2 \int_{-\infty}^{\infty} dx \left[(N_f - 1) N_f \alpha'(x)^2 - \frac{m_\pi^4}{\mu^2 N_f} \left((N_f - 1) \cos\left(\alpha(x) + \frac{\pi}{N_f} \right) + \cos\left(\frac{\pi}{N_f} - (N_f - 1)\alpha(x) \right) \right)^2 \right] \tag{4.57}$$

By introducing dimensionless coordinates as $\bar{x} = x\frac{m_\pi^2}{\mu}$, it turns out that regardless of the exact form of the wall's profile, its tension scales as

$$T \approx \frac{\nu^2 m_\pi^2}{\mu} \tag{4.58}$$

and shows a suppression by a factor or $\frac{m_\pi}{\mu}$ compared to the normal phase result $T \approx \nu^2 m_\pi$ [262].

4.2.7 Ground state energy with the axion

The effective action for two-colourQCD at finite baryon number in the presence of the Peccei-Quinn axion field $\mathcal{N}$ is

$$L_{\text{eff}} = -a\nu^2 \left(\theta - \sum_{i=1}^{N_f} \alpha_i - \delta \right)^2 - \Lambda^4 + 4\nu^2 m_\pi^2 X \cos\varphi + 2\mu^2 \nu^2 N_f \sin^2\varphi \,, \qquad \langle \mathcal{N} \rangle = e^{-i\delta/a_{PQ}} \,, \tag{4.59}$$

whose equation of motion $\theta - \sum_{i=1}^{N_f} \alpha_i - \delta = 0$ is solved for $\delta = \theta$ and $\alpha_i = 0$. This solution minimises the energy and leads to $X = N_f$. Hence, the superfluid ground state energy in presence of the axion corresponds to the known result at $\theta = 0$ [180]

$$E = -\frac{2\nu^2 N_f}{\mu^2}\left(m_\pi^4 + \mu^4\right) \ . \tag{4.60}$$

§ 4.3 Symmetry-breaking pattern and spectrum

In the section above it was determined the vacuum structure of the theory. Now, the goal is to establish the associated symmetry-breaking pattern starting with the theory without an axion. The pattern will allow us to disentangle the light degrees of freedom of the theory and it is strictly related to that in chapter 3. This analysis is kept as general as possible so that it is applicable also for the continuation of our work related to near conformal field theories in the large-charge expansion [2] developed in chapter 6.

4.3.1 Symmetry-breaking pattern without the axion

The dynamics of the theory at hand depends on three parameters: the mass of the quarks m, the chemical potential μ, and the scale of the axial anomaly a. The latter corresponds to the energy at which the pseudo-Goldstone (the S-particle) emerging from the spontaneous symmetry breaking of the axial symmetry acquires an anomalous mass. The interest here is in the low energy theory where S is kept into the spectrum. Therefore, consider the following hierarchy [7]

$$m \ll \sqrt{a} \le \mu \ll 4\pi\nu \ , \tag{4.61}$$

where the last inequality implies the validity of the chiral EFT. For $m = \mu = 0$ and in absence of the singlet S, the infrared spectrum consists of massless Goldstone bosons of the spontaneously broken chiral symmetry as summarised below.

$m = 0$
$\mu = 0$
$\sqrt{a} \gg \nu$

$2N_f^2 - N_f - 1$
Goldstones transforming under the antisymm. representation of $Sp(2N_f)$

$$SU(2N_f) \overset{2N_f^2-N_f-1}{\rightsquigarrow} Sp(2N_f)$$

When setting to zero the anomaly, and in the absence of the quark mass, the S-field becomes the Goldstone boson of the $U(1)_A$.

[7] This hierarchy of scales is typical when modelling neutron stars in 2-colour QCD at finite isospin chemical potential [96].

The full spectrum of light particles can be drawn and it is listed here in the following limits

1. **$\mathbf{m \neq 0, \mu = 0}$ and $\mathbf{\sqrt{a} \ll 4\pi v}$**

   Working in steps, one first considers the would-be pattern of spontaneous symmetry breaking according to which $SU(2N_f) \times U(1)_A$ breaks spontaneously to $Sp(2N_f)$. Then the associated $2N_f^2 - N_f$ Goldstone bosons acquire masses via the non-zero quark mass and the anomaly.

2. **$\mathbf{m = 0, \mu \neq 0}$ and $\mathbf{\sqrt{a} \ll 4\pi v}$**

   The introduction of the chemical potential breaks explicitly the final $Sp(2N_f)$ to $SU(N_f)_L \times SU(N_f)_R \times U(1)_B$ while the anomaly breaks $U(1)_A$. The relativistic Bose-Einstein condensation leads to the further spontaneous symmetry breaking $SU(N_f)_L \times SU(N_f)_R \times U(1)_B \rightsquigarrow Sp(N_f)_L \times Sp(N_f)_R$. Therefore, the final spectrum is composed of $N_f^2 - N_f - 1$ massless Goldstone bosons the massive S state due to the anomaly, and N_f^2 modes with mass proportional to the chemical potential. The latter belong to the (N_f, N_f) irreducible representation of $Sp(N_f)_L \times Sp(N_f)_R$ whereas the true Goldstones arrange themselves into three different irreducible representations: a singlet $(1,1)$, the $\left(\frac{N_f(N_f-1)}{2} - 1, 1\right)$ representation and the $\left(1, \frac{N_f(N_f-1)}{2} - 1\right)$. The sum of the degrees of freedom adds to $2N_f^2 - N_f$.

3. **$\mathbf{m \neq 0, \mu \neq 0}$ and $\mathbf{\sqrt{a} \ll 4\pi v}$**

   The situation here is involved due to the competition between the quark mass term and the baryon chemical potential. The chemical potential breaks $Sp(2N_f)$ down to $SU(N_f)_L \times SU(N_f)_R \times U(1)_B$, which, in turn, is explicitly broken by the mass term to its vectorial sub-group $SU(N_f)_V \times U(1)_B$. Finally, the superfluid vacuum breaks the latter symmetry group to $Sp(N_f)_V$ yielding to $\frac{N_f^2 - N_f}{2}$ massless Goldstone bosons as summarised below

$$
\begin{tikzcd}
SU(2N_f)\times U(1)_A \arrow[r, rightsquigarrow, "2N_f^2-N_f"] \arrow[dr, "a,\ m"'] & Sp(2N_f) \arrow[d, "\mu"] \\
& SU(N_f)_V \times U(1)_B \arrow[d, rightsquigarrow, "\frac{N_f^2-N_f}{2}", "\text{superfluid phase}"'] \\
& Sp(N_f)_V
\end{tikzcd}
$$

The case of our interest is the last one, where one has $\frac{N_f^2 - N_f}{2}$ Goldstones transforming according to the antisymmetric representation of $Sp(N_f)_V$ plus a singlet. Additionally, there is the η' like state S with mass of order $\sqrt{a}$.

The naive counting above of the number of Goldstone bosons holds correct here since there are no Goldstone bosons of type II [424] in this case. The reason is that the dimension of the representation of the Goldstone bosons is identical to the number of broken generators (see discussion in [94]).

4.3.2 Symmetry-breaking pattern with the axion

In this section, it is analysed the symmetry-breaking pattern for $m \neq 0$, $\mu \neq 0$, $a \ll 4\pi\nu$ but including the presence of the additional $U(1)_{PQ}$ symmetry discussed at the end of section 4.1. The latter is classically exact but quantum mechanically anomalous and spontaneously broken, leading to the existence of a new pseudo-Goldstone boson (the axion) with the mass of the order of the scale of the anomaly. Below there is the summary of the pattern of symmetry breaking

$$\begin{tikzcd}
SU(2N_f)\times U(1)_A\times U(1)_{PQ} \arrow[r, rightsquigarrow, "2N_f^2-N_f+1"] \arrow[d, "\mu"] \arrow[d, bend right, "m,\ a,\ a_{PQ}"'] & Sp(2N_f) \\
SU(N_f)_V\times U(1)_B \arrow[d, rightsquigarrow, "\frac{N_f^2-N_f}{2}", "\text{superfluid phase}"'] & \\
Sp(N_f)_V &
\end{tikzcd}$$

From the picture is clear that the spectrum of Goldstones remains the same as in the case without the axion with an additional singlet massive state.

In the next section, the focus is on the dispersion relations of the light modes describing the infrared dynamics. These are obtained by explicitly expanding the Lagrangian at the quadratic order in the fluctuations around the ground state.

4.3.3 Spectrum of fluctuations

To analytically determine the dispersion relations of the different relevant states around the vacuum, consider the large a/m_π^2 expansion and stop at the leading order. In this way, one recovers eqs. (69) and (84) of [180] for $\theta = 0$, and can generalize them to include the θ-angle by taking it into account via an effective quark mass matrix. Precisely, one has

$$\omega_1^2 = k^2 + \mu^2\,, \qquad \square\square \qquad \frac{1}{2}N_f(N_f+1) \tag{4.62}$$

$$\omega_2^2 = k^2 + \frac{m_\pi^4 X^2}{\mu^2 N_f^2}\,, \qquad \begin{smallmatrix}\square\\\square\end{smallmatrix} \qquad \frac{1}{2}N_f(N_f-1)-1 \tag{4.63}$$

$$\omega_3^2 = k^2 + \frac{2\left(\mu^4 N_f^2 + 3m_\pi^4 X^2\right)}{N_f^2\mu^2} + A\,, \qquad \bullet + \begin{smallmatrix}\square\\\square\end{smallmatrix} \qquad \frac{1}{2}N_f(N_f-1) \tag{4.64}$$

$$\omega_4^2 = k^2 + \frac{2\left(\mu^4 N_f^2 + 3m_\pi^4 X^2\right)}{N_f^2\mu^2} - A\,, \qquad \bullet + \begin{smallmatrix}\square\\\square\end{smallmatrix} \qquad \frac{1}{2}N_f(N_f-1) \tag{4.65}$$

$$\omega_5^2 = k^2 + M_S^2\,, \qquad \bullet \qquad 1 \tag{4.66}$$

where

$$A = \frac{2}{N_f^2\mu^2}\sqrt{\left(N_f^2\mu^4 + 3m_\pi^4 X^2\right)^2 + 4N_f^2\mu^2 m_\pi^4 k^2 X^2}\,, \tag{4.67}$$

$$M_S^2 = \frac{a\mu^4 N_f^3 + 2\mu^2 m_\pi^4 X^2}{2\mu^4 N_f^2 - 2m_\pi^4 X^2}\left(1 - \frac{m_\pi^4 X^2}{\mu^2 N_f^2}\right)\,. \tag{4.68}$$

The Young tableaux describe the irreducible representations of $Sp(N_f)$ according to which the states transform, with $\bullet$ denoting the singlet representation. The number of degrees of freedom sum to $\dim\left(\frac{U(2N_f)}{Sp(2N_f)}\right) = N_f(2N_f - 1)$, i.e the number of pseudo-Goldstones of the chiral symmetry breaking plus the η' like S-particle. For $\theta = 0$ the first four dispersion relations reduce to the ones found in [180]. ω_4 describes true Goldstone modes with speed $v_G = 1$ which parameterise the coset $\frac{SU(N_f)}{Sp(N_f)}$ and correspond to the π modes considered in [94][8]. In addition, there are modes with a mass of order μ (ω_1 and ω_3) and modes with mass $\frac{m_\pi^2 X}{\mu N_f}$.

If one wants to include the axion in the theory, the dispersion relations of the modes described by eqs.(4.62)-(4.65) remain the same with $X = N_f$, i.e. one has the spectrum at $\theta = 0$ as expected from the Peccei-Quinn mechanism. On top of that, there are the modes stemming from the mixing between the singlet S and the axion, which is described by the following inverse propagator

$$D^{-1} = \begin{pmatrix} \frac{\omega^2 - k^2}{\sin^2\varphi} - M_S^2 & -\frac{a\sqrt{N_f}\,a_{PQ}}{4\sqrt{2}v_{PQ}\sin^2\varphi} \\ -\frac{a\sqrt{N_f}\,a_{PQ}}{4\sqrt{2}v_{PQ}\sin^2\varphi} & \frac{\omega^2 - k^2}{4v^2\sin^2\varphi} - M_{\hat{a}}^2 \end{pmatrix}, \tag{4.69}$$

where

$$M_S^2 = \frac{\left(a\mu^4 N_f + 2\mu^2 m_\pi^4\right)}{2\mu^4 - 2m_\pi^4} \tag{4.70}$$

$$M_{\hat{a}}^2 = \frac{a\mu^4 a_{PQ}^2}{16v_{PQ}^2\left(\mu^4 - m_\pi^4\right)}\,. \tag{4.71}$$

The dispersion relations read

$$\omega_{6,7} = \frac{1}{2}\sqrt{4k^2 + 8v^2 M_{\hat{a}}^2\sin^2\varphi + 2M_S^2\sin^2\varphi \pm \frac{1}{v_{PQ}}\sqrt{2a^2v^2N_f a_{PQ}^2 + 4v_{PQ}^2\sin^4\varphi\,\left(M_S^2 - 4v^2M_{\hat{a}}^2\right)^2}}\,. \tag{4.72}$$

As can be seen from the inverse propagator, the S particle and the axion decouple in the anomaly-free limits $a \to 0$ and $a_{PQ} \to 0$. In the former case, the S-particle describes a pseudo-Goldstone mode with mass of order $M_S^2 = \frac{\mu^2 m_\pi^4}{\mu^4 - m_\pi^4}$, while for $a_{PQ} \to 0$ one has $M_S^2 = \frac{aN_f}{2}$ for $\mu \gg m_\pi$, in agreement with the Witten-Veneziano relation [268, 269]. On the other hand, in the limit of vanishing anomalies, the axion is massless being the

[8] These are the modes that will play the main role in chapter 6 since they dominate the large-charge dynamics.

$U(1)_{PQ}$ symmetry exact.

Let us sum up the results here presented. In this chapter the spectrum, chiral symmetry breaking patterns, and low-energy dispersion relations of two-colour QCD were explored as functions of baryon chemical potential, the topological term responsible for strong CP breaking, and quark masses. Actually ,this analysis extends to $Sp(2N)$ gauge groups with fermions in the fundamental representation. Dynamics involving two, three, six, seven, and eight light matter flavours were explicitly considered, leading to the identification of normal and superfluid ground states. The vacuum was shown to develop a complex structure due to the CP-violating topological operator, revealing novel phases. These phases were analysed, with particular focus on the dependence of the critical chemical potential on the θ-angle, which marks the transition between the normal and superfluid phases. The order of phase transitions was characterised by examining the behaviour of the CP order parameter, demonstrating that these transitions are first order.

The results have practical applications, especially in the normal phase, to θ and axion physics within composite Goldstone Higgs models. A new composite strong source of CP violation could be significant for studies on composite electroweak baryogenesis [116, 347, 348], while the analysis at non-zero chemical potential is relevant for asymmetric dark matter research and the interaction with CP violation. These predictions offer guidance and can be tested through first-principle lattice simulations at non-zero baryon chemical potential, including the effects of topological susceptibility [349, 350].

In conclusion, note that these results are valid for a number of flavours below the lower boundary of the conformal window whose value increases with the underlying number of colours of the $Sp(2N)$ gauge theory investigated here. In the large-N limit the eta-prime becomes a quasi-Goldstone boson and therefore validates the effective approach used here. The analysis is further performed respecting the hierarchies of scales of (4.61) allowing us to consider the impact of the chemical potential as a modification of the underlying pattern of chiral symmetry breaking in the vacuum.

Part III

PRELIMINARIES II: NEAR CONFORMAL DYNAMICS

Introduction to Part III

Asymptotically free gauge theories with a relatively small number of fermion degrees of freedom typically exist in a chirally broken and confining phase, characterised by a coupling that increases toward the infrared. When the number of fermion degrees of freedom is increased, the running of the coupling may slow down, potentially stopping at an infrared-attractive fixed point (IRFP). In this scenario, the theory transitions into an infrared-conformal phase. The minimum number of flavours that allows for an IRFP is often referred to as the “threshold" of the conformal window [198].

For theories with a number of flavours slightly below this sill, chiral symmetry remains broken, and the theory is still confining. However, unlike QCD, these theories are nearly conformal, with a β-function that is very small near the energy scale where chiral symmetry breaking occurs. This results in a “walking" coupling, which changes very slowly with the energy scale, as opposed to a “running" coupling.

Lattice simulations of walking theories have uncovered the existence of a flavour-singlet scalar meson that can be as light as the pions over a wide range of fermion masses. Examples include the $SU(3)$ gauge theory with $N_f = 8$ Dirac fermions in the fundamental representation or with two flavours of sextet fermions. Determining whether such a theory is chirally broken and confining or infrared conformal is challenging when the β-function is very small. For this discussion, the basic assumption will be that the mentioned models are chirally broken in the continuum limit [198].

Walking theories are particularly attractive for extensions of the Standard Model involving new strong interactions. Their renormalized coupling changes very slowly with the energy scale, even at relatively large values. This can result in large anomalous dimensions that significantly enhance the corresponding operator. This feature is beneficial for reconciling flavour physics with experimental data. Additionally, the presence of a very light scalar meson, which in technicolor-like theories is a natural candidate for the Higgs particle, is an added benefit.

These theories are also of theoretical interest. Specifically, it is intriguing to explore whether the presence of a light singlet scalar meson is connected to the small β-function. The coupling’s running indicates the breaking of classical scale invariance by the quantum theory. When the β-function is small, the quantum breaking of the dilation symmetry is correspondingly small. In the upcoming chapter, it will be discussed the construction of a low-energy effective action for the pions and the light singlet scalar meson. A consistent low-energy description must account for all light states, incorporating the scalar meson, which can be as light as the pions. Even if the pions eventually become lighter than the scalar meson in the chiral limit, this effective description remains valid when the scalar meson is much lighter than other states in the theory. The main challenge is to quantify the violations of dilation symmetry in the effective theory and relate them to the microscopic theory, ensuring that these violations are controlled by a small parameter. The light scalar, or “dilatonic meson", then becomes a pseudo-Goldstone boson of the approximate dilation symmetry in the sense explained in chapter 1.

Near Conformal Dynamics of non-abelian gauge theories

5

CHAPTER

§ 5.1 Phase diagram of non-abelian gauge theories

Non-abelian gauge theories exist in several distinct phases that can be classified according to the characteristic dependence of the potential energy on the distance between two well-separated static sources [98, 385]. The collection of all of these different behaviours, when represented, for example, in the flavour-colour space, constitutes the phase diagram of the given gauge theory. This chapter sets the stage by analysing the main features of the phase diagram of strongly coupled theories as a function of the number of colours, flavours and matter representation. Specifically, the focus is on the status of the phase diagram for $SU(N)$ gauge theories with fermionic matter transforming according to arbitrary representations of the underlying gauge group.

To this end, consider a generic gauge group with $N_f(\mathfrak{R})$ Dirac flavours that transform under the representation $\mathfrak{R}$ of the gauge group. Let us introduce some useful notation. Henceforth, $d(\mathfrak{R})$ and $d(G)$ will denote the dimensions of a given representation of the gauge group G and the dimension of the gauge group, respectively. The Lagrangian of an $SU(N)$ gauge theory reads

$$\begin{aligned}
\mathcal{L} &= \bar{\psi}\left(i\not{\mathcal{D}} - m\right)\psi - \frac{1}{4}F_{\mu\nu}\,F^{\mu\nu} \\
\not{\mathcal{D}} &\equiv \gamma^{\mu}\mathcal{D}_{\mu} \\
\mathcal{D}_{\mu} &= \partial_{\mu} + ig(\mu)A_{\mu} \\
F_{\mu\nu} &= \partial_{\mu}A_{\nu} - \partial_{\nu}A_{\mu} - g(\mu)f_{abc}\,A^{b}_{\mu}A^{c}_{\nu}
\end{aligned} \tag{5.1}$$

where implicit summation over the flavour and colour indices is considered and $g(\mu)$ is the gauge coupling at some scale μ.

In theories of strong interactions (with non-abelian gauge fields), the interaction strength, defined by the coupling constant, varies across energy scales. This phenomenon is referred to as “running".

This is due to a competition between two opposing effects. On the one hand, there is “anti-screening" caused by the nature of the charged gauge bosons, which tends to amplify interactions at shorter distances. On the other hand, matter fields tend to dampen these interactions at short distances, a process known as “screening". Thus, the coupling constant reflects the balance between these two forces.

Another key concept is chiral symmetry breaking. When this occurs below a certain energy scale, fermions gain mass, altering the dynamics of the theory. This change also impacts the behaviour of the coupling constant.

Under certain conditions, especially when there is sufficient matter present, the coupling constant can converge to a fixed value at low energies before chiral symmetry breaking occurs. This signifies the existence of a “conformal phase" where the theory behaves in a scale-invariant manner.

However, when the number of different types of matter particles is slightly below the threshold for entering this conformal phase, the coupling constant does not vary much as one changes the energy scale. It is as if it is “walking" instead of “running". The pictorial framework is shown in Figure 5.1.

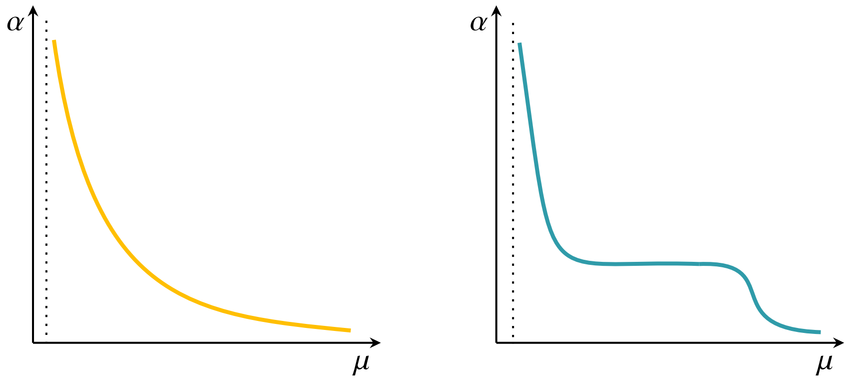

(a) QCD-like behaviour of the coupling constant as a function of the momentum (Running): strong infrared dynamics.

(b) Walking-like behaviour of the coupling constant as a function of the momentum (Walking).

Figure 5.1.: Cartoon of the coupling constant as a function of the momentum.

In essence, the behaviour of the coupling constant in strongly interacting theories reflects a complex interplay between different forces and energy scales, producing notable phenomena such as “running", “walking", and conformal phases.

Let us now delve into the mathematical details by reviewing the two loop β-function for a given non-abelian gauge theory with fermions transforming under a given representation $\mathfrak{R}$ of the gauge group [124]:

$$\mu\frac{\partial g}{\partial \mu} \equiv \beta(g) = -\beta_0\frac{g^3}{(4\pi)^2} - \beta_1\frac{g^5}{(4\pi)^4} \tag{5.2}$$

where

$$\beta_0 = \frac{11}{3}\, C_2(G) - \frac{4}{3}\, T(\mathfrak{R})\, N_f \tag{5.3}$$

$$\beta_1 = \frac{34}{3}\, C_2^2(G) - \frac{20}{3}\, C_2(G)\, T(\mathfrak{R}) - 4C_2(\mathfrak{R})\, T(\mathfrak{R})\, N_f\ . \tag{5.4}$$

Here $T^a_{\mathfrak{R}}$ denote the generators of the gauge group in the representation $\mathfrak{R}$ with $a = 1, \ldots, N^2 - 1$ and they are normalised according to $\mathrm{Tr}\{T^a_{\mathfrak{R}} T^b_{\mathfrak{R}}\} = T(\mathfrak{R})\delta^{ab}$ where $T(\mathfrak{R})$ is the trace normalisation factor. The latter is connected with the quadratic Casimir $C_2(\mathfrak{R})$ given by $T^a_{\mathfrak{R}} T^a_{\mathfrak{R}} = C_2(\mathfrak{R})\mathbb{1}$ via

$$C_2(\mathfrak{R})\ d(\mathfrak{R}) = T(\mathfrak{R})\ d(G)\ . \tag{5.5}$$

Firstly, let us observe that when the coefficient β_0 is negative the theory behaves as QED meaning that it becomes strongly interactive at high energies, losing the property of asymptotic freedom. Since this coefficient depends on the number of flavours of the matter content, one can detect the specific value of N_f above which the loss occurs. Because β_0 needs to change the sign, one simply needs to impose that

$$\beta_0(N_f^I[\mathfrak{R}]) = 0 \implies N_f^I = \frac{11}{4}\,\frac{C_2(G)}{T(\mathfrak{R})} \tag{5.6}$$

therefore, for values N_f larger than N_f^I the theory behaves as a non-abelian QED theory.

Following this reasoning, one can ask whether the coefficient β_1 also changes sign and what is the value of the number of flavours where this happens. Let us denote by N_f^{III} the latter which is obtained as

$$\beta_1(N_f) = 0 \implies N_f^{III} = \frac{17 C_2(G)}{T(\mathfrak{R})\,(10 C_2(G) + 6 C_2(\mathfrak{R}))} \tag{5.7}$$

and that, whatever the representation, is always smaller than N_f^I. This means that the two loop β-function reaches a non-trivial zero when $N_f^{III} < N_f < N_f^I$. The theory develops a Banks-Zaks infrared fixed point [199] occurring at

$$\frac{\alpha^*}{4\pi} \equiv \left(\frac{g^*}{4\pi}\right)^2 = -\frac{\beta_0}{\beta_1} = \frac{4 N_f T(\mathfrak{R}) - 11 C_2(G)}{34 C_2(G)^2 - 4 N_f T(\mathfrak{R})(5 C_2(G) + 3 C_2(\mathfrak{R})} \tag{5.8}$$

and which depends on the number of flavour: the value of the fixed point increases as N_f is decreased and disappears when $N_f = N_f^{III}$.

Hence, the dynamics at low momenta is defined by this infrared fixed point, which in turn is nonetheless sensitive to non-perturbative dynamics that may lead to the generation of particle masses. When this happens, fermions decouple from the theory and the overall picture results in the only presence of gluons which remain the sole contribution to the β-function. In this scenario, the infrared fixed point disappears, and chiral symmetry breaking is triggered [124]. Understanding the interplay between confinement, chiral dynamics, and the value of the coupling constant at the fixed point is essential.

Let us denote with α_c the value of the coupling above which a dynamical mass for the fermions generates non-perturbatively and chiral symmetry breaking occurs [124]. Solving the Schwinger-Dyson equation in the rainbow approximation, the critical value α_c is determined to be

$$\alpha_c = \frac{\pi}{3 C_2(\mathfrak{R})} \tag{5.9}$$

and therefore, if the latter value is reached, chiral symmetry breaking occurs. If α_* is met before, the coupling freezes. Whether or not this is the case can only depend on the number of flavours of the theory. There exists N_f^{II} where chiral symmetry breaking takes place and it can be obtained by imposing the value of the coupling at the fixed point to be exactly α_c, namely

$$\alpha_c \stackrel{!}{=} \alpha^* \implies N_f^{II} = \frac{C_2(G)\,(17C_2(G) + 66C_2(\mathfrak{R}))}{T(\mathfrak{R})\,(10C_2(G) + 30C_2(\mathfrak{R}))} \tag{5.10}$$

and since it is always greater compared to N_f^{III}, the interval of the number of flavours allowed for the theory to be conformal is

$$N_f^{II} < N_f < N_f^{I} \; . \tag{5.11}$$

Let us briefly pause to recap. The two-loop β function of strongly interacting theories displays a behaviour depending on both the strength of the coupling constant and the matter content, and its infrared dynamics results from the interplay between confinement and conformality. Three regions can be visualised by summarising the phase diagram as a function of the number of colours and flavours (see Figure 5.2):

- Loss of asymptotic freedom: this occurs for $N_f > N_f^I$ and the theory behaves as QED (β_0 changes sign).
- Banks-Zaks fixed point: the two loop β-function admits an interactive infrared fixed point for $N_f^{III} < N_f < N_f^I$, where N_f^{III} is the value of the number of flavours such that β_1 is zero while N_f^I the one at which $\beta_0 = 0$.
- Confinement and chiral symmetry breaking: as the coupling grows, the theory confines, chiral symmetry breaking occurs, and the fermions decouple when $N_f = N_f^{II}$ and $N_f^{III} < N_f^{II} < N_f^I$ holds.

The region of the phase diagram as a function of the number of flavours and the number of colours where the theory admits a conformal phase, i.e. the β-function admits zeros, is referred to as the *conformal window* (see Figure 5.4). Stated differently, the window in the flavour-colour space where the theory displays IR conformality is termed *conformal window*. The latter is bounded above by N_f^I and below by N_f^{II}.

Hence, one can distinguish between two (sub-)phases of the theory depending on the strength of the coupling constant and the number of matter content and they are

$$\alpha_c < \alpha^* \quad \Leftrightarrow \quad N_f^{III} < N_f < N_f^{II} \quad \text{chirally broken phase.} \tag{5.12}$$

$$\alpha_c > \alpha^* \quad \Leftrightarrow \quad N_f^{II} < N_f < N_f^{I} \quad \text{conformal window.} \tag{5.13}$$

An intuitive visual representation is shown in Figure 5.3.

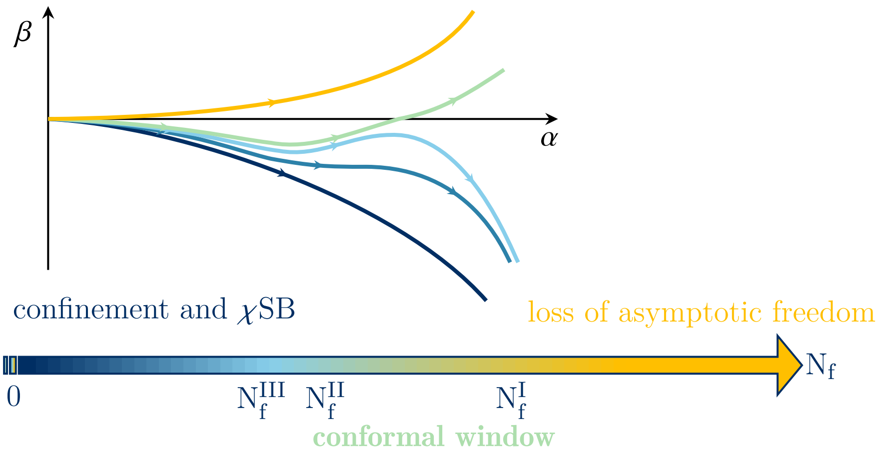

Figure 5.2.: Cartoon of the different behaviours displayed by the two loop β-function explained in the text.

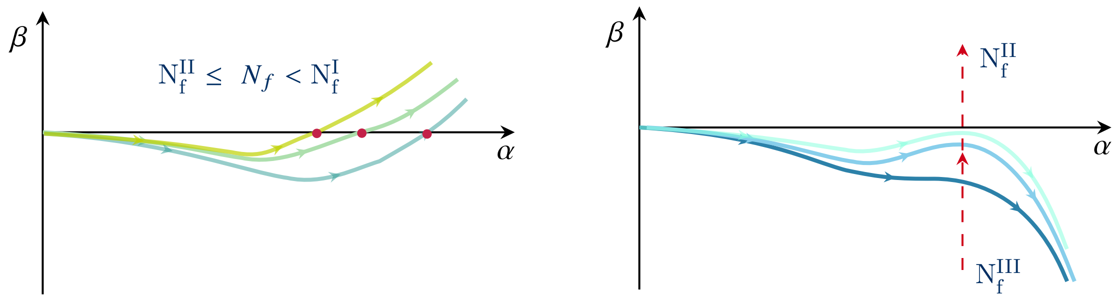

(a) β-function as a function of the coupling constant for the region $N_f^{II} \leq N_f < N_f^{I}$ for $SU(N)$ theories.

(b) Walking-like behaviour of the β-function as a function of the coupling constant. The gap to attaining the fixed point becomes smaller as N_f approaches N_f^{II}: the difference $\left|N_f - N_f^{II}\right|$ quantifies the absence of conformal invariance.

Figure 5.3.: Cartoon of the β-function as a function of the coupling constant for $SU(N)$ gauge theories.

Some comments are now required. For all the discussion the number of flavours has been treated as a continuous parameter and the end of the conformal window is a debated argument in the literature, i.e. the determination of its boundaries constitutes an active area of research [1–4, 99, 122, 124, 383, 384, 390–392, 452, 452, 453, 453–457, 459] (and references therein). Unveiling the non-perturbative physics at the lower boundary of the conformal window remains a long-standing challenge.

Additionally, the interest in theoretical and phenomenological investigations regarding the possibility that α runs towards an IR fixed point in these non-abelian gauge theories is strong [1].

[1] It is crucial to distinguish the different ways in which conformal symmetry is realised. In chapter 1, it has been stressed that conformal invariance corresponds to the vanishing of the trace of the energy-momentum tensor and that a global symmetry can be realised in two different ways: a first via a Wigner-Weyl mode where conformality is manifest and all masses of the particles go to zero and a second via a Nambu-Goldstone mode (a genuine dilaton) that is a massless scalar boson allowing all other masses to be *non-zero*. In the latter scenario, the symmetry is said to be “spontaneously broken" [223, 304].

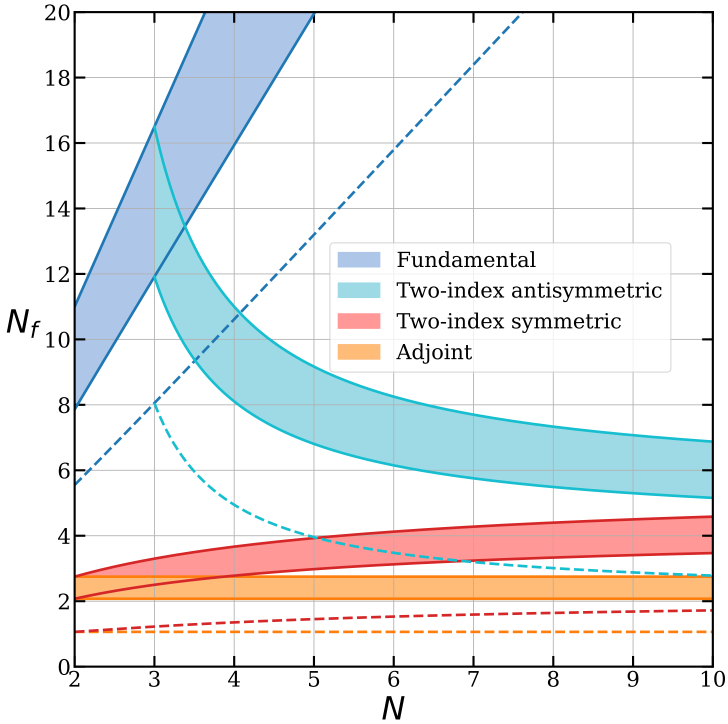

Figure 5.4.: Phase diagram for theories with fermions in the fundamental, two-index antisymmetric, two-index symmetric and adjoint representation as a function of the number of flavours and the number of colours. The shaded areas depict the corresponding conformal windows. The upper solid curve represents N_f^I (loss of asymptotic freedom) while the lower N_f^{II} (loss of chiral symmetry breaking). The dashed curves show N_f^{III} (existence of a Banks-Zaks fixed point).

5.1.1 Chiral conformal dynamics and the unitarity bound

The time has come to draw attention to another parameter in the fundamental Lagrangian: the quark mass m. As for the gauge coupling g, the discussion now is around the renormalised quantity relative to the fermion mass which is its anomalous dimension $\gamma = -\mu d \log m / d\mu$ and whose perturbative expression is

$$\gamma(g) = \frac{3C_2(G)}{2}\frac{g^2}{4\pi^2} + O\left(g^4\right) = \frac{3C_2(G)}{2\pi}\alpha + O\left(g^4\right) . \tag{5.14}$$

Since it depends on the quadratic Casimir of the adjoint representation, one can re-write the two loop β-function as follows [389]

$$\beta = -\frac{g^3}{(4\pi)^2}\frac{\beta_0 - \frac{2}{3}T(R)N_f\gamma(g^2)}{1 - \frac{g^2}{8\pi^2}C_2(G)\left(1 + \frac{2\beta_0'}{\beta_0}\right)} \quad \text{with} \quad \beta_0' = C_2(G) - T(R)N_f \tag{5.15}$$

and observe that the infrared fixed point is reached when

$$\gamma^* = \frac{3}{2}\frac{\beta_0}{T(R)N_f} \implies \gamma^* = \frac{11C_2(G) - 4T(R)N_f}{2T(R)N_f} . \tag{5.16}$$

Hence, specifying the value of the anomalous dimension at the infrared fixed point yields the last constraint to identify the conformal window. Given that the theory must adhere to conformality, it is crucial to ensure it does not include negative norm states associated with complex spinless operators. This means that their dimension must be larger than one. Therefore, since the scaling dimension associated with fermion condensate is $\Delta_{\bar{\psi}\psi} = d_{\bar{\psi}\psi} + \gamma_{\bar{\psi}\psi}$ and $\gamma_{\bar{\psi}\psi} = -\gamma$, one arrives at

$$\Delta_{\bar{\psi}\psi} = (d-1) - \gamma^* = 3 - \gamma^* \tag{5.17}$$

which, imposing the constraint to be greater than one, leads to the so-called *unitarity bound*

$$0 < \gamma^* \leq 2 \tag{5.18}$$

which leads to the maximum possible constraint for the number of flavours needed to enter the conformal window

$$N_f \geq \frac{11}{8} \frac{C_2(G)}{T(R)} . \tag{5.19}$$

The unitarity bound in (5.18) will be considered in chapter 6, chapter 7 and chapter 9.

§ 5.2 A Proposal: Unravelling the Mechanisms of Conformality Loss

The mechanism underlying the “phase transition" which these non-abelian theories undergo when passing from non-conformality to conformality is still unknown [388]. In this section one of the most widely accepted theories in literature is reviewed, mostly following the discussion in [388, 432]. Precisely, the realisation of the near conformal regime can be achieved by imaging an RG trajectory that describes a QFT starting close to a CFT and remaining as close as possible to it. If one is considering a CFT, this mechanism can be realised by the introduction of operators in the theory that consequently perturb the CFT. The flow of the new theory remains as close as possible to the original CFT if this perturbation is small. The only perturbations contemplated are those relative to relevant operators and at a given UV scale the new microscopic theory reads

$$\mathcal{L}_{\text{new}} = \mathcal{L}_{\text{CFT}} + c\, \lambda_{\text{UV}}^{d-\Delta}\, O_{\Delta} \tag{5.20}$$

where O_{Δ} denotes a scalar operator having scaling dimension $\Delta < d$. The coupling c is thus considered to be small. In other words, the smallness of this coefficient can be explained by the requirement for symmetry to be nearly preserved in the microscopic description of our theory. This essentially echoes ’t Hooft’s criterion of naturalness [461], although reformulated within the framework of CFTs [388].

To clarify the ideas, consider an RG flow of an unknown coupling λ and assume that the β-function is

$$\beta(\lambda)_{MY} = \frac{d\lambda}{dt} = -\delta - \lambda^2 + O\left(\lambda^3\right), \quad \text{with} \quad t = \log E \tag{5.21}$$

near $\lambda = 0$. In this context, δ serves as a small parameter. Then suppose that higher-order terms possess coefficients of $O(1)$, thus ensuring the reliability of (5.21) for $|\lambda| \lesssim 1$. Although $\lambda = 0$ might seem arbitrary, it is a general choice; the function β can be considered to include $\lambda - \lambda_0$ instead of only λ on the right-hand side, with the subsequent removal of λ_0 by a simple change.

Naturally, portraying the flow exclusively in terms of one coupling represents an oversimplification. The idea is to assume that other couplings affecting the flow are negligible, so their impact on the evolution of λ can be ignored.

Assuming the coupling λ to be real, the dynamics governed by the β-function (5.21) exhibits distinct behaviours depending on the sign of δ.

Let us first consider the case where $\delta < 0$. Here, two real fixed points emerge: $\lambda_\pm = \pm\sqrt{|\delta|}$. The fixed point λ_+ is classified as a UV fixed point, which means that it cannot be reached by flow from short distances. In contrast, λ_- represents an IR fixed point, accessible from both the UV fixed point and significantly negative λ values [388, 432].

Suppose that λ couples to an operator O_λ; the latter will have dimension

$$\Delta_\pm = d + \beta'(\lambda_\pm) \approx d \mp 2\sqrt{|\delta|}. \tag{5.22}$$

For $|\delta| \ll 1$ this dimension is weakly relevant at the λ_+ fixed point.

Suppose instead that $\delta > 0$. Then there is no fixed point at real λ, at least not within the region of validity of the assumed approximate β-function. A flow starting at $\lambda \sim -1$ will eventually go through to $\lambda \sim 1$, but for small δ it will slow down and linger around $\lambda \sim 0$. How much the flow lingers can be estimated by computing the RG time of passage [388]:

$$\Delta t \sim -\int_{-1}^{1} \frac{d\lambda}{\beta(\lambda)} \sim \frac{\pi}{\sqrt{\delta}}. \tag{5.23}$$

One can also use the exact solution of the β-function equation neglecting $O\left(\lambda^3\right)$ terms:

$$\lambda(t) = -\sqrt{\delta}\tan\left[\sqrt{\delta}\,(t - t_0)\right]. \tag{5.24}$$

Additionally, denoting with Λ_{UV} the scale at which the flow starts at $\lambda \sim -1$ while with Λ_{IR} the energy scale where the flow arrives at $\lambda \sim 1$ one obtains

$$\frac{\Lambda_{UV}}{\Lambda_{IR}} \sim e^{\Delta t} \sim e^{\frac{\pi}{\sqrt{\delta}}} \tag{5.25}$$

from which it is clear that the ratio of energies is huge if δ is small. This ratio and this scaling define the *walking scaling*. In Figure 5.5, the behaviour of the β-function as a function of the coupling constant for various δ is depicted. This visualisation illustrates the concept of “walking dynamics" originally proposed by Holdom [370, 398], further elaborated in [399, 440]. In simple terms, the coupling constant undergoes slow variations, or “walks", towards the infrared value, remaining relatively constant over various energies. This stability increases near the double fixed point according to δ.

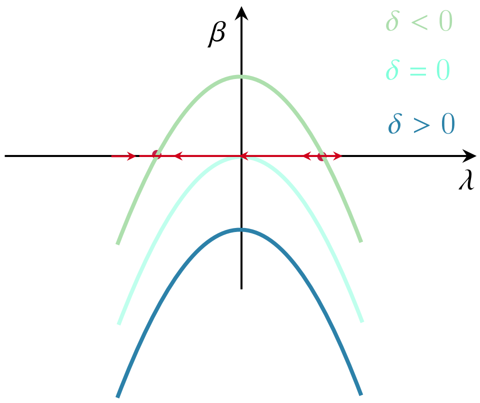

Figure 5.5.: Cartoon of the RG flow for different values of the parameter δ.

Therefore, the RG flow is fundamental to the understanding of second-order phase transitions, with critical points corresponding to the fixed points of the relevant RG equations. Near the phase transition, the characteristic energy or momentum scale μ (the inverse correlation length) approaches zero as $\mu \sim |\delta|^{\nu}$, where δ is a continuously variable parameter, and $\delta = 0$ marks the critical point. However, despite significant efforts, the physical properties at the boundary between a conformally broken and a conformally restored phase in generic gauge theories remain unknown. This problem is an important mystery yet to be solved. A well-known conjecture, known as Miransky scaling, was proposed some time ago [205, 206]. This scaling emerges under the following assumptions: i) The given gauge theory simultaneously possesses at least one non-trivial infrared fixed point and one ultraviolet fixed point; ii) Upon varying an external parameter of the theory, such as the number of flavours, the IR fixed point merges with the UV fixed point at a critical value of this parameter; iii) This merging is sufficiently smooth, allowing the nearby conformal phase to influence the conformally broken phase for values of the external parameter near the phase transition [209].

Assuming that the β-function corresponds to an underlying gauge theory involving fermions, let us proceed to investigate the scaling behaviour of the chiral condensate within the walking regime.

Being γ the anomalous dimension of the Dirac fermion mass in a given representation of an underlying gauge group, the following well-known RG equation relates the condensate at two distinct energies:

$$\langle\bar{\psi}\psi\rangle_{\mu} = \exp\left(\int_{\mu}^{\Lambda} \frac{\mathrm{d}(\ln\mu)}{\gamma(\lambda(\mu))}\right)\langle\bar{\psi}\psi\rangle_{\Lambda} = \exp\left(\int_{\lambda(\mu)}^{\lambda(\Lambda)} d\lambda\frac{\gamma(\lambda)}{\beta(\lambda)}\right)\langle\bar{\psi}\psi\rangle_{\Lambda}\,. \tag{5.26}$$

In this equation, the β-function corresponds to the “mirror" of the Miransky case in the walking region, yielding:

$$\langle\bar{\psi}\psi\rangle_{\mu} = \exp\left(\int_{\lambda(\mu)}^{\lambda(\Lambda)} d\lambda\frac{\gamma(\lambda)}{\beta(\lambda)}\right)\langle\bar{\psi}\psi\rangle_{\Lambda} \simeq \exp\left(\gamma(0)\int_{\lambda(\mu)}^{\lambda(\Lambda)} \frac{d\lambda}{\beta_{\mathrm{MY}}}\right)\langle\bar{\psi}\psi\rangle_{\Lambda} = \left(\frac{\mu}{\Lambda}\right)^{\gamma(0)}\langle\bar{\psi}\psi\rangle_{\Lambda}\,. \tag{5.27}$$

In this context, the definition of the β-function is employed, and initially, the assumption is made regarding the smoothness of the anomalous dimension of the mass operator across the phase transition. The value $\gamma(0) = \gamma(\lambda_{\mathrm{IR}} = \lambda_{\mathrm{UV}})$ denotes the anomalous dimension at the merger. The power-law amplification of the chiral condensate with energy, characteristic of walking dynamics, is subsequently obtained. As γ is assessed at the fixed point, its value remains independent of the scheme [209].

This section is concluded with a crucial observation: in this example and proposal exposed here, the role of δ can be mimicked by the difference between the number of flavours and the critical one at which the conformal window is reached for a given $SU(N)$ gauge theory. Furthermore, it is important to note that for this kind of scaling presented here, the transition between the non-conformal phase and the conformal one is supposed to be *smooth*. In particular, the nearby conformal phase is felt in the conformally broken phase for values of the external parameter near the phase transition. The suggestive picture is shown in Figure 5.6.

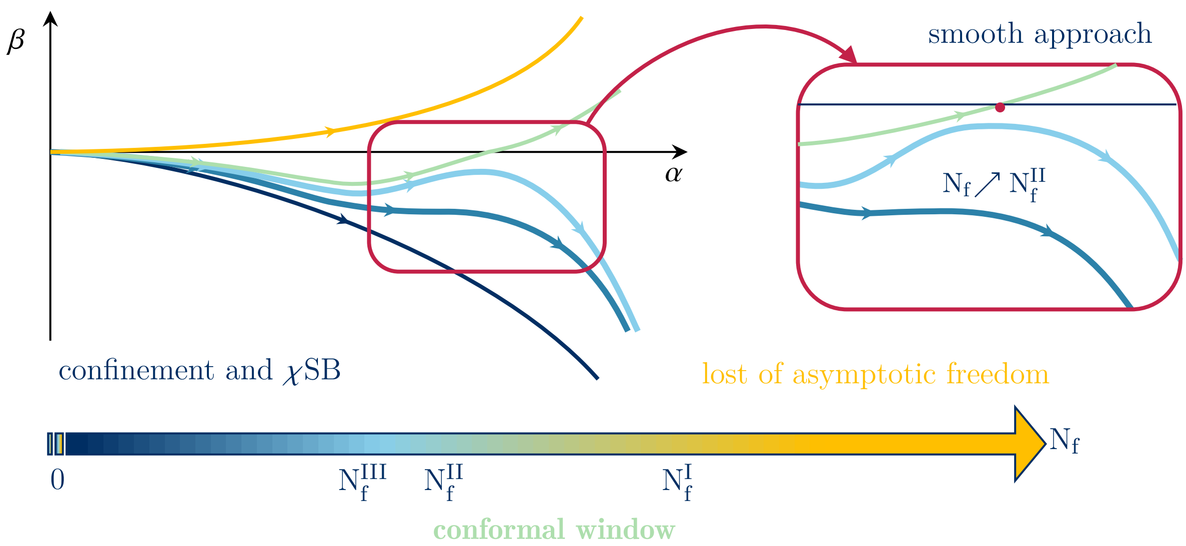

Figure 5.6.: Cartoon of the different behaviours of the β-function explained in the text.

The research topic on which this work is based is the study of the properties of near conformality of QCD-like theories. The way conformality is lost is modelled to be a small perturbation of the underlying conformal symmetry. Specifically, the transition between the conformal regime and non-conformality is essential to reproduce the walking behaviour of QCD-like theories. This transition depends on both the number of flavours of the theory and the range of energy at which the EFT is studied and is considered to be smooth. This smoothness ensures that the EFT description of the former can be obtained via a dilaton dressing. The presence of the latter, as stressed in chapter 1, non-linearly realises the conformal symmetry. The departure from the fixed point in QCD-like theories is encoded in the difference $N_f - N_f^{II}$. As a consequence, the small perturbation responsible for letting the theory feel non-conformality *is linked* to this control parameter, consequently determining the phase transition between the two regimes.

In the rest of this chapter, the motivation and the mathematical construction of a dilaton effective field theory will be presented.

§ 5.3 Light dilaton in walking gauge theories

Lattice studies of $SU(3)$ gauge theories with matter field content consisting of $N_f = 8$ fundamental (Dirac) fermions [218, 439], as well as $N_f = 2$ two-index symmetric (Dirac) fermions (sextets), have reported evidence of a light scalar singlet particle (the state $f_0(500)$) present in the spectrum, at least within the accessible range of fermion masses, whose mass is [218, 401]

$$m_{f_0} = 441 - i272 \quad \text{Mev.} \tag{5.28}$$

For a historical overview and a very comprehensive review of this topic see [386]. Let us pause for a moment to appreciate a delicate step. The question that at this point one is called to answer is the following: could there be a (pseudo)NGB (pNGB), dubbed the dilaton, linked to the spontaneous breakdown of an approximate dilation or scale symmetry within certain four-dimensional gauge theories? The $f_0(500)$ state is believed to be related to the answer to this question. Moreover, this thesis has consistently underscored that despite the particle masses vanishing, the dilation symmetry remains only in its classical form, being directly undermined by the quantum contribution of the renormalization scale. The divergence of the dilation current, j^D, mirrors the β-function $\beta(\alpha)$ proportionally, as already stressed in chapter 1 and will be reviewed in detail shortly. If this symmetry is approximate and then spontaneously broken, a light-weight dilaton could emerge as a pNGB. As a consequence, this implies that the β-function must be small which in turn means that the coupling needs to vary slowly. Gradual variation in coupling is depicted in gauge theories with non-trivial infrared fixed points.[2].

Let us recall again that *walking theories* [98] are characterised by the supercritical infrared fixed point being close to criticality, such that the scale of breaking is comparatively “small". This IRFP then dictates the behaviour of the theory across a range of momenta above the breaking scale [218]. Although the chiral-symmetry breaking scale is small compared to the scale defining UV behaviour, it represents the physical confinement scale Λ. Hence, one can reasonably infer the presence of a dilaton in the theory only if it is significantly lighter compared to this scale. In a four-dimensional field theory possessing dilation symmetry, there exists invariance under the broader group of conformal transformations. With the presence of an IRFP, the interacting theory transitions towards one characterised by conformal symmetry.

To connect the dots, this section aims to review arguments that support the possibility that a walking gauge theory can lead to the appearance of a dilaton (mostly following [218]). Therefore, let us consider an $SU(N)$ gauge theory with N_f massless Dirac fermions in the fundamental representation. Consider the Lagrangian of the theory that has been introduced in this chapter in (5.1) and consider the fields and the coupling constant to be unrenormalized. Consequently, the latter is corrected by higher-dimension, irrelevant operators [218]. Since the dominant terms are of dimension four, there is an approximate, low-energy dilation symmetry at a classical

[2] Notably, IRFPs manifest if the fermion composition of the theory weakens the fixed point, rendering it susceptible to perturbative analysis. However, in the realm of electroweak applications, the IRFP might need to be robust enough (with fermion numbers reduced sufficiently) to induce spontaneous breakdown of chiral symmetry

level. On the contrary, at a quantum level even disregarding the irrelevant operators, the dilation current j^D which is related to the symmetric energy-momentum tensor $T^{\mu\nu}$ by $J^{D\mu} = T^{\mu\nu}x_\nu$ has a non-vanishing divergence given by [387]

$$\partial_\mu j^D = T^\mu_\nu = \frac{\beta(\alpha)}{4\alpha} F^a_{\mu\nu} F^{a\mu\nu} \ , \tag{5.29}$$

where $\alpha = \alpha(\mu)$ is the renormalised gauge coupling defined at scale μ and $F^a_{\mu\nu} = \partial_\mu A^a_\nu - \partial_\nu A^a_\mu - g(Z_1/Z_2) f_{abc} A^b_\mu A^c_\nu$ with

- $A^a_\mu = Z_3^{1/2} A^a_{\mu 0}$.
- Z_2 is the fermion wave function renormalization factor: $\psi = Z_2^{1/2}\psi_0$.
- Z_1 is the fermion-gauge boson coupling renormalization factor.

Where the 0 stands for the unrenormalized coupling constant and fields. When N_f sits just below N_f^I, a perturbative infrared fixed point emerges, denoted as α^*, rendering the theory conformal in the infrared. As N_f decreases, the values of α^* increase, eventually reaching a critical strength α_c that leads to chiral symmetry breaking and confinement. Determining the critical value N_f^{II} at which this transition occurs is unlikely through perturbative methods. Although precise values for N_f^{II} remain undetermined, infrared conformal behaviour is observed across a range of N_f values, whereas chiral symmetry breaking and confinement manifest at lower values. Lattice simulations suggest that the transition at $N_f = N_f^{II}$ is of second order or higher [455] (and references therein).

Stressing again, walking behaviour ensues when N_f approaches but remains below N_f^{II} it follows that $0 < N_f^{II} - N_f \ll N_f^{II}$. Consequently, one anticipates $0 < \alpha^* - \alpha_c \ll \alpha_c \leq O(1)$. The chiral symmetry breaking and confinement scales match the magnitude of the scale Λ where $\alpha(\mu)$ and α_c converge [125, 218, 385]. This scale is much smaller than the one defining perturbative ultraviolet behaviour as N_f approaches N_f^{II}, while α is controlled by the infrared fixed point over scales above Λ.

In its simplest guess, when $N_f > N_f^{II}$ the β-function has a linear zero [218, 445]

$$\beta(\alpha) \approx -s(\alpha^* - \alpha) + O\Big((\alpha^* - \alpha)^2\Big) \tag{5.30}$$

where $s > 0$ is the slope at $\alpha^* = \alpha$. Therefore, this expression governs the evolution of α as $\mu \to \Lambda$ for a range of μ above Λ. Solving the equation gives

$$\alpha \approx \alpha^* - (\alpha^* - \alpha)\left(\frac{\mu}{\Lambda}\right)^s \implies \beta(\alpha) \approx s(\alpha^* - \alpha)\left(\frac{\mu}{\Lambda}\right)^s \ . \tag{5.31}$$

Hence, the β-function is small for the range $0 < \alpha^* - \alpha_c \ll \alpha_c$ when μ is above Λ. Additionally, this result suggests that conformal perturbation theory can be used to compute the mass of the dilaton in analogy to that of the pions in QCD.

First, let us review the derivation of the partially conserved axial current (PCAC) formula for the pion mass. The pion decay constant is defined via [53]

$$\big\langle 0 \big| j^{5a}_\mu(x) \big| \pi^b(p) \big\rangle = -iF_\pi \delta^{ab} p_\mu e^{-ipx} \tag{5.32}$$

and since

$$\partial^\mu j_\mu^{5a} = 2m j^{5a} \tag{5.33}$$

then

$$\left\langle 0 \middle| j_\mu^{5a}(0) \middle| \pi^b(p=0) \right\rangle = -\frac{F_\pi m_\pi^2}{2m} \delta^{ab} \ . \tag{5.34}$$

At this point, using the local version of $\left[iQ^{5a}, j^{5b}\right] = \delta^{ab}\bar{\psi}\psi$ and approximate current conservation one has the PCAC formula for the pion mass

$$m_\pi^2 \simeq -\frac{2m \langle 0|\bar{\psi}\psi|0\rangle}{F_\pi^2} \tag{5.35}$$

this expression is μ-independent since the anomalous dimension $\gamma(\mu)$ of the operator j^{5a} is opposite of that of $m = m(\mu)$. The same procedure can be repeated for deriving the mass of the dilaton based on a partially conserved dilation current, PCDC. In this way, the scale-symmetry-breaking term is chosen to obtain a scale current proportional to the dilaton field. To this end, one assumes the existence of a dilaton state $|\sigma(p)\rangle$ and that $N_f \lesssim N_f^{II}$ so if $|0\rangle$ denotes the vacuum state corresponding to spontaneously broken chiral and dilation symmetry, then [218]

$$\langle 0|T^{\mu\nu}(x)|\sigma(p)\rangle = \frac{f_\sigma}{3}(p^\mu p^\nu - g^{\mu\nu}p^2)e^{-ipx} \tag{5.36}$$

with $p^2 = m_\sigma^2$. The role analogous played by $\bar{\psi}\psi(x)$ will be now taken by $F^a_{\mu\nu}F^{a\mu\nu}(x)$. However, while $\langle 0|F^a_{\mu\nu}F^{a\mu\nu}(x)|\sigma(p)\rangle$ is finite, $\langle 0|F^a_{\mu\nu}F^{a\mu\nu}(x)|0\rangle$ is not since it plays the defining role in spontaneous dilation-symmetry breaking. Nevertheless, this piece will be removed by subtraction scheme. So, one considers $\mu = \lambda\Lambda$ with $\lambda \geq 1$ such that $\alpha(\lambda\Lambda) \approx \alpha(\Lambda)$ and defines

$$[T^\mu_\mu]_\Lambda = \frac{\beta(\alpha)}{4\alpha}F^a_{\mu\nu}F^{a\mu\nu} - \langle 0|\frac{\beta(\alpha)}{4\alpha}F^2|0\rangle_{p\geq\lambda\Lambda} \ . \tag{5.37}$$

At this point [218], one uses the fact that the underlying theory is approximately conformal at momentum scales of order Λ and that the operator $[T^\mu_\mu]_\Lambda$ has vanishing anomalous dimension so that $\left[i[Q]_\Lambda, [T^\mu_\mu]_\Lambda\right] \simeq 4[T^\mu_\mu]_\Lambda$. Making use of the local version of this commutation relation and using $\partial_\mu[D^\mu(x)]_\Lambda \simeq 0$ one has

$$i\partial_\mu \langle 0|\mathcal{T}[D^\mu(x)]_\Lambda[T^\mu_\mu(0)]_\Lambda|0\rangle \simeq 4\delta^4(x)\langle 0|[T^\mu_\mu]_\Lambda|0\rangle \ . \tag{5.38}$$

Therefore, the PCDC formula for the dilaton mass reads

$$m_\sigma^2 \simeq -\frac{4}{f_\sigma^2}\langle 0|[T^\mu_\mu]_\Lambda|0\rangle \ . \tag{5.39}$$

Now, for an order of magnitude estimate, it is reasonable to take $f_\sigma \simeq \Lambda$ and then to use the simplest assumption that the IRFP is described by a linear zero of the β-function. Hence

$$m_\sigma^2 \simeq \frac{s(\alpha^* - \alpha_c)}{\alpha_c}\Lambda^2 \simeq \frac{N_f^{II} - N_f}{N_f^{II}}\Lambda^2 \tag{5.40}$$

which in the limit $N_f \to N_f^{II}$, since $\Lambda \to 0$, the dilaton mass vanishes more rapidly than the order parameter $\langle 0|[F^a_{\mu\nu}F^{a\mu\nu}]_\Lambda|0\rangle$.

To summarise, this section shows that in scenarios where gauge theories are controlled by an approximate fixed point in the infrared (i.e. walking behaviour), the explicit breaking of conformal symmetry at these scales is minimal. If confinement and spontaneous chiral symmetry breaking occur at a certain infrared scale, the breaking of the approximate conformal symmetry could result in the emergence of a dilaton. Its mass may be significantly smaller than the confinement scale, making it a potential candidate for detection at the LHC [52]. This reasoning encourages the investigation of dilaton dynamics and its role in low-energy gauge theory. Thus, the next section formalises these concepts mathematically, integrating different approaches from the literature.

§ 5.4 A dilaton effective field theory

Throughout this thesis, the dilaton has been presented as a neutral Nambu-Goldstone boson resulting from the spontaneous breaking of scale invariance. It has long been considered a potential player in fundamental physics (see, e.g., [53, 339]). However, a probable loophole stems from the fact that if an approximate symmetry under scale transformations emerges over a certain energy range and if the forces cause this symmetry to be violated by the system's ground state (the vacuum), the natural outcome would be the presence of an approximate, light dilaton.

On the one hand, the previous idea seems reasonable if the explicit breaking is small so that one can talk about “approximate" scale invariance that can in turn be spontaneously broken. On the other hand, at the quantum level, the process of explicit breaking appears with both fixed dimensionful parameters in the Lagrangian and via renormalisation. This process generates a confinement scale Λ for the case of QCD-like theory. The existence alone of this scale explicitly breaks dilation symmetry.

Therefore, since approximate scale invariance appears only at higher energies there is apparently no reason to expect the presence of an approximate dilaton in the spectrum [218, 445, 446, 460, 477]. However, as the number of light fermions in a gauge theory increases, the running of the gauge coupling slows down (see Figure 5.6). It has been speculated that this can lead to the development of an approximate dilation symmetry, which is then spontaneously broken at scales relevant to bound-state formation [438–440]. Recent lattice studies have supported this idea, suggesting the presence of an approximate dilaton. In this scenario, gauge theories exhibit both confinement and near conformal behaviour.

Motivated by the possibility that a dilaton could be associated with the state $f_0(500)$ [386], an effective field theory framework extending the field content of the chiral Lagrangian has been developed through the last decades. This framework includes a dilaton field σ along with the pseudo-Nambu-Goldstone boson fields π, as discussed for example in [226, 475, 476] and references therein. Dilaton EFTs (dEFTs)[3] are of general interest, extending beyond the study of $SU(3)$ lattice gauge theories. For example, the

[3] See [234] for a pedagogical introduction

Higgs particle might originate as a light dilaton in extensions of the Standard Model of particle physics. Suggestions in this direction are found in Refs. [123, 477], with revivals in the context of compositeness and dynamical electroweak symmetry breaking or in new suggestive proposals [304, 305].

Accordingly, in the remainder of this preliminary chapter, there will be a quick round-up of dEFTs well-established in literature and of interest for this thesis work and, of course, for the remaining chapters of the latter. The presentation of these topics mainly follows [53,198,228], reviewing their works as they did. The proposals will be addressed neutrally, highlighting the authors' perspectives and differing scientific reasons. Each proposal's advantages and disadvantages, along with the scientific reasoning, will be highlighted. Additionally, the thesis will clearly explain why one proposal is favoured over the others.

5.4.1 A first example: the Coleman dEFT

In [53], Coleman discusses a simple phenomenological Lagrangian where the scale invariance (thus conformal invariance in the sense clarified in chapter 1) is realised as a Nambu-Goldstone symmetry. The basic idea consists of considering a scalar field χ transforming in the conventional way under scale transformations

$$\chi(x) \mapsto e^{\alpha}\chi(e^{\alpha}x) \tag{5.41}$$

and then introduce a new field σ defined as

$$\chi = \frac{e^{-f\sigma}}{f} \tag{5.42}$$

with f a constant having the measure of length. This new field transforms non-linearly. Hence, a scale-invariant (conformally invariant) Lagrangian for σ is simply

$$\mathcal{L} = \frac{1}{2}\partial\chi\partial\chi = \frac{1}{2}\partial\sigma\partial\sigma e^{-2f\sigma} \ . \tag{5.43}$$

The field σ can be used to make manifestly scale-invariant any Lagrangian by multiplying the scale-breaking parts by the appropriate powers of $e^{-f\sigma}$. For the moment, σ is massless: it is the Goldstone boson of scale invariance. However, one can choose the scale-symmetry breaking term to obtain the scale current proportional to σ. A naive and simple guess made by Coleman is the following potential

$$V(\sigma) = -\frac{m_\sigma^2}{16f^2}\left(1 - 4f\sigma - e^{-4f\sigma}\right) \tag{5.44}$$

that when expanded in powers of σ reads

$$V(\sigma) = \frac{m_\sigma^2}{2}\sigma^2 + \mathcal{O}\left(\sigma^3\right) \tag{5.45}$$

which is exactly in the form of a mass term for the σ field.

5.4.2 Power counting scheme: a dEFT via a triple limit

As a second proposal, let us go through the work of [222, 224, 236, 238, 239, 301, 445, 460]. The discussion will mainly follow [198].

To set the stage, let us first stress an important difference between chiral symmetry breaking, dilation breaking, and conformal breaking. In fact, in the case of chiral symmetry, the fermion mass m is a parameter that can be continuously adjusted so that, as m approaches zero, exact chiral symmetry is restored and the pions become massless. In contrast, while scale invariance is softly broken by the fermion mass, its breaking by the scale dependence of the renormalized coupling constitutes a hard breaking. Even if the fermion mass is set to zero, there is no other parameter to continuously control the explicit breaking of scale invariance encoded in the β-function. Furthermore, for confinement and chiral symmetry breaking to ultimately occur, the coupling must continue to grow as the energy scale decreases. Thus, the hard breaking of dilation symmetry by the running (or walking) of the coupling is fundamentally different from the soft breaking of chiral symmetry by a fermion mass term.

As stressed by the authors, a similar concept comes from the effective low-energy treatment of the anomalous axial symmetry $U(1)_A$. In this scenario, there is no way to "turn off" the anomaly within a given theory. To address this, one considers the large-N limit, where the number of colours N is taken to infinity while the number of flavours remains fixed [260, 261, 338, 357, 462, 463]. In this limit, the axial anomaly becomes negligible, and the flavour-singlet pseudo-scalar meson eventually becomes as light as the pions[4].

Let us define a reference scale to measure dimensionful quantities in the effective theory. This reference infrared scale will be set using one of the decay constants, either the pion decay constant F_π or the dilatonic meson decay constant f, in the chiral limit. The large-N scaling behaviour of these two quantities is given by the two-point function of j^{5a}_μ or $T_{\mu\nu}$ and reads

$$F_\pi \sim \sqrt{N} \quad \text{and} \quad f \sim N \tag{5.46}$$

which in turn can be used to set the dynamical IR scale Λ_{IR} as

$$\Lambda_{IR} \sim \frac{4\pi F_\pi}{\sqrt{N}} \sim \frac{4\pi f}{N}\,, \tag{5.47}$$

and it is used to construct the power counting of the usual order-by-order construction of the effective Lagrangian

$$\frac{m}{\Lambda_{IR}} \sim \frac{q^2}{\Lambda_{IR}} \tag{5.48}$$

where δ is used to label the small expansion parameter of the effective theory while q^2 is the square of the momentum of the Goldstones and m is the fermion mass. As already anticipated in chapter 3, the leading-order effective Lagrangian consists of terms coming in powers of q^2/Λ_{IR} while the next-to-leading order terms are q^2/Λ_{IR} squared and so on.

Crucial here is the following observation. In $SU(N)$ gauge theories with N_f Dirac

[4] For further details see appendix C.

fermions in the fundamental representation, the so-called Veneziano limit is defined as the limit where $N \to \infty$ while keeping $\epsilon = \frac{N_f}{N}$ fixed. For the fundamental representation, asymptotic freedom is lost when $\epsilon = \frac{11}{2}$ and the conformal window is indeed guaranteed for $\lim_{N\to\infty} \frac{N_f^{II}}{N} \equiv \epsilon^{II} < \epsilon < \frac{11}{2}$. Hence, the corresponding chiral broken phase is defined by $\epsilon < \epsilon^{II}$. N and N_f are integers but in the Veneziano limit ϵ becomes a continuous parameter.

In constructing the dEFT here reviewed, the three small parameters of the low-energy expansion are

$$i)\ \frac{m}{\Lambda_{IR}}, \qquad ii)\ \frac{1}{N}, \qquad iii)\ \epsilon - \epsilon^{II}. \tag{5.49}$$

Being $iii)$ the result of the large-N limit, the quantity $\epsilon - \epsilon^{II}$ cannot be parametrically smaller than $ii)$: This means that $i)$ and $ii)$ can be arbitrarily small independently of each other, but the same is not true for the condition $iii)$ since it depends on $ii)$. One can assert that the behaviour of the pion mass reads

$$\frac{m_\pi^2}{\Lambda_{IR}^2} \sim \frac{m}{\Lambda_{IR}} \frac{(\epsilon - \epsilon^{II})^0}{N^0} \sim \frac{m}{\Lambda_{IR}}\ . \tag{5.50}$$

These premises establish the fundamental principles for this subsection. Let us rewind the tape and start the discussion from the beginning to appreciate the flow and the construction of a dilaton effective field theory[5].

The massless microscopic theory possesses chiral symmetry, which, when spontaneously broken, results in Nambu-Goldstone bosons known as pions. Upon introducing a non-zero mass for the fermions, the pions acquire mass but remain the lightest asymptotic states as long as the fermion mass is sufficiently small. Consider N_f Dirac fermions in the fundamental representation, a complex representation when $N \geq 3$. Following chapter 3, the symmetry breaking pattern is $SU(N_f)_L \times SU(N_f)_R \to SU(N_f)_V$, with $SU(N_f)_V$ being the diagonal sub-group. The Lagrangian of the microscopic theory is

$$\mathcal{L}_{\text{MIC}}(\chi) = -\frac{1}{4}F^2 + \bar{\psi}\, \not{D}\psi + \bar{\psi}_R \chi^\dagger \psi_L + \bar{\psi}_L \chi \psi_R\ , \tag{5.51}$$

where χ is an $N_f \times N_f$ matrix-valued spurion, acting as an external source field and $\psi_{R,L} = \frac{1}{2}(1 \pm \gamma_5)\psi$ and $\bar{\psi}_{R,L} = \frac{1}{2}\bar{\psi}(1 \mp \gamma_5)$. Let us recall that under a chiral rotation, they transform as

$$\psi_{L,R} \to g_{L,R}\psi_{L,R}, \quad \bar{\psi}_{L,R} \to \bar{\psi}_{L,R} g_{L,R}^\dagger, \quad \chi \to g_L \chi g_R^\dagger \tag{5.52}$$

where $g_{L,R} \in SU(N_f)_{L,R}$. The Lagrangian $\mathcal{L}_{\text{MIC}}(\chi)$ remains invariant under the chiral transformation applied to all fields, including the spurion. Setting the external source $\chi(x) = 0$, $\mathcal{L}_{\text{MIC}}(0)$ corresponds to the Lagrangian of the massless theory. Alternatively, setting the chiral source to a non-zero value $\chi(x) = m$, $\mathcal{L}_{\text{MIC}}(m)$ loses chiral invariance, exhibiting explicit (soft) breaking of chiral symmetry via the fermion mass term, indicated by $\delta\mathcal{L}_{\text{MIC}}(m) = m\delta(\bar{\psi}\psi)$. The chiral spurion has a dual role: encoding explicit chiral symmetry breaking from the mass term while assigning chiral transformation properties to the mass matrix, maintaining the Lagrangian of the massive theory formally invariant. These transformation properties will constrain the structure of the chiral

[5] Part of this dissertation covers arguments of chapter 3.

Lagrangian [198].

This section aims to construct an effective field theory that incorporates the dilaton field. In doing this, one needs to write down the theory in terms of the meson fields that possess the same properties as the microscopic ones. Hence, let us first recall that the Lagrangian of the low-energy effective theory is (at leading order)

$$\mathcal{L}_{\mathrm{EFT}} = \frac{F_\pi^2}{4}\,\mathrm{Tr}\{\partial_\mu \Sigma^\dagger \partial_\mu \Sigma\} - \frac{F_\pi^2 B}{2}\,\mathrm{Tr}\{\chi^\dagger \Sigma + \Sigma^\dagger \chi\}\ , \tag{5.53}$$

which depends on two low-energy constants (LECs): F_π and B. The effective field Σ_{ij} is identified with the fermion bilinear $\mathrm{Tr}\{\psi_{L,i}\psi_{R,j}\}$, inheriting its transformation properties

$$\Sigma \to g_L \Sigma g_R^\dagger\ . \tag{5.54}$$

For $\chi(x) = m > 0$:

$$\mathcal{L}_{\mathrm{EFT}} = -F_\pi^2 B m N_f + \mathrm{Tr}\{(\partial_\mu \pi)^2 + 2mB\pi^2\} + O(\pi^4) \tag{5.55}$$

where the non-linear field $\Sigma(x) = \exp(2i\pi(x)/F_\pi)$ is expanded around its classical vacuum $\langle\Sigma\rangle = 1$. At tree level, B is linked to the pion mass and F_π is the pion decay constant in the chiral limit (up to normalisation conventions).

The leading-order chiral Lagrangian contains only two terms because the chiral Lagrangian provides a systematic expansion in the external momenta and fermion mass, as outlined in chapter 3. Denoting the small expansion parameter by δ, the power counting is

$$\frac{q^2}{\Lambda^2} \sim \frac{m}{\Lambda} \sim \delta \tag{5.56}$$

where q^2 represents the inner product of any two external momenta, and $\Lambda = 4\pi F_\pi$ is the reference scale, typically identified as the ultraviolet cut-off of the chiral Lagrangian. This approach works because the mass of the pions, which sets the energy scale for the effective Lagrangian, tends to zero in the chiral limit. At leading order, terms of order δ^1 are considered, yielding only the two operators in (5.53).

Having recalled the power counting of the low-energy theory, let us now turn our attention to scale transformations, acting on coordinates and fields [198]. Given a field $\Phi(x)$, its variation under an infinitesimal dilation is

$$\delta\Phi = x^\mu \partial_\mu \Phi + \Delta\Phi \tag{5.57}$$

where Δ is the scaling dimension of Φ. In a theory with gauge and fermion fields (but no elementary scalar fields), in chapter 1 was shown that the dilation current is given by

$$j_\mu^D = x^\nu T_{\mu\nu} \tag{5.58}$$

where $T_{\mu\nu}$ is the energy-momentum tensor. Hence, the dilation current equals the trace of the energy-momentum tensor

$$\partial_\mu j_\mu^D = T_\mu^\mu \equiv -T\ , \tag{5.59}$$

where $T = T_{\rm cl} + T_{\rm an}$, with

$$T_{\rm cl}(m) = m\bar{\psi}\psi, \quad T_{\rm an}(m) = \frac{\beta(g^2)}{4g^2}F^2 + \gamma m\bar{\psi}\psi \ . \tag{5.60}$$

Therefore, it *suffices* to introduce a spurion field that mimics the role of χ in the chiral effective field theory. Precisely, it shall be the field responsible for the explicit breaking of scale invariance between the microscopic theory and the effective one. Following the example of chiral perturbation theory, the first task is to formally restore dilation invariance in the microscopic theory by introducing a new spurion field $\sigma(x)$. Unlike the homogeneous transformation rule, the infinitesimal variation of the dilaton field is given by

$$\delta\sigma = x^\mu\partial_\mu\sigma + 1 \ , \tag{5.61}$$

note that it appears an inhomogeneous term that will play a crucial role.

Consequently, the Lagrangian of the microscopic theory is modified to

$$\mathcal{L}_{\rm MIC}(\sigma,\chi) = \mathcal{L}_{\rm MIC}(\chi) + \sigma T_{\rm an}(\chi) + O(\sigma^2) \tag{5.62}$$

where $T_{\rm an}(\chi)$ is obtained by replacing $m \to \chi(x)$. Due to scale transformation properties, the classical variation of the Lagrangian is absent.

At this point, an important step needs to be stressed. There is a first difference in this construction compared to the chiral EFT reviewed previously. In fact if on the one hand, in this latter case, setting $\chi(x) = 0$ reproduces the massless theory with exact chiral symmetry on the other the same does not hold for scale symmetry. Setting $\chi(x) = \sigma(x) = 0$, the quantum variation of the massless theory becomes $-T_{\rm an}(0)$, indicating the trace anomaly $\frac{\beta(g^2)}{4g^2}F^2$. One concludes that the massless quantum theory is not scale invariant because the coupling runs.

Having outlined the key differences let us introduce a new effective field for the dilatonic meson, denoted $\tau(x)$, whose transformation rule is

$$\delta\tau = x^\mu\partial_\mu\tau + 1 \ . \tag{5.63}$$

Notably, this rule includes an inhomogeneous term and both σ and τ are invariant under chiral transformations.

Equipped with everything discussed so far, let us build the dEFT in the next subsection.

The construction of the leading-order effective Lagrangian

The leading-order effective Lagrangian is constructed by writing down all possible operators that depend on the effective fields Σ and τ, and on the source fields χ and σ, which are invariant under both chiral and scale transformations. Using the same power counting as for the chiral Lagrangian (terms of order δ^1) the resulting leading-order Lagrangian is [460]

$$\tilde{\mathcal{L}} = \tilde{\mathcal{L}}_\pi + \tilde{\mathcal{L}}_\tau + \tilde{\mathcal{L}}_m + \tilde{\mathcal{L}}_d \tag{5.64}$$

where

$$\begin{aligned}
\tilde{\mathcal{L}}_\pi &= \frac{F_\pi^2}{4} V_\pi(\tau-\sigma)e^{2\tau}\,\mathrm{Tr}\{\partial_\mu\Sigma^\dagger\partial_\mu\Sigma\} \quad \text{pions' kinetics}\\
\tilde{\mathcal{L}}_\tau &= \frac{f_\tau^2}{2} V_\tau(\tau-\sigma)e^{2\tau}(\partial_\mu\tau)^2 \quad \text{dilatonic meson's kinetics}\\
\tilde{\mathcal{L}}_m &= -\frac{F_\pi^2 B_\pi}{2} V_M(\tau-\sigma)e^{y\tau}\,\mathrm{Tr}\{\chi^\dagger\Sigma+\Sigma^\dagger\chi\} \quad \text{chiral mass term}\\
\tilde{\mathcal{L}}_d &= f_\tau^2 B_\tau V_d(\tau-\sigma)e^{4\tau}\ ,
\end{aligned} \tag{5.65}$$

where $\tilde{\mathcal{L}}_d$ accounts for the self-interactions of the dilatonic meson. Note that the exponent y in $\tilde{\mathcal{L}}_m$ compensates for the dependence of the transformation rule of the renormalized chiral source on the mass anomalous dimension.

The new effective Lagrangian is a prototype, as it faces the issue of arbitrary potentials V_π, V_τ, V_M, V_d. These potentials are present because the inhomogeneous terms in the variations of σ and τ cancel out in the difference $\tau-\sigma$, making any function $V(\tau-\sigma)$ to transform homogeneously with a zero scaling dimension, similar to the non-linear field Σ [222]. However, the abelian dilation symmetry does not impose algebraic constraints on the form of the $V(\tau-\sigma)$ potentials [198]. This is another difference with the Σ-dependent terms, whose structure is algebraically constrained by the unitarity of Σ and the non-abelian nature of chiral symmetry.

The four potentials in the leading-order Lagrangian can be Taylor-expanded but in doing so, infinitely many parameters are introduced, undermining predictive power. To prevent this, a re-examination of the dynamics is necessary. To effectively Taylor expand, the chiral power counting must be extended to impose a hierarchy on the Taylor coefficients of these potentials.

At this point, the power count (5.49) is invoked. First, observe that differentiating the Lagrangian of the microscopic theory with respect to the dilaton source $\sigma(x)$, and then setting the sources to zero gives

$$\frac{\partial}{\partial\sigma(x)}\mathcal{L}_{\mathrm{MIC}}\Big|_{\sigma=\chi=0} = T_{\mathrm{an}}(x)\Big|_{\chi=0} = \frac{\beta(\tilde{\alpha})}{4\tilde{\alpha}}F^2(x) = O(\delta)\ , \tag{5.66}$$

where the last equality follows from the central assumption that $\beta\sim\epsilon-\epsilon^{II}$.

Secondly, the goal is to match suitable correlation functions of the microscopic and the effective theory, setting $\sigma=0$ in the end. Let us recall that from the perspective of the effective field theory, taking n derivatives of the Lagrangian with respect to σ probes the n-th derivative of the potentials, $V^{(n)}$. Therefore, in terms of the Taylor expansion:

$$V=\sum_{n=0}^{\infty}\frac{c_n}{n!}(\tau-\sigma)^n, \tag{5.67}$$

probing c_k for $k\geq n$ [301]. Ultimately [445], the Taylor coefficients adhere to the power-counting hierarchy [6]

$$c_n = O(\delta^n)\ . \tag{5.68}$$

[6] It is important to note that while the effective theory allows for multiple σ derivatives at the same spacetime point, this is disallowed in the microscopic theory. This discrepancy is not problematic, as the effective theory pertains to hadrons, which are not point-like objects, and thus cannot resolve spacetime distances smaller than $1/\Lambda$.

The leading-order Lagrangian now consists of terms of order δ according to the power counting (5.49). Consequently, V_π, V_τ, and V_M can be discarded, as $\tilde{\mathcal{L}}_\pi$, $\tilde{\mathcal{L}}_\tau$, and $\tilde{\mathcal{L}}_M$ are already $O(\delta)$ without them. Only in V_d it is necessary to consider the first non-trivial order in its expansion. After setting $\sigma = 0$ and $\chi = m$, the leading-order Lagrangian is

$$\mathcal{L} = \mathcal{L}_\pi + \mathcal{L}_\tau + \mathcal{L}_m + \mathcal{L}_d \,, \tag{5.69}$$

where

$$\begin{aligned}
\mathcal{L}_\pi &= \frac{F_\pi^2}{4} e^{2\tau}\, \mathrm{Tr}\{\partial_\mu \Sigma^\dagger \partial_\mu \Sigma\}, \\
\mathcal{L}_\tau &= \frac{f_\tau^2}{2} e^{2\tau} (\partial_\mu \tau)^2, \\
\mathcal{L}_m &= -\frac{F_\pi^2 B_\pi}{2} e^{y\tau} m \,\mathrm{Tr}\{\Sigma + \Sigma^\dagger\}, \\
\mathcal{L}_d &= f_\tau^2 B_\tau e^{4\tau} (c_0 + c_1 \tau).
\end{aligned} \tag{5.70}$$

where the exponent y in $\mathcal{L}_m$ is exactly $\Delta_{\bar{\psi}\psi}$ appearing in (5.17), that is, $y = 3 - \gamma^*$. Combining the discussion in section 5.1.1 and section 5.2, if the transition into the conformal window is sufficiently smooth for γ, it can be shown that $\gamma = \gamma^*$ in the transformation rule of the renormalized chiral source, where γ^* is the IRFP value of the anomalous mass dimension at the edge of the conformal window.

One can explicitly manifest the expected dependence on $\epsilon - \epsilon^{II}$ of the trace anomaly in the coefficients c_n. This means that (5.67) is rearranged as

$$V = \sum_{n=0}^{\infty} \sum_{k=0}^{\infty} \frac{\tilde{c}_{nk}\, (\epsilon - \epsilon^{II})^k}{n!} (\tau - \sigma)^n \tag{5.71}$$

where $\tilde{c}_{nk}$ are independent on the three expansion parameters m, $1/N$ and $\epsilon - \epsilon^{II}$. Therefore, the parameter c_1 is the only parameter of the leading-order Lagrangian that accounts for the hard breaking of scale invariance via the walking of the coupling in the microscopic theory. The role of $\tilde{c}_{00}$, the leading-order term in the expansion of V, is more subtle. The $\tilde{c}_{00}$-dependent term is the only part of the entire Lagrangian that is $O(1)$. All other terms begin at $O(m/\Lambda_{IR})$, which aligns with how the leading-order Lagrangian typically scales according to low-energy power counting.

As shown in [222], a redefinition of the τ field allows setting $c_0 = -c_1/4$. This is equivalent to setting $\tilde{c}_{00} = 0$ and $\tilde{c}_{01} = -\tilde{c}_{11}/4$. After the redefinition, the leading-order potential is $O(m/\Lambda_{IR})$ and reads

$$\mathcal{L}_d = f_\tau^2 B_\tau e^{4\tau} c_1 \left(\tau - \frac{1}{4}\right). \tag{5.72}$$

For the rest of this work, the previous expression will be re-written by a redefinition of τ as $\tau = -f\sigma$ (to uniform the notation) and by identifying $f_\tau^2 B_\tau c_1 = m_\sigma^2/4f^2$, so that (5.72) becomes

$$V(\sigma) = -\frac{m_\sigma^2 e^{-4f\sigma}}{16 f^2} (1 + 4f\sigma) \,. \tag{5.73}$$

5.4.3 A dEFT on general grounds

The time has come to review another pillar proposal for the dilaton dynamics. Understanding the underlying premises and assumptions is crucial; the subsequent discussion follows [225] based on [234, 302].

The model that is now presented assumes that the strongly coupled dynamics of the underlying nearly conformal gauge theory can be described by a dilaton EFT which satisfies the following conditions:

1. The EFT exhibits scale invariance across a finite range of scales. At long distances, the dynamics generate a space of degenerate, distinct vacua, parameterised by a scalar field χ (see chapter 1). This scale invariance is spontaneously broken by a non-zero vacuum expectation value F_χ for this field χ, resulting in the formation of a massless scalar particle, the dilaton, whose couplings are indeed defined by F_χ.
2. Scale invariance is explicitly broken *while keeping F_χ fixed*. The dilaton is given a small mass m_χ, thereby suppressing this explicit breaking [218].
3. The EFT incorporates an internal continuous global symmetry with Lie group G, spontaneously broken to a sub-group H. The spectrum includes a set of pNGBs with couplings determined by their decay constant F_π.
4. The introduction of a tunable mass m_π for the pNGBs associated with the spontaneous breaking of G breaks the global symmetry G. This mass also explicitly breaks scale invariance through an operator with scaling dimension y.
5. The vacuum of the theory is primarily determined by a single operator in the EFT with scaling dimension Δ when performing the limit $m_\pi \to 0$.

Therefore, according to these hypotheses, the authors claim that an EFT can be constructed by starting with an exact scale-invariant theory which possesses a moduli space of vacua that are degenerate and such that scale invariance is spontaneously broken [225]. Additionally, this EFT can be *weakly* deformed by introducing perturbations explicitly breaking the scale invariance. The key point is to give a scaling dimension Δ to the operator working as the source of explicit symmetry breaking *and* this scaling dimension is considered to be unknown and to be fitted from lattice data. Precisely, the approach developed here follows section 5.2 where the starting point is a specific physical model for the mechanism that drives the transition into the conformal window. According to this model, massless theories near the edge of the conformal window are governed in the infrared by a phenomenological Lagrangian of the form

$$\mathcal{L} = \mathcal{L}_{\rm CFT} + \lambda_O O \tag{5.74}$$

where O, with dimension Δ, is responsible for the transition conformal/non-conformal. Concretely, one can perform a similar analysis of the previous section by introducing a spurion field $\xi(x)$ that is chiral symmetry invariant but transforms as follows

$$\xi(x) \to e^{-\alpha(\Delta-4)}\, \xi(e^\alpha x) \tag{5.75}$$

under a scale transformation $x \to e^{\alpha}x$. Specifically, the coupling λ_O is promoted to a spurion field $\xi(x)$. According to the above scaling transformations, the overall Lagrangian is formally invariant under the action of dilations. Moreover, note also that scale invariance is explicitly broken in the EFT by considering $\xi(x)$ to be a constant scale. As a consequence, the construction of this potential *does not demand* to describe the dynamics of QCD far away from the conformal window. To better appreciate this point, let us start by observing that in principle one can construct this potential from the following general expression

$$V(\chi) = \chi^4 \sum_{n=0}^{\infty} b_n \left(\xi\chi^{\Delta-4}\right)^n \ . \tag{5.76}$$

If one aims to extend chiral perturbation theory to include the dilaton it is necessary to consider a new small parameter to control the dilaton mass and its interactions. Careful attention is required for scale transformations as they affect both fields and coordinates. This immediately leads to the awareness that a quartic potential for the (effective) dilaton field is consistent with scale invariance. This term does not violate any symmetries of the pion-dilaton EFT and, as a result, the power counting will inevitably allow this potential to appear in the EFT with a $O(1)$ coupling [460].

In other words, it is the absence of suppression for the quartic potential by any small parameter that undermines the possibility of a systematic expansion for the pion-dilaton EFT.

Since an alternative approach is shown, it is important to stress that even though it shares the same goal as the previous one in investigating the dynamics of the dilaton, they differ in the spirit of constructing such a theory. The one already presented in the previous subsection aims to develop a power counting scheme legitimating the presence of all terms in the EFT while here the aim is not to focus on fine details of the theory but to provide a clear understanding of the overall phenomenon.

After fixing the spurion field $\langle\xi\rangle = \lambda_O$, the above potential explicitly breaks the scale invariance except for the coupling b_0 which is parametrically $O(1)$. The acknowledgement of ignorance about the value of Δ translates into the need to encode the smallness of the explicit break in the smallness of λ_O. It is thus reasonable to expand (5.76) up to terms $O(\lambda_O)$ so that [460]

$$V = b_0\chi^4 + \lambda_O b_1\chi^{\Delta} \tag{5.77}$$

and after expanding around the vev that here it is denoted with F_χ, one arrives at the following relation

$$F_\chi^{4-\Delta} = -\frac{\Delta}{4}\frac{\lambda_O b_1}{b_0} \tag{5.78}$$

that is used to write down the expression for the dilaton mass which in turn reads [228, 444, 446, 460]

$$m_\sigma^2 = 4b_0F_\chi^2(4-\Delta) \ . \tag{5.79}$$

The overall expansion mimics the one in terms of the pion mass in the usual chiral lagrangian where the latter is indeed an expansion in the parameter $m_\pi^2/(4\pi F_\pi)^2$. Since the pion mass squared is proportional to the quark mass at tree level, this ratio can be considered arbitrarily small. Hence, it can work as the regulator of a systematic low-energy expansion. Following the same reasoning, the power counting that one is employing here, $q^2 \sim m \sim \lambda_O$, leads to the following ratio to control the low-energy expansion

$$\frac{m_\sigma^2}{(4\pi F_\chi)^2} = \frac{b_0(4-\Delta)}{4\pi^2} \,. \tag{5.80}$$

However, this ratio is not parametrically small and neither it can be rendered so because of the presence of the parameter b_0. The latter, being the coupling of a scale-invariant term (and thus *acceptable a priori* in the theory), is de facto a $O(1)$ parameter.

Nevertheless, one can approach the construction of a dilaton effective field theory to grasp the physical description, disregarding a precise counting since the details of the theory are indeed unknown. Within this spirit, the key point for this construction is the second condition listed at the beginning of this subsection. One can admit that F_χ is fixed, m_σ is tunable, and *arbitrarily small* so that the ratio m_σ^2/F_χ^2 is also parametrically small. In other words, a key feature of the other EFT that now will be presented stands in tuning the dilaton mass (the explicit breaking of scale symmetry) as small as necessary while keeping F_χ fixed. In this limit, the space of vevs becomes a moduli space, presumably reflecting a similar feature in the underlying gauge theory. As shown in the previous subsections, common reasoning is that the explicit breaking in the underlying theory, and consequently in the EFT, can be made arbitrarily small by tuning the number of flavours N_f close to the critical value N_f^{II}. At this critical value, confinement transitions to IR conformality, with the emergence of fixed points. Here, instead of a precise power counting scheme, the following proposal focusses only on the EFT, employing condition 1 and condition 2 of the list as one of its fundamental principles [228, 446].

Therefore, let us go back to (5.76), demoting $\xi(x)$ to λ_O and observe that it can be re-written as [225]

$$V(\chi) = \chi^4 \sum_{n=0}^{\infty} \underbrace{(-1)^n \sum_{r=n}^{\infty} b_r \left(\xi F_\chi^{\Delta-4}\right)^r \frac{r!}{n|(r-n)!}}_{\equiv a_n} \left(\xi F_\chi^{\Delta-4}\right)^n \left[1-\left(\frac{\chi}{F_\chi}\right)^{\Delta-4}\right]^n \,. \tag{5.81}$$

Then, one truncates this potential at the linear order obtaining

$$V(\chi) = a_0\chi^4 + a_1\lambda_O\, \chi^4 F_\chi^{\Delta-4}\left[1-\left(\frac{\chi}{F_\chi}\right)^{\Delta-4}\right] + O\left(\lambda_O^2\right) \tag{5.82}$$

and, along the lines of condition 1 and 2, one arrives at

$$\lambda_O = \frac{4a_0}{a_1}\frac{F_\chi^{4-\Delta}}{\Delta-4}\,, \qquad m_\chi^2 = -4a_0\Delta F_\chi^2\,, \tag{5.83}$$

in terms of which the truncated potential reads

$$V(\chi) = \frac{m_\chi^2}{4(4-\Delta)F_\chi^2}\chi^4\left[1-\frac{4}{\Delta}\left(\frac{\chi}{F_\chi}\right)^{\Delta-4}\right] \,. \tag{5.84}$$

This suggested potential [223, 444] is made up of two contributions: a scale-invariant term proportional to χ^4, and a term proportional to χ^Δ, capturing the leading-order effect of scale deformation in the underlying theory. The normalisation of the coefficients ensures that the potential has a minimum at $\chi = F_\chi > 0$, with curvature m_χ^2.

Several comments are now necessary. The key observation refers to the second relation in (5.83), similar to (5.79) and (5.80), from which one observes that a_0 is proportional to the ratio m_χ^2/F_χ^2. As already outlined at the beginning of this subsection, this seems a loophole since the latter ratio cannot be considered parametrically small on general grounds. However, the crucial aspect of this construction stands in the second condition mentioned at the beginning of this subsection. Specifically, it is assumed that F_χ is fixed, while m_χ remains tunable and can be made *arbitrarily small*, ensuring that the ratio m_χ^2/F_χ^2 is also parametrically small. In fact, (5.84) explicitly reads as an expansion in the ratio m_χ^2/F_χ^2.

Finally, the approach discussed in the previous subsection that involves precise power counting can actually be obtained by (5.84) considering a small deformation that drives the theory away from conformality. Exactly, a marginal deformation means $\Delta \to 4$ in (5.84). However, the above potential (5.73) is the result of a precise power counting scheme that is not the same as the one used here. If one wants to re-deriving it from (5.76), one shall assume that $\Delta - 4$ is proportional to $\epsilon^{II} - \epsilon$ at the sill of the conformal window. Then, since the latter difference is small, $\Delta - 4$ is small as well. The immediate consequence is that the spurion used here $\xi(x)$ is not appropriate for the power counting but

$$\xi(x) = \lambda_{\mathcal{O}} e^{-(\Delta-4)\sigma(x)} \tag{5.85}$$

is more suitable since the spurion field is multiplied by a small parameter, $\Delta - 4$ [460].

For the upcoming chapters, the previous potential is re-written using the relation (5.42) as

$$V(\sigma) = \frac{m_\sigma^2 e^{-4f\sigma}}{4(4-\Delta)f^2}\left(1 - \frac{4}{\Delta} e^{-(\Delta-4)f\sigma}\right). \tag{5.86}$$

where $f = 1/F_\chi$ and m_σ is the mass of the dilaton field σ.

5.4.4 Merging all the pictures: the agnostic dEFT

To conclude this preliminary chapter, in this subsection the table for the framework used in chapter 6, chapter 7 and chapter 9 is prepared. To this aim, let us first observe that for all the different constructions of a dEFT presented in this section, the overall Lagrangian density is comparatively simple. In addition to kinetic terms, it contains two other types of terms that are responsible for the explicit breaking of scale invariance: a scalar potential $V(\sigma)$ for the dilaton field, and an additional operator dependent on both the pNGBs and dilaton fields, which generates masses for the pNGBs. The latter is necessary because the lattice formulation of the gauge theories of interest requires a mass term for the fermions, explicitly breaking both scale invariance and chiral symmetry. Generally, as emphasised at length in this thesis, explicit breaking of the dilation symmetry is taken into account, introducing a potential term for σ. The construction of the dilaton potential and the related power counting have been discussed multiple times in the literature and also reviewed in this last section [52, 219, 222, 224, 227, 228, 235]. To sum up, several works [52, 219, 227, 228] considered the breaking of conformality as the result of perturbing a CFT with a relevant operator O with conformal dimension Δ, i.e. possible sources of explicit conformal breaking can be modelled by perturbing the underlying conformal theory via

$$\mathcal{L}_{\mathrm{CFT}} \to \mathcal{L}_{\mathrm{CFT}} + \delta\mathcal{L}_O \quad \text{where} \quad \delta\mathcal{L}_O = \lambda_O O \,, \tag{5.87}$$

with O an operator with dimension $\Delta \neq 4$ and λ_O the associated coupling. This is exactly in the same spirit as the one proposed in section 5.2 and it is the approach that it is used in chapter 6, chapter 7 and chapter 9. The presence of such an operator generates the following effective dilaton potential [52, 226, 227, 232, 443, 444]

$$V(\sigma) = f^{-4}\, e^{-4\sigma f} \sum_{n=0}^{\infty} c_n\, e^{-n(\Delta-4)f\sigma} \,, \tag{5.88}$$

where the coefficients c_n depend on the microscopic theory and scale as $c_n \sim \lambda_O^n$ [52, 227, 232, 444].

In the present work, the interest is on those scenarios where the explicit conformal breaking is small which, in turn, can be realised when $\lambda_O \ll 1$ and/or $\Delta \to 4$. In the first case, one can truncate the expansion (6.8) and obtain [52, 223, 227, 232, 444]

$$V(\sigma) = \frac{m_\sigma^2 e^{-4f\sigma}}{4(4-\Delta)f^2}\left(1 - \frac{4}{\Delta} e^{-(\Delta-4)f\sigma}\right) + O(\lambda_O^2) \,, \tag{5.89}$$

which is obtained by retaining only the first two terms in eq.(5.88) (exactly equation (5.86)). Then the coefficients c_0 and c_1 are fixed requiring $\sigma_0 \equiv \langle\sigma\rangle = 0$ and defining the dilaton mass as $m_\sigma^2 \equiv \left.\frac{\partial^2 V(\sigma)}{\partial\sigma^2}\right|_{\sigma=\langle\sigma\rangle}$. Concretely, the first two unknown coefficients have been fixed by requiring that the ground state occurs for $\sigma = 0$ and that the mass squared of σ on the ground state is m_σ^2. These constraints link the c_0 and c_1 coefficients as follows

$$\frac{c_1}{c_0} = -\frac{4}{\Delta} \,, \quad \text{with} \quad c_0 = \frac{f^2\, m_\sigma^2}{4(4-\Delta)} \,. \tag{5.90}$$

The potential (5.89) has been considered in various recent studies of QCD-like theories in the near conformal regime [2, 219, 226–228, 234, 302] as well as in the description of dense skyrmion matter [4, 325, 327]. In the EFT spirit, the nature of the conformal breaking deformation and its conformal dimension Δ are left unspecified [7]. When $\Delta = 2$ eq.(5.89) reduces to the usual ϕ^4 Higgs-like potential whereas when Δ vanishes the coefficient c_1 becomes parametrically larger than c_0 and for $\Delta = 0$ the potential (5.89) diverges.

The power counting leading to eq.(5.89) is[8]

$$q^2 \sim m \sim m_\sigma^2 \quad \text{with} \quad m \quad \text{the quark mass.} \tag{5.91}$$

[7] The potential (5.89) has also been related to the gluon condensate $\langle G^2\rangle$ and the usual soft dilaton theorems [223, 227]. However, it has recently been argued that the only value of Δ consistent with the soft theorems is $\Delta = 2$ [365].

[8] See [228] for a detailed discussion of the power counting associated with the dilaton potential eq.(5.89).

Moreover, in QCD-like theories one naturally expects that the conformal-breaking parameter m_σ^2 depends on $N_f - N_f^{II}$ [123].

The case of $\Delta = 0$ must be handled with care. Here, one must retain at least one extra term in (5.88), namely the one with the c_2 coefficient. The c_1 term becomes a σ independent constant that can be set to zero. Imposing the very same conditions adopted earlier, one arrives at

$$V^{(1)}_{\Delta\to 0}(\sigma) = \frac{m_\sigma^2 \cosh(4f\sigma)}{16f^2} \,, \tag{5.92}$$

where now $c_0 = c_2 = \frac{f^2 m_\sigma^2}{32}$ and $c_1 = 0$. In this limit, the final dilaton potential preserves a Z_2 symmetry whose existence depends on the structure of the specific underlying CFT and its deformation. On the other hand, expanding eq.(5.89) around $\Delta = 0$ leads to

$$V^{(2)}_{\Delta\to 0}(\sigma) = -\frac{m_\sigma^2}{4\Delta_O f^2} - \frac{m_\sigma^2}{16f^2}\left(-4f\sigma - e^{-4f\sigma} + 1\right) + O\left(\Delta_O\right) \tag{5.93}$$

and by subtracting the infinite constant appearing in the expansion one obtains the dilaton potential considered in the classic work of Coleman (in equation (5.44)) [53]

$$V(\sigma) = -\frac{m_\sigma^2}{16f^2}\left(1 - 4f\sigma - e^{-4f\sigma}\right) \,. \tag{5.94}$$

Another case where the explicit breaking of scale symmetry is small occurs when the perturbing operator O is nearly marginal. In this case, it is possible to expand eq.(5.88) in powers of $(\Delta - 4)$ obtaining

$$V_{\Delta\to 4}(\sigma) = -\frac{m_\sigma^2 e^{-4f\sigma}}{16f^2}(1 + 4f\sigma) + O\left((\Delta - 4)^2\right) \,, \tag{5.95}$$

where here the dilaton mass is related to the c_n coefficients as

$$m_\sigma^2 = \frac{4}{f^2}(\Delta - 4)\sum_{n=1}^{\infty} n c_n \,. \tag{5.96}$$

The above potential is exactly that appearing in equation (5.73) which has also been constructed in a series of recent papers [222, 224, 235–238] which, as summarised in section 5.4.2, make use of the Veneziano limit and assume the following power counting

$$q^2 \sim m \sim \frac{\left(N_f - N_f^{II}\right)}{N} \sim \frac{1}{N} \,. \tag{5.97}$$

Furthermore, the authors of [222, 224, 235–239, 301, 303] argued that eq.(5.95) is the only consistent potential for QCD-like theories. Moreover, at the considered order in the EFT expansion, eq.(5.95) coincides with the potential derived in [304] starting from the partially conserved dilation current (PCDC) relation and has often been employed to describe dense Skyrmion matter, see e.g. [314, 315, 318, 321, 323].

Crucially, since Eq.(5.95) can be seen as a subcase (the $\Delta \to 4$ limit) of eq.(5.89), in this work the generic form of the dilaton potential appearing in eq.(5.89) is considered to encompass all the proposals considered in the literature to keep the analysis as general as possible without committing to a specific model. Therefore, to conclude this section, for the sake of completeness, it is worth mentioning other potentials appearing in the literature regarding dilaton effective field theories. The following discussion points to a different speculation than the one carried out in this chapter and throughout this thesis work. The main idea starts with the consideration that conformality can be realised via a NG mode, the dilaton, specifying that the symmetry is *hidden* rather than spontaneously broken. As a consequence, particle masses and scale condensates (the quark condensate for example) can be generated dynamically when the conformal limit is reached, namely as soon as $\alpha \to \alpha_*$. Hence, the main difference lies in contemplating a scenario where walking does not occur: for values of N_f smaller than N_f^{II}, i.e. outside the conformal window, a fermion condensate is formed at non-zero coupling and *remains non-zero* at the fixed point [304], as shown in Figure 5.7.

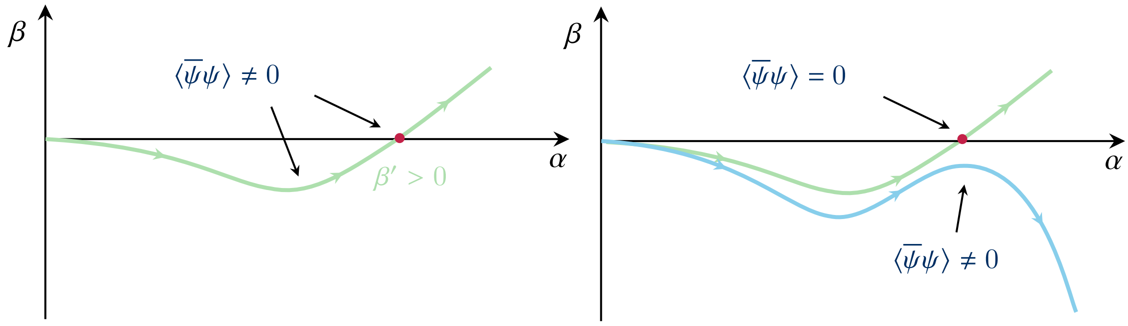

Figure 5.7.: Cartoon of the two different scenarios where a fermion condensate forms and remains non-vanishing at the fixed point (left) and becomes zero for the walking theories (right).

The spirit of this line of research is found also in those scenarios in which a new phase below the conformal window is conjectured in addition to the confinement (QCD phase) and conformal phase. This new phase is called *conformal dilaton phase* and is characterised by hadrons still carrying a mass even though the theory is conformal. The mechanism enabling this occurrence is the spontaneous breaking of conformal symmetry, where the corresponding Goldstone boson, the dilaton, restores the dilation Ward identity [305]. The potential suggested by the authors of [304] reads

$$V(\sigma) = \frac{m_\sigma^2}{4(4+\beta')f} - \frac{m_\sigma^2 e^{-4\sigma f}}{4f\beta'}\left(1 + \frac{4}{4+\beta'}e^{-\beta'\sigma f}\right) \tag{5.98}$$

with β' being the slope of the β-function as can be seen in Figure 5.7. Since the authors describe the RG flow in the proximity of an IR fixed point in Figure 5.7, the slope β' is positive. In the framework described in this subsection, this situation is exactly the opposite: the sign of $\beta' = \Delta - 4$ is dictated by the scaling dimension of an *irrelevant* operator rather than a *relevant* one. Furthermore, the first term on the right side of (5.98) is exactly the divergent constant that appears in (5.93).

5.4.5 More on the quartic potential: a cosmological constant contribution

Let us conclude this chapter with a brief detour into the conceptual question of whether spontaneous symmetry breaking of scale invariance is necessarily tied to explicit symmetry breaking, and if so, how. Firstly, by definition, spontaneous symmetry breaking occurs when the Goldstone boson associated with the broken symmetry acquires a vacuum expectation value, implying the existence of a moduli space for it. One might ask whether scale invariance can be spontaneously broken when the underlying theory is also exactly conformal.

This subsection aims to review an intriguing proposal appearing in [364], which addresses this question. Within the broader context of this chapter, the discussion is whether spontaneous symmetry breaking occurs within the conformal window. This ties into [460]'s criticism of the potential proposed by [225, 234, 302], as will soon be explained.

When a theory is exactly conformal, it either does not break scale invariance, or if it does, the breaking is arbitrary, occurring along what is known as a "preferred flat direction" [364]. For scale invariance to truly be broken in this case, there must also be explicit symmetry breaking, ensuring that this flat direction exists. Moreover, this contribution must stay sufficiently small to preserve scale invariance in the renormalization group flow. In other words, the β-function, which tracks this explicit breaking encoding the running of the coupling associated with the operator that perturbs conformal invariance, must stay small at the scale where spontaneous breaking occurs [364].

One plausible scenario is that conformality is spontaneously broken along a flat direction, which is then lifted by a potential generated via a small external coupling. This coupling, while breaking scale invariance explicitly, has a non-zero but small β-function. To refine our understanding, an important consideration is whether a light dilaton can emerge without the need for fine-tuning.

Interestingly, this scenario finds its footing in a four-dimensional theory, where a large mistuning can be understood in terms of a dilaton potential. As discussed earlier, scale invariance permits an unsuppressed quartic (non-derivative) self-interaction term for the dilaton, since a 4-dimensional operator in the action is scale invariant. In the case of a supersymmetric model, [366] presents a compelling idea: the quartic term becomes mildly energy-dependent through an explicit breaking of scale invariance, where the β-function remains small, though the coupling itself need not be.

In this framework, spontaneous symmetry breaking happens when the effective dilaton quartic term vanishes. Naturally, if the β-function remains small at the point of spontaneous breaking, the dilaton can be light. In summary, as long as the β-function of the perturbation remains small, spontaneous breaking of scale invariance will occur naturally, even in the absence of an obvious flat direction. In a sense, this mechanism ensures the existence of an approximate moduli space, providing a way forward without requiring the fine-tuning that would otherwise be needed.

The central question now is how to achieve an almost vanishing quartic coupling. The answer lies in coupling the theory to gravity. Specifically, the value of the potential at its minimum can correspond to the cosmological constant. Furthermore, it is understood that this constant is generated during the phase transition from a scale-invariant theory to its broken phase [364].

As a result of this connection, if the β- function remains small, the value of the potential at the minimum is suppressed, and consequently, the contribution to the cosmological constant is also reduced. In the remainder of this chapter, there will be a review of the basic ideas of the work of [364, 366], where the authors may have paved the way for the existence of a parametrically light dilaton in a scenario of dynamical spontaneous symmetry breaking of scale invariance, complete with hierarchical scales.

In short, coupling the theory to gravity offers a way to lower the potential at the minimum, which could explain a reduced cosmological constant and potentially lead to a light dilaton, a crucial feature in a scenario where spontaneous symmetry breaking happens at different energy scales.

Let us now consider the mathematical framework. As previously highlighted, a term like

$$\Lambda_0 \chi^4$$

is perfectly valid in a non-linearly realised, spontaneously broken, scale-invariant theory (this is exactly the C-term introduced at the end of chapter 2). However, if the theory is to be exactly conformal, one must set $\Lambda_0 = 0$. The reasoning is straightforward: if $\Lambda_0 > 0$, the minimum of the dilaton potential occurs at $\chi = 0$, which means that spontaneous symmetry breaking does not take place. On the other hand, if $\Lambda_0 < 0$, the minimum is reached as $\chi \to \infty$, leading to a breakdown of scale invariance. Therefore, with $\Lambda_0 = 0$, χ becomes a flat direction.

This raises a critical point: the possibility that such a scenario occurs. More precisely, how plausible is it for $\Lambda_0 = 0$? Λ_0 could be scale-dependent, and by introducing an external coupling, it becomes possible for SSB to occur when $\Lambda_0 \sim 0$. The running coupling drives the value of Λ_0 closer to zero, and when it reaches this critical point, spontaneous breaking of scale invariance occurs. However, to stabilise the scale, some explicit breaking must be introduced. This is achieved by adding an operator O having dimension Δ that perturbs the theory via a coupling λ_O.

As the perturbing coupling grows through renormalization group running, the effective quartic term for the dilaton gradually decreases. At the point where this quartic term vanishes, scale invariance breaks, and the perturbing operator condenses, stabilising the minimum of the dilaton potential at hierarchically small scales [364].

At this point, the smallness of the β-function becomes crucial. A small β-function ensures that the dilaton does not acquire a large mass. The work presented in [364] demonstrates that achieving a suppressed dilaton mass squared and a minimised value of the dilaton potential at its minimum is feasible if the perturbing operator is nearly marginal. If this operator remains close to marginal, even at large couplings, both quantities will be significantly reduced [364].

This discussion is connected to the content of this section; to be more precise, it strictly regards the relation between c_0 and c_1 in (5.90) along with the discussion right after (5.80). Condition (5.90) requires the two coefficients to be of the same order, which is not a natural condition in the absence of further constraints. In addition, the condition of having a parametrically light dilaton in the spectrum is linked to the necessary condition of having a parametrically small c_0. The latter argument, as seen by the above discussion, is also linked to the " smallness of the cosmological term" which in turn is equivalent to requiring the existence of a moduli space in the CFT. It is acknowledged that in the above arguments, this occurs in supersymmetric theory by requiring a large amount of fine-tuning [366]. An important theoretical open question nowadays is whether or not such behaviour also occurs in QCD-like theories below the lower edge of the conformal window.

To bring this chapter to a close, it is important to emphasise again that in a theory where scale invariance remains unbroken explicitly, spontaneous breaking of the symmetry can only occur if the cosmological constant is zero. This condition, as discussed earlier, allows for the existence of a moduli space. In chapter 6 and in chapter 7, a cosmological term has been considered, and deformations to the conformal field theory have been introduced by adding sources of conformal breaking, enabling the presence of an approximate moduli space.

In this section, the general structure of the dilaton potential and common approximations found in the literature were reviewed. Subsequent chapters will examine theories admitting the existence of an approximate moduli space and introduce sources that explicitly break scale invariance, which in turn generate a non-trivial dilaton potential. The process begins by adding a cosmological constant term to the model, as this is the simplest coupling consistent with conformal invariance (see the end of chapter 2). This term can also be understood as the first term in the infinite-series expansion of the dilaton potential.

It should be stressed that, in the presence of a dilaton potential, conformal invariance becomes only an approximate symmetry of the theory. As a result, the state-operator correspondence no longer holds exactly, and the scaling dimension is no longer equivalent to the ground state energy on the cylinder. In chapter 6 and chapter 7, it will be shown that failure of the state-operator correspondence generally leads to geometric-dependent terms in the scaling dimension, which disappear in the limit of exact conformal invariance, where the scaling and conformal dimensions coincide.

Concretely, the theories introduced in chapter 3 will be generalised by including in the action both the cosmological constant term and the dilaton potential, with the quartic self-coupling being absorbed into the definition of the cosmological constant. This sets the stage for a deeper exploration of how these terms influence the breaking of scale invariance and the structure of the theory.

This chapter is crucial for examining the near-conformality of QCD and QCD-like theories, central to this thesis. Precisely, chapter 7 aims to investigate the QCD phase diagram at finite isospin density in the presence of the θ-angle (see appendix C) at the bottom of the conformal window for the case of three colours and for quarks transforming according to the fundamental representation. In contrast, chapter 6 focusses on a similar study, but for the case of two colours and in the presence of non-zero baryon density. Last but not least, chapter 9 is centred on the study of the near conformal regime for the case of $N_f = 2$. The study of the bottom edge of the conformal window in this case can be realised in multiple ways when the number of colours is large. In Figure

5.8 there is a visual representation of the case studied in the aforementioned chapters.

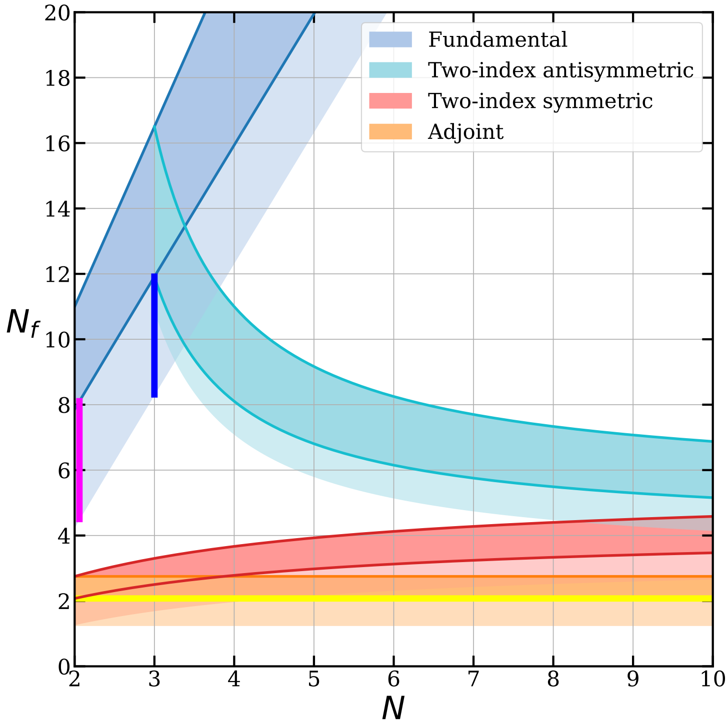

Figure 5.8.: Cartoon of the conformal windows for different representations of $SU(N)$ along with a sketch of the region of near conformality at the bottom edge of each of them. The straight lines represent the cases studied in chapter 6 (vertical magenta line), chapter 7 (vertical blue line) and in chapter 9 (horizontal yellow line).

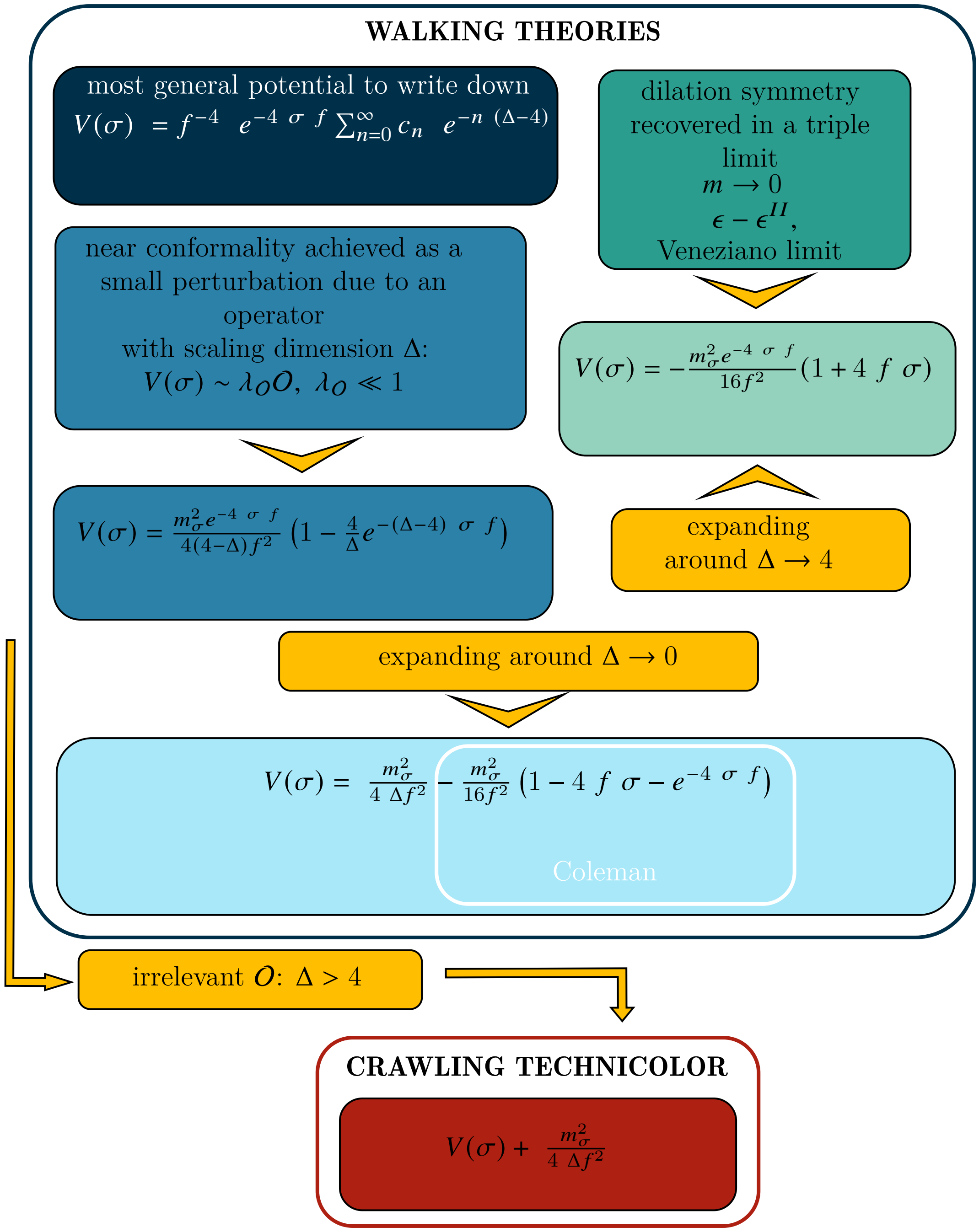

Figure 5.9.: Concept map of all the dilaton potentials discussed in this chapter and their connections.

Part IV

NEAR CONFORMAL DYNAMICS OF QCD-LIKE AND QCD THEORIES AT NON-ZERO BARYON AND ISOSPIN DENSITY

Introduction to Part III

As already stressed, the unveiling of near conformal properties of QCD has attracted much interest over the past several decades. This exploration was spurred by the seminal work of Banks and Zaks [199] who discovered the existence of a perturbative infrared fixed point in massless QCD for a number of flavours N_f just below the loss of asymptotic freedom. As one decreases N_f relative to the fixed number of colours N, one expects the theory to undergo a quantum phase transition below a critical number of flavours N_f^{II}, as explained in chapter 5. As previously anticipated, this dynamics is also known as *walking dynamics* since the underlying gauge coupling has a region in the renormalisation group flow where the coupling is almost constant and therefore walks rather than displaying running behaviour. It is worth mentioning that this walking behaviour has recently been shown to mathematically describe the endemic state of pandemics [200] using the epidemic renormalization group approach [10, 11, 201].

Several key questions are related to the dynamics near the lower boundary of the conformal window. These range from a precise determination of its lower edge to the characterisation of the quantum phase transition. Let us also mention that one exciting possibility concerning the transition is to lose conformality à la Berezinskii-Kosterlitz-Thouless (BKT) [202–204]. The latter occurs in two dimensions and was envisioned for four dimensions in [205–208]. An alternative scenario considers the quantum transition to be a jumping one [209]. The first possibility leads to infrared non-conformal physics displaying premonitory signs of near conformality that can be observed, as learnt from chapter 5, in the power-law scaling of certain phenomenologically relevant operators [210–212].

In terms of the spectrum of the theory, in the confining and chiral symmetry broken phase occurring below but near the lower end of the conformal window, besides the ordinary Goldstones, it has long been argued [213–216], as reviewed at length in chapter 5, that another precursor of a smooth quantum phase transition is the occurrence of a dilaton in the theory. In chapter 5 it has been explained that a first description at the effective Lagrangian level goes back to the work of Coleman [53] and for walking dynamics has been considered in [123, 124, 216–218]. Recent investigations via effective approaches in different dynamical regimes have appeared in [2, 4, 94, 219–228]. An explicit calculable example has been discussed in [229] where it was possible to demonstrate the emergence of a dilaton in a near CFT alongside a precise study of all the relevant scales emerging once conformality is lost[9].

Complementary ways to isolate the dilaton properties and more generally to learn about the near conformal dynamics of QCD are therefore vital to corner the properties of the flavour-driven quantum phase transition. In reality, fixed-charge sectors offer novel opportunities to investigate near conformal dynamics providing precious information on the sectors responsible for breaking conformality.

It was introduced in chapter 1 that central quantities in any CFT are scaling dimensions of local operators. By the state-operator correspondence [36] these are the energies of the corresponding states on a non-trivial gravitational background. For example, armed with the notions introduced in chapter 2, the scaling dimension of the lowest-lying operator of charge Q, denoted with Δ_Q, is mapped into the ground state energy E_Q on the cylinder via the relation

$$\Delta_Q = R\, E_Q \ , \tag{5.99}$$

with R the radius of the cylinder. Additionally, following the discussion in chapter 2, in the large charge limit one can compute scaling dimensions of fixed charge operators using semiclassical computations [75, 82, 88, 93, 240–248]. Intriguingly, the large charge framework allows to perform analytical calculations in strongly coupled quantum field theories and its predictions have been tested via numerical Monte Carlo simulations in [240, 249–252]. Additionally, for fixed charge physics [75, 82, 93, 243, 244, 253–256] the dilaton (also referred to as the radial mode in the sense explained in section 2.4.4) was introduced [94, 241] in the absence of the topological θ-term. In this thesis work, this same analysis is extended to include topological sectors of the theory. Specifically, in chapter 6 and in chapter 7, the lighthouse of the discussion is made of [2, 94, 241] and the contents extend this relation to near conformal field theories by introducing the quantity:

$$\boldsymbol{\Delta}_Q^{ex} \equiv R\, E_Q = \Delta_Q + \quad \text{near CFT terms} \ . \tag{5.100}$$

The near CFT terms depend on the way the CFT is deformed. In the case at hand, there are two sources of conformal breaking: one stemming from an explicit quark mass term and the other from the occurrence of an operator of dimension Δ inducing a dilaton potential, in the sense explained in chapter 5 and in particular in section 5.2.

The near conformal corrections are expressed in powers of the dilaton and pion masses. The θ-angle dependence is explicitly encoded in the pion mass. The novel scalings in the charge of the near conformal corrections are expressed in terms of the quark mass operator anomalous dimension γ and the one characterising the dilaton potential Δ.

Precisely, throughout Part III, applications of the large charge formalism generalised to conformal theories featuring a dilaton in the spectrum are presented. These investigations are presented by providing a precise correspondence between the dilaton properties and the large charge operator spectrum in theories featuring an approximate moduli space. In particular, it will be shown that the large charge limit simplifies considerably the dilaton potential allowing for making model-independent predictions for the Q-scaling of near conformal corrections to observables in the large charge sector

[9] A complementary analysis of the mass-induced confinement for gauge-fermion theories near the lower edge of the conformal window was performed in [230]. One can also use first principle lattice simulations to disentangle the dilaton properties. However, this is a difficult task since its quantum numbers are the ones of the vacuum and therefore it is subject to large numerical noise. Nevertheless, there have been attempts to fit effective approaches to lattice data (see, e.g., [224, 231–239]).

of the theory.

This same analysis is carried out both in chapter 6 and chapter 7. In the former, there is an attempt to study the dependence of near conformal scaling dimensions including the impact of the θ-angle for two-colour QCD with fixed baryon charge. Building on the bridge between QCD-like and QCD theories introduced in chapter 3, the aim is to gain precious information on the near conformal strongly coupled dynamics of two-colour QCD for previously inaccessible sectors of the theory, i.e., the ones with large baryon charge and non-vanishing θ-angle [257], including the presence of axions [102–107, 258, 259]. This is achieved by employing and extending the formalism developed in [1, 94, 241]. Instead, in chapter 7 the theory is the three-colour QCD and it is the isospin charge to be fixed.

In Figure 5.10 and Figure 5.11 the flowcharts summarise the contents of chapter 6 and chapter 7, respectively.

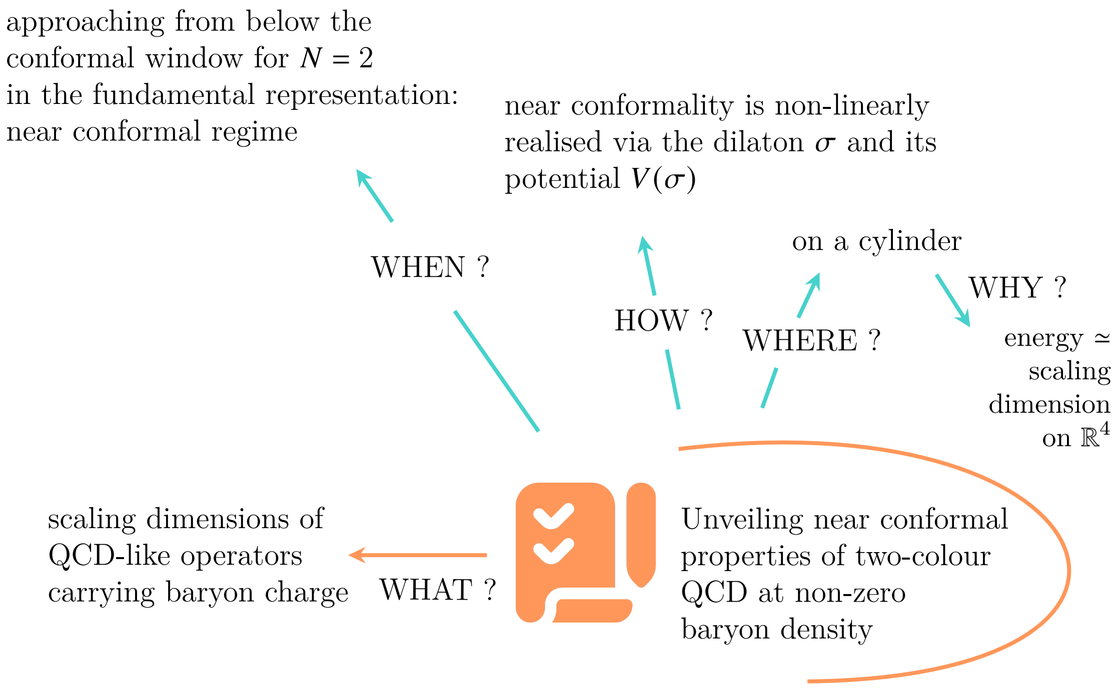

Figure 5.10.: Concept map of the contents of chapter 6.

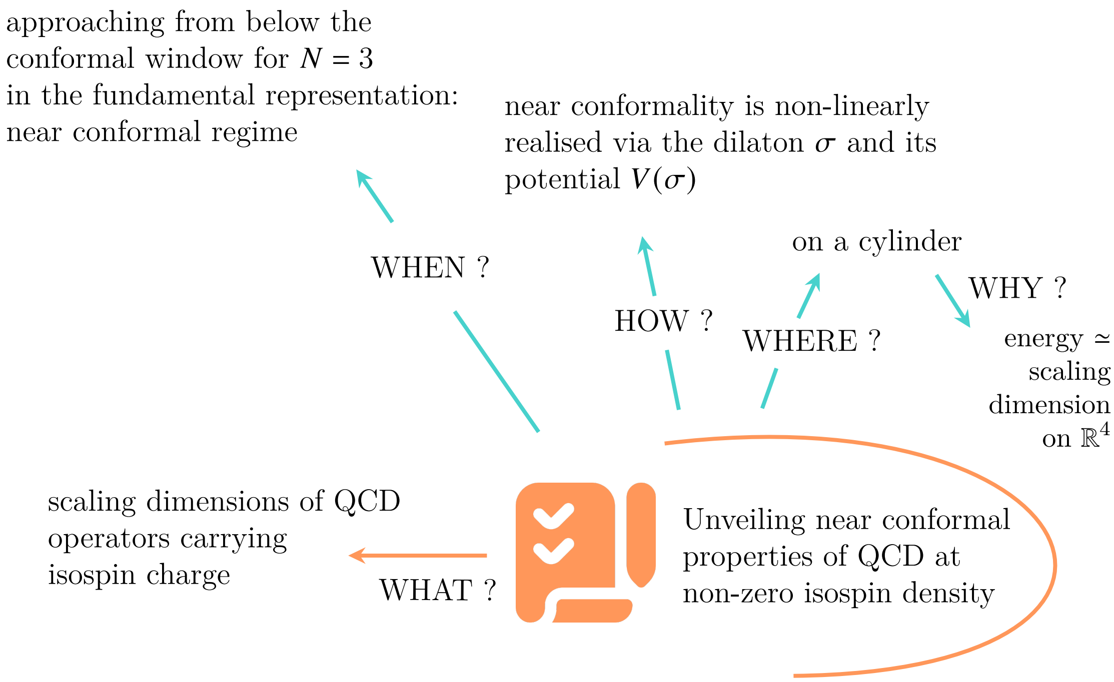

Figure 5.11.: Concept map of the contents of chapter 7.

Charging the conformal window of two-colour QCD at non-zero θ-angle and baryon density

6
Chapter

This chapter reviews the results obtained in [2]. The impact of the θ-angle and axion physics on the near conformal dynamics of the large-charge baryon sector of $SU(2)$ gauge theories with N_f fermions in the fundamental representation is determined. An effective approach featuring Goldstone and dilaton degrees of freedom, augmented by the topological terms in the theory, is employed. The effects of different dilaton potentials, including those allowing for a systematic counting scheme, are investigated. Via state-operator correspondence, corrections to the expected conformal dimensions of the lowest large-charge operators are computed as a function of the θ-term and dilaton potential.

§ 6.1 Chiral Lagrangian near the conformal window

6.1.1 Axion and θ-angle Chiral Lagrangian

Following discussions in chapter 3 and chapter 4, this chapter opens with the effective Lagrangian describing two-colour QCD at finite baryon density that it is re-written below

$$\begin{aligned}\mathcal{L} &= \nu^2 Tr\{\partial_\mu \Sigma \partial^\mu \Sigma^\dagger\} + 4\mu\nu^2 Tr\{B\Sigma^\dagger \partial_0 \Sigma\} + m_\pi^2 \nu^2 Tr\{M\Sigma + M^\dagger \Sigma^\dagger\} \\ &+ 2\mu^2\nu^2 \left[Tr\{\Sigma B^T \Sigma^\dagger B\} + Tr\{BB\}\right] .\end{aligned} \tag{6.1}$$

Let us recall that $\Sigma(t,x)$ is a matrix field that transforms in the two-index antisymmetric representation of $SU(2N_f)$, $4\pi\nu$ is the energy scale of the chiral symmetry breaking and μ is the baryonic chemical potential. The mass M and baryon charge B matrices are given by

$$M = \begin{pmatrix} 0 & -\mathbb{1}_{N_f} \\ \mathbb{1}_{N_f} & 0 \end{pmatrix} , \qquad B = 1/2 \begin{pmatrix} \mathbb{1}_{N_f} & 0 \\ 0 & -\mathbb{1}_{N_f} \end{pmatrix} . \tag{6.2}$$

To take into account the θ-angle physics and the axial anomaly, the above needs to be augmented by the following term [431]

$$\Delta\mathcal{L}_\theta = -av^2\left(\theta - \frac{i}{4}Tr\{\log\Sigma - \log\Sigma^\dagger\}\right)^2 \tag{6.3}$$

while in the presence of the Peccei-Quinn axion field N [258, 259] one has to add

$$\Delta\mathcal{L}_{\hat{a}} = v_{PQ}^2\partial_\mu N\partial^\mu N^\dagger - av^2\left(\theta - \frac{i}{4}Tr\{\log\Sigma - \log\Sigma^\dagger\} - \frac{i}{4}a_{PQ}(\log N - \log N^\dagger)\right)^2 , \tag{6.4}$$

where $\sqrt{a}$ and $\sqrt{a_{PQ}}$ are the scales of the anomalous $U(1)_A$ and $U(1)_{PQ}$ symmetries, respectively, while v_{PQ} is the scale of the spontaneous symmetry breaking of $U(1)_{PQ}$[1].

6.1.2 Near Conformal Chiral Lagrangian: The dilaton story

The aim of this chapter is the investigation of the near conformal window properties of the theory presented in chapter 4. Hence, to smoothly approach the conformal phase of the theory, recalling discussion made in chapter 1 and chapter 5, one non-linearly realises scale invariance by *dressing* the Lagrangian via a dilaton field $\sigma(x)$. The latter partially serves as a conformal compensator [52, 53, 123, 216–218, 438–440].

Therefore, under a scale transformation $x \mapsto e^\alpha x$, each operator O_k of dimension k is assumed to transform as follows

$$O_k \mapsto e^{(k-4)\sigma f}\, O_k , \tag{6.5}$$

where f is the order parameter of the spontaneous scale symmetry breaking whose pseudo-Goldstone boson transforms as

$$\sigma \mapsto \sigma - \frac{\alpha}{f} . \tag{6.6}$$

Specifically, here the fermion-induced mass term operator is assumed to have dimension $y = 3 - \gamma$, with γ being the anomalous dimension of the fermion condensate constrained to be $0 < \gamma < 2$ by the unitarity bound (see chapter 5). However, around $\gamma \simeq 1$ the underlying four fermion operator becomes near marginal and therefore one can safely concentrate the following analysis in the interval $0 < \gamma < 1$.

However, in the absence of the underlying quark mass, the underlying conformal symmetry can break due to the emergence of another operator O with scaling dimension Δ just below the critical number of matter fields below which conformality is lost. This dynamics is encoded in the dilaton potential. This amounts to adding to the CFT the following Lagrangian term:

$$\delta L_O = \lambda_O O . \tag{6.7}$$

Here λ_O is the associated coupling to the Lagrangian. One expects this operator to be, for example, related to the emergence of a quasi-relevant four-fermion interaction [205, 208, 432, 433].

[1] For more details see appendix C.

Let us recall the discussion in section 5.4.4. The general form of the dilaton potential is

$$V(\sigma) = f^{-4}\, e^{-4\sigma f} \sum_{n=0}^{\infty} c_n\, e^{-n(\Delta-4)f\sigma} \;, \tag{6.8}$$

as can be shown by introducing a spurion field taking into account the explicit breaking of conformal symmetry [52, 443, 444, 446]. Here Δ is the scaling dimension of O while the c_n depend on the given theory. Since the goal consists in describing near conformal dynamics, the basic assumption henceforth is to assume that the explicit breaking is small. This can be realized when $\lambda_O \ll 1$ and/or O is near marginal. In the former case, one expects $c_n \sim \lambda_O^n$.

Inspired by the above ordering one could truncate the expansion (6.8) to the first two terms and obtain [52]

$$V(\sigma) = \frac{m_\sigma^2 e^{-4f\sigma}}{4(4-\Delta)f^2}\left(1 - \frac{4}{\Delta} e^{-(\Delta-4)f\sigma}\right) + O(\lambda_O^2) \;. \tag{6.9}$$

Here the first two unknown coefficients have been fixed by requiring that the ground state occurs for $\sigma = 0$ and that the mass squared of σ on the ground state is m_σ^2. These constraints link the c_0 and c_1 coefficients as follows

$$\frac{c_1}{c_0} = -\frac{4}{\Delta}\;, \quad \text{with} \quad c_0 = \frac{f^2\, m_\sigma^2}{4(4-\Delta)} \;. \tag{6.10}$$

The coefficient of the cosmological constant c_0 is thereby forced to be of the same order as the first coefficient of the series $c_1 \sim \lambda_O$. This potential has been used in recent investigations [446], including comparisons with lattice simulations [228]. Assuming $\Delta = 2$ one recovers the usual ϕ^4 Higgs-like potential while in the $\Delta \to 0$ limit one obtains

$$V_{\Delta\to 0}(\sigma) = -\frac{m_\sigma^2}{4\Delta f^2} - \frac{m_\sigma^2}{16 f^2}\left(-4f\sigma - e^{-4f\sigma} + 1\right) + O\left(\Delta\right) \;. \tag{6.11}$$

The order $O\left(\Delta^0\right)$ term in the above expression coincides with the dilaton potential considered in the pioneering work of Coleman [53].

Another interesting limit is the one for which the deformation itself is nearly marginal $\Delta \to 4$. Here one expands eq.(6.8) in powers of $\Delta - 4$ obtaining

$$V(\sigma) = -\frac{m_\sigma^2 e^{-4f\sigma}}{16 f^2}(1 + 4f\sigma) + O\left((\Delta-4)^2\right) \;. \tag{6.12}$$

In fact, one can satisfy the conditions that the potential is minimised for $\sigma = 0$ and that at the leading order in $\Delta - 4$ the mass for the dilaton is m_σ without assuming an expansion in λ_O. The same potential can be derived from (6.9) in the double limit $\Delta \to 4$ and $\lambda_O \to 0$.

Before continuing with the discussion, let us stress that the potential in (6.12) obtained central stage in a series of interesting papers by Golterman and Shamir [222, 224, 236, 239, 301, 303, 434]. As already reviewed, in these works the authors considered a dilaton EFT featuring the following counting in the parameters $p^2 \sim m \sim N_f - N_f^{II} \sim 1/N$. N_f^{II} is taken to be the critical number of fermions marking the onset of the IR fixed point, and

m is the quark mass.

While (6.9) holds generally without specifying the scaling dimension Δ, this chapter will focus on the established potentials for $\Delta \to 4$, $\Delta = 2$, and $\Delta \to 0$. In the latter case, the divergent constant in eq.(6.11) will be ignored.

6.1.3 Baryon charging the Dilaton-θ-Axion-Chiral Lagrangian

Armed with the notions of chapter 1 and chapter 2, to access the (near) conformal dynamics of large charge operators let us consider our system on a manifold $\mathcal{M}$ with volume V and curvature R such that the underlying new scale of the theory is $\Lambda_Q = (Q/V)^{1/3}$ where Q is the fixed baryon charge. Concretely, here the manifold is taken to be $\mathcal{M} = \mathbb{R} \times S^{d-1}$. Let us recall here that the advantage of having performed such a map is that, in the conformal limit $m_\pi = m_\sigma = 0$, one can now consider the state-operator correspondence which links the conformal data Δ_Q to the ground state energy E_Q at fixed Q of the theory on the cylinder as

$$\Delta_Q = RE_Q \,, \qquad E_Q = \mu Q - \mathcal{L} \,, \tag{6.13}$$

where Δ_Q is the scaling dimension of the lowest-lying operator with baryon charge Q, E_Q is the ground state energy on $\mathbb{R} \times S^{d-1}$ at fixed charge, R is the radius of S^{d-1}, and μ is the baryon chemical potential.

In chapter 3 it was shown that, as customary, the chemical potential is introduced into the covariant derivative as the zero-component of a gauge field. The dynamics of the theory is controlled by various energy scales. These are the chemical potential μ, the mass of the quarks m, the scale of the axial anomaly a, the scales of chiral and conformal symmetry breaking v and f, respectively, and the explicit conformal symmetry breaking scale m_σ. One can envision different counting schemes respecting the following hierarchy

$$m_\pi \,, m_\sigma \ll \mu \ll 4\pi v \,. \tag{6.14}$$

The first inequality implies that the theory is in the broken phase where pion condensation occurs [1] while the last inequality ensures the applicability of the chiral EFT at finite chemical potential.

Therefore, after taking into account the background geometry and the dressing with the dilaton one arrives at the following two Lagrangians [53, 82, 88, 241, 267]

$$\begin{aligned}\mathcal{L}_{\theta,\sigma} = {} & v^2 Tr\{\partial_\mu \Sigma \partial^\mu \Sigma^\dagger\}\, e^{-2\sigma f} + 4\mu v^2 Tr\{B\Sigma^\dagger \partial_0 \Sigma\}\, e^{-2\sigma f} + m_\pi^2 v^2 Tr\{M\Sigma + M^\dagger \Sigma^\dagger\}\, e^{-y\sigma f} + \\ & + 2\mu^2 v^2 \left[Tr\{\Sigma B^T \Sigma^\dagger B\} + Tr\{BB\}\right]\, e^{-2\sigma f} - a v^2 \left(\theta - \frac{i}{4} Tr\{\log \Sigma - \log \Sigma^\dagger\}\right)^2 e^{-4\sigma f} + \\ & + \frac{1}{2}\left(\partial_\mu \sigma \partial^\mu \sigma - \frac{\mathcal{R}}{6 f^2}\right) e^{-2\sigma f} - V(\sigma) - \Lambda_0^4\, e^{-4\sigma f} \,,\end{aligned} \tag{6.15}$$

and

$$
\begin{aligned}
\mathcal{L}_{\hat{a},\sigma} = {} & v^2 Tr\{\partial_\mu \Sigma \partial^\mu \Sigma^\dagger\}\ e^{-2\sigma f} + 4\mu v^2 Tr\{B\Sigma^\dagger \partial_0 \Sigma\}\ e^{-2\sigma f} + m_\pi^2 v^2 Tr\{M\Sigma + M^\dagger \Sigma^\dagger\}\ e^{-y\sigma f} \\
& + 2\mu^2 v^2 \left[Tr\{\Sigma B^T \Sigma^\dagger B\} + Tr\{BB\}\right]\ e^{-2\sigma f} + v_{PQ}^2 \partial_\mu N \partial^\mu N^\dagger\ e^{-2\sigma f} + \\
& - a v^2 \left(\theta - \frac{i}{4} Tr\{\log\Sigma - \log\Sigma^\dagger\} - \frac{i}{4} a_{PQ} (\log N - \log N^\dagger)\right)^2\ e^{-4\sigma f} + \\
& + \frac{1}{2}\left(\partial_\mu \sigma \partial^\mu \sigma - \frac{\mathcal{R}}{6f^2}\right)\ e^{-2\sigma f} - V(\sigma) - \Lambda_0^4\ e^{-4\sigma f}\ ,
\end{aligned}
\tag{6.16}
$$

where for later convenience, the bare cosmological constant Λ_0 was included.

Following the discussions in chapter 3 and more details in appendix B[2], Δ_Q can then be computed via a semiclassical expansion in the double scaling limit

$$
\Lambda_0 f \to 0\ , \quad Q \to \infty\ , \quad Q(\Lambda_0 f)^4 = \text{fixed}\ . \tag{6.17}
$$

This can be seen by considering the expectation value of the evolution operator $U = e^{-HT}$ in an arbitrary state $|Q\rangle$ with charge Q

$$
\langle U\rangle_Q \equiv \langle Q|e^{-HT}|Q\rangle \underset{T\to\infty}{\longrightarrow} \mathcal{N} e^{-E_Q T} = \mathcal{N} e^{-\frac{\Delta_Q^*}{r} T}\ , \tag{6.18}
$$

with H the Hamiltonian, T the time interval, and $\mathcal{N}$ an unimportant normalization factor. Then one can re-scale the fields as $\Sigma \to v f \Sigma$ and $e^{-f\sigma} \to \sqrt{Q} e^{-f\sigma}$ to exhibit Q as a new counting parameter in the path integral expression for $\langle U\rangle_Q$. Accordingly, the scaling dimension of the lowest-lying operator assumes the following form

$$
R E_Q = \Delta_Q = \sum_{j=-1} \frac{1}{Q^j} \Delta_j \left(Q(\Lambda_0 f)^4\right)\ . \tag{6.19}
$$

The leading order Δ_{-1} of the above expression corresponds to the expression obtained in (2.60) which is the leading order in the large charge expansion given by the classical ground state energy on the cylinder multiplied by its radius. Furthermore, the next-to-leading order Δ_0 is determined by the fluctuations around the classical trajectory. For more details, see [75, 243, 244].

However, the theory considered is not conformal but it is interpreted as near conformal in the sense that the underlying conformal theory is slightly perturbed by operators driving the theory away from conformality such as $V(\sigma)$. This in turn implies that when considering the theory on the cylinder and in particular when computing the ground state energy on this manifold, there will be terms proportional to the parameters that encode explicit symmetry breaking, such as the pion mass and the dilaton mass. However, let us stress that under the assumption that these parameters are small, the explicit breaking of conformality is small and this leads to the central conjecture of an *approximate* state-operator correspondence so that it is natural to consider the following quantity

$$
\boldsymbol{\Delta}_Q^{ex} = R E_Q^{ex} \equiv \Delta_Q + \text{corrections to the CFT.} \tag{6.20}
$$

[2] The discussion concluding this section was not originally presented in our work [2] but it was here added in light of progress and further discussions made in our subsequent paper [3].

Having set the stage, the calculations can proceed.

§ 6.2 The vacuum structure and semiclassical expansion

In this section, the focus is on the classical ground state energy of the theory which, according to the state-operator correspondence, gives the leading order in the large-charge expansion for the scaling dimension of the lowest-lying operator with baryon charge Q. As discussed in detail in chapter 3 and chapter 4 the ground state takes the following form

$$\Sigma_0 = U(\alpha_i)\Sigma_c \tag{6.21}$$

with

$$\begin{aligned} &U(\alpha_i) = \mathrm{diag}\{e^{-i\alpha_1}, \dots, e^{-i\alpha_{N_f}}, e^{-i\alpha_1}, \dots, e^{-i\alpha_{N_f}}\} \quad \text{and} \\ &\Sigma_c = \begin{pmatrix} 0 & \mathbb{1}_{N_f} \\ -\mathbb{1}_{N_f} & 0 \end{pmatrix} \cos\varphi + i \begin{pmatrix} \mathcal{I} & 0 \\ 0 & \mathcal{I} \end{pmatrix} \sin\varphi \quad \text{with} \quad \mathcal{I} = \begin{pmatrix} 0 & -\mathbb{1}_{N_f/2} \\ \mathbb{1}_{N_f/2} & 0 \end{pmatrix}, \end{aligned} \tag{6.22}$$

where the alignment angle φ and the Witten variables α_i are determined by the equations of motion.

Replacing this vacuum ansatz, the Lagrangian (6.15) becomes

$$\begin{aligned} \mathcal{L}_{\theta,\sigma}\left[\Sigma_0, \sigma_0\right] = &-e^{-4f\sigma_0}\Lambda_0^4 - V(\sigma_0) - \frac{\mathcal{R}\, e^{-2f\sigma}}{12 f^2} + 4 m_\pi^2 v^2 X \cos\varphi\, e^{-f\sigma_0 y} \\ &+ 2\mu^2 N_f v^2 e^{-2f\sigma_0} \sin^2\varphi - a v^2 e^{-4f\sigma_0}\bar{\theta}^2 , \end{aligned} \tag{6.23}$$

where

$$\bar{\theta} \equiv \theta - \sum_i^{N_f} \alpha_i , \qquad X \equiv \sum_i^{N_f} \cos\alpha_i . \tag{6.24}$$

The respective equations of motion are

$$N_f \mu^2 e^{-2f\sigma_0} \cos\varphi - m_\pi^2 X e^{-f\sigma_0 y} = 0 \tag{6.25}$$

$$a e^{-4f\sigma_0}\bar{\theta} - 2 m_\pi^2 \sin\alpha_i \cos\varphi e^{-f\sigma_0 y} = 0 , \qquad i = 1, .., N_f \tag{6.26}$$

$$\begin{aligned} &\frac{\mathcal{R} e^{-2f\sigma_0}}{6f} + 4 a f v^2 e^{-4f\sigma_0} Y^2 + 4 f \Lambda_0^4 e^{-4f\sigma_0} - \left.\frac{\partial V(\sigma)}{\partial\sigma}\right|_{\sigma=\sigma_0} + \\ &-4 f \mu^2 N_f v^2 e^{-2f\sigma_0} \sin^2\varphi - 4 f m_\pi^2 v^2 y X \cos\varphi e^{-f\sigma_0 y} = 0 \end{aligned} \tag{6.27}$$

$$4\mu N_f v^2 e^{-2f\sigma_0} \sin^2\varphi = \frac{Q}{V} . \tag{6.28}$$

Now, these equations are solved in the large Q expansion; focussing on the two extreme cases $\gamma \ll 1$ and $1 - \gamma \ll 1$, one finds the following expressions for the ground state energy

- $\mathrm{V}_{\Delta\to 0}(\sigma)$

$$\begin{aligned}\tilde{E}^{\gamma\ll 1} &= \frac{c_{4/3}Q^{4/3}}{\tilde{V}^{1/3}} + Q^{2/3}\tilde{V}^{1/3}\left\{c_{2/3}\tilde{R} - \frac{X_{00}^2}{4\pi^2 N_f^3 c_{4/3}^4}\left(\frac{9m_\pi^2}{32\nu}\right)^2\left[1-\gamma\left(\frac{2}{3}\log Q - \log\left(\frac{32N_f\nu^2\pi^2 c_{4/3}\tilde{V}^{2/3}}{3}\right)\right.\right.\right.\\ &\left.\left.\left.-\frac{X_{10}}{X_{00}}\right)+\mathcal{O}\left(\gamma^2\right)\right]\right\} - \tilde{V}\log Q\left\{\frac{16\pi^2}{9}N_f c_{2/3}c_{4/3}\nu^2 m_\sigma^2 - \frac{\gamma}{3\pi^2 N_f^4 c_{4/3}^5}\left(\frac{9m_\pi^2}{32\nu}\right)^2\left[\frac{5}{8\pi^2 c_{4/3}^4 N_f^2}\left(\frac{9m_\pi^2}{32\nu}\right)^2 X_{00}^4\right.\right.\\ &\left.\left.-c_{2/3}\tilde{R}N_f X_{00}^2 + \frac{9X_{00}X_{01}}{32c_{4/3}}\right]+\mathcal{O}\left(\gamma^2\right)\right\}+\mathcal{O}\left(Q^0\right) \quad \text{and}\\ \tilde{E}^{1-\gamma\ll 1} &= \frac{c_{4/3}Q^{4/3}}{\tilde{V}^{1/3}} + c_{2/3}Q^{2/3}\tilde{R}\tilde{V}^{1/3} - \left[\frac{16}{9}\pi^2 m_\sigma^2 N_f c_{2/3}c_{4/3}\nu^2 + \frac{9(1-\gamma)X_{00}^2 m_\pi^4}{64c_{4/3}^3 N_f^2} + \mathcal{O}\left((1-\gamma)^2\right)\right]\tilde{V}\log Q + \mathcal{O}\left(Q^0\right),\end{aligned} \tag{6.29}$$

- $\mathrm{V}_{\Delta=2}(\sigma)$

$$\begin{aligned}\tilde{E}_Q^{\gamma\ll 1} &= \frac{c_{4/3}Q^{4/3}}{\tilde{V}^{1/3}} + Q^{2/3}\tilde{V}^{1/3}\left\{c_{2/3}\tilde{R} - \frac{1}{2}c_{2/3}m_\sigma^2 - \frac{X_{00}^2}{4\pi^2 N_f^3 c_{4/3}^4}\left(\frac{9m_\pi^2}{32\nu}\right)^2\left[1-\gamma\left(\frac{2}{3}\log Q - \frac{X_{10}}{X_{00}}\right.\right.\right.\\ &\left.\left.\left.-\log\left(\frac{32N_f\nu^2\pi^2 c_{4/3}\tilde{V}^{2/3}}{3}\right)+\mathcal{O}\left(\gamma^2\right)\right)\right]\right\} + \left\{\frac{\gamma}{3\pi^2 N_f^4 c_{4/3}^5}\left(\frac{9m_\pi^2}{32\nu}\right)^2\left[\frac{5}{8\pi^2 c_{4/3}^4 N_f^2}\left(\frac{9m_\pi^2}{32\nu}\right)^2 X_{00}^4\right.\right.\\ &\left.\left.-c_{2/3}\tilde{R}N_f X_{00}^2 + \frac{9X_{00}X_{01}}{32c_{4/3}}\right]+\mathcal{O}\left(\gamma^2\right)\right\}\tilde{V}\log Q + \mathcal{O}\left(Q^0\right) \quad \text{and}\\ \tilde{E}_Q^{1-\gamma\ll 1} &= \frac{c_{4/3}}{\tilde{V}^{1/3}}Q^{4/3} + c_{2/3}Q^{2/3}\tilde{R}\tilde{V}^{1/3} - \frac{m_\sigma^2 c_{2/3}Q^{2/3}\tilde{V}^{1/3}}{2} - \left[\frac{9(1-\gamma)m_\pi^4 X_{00}^2}{64N_f^2 c_{4/3}^3} + \mathcal{O}\left((1-\gamma)^2\right)\right]\tilde{V}\log Q + \mathcal{O}\left(Q^0\right),\end{aligned} \tag{6.30}$$

- $\mathrm{V}_{\Delta\to 4}(\sigma)$

$$\tilde{E}_Q^{\gamma\ll 1} = \frac{c_{4/3}Q^{4/3}}{\tilde{V}^{1/3}}\left[1 + m_\sigma^2\frac{c_{2/3}}{256\pi^2\nu^2 N_f c_{4/3}^2}\left(4\log\left(\frac{3\sqrt{\frac{3}{2}}Q}{128\pi^3 c_{4/3}^{3/2}\nu^3\tilde{V}N_f^{3/2}}\right)-3\right)+\mathcal{O}\left(m_\sigma^4\right)\right] \tag{6.31}$$

$$\begin{aligned}&+c_{2/3}Q^{2/3}\tilde{R}\tilde{V}^{1/3}\left\{1 - \frac{X_{00}^2}{4\pi^2 N_f^3 c_{2/3}c_{4/3}^4\tilde{R}}\left(\frac{9m_\pi^2}{32\nu}\right)^2\left[1-\gamma\left(\frac{2}{3}\log Q - \frac{X_{10}}{X_{00}} - \log\left(\frac{32N_f\nu^2\pi^2 c_{4/3}\tilde{V}^{2/3}}{3}\right)\right)\right]\right.\\ &\left.-\frac{m_\sigma^2}{(8c_{4/3}\pi\nu)^2 N_f}c_{2/3}\log\left(\frac{3\sqrt{\frac{3}{2}}Q}{128\pi^3 c_{4/3}^{3/2}\nu^3\tilde{V}N_f^{3/2}}\right)+\mathcal{O}\left(m_\sigma^4, m_\sigma^2\gamma, \gamma^2\right)\right\} + \tilde{V}\log Q\left\{\frac{\gamma}{3\pi^2 N_f^4 c_{4/3}^5}\left(\frac{9m_\pi^2}{32\nu}\right)^2\right.\end{aligned} \tag{6.32}$$

$$\begin{aligned}&\left.\times\left[\frac{5}{8\pi^2 c_{4/3}^4 N_f^2}\left(\frac{9m_\pi^2}{32\nu}\right)^2 X_{00}^4 - c_{2/3}\tilde{R}N_f X_{00}^2 + \frac{9X_{00}X_{01}}{32c_{4/3}}\right] + \frac{14c_{2/3}^3 m_\sigma^2\tilde{R}^2}{(32\pi\nu)^2 N_f c_{4/3}^3}\right\}+\mathcal{O}\left(Q^0\right)\\ \tilde{E}_Q^{1-\gamma\ll 1} &= \frac{c_{4/3}Q^{4/3}}{\tilde{V}^{1/3}}\left[1 + \frac{m_\sigma^2 c_{2/3}}{256\pi^2 N_f c_{4/3}^2\nu^2}\left(4\log\left(\frac{3\sqrt{\frac{3}{2}}Q}{128\pi^3 c_{4/3}^{3/2}\nu^3\tilde{V}N_f^{3/2}}\right)-3\right)+\mathcal{O}\left(m_\sigma^4\right)\right]\\ &+c_{2/3}Q^{2/3}\tilde{R}\tilde{V}^{1/3}\left[1 - \frac{c_{2/3}m_\sigma^2}{(8c_{4/3}\pi\nu)^2 N_f}\log\left(\frac{3\sqrt{\frac{3}{2}}Q}{128\pi^3 c_{4/3}^{3/2}\nu^3\tilde{V}N_f^{3/2}}\right)+\mathcal{O}\left(m_\sigma^4\right)\right]\\ &+\tilde{V}\log Q\left\{\frac{14c_{2/3}^2 m_\sigma^2\tilde{R}^2}{(32\pi\nu)^2 N_f c_{4/3}^3} - \frac{9(1-\gamma)m_\pi^4 X_{00}^2}{64N_f^2 c_{4/3}^3} + \mathcal{O}\left(m_\sigma^4, m_\sigma^2(1-\gamma), (1-\gamma)^2\right)\right\}+\mathcal{O}\left(Q^0\right),\end{aligned} \tag{6.33}$$

where

$$c_{4/3} = \frac{3}{8}\left(\frac{\Lambda^2}{\pi N_f v^2}\right)^{2/3}, \quad c_{2/3} = \frac{1}{4f^2}\left(\frac{\pi^2}{N_f v^2 \Lambda^4}\right)^{1/3}, \quad \tilde{R} = \frac{\mathcal{R}}{6}, \quad \tilde{V} = \frac{V}{2\pi^2}, \quad \Lambda^4 \equiv \begin{cases} \Lambda_0^4 + \frac{m_\sigma^2}{16f^2} & \Delta \to 0 \\ \Lambda_0^4 + \frac{m_\sigma^2}{8f^2} & \Delta = 2 \\ \Lambda_0^4 & \Delta \to 4 \end{cases} \tag{6.34}$$

and X is double-expanded first in γ and then also in $1/Q$ as follows

$$\begin{aligned} X &= X_0 + X_1\gamma + O\left(\gamma^2\right), \qquad & X_k &= X_{k0} + \frac{X_{k1}}{Q^{2/3}} + O\left(Q^{-4/3}\right), \qquad & &\text{for } \gamma \ll 1 \\ X &= X_0 + X_1(1-\gamma) + O\left((1-\gamma)^2\right), \qquad & X_k &= X_{k0} + \frac{X_{k1}}{Q^{4/3}} + O\left(Q^{-2}\right), \qquad & &\text{for } 1-\gamma \ll 1\,. \end{aligned} \tag{6.35}$$

Within the same double expansion, one can solve for $\bar{\theta}$. In particular, the steps include to solve the equation of motion, that at the leading order in this expansion, yields $\bar{\theta}_{00}(\alpha_i) = 0$. Henceforth, the latter is interpreted as double-expanding the α_i. With a slight abuse of notation, in the following the same name for the coefficients of the expansions around $\gamma = 0$ and $1-\gamma = 0$ is used. Interestingly, in the latter case there is no term of order $O\left(Q^{-2/3}\right)$.

For $\theta = 0$ eq.(6.29) reproduces the results in [94] [3]. When the theory is conformal (i.e. $m_\pi = m_\sigma = 0$), the θ-dependence disappears and the scaling dimension depends only on dimensionless coefficients as

$$\tilde{\Delta}_Q = \tilde{V}^{1/3}\tilde{E}_Q = c_{4/3}Q^{4/3} + c_{2/3}Q^{2/3} + O\left(Q^0\right), \tag{6.36}$$

in agreement with the general form of the large-charge expansion for generic non-supersymmetric CFTs [93], as discussed in chapter 2. As first pointed out in [241], the deviations from conformality lead to corrections depending on the background geometry and involve the appearance of logarithms of Q.

From eq.(6.29), one can observe that θ does not affect the leading order in the large-charge expansion. Moreover, the θ-vacuum is determined by X_{00} which can be obtained by solving $\bar{\theta}_{00}(\alpha_i) = 0$ in terms of the α_i. In particular, $X_{00} = \sum_i^{N_f} \cos\alpha_{i00}$ (with the obvious notation) where the α_{i00}s are the solutions found in chapter 4 for the α_i variables at the leading order in $\frac{m_\pi^2}{a}$ and henceforth one refers to such results in the text. In particular, in the $1-\gamma \ll 1$ case, the minimum energy is achieved when X_{00}^2 is maximised due to the minus sign in front of the $\log Q$ term in the energy (6.29).
It follows that the problem of maximising X_{00} in terms of the α_{i00} is equivalent to the problem studied in chapter 4 of maximising X^2 in terms of the α_i which determines the vacuum structure of the superfluid phase of theory in absence of the dilaton.
In other words, the results of chapter 4 apply here by replacing $X \to X_{00}$ and $\alpha_i \to \alpha_{i00}$ and the θ-dependence of the vacuum in the presence of the dilaton is identical to the case without it.

Interestingly, when $\gamma \ll 1$ the situation is more subtle since the leading θ-dependent contribution is of the form $X_{00}^2\left(\frac{2}{3}\gamma\log Q - 1\right)$. Therefore, at fixed γ there exists a critical

[3] Precisely, this expression corrects a few misprints in eqs.(23) and (24) of [94]. The corrected expression for $\theta = 0$ will be given in Sec.6.2.1

charge below/above which the θ-vacuum has to maximise/minimise X_{00}^2.
In other words, there is a phase transition in the large-charge regime as Q crosses

$$Q_c = e^{\frac{3}{2\gamma}} \,. \tag{6.37}$$

Therefore, for $Q < Q_c$ the θ-vacuum will be analogous to the $1-\gamma \ll 1$ case. One expects this to be the natural limit here as well given that for charges very larger than Q_c one should start exploring the UV asymptotically free fixed point rather than the IR interacting one.

As already shown in chapter 4, the α_{i00} assume the following expressions that solve eq.(6.26):

$$\alpha_{i00} = \begin{cases} \pi - \alpha, & i = 1, \dots, n \\ \alpha, & i = n+1, \dots, N_f \end{cases} \tag{6.38}$$

where α is given by

$$\alpha = \frac{\theta + (2k-n)\pi}{(N_f - 2n)}, \quad k = 0, \dots, N_f - 2n - 1\,, \quad n = 0, ..., \left[\frac{N_f - 1}{2}\right] . \tag{6.39}$$

Furthermore, let us recall that X_{00}^2 is always maximised by solutions with $n = 0$. For even N_f the ground state solutions have $\alpha_{i00} = \frac{\theta}{N_f}$ in the interval $\theta \in [0, \pi]$ and $\alpha_{i00} = \frac{\theta - 2\pi}{N_f}$ for $\theta \in [\pi, 2\pi]$. The energies stemming from the two solutions cross at $\theta = \pi$ where for $N_f > 2$ one has spontaneous CP symmetry breaking.

For odd N_f, the solutions that maximise X_{00}^2 are $\alpha_{i00} = \frac{\theta}{N_f}$ (for $\theta \in [0, \frac{\pi}{2}]$), $\alpha_{i00} = \frac{\theta-\pi}{N_f} + \pi$ (for $\theta \in [\frac{\pi}{2}, \frac{3\pi}{2}]$) , $\alpha_{i00} = \frac{\theta - 2\pi}{N_f}$ (for $\theta \in [\frac{3\pi}{2}, 2\pi]$).
In particular, this entails that for odd N_f, CP is conserved at $\theta = \pi$ since the vacuum is non-degenerate, while one has two first-order phase transitions at $\theta = \frac{\pi}{2}$ and $\theta = \frac{3\pi}{2}$.

This section is concluded by determining the θ-dependent parameters entering the ground state energy for $\gamma \ll 1$ case when $Q < Q_c$ where $X_{00} = N_f \cos\alpha$ that read

$$X_{00} = N_f \cos\left(\frac{\theta + 2k\pi}{N_f}\right) \tag{6.40}$$

$$X_{01} = \frac{9 m_\pi^4 \sin^2\left(\frac{\theta+2k\pi}{N_f}\right)\cos\left(\frac{\theta+2k\pi}{N_f}\right)}{8\ a\ c_{4/3}^2} \tag{6.41}$$

$$\bar{\theta}_{01} = \frac{m_\pi^2 X_{00} \sin\left(\frac{\theta+2\pi k}{N_f}\right)}{a N_f} \tag{6.42}$$

$$\bar{\theta}_{11} = \frac{3 m_\pi^2 \sin\left(\frac{2(\theta+2\pi k)}{N_f}\right)\log\left(\frac{8192\pi^2 c_{4/3}^3 N_f^3 \nu^6}{27 Q^2}\right)}{32\ a\ c_{4/3}^2} \tag{6.43}$$

$$X_{10} = X_{11} = \bar{\theta}_{00} = \bar{\theta}_{10} = 0 \tag{6.44}$$

where the value of k relevant for a given value of θ has to be taken in accordance with the previous discussion.

6.2.1 Ground state energy with the axion

Here, the heart of the discussion is the theory in the presence of the axion field described by eq.(6.16). So, let us consider the ansatz (6.22) for the ground state of Σ and [266]

$$\langle N \rangle = e^{-i\delta/a_{PQ}} \tag{6.45}$$

for the axion field. This leads us to study the Lagrangian

$$\begin{aligned}\mathcal{L}\left[\Sigma_0,\sigma_0,\delta\right] = &-a\nu^2 e^{-4f\sigma_0}(\bar{\theta}-\delta)^2 - e^{-4f\sigma_0}\left(\Lambda^4 - \frac{m_\sigma^2}{16f^2}\right) - V(\sigma_0) + \\ &+ 2\nu^2 m_\pi^2 X\cos\varphi\; e^{-f\sigma_0 y} + 2\mu^2\nu^2 N_f e^{-2f\sigma_0}\sin^2\varphi \; - \frac{\mathcal{R}e^{-2f\sigma_0}}{12f^2}\end{aligned} \tag{6.46}$$

and the corresponding EOMs

$$\frac{\delta\mathcal{L}}{\delta\alpha} = \frac{\delta\mathcal{L}}{\delta\varphi} = \frac{\delta\mathcal{L}}{\delta\sigma_0} = \frac{\delta\mathcal{L}}{\delta\delta} = 0, \qquad \frac{\delta\mathcal{L}}{\delta\mu} = \frac{Q}{V}\ . \tag{6.47}$$

The main difference with the axion-less case is expressed in the equations for the α_i and δ

$$ae^{-4f\sigma_0}(\bar{\theta}-\delta) - 2m_\pi^2 \sin\alpha_i \cos\varphi e^{-f\sigma_0 y} = 0\,, \qquad i = 1,..,N_f \tag{6.48}$$

$$\delta - \bar{\theta} = 0\ . \tag{6.49}$$

These equations can be solved as $\delta = \theta$ and $\alpha_i = 0$. Thus, the θ-dependence disappears from the ground state energy and there is no CP violation since $(\bar{\theta} - \delta) = 0$. In fact, by construction, the axion realises the Peccei-Quinn solution of the strong CP problem [258,259] (for details, see appendix C) and, as a consequence, the classical solutions are equivalent to the ones at $\theta = 0$ which are obtained by setting $X_{00} = N_f$ and $X_{01} = \bar{\theta}_{01} = 0$ in eqs.(6.29), (6.30), (6.31).

For instance, in the $V_{\Delta=0}(\sigma)$ case, one obtains the results in [94]

$$\begin{aligned}\tilde{E}_Q^{\gamma\ll1} = &\frac{c_{4/3}Q^{4/3}}{\tilde{V}^{1/3}} + Q^{2/3}\tilde{V}^{1/3}\left\{c_{2/3}\tilde{R} - \frac{1}{4\pi^2 N_f c_{4/3}^4}\left(\frac{9m_\pi^2}{32\nu}\right)^2\left[1-\gamma\left(\frac{2}{3}\log Q - \log\left(\frac{32N_f\nu^2\pi^2 c_{4/3}\tilde{V}^{2/3}}{3}\right)\right)\right]\right\} + \\ &- \tilde{V}\log(Q)\left\{\frac{16\pi^2}{9}N_f c_{2/3}c_{4/3}\nu^2 m_\sigma^2 - \frac{\gamma}{3\pi^2 N_f^2 c_{4/3}^5}\left(\frac{9m_\pi^2}{32\nu}\right)^2\left[\frac{5}{8\pi^2 c_{4/3}^4}\left(\frac{9m_\pi^2}{32\nu}\right)^2 - c_{2/3}\tilde{R}N_f\right]\right\}\end{aligned} \tag{6.50}$$

for the case of $\gamma \ll 1$, while for $1-\gamma \ll 1$

$$\tilde{E}_Q^{1-\gamma\ll1} = \frac{c_{4/3}Q^{4/3}}{\tilde{V}^{1/3}} + c_{2/3}Q^{2/3}\tilde{R}\tilde{V}^{1/3} - \frac{9(1-\gamma)m_\pi^4\tilde{V}\log Q}{64c_{4/3}^3} - \frac{16}{9}\pi^2 m_\sigma^2 N_f c_{2/3}c_{4/3}\nu^2\tilde{V}\log Q\ . \tag{6.51}$$

What differs from [94] is the presence of a light axion in the spectrum which one must take into account when considering the second-order expansion.

§ 6.3 Second-order expansion in the near conformal regime

The spectrum of the theory in the absence of the dilaton field has been detailed in chapter 3 and chapter 4. There, it was observed that the theory is characterized by the symmetry-breaking pattern

$$SU(2N_f)\times U(1)_A \overset{2N_f^2-N_f}{\rightsquigarrow} Sp(2N_f) \longrightarrow SU(N_f)_V\times U(1)_B \overset{\frac{N_f^2-N_f}{2}}{\rightsquigarrow} Sp(N_f)_V \tag{6.52}$$

where $\rightsquigarrow$ and $\longrightarrow$ denote, respectively, spontaneous and explicit breaking. In fact, the axial symmetry is explicitly broken by the anomaly and therefore the would-be Goldstone boson is massive. Let us recall that the further explicit breaking is due to the introduction of a baryon charge while the last spontaneous breaking is the superfluid transition.

In the absence of the dilaton, the spectrum of light modes is composed of $\frac{1}{2}N_f(N_f-1)$ massless Goldstones with speed $v_G=1$ that parameterises the coset $\frac{SU(N_f)}{Sp(N_f)}$. They arrange themselves in the antisymmetric representation of the unbroken $Sp(N_f)$ plus a singlet which is denoted as π_0. In addition, one finds $\frac{1}{2}N_f(N_f-1)-1$ pseudo-Goldstones with mass $\frac{m_\pi^2 X}{\mu N_f}$ plus a pseudo-Goldstone mode stemming from the would-be spontaneous breaking of $U(1)_A$ which here is called the S (singlet) mode. As mentioned above, the $U(1)_A$ symmetry is quantum mechanically anomalous, and therefore the latter mode acquires a mass contribution proportional to the scale of the anomaly, $\sqrt{a}$.

The rest of the spectrum is given by gapped modes with a mass of order μ which, for the purposes of this chapter, will not be considered since they decouple from the large-charge dynamics.

It is interesting to analyse how the spectrum changes when (near)conformal dynamics is realised through the dilaton dressing. In particular, conformal invariance dictates the existence of a massless mode with speed $v_G=\frac{1}{\sqrt{d-1}}=\frac{1}{\sqrt{3}}$ [241] as stressed in chapter 2.

Specifically, the latter arises from the mixing between the singlet mode π_0 with the dilaton that acts as its "radial mode" and changes its speed from $v_G=1$ to $v_G=\frac{1}{\sqrt{3}}$, as anticipated in chapter 1. In general, the infrared dynamics of this mode can be described using a conformally invariant four-derivative action of the type $\mathcal{L}_{NLSM}=k_4(\partial_\mu\chi\partial^\mu\chi)^2$. In turn, the latter can be seen as the heavy dilaton limit of the two-derivative action $\mathcal{L}_2=v^2(\partial_\mu\chi\partial^\mu\chi)$ after dressing it with the dilaton [82, 88, 241, 267] (see the discussion in section 2.4.4).

Having in mind the hierarchy of scales $m_\pi, m_\sigma \ll \sqrt{a}\le\mu\ll 4\pi v$, the focus is on the spectrum of light modes i.e. the modes whose mass is smaller than the chemical potential in the large-charge limit. To this end, let us start by considering the modes with mass $\frac{m_\pi^2 X}{\mu N_f}$. These cannot mix with the dilaton and, therefore, their dispersion relation in the near conformal phase can be obtained by generalizing the non-conformal expression of chapter 4 to include the expectation value of the dilaton as

$$\omega_1^2=k^2-\frac{m_\pi^4X^2e^{-2f\sigma_0(y-2)}}{\mu^2N_f^2}\,, \tag{6.53}$$

which matches eq.(59) of [1] when $f = 0$.

For $y = 2$ this mode has a squared mass $\frac{m_\pi^4 X^2}{\mu^2 N_f^2}$, whereas in the limit $y = 3$ one has

$$\omega_1^2 = k^2 - \frac{27 m_\pi^4 X_{00}^2}{512\pi^2\nu^2 N_f^3 c_{4/3}^3} + \mathcal{O}\left(Q^{-2/3}\right) . \tag{6.54}$$

To study the remaining light modes, one expands around the vacuum solution,

$$\Sigma = e^{i\Omega}\Sigma_0 e^{i\Omega^t} , \tag{6.55}$$

where Σ_0 is the classical solution (6.22) while the fluctuations are organized in the matrix Ω as

$$\Omega = \begin{pmatrix} \pi & 0 \\ 0 & -\pi^t \end{pmatrix} + \tilde{\beta} S \begin{pmatrix} \mathbb{1}_{N_f} & 0 \\ 0 & \mathbb{1}_{N_f} \end{pmatrix}, \quad \tilde{\beta} \equiv \frac{1}{\sqrt{2N_f}} , \tag{6.56}$$

where $\pi = \sum_{a=0}^{\dim\frac{U(N_f)}{Sp(N_f)}} \pi^a T_a$ belongs to the algebra of the coset space $\frac{U(N_f)}{Sp(N_f)}$. The normalisation condition on the generators is $Tr\left\{T_a T_b\right\} = \frac{\delta_{ab}}{2}$. Using the results contained in appendix D the result reads

$$Tr\left\{\partial_\mu\Sigma\partial^\mu\Sigma^\dagger\right\} = 4\sin^2\varphi\ \partial_\mu\pi^a\partial^\mu\pi^a + 8N_f\tilde{\beta}^2\partial_\mu S\partial^\mu S \tag{6.57}$$

$$Tr\left\{B\Sigma\partial_0\Sigma^\dagger\right\} = -2i\sqrt{2N_f}\sin^2\varphi\partial_0\pi^0 \tag{6.58}$$

$$Tr\left\{M\Sigma + M^\dagger\Sigma^\dagger\right\} = 2N_f\cos\varphi\left(X\cos\left(\sqrt{\frac{2}{N_f}}S\right) + Z\sin\left(\sqrt{\frac{2}{N_f}}S\right)\right) \tag{6.59}$$

$$Tr\left\{\log\Sigma - \log\Sigma^\dagger\right\} = 8iN_f\tilde{\beta}S - \sum_i^{N_f}\alpha_i , \tag{6.60}$$

where $Z \equiv \sum_{i=1}^{N_f}\sin\alpha_i$.

Finally, by expanding the dilaton field around its background solution as $\sigma \to \sigma_0 + \hat{\sigma}(t,\mathrm{x})$, one obtains the quadratic Lagrangian

$$\frac{\mathcal{L}}{4\nu^2\sin^2\varphi\ e^{-2\sigma_0 f}} = \begin{pmatrix} \pi^0 & \hat{\sigma} & S \end{pmatrix} D^{-1}\begin{pmatrix} \pi^0 \\ \hat{\sigma} \\ S \end{pmatrix} + \sum_{a=1}^{\dim\left(\boxminus\right)} \partial^\mu\pi^a\partial_\mu\pi^a \tag{6.61}$$

with the inverse propagator D^{-1} defined as

$$D^{-1} = \begin{pmatrix} \omega^2 - k^2 & i\omega\mu f\sqrt{2N_f} & 0 \\ -i\omega\mu f\sqrt{2N_f} & \frac{\omega^2-k^2}{8\nu^2\sin^2\varphi} - M_\sigma^2 & \frac{1}{2}I_{\hat{\sigma}s} \\ 0 & \frac{1}{2}I_{\hat{\sigma}s} & \frac{\omega^2-k^2}{\sin^2\varphi} - M_s^2 \end{pmatrix}, \qquad I_{\hat{\sigma}S} = \frac{\sqrt{2}f\mu^2 m_\pi^4\sqrt{N_f}XyZ}{m_\pi^4X^2 - \mu^4N_f^2e^{2f\sigma_0(y-2)}} \tag{6.62}$$

where the Lagrangian masses for the dilaton field are given by

- $V_{\Delta\to 0}(\sigma)$

$$M_\sigma^2 = -\frac{f^2\mu^2 N_f e^{-6f\sigma_0}\left(v^2 m_\pi^4 X^2\left(y^2-2\right)e^{6f\sigma_0} + 2\mu^4 v^2 N_f^2 e^{2f\sigma_0(y+1)} - 4\Lambda^4\mu^2 N_f e^{2f\sigma_0 y}\right)}{2v^2\left(\mu^4 N_f^2 e^{2f\sigma_0(y-2)} - m_\pi^4 X^2\right)} \tag{6.63}$$

- $V_{\Delta=2}(\sigma)$

$$M_\sigma^2 = -\frac{\mu^2 e^{-f\sigma_0 y}}{8v^2\left(\mu^4 e^{2f\sigma_0} - m_\pi^4 X^2\right)}\Big[-8f^2 e^{f\sigma_0 y}\left(2\mu^2\left(av^2\bar{\theta}^2+\Lambda^4\right) + m_\pi^4 N_f v^2 X^2\right) + 4f^2 m_\pi^4 N_f v^2 X^2 y^2 e^{3f\sigma_0}$$
$$+\mu^2 e^{f\sigma_0(y+2)}\left(8f^2\mu^2 N_f v^2 + m_\sigma^2\right)\Big] \tag{6.64}$$

- $V_{\Delta\to 4}(\sigma)$

$$M_\sigma^2 = -\frac{\mu^2\left(4f^2\left(4\mu^2\left(av^2\bar{\theta}^2+\Lambda^4\right) + m_\pi^4 N_f v^2 X^2\left(2-y^2 e^{-f\sigma_0(y-3)}\right) - 2\mu^4 N_f v^2 e^{2f\sigma_0}\right) - 4f\mu^2 m_\sigma^2\sigma_0 + \mu^2 m_\sigma^2\right)}{8v^2\left(m_\pi^4 X^2 - \mu^4 e^{2f\sigma_0}\right)} \tag{6.65}$$

while the mass of the S-mode is the same for all three potentials and reads

$$M_S^2 = \frac{a\mu^4 N_f^3 e^{2f\sigma_0(y-1)} + 2\mu^2 m_\pi^4 X^2 e^{4f\sigma_0}}{2\mu^4 N_f^2 e^{2f\sigma_0 y} - 2m_\pi^4 X^2 e^{4f\sigma_0}}\ . \tag{6.66}$$

The π^a represent Goldstone modes with sound speed $v_G{=}1$ transforming in the antisymmetric representation of $Sp(N_f)$ analogous to the ones found in absence of the dilaton field in chapter 4.

The field π_0 corresponds to the Goldstone mode of the coset $\frac{SU(N_f)}{Sp(N_f)}$ that transforms as a singlet of $Sp(N_f)$. For this reason, it mixes with the dilaton and S according to eq.(6.62). At this point, one can investigate whether eq.(6.66) is in agreement with the Witten-Veneziano relation [338, 423] presented in chapter 3. The latter constrains the mass squared of the S-particle to be proportional to the number of flavours and the topological susceptibility in the limit $m_\pi \to 0$. Indeed, this agrees with the limit of eq.(6.66) [4]

$$\lim_{\sigma_0\to 0,\ m_\pi\to 0}(6.66) \implies M_S^2 = \frac{aN_f}{2}\ . \tag{6.67}$$

Additionally, for $\sigma_0 \to 0$

$$\lim_{\sigma_0\to 0}(6.66) \implies M_S^2 = \frac{a\mu^4 N_f^3 + 2\mu^2 m_\pi^4 X^2}{2\mu^4 N_f^2 - 2m_\pi^4 X^2}\ , \tag{6.68}$$

in agreement with (4.70).

The remaining dispersion relations are obtained by solving the equation $\det(D^{-1}) = 0$. As a result, there are one massless degree of freedom and two gapped modes. In what follows, there are explicit expressions for the dispersion relations at the two extrema of the dimension of the fermion condensate $\gamma = 0$ and $\gamma = 1$ in the limit of small momenta and within the large-charge expansion.

[4] The definition of M_S used here differs by a factor of 2 from the usual conventions.

For the sake of simplicity, only the case $\Delta \to 0$ is presented. For the massless mode one obtains

$$\gamma = 0: \quad \omega_2 = \sqrt{\frac{9f^2 m_\pi^8 X_0^2 Z_0^2 e^{-4f\sigma_0} - 2\mu^4 M_\sigma^2 M_S^2 N_f^3 \sin^4\varphi}{9f^2 m_\pi^8 X_0^2 Z_0^2 e^{-4f\sigma_0} - 2\mu^4 M_S^2 N_f^3 \sin^4\varphi \ \left(2f^2\mu^2 N_f + M_\sigma^2\right)}}\, k + \mathcal{O}\left(k^2\right) \tag{6.69}$$

$$\gamma = 1: \quad \omega_2 = \sqrt{\frac{2f^2 m_\pi^8 N_f X_0^2 Z_0^2 - \mu^4 M_\sigma^2 M_S^2 \sin^4\varphi}{2f^2 N_f \left(m_\pi^8 X_0^2 Z_0^2 - \mu^6 M_S^2 \sin^4\varphi\right) - \mu^4 M_\sigma^2 M_S^2 \sin^4\varphi}}\, k + \mathcal{O}\left(k^2\right) \tag{6.70}$$

where Z is expanded in γ and $1-\gamma$ as for X in eq.(6.35) and kept only the leading term. In the large-charge limit, the above reduces to

$$\gamma = 0: \quad \omega_2 = k\left[\frac{1}{\sqrt{3}} + \frac{\sqrt{3}\, X_{00}^2}{\left(2\pi^2\right)^{2/3} c_{4/3}^5 N_f^3}\left(\frac{9m_\pi^2}{128\pi\nu}\right)^2 \left(\frac{V}{Q}\right)^{2/3} + \ldots\right] + \mathcal{O}\left(k^2\right) \tag{6.71}$$

$$\gamma = 1: \quad \omega_2 = k\left[\frac{1}{\sqrt{3}} + 1\left(\frac{2^{5/3} c_{2/3}\nu^2 m_\sigma^2}{3\sqrt{3}\pi^{2/3}} + \frac{9\sqrt{3} m_\pi^4 X_{00}^2}{128\sqrt[3]{2}\pi^{8/3} c_{4/3}^4 N_f^2}\right)\left(\frac{V}{Q}\right)^{4/3} + \ldots\right] + \mathcal{O}\left(k^2\right) . \tag{6.72}$$

These results agree with those in [94] for $\theta = 0$ i.e. $X_{00} = N_f$ (see Sec.6.3.1 for further details). At the conformal point $m_\sigma = m_\pi = 0$, eqs.(6.71) and (6.72) describe the expected conformal phonon whose speed approaches the value $v_G = \frac{1}{\sqrt{3}}$ as $Q \to \infty$ [241].

For the massive modes described by eq.(6.62), the dispersion relations are written as an expansion for small momenta

$$\omega_3 = M_3 + v_3 k^2 + \ldots \tag{6.73}$$

$$\omega_4 = M_4 + v_4 k^2 + \ldots . \tag{6.74}$$

In the $\gamma = 0$ case one has

$$M_{3,4} = \frac{1}{\sqrt{2}}\sqrt{8\nu^2\sin^2\varphi\left(2f^2\mu^2 N_f + M_\sigma^2\right) + M_S^2\sin^2\varphi \pm \frac{\sqrt{144f^2\nu^2 m_\pi^8 X_0^2 Z_0^2 e^{-4f\sigma_0} + \mu^4 N_f^3 \sin^4\varphi\left(M_S^2 - 8\nu^2\left(2f^2\mu^2 N_f + M_\sigma^2\right)\right)^2}}{\mu^2 N_f^{3/2}}} \tag{6.75}$$

$$v_{3,4} = \frac{\mu^4 N_f^3 e^{4f\sigma_0}\left(-2M_{3,4}^2\sin^2\varphi\left(8\nu^2\left(f^2\mu^2 N_f + M_\sigma^2\right) + M_S^2\right) + 3M_{3,4}^4 + 8\nu^2 M_\sigma^2 M_S^2 \sin^4\varphi\right) - 36f^2\nu^2 m_\pi^8 X_0^2 Z_0^2}{2M_{3,4}\mu^4 N_f^3 e^{4f\sigma_0}\left(8\nu^2\sin^2\varphi\left(M_S^2\sin^2\varphi - 2M_{3,4}^2\right)\left(2f^2\mu^2 N_f + M_\sigma^2\right) - 2lM_{3,4}^2 M_S^2\sin^2\varphi + 3M_{3,4}^4\right) - 72M_{3,4}f^2\nu^2 m_\pi^8 X_0^2 Z_0^2} \tag{6.76}$$

which in the large-charge limit yields

$$\omega_3 = \frac{8\, 2^{5/6}\pi^{2/3} f c_{4/3}\nu\sqrt{N_f}}{\sqrt{3}}\left(\frac{Q}{V}\right)^{1/3} + \frac{\left(640\pi^2 k^2 N_f^2 c_{4/3}^3 - 567 f^2 m_\pi^4 X_{00}^2\right)}{2048\, 2^{5/6}\sqrt{3}\pi^{8/3} f c_{4/3}^4 \nu N_f^{5/2}}\left(\frac{V}{Q}\right)^{1/3} + \ldots \tag{6.77}$$

$$\omega_4 = \frac{\sqrt{3a}}{4\, 2^{2/3}\pi^{1/3}\sqrt{c_{4/3}}\nu}\left(\frac{Q}{V}\right)^{1/3} + \left[\frac{9\sqrt{3}m_\pi^4 X_{00}^2\left(9a+256\pi^2 c_{4/3}^3\nu^2\right)}{4096\, 2^{10/3}\pi^{11/3}\sqrt{a}c_{4/3}^{11/2}\nu^3 N_f^3} + \frac{2^{5/3}\pi^{1/3}k^2\sqrt{c_{4/3}}\nu}{\sqrt{3}\sqrt{a}}\right]\left(\frac{V}{Q}\right)^{1/3} + \dots \tag{6.78}$$

For the case $\gamma = 1$, the mass and speed of the massive modes are given by

$$M_{3,4} = \frac{\sin\varphi}{\sqrt{2}}\sqrt{8\nu^2\left(2f^2\mu^2N_f + M_\sigma^2\right) + M_S^2 \pm \sin^2\varphi\sqrt{\frac{64f^2\nu^2m_\pi^8X_0^2Z_0^2 + \mu^4N_f^3\sin^4\varphi\left(M_S^2 - 8\nu^2\left(2f^2\mu^2N_f + M_\sigma^2\right)\right)^2}{\mu^4N_f^3\sin^8\varphi}}} \tag{6.79}$$

$$v_{3,4} = \frac{\mu^4\left(-2M_{3,4}^2\sin^2\varphi\left(8\nu^2\left(f^2\mu^2N_f + M_\sigma^2\right) + M_S^2\right) + 3M_{3,4}^4 + 8\nu^2M_\sigma^2M_S^2\sin^4\varphi\right) - 16f^2\nu^2m_\pi^8N_fX_0^2Z_0^2}{\text{Den}} \tag{6.80}$$

$$\begin{aligned}\text{Den} = {}& 2M_{3,4}^3\mu^4\left(3M_{3,4}^2 - 2M_S^2\sin^2\varphi\right) - 16M_{3,4}\nu^2\big[2f^2N_f\left(\mu^6\sin^2\varphi\left(2M_{3,4}^2 - M_S^2\sin^2\varphi\right)m_\pi^8X_0^2Z_0^2\right)\\ &+ \mu^4M_\sigma^2\sin^2\varphi\left(2M_{3,4}^2 - M_S^2\sin^2\varphi\right)\big]\end{aligned} \tag{6.81}$$

whose large-charge limit gives

$$\omega_3 = \frac{8\, 2^{5/6}\pi^{2/3}f\nu\sqrt{N_f}c_{4/3}}{\sqrt{3}}\left(\frac{Q}{V}\right)^{1/3} + \frac{5k^2}{16\, 2^{5/6}\sqrt{3}\pi^{2/3}f\nu\sqrt{N_f}c_{4/3}}\left(\frac{V}{Q}\right)^{1/3} + \dots \tag{6.82}$$

$$\omega_4 = \frac{\sqrt{3a}}{4\, 2^{2/3}\pi^{1/3}\sqrt{c_{4/3}}\nu}\left(\frac{Q}{V}\right)^{1/3} + \frac{2^{5/3}\pi^{1/3}k^2\sqrt{c_{4/3}}\nu}{\sqrt{3}\sqrt{a}}\left(\frac{V}{Q}\right)^{1/3} + \dots \tag{6.83}$$

Notice that the $\gamma = 1$ case leads to enhanced suppression of the θ-dependence in the large-charge limit compared to the $\gamma = 0$ case as already observed at the classical level.

6.3.1 Second-order expansion with the axion

Similarly to the previous section, to take into consideration the fluctuations of the axion field, the parameterisation of the fluctuations of the Σ field are the same as in (7.39) while the axion reads [266]

$$N(x) = e^{i\hat{a}(x)/v_{PQ}}\ \langle N\rangle \tag{6.84}$$

with $\langle N\rangle$ given by eq.(6.45). Therefore, (6.16) gives another term to consider with respect to the previous section which is

$$-\frac{i}{2}a_{PQ}(\log N - \log N^\dagger) = \frac{a_{PQ}}{v_{PQ}}\hat{a} - \delta\ . \tag{6.85}$$

As a consequence, there are again modes with dispersion relation (6.53) with $X_{00} = N_f$, while the remaining light fluctuations are described by the Lagrangian below

$$\begin{aligned}\mathcal{L} = {}& 4\nu^2\sin^2\varphi\partial_\mu\pi^a\partial^\mu\pi^a e^{-2\sigma f} + 4\nu^2\partial_\mu S\partial^\mu S e^{-2\sigma f} + 8\sqrt{2N}\mu\nu^2\sin^2\varphi\ \partial_0\pi^0 e^{-2\sigma f}\\ &+ 2\nu^2\mu^2N_f\sin^2\varphi e^{-2\sigma f} + 2N_f^2\nu^2m_\pi^2\cos\varphi\cos\left(\sqrt{\frac{2}{N_f}}S\right)e^{-y\sigma f} - a\nu^2\left(\bar{\theta} + \sqrt{2N_f}S + \frac{a_{PQ}}{2v_{PQ}}\hat{a} - \delta\right)^2 e^{-2\sigma f}\end{aligned}$$

$$-\Lambda_0^4 e^{-4\sigma f} - \frac{\mathcal{R}}{12 f^2} e^{-2\sigma f} + (\partial_\mu \hat{a}\, \partial^\mu \hat{a}) e^{-2\sigma f} + \frac{1}{2}(\partial_\mu \sigma \partial^\mu \sigma) e^{-2\sigma f} - V(\sigma)\,, \tag{6.86}$$

from which one obtains the normalised quadratic Lagrangian as

$$\frac{\mathcal{L}}{4v^2 \sin^2\varphi\; e^{-2\sigma_0 f}} = \begin{pmatrix} \pi^0 & \hat{\sigma} & S & \hat{a} \end{pmatrix} D^{-1} \begin{pmatrix} \pi^0 \\ \hat{\sigma} \\ S \\ \hat{a} \end{pmatrix} + \sum_{a=1}^{\dim(\square)} \partial^\mu \pi^a \partial_\mu \pi^a \tag{6.87}$$

where the inverse propagator D^{-1} is given by

$$D^{-1} = \begin{pmatrix} \omega^2 - k^2 & i\omega\mu f\sqrt{2N_f} & 0 & 0 \\ -i\omega\mu f\sqrt{2N_f} & \frac{\omega^2-k^2}{8v^2\sin^2\varphi} - M_\sigma^2 & 0 & 0 \\ 0 & 0 & \frac{\omega^2-k^2}{\sin^2\varphi} - M_S^2 & \frac{I_{S\hat{a}}}{2} \\ 0 & 0 & \frac{I_{S\hat{a}}}{2} & \frac{\omega^2-k^2}{4v^2\sin^2\varphi} - M_{\hat{a}}^2 \end{pmatrix}. \tag{6.88}$$

The Lagrangian masses appearing in D^{-1} are

- $\mathrm{V}_{\Delta\to 0}(\sigma)$

$$M_\sigma^2 = -\frac{f^2\mu^2 e^{-2f\sigma_0(y-2)}\left(v^2 m_\pi^4 N_f\left(y^2-2\right)e^{2f\sigma_0(y-2)} + 2\mu^4 v^2 N_f e^{4f\sigma_0(y-2)} - 4\Lambda^4\mu^2 e^{2f\sigma_0(2y-5)}\right)}{2v^2\left(\mu^4 e^{2f\sigma_0(y-2)} - m_\pi^4\right)}, \tag{6.89}$$

- $\mathrm{V}_{\Delta=2}(\sigma)$

$$M_\sigma^2 = -\frac{4f^2\mu^2v^2m_\pi^4N_f\left(y^2-2\right) + \mu^4 e^{2f\sigma_0(y-2)}\left(8f^2\mu^2v^2N_f + m_\sigma^2\right) - 16f^2\Lambda^4\mu^4 e^{2f\sigma_0(y-3)}}{8v^2\left(\mu^4 e^{2f\sigma_0(y-2)} - m_\pi^4\right)}, \tag{6.90}$$

- $\mathrm{V}_{\Delta\to 4}(\sigma)$

$$M_\sigma^2 = -\frac{2f^2\mu^2v^2m_\pi^4N_f\left(y^2-2\right) + \mu^4 e^{2f\sigma_0(y-3)}\left(m_\sigma^2(2f\sigma_0-1) - 8f^2\Lambda^4\right) + 4f^2\mu^6v^2N_f e^{2f\sigma_0(y-2)}}{4v^2\left(\mu^4 e^{2f\sigma_0(y-2)} - m_\pi^4\right)} \tag{6.91}$$

for the dilaton and

$$M_S^2 = \frac{a\mu^4 N_f e^{2f\sigma_0(y-1)} + 2\mu^2 m_\pi^4 e^{4f\sigma_0}}{2\mu^4 e^{2f\sigma_0 y} - 2m_\pi^4 e^{4f\sigma_0}}, \tag{6.92}$$

$$M_{\hat{a}}^2 = \frac{a\, a_{PQ}^2 e^{-2f\sigma_0}}{16v_{PQ}^2\left(1 - \frac{m_\pi^4 e^{-2f\sigma_0(y-2)}}{\mu^4}\right)} \tag{6.93}$$

for the remaining modes. The interaction term between the S-particle and the fluctuation of the axion $\hat{a}$ is

$$I_{S\hat{a}} = -\frac{\sqrt{N_f}\; a\mu^4 a_{PQ} e^{2f\sigma_0(y-3)}}{2\sqrt{2}v_{PQ}\left(\mu^4 e^{2f\sigma_0(y-2)} - m_\pi^4\right)}\,. \tag{6.94}$$

The inverse propagator (6.88) takes the form of a block matrix. The upper left 2×2 block represents the mixing between π_0 and the $\hat{\sigma}$ in the absence of the θ-angle. Diagonalising it, the result comprises both a massless and a gapped mode with dispersion relations given by

$$\omega_{5.6} = \sqrt{k^2 + 4\nu^2 \sin^2\phi \left(2f^2\mu^2 N_f + M_\sigma^2 \pm \sqrt{\frac{f^2k^2\mu^2 N_f \csc^2\phi}{\nu^2} + \left(2f^2\mu^2 N_f + M_\sigma^2\right)^2} \right)} \tag{6.95}$$

The spectrum in the Δ→0 case has been previously studied in [94]. In that case, the explicit expression of the dispersion relation of the massless mode in the two extreme cases $\gamma = 0$ and $\gamma = 1$ reads

$$\gamma = 0: \quad \omega_5 = \frac{k}{\sqrt{3}} + k\,\frac{\sqrt{3}}{\left(2\pi^2\right)^{2/3} c_{4/3}^5 N_f} \left(\frac{9m_\pi^2}{128\pi\nu}\right)^2 \left(\frac{V}{Q}\right)^{2/3} + \dots \tag{6.96}$$

$$\gamma = 1: \quad \omega_5 = \frac{k}{\sqrt{3}} + k\left[\frac{2\,2^{2/3} c_{2/3}\nu^2 m_\sigma^2 N_f}{3\sqrt{3}\pi^{2/3}} + \frac{9\sqrt{3}m_\pi^4}{256\sqrt[3]{2}\pi^{8/3}c_{4/3}^4}\right]\left(\frac{V}{Q}\right)^{4/3} + \dots \tag{6.97}$$

The above results correct a typo in eqs.(53) and (54) of [94]. The gapped mode arising from the mixing between π_0 and the dilaton has a mass of order $O(\mu)$. The lower right 2×2 block describes the mixing between the S mode and the axion $\hat{a}$ and by diagonalising it one obtains the dispersion relations of the propagating modes which read

$$\omega_{7,8} = \frac{1}{2}\sqrt{4k^2 + 2\sin^2\varphi\left(4\nu^2 M_{\hat{a}}^2 + M_S^2\right) \pm \frac{e^{-2f\sigma_0}}{\nu_{PQ}}\sqrt{2a^2\nu^2 N_f a_{PQ}^2 + 4\nu_{PQ}^2 \sin^4\varphi\, e^{4f\sigma_0}\left(M_S^2 - 4\nu^2 M_{\hat{a}}^2\right)^2}}\,. \tag{6.98}$$

For $f = 0$ the above reproduces the dispersion relations in absence of the dilaton, see chapter 4. Finally, in the following there are the explicit results for these dispersion relations in the Δ→0 case. For $\gamma = 0$ and in the large-charge expansion:

$$\begin{aligned}\omega_7 = {} & \frac{\sqrt{\frac{3a\tilde{\nu}}{c_{4/3}N_f}}}{8^{21/6}\pi^{1/3}\nu_{PQ}\nu}\left(\frac{Q}{V}\right)^{1/3} + \frac{3^5}{16^4}\frac{\sqrt{a}m_\pi^4\sqrt{\tilde{\nu}_{PQ}}}{2^{2/3}\sqrt{3}\pi^{11/3}\nu_{PQ}c_{4/3}^{11/2}\nu^3 N_f^{3/2}}\left(\frac{V}{Q}\right)^{1/3} + \\ & + \frac{\sqrt{N_f}\nu_{PQ}\left[\nu_{PQ}^2\left(512\pi^2k^2c_{4/3}^3\nu^2 N_f + 27m_\pi^4\right) + 256\pi^2k^2c_{4/3}^3\nu^4 a_{PQ}^2\right]}{\sqrt{3a}\pi^{5/3}c_{4/3}^{5/2}\nu\tilde{\nu}_{PQ}^{3/2}}\left(\frac{V}{Q}\right)^{1/3} + \dots\end{aligned} \tag{6.99}$$

$$\begin{aligned}\omega_8 = {} & \frac{\sqrt{512\pi^2k^2c_{4/3}^3N_f\tilde{\nu} + 27m_\pi^4 a_{PQ}^2}}{16\pi c_{4/3}^{3/2}\sqrt{2\tilde{\nu}N_f}} + \\ & + \frac{3^3 m_\pi^8 a_{PQ}^2 N_f^{5/2}\left(27a\tilde{\nu}^2 - 2048\pi^2\nu_{PQ}^4 c_{4/3}^3\nu^2 N_f^2\right)}{16^3\cdot 8^2\cdot 2^{1/6}\pi^{13/3}ac_{4/3}^{13/2}\nu^2\tilde{\nu}^{5/2}\sqrt{512\pi^2k^2c_{4/3}^3N_f\tilde{\nu} + 27m_\pi^4 a_{PQ}^2}}\left(\frac{V}{Q}\right)^{2/3} + \dots\end{aligned} \tag{6.100}$$

while for $\gamma = 1$:

$$\omega_7 = \frac{\sqrt{3\tilde{\nu}}}{8\cdot 2^{1/6}\nu_{PQ}\pi^{1/3}\nu\sqrt{N_f c_{4/3}}}\left(\frac{Q}{V}\right)^{1/3} + \frac{4\cdot 2^{1/6}\pi^{1/3}\nu_{PQ}k^2\sqrt{c_{4/3}}\nu\sqrt{N_f}}{\sqrt{3a\tilde{\nu}}}\left(\frac{V}{Q}\right)^{1/3} + \dots \tag{6.101}$$

$$\omega_8 = k + \frac{9v^2 m_\pi^4 a_{PQ}^2}{32\ 2^{2/3}\pi^{4/3} k c_{4/3}^2 \tilde{v}} \left(\frac{V}{Q}\right)^{2/3} + \dots \tag{6.102}$$

with $\tilde{v} \equiv 2v_{PQ}^2 N_f + a_{PQ}^2 v^2$.

The upshot of this subsection is that the effect of eliminating the θ-angle via the axion, in the large-charge regime, is the introduction of a new light state affecting the spectrum and dynamics of the theory expressed in the new dispersion relations ω_7 and ω_8.

6.3.2 Conformal dimension and vacuum energy of type I Goldstones

As eq.(6.36) illustrates, in the conformal limit $m_\pi = m_\sigma = 0$, the scaling dimension of the lowest-lying operator with baryon charge Q takes the form predicted by the large-charge EFT [82, 88]

$$k_{4/3} Q^{4/3} + k_{2/3} Q^{2/3} + k_0 \log Q + O\left(Q^0\right), \tag{6.103}$$

where the coefficients that appear should not be confused with $c_{4/3}$ and $c_{2/3}$ introduced in eq.(6.34). Instead, the latter should be viewed as the leading order of a semiclassical expansion of the former, generated by integrating out the heavy degrees of freedom when building the large charge EFT. Inspectively, the parameter controlling the leading quantum correction to the classical result (6.29) is

$$\frac{c_{4/3}}{c_{2/3}^2} = \frac{6}{\pi^2} f^4 \Lambda^4 . \tag{6.104}$$

This can be traced back to the observations made in [241] and reviewed in section 2.4.4, where the authors mapped a dilaton-dressed 2-derivative action with $U(1)$ symmetry (analogous to the π_0, $\hat{\sigma}$ sub-sector of the present theory) to the familiar $\lambda\phi^4$ model with quartic coupling $\lambda = f^4\Lambda^4$. In fact, it is known that within this model the Wilson coefficient of the large charge EFT can be computed as a semiclassical expansion in λ by considering the double-scaling limit $Q \to \infty$, $\lambda \to 0$ with 't Hooft-like coupling λQ fixed [75, 243] (for more and a little review, see appendix B). However, as observed in [247], the knowledge of the spectrum of gapless modes is enough to compute exactly the k_0 coefficient in eq.(6.103), which is related to the renormalization of their vacuum energy. In this chapter, the massless spectrum described by the large charge EFT is composed of the $\frac{1}{2}N_f(N_f-1)-1$ modes with dispersion relation $\omega_1$and the $\frac{1}{2}N_f(N_f-1)$ π^a modes. In the conformal limit, these are $N_f^2 - N_f - 1$ type I Goldstone bosons of the spontaneous symmetry breaking (see chapter 4)

$$SU(N_f)_L \times SU(N_f)_R \times U(1)_B \times U(1)_A \rightsquigarrow Sp(N_f)_L \times Sp(N_f)_R \tag{6.105}$$

and all have sound speed $v_G = 1$ with the exception of the conformal mode π_0 with $v_G = \frac{1}{\sqrt{3}}$. The singlet mode S is not included as it decouples due to the axial anomaly. Following discussion in chapter 2, the action describing a type I Goldstone field χ at low energy is

$$S_G = \int_{\mathcal{M}} \mathrm{d}t\mathrm{d}\mathbf{x} \left(\frac{1}{2}(\partial_t \chi)^2 + \frac{v_G^2}{2}(\boldsymbol{\nabla}\chi)^2 \right) , \tag{6.106}$$

and its one-loop vacuum energy reads

$$E_{\text{Casimir}} = \frac{1}{2} Tr\{\log\left(-\partial_t^2 - v_G^2 \nabla^2\right)\} = \frac{1}{4\pi} \int_{-\infty}^{\infty} \mathrm{d}\omega \sum_{\mathbf{p}} \log\left(\omega^2 + v_G^2 E^2(\mathbf{p})\right) = \frac{v_G}{2} \sum_{\mathbf{p}} E(\mathbf{p}) \tag{6.107}$$

where $E(\mathbf{p})^2$ are the eigenvalues of the Laplacian on the sphere, i.e. $\nabla^2 f_{\mathbf{p}}(\mathbf{r}) + E^2(\mathbf{p}) f_{\mathbf{p}}(\mathbf{r}) = 0$. Being this contribution of order Q^0, in odd dimension is not renormalized by the classical vacuum energy and is, therefore, universal to all the CFT whose large-charge dynamics realise the same conformal superfluid phase [82, 93].

In contrast, for an even number of spacetime dimensions, there is a universal $Q^0 \log Q$ term arising from the renormalization of the energy. In fact, as shown in [247], in dimensional regularization E_G has a pole for $d \to 4$ that is linked to a calculable logarithm of the charge with coefficient $-\frac{v_G}{48}$.
Hence

$$k_0 = -\frac{1}{48} \left(\frac{1}{\sqrt{3}} + (N_f + 1)(N_f - 2) \right) . \tag{6.108}$$

This is a robust non-perturbative prediction of the large-charge approach which would be interesting to test via lattice simulations.

§ 6.4 The scaling dimensions and the near conformal corrections

Using the state-operator correspondence one can generalise the corrections determined in [94, 241] to the large-charge quasi-anomalous dimension Δ as a function of the dilaton, fermion mass, and background geometry to include the impact of the θ angle, axion physics, and dilaton potential yielding:

- $V_{\Delta\to 0}(\sigma)$, $\gamma \ll 1$

$$\frac{\tilde{\Delta}_Q^{ex}}{\tilde{\Delta}_Q} = 1 - \left(\frac{9m_\pi^2}{32\pi\nu}\right)^2 \frac{1-\gamma\log\left(\frac{3\rho^{2/3}}{16(2\pi^2)^{1/3}c_{4/3}\nu^2 N_f}\right)}{4c_{4/3}^5 N_f} \cos^2\left(\frac{\theta+2\pi k}{N_f}\right)\left(\frac{1}{2\pi^2\rho}\right)^{2/3}$$
$$+ \frac{\gamma}{c_{4/3}^6 N_f}\cos^2\left(\frac{\theta+2\pi k}{N_f}\right)\left(\frac{27m_\pi^4 \sin^2\left(\frac{\theta+2\pi k}{N_f}\right)}{256\, a\, c_{4/3}^3 N_f^2} + \frac{5\left(\frac{9m_\pi^2}{64\pi\nu}\right)^2\cos^2\left(\frac{\theta+2\pi k}{N_f}\right)}{6c_{4/3}^4 N_f} - \frac{c_{2/3}}{2}\left(\frac{2\pi^2\rho}{Q}\right)^{2/3}\right)$$
$$\times \left(\frac{9m_\pi^2}{32\pi\nu}\right)^2\left(\frac{1}{2\pi^2\rho}\right)^{4/3}\log Q - \frac{16}{9}\pi^2 c_{2/3}\nu^2 N_f m_\sigma^2 \left(\frac{1}{2\pi^2\rho}\right)^{4/3}\log Q \tag{6.109}$$

- $V_{\Delta\to 0}(\sigma),\ (1-\gamma)\ll 1$

$$\frac{\tilde{\Delta}_Q^{ex}}{\tilde{\Delta}_Q}=1-\frac{9m_\pi^4}{64c_{4/3}^4}(1-\gamma)\cos^2\left(\frac{\theta+2\pi k}{N_f}\right)\left(\frac{1}{2\pi^2\rho}\right)^{4/3}\log Q-\frac{16}{9}\pi^2 c_{2/3}\nu^2 N_f m_\sigma^2\left(\frac{1}{2\pi^2\rho}\right)^{4/3}\log Q\,. \tag{6.110}$$

- $V_{\Delta=2}(\sigma),\ \gamma\ll 1$

$$\begin{aligned}\frac{\tilde{\Delta}_Q^{ex}}{\tilde{\Delta}_Q}=1&-\left(\frac{9m_\pi^2}{32\pi\nu}\right)^2\frac{1-\gamma\log\left(\frac{3\rho^{2/3}}{16(2\pi^2)^{1/3}c_{4/3}\nu^2N_f}\right)}{4c_{4/3}^5N_f}\cos^2\left(\frac{\theta+2\pi k}{N_f}\right)\left(\frac{1}{2\pi^2\rho}\right)^{2/3}-\frac{c_{2/3}m_\sigma^2}{2c_{4/3}}\left(\frac{1}{2\pi^2\rho}\right)^{2/3}\\&+\frac{\gamma}{c_{4/3}^6N_f}\cos^2\left(\frac{\theta+2\pi k}{N_f}\right)\left(\frac{27m_\pi^4\sin^2\left(\frac{\theta+2\pi k}{N_f}\right)}{256\ a\ c_{4/3}^3N_f^2}+\frac{5\left(\frac{9m_\pi^2}{64\pi\nu}\right)^2\cos^2\left(\frac{\theta+2\pi k}{N_f}\right)}{6c_{4/3}^4N_f}-\frac{c_{2/3}}{2}\left(\frac{2\pi^2\rho}{Q}\right)^{2/3}\right)\\&\times\left(\frac{9m_\pi^2}{32\pi\nu}\right)^2\left(\frac{1}{2\pi^2\rho}\right)^{4/3}\log Q\end{aligned} \tag{6.111}$$

- $V_{\Delta=2}(\sigma),\ (1-\gamma)\ll 1$

$$\frac{\tilde{\Delta}_Q^{ex}}{\tilde{\Delta}_Q}=1-\frac{c_{2/3}m_\sigma^2}{2c_{4/3}}\left(\frac{1}{2\pi^2\rho}\right)^{2/3}-\frac{9m_\pi^4}{64c_{4/3}^4}(1-\gamma)\cos^2\left(\frac{\theta+2\pi k}{N_f}\right)\left(\frac{1}{2\pi^2\rho}\right)^{4/3}\log Q\,. \tag{6.112}$$

- $V_{\Delta\to 4}(\sigma),\ \gamma\ll 1$

$$\begin{aligned}\frac{\tilde{\Delta}_Q^{ex}}{\tilde{\Delta}_Q}=1&-\frac{c_{2/3}m_\sigma^2}{256\pi^2c_{4/3}^2\nu^2N_f}\left(3-4\log\left(\frac{3\sqrt{\frac{3}{2}}\rho}{64\pi c_{4/3}^{3/2}\nu^3N_f^{3/2}}\right)\right)+\frac{c_{2/3}^2m_\sigma^2}{256\pi^2c_{4/3}^3\nu^2N_f}\left(3-8\log\left(\frac{3\sqrt{\frac{3}{2}}\rho}{64\pi c_{4/3}^{3/2}\nu^3N_f^{3/2}}\right)\right)\frac{1}{Q^{2/3}}\\&-\left(\frac{9m_\pi^2}{32\pi\nu}\right)^2\frac{1-\gamma\log\left(\frac{3\rho^{2/3}}{16(2\pi^2)^{1/3}c_{4/3}\nu^2N_f}\right)}{4c_{4/3}^5N_f}\cos^2\left(\frac{\theta+2\pi k}{N_f}\right)\left(\frac{1}{2\pi^2\rho}\right)^{2/3}\end{aligned} \tag{6.113}$$

- $V_{\Delta\to 4}(\sigma),\ (1-\gamma)\ll 1$

$$\frac{\tilde{\Delta}_Q^{ex}}{\tilde{\Delta}_Q}=1-\frac{c_{2/3}m_\sigma^2}{256\pi^2c_{4/3}^2\nu^2N_f}\left(3-4\log\left(\frac{3\sqrt{\frac{3}{2}}\rho}{64\pi c_{4/3}^{3/2}\nu^3N_f^{3/2}}\right)\right)+\frac{c_{2/3}^2m_\sigma^2}{256\pi^2c_{4/3}^3\nu^2N_f}\left(3-8\log\left(\frac{3\sqrt{\frac{3}{2}}\rho}{64\pi c_{4/3}^{3/2}\nu^3N_f^{3/2}}\right)\right)\frac{1}{Q^{2/3}} \tag{6.114}$$

Here $\tilde{\Delta}$ is the conformal dimension at the fixed point at leading order in the semiclassical expansion and $\rho\equiv Q/V$ is the charge density.

This chapter closes with a few comments in the following.

a) The effects coming from different values of Δ of the underlying operator responsible for conformal breaking are the main protagonists of this analysis. These are encoded in the dilaton potential and their results are summarised in the magenta part of the deformed conformal dimensions. The first observation is that all corrections are universally proportional to the dilaton squared mass, while the dependence on Δ is encoded in both the coefficient and the scaling dependence on the charge (density) of the term m_σ^2.

For $\Delta \to 0$ the leading conformal breaking term scales with $\nu^2\rho^{-4/3}\log Q$ [241] while for $\Delta = 2$ and $\Delta = 4$ one has respectively, $\rho^{-2/3}$ and $\nu^{-2}\log(\rho/\nu^3)$ at fixed but large charge density.

b) Conformal breaking due to the introduction of the π mass, to the chiral and conformal lagrangian order that is considered, yields an additive contribution to the deformed anomalous dimensions with respect to the dilaton one. This contribution is independent of the value of Δ and is universally proportional to the fourth power of the pion mass (i.e. quadratic in the underlying fermion masses).

However, its contribution depends on the value of the anomalous dimension of the fermion-antifermion condensate operator controlled by γ. In the $\Delta \to 0$ case the zero θ-angle expression was determined in [94] while here, for the first time, its θ-angle dependence is shown. These terms are highlighted in violet. For $\Delta \to 4$ there are still these terms, but they are subleading at large charge density with respect to the dilaton contribution. However, they are naturally there when the dilaton mass vanishes.

Scaling results for charged sectors of near conformal QCD

7

CHAPTER

At this stage, after several introductory chapters on the methodology and theories that form the focus of this thesis, the framework is now established to examine three-colour QCD. This chapter, based on [3], reveals the discovery of near conformal properties of finite isospin density QCD by the determination of the classical ground state energy on a cylinder via the semiclassical large charge expansion. In the conformal limit this energy maps, via state-operator correspondence, to the scaling dimension of the lowest-lying operator of fixed isospin charge Q. The leading near conformal corrections at the lower boundary of the QCD conformal window are shown. The characteristic Q-scalings due to the near conformal corrections are induced by the quark mass operator anomalous dimension γ as well as the conformal dimension Δ of the operator responsible for dynamically deforming QCD away from the conformal window. Furthermore, the pattern of symmetry breaking, the associated physical spectrum, and their dispersion relations follow. These results will also help to determine the next-to-leading order large charge contributions. Last but not least, the $\mu - \theta$ QCD phase diagram is also discussed.

§ 7.1 Chiral Lagrangian at finite isospin and θ-angle: notation and conventions

The low-energy dynamics of QCD at finite generalised isospin density is described by the chiral Lagrangian below

$$\begin{aligned}\mathcal{L} = \nu^2 Tr\{\partial_\mu \Sigma \partial^\mu \Sigma^\dagger\} + m_\pi^2 \nu^2 Tr\{M\Sigma + M^\dagger \Sigma^\dagger\} + 2i\mu\nu^2 Tr\{I\partial_0 \Sigma\Sigma^\dagger - I\Sigma^\dagger \partial_0 \Sigma\} \\ + 2\mu^2 \nu^2 Tr\{II - \Sigma^\dagger I \Sigma I\}\ .\end{aligned} \tag{7.1}$$

Here ν is half the pion decay constant, μ is the (generalised) isospin chemical potential, and

$$\Sigma = e^{i\varphi/\nu}\,, \qquad \varphi = \Pi^a T^a + \frac{S}{\sqrt{N_f}}\,, \tag{7.2}$$

with T^a the $SU(N_f)$ generators normalised as $\mathrm{Tr}\{T^aT^b\} = \delta^{ab}$. The mass matrix and the charge generator read

$$M = \mathbb{1}_{N_f}\,, \qquad I = \frac{1}{2}\begin{pmatrix} \mathbb{1}_{N_f/2} & 0 \\ 0 & -\mathbb{1}_{N_f/2} \end{pmatrix}\,, \tag{7.3}$$

where, as in chapter 4, let us assume degenerate Goldstone bosons of mass m_π. The matrix I generalises the concept of isospin in the multi-flavour theory, with the two-flavour case being the conventional QCD isospin. In this chapter, the focus is on the dynamics of the theory at finite charge density, with the charge defined via the generator I with μ being the associated chemical potential.

Finally, as fully detailed in [260, 261], the CP-violating topological sector is included through the θ-angle term

$$\Delta\mathcal{L}_\theta = -av^2\left(\theta - \frac{i}{2}Tr\{\log\Sigma - \log\Sigma^\dagger\}\right)^2\,. \tag{7.4}$$

Let us stress again that the introduction of the above term is well-justified only in the large number of colours limit (see also the summary of chapter 4). However, the discussion of the phase diagram of the theory in the next section is at leading order in an expansion in m_π^2/a. Since this is equivalent to incorporating the θ-angle directly in the mass term (as done in e.g. [262–264]), the corresponding analysis does not rely on the large N limit. On the other hand, when studying the dispersion relation of the eta prime mode in section 7.5, the use of the large-N limit is implied.

§ 7.2 Phase diagram in the μ-θ plane

In the absence of the θ-angle, the ground state of our theory generalises the $N_f = 2$ case examined in detail in [80] and reviewed in section 3.4.1 and takes the form

$$\Sigma_c = \mathbb{1}_{N_f}\cos\varphi + i\Sigma_I\sin\varphi\,, \tag{7.5}$$

with

$$\Sigma_I = \begin{pmatrix} 0 & \mathbb{1}_{N_f/2} \\ \mathbb{1}_{N_f/2} & 0 \end{pmatrix}\cos\eta + i\begin{pmatrix} 0 & -\mathbb{1}_{N_f/2} \\ \mathbb{1}_{N_f/2} & 0 \end{pmatrix}\sin\eta\,. \tag{7.6}$$

As stressed in section 3.4.1 [179], the minimisation of the potential results from the competition of two terms in the right-hand side of eq.(7.5) which individually minimise, respectively, the mass and isospin terms in the potential. Their contribution is weighted by the angle φ which is determined by the equations of motion. Moreover, it can be shown that the isospin term in the potential is minimised when Σ_I satisfies $I\Sigma_I = -\Sigma_I I$. Following discussion in chapter 4, to take into account the effect of the θ-angle on the vacuum state, let us introduce the Witten variables α_i [260] so that the ground state reads

$$\Sigma_0 = U(\alpha_i)\Sigma_c\,, \text{ with } U(\alpha_i) = \mathrm{diag}\{e^{-i\alpha_1}, \dots, e^{-i\alpha_{N_f}}\}\,. \tag{7.7}$$

It is useful to again define the quantities

$$\bar{\theta} = \theta - \sum_{i}^{N_f} \alpha_i \ , \ \ X = \sum_{i=1}^{N_f} \cos \alpha_i \ , \tag{7.8}$$

in terms of which the Lagrangian of the theory evaluated on the ground state ansatz reads

$$\mathcal{L}[\Sigma_0] = 2m_\pi^2 \nu^2 X \cos\varphi + N_f \mu^2 \nu^2 \sin^2\varphi - a\nu^2\bar{\theta}^2 \, . \tag{7.9}$$

The angle φ and the Witten variables α_i are determined by the EOM as

$$\sin\varphi \left(N_f \cos\varphi - \frac{m_\pi^2 X}{\mu^2} \right) = 0 \ , \tag{7.10}$$

$$m_\pi^2 \sin\alpha_i \cos\varphi = a\bar{\theta} \ , \ \ i = 1, \ldots, N_f \ , \tag{7.11}$$

while the angle η does not appear in the equation of motion, meaning that there is a residual unbroken $U(1)$ isospin vector-symmetry. However, choosing a specific value of η amounts to the further spontaneous breaking of this leftover $U(1)$. The first EOM has two solutions, namely $\varphi = 0$ and $\cos\varphi = \frac{m_\pi^2 X}{N_f \mu^2}$. Recalling the discussion in chapter 3 when the latter is realised, the theory is in a superfluid phase characterised by pion condensation. The energy density of the system in the two phases reads

$$\begin{aligned} \mathcal{E}(\theta) &= -2m_\pi^2 \nu^2 X + a\nu^2\bar{\theta}^2 && \text{normal phase} \quad (\varphi = 0) \\ \mathcal{E}(\theta) &= -\frac{m_\pi^4 \nu^2}{N_f \mu^2} X^2 - N_f \nu^2 \mu^2 + a\nu^2\bar{\theta}^2 && \text{superfluid phase} \left(\cos\varphi = \frac{m_\pi^2 X}{N_f \mu^2} \right) . \end{aligned} \tag{7.12}$$

When $a \gg m_\pi^2$ the θ-dependence results in an effective pion mass $m_\pi^2(\theta) = m_\pi^2 X/N_f$. The EOMs and the expression for the vacuum energy of the system are very similar to the ones shown in chapter 4 for two-colour QCD with finite baryon density. At $\theta = 0$ the normal to superfluid phase transition occurs at a critical value of the chemical potential $\mu_c = m_\pi$. Since the θ-vacuum may differ in the two phases, to study the superfluid transition at non-vanishing values of θ, let us first determine the θ-dependence. Therefore, eq.(7.11) is solved as in chapter 4 by expanding in powers of m_π^2/a that is taken to be small. Specifically, at the leading order in m_π^2/a:

$$\alpha_i = \begin{cases} \pi - \alpha(\theta) \, , & i = 1, \ldots, n \\ \alpha(\theta) \, , & i = n+1, \ldots, N_f \, , \end{cases} \tag{7.13}$$

where

$$\alpha(\theta) = \frac{\theta + (2k - n)\pi}{(N_f - 2n)}, \quad k = 0, \ldots, N_f - 2n - 1 \, , \quad n = 0, ..., \left[\frac{N_f - 1}{2} \right] . \tag{7.14}$$

Here, again, the parameters n and k label the various solutions to the EOMs. The interval of values for k is constrained because at fixed n the solutions are periodic in k of period $N_f - 2n$. In the normal phase the energy is minimised when X is maximized. As has been shown in chapter 4 the solution minimising the energy has $n = 0$ and the following values of $\alpha(\theta)$

$$\alpha(\theta) = \begin{cases} \frac{\theta}{N_f} , & \theta \in [0, \pi] \\ \frac{\theta - 2\pi}{N_f} , & \theta \in [\pi, 2\pi] , \end{cases} \tag{7.15}$$

which correspond, respectively, to $k = 0$ and $k = N_f - 1$.

The physics at $\theta = \pi$ deserves further discussion. In fact, the Lagrangian possesses CP symmetry when $\theta = \pi$ but the latter is spontaneously broken by the vacuum leading to the well-known Dashen's phenomenon [265]. In fact, at $\theta = \pi$ the two solutions for $\alpha(\theta)$ in eq.(7.15) have the same energy leading to degenerate vacua connected by a CP transformation. The situation in which the ground state energy as a function of θ for the template case $N_f = 2$ is exactly the one depicted in Fig.4.1.(a) as well as a plot of the CP order parameter $\langle F\widetilde{F}\rangle$ associated with the pseudo-scalar glueball condensate of Fig. 4.2.(a).

In the superfluid phase, the EOM becomes

$$\frac{m_\pi^4}{N_f \mu^2} X \sin\alpha_i = a\bar{\theta} \, , \quad i = 1, \ldots, N_f \tag{7.16}$$

and admits the same solution (7.14) at the leading order in the natural expansion parameter $\frac{m_\pi^4}{a\mu^2}$. The crucial difference from the normal phase is that the energy now depends quadratically instead of linearly on X. The situation is analogous to the case of two-colour QCD at finite baryon charge investigated in chapter 4 for even N_f. As has been found there, the ground state solution is the same as the normal phase given by eq.(7.15). Consequently, for $N_f > 2$, at the crossing point $\theta = \pi$, spontaneous breaking of CP occurs. On the other hand, for $N_f = 2$ the two solutions $\alpha(\theta) = \frac{\theta}{N_f}$ and $\alpha(\theta) = \frac{\theta - 2\pi}{N_f}$ have a degenerate energy for all values of θ. As a consequence, physics is analytic at $\theta = \pi$ and Dashen's phenomenon does not occur [1,163]. The θ-vacuum in the superfluid phase in the two-flavour case is illustrated in Fig.4.1.

Note that the pair of completely degenerate solutions remains such for all orders in $\frac{m_\pi^4}{a\mu^2}$. In fact, given the EOM (7.16) for a certain $\alpha(\theta)$

$$\frac{m_\pi^4}{2a\mu^2} \sin(2\alpha(\theta)) = \theta - 2\alpha(\theta) \, , \tag{7.17}$$

the same EOM is valid for $\alpha(\theta) + \pi$, upon shifting the θ-angle as $\theta \to \theta + 2\pi$. However, this shift leaves the physics unchanged. Finally, let us investigate the critical value of the isospin chemical potential where the superfluid phase transition occurs. For $m_\pi^2 \ll a$, the latter occurs at a critical value of the chemical potential given by

$$\mu_c = m_\pi(\theta) = m_\pi \left[\sqrt{\left| \cos\frac{\theta}{N_f} \right|} + O\left(\frac{m_\pi^2}{a} \right) \right] , \tag{7.18}$$

which is of particular interest when $N_f = 2$ at $\theta = \pi$. In fact, μ_c is almost zero, as the effective pion mass $m_\pi^2(\theta) \sim m_\pi^2 |\cos(\theta/2)|$ vanishes identically. Concretely, at $\theta \sim \pi$ one has

$$\mu_c \sim m_\pi \sqrt{\frac{m_\pi^2}{a} + \frac{|\phi|}{2}} \, , \qquad \phi \equiv \theta - \pi \, . \tag{7.19}$$

On the other hand, a vanishing pion mass at the effective Lagrangian level raises an apparent paradox, since it would imply no explicit breaking of chiral symmetry. However, let us again stress that there is no chiral symmetry restoration in the fundamental QCD Lagrangian at $\theta = \pi$. The apparent paradox is solved by pointing out that the global flavour symmetry is still broken when including higher-order mass terms in the effective Lagrangian as explained in detail in [263, 264] and presented in chapter 4.

§ 7.3 Dilaton augmented chiral Lagrangian and the large charge expansion

The stage is set in this section, which focusses on the dynamics near the lower edge of the conformal window to determine the ground state energy of charged states on a non-trivial background that can be associated with scaling dimensions of QCD operators carrying (generalised) isospin charge. Of course, the procedure is always the same where first step is to upgrade the chiral Lagrangian to a conformally invariant theory via the introduction of the dilaton field that non-linearly realises scale invariance. The latter is enforced at the effective action level by coupling σ to each operator O_k of dimension k appearing in the Lagrangian as [52, 53]

$$O_k \mapsto e^{(k-4)\sigma f}\, O_k \,. \tag{7.20}$$

Of course, as already done in chapter 6, explicit breaking of the latter can be taken into account, introducing a potential term for σ. Following chapter 5, the breaking of conformality is here considered as the result of perturbing a CFT with a relevant operator O with conformal dimension Δ, i.e.

$$\mathcal{L}_{\text{CFT}} \to \mathcal{L}_{\text{CFT}} + \lambda_O O \,, \tag{7.21}$$

with λ_O the corresponding coupling.

The key point here is that unlike in the previous chapter 6, Δ will not be fixed to investigate the cases introduced in chapter 5. Instead, the treatment will remain on a general level, and it will later be shown how the large charge expansion allows for a general result, with the charge acting as a new tunable parameter governing the final expression. In particular, the non-conformal corrections do depend on the specific form of the potential deforming the CFT, but they are accompanied by a scaling in charge that holds more generally.

Let us employ the large charge expansion framework [75, 82, 93] (see chapter 2) to determine the scaling dimension of the lowest-lying operator with charge Q. Precisely, the approximate Weyl invariance of the near conformal theory is used to map the latter onto the cylinder $\mathbb{R} \times S^3$. The volume, the radius and the Ricci scalar of S^3 are denoted as V, R, and $\mathcal{R} = \frac{6}{R^2}$, respectively.

The dilaton-pion effective Lagrangian on $\mathbb{R}\times S^3$ reads

$$\begin{aligned}\mathcal{L}_\sigma &= v^2 Tr\{\partial_\mu\Sigma\partial^\mu\Sigma^\dagger\}\, e^{-2\sigma f} + m_\pi^2 v^2 Tr\{M\Sigma + M^\dagger\Sigma^\dagger\}\, e^{-y\sigma f} + 2\mu^2 v^2 Tr\{II - \Sigma^\dagger I\Sigma I\}e^{-2\sigma f} \\ &+ 2i\mu v^2 Tr\{I\partial_0\Sigma\Sigma^\dagger - I\Sigma^\dagger\partial_0\Sigma\}e^{-2\sigma f} - av^2\left(\theta - \frac{i}{2}Tr\{\log\Sigma - \log\Sigma^\dagger\}\right)^2 e^{-4\sigma f} - \Lambda_0^4\, e^{-4\sigma f} \\ &+ \frac{1}{2}\left(\partial_\mu\sigma\partial^\mu\sigma - \frac{\mathcal{R}}{6f^2}\right) e^{-2\sigma f} - V(\sigma)\,,\end{aligned} \tag{7.22}$$

where Λ_0 is again the bare cosmological constant. The inclusion of this term is convenient in the sense explained in section 2.4.4 and in appendix B and already discussed in chapter 6. Let us recall that Δ_Q can be computed via a semiclassical expansion in the double scaling limit

$$\Lambda_0 f \to 0\,, \quad Q\to\infty\,, \quad Q(\Lambda_0 f)^4 = \text{fixed} \tag{7.23}$$

and the leading order result corresponds to $\tilde{\Delta}_Q$ and is given by the classical ground state energy on $\mathbb{R}\times S^3$ whereas the next-to-leading order is determined by the fluctuations around the classical trajectory.

Since in the near conformal regime the state-operator correspondence is only approximate, one actually computes $\tilde{\boldsymbol{\Delta}}_Q^{ex}$ that will be equal to $\tilde{\Delta}_Q$ plus corrections that disappear as the pion and dilaton masses vanish. Precisely, deviations from conformality will be encoded in a set of contributions that depend on the spacetime geometry due to the lack of Weyl invariance. Therefore, in the next section, it will determined the classical ground state energy $\tilde{\boldsymbol{\Delta}}_Q^{ex}$.

§ 7.4 Large charge expansion: leading order

As anticipated in the previous section, the state-operator correspondence is pivotal to deduce the scaling dimension for the lowest-lying operator with (generalised) isospin charge Q. This is achieved by determining the energy associated with the vacuum structure inducing the superfluid phase transition. Hence, let us evaluate the Lagrangian (7.22) on the ansatz (7.7), it reads

$$\begin{aligned}\mathcal{L}_\sigma\,[\Sigma_0,\sigma_0] &= -e^{-4f\sigma_0}\Lambda_0^4 - V(\sigma_0) - \frac{\mathcal{R}\, e^{-2f\sigma_0}}{12f^2} + 2m_\pi^2 v^2 X\cos\varphi\, e^{-f\sigma_0 y} \\ &+ N_f\mu^2 v^2 e^{-2f\sigma_0}\sin^2\varphi - av^2 e^{-4f\sigma_0}\bar{\theta}^2\,,\end{aligned} \tag{7.24}$$

where σ_0 denotes the classical dilaton solution. It is worth noticing that, replacing $m_\pi \to \sqrt{2}\,m_\pi$ and $\mu\to\sqrt{2}\,\mu$, the resulting expression is identical to that found for two-colour QCD at finite baryon density, as explored in chapter 6. However, throughout this chapter, the results already obtained in chapter 6 are further extended since here, rather than concentrating on specific values of Δ and y, the dilaton potential considered is directly that of eq. (5.89).

Specifically, as explained in section 5.4.4, the intention is to avoid committing to a specific potential, instead acknowledging the lack of detailed understanding regarding the underlying mechanism and a precise counting scheme for the dEFT construction. This approach is taken to maintain the discussion in the broadest possible terms. As will be demonstrated later, the presented results are valid on general grounds due to the presence of the isospin charge and the large charge framework. Moreover, the near conformal contributions obtained depend solely on the charge-expansion power and the dilaton mass. Therefore, while different potentials discussed in chapter 5 and considered in chapter 6 yield different numerical constants, the Q-scaling of the results remains unchanged.

Having this in mind, then the classical ground state energy is computed by solving the EOM

$$\frac{\delta\mathcal{L}}{\delta\alpha} = \frac{\delta\mathcal{L}}{\delta\varphi} = \frac{\delta\mathcal{L}}{\delta\sigma_0} = 0, \quad \frac{\delta\mathcal{L}}{\delta\mu} = \frac{Q}{V}\,, \tag{7.25}$$

explicitly:

$$\sin\varphi(N_f\mu^2 e^{-2f\sigma_0}\cos\varphi - m_\pi^2 X e^{-f\sigma_0 y}) = 0\,, \tag{7.26}$$

$$a e^{-4f\sigma_0}\bar{\theta} - m_\pi^2 \sin\alpha_i \cos\varphi e^{-f\sigma_0 y} = 0\,, \qquad i = 1, .., N_f\,, \tag{7.27}$$

$$\begin{aligned}\frac{\mathcal{R}e^{-2f\sigma_0}}{6f} &+ 4af\nu^2 e^{-4f\sigma_0}\bar{\theta}^2 + 4f\Lambda_0^4 e^{-4f\sigma_0} - \left.\frac{\partial V(\sigma)}{\partial\sigma}\right|_{\sigma=\sigma_0} + \\ &-2fN_f\mu^2\nu^2 e^{-2f\sigma_0}\sin^2\varphi - 2fym_\pi^2\nu^2 X\cos\varphi e^{-f\sigma_0 y} = 0\,,\end{aligned} \tag{7.28}$$

$$2N_f\mu\nu^2 e^{-2f\sigma_0}\sin^2\varphi = \frac{Q}{V}\,, \tag{7.29}$$

where the last equation defines the isospin charge density. To determine the classical ground state energy on the cylinder one needs to solve the above EOM in the variables φ, α_i, σ_0 and μ and plug the solution into eq.(7.24). However, since the EOM are transcendental equations, it is not straightforward to find their exact solutions.

Therefore, this issue is overcome by solving the EOM perturbatively in positive powers of the parameters m_σ^2 and m_π^2. Specifically, one expands the variables as $x = x_0 + x_1 m_\sigma^2 + x_2 m_\pi^2 + x_3 m_\sigma^4 + x_4 m_\pi^4 + x_5 m_\sigma^2 m_\pi^2 + \mathcal{O}\left(m_\sigma^6, m_\pi^6, m_\sigma^4 m_\pi^2, m_\sigma^2 m_\pi^4\right)$ where $x = \{\mu, \varphi, \sigma_0, \alpha_i\}$ and determines the coefficients of the expansion by solving the EOM order by order. The result reads

$$\begin{aligned}\Delta_Q^{ex} = &\frac{\pi^2}{8f^2}\left(6N_f(f\nu\mu R)^2 + 1\right)\left(\frac{2N_f(f\nu\mu R)^2 - 1}{f^2\Lambda^4}\right) + m_\sigma^2\,\frac{\pi^2 2^{1-\Delta}R^{4-\Delta}}{(\Delta-4)\Delta f^2}\left(\frac{2N_f(f\nu\mu R)^2 - 1}{f^2\Lambda^4}\right)^{\Delta/2} \\ &- m_\pi^4 N_f\cos^2(\alpha(\theta))\,2^{2\gamma-3}\left(\frac{\pi\nu R^{\gamma+1}}{\mu R}\right)^2\left(\frac{2N_f(f\nu\mu R)^2 - 1}{f^2\Lambda^4}\right)^{2-\gamma} + \mathcal{O}\left(m_\sigma^4, m_\pi^8, m_\sigma^2 m_\pi^4\right)\,,\end{aligned} \tag{7.30}$$

where μ is related to Q as

$$\mu R = \frac{\left(6\pi^4\nu^2 N_f\right)^{1/3} + \left(\sqrt{81f^6\Lambda^8 Q^2 - 6\pi^4\nu^2 N_f} + 9f^3\Lambda^4 Q\right)^{2/3}}{f\left(6\pi\nu^2 N_f\right)^{2/3}\left(\sqrt{81f^6\Lambda^8 Q^2 - 6\pi^4\nu^2 N_f} + 9f^3\Lambda^4 Q\right)^{1/3}}\,. \tag{7.31}$$

The first term in (7.30) represents the scaling dimension in the conformal limit $m_\pi = m_\sigma = 0$ which depends only on the dimensionless combination μR (7.31). The latter is determined by the value of the charge Q via eq.(7.31) and, therefore, the first term in eq.(7.30) is insensitive to the spacetime geometry. Noticeably, the leading correction in the pion mass is of order m_π^4 and its dependence on the geometry is tied to the anomalous dimension of the chiral condensate through the universal factor $R^{2(\gamma+1)}$. Remarkably, the whole θ-dependence is encoded in the factor $\cos^2(\alpha(\theta))$ with $\alpha(\theta)$ given in eq.(7.15). The first term in the dilaton potential (5.89) redefines the cosmological constant as

$$\Lambda^4 \equiv \Lambda_0^4 + \frac{m_\sigma^2}{4f^2(4-\Delta)} \,. \tag{7.32}$$

The contribution stemming from the second term in the dilaton potential (5.89) has been expanded in powers of m_σ with the leading order quadratic in the dilaton mass. The latter exhibits a universal dependence on the radius of the sphere via the factor $R^{4-\Delta}$. It is interesting to further expand these results (7.30) in the large charge limit $Q(\Lambda_0 f)^4 \gg 1$ where one can make contact with the universal predictions of the large charge effective field theory (EFT) [82, 93]. Hence, in this expansion, the previous result reads

$$\tilde{\boldsymbol{\Delta}}_Q^{ex} = \tilde{\Delta}_Q + \left(\frac{m_\sigma}{4\pi\nu}\right)^2 Q^{\frac{\Delta}{3}} B_1 + \left(\frac{m_\pi}{4\pi\nu}\right)^4 \cos^2(\alpha(\theta))\, Q^{\frac{2}{3}(1-\gamma)} B_2 + O\left(m_\sigma^4, m_\pi^8, m_\sigma^2 m_\pi^4\right) , \tag{7.33}$$

where B_1 and B_2 are

$$B_1 = \frac{c_{2/3} 2^{9-2\Delta} 3^{\frac{\Delta}{2}-1} (\pi\nu R)^{4-\Delta} \left(c_{4/3} N_f\right)^{1-\frac{\Delta}{2}}}{(\Delta-4)\Delta} \left(1 - \frac{\Delta\, c_{2/3}}{4c_{4/3}} Q^{-2/3} + O\left(Q^{-4/3}\right)\right) , \tag{7.34}$$

$$B_2 = -\, 3^{4-\gamma} 2^{4\gamma-3} \pi^{2\gamma+2} c_{4/3}^{\gamma-4} N_f^{\gamma-1} (\nu R)^{2(\gamma+1)} \left(1 + \frac{(\gamma-4)c_{2/3}}{2c_{4/3}} Q^{-2/3} + O\left(Q^{-4/3}\right)\right) , \tag{7.35}$$

while

$$\tilde{\Delta}_Q = c_{4/3} Q^{4/3} + c_{2/3} Q^{2/3} + O\left(Q^0\right) \tag{7.36}$$

is the scaling dimension in the conformal limit at the leading order in the double scaling limit (7.23), which depends only on the dimensionless coefficients defined below

$$c_{4/3} = \frac{3}{8}\left(\frac{2\Lambda^2}{\pi N_f \nu^2}\right)^{2/3} , \quad c_{2/3} = \frac{1}{4f^2}\left(\frac{2\pi^2}{N_f \nu^2 \Lambda^4}\right)^{1/3} . \tag{7.37}$$

The conformal dimension $\tilde{\Delta}_Q$ exhibits the general structure predicted by the large charge EFT. The non-conformal corrections feature a characteristic Q-scaling which has been made manifest in eq.(7.33) and depends on the parameters γ and Δ encoding the explicit breaking of scale invariance. Additionally, the near conformal corrections come as a product of two contributions: a first where there is encoded information about the geometry of the system and a second one that carries the general information about the large charge expansion. In this sense, eq.(7.33) is independent of the specific model used to describe the dilaton potential: the corrections are influenced by the presence of the dilaton mass and the charge expansion, with the specific form of the potential potentially altering the factor B_1 by constant factors.

§ 7.5 Symmetry-breaking pattern and spectrum of fluctuations

Let us now move to determine first the symmetry-breaking pattern and then the spectrum of the theory. Fixing the generalised isospin charge results in

$$SU(N_f)_L \times SU(N_f)_R \times U(1)_V \overset{N_f^2-1}{\rightsquigarrow} SU(N_f)_V \times U(1)_V \longrightarrow SU\left(\frac{N_f}{2}\right)_u \times SU\left(\frac{N_f}{2}\right)_d \times U(1)_I \times U(1)_V$$
$$\overset{\frac{N_f^2}{4}}{\rightsquigarrow} SU\left(\frac{N_f}{2}\right)_{ud} \times U(1)_V\,, \tag{7.38}$$

where $\rightsquigarrow$ and $\longrightarrow$ denote, respectively, spontaneous and explicit breaking. The first stage is the usual chiral symmetry breaking with the ABJ anomaly already taken into account in the breaking of the axial symmetry. The further explicit breaking is owing to the introduction of the isospin charge, while the last spontaneous breaking is associated with pion condensation and the superfluid phase transition.

In the absence of the dilaton, the spectrum of light modes is composed of $N_f^2/4$ massless Goldstone bosons with speed $v_G = 1$ that parameterise the coset $G/H = \dfrac{SU(N_f/2)_u \times SU(N_f/2)_d \times U(1)_I \times U(1)_V}{SU(N_f/2)_{ud} \times U(1)_V}$. These modes arrange themselves in the adjoint representation of the stability group $SU(N_f/2)_{udV} \times U(1)_V$ plus a singlet which we denote as π_3 since it is associated with the spontaneous breaking of $U(1)_I$ i.e. to the third Pauli matrix in the $N_f = 2$ case. In addition, a pseudo-Goldstone mode stems from the would-be spontaneous breaking of $U(1)_A$ which we call the S (singlet) mode and it is related to the η'-meson [266]. As mentioned above, the $U(1)_A$ symmetry is quantum mechanically anomalous, and therefore the latter mode acquires a mass proportional to the scale of the anomaly $\sqrt{a}$.

In what follows, only the spectrum of Goldstone bosons will be taken into account since they control the large charge dynamics. Specifically, the interest is in analysing how the spectrum of light modes changes when (near)conformal dynamics is realised through the dilaton dressing. Precisely, conformal invariance dictates the existence of a massless mode with speed $v_G = \frac{1}{\sqrt{d-1}} = \frac{1}{\sqrt{3}}$ [82, 267]. As will be shown, the latter arises from the mixing between the singlet π_3 with the dilaton that acts as its “radial mode" and changes its speed from $v_G = 1$ to $v_G = \frac{1}{\sqrt{3}}$, that is exactly the situation depicted in chapter 2 and already obtained in chapter 6.

In the following, as done in chapter 6, the hierarchy of scales $m_\pi, m_\sigma \ll \mu \ll 4\pi\nu$ is considered since it ensures the validity of chiral perturbation theory and assumes a small deviation from conformality. To determine the spectrum of the fluctuations, one expands around the vacuum solution as

$$\Sigma = e^{\frac{2i}{\sqrt{N_f}} S \mathbb{1}_{N_f}} e^{i\Omega} \Sigma_0 e^{-i\Omega^\dagger}\,, \tag{7.39}$$

where Σ_0 is the classical solution (7.5) while the fluctuations are organized in the matrix

Ω as

$$\Omega = \begin{pmatrix} \pi & 0 \\ 0 & -\pi^T \end{pmatrix} . \tag{7.40}$$

Here $\pi = \sum_{a=0}^{\dim \mathrm{G/H}} \pi^a t_a$ where the sum runs over all the generators of the coset G/H that is normalized as $Tr\,\{t_a t_b\} = \frac{\delta_{ab}}{2}$. After some manipulations, one obtains

$$Tr\left\{\partial_\mu \Sigma \partial^\mu \Sigma^\dagger\right\} = 4\sin^2\varphi\; \partial_\mu \pi^a \partial^\mu \pi^a + 4\partial_\mu S \partial^\mu S\,, \tag{7.41}$$

$$Tr\left\{I\partial_0 \Sigma\Sigma^\dagger - I\Sigma^\dagger \partial_0 \Sigma\right\} = 4iTr\,\{I\partial_0 \nu\}\sin^2\varphi = 2i\sqrt{N_f}\,\partial_0 \pi^3 \sin^2\varphi\,, \tag{7.42}$$

$$Tr\left\{M\Sigma + M^\dagger \Sigma^\dagger\right\} = 2\cos\varphi\left[X\cos\left(\frac{2}{\sqrt{N_f}}S\right) + Z\sin\left(\frac{2}{\sqrt{N_f}}S\right)\right]\,, \tag{7.43}$$

$$Tr\left\{\log\Sigma - \log\Sigma^\dagger\right\} = 4i\sqrt{N_f}S - 2i\sum_i^{N_f}\alpha_i\;, \tag{7.44}$$

where $Z \equiv \sum_{i=1}^{N_f}\sin\alpha_i$. Finally, the dilaton field is expanded around its background solution as $\sigma \to \sigma_0 + \hat\sigma(t,\mathrm{x})$. It is easy to show that the π_a modes corresponding to the Goldstone modes transforming according to the adjoint representation of $SU(N_f/2)$ have trivial dispersion relations $\omega = k$. On the other hand, the Goldstone boson which is a singlet of $SU(N_f/2)$ mixes with the dilaton and the S. The corresponding dispersion relations are obtained by solving $\det D^{-1} = 0$ where the inverse propagator D^{-1} is given by

$$D^{-1} = \begin{pmatrix} \omega^2 - k^2 & i\omega\mu f\sqrt{N_f} & 0 \\ -i\omega\mu f\sqrt{N_f} & \frac{\omega^2-k^2}{8\nu^2\sin^2\varphi} - M_\sigma^2 & \frac{1}{2}I_{\hat\sigma s} \\ 0 & \frac{1}{2}I_{\hat\sigma s} & \frac{\omega^2-k^2}{\sin^2\varphi} - M_s^2 \end{pmatrix}\,, \tag{7.45}$$

with

$$I_{\hat\sigma S} = \frac{f\mu^2\sqrt{N_f}\left(4a\mu^2\bar\theta N_f^2 e^{-2f\sigma_0\gamma} - m_\pi^4 XZ(3-\gamma)\right)}{\left(\mu^4 N_f^2 e^{2f\sigma_0(1-\gamma)} - m_\pi^4 X^2\right)}\,, \tag{7.46}$$

$$\begin{aligned} M_\sigma^2 = \frac{\mu^2 N_f}{8\nu^2}\Bigg[& \frac{\Delta\mu^2 N_f m_\sigma^2 e^{-f(\Delta-2)\sigma}}{(\Delta-4)\left(\mu^4 N_f^2 - m_\pi^4 X^2 e^{2(\gamma-1)f\sigma}\right)} \\ & + \frac{2f^2\left(2\mu^2 N_f\left(\mu^2\nu^2 N_f e^{2f\sigma} - 4\left(a\nu^2\bar\theta^2 + \Lambda^4\right)\right) + ((\gamma-6)\gamma+7)\nu^2 m_\pi^4 X^2 e^{2\gamma f\sigma}\right)}{m_\pi^4 X^2 e^{2\gamma f\sigma} - \mu^4 N_f^2 e^{2f\sigma}}\Bigg]\,, \end{aligned} \tag{7.47}$$

$$M_S^2 = \frac{a\mu^4 N_f^3 + \mu^2 m_\pi^4 X^2 e^{2\gamma f\sigma_0}}{\mu^4 N_f^2 e^{2f\sigma_0} - m_\pi^4 X^2 e^{2\gamma f\sigma_0}}\,. \tag{7.48}$$

Note that eq.(7.48) is consistent with the Witten-Veneziano relation [268, 269]. In fact, in the $m_\pi \to 0$ limit, M_S^2 reduces to

$$\lim_{\sigma_0\to 0,\ m_\pi\to 0}(7.48) \implies M_S^2 = aN_f\ . \tag{7.49}$$

The remaining dispersion relations are obtained by solving the equation $\det(D^{-1}) = 0$. The results describe two gapped modes $\omega_{1,2}$ with mass

$$M_{1,2}^2 = -\frac{1}{2}\sin^2\varphi\left[M_S^2 + 8\nu^2 f^2\mu^2 N_f + 8\nu^2 M_\sigma^2 \pm \sqrt{\left(M_S^2 - 8\nu^2\left(f^2\mu^2N_f + M_\sigma^2\right)\right)^2 + 8\nu^2 I_{\hat\sigma S}^2}\right] \tag{7.50}$$

and a massless mode ω_3 with speed given by

$$v_3^2 = \frac{I_{\hat\sigma s}^2 - 4M_\sigma^2 M_S^2}{I_{\hat\sigma s}^2 - 4M_S^2\left(M_\sigma^2 + f^2N_f\mu^2\right)}\ . \tag{7.51}$$

In parallel with the previous section, one can determine the dispersion relations considering corrections in both m_σ^2 and m_π^2. According to this expansion, the obtained result is

$$\begin{aligned}\omega_i^2 = \omega_i^{2*} &+ \left(\frac{N_f\mu^2\nu^2}{2\Lambda^4}\right)^{\frac{\Delta-2}{2}} m_\sigma^2 D_1(\omega_i^{2*},\Delta) + \left(\frac{N_f\mu^2\nu^2}{2\Lambda^4}\right)^{-\gamma-3} m_\pi^4\cos^2(\alpha(\theta))D_2(\omega_i^{2*},\gamma)\\ &+\mathcal{O}\left(m_\sigma^4, m_\pi^8, m_\sigma^2 m_\pi^4\right)\ , \qquad \text{for } i = 1,2,3\,. \end{aligned}\tag{7.52}$$

The coefficients D_1 and D_2 read

$$\begin{aligned} D_1(\omega_i^{2*},\Delta) = {}& \frac{1}{12(\Delta-4)f^2\left(\mu^2\nu^2N_f\left(aN_f\left(6f^2\mu^2\nu^2N_f + k^2 - \omega_i^{2*}\right) + 8f^2\Lambda^4\left(2k^2 - 3\omega_i^{2*}\right)\right) + 3\Lambda^4\left(k^2-\omega_i^{2*}\right)^2\right)}\\ &\times\left[aN_f\left(2f^2\mu^2\nu^2N_f\left((3\Delta-10)k^2 - 3(\Delta-2)\omega_i^{2*}\right) - \left(k^2-\omega_i^{2*}\right)^2\right)\right.\\ &\left.+4f^2\Lambda^4\left(k^2-\omega_i^{2*}\right)\left((3\Delta-8)k^2 - 3\Delta\omega_i^{2*}\right)\right]\ , \end{aligned}\tag{7.53}$$

$$\begin{aligned} D_2(\omega_i^{2*},\gamma) = {}& \frac{\mu^4\nu^8\Lambda^{-4(\gamma+4)}(\mu\nu)^{2\gamma}N_f^{\gamma+4}}{96\left(\mu^2\nu^2N_f\left(aN_f\left(k^2-\omega_i^{2*}\right) + 8f^2\Lambda^4\left(2k^2-3\omega_i^{2*}\right)\right) + 6af^2\mu^4\nu^4N_f^3 + 3\Lambda^4\left(k^2-\omega_i^{2*}\right)^2\right)}\\ &\times\left[-2(\gamma(3\gamma-10)-5)f^2\Lambda^{4\gamma}\mu^{2-2\gamma}\left(k^2-\omega_i^{2*}\right)\left(\nu^2N_f\right)^{1-\gamma}\left(a\mu^2\nu^2N_f^2 + 2\Lambda^4\left(k^2-\omega_i^{2*}\right)\right)\right.\\ &+3\left(k^2-\omega_i^{2*}\right)^2\left(\frac{\mu^2\nu^2N_f}{\Lambda^4}\right)^{-\gamma}\left(a\mu^2\nu^2N_f^2 + 2\Lambda^4\left(k^2-\omega_i^{2*}\right)\right) - 16(\gamma-1)f^2\omega_i^{2*}\Lambda^{4\gamma}\mu^{2-2\gamma}\left(\nu^2N_f\right)^{1-\gamma}\\ &\times\left(a\mu^2\nu^2N_f^2 + 2\Lambda^4\left(k^2-\omega_i^{2*}\right)\right) + \Lambda^{4\gamma}(\mu\nu)^{-2\gamma}N_f^{-\gamma}\left(4f^2\mu^2\nu^2N_f\left(k^2-3\omega_i^{2*}\right) + \left(k^2-\omega_i^{2*}\right)^2\right)\\ &\left.\times\left(6\Lambda^4\left(k^2+\mu^2-\omega_i^{2*}\right) - a(\gamma-7)\mu^2\nu^2N_f^2\right)\right] \end{aligned}\tag{7.54}$$

while the dispersion relations in the conformal limit $m_\pi = m_\sigma = 0$ have the simple form

$$\omega_1^{2*} = k^2 + 6f^2\mu^2\nu^2N_f + 2f\mu\nu\sqrt{N_f\left(9f^2\mu^2\nu^2N_f + 2k^2\right)}\,, \tag{7.55}$$

$$\omega_2^{2*} = k^2 + \frac{a\mu^2 v^2 N_f^2}{2\Lambda^4}, \tag{7.56}$$

$$\omega_3^{2*} = k^2 + 6f^2\mu^2 v^2 N_f - 2f\mu v\sqrt{N_f\left(9f^2\mu^2 v^2 N_f + 2k^2\right)}, \tag{7.57}$$

where one can recognize the expected mode with a square mass of order a stemming from the axial anomaly as well as a gapped mode with mass $12N_f f^2\mu^2 v^2$ and a Goldstone boson with speed $v_3^2 = \frac{1}{3}$, as dictated by scale invariance. The explicit expression for $M_{1,2}^2$ and v_3^2 are

$$\begin{aligned} v_3^2 =& \frac{1}{3} + m_\sigma^2 \left(\frac{N_f\mu^2 v^2}{2\Lambda^4}\right)^{\Delta/2} \frac{\Lambda^4}{9f^2 N_f^2 \mu^4 v^4} \\ &- m_\pi^4 \cos^2(\alpha(\theta)) \left(\frac{N_f\mu^2 v^2}{2\Lambda^4}\right)^{-\gamma-3} \frac{\mu^4 v^8 N_f^2}{144\Lambda^{16}}(\gamma-3)(\gamma+1) + O\left(m_\sigma^4, m_\pi^8, m_\sigma^2 m_\pi^4\right), \end{aligned} \tag{7.58}$$

$$\begin{aligned} M_1^2 =& 12N_f f^2\mu^2 v^2 + m_\sigma^2 \left(\frac{N_f\mu^2 v^2}{2\Lambda^4}\right)^{\Delta/2} \frac{\Delta}{\Delta-4}\left(\frac{2\Lambda^4}{N_f\mu^2 v^2}\right) \\ &- m_\pi^4 \cos^2(\alpha(\theta)) \left(\frac{N_f\mu^2 v^2}{2\Lambda^4}\right)^{-\gamma-3} \frac{f^2\mu^6 v^{10} N_f^3}{8\Lambda^{16}}(\gamma^2 - 6\gamma + 7) + O\left(m_\sigma^4, m_\pi^8, m_\sigma^2 m_\pi^4\right), \end{aligned} \tag{7.59}$$

$$\begin{aligned} M_2^2 =& \frac{a\mu^2 v^2 N_f^2}{2\Lambda^4} - m_\sigma^2 \left(\frac{N_f\mu^2 v^2}{2\Lambda^4}\right)^{\Delta/2} \frac{a}{6(\Delta-4)f^2\mu^2 v^2} \\ &- m_\pi^4 \cos^2(\alpha(\theta)) \left(\frac{N_f\mu^2 v^2}{2\Lambda^4}\right)^{-\gamma-3} \frac{\mu^6 v^8 N_f^2}{96\Lambda^{20}}\left(a(\gamma-4)v^2 N_f^2 - 6\Lambda^4\right) + O\left(m_\sigma^4, m_\pi^8, m_\sigma^2 m_\pi^4\right). \end{aligned} \tag{7.60}$$

§ 7.6 Casimir energy contribution to Δ_Q in the conformal limit

This chapter comes to an end by presenting the next-to-leading order contributions to the energy. The discussion is analogous to the one carried out in chapter 6, but is here repeated for completeness. Of course, here the theory studied is different and consequently characterised by a different symmetry breaking pattern. Therefore, as discussed in section 7.3, in the conformal limit $m_\pi = m_\sigma = 0$ the results (7.33) correspond to the leading contribution to the conformal dimension of the lowest-lying charge Q operator in the double scaling limit (7.23). However [82], Δ_Q can also be computed in the strongly coupled regime by constructing an EFT for the relativistic Goldstone modes stemming from the spontaneous symmetry breaking induced by fixing the charge. In $d = 4$ dimensions, the large charge EFT predicts [82, 247]

$$k_{4/3}Q^{4/3} + k_{2/3}Q^{2/3} + k_0 \log Q + O\left(Q^0\right), \tag{7.61}$$

where the coefficients $k_{4/3}$ and $k_{2/3}$ are related to the Wilson coefficients of the EFT and cannot, therefore, be computed within the EFT approach. The calculated coefficients $c_{4/3}$ and $c_{2/3}$ given in eq.(7.37) can be seen as the leading contribution to $k_{4/3}$ and $k_{2/3}$

in a perturbative expansion of the latter around $(\Lambda_0 f)^4 = 0$ [75].

On the other hand, the coefficient k_0 is a purely quantum contribution related to the Casimir energy of the relativistic Goldstone bosons [1]. Importantly, its value is universal being entirely determined by symmetry and the number of spacetime dimensions.

In particular, it can be computed exactly from the knowledge of the low-energy spectrum. In fact, consider the low-energy action for a Goldstone mode χ

$$S_G = \int_{\mathcal{M}} \mathrm{d}t\, \mathrm{d}\mathbf{x} \left(\frac{1}{2}(\partial_t \chi)^2 + \frac{v_G^2}{2}(\boldsymbol{\nabla}\chi)^2 \right) . \tag{7.62}$$

The corresponding Casimir energy is given by

$$E_{\text{Casimir}} = \frac{1}{2} Tr\{\log\left(-\partial_t^2 - v_G^2 \nabla^2 \right)\} = \frac{1}{4\pi}\int_{-\infty}^{\infty} \mathrm{d}\omega \sum_{\mathbf{p}} \log\left(\omega^2 + v_G^2 E^2(\mathbf{p})\right) = \frac{v_G}{2}\sum_{\mathbf{p}} E(\mathbf{p}) . \tag{7.63}$$

Here, $E^2(\mathbf{p})$ denotes the eigenvalues of the Laplacian operator on S^3 (see chapter 2). The above contribution scales as Q^0 and exhibits a pole for $d \to 4$ in dimensional regularization. The latter is related to a $\log Q$ term with a universal coefficient $-\frac{v_G}{48}$ stemming from the renormalization of the vacuum energy [247]. Hence, we simply need to sum the contributions of the various Goldstone bosons to calculate k_0. The symmetry breaking pattern in the chiral limit reads

$$\begin{aligned} & SU(N_f)_L \times SU(N_f)_R \times U(1)_V \times U(1)_A \\ & \to SU\left(\frac{N_f}{2}\right)_{uL} \times SU\left(\frac{N_f}{2}\right)_{dL} \times SU\left(\frac{N_f}{2}\right)_{uR} \times SU\left(\frac{N_f}{2}\right)_{dR} \times U(1)_I \times U(1)_V \\ & \overset{\frac{3}{4}N_f^2-2}{\rightsquigarrow} SU\left(\frac{N_f}{2}\right)_{ud} \times U(1)_V . \end{aligned} \tag{7.64}$$

The resulting $\frac{3}{4}N_f^2 - 2$ Goldstone bosons have speed $v_G = 1$ except the π^3 mode which has $v_G = \frac{1}{\sqrt{3}}$. Hence

$$k_0 = -\frac{1}{48}\left(\frac{1}{\sqrt{3}} + \frac{3}{4}N_f^2 - 3\right) . \tag{7.65}$$

This chapter brings part IV to a close, during which intriguing results regarding the study of phase diagrams of topological QCD and QCD-like theories in zero-temperature sectors and with fixed charge near their respective conformal windows have been presented.

[1] The value of k_0 can also be obtained by computing the next-to-leading order Δ_0 of the expansion (6.19).

Part V

NEAR CONFORMAL DYNAMICS OF SOLITONS

Introduction to Part IV

It has long been stressed that strong dynamics is notoriously hard to tackle both analytically and numerically. Over several decades, methodologies have been devised to access different dynamical regimes of strongly interacting theories. At sufficiently low energies, chiral Lagrangians have been shown to faithfully describe the dynamics of specific strongly-coupled underlying theories in terms of their Goldstone bosons. This approach has produced precious information on the dynamics and spectrum of various models of which Quantum Chromodynamics is the time-honoured example. The approach is also routinely employed to obtain (and extract information from) first-principles numerical simulations. Another remarkable property of chiral Lagrangians is that their non-perturbative solutions describe extended objects that, depending on the boundary conditions (BCs), can be identified with distinct physical configurations, from crystals to branes and spheres.

A first introduction to the topic is offered in chapter 8. The spherical case (the hedgehog solution) is the oldest example dating back to the pioneering work of Skyrme [185]. Once the topological sector of the theory is taken into account [270, 271] the properly quantized hedgehog solutions describe half-integer states with topological charge identified as the baryon number. These extended states are taken to be the nucleons of the underlying theory.

Astonishingly, the same model can simultaneously describe mesonic degrees of freedom and their scattering properties as well as the spectrum and form factors of extended baryonic states including the Goldstone boson scattering off them. Therefore, the same effective Lagrangian coefficients control both the pion dynamics as well as the baryon spectrum and form factors. The operators of the chiral effective Lagrangian can be organised in the number of derivative and pion masses. The solitonic solutions can be mapped into baryon states of the underlying QCD-like dynamics at large number of colours. The dependence on the number of colours is naturally encoded in the pion decay constant and depends on the underlying fermion representation with respect to the asymptotically free gauge group.

The Skyrme model has also been enriched by adding at the Lagrangian level massive vector mesons that have been shown to play an important role, not only to give a deeper understanding of the origin of the Skyrme term but also for the associated phenomenological consequences [272–275]. Lastly, a less explored avenue that still deserves much attention, especially after the renewed experimental interest in heavy baryon spectroscopy and transitions [276–278], is the study of heavy baryons as bound states of a Skyrme soliton and heavy mesons [279–291]. However, the original idea pioneered by Callan and Klebanov [279] and first tailored for baryons made by one strange quark and two light quarks could account only for half of the physical states possible in QCD. The issue was resolved analytically in [292] by consistently introducing excited heavy mesons. When working with heavy quarks such as the charm and the bottom ones the approach hugely benefits from the marriage between the large number of colours dynamics and the celebrated heavy-quark limit of QCD [293–299].

Beyond the traditional phenomenological nuclear and particle physics applications, in chapter 9 there is a systematical investigation of the solitonic dynamics when the underlying gauge-fermion theory is near conformal. The phase diagram structure for QCD and QCD-like theories appeared in [122, 124] and has been summarised so far in this thesis. Let us again recall that at the lower edge of the conformal window, the theory undergoes a quantum phase transition from an infrared CFT to a phase characterised by both conformal and chiral symmetry breaking [205, 206]. When the transition is sufficiently smooth, close to the lower end of the conformal window, the theory exhibits a near conformal phase characterised by the existence of a region of the renormalization group flow in which the coupling remains nearly constant, signalling the occurrence of *walking dynamics* [210–212].

As stressed many times in this thesis, the infrared dynamics of the near conformal theory can be modelled by augmenting the standard chiral Lagrangian via the introduction of a new light scalar degree of freedom with the same quantum numbers of the vacuum which is commonly referred to as the *dilaton* or *radion*. In this scenario, the dilaton is the Goldstone boson stemming from the spontaneous breaking of scale invariance whereas sources of explicit conformal breaking leading to the near conformal phase can be encoded in the effective dilaton potential. The aforementioned phenomenological applications have motivated several investigations of the resulting dilaton effective field theory [123, 219–228, 239, 300–305].

In chapter 9 several classes of extended objects emerging as solitons of the dilaton augmented EFT are presented. Precisely, this last part will focus on crystal, brane, and sphere phases constituted respectively by ordered arrays of hadronic tubes, layers, and spherical hedgehog solitonic solutions at non-vanishing baryon number.

Until very recently, it was considered hard to construct analytical solutions representing baryonic condensates in the low-energy limit of QCD. However, in references [306–309, 309–313] an exact method has been introduced to build hadronic solitons. These solutions disclose intriguing non-perturbative features of the finite-density phase diagram. For these reasons, it is very interesting to analyse what happens when the dilatonic degree of freedom is taken into account.

Skyrmions under the effects of dilaton dynamics have already been employed to describe dense nuclear matter such as the core of neutron stars [314–322]. In this framework, conformal invariance is seen as an emergent hidden symmetry of real-world QCD at high densities. Starting from the pioneering work of G.E. Brown and M. Rho [323], who introduced the dilaton mode to derive a series of scaling relations among the values of decay constants and masses in vacuum and at finite density, the dilaton EFT is considered to be a key ingredient for studying Skyrmion matter in extreme conditions.

These relations are shown to be modified when considering generalised EFTs [324].

While earlier works considered a simplified version of the effective action, the construction has later been refined in [325] and since then the dilaton EFT has become one of the building blocks of the generalised nuclear effective field theory (GnEFT), which aims at the description of hadronic matter from low to compact star densities (see e.g. [326, 327] for recent reviews). However, no comprehensive analysis of the spherical Skyrmion properties in near conformal theories has been performed.

The overarching goal of chapter 9 is to combine numerical and analytical methods to perform a systematic investigation of Skyrmion solutions in the presence of dilatonic dynamics. Applications range from the dynamics of QCD-like theories close to the lower end of the conformal window to nuclear matter in extreme regimes.

After introducing the dilaton augmented EFT in section 9.1, a systematic numerical analysis is presented in section 9.2. The standard hedgehog ansatz [270] is employed and relevant physical quantities such as the Skyrmion profile, mass, and size are determined as a function of the physical parameters responsible for deviations from conformal dynamics. These are the anomalous dimension of the quark mass operator, the dilaton mass, and the conformal dimension of the relevant operator triggering the RG flow away from the infrared fixed point. An intricate dependence of the solitonic properties on these parameters as a consequence of the competition of dilaton and pion mass terms is unveiled.

In section 9.3, the impact of the dilaton on the Skyrmion crystals investigated in [310–313] is studied. After briefly reviewing the analytical solution in the absence of the dilaton, it is shown that even for the emerging hadronic tubes there exists a special parameter point where the coupled second-order equation of motions reduce to a first-order system (again without a BPS bound on the energy). Additionally, the presence of the dilaton spatially separates the baryon and isospin charge distributions similarly to spin-charge separation discussed in [328, 329].

Finally, it has been proposed that nuclear matter at low temperatures may exist in non-uniform brane-like structures which may be realised in the crusts of neutron stars [330]. In fact, these configurations appear as ground states in numerical simulations where nucleons are treated as classical bodies with pairwise interactions (see e.g. [331] for a recent review). Intriguingly, a class of analytic solutions of the Skyrme model describing solitonic brane configurations has been discovered in [306–309, 313]. Although it is tempting to identify these exact solutions with the results of the numerical studies, establishing a quantitative connection is not straightforward. In particular, a full quantisation of the solitonic solutions appears to be extremely involved [309], and, therefore, their phenomenological relevance remains an interesting open problem that lies beyond the scope of the present work. Instead, inspired by the possible emergent scale symmetry in dense Skyrmion matter, chapter 9 studies the impact of the dilaton on the analytic brane solutions.

The appendix E summarises the numerical results for the spherical Skyrmion solutions.

Preliminaries III: Introduction to topological Solitons and the Skyrme model

8

CHAPTER

§ 8.1 An invitation

With the advent of gravitational wave and multi-messenger astronomy, constraints on the equation of state (EOS) of neutron stars describing strongly interacting matter at finite density have significantly improved over the past decade. Moreover, upcoming gravitational wave measurements from neutron star mergers with enhanced precision from LIGO/Virgo are expected to impose even stricter constraints on the EOS [332].

The non-perturbative nature of QCD at small and intermediate energy or density regimes makes computing the properties of nuclear matter from the first principles extremely challenging. As stressed in chapter 3, while perturbative methods are applicable at asymptotically high densities, lattice QCD, the main non-perturbative computational tool, can be used for arbitrarily low temperatures but is limited to small densities due to the fermion sign problem. Consequently, the QCD phase diagram at sufficiently high (but not asymptotically high) densities remains poorly understood. This leads to significant theoretical uncertainty regarding basic observables, such as the relevant degrees of freedom or the EOS in this regime. This uncertainty is particularly relevant for matter in the interior of neutron stars.

Standard nuclear physics methods, such as relativistic mean field theory [333] and chiral perturbation theory, can be utilised to study the QCD phase diagram in the intermediate density regime. These theories are EFTs that use nucleons and mesons as their fundamental fields, rather than the quarks and gluons of QCD.

In fact, around sixty years ago, a novel approach to quantum field theory emerged and gained popularity. Physicists and mathematicians began to seriously study the classical field equations in their fully non-linear form, interpreting some of the solutions as candidates for particles in the theory [334, 335]. These particles were previously unrecognised and differ from the elementary particles that arise from the quantization of the wave-like excitations of the fields. Their properties are largely determined by the classical equations, although it is possible to systematically treat quantum corrections.

A defining characteristic of these new particle-like solutions is their topological structure, which differentiates them from the vacuum. When one considers quantum excitations around the vacuum, these are associated with smooth deformations of the field that do not alter its topology. Consequently, conventional elementary particles of quantum field theory, such as photons, lack topological structure. In contrast, the stability of these new particles arises from their topological properties. Although they may possess significant energy, they cannot simply decay into multiple elementary particles [334].

In many instances, the topological nature of a field can be described by a single integer, denoted henceforth as B, known as the topological charge. This charge typically represents a topological degree or a generalised winding number of the field. The topological charge B corresponds to the net number of this new type of particle, with energy increasing as $|B|$ grows. The fundamental particle is characterised by $B = 1$; the minimal energy field configuration with $B = 1$ is classically stable, as it cannot decay into a topologically trivial field. Its energy density is smooth and concentrated within a finite region of space. This type of field configuration is known as a topological soliton or simply a soliton [334].

Typically, there exists a reflection symmetry that reverses the sign of B, resulting in the existence of an anti-soliton with $B = -1$. Soliton–anti-soliton pairs can either annihilate or be produced in pairs. Field configurations with $B > 1$ are understood as multi-soliton states [335].

The length scale and energy of a soliton depend on the coupling constants in the Lagrangian and field equations. In a Lorentz-invariant theory, and using units where the speed of light is unity, the energy of a soliton is identified with its rest mass. In contrast, the mass of elementary particles is proportional to the Planck constant $\hbar$ (which is sometimes not recognised due to the choice of units). Quantum effects become negligible as $\hbar \to 0$. In this limit, the topological soliton has a finite mass, while the mass of elementary particles goes to zero. Moreover, the quantum corrections to the soliton mass also approach zero.

Historically, the first example of a topological soliton model of a particle was the Skyrmion [185]. The Skyrmion originated from the Yukawa model, a field theory for spin-$\frac{1}{2}$ nucleons (protons and neutrons) and the three types of spinless pions $\{\pi^+, \pi^-, \pi^0\}$, where the relatively heavy nucleons interact through pion exchange. Skyrme proposed that nucleons in a nucleus move within a non-linear, classical pion medium, leading him to reconsider the pion interaction terms. Symmetry arguments led him to a specific form of the Lagrangian for the three-component pion field, which had a topological structure allowing a topologically stable soliton solution of the classical field equation, distinct from the vacuum. This Skyrmion possesses rotational degrees of freedom, and Skyrme realised that upon quantization, these degrees of freedom could result in states with spin-$\frac{1}{2}$. Thus, a purely bosonic field theory could produce spin-$\frac{1}{2}$ fermionic states, identifiable as nucleons (the details are beyond the scope of this thesis).

The Skyrme model is potentially a low-energy approximation of QCD. When quarks are ignored, the theory reduces to a pure gauge theory with the gauge group $SU(3)$, whose classical field equation is the Yang-Mills equation. In three spatial dimensions, this equation does not have soliton solutions. However, in four spatial dimensions, the Yang-Mills equation has topological soliton solutions known as instantons.

Specifically, the Skyrme model is a non-linear theory of pions in three spatial dimensions, with the Skyrme field, $U(t, x)$, being an $SU(2)$-valued scalar. Although it does not involve quarks, it can be considered an approximate, low-energy effective theory of QCD, becoming exact as the number of quark colours becomes large. Remarkably, and this was Skyrme's main motivation for developing and studying this model, it has topological soliton solutions that can be interpreted as baryons.

Before presenting the dynamics of Skyrmions, let us take a moment to review the topological features of non-linear field theories and explore how the concept of topological solitons arises from them. The following discussion is mainly based on [334] and [165].

§ 8.2 Warm up: linear scalar field theories

To set the stage, let us start the discussion with the simplest scenario of linear scalar fields [334, 335]. Consider a linear scalar field $\Phi : \mathbb{R}\times\mathbb{R}^d \to \mathbb{R}^n$ taking values in $\mathbb{R}^n$, i.e. the flat space in n dimensions. For this field, one can consider the following Lagrangian

$$L = \int \mathcal{L}\, d^d x = \int \left(\frac{1}{2}(\partial_0\Phi)^2 - \frac{1}{2}\nabla\Phi\nabla\Phi - U(\Phi)\right) d^d x \tag{8.1}$$

with $U(\Phi)$ some regular function of the field Φ. The first term appearing on the right-hand side of (8.1) is the kinetic energy while the remaining two represent $-V$, with V the potential energy. The corresponding field equations are obtained via the action principle. Therefore, one needs to solve $\delta S = 0$ with

$$S = \int_{t_1}^{t_2} L dt \tag{8.2}$$

the action, so that

$$\delta S = \int_{t_1}^{t_2}\left[\int \left(\frac{\partial\mathcal{L}}{\partial\partial_0\Phi}\partial_0\delta\Phi + \frac{\partial\mathcal{L}}{\partial\nabla\Phi}\nabla\delta\Phi + \frac{\partial\mathcal{L}}{\partial\Phi}\delta\Phi\right) d^d x\right] dt = 0\ . \tag{8.3}$$

After partial integration, the above is satisfied for all possible $\delta\Phi$ if

$$-\partial_0\frac{\partial\mathcal{L}}{\partial\partial_0\Phi} - \nabla\frac{\partial\mathcal{L}}{\partial\nabla\Phi} + \frac{\partial\mathcal{L}}{\partial\Phi} = 0\ , \tag{8.4}$$

that results in the following field equation

$$\partial_0\partial_0\Phi - \nabla^2\Phi + \frac{\mathrm{d}U}{\mathrm{d}\Phi} = 0\ . \tag{8.5}$$

One may discuss the energy of this system which means to study the configurations of the field such that the potential energy achieves a minimum. To this aim, let us make a digression on the vacuum manifold of the theory. First of all, let us consider Φ to be a multiplet $\Phi = (\Phi_1, \ldots, \Phi_n)$ of n fields defined on Minkowski spacetime. Hence, the vacuum manifold of the theory is defined as the sub-manifold $\mathcal{V} \subset \mathbb{R}^n$ where the potential $U(\Phi)$ has a minimum. The function $U(\Phi)$ can always be shifted by an overall constant since this does not affect the dynamics, i.e. the field equation. Due to this property, without loss of generality, one can assume that $U_{min} = 0$.

Given this definition of $\mathcal{V}$, a vacuum configuration is a field configuration constant in space and time taking its value in the vacuum manifold. Generally, linear fields can be classified depending on their vacuum configurations.

Since by a linear field, one just means to consider a field taking values on flat spacetime, to simplify the discussion that now will come (the focus will be on static fields) from now on let us consider this field $\Phi : \mathbb{R}^d \to \mathbb{R}^n$.

Since these vacuum configurations should lead to finite energy field configurations that are *physical*, one has to demand that the potential contribution is finite

$$\int U(\Phi)\ d^d x < \infty \tag{8.6}$$

so that the total energy

$$E = \int \left(\frac{1}{2}\,(\nabla\Phi)^2 + U(\Phi)\right)\ d^d x \tag{8.7}$$

is finite too. This request translates into demanding precise constraints for the values of the field configuration at finite points and the boundary condition

$$\Phi(x) \in \mathcal{V} \quad \forall x \in S^d_\infty\ , \tag{8.8}$$

where $S^d_\infty = \mathbb{R}^d \cup \{\infty\}$.

8.2.1 Homotopy

The above conclusion defines a map from the sphere at spatial infinity to the vacuum manifold, $\Phi^\infty : S^d_\infty \to \mathcal{V}$. To be precise, at any given time, a field configuration can be seen as a map from the manifold X on which the field is defined to the target manifold Y on which it is valued [165].

Definition 8.2.1

> *Two maps, Φ_A and Φ_B, that are related by a continuous transformation are called homotopic, and the continuous transformation is called homotopy. Then the two maps are said to define the homotopy class as the class of equivalence defined by all mappings that are homotopic to it.*

In general, Φ_A can be viewed as an element of the space of continuous maps denoted $\mathrm{Maps}(X \to Y)$, which is typically disconnected. Each connected component corresponds to a different homotopy class of maps [165]. In particular, any property that depends only on the homotopy class of the map, rather than on the specific map A itself, will remain conserved over time. Such conserved quantities are referred to as *topological invariants*.

The number of homotopy classes of maps between two manifolds X and Y is determined by the topology of the manifolds. Specifically, when the base manifold is a d-dimensional sphere, the number of homotopy classes of maps from S^d to Y is given by the d-th homotopy group of Y, denoted as $\pi_d(Y)$.

In the case explored in this section, the boundary condition Φ^∞ is a map that can therefore be classified by an element of the homotopy group $\pi_d(\mathcal{V})$. So, since two field configurations Φ and $\tilde{\Phi}$ with different asymptotic data Φ^∞ and $\tilde{\Phi}^\infty$ are homotopic if Φ^∞ is homotopic to $\tilde{\Phi}^\infty$, one can classify the field configurations $\Phi(x)$ based on the same element of the homotopy group $\pi_d(\mathcal{V})$.

If a linear scalar field is the only field in the theory, then the corresponding topological objects in dimensions $1, 2$ and 3 (assuming they exist) are known as kinks, global vortices, and global monopoles.

§ 8.3 Non-linear scalar field theories

Since this warm-up has set the stage, let us now consider the non-linear scalar field theory, which is a slightly more difficult type of field theory. In this scenario, the field Φ takes its values on a target manifold Y that is closed and non-trivial. In non-linear field theory, a minimal energy configuration (classically stable) where the energy density is smooth and localised within a finite region of space is referred to as a *soliton*.

These stable field configurations are known as *topological solitons* when their stability can be explained using topological arguments. They represent field configurations that are homotopically distinct from the vacuum. The stability of topological solitons arises from the existence of different homotopy classes, meaning that the target manifold has a non-trivial homotopy group.

In general, different solitonic configurations corresponding to different topological sectors (i.e. homotopy equivalence classes) are characterised by their associated topological invariants [165]. Before continuing with the discussion, let us pause for a moment to introduce the pivotal notion of the *topological degree*.

8.3.1 Topology: the winding number

Consider any two compact, oriented manifolds X and Y having the same dimension d.

Definition 8.3.1

The topological degree of a differential map $\Psi : X \mapsto Y$ is defined as

$$deg\,\Psi = \frac{1}{Vol(Y)} \int_X \Psi^*(\Omega) \ \in \mathbb{N}\,, \tag{8.9}$$

where Ω is a volume form on the manifold Y and $Vol(Y) = \int_Y \Omega$ and $\Psi^*(\Omega)$ is its pullback to X and defines a volume form on X. The topological degree is independent of the form of Ω and invariant under homotopy transformations.

As a consequence, the topological degree is the same for any other map in the same homotopy class of Ψ. The homotopy-invariant nature of the topological degree arises because the latter is an integer and therefore cannot change under continuous deformations. The topological degree represents the number of times the target manifold wraps around the base manifold under the mapping Ψ. For this reason, it is also referred to as the *winding number* [165].

8.3.2 Topological solitons

First of all, to identify topological soliton solutions in a given field theory, it is essential to examine whether or not the theory possesses the necessary topological structure [335]. Following the discussion in [334, 335], let us consider a scalar field theory defined in a flat space, $X = \mathbb{R}^d$, with no additional boundary conditions. In the case of a linear theory, any field configuration $\Phi(x)$ can be continuously deformed by the homotopy $(1-\lambda)\Phi$, with $\lambda \in [0,1]$, making all configurations homotopic to the trivial one, $\Phi = 0$. Therefore, linear fields without constraints are topologically trivial in flat space.

For non-linear fields, field configurations are mappings from $\mathbb{R}^d$ to a target space Y, and since $\mathbb{R}^d$ is contractible to a point, the only topological invariant is the connected component of Y where the field takes its value. As a result, the field configurations are classified by $\pi_0(Y)$, the set of connected components of Y.

In classical field theories in flat space, both non-linear interactions and non-trivial boundary conditions for the field configurations are necessary for the existence of topological solitons [165]. However, these conditions do not guarantee the presence of stable topological solitons in a given theory.

Therefore, let us now turn our attention to field configurations with localised finite energy density, meaning configurations where the energy density decays rapidly as $|x| \to \infty$. This requirement is equivalent to imposing certain boundary conditions on the field configurations, which in turn influence their topological classification [165].

It is necessary to assume that the field becomes constant at spatial infinity, namely:

$$\Phi(x) = y_0,\ \forall x \in S^d_\infty \tag{8.10}$$

or equivalently,

$$\Phi^\infty \equiv y_0\ , \tag{8.11}$$

where $y_0 \in Y$ is an arbitrary constant value. This boundary condition enables the topological compactification of flat space $\mathbb{R}^d$ to S^d_∞ via stereographic projection, which in turn is homeomorphic to the d-dimensional sphere [165]. The stereographic projection is a smooth and bijective mapping between a plane and a sphere, except at one point, the projection point, which is the north pole of the d-dimensional sphere S^d. By assigning this north pole to a point at spatial infinity in the plane $\mathbb{R}^d$, a method for topological compactification of $\mathbb{R}^d$ to S^d is established.

Thus, a map $\Phi : \mathbb{R}^d \to Y$ with the boundary condition that the point at infinity is mapped to y_0 is homotopically equivalent to a based map $\Phi : S^d \to Y$, where y_0 is the base point of the target space Y and the north pole p is the base point of the domain S^d. In other words, the field $\Phi : \mathbb{R}^d \to Y$ extends to a continuous based map $\Phi : S^d \to Y$, which can be classified by an element of the homotopy group $\pi_d(Y)$.

In a chiral effective theory where mesons are represented as coordinates in the chiral coset space, finite energy solitons in $3+1$ dimensions are possible due to the non-trivial nature of the third homotopy group of this space [336]:

$$\pi_3\left(\frac{SU(N_f)_L \times SU(N_f)_R}{SU(N_f)_V}\right) = \pi_3(SU(2)) = \mathbb{Z} \, . \tag{8.12}$$

Such solitons are typically referred to as *Skyrmions*, named after Tony R. Skyrme, who introduced them as models for baryons before the development of QCD [185]. Consequently, the topological charge associated with a Skyrmion is identified with the baryon number.

Derrick's theorem, introduced in the next section, provides a way to intuit if a field theory admits topological solitons without solving the field equation.

§ 8.4 Derrick's scaling argument

Let us consider a static field Φ and the corresponding total energy (8.7). According to the discussion above, the field configuration Φ cannot be a solution of the corresponding field equation if the energy functional is not stationary against all variations including spatial re-scaling. Therefore, if the latter condition is not met, there can be no solutions of the corresponding field equation and especially no topological solitons. Hence, it suffices to study the possibility that the functional energy is stationary to guarantee the existence of topological solutions. This is indeed the core of Derrick's theorem which is a non-existence theorem since it can rule out the existence of topological solitons in certain field theories but cannot prove their existence.

Derrick's theorem

The presence of topological solitons is ruled out if the stationarity of the functional energy against all variations of the field configuration, including spatial re-scaling, is not met.

To understand this theorem, let us consider the case of linear scalar field theories in several dimensions. Firstly, as already seen in the course of this thesis, spatial re-scaling means

$$\Phi(x) \mapsto \Phi(\mu x) \quad \text{with} \quad \mu \in (0, \infty) \tag{8.13}$$

so that, if the energy functional is of the form

$$E(\Phi(x)) = \int \Big[W(\Phi(x))\nabla\Phi(x)\nabla\Phi(x) + U(\Phi(x))\Big]\, d^d x = E_2 + E_0, \quad W(\Phi) \quad \text{positive function} \tag{8.14}$$

after a spatial re-scaling, it reads

$$e(\mu) = E(\Phi(\mu x)) = \int \Big[W(\Phi(\mu x))\nabla\Phi(\mu x)\nabla\Phi(\mu x) + U(\Phi(\mu x))\Big]\, d^d x = \mu^{2-d} E_2 + \mu^{-d} E_0 \, . \tag{8.15}$$

At this point, consider an arbitrary, finite-energy field configuration $\Phi(x)$ that differs from the vacuum state. For this field configuration, the energy $e(\mu)$ of the rescaled field

$\Phi(\mu x)$ can be computed. According to Derrick's theorem, if this function $e(\mu)$ has no stationary points, then no static, finite-energy solutions of the field equation exist in this theory, except for the vacuum configuration. In such a case, no topological soliton can exist within the framework of this field theory. The vacuum configuration avoids Derrick's theorem in all dimensions because this field is constant in both space and time by definition, resulting in the vanishing of the coefficient E_2, which represents the gradient energy [335]. Additionally, the potential term $U(\phi)$ vanishes for the vacuum configuration, meaning that $E_0 = 0$, i.e., the energy contribution from the potential term also disappears. As a result, the vacuum configuration is a stationary point of the function $e(\mu)$ in all spatial dimensions. To conclude this section, it is worth mentioning that there are ways to avoid Derrick's theorem. For example, one can include in the theory higher order derivatives terms. For instance, one may consider

$$\mathcal{L} = W_1(\Phi)|\nabla\Phi|^2 + W_2(\Phi)|\nabla\Phi|^4 + \cdots \implies E = E_2 + E_4 + \dots \; . \tag{8.16}$$

that leads to

$$e(\mu) = \mu^{2-d}E_2 + \mu^{4-d}E_4 \tag{8.17}$$

which in turn admits a finite value for a finite $\mu \neq 0$.

§ 8.5 The Skyrme Model

The time is ripe to present the Skyrme model. The Skyrme model is a non-linear field theory for a scalar field U taking values in the $SU(N_f)$ Lie group, N_f being the flavour number. Despite the scalar nature of U, the solitons of the theory are interpreted as baryons. Precisely, Skyrme's original motivation was to reproduce baryons as topological soliton solutions from a purely mesonic field theory [336]. In its simplest version, the basic fields of the Skyrme model are just the pion fields combined in an $SU(2)$ valued field U,

$$U = \sigma\mathbb{1} + i\,\pi_a\tau^a \tag{8.18}$$

with τ_a being the Pauli matrices, $a = 1, 2, 3$. The action of the Skyrme model in $(3+1)$ dimensions is

$$I = \int d^4x\sqrt{-g}\left[\frac{K}{4}Tr\left\{R_\mu R^\mu + \frac{\lambda}{8}\,F_{\mu\nu}F^{\mu\nu}\right\}\right] \quad \text{with} \quad R_\mu = U^{-1}\nabla_\mu U \quad \text{and} \quad F_{\mu\nu} = \left[R_\mu, R_\nu\right] \tag{8.19}$$

where ∇_μ is the Levi-Civita covariant derivative while g is the metric determinant. The constants K and λ are positive coupling constants and are fixed by comparison with experimental data [270–272]. The first term of the Skyrme action is mandatory to describe pions, while the second is the only covariant term leading to second-order field equations in time which supports the existence of Skyrmions in four dimensions. The variation of the action with respect to the field U gives the field equations

$$\nabla^\mu\left(R_\mu + \frac{\lambda}{4}\left[R^\nu, F_{\mu\nu}\right]\right) = 0 \tag{8.20}$$

that are 3 non-linear coupled second-order differential equations. Moreover, the topological charge is defined as

$$B = \frac{1}{24\pi^2}\int_\Sigma \rho_B , \qquad \rho_B = \epsilon^{ijk} Tr\left\{\left(U^{-1}\partial_i U\right)\left(U^{-1}\partial_j U\right)\left(U^{-1}\partial_k U\right)\right\} . \tag{8.21}$$

Furthermore, the presence of a topological charge alone is insufficient to guarantee stable topological solitons, as Derrick's theorem must also be circumvented. The static Skyrme energy can be broken down into two components, $E = E_2 + E_4$, corresponding to terms that are quadratic and quartic in the spatial derivatives of the Skyrme field. When the spatial coordinates are rescaled as $x \to \mu x$, the energy transforms into:

$$e(\mu) = \frac{E_2}{\mu} + \mu E_4 . \tag{8.22}$$

These two terms scale oppositely, leading to a minimum energy value for a finite $\mu \neq 0$. This suggests that a soliton will have a well-defined size, preventing it from expanding infinitely or collapsing to a single point. For any static solution, particularly a Skyrmion, which represents the lowest energy state in a given topological sector, $e(\mu)$ reaches its minimum at $\mu = 1$. At this point, the quadratic and quartic energy contributions are exactly balanced.

This clarifies why the model including only the first term in equation (8.19) does not support stable solitons. The stability issue is resolved by including the second term in equation (8.19), known as the Skyrme term. The Skyrme term enables the existence of static solitonic solutions with finite energy and topological charge, representing the Baryonic charge, i.e. Skyrmions (see [335] and references therein)[1]. Furthermore, the Skyrme term is not the only method to circumvent Derrick's argument. Another way to avoid it is by constructing a time-dependent ansatz for the matter fields, ensuring that the corresponding energy density remains stationary.

Let us conclude this section by presenting some applications of the theory. As already said, the model was introduced to describe baryons as topological solitons, the Skyrmions, of the field U. The argument for identifying Skyrmions with baryons and nuclei was further strengthened in the large-N limit of QCD [260, 337, 338], where the theory becomes an effective weakly interacting model of mesons, and baryons exhibit the typical properties of solitons. The Skyrme model naturally incorporates several key aspects of strong interaction physics, such as chiral symmetry and its breaking, the conservation of baryon number, and the extended nature of nucleons. This extended nature helps avoid short-distance singularities in nucleon-nucleon interactions. Additionally, the model naturally incorporates the spin-statistics theorem, where Skyrmions quantized with half-integer spin are fermions, and those with integer spin are bosons[2].

Skyrme's concept of baryons as topological solitons is also shared by other approaches. Holographic models based on the conjectured gauge/gravity duality have proven useful for studying the non-perturbative regimes of QCD-like theories, for instance.

[1] However, the original arguments in [335] that establish the identification of the topological charge (8.21) with the baryonic charge do not explicitly require the Skyrme term.
[2] A recent review can be found in [335] since this topic is not explored in this work.

Another related approach involves the development of generalised nuclear effective theories over the last two decades. These theories preserve the field content and topological structure of the Skyrme model at low energies while evolving toward an effective theory compatible with QCD symmetries at higher energies (for a recent review, see [326]). This transition is achieved by coupling the Skyrme field to the dilaton [339] and an infinite tower of vector mesons via hidden local symmetry [340]. In these theories, the fields flow from a spontaneously broken phase to an unbroken one. As a result, these nuclear effective theories retain some topological structures of the Skyrme model, although their dynamic content is more complex and difficult to calculate. Consequently, instead of performing full numerical simulations, it is sometimes assumed that these theories inherit topological structures from the Skyrme model, and the implications of these assumptions are explored using more conventional nuclear physics methods.

8.5.1 Applications: Nuclear Pasta in Neutron Stars

This chapter is concluded by introducing the *nuclear pasta* [165]. Topological soliton studies apply to astrophysics, particularly in analysing the nuclear matter of neutron stars. Neutron stars represent the final stage in the life cycle of a massive star. Stars reach this stage when internal thermonuclear fusion can no longer counterbalance gravitational forces, resulting in a supernova that ejects most of the star's mass, leaving behind a dense core. If the remnant core exceeds the Chandrasekhar limit, gravity becomes strong enough to overcome the electron degeneracy pressure, compressing the star to nuclear densities. During this collapse, many electrons and protons combine to form neutrons through electron capture, resulting in a neutron-rich core, hence the term “neutron star" [331].

A neutron star is electrically neutral, composed of neutrons, protons, and electrons, with the charges of protons balanced by electrons. The mass of neutron stars ranges between 1 and 3 solar masses, with a radius of approximately 10 km and an average density of around $10^{15} g/cm^3$, which is about 20 times that of normal atomic nuclei [165][3].

At low temperatures and sub-saturation densities, nuclear matter can form non-uniform structures known as “pasta", and it is believed that neutron star crusts may exhibit these configurations. The pasta structures in nuclear systems have been analysed using various models [331]. These structures are thought to arise from the interaction between nuclear and Coulomb forces, which are both attractive and repulsive. Changes in density, temperature, and proton fraction lead to transitions from a uniform phase in the core to configurations with voids filled by small *gnocchi-like* clusters, *lasagna-like* nuclear layers, *spaghetti-like* rods embedded in nuclear gas, and eventually to a gaseous phase with dissolved nuclear matter [331].

Having introduced these concepts and their possible applications, the subsequent

[3] It has been established that the outer layer of neutron stars, a 1-km-thick crust, contains neutron-rich nuclear matter immersed in a sea of electrons. The density within the crust varies, starting from normal nuclear density ($\sim 3{\times}10^{14} g/cm^3$) at a depth of about 1 km, down to neutron drip density ($\sim 4{\times}10^{11} g/cm^3$) at approximately half a kilometre, and finally to very low densities in the outer envelope [165].

chapter will take care of an in-depth analysis of the impact of dilaton dynamics on topological soliton configurations of nuclear pasta: the spaghetti and lasagna configurations.

The Dilatonic Dynamics of Baryonic Crystals, Branes and Spheres

Chapter 9

In this chapter, the impact of dilatonic dynamics on Skyrme spheres, crystals, and branes is systematically analysed. Precisely, the effects of the dilatonic model parameters, which encompass different underlying near conformal dynamics, on the macroscopic properties of Skyrmions, such as their mass and radius, are discussed. The results that will be here shown, based on [4], are expected to have wide implications, ranging from the study of near conformal dynamics stemming from QCD-like theories to phenomenological investigations of nuclear matter in extreme regimes.

§ 9.1 Dilaton dressing of the chiral Lagrangian

This chapter opens with a brief recap of the Skyrme model introduced in chapter 8. The Skyrme Lagrangian for $N_f = 2$ massive flavours in four dimensions reads

$$I[U] = \int d^4x\sqrt{-g}\,\frac{K}{2}\,\mathrm{Tr}\left\{\frac{1}{2}R_\mu R^\mu + \frac{\lambda}{16}F_{\mu\nu}F^{\mu\nu} + \frac{m_\pi^2}{2}\left(U + U^\dagger\right)\right\}\ , \tag{9.1}$$

$$R_\mu = U^{-1}\nabla_\mu U = R^j_\mu t_j\ , \quad F_{\mu\nu} = \left[R_\mu, R_\nu\right]\ . \tag{9.2}$$

Here $U \in SU(2)$, ∇_μ is the covariant derivative, and $t_a = i\sigma_a$ are the generators of the $SU(2)$ algebra, σ_a being the Pauli matrices. Here, the model presented in chapter 8 is now enriched with the mass term, precisely m_π is the pion mass while K is related to the meson decay constant via $F_\pi = \sqrt{K}$. The above theory can describe low-energy QCD or any other underlying quantum field theory featuring the same pattern of chiral symmetry breaking.

The theory admits a conserved topological current J_μ given by

$$J^\mu = \epsilon^{\mu\nu\lambda\rho}\,\mathrm{Tr}(R_\nu R_\lambda R_\rho)\ . \tag{9.3}$$

Integrating the zero-component of J^μ on a time-slice surface Σ the topological charge reads

$$B = \frac{1}{24\pi^2}\int_\Sigma \epsilon^{ijk}\,\mathrm{Tr}(R_i R_j R_k)\ . \tag{9.4}$$

This quantity corresponds to the winding number associated with U and is interpreted as the baryon number. The classical equations of motion are obtained by performing the functional variation with respect to U, yielding

$$\nabla_\mu \left(R^\mu + \frac{\lambda}{4}[R_\nu, F^{\mu\nu}] \right) - \frac{m_\pi^2}{2}\left(U - U^\dagger \right) = 0 \,. \tag{9.5}$$

These correspond to a set of three non-linear coupled partial differential equations.

Furthermore, following the discussion in chapter 6 and chapter 7, the explicit breaking of conformal symmetry stemming from the presence of quark masses is also taken into account. This is achieved by assuming that the mass term has dimension $y = 3 - \gamma$ where $0 < \gamma < 2$ is the anomalous dimension of the chiral condensate and its range is limited by the unitarity bound. Moreover, since for $\gamma \simeq 1$ the underlying four fermion operator becomes nearly marginal so that only the interval $0 < \gamma < 1$ will be considered.

Therefore, the starting point of this chapter is the following dilaton augmented chiral Lagrangian

$$\begin{aligned} I[U,\sigma] = \int d^4x\sqrt{-g}\Bigg[& \frac{K}{2}\,\mathrm{Tr}\left(\frac{1}{2}R^\mu R_\mu e^{-2\sigma f} + \frac{\lambda}{16}F_{\mu\nu}F^{\mu\nu} + \frac{m_\pi^2}{2}\left(U + U^\dagger \right) e^{-y\sigma f} \right) \\ & - \frac{1}{2}e^{-2\sigma f}\nabla_\mu\sigma\nabla^\mu\sigma - V(\sigma) \Bigg] \,, \end{aligned} \tag{9.6}$$

with $V(\sigma)$ being the one in (5.89). Although the number of flavours is two, let us recall from the discussion in chapter 5 that conformality can be realised with such a small number of flavours in a number of theories, such as those with fermions in the two-index symmetric or antisymmetric representation of the gauge group, as first shown in [122] and generalised in [124]. In any case, here the focus is on the impact of the novel dilatonic dynamics on time-honoured solitons first discussed for the two and three flavour cases.

In order to investigate these extended objects one starts with the equations of motion that read

$$\nabla_\mu \left(R^\mu e^{-2\sigma f} + \frac{\lambda}{4}[R_\nu, F^{\mu\nu}] \right) - \frac{m_\pi^2}{2}\left(U - U^\dagger \right) e^{-y\sigma f} = 0 \,, \tag{9.7}$$

$$\begin{aligned} & \nabla_\mu \left(e^{-2\sigma f}\nabla^\mu\sigma \right) + f\nabla^\mu\sigma\nabla_\mu\sigma e^{-2\sigma f} - \partial_\sigma V(\sigma) - \frac{K}{2} f\,\mathrm{Tr}\, R_\mu R^\mu e^{-2\sigma f} \\ & - \frac{K}{4} y f m_\pi^2\,\mathrm{Tr}\left(U + U^\dagger \right) e^{-y\sigma f} = 0 \,, \end{aligned} \tag{9.8}$$

while the stress-energy tensor $T_{\mu\nu} = -\frac{2}{\sqrt{-g}}\frac{\partial\sqrt{-g}\mathcal{L}}{\partial g^{\mu\nu}}$ is given by

$$\begin{aligned} T_{\mu\nu} = -\frac{K}{2}\,\mathrm{Tr}\Bigg[& \left(R_\mu R_\nu - \frac{1}{2}g_{\mu\nu}R_\alpha R^\alpha \right) e^{-2\sigma f} + \frac{\lambda}{4}\left(g^{\alpha\beta}F_{\mu\alpha}F_{\nu\beta} - \frac{1}{4}g_{\mu\nu}F_{\alpha\beta}F^{\alpha\beta} \right) \\ & - \frac{m_\pi^2}{2}g_{\mu\nu}\left(U + U^\dagger \right) e^{-y\sigma f} \Bigg] - \left(-\nabla_\mu\sigma\nabla_\nu\sigma + \frac{1}{2}g_{\mu\nu}(\nabla\sigma)^2 \right) e^{-2\sigma f} - g_{\mu\nu}V(\sigma) \,. \end{aligned} \tag{9.9}$$

The presence of the mass term shifts the value of the minimum of the dilaton potential from $\sigma = 0$ to a finite value $\langle\sigma\rangle = \sigma_f$. The latter is determined by the equation

$$\partial_\sigma V(\sigma)|_{\sigma=\sigma_f} + Kyfm_\pi^2 e^{-yf\sigma_f} = 0 \,. \tag{9.10}$$

This leads to new values for the decay constants and the masses of all the states appearing in the Lagrangian satisfying certain scaling relations [224,226,232,303]. Equipped with the above, let us now investigate several classes of solitonic configurations starting with the celebrated hedgehog solution.

§ 9.2 Dilaton augmented hedgehog Skyrmions

9.2.1 Setup

In this section, the modification to the time-honoured hedgehog solution in the presence of dilatonic dynamics is investigated. Let us start with a general parameterisation for $U(x)$

$$\begin{gathered} U^{\pm 1}\left(x^\mu\right) = \cos(\alpha)\mathbb{1}_{2\times 2} \pm \sin(\alpha) n^a t_a \,, \\ n^1 = \sin(\Theta)\cos(\Phi), \quad n^2 = \sin(\Theta)\sin(\Phi), \quad n^3 = \cos(\Theta) \,, \end{gathered} \tag{9.11}$$

where $\mathbb{1}_{2\times 2}$ is the 2×2 identity matrix and $\alpha(x)$, $\Theta(x)$ and $\Phi(x)$ are the three scalar degrees of freedom of $SU(2)$. The hedgehog ansatz for $SU(2)$ in spherical coordinates $\{r, \theta, \phi\}$ reads

$$\alpha = \alpha(r), \quad \Theta = \theta, \quad \Phi = \phi \,. \tag{9.12}$$

The energy and topological charge densities are respectively given by

$$\begin{aligned} \epsilon = T_{00} = {} & \frac{1}{2} e^{-2f\sigma} \left(\frac{2K \sin^2(\alpha)}{r^2} + K\alpha'^2 + \sigma'^{\,2} \right) + \frac{\lambda K \alpha'^2 \sin^2(\alpha)}{r^2} \\ & + \frac{\lambda K \sin^4(\alpha)}{2r^4} - K m_\pi^2 \cos(\alpha) e^{-fy\sigma} + V(\sigma) \,, \end{aligned} \tag{9.13}$$

$$\rho_B = J^0 = -\frac{12\alpha' \sin^2(\alpha)}{r^2} \,, \tag{9.14}$$

where the prime denotes the derivative with respect to the radial coordinate. The baryon mass M_S and charge B are respectively obtained by integrating the energy and charge densities of the solution over the whole spacetime, that is

$$M_s = 4\pi \int_0^\infty r^2 \epsilon \, dr \,, \qquad B = \frac{1}{6\pi} \int_0^\infty r^2 \rho_B \, dr \,. \tag{9.15}$$

A measure of the size of the solitonic object is given by the root mean square radius of the baryon charge $\langle r^2\rangle^{1/2}$ defined as

$$\langle r^2\rangle^{1/2} \equiv \left(\frac{1}{6\pi}\int_0^\infty \rho_B\, r^4\, \mathrm{d}r\right)^{1/2} = \sqrt{-\frac{2}{\pi}\int_0^\infty r^2 \sin^2(\alpha)\alpha' dr}\ . \tag{9.16}$$

Inserting the hedgehog ansatz in (9.5) and (9.8) the following set of coupled second order differential equations is obtained

$$\begin{aligned}&\left(2\lambda e^{2f\sigma}\sin^2(\alpha)+r^2\right)\alpha'' - 2r\alpha'\left(fr\sigma'-1\right) + \frac{\lambda e^{2f\sigma}\sin(2\alpha)\left(r^2\alpha'^2-\sin^2(\alpha)\right)}{r^2} - \sin(2\alpha)\\ &- m_\pi^2 r^2\sin(\alpha)e^{-f(y-2)\sigma} = 0\ ,\end{aligned} \tag{9.17}$$

$$\sigma'' - f\sigma'^2 + \frac{2}{r}\sigma' - e^{2f\sigma}\partial_\sigma V(\sigma) + fK\alpha'^2 + \frac{2}{r^2}fK\sin^2(\alpha) - Kfm_\pi^2 y\cos(\alpha)e^{f(2-y)\sigma} = 0\ . \tag{9.18}$$

In the next section, the above equations are numerically solved to investigate the dependence of the Skyrmion properties on the parameters Δ, m_σ, y encoding the explicit breaking of conformal invariance.

9.2.2 Numerical solutions

To study the impact of dilatonic dynamics, the EOMs (9.17) and (9.18) are numerically solved in the sector of topological charge $B = 1$. All the dimensionful quantities are measured in units of $\sqrt{K}$ (in QCD $\sqrt{K} = 93$MeV) and as a starting point the following QCD-inspired values [232, 270, 314] are considered:

$$f = 0.29\,, \qquad \lambda = \frac{1}{4.75^2}\,, \qquad m_\pi = \frac{140}{93}\ . \tag{9.19}$$

Then, the EOMs are solved for different values of the parameters Δ, m_σ, y. In particular, $m_\sigma = 1, 2, \ldots, 10$ and $\Delta = 1, 1.2, 1.4, \ldots, 3.8$. In addition, the limiting cases $\Delta \to 4$ and $\Delta \to 0$ corresponding to the dilaton potentials (5.95) and (5.94), respectively, are encompassed. For every value of Δ and m_σ, the profile functions $\alpha(r)$ and $\sigma(r)$, the baryon mass M_S, and the root mean square radius of the baryon charge $\langle r^2\rangle^{1/2}$ are determined. Since the topologically trivial vacuum exhibits a divergent zero-point energy, in the following M_S will denote the energy difference between the solutions with $B = 1$ and $B = 0$. To simplify the presentation, at the moment let us set $y = 5/2$ while later analysis provides the discussion of the dependence on the anomalous dimension of the chiral condensate. However, it will be shown that all the conclusions below apply to any value of y in the range $2 < y < 3$.

To set the boundary conditions one imposes that for $r \to \infty$ the fields approach the topologically trivial vacuum. Let us recall that at fixed values of time, the field $U(r)$ defines a map from the spatial manifold $\mathbb{R}^3$ to the isospin manifold S^3 with the boundary condition that $U(r)$ goes to its trivial vacuum for asymptotically large distances. In other words

$$U(r\to\infty) = \mathbb{1} \implies \alpha(r\to\infty) = 0\,, \qquad U(0) = -\mathbb{1} \implies \alpha(0) = \pi\ , \tag{9.20}$$

where the latter condition fixes the baryon charge to unity [270]. Analogously, one imposes $\sigma(r \to \infty) \to \sigma_f$ with σ_f given in eq.(9.10). Since σ_f depends on the values of the parameters that are varied, this can be seen as a fixed BC for the normalized variable

$$\chi(r) \equiv e^{-f(\sigma(r)-\sigma_f)}, \tag{9.21}$$

namely $\chi(r \to \infty) \to 1$. Note that one of the main differences with respect to earlier numerical studies [314,315] is that here there is the dependence of σ_f on the pion mass. Finally, $\chi'(0) = 0$ is imposed in line with previous investigations [314,315].

The following discussion refers to the study the dilaton potential (5.89) for $1 \leq \Delta < 4$ and its $\Delta \to 4$ limit (5.95) for $\Delta = 4$. Additionally, values of Δ smaller than 1 will not be considered since the potential (5.89) is ill-defined in the $\Delta \to 0$ limit.

Figure 9.1 shows the dilaton profile $\chi(r)$ for $\Delta = 1,\ 2,\ 3$ and $m_\sigma = 1, \ldots, 10$. The general trend displayed in the figures can be summarized as follows.

1. At fixed Δ the dilaton profile flattens towards its asymptotic value $\chi = 1$ as m_σ increases [1].

2. At fixed m_σ the dilaton profile flattens towards its asymptotic value $\chi = 1$ as Δ decreases.

The profile $\alpha(r)/\pi$ is depicted in Figure 9.2 for the same choice of the parameters. As m_σ increases the dilaton decouples from the dynamics and $\alpha(r)$ converges rapidly to the solution obtained in the absence of the dilaton. In general, the solutions exhibit little dependence on Δ.

The results for M_S are collected in appendix E and illustrated in Figure 9.3 for $m_\sigma = 3, 5, 7, 10$. For all the values of the parameters, the relative numerical error is less than 0.5% where such a value should be seen as a conservative upper limit. One can see that at fixed values of m_σ the baryon mass gets smaller as Δ increases. On the other hand, the dependence of M_S on m_σ at fixed Δ is not monotonic. In fact, M_S first decreases with increasing m_σ till it reaches its minimum for $m_\sigma \sim 5$ after which it climbs towards its Skyrme model value $M_{\text{Skyrme}} = 15.67$. This behaviour is illustrated in Figure 9.4. A change in the behaviour of the solutions around $m_\sigma = 5$ can be also seen by analyzing the values of $\langle r^2 \rangle^{1/2}$ which are given in Table E.2 and Table E.4 in appendix E. In fact, $\langle r^2 \rangle^{1/2}$ increases with increasing m_σ till $m_\sigma \sim 5$ and then starts getting smaller for higher values of the dilaton mass. Moreover, while $\langle r^2 \rangle^{1/2}$ grows monotonically with Δ for $m_\sigma = 1, 2, \ldots, 5, 6$, the opposite holds for $m_\sigma = 7, 8, 9, 10$ as can be seen from Figure 9.3 [2].

Finally, it is important to stress that the dependence of the Skyrmion properties on both Δ and m_σ becomes quickly milder as one increases m_σ implying that *the dilaton decouples rapidly from the dynamics once its mass exceeds m_π*. For instance, while for $m_\sigma = 1$ both M_S and $\langle r^2 \rangle^{1/2}$ differ more than 20% from their values in the absence of the dilaton, such a difference reduces to less than 3% for $m_\sigma \geq 3$.

[1] The case $m_\sigma = 1$ constitutes an exception since in this case the dilaton profile stays below the one obtained for $m_\sigma = 2$ only for small values of the radius.

[2] However, for $m_\sigma = 6$, the root mean square radius shows almost no dependence on Δ.

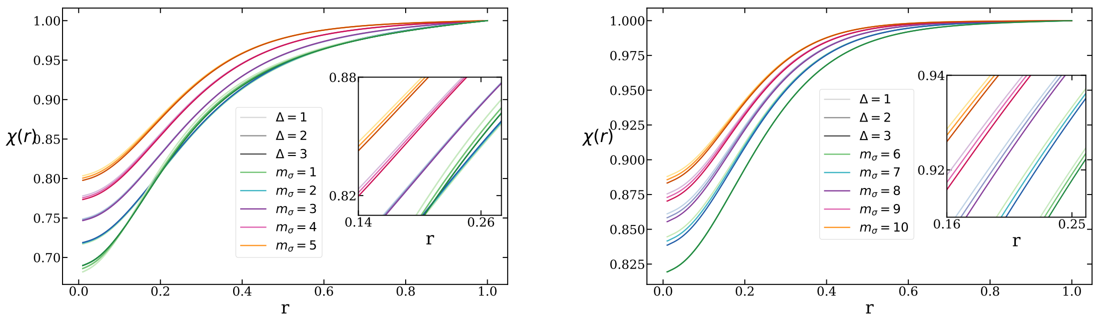

Figure 9.1.: Dilaton profile $\chi(r)$ for $\Delta = 1, 2, 3$ and $m_\sigma = 1, 2, 3, 4, 5$ (*left panel*) and $m_\sigma = 6, 7, 8, 9, 10$ (*right panel*).

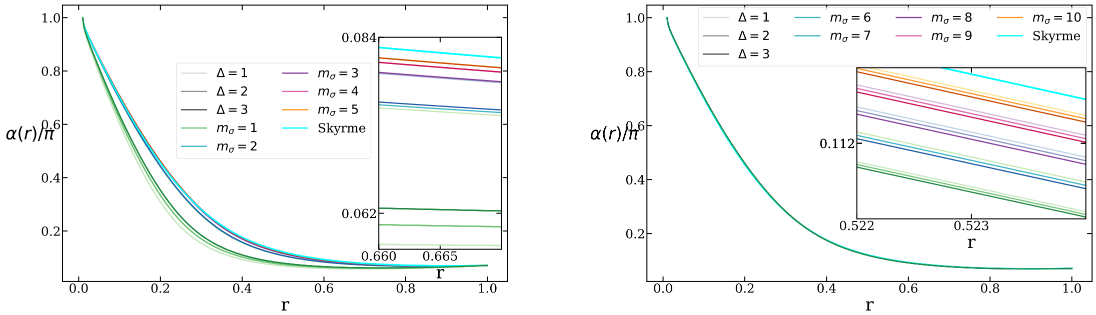

Figure 9.2.: Skyrmion profile $\alpha(r)$ for $\Delta = 1, 2, 3$ and $m_\sigma = 1, 2, 3, 4, 5$ (*left panel*) and $m_\sigma = 6, 7, 8, 9, 10$ (*right panel*).

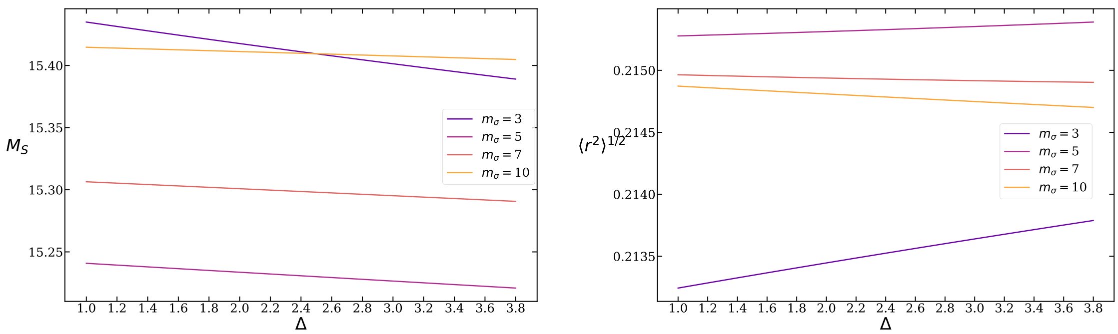

Figure 9.3.: M_S (*left*) and $\langle r^2 \rangle^{1/2}$ (*right*) as a function of Δ for $m_\sigma = 3, 5, 7, 10$.

Skyrmions in the $\Delta \to 0$ limit

As previously discussed, the potential (5.89) diverges in the $\Delta \to 0$ limit. For completeness, here also the solitonic solution in the presence of the potential (5.94) is discussed, which can be seen as a regularized version of the $\Delta = 0$ case. To this end, the values of the parameters considered in the previous section are still adopted.

The profiles of the fields are displayed in Figure 9.5. Their behaviour as m_σ varies is similar to the one discussed in the $1 \leq \Delta \leq 4$ case with the dilaton profile becoming more flat and converging faster to $\chi = 1$ as m_σ increases while $\alpha(r)$ converges quickly to the Skyrme model profile. However, note the exception in the dilaton profile for small values

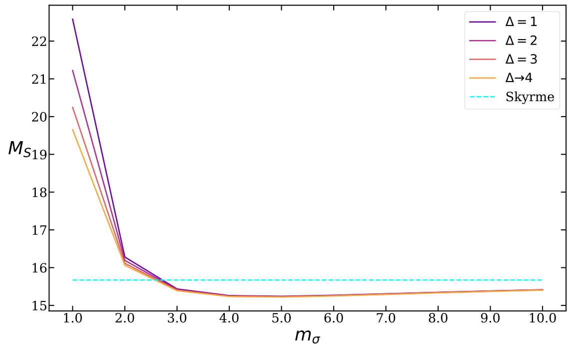

Figure 9.4.: The Skyrmion mass M_S as a function of the dilaton mass m_σ for $\Delta = 1$ (*purple*), $\Delta = 2$ (*red*), $\Delta = 3$ (*orange*), and $\Delta = 4$ (*yellow*). The dashed line marks the value of the Skyrmion mass in the absence of the dilaton ($M_{\text{Skyrme}} = 15.67$ in units of $\sqrt{K}$).

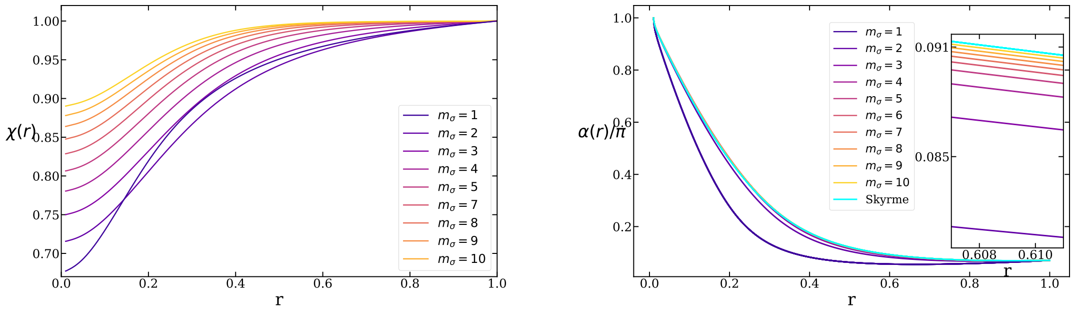

Figure 9.5.: Dilaton profile $\chi(r)$ (*left*) and $\alpha(r)/\pi$ (*right*) for $m_\sigma = 1, 2, 3, 4, 5, 6, 7, 8, 9, 10$.

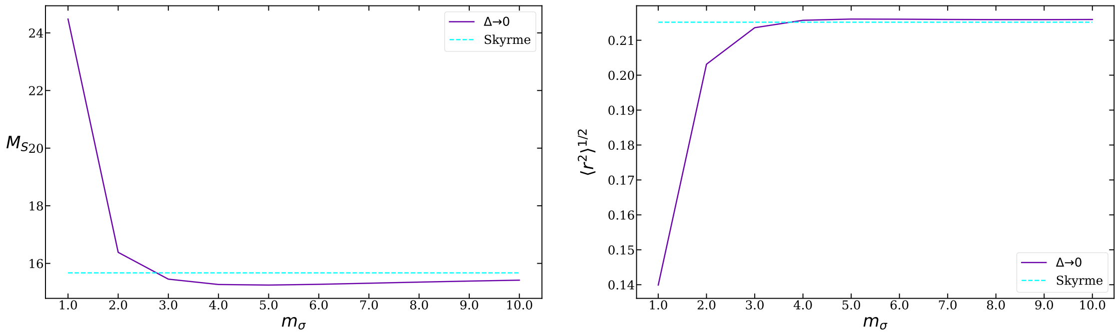

Figure 9.6.: The Skyrmion mass M_S (*left*) and $\langle r^2\rangle^{1/2}$ (*right*) as a function of the dilaton mass m_σ. The dashed line marks the values obtained in the absence of the dilaton $M_{\text{Skyrme}} = 15.67$ and $\langle r^2\rangle^{1/2}_{\text{Skyrme}} = 0.215$.

of m_σ, with the $m_\sigma = 1$ profile staying below the $m_\sigma = 2$ one only for small values of r. The behaviour of the Skyrmion mass and the root mean square radius as a function of m_σ is illustrated in Figure 9.6 and mimics the one found in the previous section. In fact, M_S decreases, reaches its minimum around $m_\sigma \sim 5$, and then grows toward the Skyrme model value. At the same time $\langle r^2\rangle^{1/2}$ mirrors such a behaviour. Our results for M_S and $\langle r^2\rangle^{1/2}$ are listed in App.E.0.2.

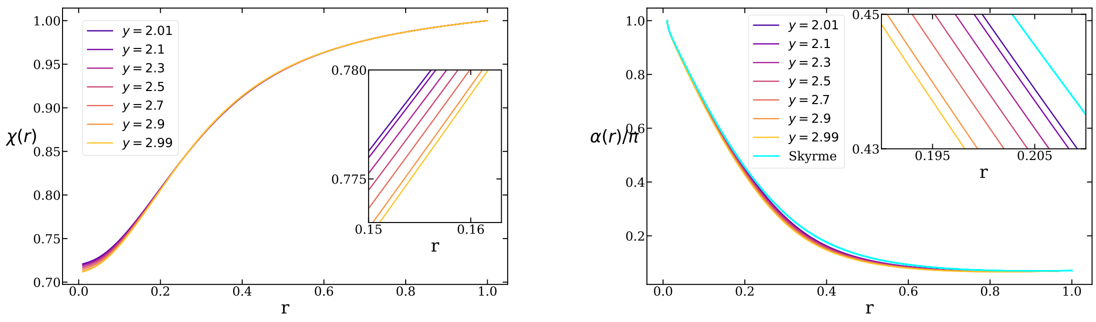

Figure 9.7.: Dilaton profile $\chi(r)$ (*left*) and $\alpha(r)/\pi$ (*right*) for $m_\sigma = 2$ and $\Delta = 1$.

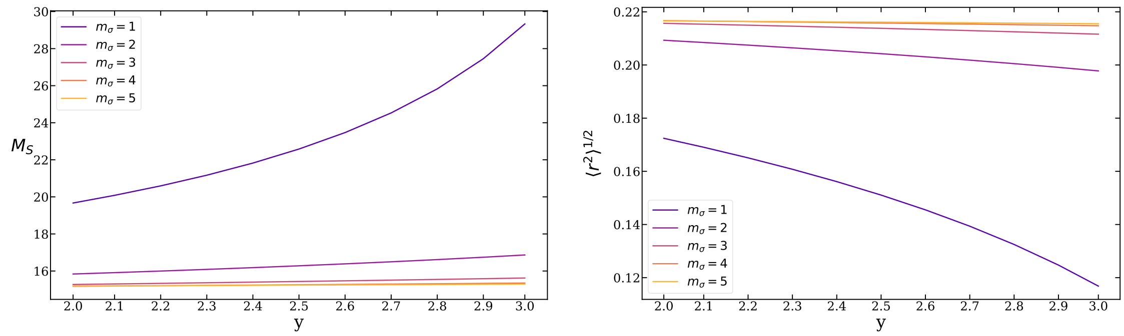

Figure 9.8.: M_S (*left*) and $\langle r^2 \rangle^{1/2}$ (*right*) as a function of y for $\Delta = 1$ and $m_\sigma = 1, 2, 3, 4, 5$.

The role of the anomalous dimension of the chiral condensate

The time is ripe to discuss the impact of the anomalous dimension of the chiral condensate on the Skyrmion properties, i.e. the dependence on y. First, note that all the conclusions drawn for the $y = 5/2$ case in the previous sections hold for every $2 < y < 3$. The dilaton profile $\chi(r)$ becomes flatter and converges earlier to its asymptotic value as y decreases. At the same time, the Skyrmion profile $\alpha(r)$ approaches the profile in the absence of the dilaton as y decreases signaling the decoupling of $\sigma(r)$ from the dynamics. Figure 9.7 illustrates this behaviour showing the profiles obtained for $\Delta = 1$ and $m_\sigma = 2$ and different values of y.

M_S and $\langle r^2 \rangle^{1/2}$ get, respectively, larger and smaller as y varies from $y = 2$ to $y = 3$, as shown in Figure 9.8. Moreover, the dependence on y gets weaker as the dilaton decouples for larger m_σ. Finally, the results for M_S and $\langle r^2 \rangle^{1/2}$ confirm that *the dilaton decouples faster for smaller* y. For instance, this can be seen by looking at how the dependence of M_S (and $\langle r^2 \rangle^{1/2}$) on both Δ and m_σ becomes softer as y decreases. This last point is exemplified in Figure 9.9.

Numerical solutions in the chiral limit

The numerical analysis carried out above concludes now with a brief discussion of the solitonic solution in the chiral limit $m_\pi = 0$. Here the topological trivial vacuum state occurs for $U = \mathbb{1}$ and $\sigma = 0$. Therefore, the BC for $\chi(r)$ at infinity no longer depends on the value of m_σ and Δ. Keeping the same numerical values adopted in Sec.9.2.2

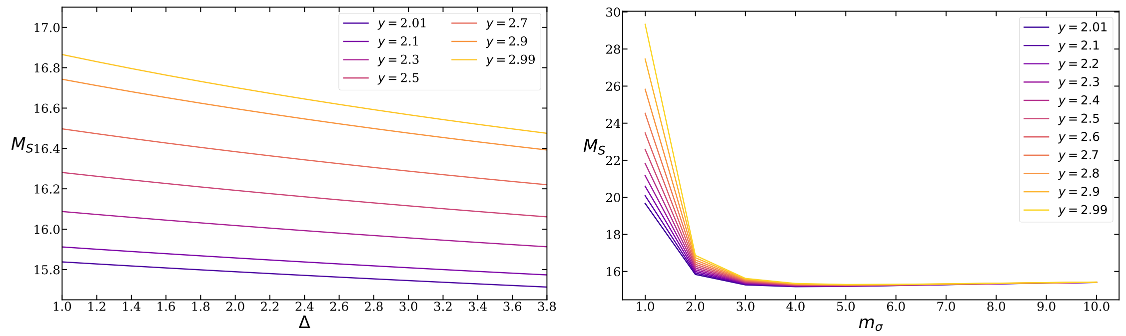

Figure 9.9.: The Skyrmion mass M_S as a function of Δ for $m_\sigma = 2$ and $y = 2.01, 2.1, 2.3, 2.5, 2.7, 2.9, 2.99$ (*left*) and as a function of m_σ for $\Delta = 1$ and $y = 2.01, 2.1, 2.3, 2.5, 2.7, 2.9, 2.99$ (*right*).

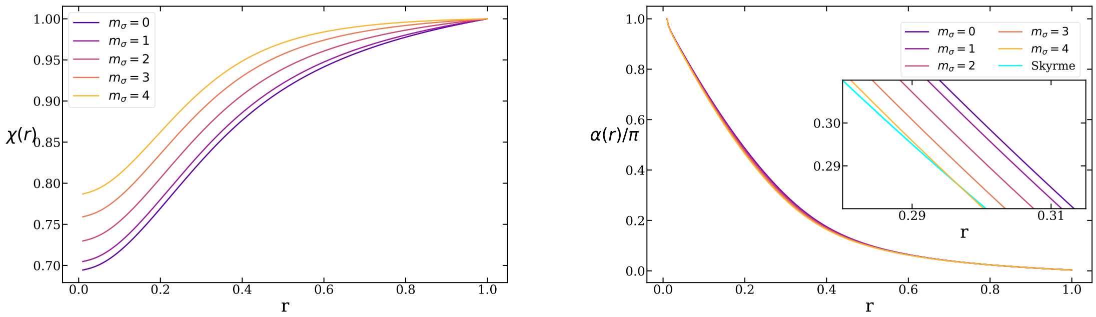

Figure 9.10.: Dilaton $\chi(r)$ (*left*) and $\alpha(r)/\pi$ (*right*) profiles for $\Delta = 1$ and $m_\sigma = 0, 1, 2, 3, 4$.

the EOM are solved for $\Delta = 1, 1.2 \ldots, 4$ and $m_\sigma = 0, 1, 2, 3, 4$. The first observation is that all the solitonic properties are nearly independent on Δ for any value of m_σ. This is a direct consequence of the fact that the dilaton ground state value vanishes for any Δ. The dilaton $\chi(r)$ and $\alpha(r)/\pi$ profiles are displayed in Figure 9.10 for $\Delta = 1$ and $m_\sigma = 0, 1, 2, 3, 4$. Analogously to the $m_\pi \neq 0$ case, the dilaton profile progressively flattens as one increases its mass exhibiting a faster convergence to unity. At the same time, the associated $\alpha(r)/\pi$ profile shows almost no dependence on m_σ. The baryon mass M_S is shown in Figure 9.11. The dependence on Δ is similar (M_S gets smaller as Δ increases) but much weaker than in the $m_\pi \neq 0$ case for all values of m_σ. For instance, for $m_\sigma = 1$ the relative variation of the solitonic mass along the whole range of values of Δ is only $\sim 0.07\%$, to be compared with $\sim 15\%$ obtained for $m_\pi = 140/93$ in Sec.9.2.2. Moreover, the dependence on m_σ of both M_S and $\langle r^2 \rangle^{1/2}$ is such that now the solitonic mass increases and the radius decreases towards the dilaton-decoupled limit as shown in Figure 9.12. In the case of a non-vanishing m_π it is the solitonic mass that decreases while the radius increases.

9.2.3 Analytical solution in the massless case

In the case of the chiral Lagrangian alone, the spherical hedgehog ansatz leads to a differential equation that can only be solved using numerical methods. Quite remarkably,

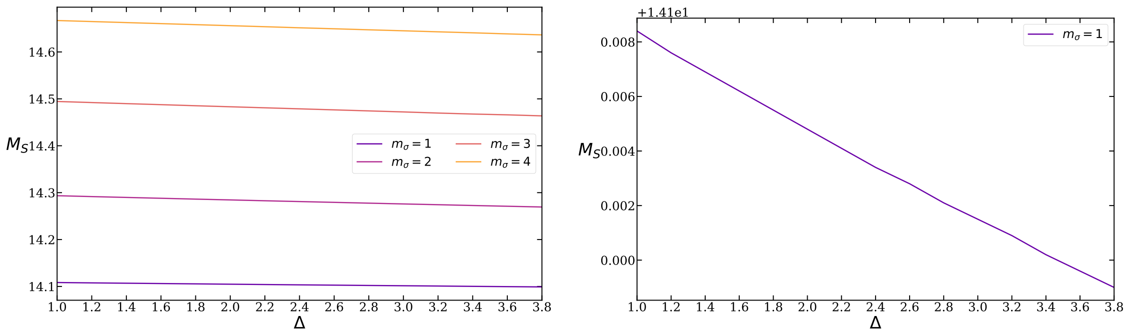

Figure 9.11.: Skyrmion mass M_S as a function of Δ for $m_\sigma = 1, 2, 3, 4$ (*left*) and a detail of the $m_\sigma = 1$ line (*right*).

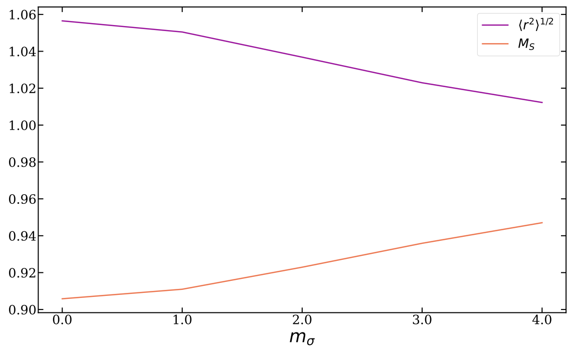

Figure 9.12.: Skyrmion mass M_S and root mean square radius $\langle r^2 \rangle^{1/2}$ normalized at their values in the absence of the dilaton ($M_{\mathrm{Skyrme}} = 15.49$ and $(\langle r^2 \rangle^{1/2}_{\mathrm{Skyrme}} = 0.213)$ as a function of m_σ.

when the coupling with the dilaton is not neglected it is possible to find an analytical solution for a special value of the couplings f and K due to an interesting phenomenon, namely *"BPS-like equations without a BPS bound*". In fact, when $f^2 K = 7/8$, the second order field equations can be reduced to a first order system even though there is no BPS bound on the energy of the system. The equations of motion (9.7) and (9.8) in the absence of mass and Skyrme term reduce to two non-linear coupled ODEs

$$r^2 \alpha'' - 2r\alpha' \left(f r \sigma' - 1 \right) - \sin(2\alpha) = 0 \, , \tag{9.22}$$

$$r^2 \sigma'' + r \left(f K r \alpha'^2 + \sigma' \left(2 - f r \sigma' \right) \right) + 2 f K \sin^2(\alpha) = 0 \, . \tag{9.23}$$

For later convenience, let us change variables as $\rho = \log r$ and $\frac{\partial \sigma}{\partial \rho} \to \frac{\partial \sigma}{\partial \rho} + \frac{1}{2f}$ and rewrite the EOMs as

$$\ddot{\alpha} - 2f \dot{\alpha} \dot{\sigma} - \sin(2\alpha) = 0 \, , \tag{9.24}$$

$$\ddot{\sigma} - f \dot{\sigma}^2 + f K \dot{\alpha}^2 + 2 f K \sin^2(\alpha) + \frac{1}{4f} = 0 \, , \tag{9.25}$$

where the dot denotes the derivative with respect to t. Noticeably, when $f^2K = \frac{7}{8}$ one can find a first order system implying the EOM

$$\alpha' = \frac{\sqrt{2}}{r}\cos(\alpha)\ , \tag{9.26}$$

$$\sigma' = -\frac{\sqrt{2}}{fr}\sin(\alpha) + \frac{1}{2fr}\ . \tag{9.27}$$

Therefore, the analytical solution of the EOM reads

$$\alpha_\pm(r) = n\pi + 2\tan^{-1}\left(1 - \frac{2c_1}{c_1 \pm \left(\frac{r}{r_0}\right)^{\sqrt{2}}}\right), \qquad n \in \mathbb{Z}\ , \tag{9.28}$$

$$\sigma_\pm(r) = \frac{1}{f}\left\{c_2 + \frac{1}{2}\log\left(\frac{r}{r_0}\right) + \log\left[\cos\left(2\tan^{-1}\left(1 - \frac{2c_1}{c_1 \pm \left(\frac{r}{r_0}\right)^{\sqrt{2}}}\right)\right)\right]\right\}\ , \tag{9.29}$$

where the plus and minus signs apply for $c_1 > 0$ and $c_1 < 0$, respectively. The topological charge associated with this solution is $B = -1$. Conventional solitonic solutions of the chiral Lagrangian with negative winding numbers are called *antiskyrmions*. The energy density of the solution reads

$$\epsilon = \frac{e^{-2c_2}}{8c_1^2 f^2 r^2}\left(\frac{r}{r_0}\right)^{-2\sqrt{2}-1}\left[\left(\sqrt{2}+4\right)c_1^4 - \left(\sqrt{2}-4\right)\left(\frac{r}{r_0}\right)^{4\sqrt{2}}\right]\ , \tag{9.30}$$

and diverges at the origin as $r^{-2\sqrt{2}-3}$ due to the dilaton profile $\chi(r)$ being singular in $r = 0$. Moreover, even excluding the singularity at $r = 0$, the total energy would still diverge since the energy density does not decrease fast enough at large r.

§ 9.3 Dilaton augmented Crystals

This section opens with a review of the strategies to find analytical solutions describing arrays of tubes of baryons with non-trivial topological charge on flat space-time [310–313] and then a generalisation of the solutions in the presence of the dilaton is presented. The qualitative behaviour of these exact solutions suggests they may be relevant for describing nuclear pasta states [330, 331].

9.3.1 Crystals without the dilaton

Consider the action (9.2) in the absence of the Skyrme and mass terms and retain the same general parameterization for $U(x)$ given in (9.11). The equations of motions (9.5) constitute the following set of three non-linear coupled PDEs

$$-\Box\alpha + \sin(\alpha)\cos(\alpha)\left(\nabla_\mu\Theta\nabla^\mu\Theta + \sin^2(\Theta)\nabla_\mu\Phi\nabla^\mu\Phi\right) = 0 \,, \tag{9.31}$$

$$\sin^2(\alpha)\Box\Theta + 2\sin(\alpha)\cos(\alpha)\nabla_\mu\alpha\nabla^\mu\Theta - \sin^2(\alpha)\sin(\Theta)\cos(\Theta)\nabla_\mu\Phi\nabla^\mu\Phi = 0 \,, \tag{9.32}$$

$$\sin^2(\alpha)\sin^2(\Theta)\Box\Phi + 2\sin(\alpha)\cos(\alpha)\sin^2(\Theta)\nabla_\mu\alpha\nabla^\mu\Phi + 2\sin^2(\alpha)\sin(\Theta)\cos(\Theta)\nabla_\mu\Theta\nabla^\mu\Phi = 0 \,, \tag{9.33}$$

where any ansatz for the parameters of U in terms of the coordinates has yet been made. Here the topological charge density $\rho_B \equiv J^0$ takes the form

$$\rho_B = 12\sin^2(\alpha)\sin(\Theta)d\alpha \wedge d\Theta \wedge d\Phi \,. \tag{9.34}$$

From this expression, one observes that in order to have $d\alpha \wedge d\Theta \wedge d\Phi \neq 0$ the fields α, Θ, and Φ must be independent. Additionally, in order to decouple the previous set of equations one imposes

$$\nabla_\mu\Phi\nabla^\mu\alpha = \nabla_\mu\alpha\nabla^\mu\Theta = \nabla_\mu\Phi\nabla^\mu\Phi = \nabla_\mu\Theta\nabla^\mu\Phi = 0 \,. \tag{9.35}$$

To proceed, let us confine the system into a box described by the line element

$$ds^2 = -dt^2 + L_x^2dx^2 + L_y^2dy^2 + L_z^2dz^2 \,, \tag{9.36}$$

where $\{x, y, z\}$ are dimensionless coordinates having the range

$$0 \leq x \leq 2\pi, \quad 0 \leq y \leq \pi, \quad 0 \leq z \leq 2\pi \,. \tag{9.37}$$

The condition (9.35) is then realised by considering the ansatz

$$\alpha = \alpha(x), \quad \Theta = qy, \quad \Phi = p\left(\frac{t}{L_z} - z\right), \quad q = 2v + 1, \quad v, p \in \mathbb{Z} \,, \tag{9.38}$$

such that the equations of motion reduce to a single integrable ODE for the profile $\alpha(x)$

$$\partial_x\left[\frac{1}{2}(\alpha')^2 - V(\alpha) - E_0\right] = 0, \quad V(\alpha) = -\frac{q^2L_x^2}{2L_y^2}\cos(2\alpha) \,, \tag{9.39}$$

where E_0 is an integration constant that depends on the boundary conditions for α. The explicit solution can be written in terms of a certain Jacobi elliptic function. The corresponding topological charge density reads

$$\rho_B = \frac{3qp\sin(qy)}{L_xL_yL_z}\partial_x(2\alpha - \sin(2\alpha)) \,. \tag{9.40}$$

By considering the boundary conditions for α

$$\alpha(2\pi) - \alpha(0) = n\pi \,, \qquad n \in \mathbb{Z} \,, \tag{9.41}$$

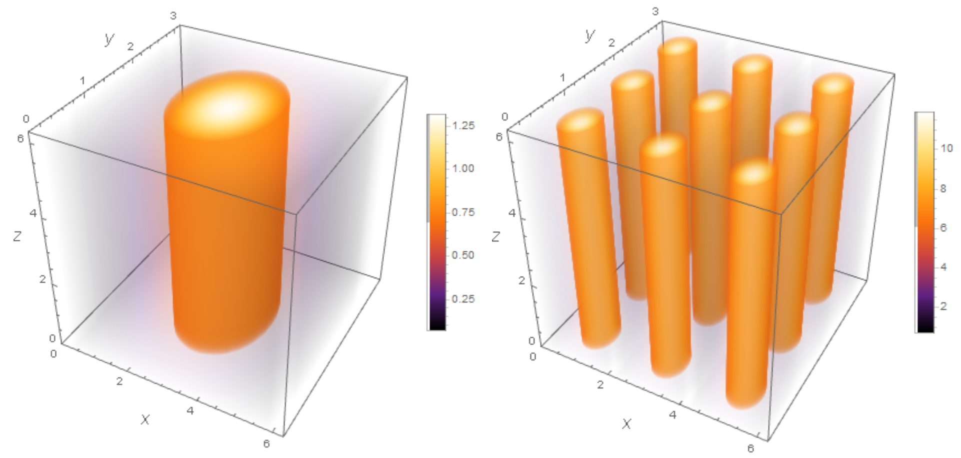

Figure 9.13.: Energy density of the solution (9.39) for $p = q = n = 1$ (*left*) and $p = q = n = 3$ (*right*). In both cases, $K = L_x = L_z = 1$ and $L_y = 2$.

then the topological charge is given by $B = np$. Therefore the baryon charge can be an arbitrary integer number. This solution describes stationary soliton crystals with the shape of ordered arrays of baryonic tubes carrying topological charge. Here the integer p can be interpreted as the baryonic charge per unit of length in the z-direction per tube. This can be seen by looking at the energy density of the solution $\epsilon \equiv T_{00}$

$$\epsilon = \frac{1}{2}K\left(\frac{\alpha'^2}{L_x^2} + \sin^2(\alpha)\left(\frac{q^2}{L_y^2} + \frac{2p^2\sin^2(qy)}{L_z^2}\right)\right) , \tag{9.42}$$

which is depicted in Figure 9.13.

9.3.2 Crystals with the dilaton

This subsection aims to study the effect of the dilaton on the solutions considered in the previous section [3]. In particular, consider U given by equations (9.11) and (9.38) and assume that the dilaton field depends only on the x coordinate, i.e. $\sigma = \sigma(x)$. Consequently, the field equations reduce to two coupled non-linear ODE for $\alpha(x)$ and $\sigma(x)$

$$\alpha'' - 2f\alpha'\sigma' - \frac{L_x^2}{2L_y^2}q^2\sin(2\alpha) - L_x^2 m_\pi^2 \sin(\alpha)e^{-f(y-2)\sigma} = 0 , \tag{9.43}$$

$$\sigma'' + fK\alpha'^2 - f\sigma'^2 + \frac{L_x^2}{L_y^2}fKq^2\sin^2(\alpha) - L_x^2 e^{2f\sigma}\partial_\sigma V(\sigma) - KfL_x^2 m_\pi^2 y\cos(\alpha)e^{-f(y-2)\sigma} = 0 . \tag{9.44}$$

[3] Differently from the conventional static Skyrmions discussed in [341] and [342], the crystal configurations are stationary rather than static as studied in [310, 312]. For the crystal solutions without dilaton the question of stability was discussed in [310] where the author showed that the solutions are stable under perturbations of the profile which keep the structure of the ansatz.

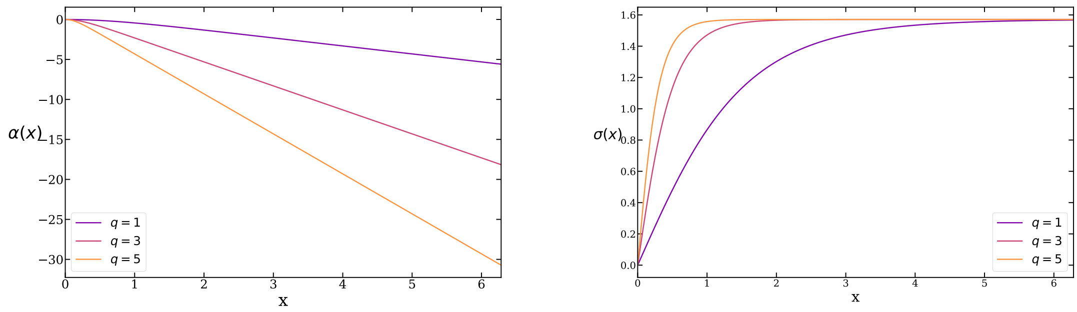

Figure 9.14.: The profiles $\alpha(x)$ (*left*) and $\sigma(x)$ (*right*) for $q = 1, 3, 5$.

The topological charge is given by eq.(9.40) while the energy density evaluated on this ansatz reads

$$\epsilon = \frac{1}{2}Ke^{-2f\sigma}\left(\sin^2(\alpha)\left(\frac{q^2}{L_y^2}+\frac{2p^2\sin^2(qy)}{L_z^2}\right)+\frac{\alpha'^2}{L_x^2}\right)+\frac{e^{-2f\sigma}\sigma'^2}{2L_x^2}-Km_\pi^2\cos(\alpha)e^{-fy\sigma}+V(\sigma)\,, \tag{9.45}$$

and reduces to eq.(9.42) for $\sigma = m_\pi = 0$. Let us proceed by focusing on the massless case $m_\pi = m_\sigma = 0$, which unlike the massive case can be partially addressed analytically. In fact, it is quite remarkable that at the special parameter point, $f^2K = 1$ the field equations (9.43) and (9.44) can be reduced to a system of first order ODEs given by

$$\alpha' = q\cos(\alpha)\,, \qquad \sigma' = -\frac{q}{f}\sin(\alpha)\,, \tag{9.46}$$

where for the sake of simplicity $L_x = L_y$. This can also be seen by noting that the EOMs (9.43) and (9.44) coincide with the EOMs (9.24) and (9.25) for the hedgehog ansatz up to a constant term $\frac{1}{4f}$ in eq.(9.25). The latter shifts the special combination of parameters from $f^2K = 7/8$ to $f^2K = 1$ reducing the second order equations of motion to the above set of first order ones yielding the solutions

$$\alpha(x) = 2\arctan\left(\tanh\left(\frac{1}{2}(c_1+qx)\right)\right)\,, \tag{9.47}$$

$$\sigma(x) = -\frac{1}{f}\left[c_2 + 2\,\mathrm{arctanh}\left(\tanh^2\left(\frac{1}{2}(c_1+qx)\right)\right)\right]\,, \tag{9.48}$$

where c_1 and c_2 are the integration constants. The behaviour of these solutions is shown in Figure 9.14. All the integration constants stemming from the second order original EOM can be restored to write the solution as

$$\alpha(x) = n\pi + \arctan\left(d_1e^{qx}+d_2e^{-qx}\right)\,, \qquad n\in\mathbb{Z}\,, \tag{9.49}$$

$$\sigma(x) = -\frac{1}{f}\left(c_2+\frac{1}{2}\log\left((d_1e^{qx}+d_2e^{-qx})^2+1\right)\right)\,. \tag{9.50}$$

When the parameter p is an integer it is possible to have an integer topological charge B only by considering a box that has an infinite length in the x direction. In such a case, $B = p$ but the total energy carried by the solution diverges. This is in contrast with the

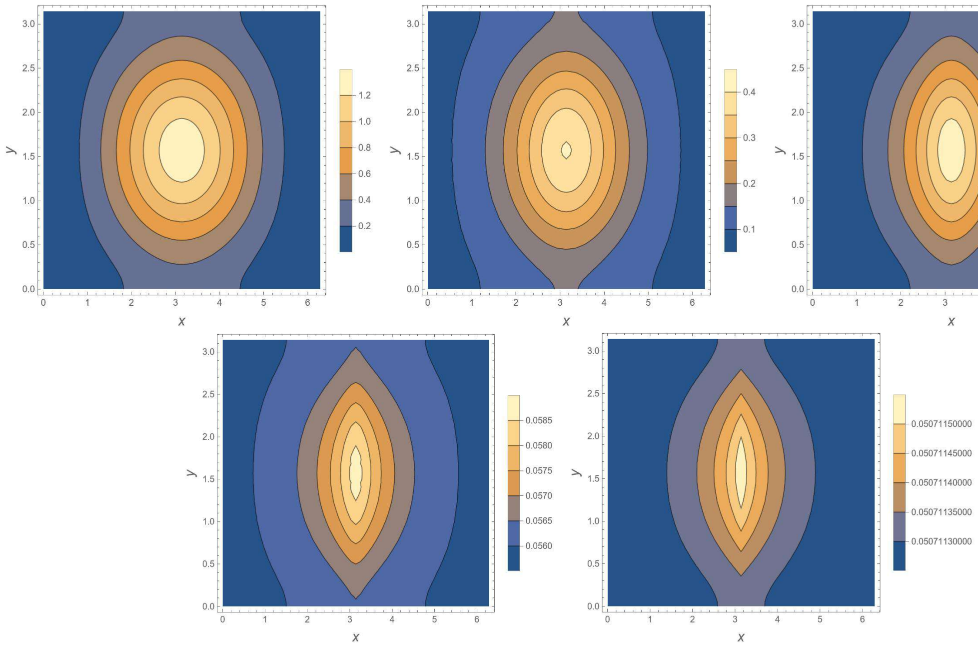

Figure 9.15.: Contour plot of the energy density in the $x-y$ plane for $m_\pi = m_\sigma = 0$ varying $X = f^2K$. From left to right and top to bottom: $X = 0, 0.3, 0.6, 0.9, 1$. As X goes from 0 to 1 the results interpolate between the analytical solution found in [310–313] in the absence of the dilaton field and the solution (9.47).

solution in the absence of the dilaton field, where for $p \in \mathbb{Z}$ one can confine an arbitrary amount of topological charge in a finite-size box and the corresponding energy is finite. On the other hand, one can relax the condition $p \in \mathbb{Z}$ and determine the value of p such that a certain amount of topological charge is confined in a finite-size box. Without losing generality, considering $0 \leq x \leq 2\pi$ and imposing BCs $\alpha(0) = 0$ and $\alpha(2\pi) = s$ with $0 < s < \pi/2$, leads to the topological charge

$$B = -2 \int_{\alpha(0)}^{\alpha(2\pi)} \frac{p}{\pi} \sin^2(\alpha)\, d\alpha \,. \tag{9.51}$$

Hence $B \in \mathbb{Z}$ can be achieved when

$$p = \frac{2\pi B}{\sin(2s) - 2s} \,. \tag{9.52}$$

The behaviour of the solution for different values of $X \equiv f^2K$ can also be investigated numerically. The corresponding energy density is shown in Figure 9.15. At $X = 0$ the EOM decouple; the dilaton solution is $\sigma(x) = c_1 - \log(c_2 + x)$, $\{c_1, c_2\} \in \mathbb{R}$ while $\alpha(x)$ solves eq.(9.39) yielding a field configuration with localized energy and integer topological charge. On the other hand, for $X = 1$ the analytical solution (9.47) has an energy that grows indefinitely for increasing x. The physical impact of this solution will be discussed below.

9.3.3 Stability analysis

Here a nontrivial test of the stability of the crystal solutions in the presence of the dilaton is presented. In many situations when the hedgehog property holds, i.e., the equations of motion reduce to a single equation for the soliton profile, the most “dangerous" perturbations are those that keep the structure of the ansatz since they are likely to lead to a lower energy state [343, 344]. In the presence of the dilaton, these perturbations are of the following form

$$\alpha = \alpha_0(r) + \varepsilon u(r), \tag{9.53}$$

$$\sigma = \sigma_0(r) + \varepsilon v(r), \tag{9.54}$$

where α_0 and σ_0 solve Eq.(9.46) and $0 \leq \varepsilon \ll 1$. These perturbations do not involve the isospin degrees of freedom Θ and Φ. A straightforward computation shows that the linearized EOMs for $u(r)$ and $v(r)$ always have a zero-mode $u(r) = \nabla_r \alpha_0(r)$ and $v(r) = \nabla_r \sigma_0(r)$. The contribution of this configuration to the density energy is given by

$$\delta E = \frac{2Kq}{L^2} \varepsilon e^{-2f\sigma_0(r)} \sin(\alpha_0(r)) \left(p^2 \sin^2(\theta q) + q^2 \right) \geq 0 \, . \tag{9.55}$$

Therefore, the present solutions are stable under the above potentially dangerous perturbations.

9.3.4 Isospin-Charge Separation

A further intriguing feature of the effective chiral Lagrangian dressed with the dilaton is the following. In the solutions without dilaton [310–313] the peaks corresponding to the local maxima of the topological charge density are in the same locations as the peaks corresponding to the local maxima of the isospin charge density (as one can also check via a direct computation). On the other hand, the isospin current (which is the Noether current associated with the $SU(2)$ isospin rotations of the theory) is deformed by the presence of the dilaton while the definition of the topological charge density does not change (being the usual baryon charge). This implies that the local maxima of these two relevant quantities no longer coincide. Indeed, by setting for simplicity $L_x = L_y = L_z \equiv L$, the topological charge density reads

$$\rho_B = \frac{12pq}{L^3} \sin(yq) \alpha'(x) \sin^2(\alpha(x)) \, , \tag{9.56}$$

while the isospin charge density is

$$\rho_I = K \, \mathrm{Tr}(R^0 \tau_3) e^{-2f\sigma(x)} = \frac{2Kp}{L} e^{-2f\sigma(x)} \sin^2(yq) \sin^2(\alpha(x)) \, . \tag{9.57}$$

In Figure 9.16 there is a comparison between the two charge densities to illustrate the different positions of the peaks.

This “separation" of the peaks of baryonic and isospin charge densities could open

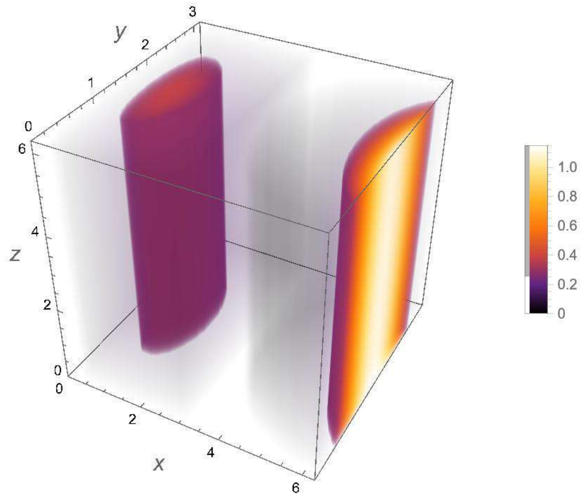

Figure 9.16.: Topological (*left*) and isospin (*right*) charge densities for $L = B = q = 1$ and $\alpha(2\pi) = s = \frac{\pi}{4}$.

the interesting possibility of defining the analogue of the well-known phenomenon in condensed matter physics called *spin-charge separation* (see e.g. [328, 329] and references therein). In the condensed matter version of this phenomenon, due to the presence of strong correlations, spin and charge may cease to be tied generating independent branches of excitations. In the present case, it could be possible to observe isospin-baryon charge separation due to the presence of the dilaton which can support excitations that change directly the isospin and only indirectly the baryon charge density.

§ 9.4 Dilaton augmented Branes

In [306–309, 313], another family of analytical solutions of the massless chiral Lagrangian has been discovered. These are again obtained by confining the theory in a box according to the metric eq.(9.36) and considering the following ansatz

$$U = e^{\frac{1}{2}py\tau_3}e^{\frac{1}{4}x\tau_2}e^{\frac{1}{2}\tau_3 F(t,z)}\,, \qquad p \in \mathbb{Z}\,. \tag{9.58}$$

The above represents a particular instance of Euler angles parametrization for $SU(2)$ which implies the following range for x and y [345, 346]

$$0 \leq y \leq \pi\,, \qquad 0 \leq x \leq 2\pi\,. \tag{9.59}$$

Without losing generality one can also consider

$$0 \leq z \leq 2\pi\,. \tag{9.60}$$

The topological charge density is given by

$$\rho_B = \frac{3p}{4L_xL_yL_z}\sin\left(\frac{x}{2}\right)\partial_z F\,. \tag{9.61}$$

The periodicity of physical observables along with the properties of the Euler angles parameterization fixes the boundary condition satisfied by $F(t,z)$ as

$$F(t, z = 0) - F(t, z = 2\pi) = \pm 8\pi q\,, \qquad q \in \mathbb{Z}\,. \tag{9.62}$$

As a consequence, the topological charge reads

$$B = -\frac{p}{8\pi}(F(t, z = 0) - F(t, z = 2\pi)) = pq\,. \tag{9.63}$$

Noticeably, for $m_\pi = 0$ the EOMs (9.5) evaluated on the ansatz (9.58) reduce to the field equation of a free massless scalar in $d = 2$ dimensions [309]

$$\left(\partial_t^2 - \frac{1}{L_z^2}\partial_z^2\right) F(t,z) = 0\,. \tag{9.64}$$

The general solution to the previous equations can be decomposed as the sum of two independent modes $F = F_+\left(\frac{t}{L_z} + z\right) + F_-\left(\frac{t}{L_z} - z\right)$. The latter can be generically written using the following representation

$$F_+ = \phi_+^0 + v_+\left(\frac{t}{L_z} + z\right) + \sum_{n\neq 0}\left[a_n^+ \sin\left(\frac{t}{L_z} + z\right) + b_n^+ \cos\left(\frac{t}{L_z} + z\right)\right]\,, \tag{9.65}$$

$$F_- = \phi_-^0 + v_-\left(\frac{t}{L_z} - z\right) + \sum_{n\neq 0}\left[a_n^- \sin\left(\frac{t}{L_z} - z\right) + b_n^- \cos\left(\frac{t}{L_z} - z\right)\right]\,, \tag{9.66}$$

with coefficients $\phi_\pm^0, v_\pm, a_n^\pm, b_n^\pm$. In this way, the topological charge (9.63) is non zero when $v_+ - v_- \neq 0$, additionally the coefficients $v_\pm$ have to be chosen such that

$$F(t, \phi = 0) = \phi_0^+ + \phi_0^- + (v_+ + v_-)\,\frac{t}{L_z} \quad \Rightarrow \quad v_+ + v_- = 0\,, \tag{9.67}$$

$$F(t, \phi = 2\pi) = \phi_0^+ + \phi_0^- + (v_+ - v_-)\,2\pi \quad \Rightarrow \quad v_+ - v_- = 4q\,. \tag{9.68}$$

The energy density of the solution reads

$$\epsilon = \frac{K}{8}\left[\frac{1}{4}\left(\frac{1}{L_x^2} + \frac{4p^2}{L_y^2}\right) + (\partial_t F)^2 + \frac{1}{L_z^2}\,(\partial_z F)^2\right]\,, \tag{9.69}$$

and is illustrated in Figure 9.17. One can see that this solution describes modulated layers of nuclear matter.

The inclusion of the Skyrme term yields an additional equation

$$(\partial_t F)^2 - \frac{1}{L_z^2}\,(\partial_z F)^2 = \left(\partial_t F - \frac{1}{L_z}\partial_z F\right)\left(\partial_t F + \frac{1}{L_z}\partial_z F\right) = 0\,, \tag{9.70}$$

with solution $F(t,z) = F\left(z \pm \frac{t}{L_z}\right)$. On the other hand, the equations of motion do not admit any solution of the form (9.58) when $m_\pi \neq 0$.

Equipped with the above, let us now investigate the impact of the dilaton on this class of topologically non-trivial solutions of the chiral and Skyrme models in the chiral limit $m_\pi = 0$. Assuming $\sigma = \sigma(t,z)$, the EOM are

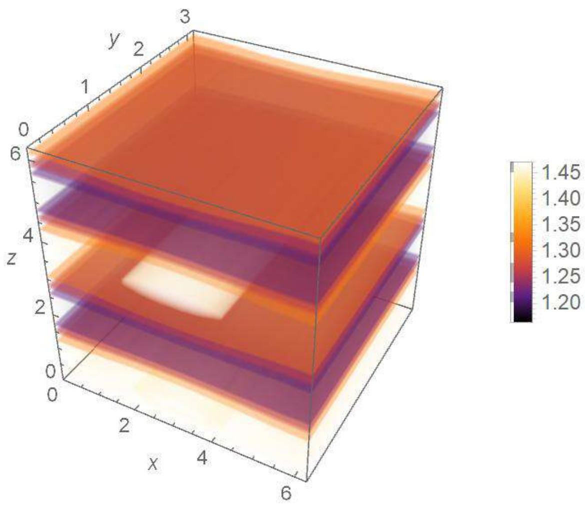

Figure 9.17.: Energy density of a solution of the EOMs (9.64) exhibiting a layer structure. Here $F = F_+(\frac{t}{L_z} + z) = \cos\left(\frac{t}{L_z} + z\right)$.

$$\partial_t^2 F - \frac{1}{L_z^2}\partial_z^2 F = 0\,, \tag{9.71}$$

$$(\partial_t F)^2 - \frac{1}{L_z^2}(\partial_z F)^2 = 0\,, \tag{9.72}$$

$$\partial_z F\ \partial_z\sigma - L_z^2\partial_t F\ \partial_t\sigma = 0\,, \tag{9.73}$$

$$\partial_t^2\sigma - \frac{1}{L_z^2}\partial_z^2\sigma - f\left((\partial_t\sigma)^2 - \frac{1}{L_z^2}(\partial_z\sigma)^2\right) - \frac{fk}{16}\left(\frac{4p^2}{L_y^2} + \frac{1}{L_x^2}\right) + e^{2f\sigma}\partial_\sigma V(\sigma) = 0\,. \tag{9.74}$$

The baryon charge does not depend on the dilaton and, therefore, it is still given by eq.(9.63). The energy density reads

$$\epsilon = \frac{Ke^{-2f\sigma}\left(4L_x^2L_y^2\left(L_z^2\partial_t F^2 + \partial_z F^2\right) + L_z^2\left(L_y^2 + 4L_z^2p^2\right)\right)}{32L_x^2L_y^2L_z^2} + \frac{e^{-2f\sigma}\left(L_z^2\partial_t\sigma^2 + \partial_z\sigma^2\right)}{2L_z^2}$$
$$+\frac{\lambda K\left(\left((L_z^2\partial_t F^2 + \partial_z F^2\right)\left(L_y^2 + 4L_x^2p^2\sin^2\left(\frac{r}{2}\right)\right) + L_z^2p^2\right)}{128L_x^2L_y^2L_z^2} + V(\sigma)\,. \tag{9.75}$$

9.4.1 Branes in the conformal limit

To begin with, consider the scenario where both the Skyrme term and the dilaton potential are zero. In this case, the EOM for the brane ansatz (9.58) admits an analytical solution carrying topological charge where the U and σ fields are, respectively, static and

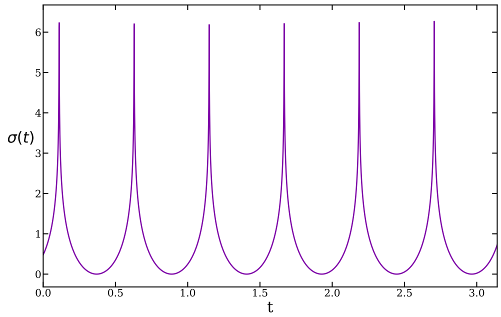

Figure 9.18.: Time evolution of the dilaton solution eq.(9.76).

homogeneous. It reads

$$F(z) = c_1 + c_2 z\,, \qquad \sigma(t) = \frac{1}{f}\left\{d_1 - \log\left|\cos\left(\frac{\sqrt{K}\sqrt{4c_2^2 L_y^2 L_x^2 + L_z^2\left(L_y^2 + 4L_x^2 p^2\right)}\,(d_2 + ft)}{4L_y L_x L_z}\right)\right|\right\}\,, \tag{9.76}$$

where c_1, c_2, d_1, and d_2 are arbitrary integration constants. The boundary conditions (9.62) for $F(z)$ impose $c_2 = 4q$ whereas the energy density evaluated on the solution is both homogeneous and static

$$\epsilon = \frac{K}{32L_y^2 L_x^2 L_z^2} e^{-2d_1}\left[L_y^2\left(64L_x^2 q^2 + L_z^2\right) + 4L_x^2 L_z^2 p^2\right]\,. \tag{9.77}$$

Moreover, since the U field is static, the isospin charge density of this solution vanishes identically. The time evolution of the dilaton field is depicted in Figure 9.18. Note that this solution is non-analytic in time due to a series of branch-cut singularities lying at

$$ft = \frac{2L_y L_x L_z\, \pi(2n+1)}{\sqrt{K}\sqrt{L_y^2\left(64L_x^2 q^2 + L_z^2\right) + 4L_x^2 L_z^2 p^2}} - d_2\,, \qquad n \in \mathbb{Z}\,. \tag{9.78}$$

It is possible to construct another analytical solution to the EOM of the massless chiral Lagrangian where, akin to the case without the dilaton, $F(z,t)$ can be expressed as a particular linear combination of left- and right-moving modes

$$\begin{aligned} F(t,z) &= c_1 + c_2\left[\left(z + \frac{t}{L_z}\right) - A\left(z - \frac{t}{L_z}\right)\right]\,, \\ \frac{\sigma(t,z)}{\sqrt{k}} &= d_1 + d_2\left[\left(z + \frac{t}{L_z}\right) + A\left(z - \frac{t}{L_z}\right)\right]\,, \end{aligned} \tag{9.79}$$

where

$$A = \frac{L_z^2\left(L_y^2 + 4L_x^2 p^2\right)}{16L_t^2 L_x^2\left(c_2^2 + 4d_2^2\right)}\,. \tag{9.80}$$

However, for $d_2 \neq 0$ the energy of this solution either grows or decays exponentially in time depending on the boundary conditions. Note that, when $d_2 = 0$ the solution for the dilaton is a constant and the energy of the solution is exactly twice of (9.77).

There are no nontrivial solutions with U given by eq.(9.58) for $m_\pi \neq 0$. Moreover, when $m_\sigma = 0$ there are no solutions of the EOMs when adding the Skyrme term together with dilatonic dynamics. However, as will be shown in the next section, for non-vanishing dilaton mass one is able to find analytical solutions with the ansatz eq.(9.58) including the Skyrme term.

9.4.2 Branes in the near conformal Skyrme model

The goal in this section is to study the most general solution of the EOM (9.71) of the dilaton augmented Skyrme model including the Skyrme term [4]. This is of the form

$$F(t,z) \equiv F\left(\frac{t}{L_z} \pm z\right) , \qquad \sigma(t,z) = c \, , \tag{9.81}$$

where for a dilaton potential of the form (5.89) the dilaton vev c is determined by the equation

$$\chi_0^{\Delta-2} + \frac{\beta(\Delta-4)}{m_\sigma^2} - \chi_0^2 = 0 \, , \qquad \chi_0 \equiv e^{-cf} \, , \tag{9.82}$$

where

$$\beta = \frac{1}{16} f^2 K \left(\frac{4p^2}{L_y^2} + \frac{1}{L_x^2}\right) . \tag{9.83}$$

The properties of the soliton affect the dilaton vev through the value of the parameter p which is related to the topological charge via eq.(9.63). For $m_\sigma \to \infty$ the solution is $c = 0$. On the other hand, when $\Delta \to 4$ or $m_\sigma \to 0$ the vev becomes undetermined since the potential vanishes. In the special cases $\Delta \to 0, 4$ and $\Delta = 2$ the dilaton vev reads

$$2fc = \begin{cases} \sinh^{-1}\left(\frac{2\beta}{m_\sigma^2}\right) & \Delta \to 0 \\ -\log\left(1 - \frac{2\beta}{m_\sigma^2}\right) & \Delta = 2 \\ -W(-\frac{2\beta}{m_\sigma^2}) & \Delta \to 4 \, , \end{cases} \tag{9.84}$$

where $W(x)$ denotes the Lambert W function. Only in the $\Delta = 0$ case c is real for arbitrary values of the dilaton mass. For $\Delta = 2$ the vev exhibits a branch cut singularity at $m_\sigma^2 = 2\beta$ and the solution is complex for smaller masses. Analogously, in the $\Delta \to 4$ case the solution is real only for $m_\sigma^2 > 2e\beta$.

[4] The brane configurations here are constructed *in the presence of a stabilizing Skyrme term.* This guarantees from the outset the stability of the brane configurations even in the infinite volume limit.

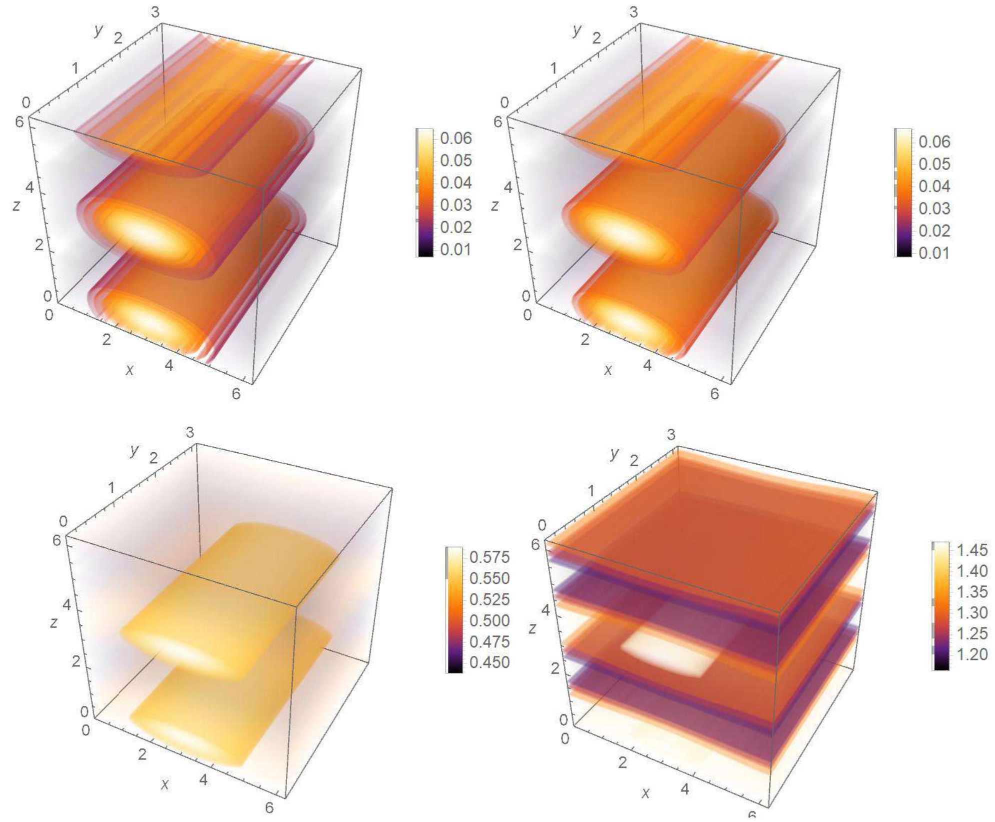

Figure 9.19.: Energy density of the solution (9.81) for $\Delta \to 0$ and different values of the dilaton mass. Here $m_\sigma/\sqrt{K} = 0.001$ (*top-left*), 0.05 (*top-right*), 1 (*bottom-left*), and 20000 (*bottom-right*). As m_σ is increased the dilaton decouples from the dynamics as can be seen by comparing the $m_\sigma/\sqrt{K} = 20000$ case to Figure 9.17. Here choose $F(\frac{t}{L_z}+z) = \cos\left(\frac{t}{L_z}+z\right)$.

The energy density carried by the solution for a generic Δ is

$$\epsilon = \frac{K}{32} e^{-2cf} \left(\frac{8F'\left(\frac{t}{L_z}+\phi\right)^2}{L_z^2} + \frac{4p^2}{L_y^2} + \frac{1}{L_x^2} \right) + \frac{K\lambda \left(2F'\left(\frac{t}{L_z}+\phi\right)^2 \left(L_y^2 + 4L_x^2 p^2 \sin^2\left(\frac{r}{2}\right)\right) + L_z^2 p^2 \right)}{128 L_x^2 L_y^2 L_z^2} + V(c) \ . \tag{9.85}$$

As shown in Figure 9.19, this solution describes ordered layers of matter analogously to the case without dilaton previously described. The dilaton vev suppresses the energy density of the U field while adding a homogeneous contribution proportional to m_σ^2. As a consequence, the overall effect of the dilaton is to smooth out the layer structure.

Analogous solutions exist in the absence of the Skyrme term. In fact, one can now look for solutions of the form

$$F(t,z) \equiv F_+\left(\frac{t}{L_z}+z\right) + F_-\left(\frac{t}{L_z}-z\right) , \qquad \sigma(t,z) = c \ . \tag{9.86}$$

Note that differently from eq.(9.81), this is not the most general solution to the EOM. By plugging the above into the EOM (9.71) with $\lambda = 0$ one has

$$fKL_z^2\left(L_y^2 + 4L_x^2p^2\right) - 16L_y^2L_x^2\left[L_z^2 e^{2cf}\frac{\partial V(\sigma)}{\partial\sigma}\bigg|_{\sigma=c} - fKF'_+\left(\frac{t}{L_z}+\phi\right)F'_-\left(\phi-\frac{t}{L_z}\right)\right] = 0\,, \tag{9.87}$$

which admits solutions if and only if

1. Either F_+ or F_- vanishes.
2. Both F_+ and F_- are linear functions of their argument.

In the first case, the solution is equal to the one in the presence of the Skyrme term with the dilaton vev given by eq.(9.84). In the second scenario instead

$$F(t,z) = a_0 + a_1\left(\frac{t}{L_z}+\phi\right) + a_2\left(\frac{t}{L_z}-\phi\right)\,, \tag{9.88}$$

and the dilaton vev is again determined by eq.(9.82) with β now given by

$$\beta = \frac{f^2K\left(16a_1a_2L_y^2L_x^2 + L_z^2\left(L_y^2+4L_x^2p^2\right)\right)}{16L_y^2L_x^2L_z^2}\,. \tag{9.89}$$

For $m_\sigma = 0$ this reduces to the solution (9.79) with $d_2 = 0$.

The ink dries in this chapter, where numerical and analytical methods were used to perform a thorough investigation of Skyrmion solutions featuring dilatonic dynamics. Using the dilaton-dressed chiral Lagrangian, the study shed light on how varying near conformal control parameters affect key physical quantities such as the Skyrmion profile, mass, and size. An intriguing link was discovered between these properties and the dilaton mass, with a standout finding being a quick dilaton decoupling when its mass exceeds that of the pion. Moreover, the impact of dilatonic dynamics was also studied on Skyrmion crystals. An additional feature observed, due to the presence of the dilaton, is the spatial separation of the baryon and isospin charge distributions, resembling the spin-charge separation phenomenon.

Let us also mention that one of the original appeals of brane solutions, without the dilaton, lies in their ability to be analytically derived from the equations of motion. The results demonstrate that it remains possible to obtain analytic solutions even with dilaton dynamics. In this chapter, this direction was further pushed and dilaton-modified solitonic branes were considered, showing that the soliton profile remains unchanged by the presence of the dilaton, while the latter acquires a homogeneous vacuum expectation value. As a final remark, let us stress that since near conformal dynamics have been suggested in various studies to play a role in nuclear matter, especially in the cores of compact stars, the findings in this chapter were presented using QCD-inspired parameters.

Conclusions

10

Chapter

It ain't what you don't know that gets you in trouble
It's what you know for sure that just ain't so
— Mark Twain

In conclusion, a central theme reiterated in this thesis is that the exploration of Nature's fundamental forces remains a complex and continuous endeavour, with strongly coupled theories representing some of the most complex problems in theoretical physics. As the literature has long since confirmed and as this study has consistently highlighted, despite considerable progress in recent decades, QCD still presents major unresolved questions. The theory remains enigmatic, particularly with regard to its physical spectrum, the interplay between chiral symmetry breaking and confinement, and its phase structure under varying conditions of temperature, matter density, and light fields, all influenced by a coupling that grows as the infrared scale is approached.

A key tool for unravelling these complexities is to study the phase diagram, an established avenue in research, which maps the behaviour of matter under different conditions and illustrates transitions between phases, often tied to changes in symmetry. The theory poses difficulties in extreme conditions, but the topic of interest in this work concerns ultrahigh-density environments.

Despite extensive efforts, the full mapping of the QCD phase diagram continues to captivate researchers because of its relevance in both theoretical and astrophysical contexts. However, significant obstacles remain to studying QCD from the first principles. Lattice QCD simulations are effective at zero and finite temperatures, but they encounter a "sign problem" at finite baryon densities. This makes it difficult to apply standard computational methods, creating a significant barrier to further progress. Ongoing research is focused on overcoming these challenges, but QCD at finite baryon densities remains one of the most formidable puzzles in modern theoretical physics.

Due to the current inability to directly simulate QCD at finite baryon density on the lattice, researchers have turned to alternative approaches by studying QCD-like theories that avoid the sign problem. This thesis casts a spotlight on understanding the dynamics of charged sectors of strongly interacting theories, at zero temperature, by studying the behaviour of the lightest particles that emerged in these systems. A key aim was to explore the mathematical structure of phase diagrams, shaped by various physical parameters involved.

Specifically, by reducing the number of colours in QCD, it became possible to rigorously describe vacuum properties and explore phenomena at high baryon densities, including phase transitions. Additionally, even though there are differences, two-colour QCD and three-colour QCD share numerous common properties. As a result, lattice simulations of two-colour QCD offer valuable insights into the behaviour of dense three-colour QCD. One such example is diquark condensation in dense matter. This thesis first focused on two-colour QCD with fundamental quarks. The theory has been presented in chapter 3 and it was emphasised that it is worth exploring since, in this case, the pseudoreality of quark fields ensures a positive fermion determinant for an even number of flavours, thus eliminating the sign problem.

This was the motivation behind chapter 4, where there was the investigation of the spectrum, the pattern of chiral symmetry breaking, and the dispersion relations at low energy of two-colour QCD as a function of the baryon chemical potential, the topological term responsible for strong CP breaking as well as the quark masses. Actually, the analysis is applicable to $Sp(2N)$ gauge groups with fermions in the fundamental representation. Moreover, chapter 4 explicitly considered the dynamics stemming from two, three, six, seven and eight light matter flavours and determined the normal and superfluid ground state. One of the main results shown is that the vacuum acquires a rich structure originating from the presence of the CP violating topological operator, revealing novel phases. The latter were analysed, as well as the dependence of the critical chemical potential on the θ-angle, delineating the boundary between the normal phase and the superfluid phase. The results are readily applicable, in the normal phase, to the θ and axion physics of composite Goldstone Higgs models. In particular, a new composite strong source of CP violation can be relevant to investigate composite electroweak baryogenesis [116, 347, 348], while non-zero chemical potential analysis is useful for studying asymmetric dark matter [116, 120, 121] and the interplay with CP violation. The main results of the chapter can guide and be tested by first-principle lattice simulations at non-zero baryon chemical potential, but also including the effects of the topological susceptibility [349, 350].

The same theory was further investigated in chapter 6 in proximity of its conformal window, where the infrared dynamics is orchestrated by the interplay of chiral symmetry breaking and conformal invariance. Precisely, asymptotically free gauge theories can achieve conformality in the infrared depending on both the number of flavours and colours whose detailed theoretical description was the heart of chapter 5. In fact, following the notions reviewed in chapter 5, the underlying dynamics was modelled via an effective approach that encapsulates the light degrees of freedom of the theory augmented by a dilaton state. Therefore, the main focus was to address the region of the theory where there is near conformality, bearing in mind that fixed-charge sectors offer novel opportunities to investigate near conformal dynamics. Therefore, to access non-perturbative information of the (near) conformal fixed baryon-charge sector of the theory it was employed the large-charge approach that has been reviewed in chapter 2. Precisely, using the state-operator correspondence it was possible to generalise the corrections determined in [94, 241] to the large-charge quasi-anomalous dimension as a function of the dilaton, fermion mass, and background geometry to include the impact of the θ-angle, axion physics, and dilaton potential. Therefore, chapter 6 studied the impact of the θ-angle and axion physics in the large-charge limit of near conformal symplectic gauge theories with fermion matter in the fundamental representation. Furthermore, the results presented in chapter 4 and in chapter 6 are valid for a number of flavours below the lower boundary of the conformal window whose value increases with the underlying number of colours of the $Sp(2N)$ gauge theory investigated there. In the large-N limit the eta-prime becomes a quasi-Goldstone boson and, therefore, validates the effective approach used. The analysis is further performed respecting the hierarchies of scales, allowing us to consider the impact of the chemical potential as a modification of the underlying pattern of chiral symmetry breaking in the vacuum.

This line of research involving the investigation of determining the leading near conformal corrections to quasi-anomalous dimensions of operators carrying fixed charge at the lower boundary of the conformal window was also extended to three-colour QCD at finite isospin in chapter 7. There again, the methodology used to tackle the challenge was the semiclassical approach of the large charge expansion. In fact, the charge works as a new tunable parameter that first enables us to access the extreme density regime of the theory and second provides precious information on the sectors responsible for breaking conformality. Once more, the result was that the near conformal contributions are proportional to those parameters responsible for dynamically deforming QCD away from the conformal window. Furthermore, chapter 7 showed the pattern of symmetry breaking, the associated physical spectrum, and their dispersion relations. These latter results helped to determine the next-to-leading-order large charge contributions.

Since the core of this work centres on ultrahigh-density environments, the exploration of this theory continues in chapter 9, where the focus shifts to other valuable EFTs that depict low-energy QCD in the non-zero isospin regime. This latter environment mirrors the extreme conditions found in neutron star cores, which serve as a natural laboratory for exploring these regimes, even though the behaviour of matter at their cores remains largely unknown. In such conditions, temperature plays a less significant role; however, understanding dense matter is crucial to filling gaps in the QCD phase diagram.

It is widely believed that nuclear matter can form non-uniform structures known as nuclear pasta and it is thought that neutron star crusts may exhibit these intriguing configurations. For this reason, in chapter 9, numerical and analytical methods have been used to perform a thorough investigation of Skyrmion solutions featuring dilatonic dynamics. Employing the dilaton-dressed chiral Lagrangian, the impact on relevant physical quantities such as the traditional Skyrmion profile, mass, and size stemming from varying the near conformal controlling parameters was addressed. What was shown is an intriguing dependence of these physical properties on the dilaton mass. A notable result is the observation of a quick dilaton decoupling when its mass exceeds that of the pion one. The decoupling is further enhanced at large values of the anomalous dimension of the chiral condensate.

Furthermore, the impact of dilatonic dynamics on Skyrmion crystals and the identification of a special parameter point was presented, linked to the case of the traditional Skyrmion above, for which the second-order differential equations also reduce to a set of first-order ones. Here another observed feature, stemming from the presence of the dilaton, is that the latter spatially separates the baryon and isospin charge distributions similarly to the spin-charge separation phenomenon. Lastly, also dilaton-modified solitonic branes were considered, and it was shown that the soliton profile is unaltered by the presence of the dilaton, while the latter acquires a homogeneous vacuum expectation value.

While a complete and comprehensive understanding of the intricacies of the theory remains elusive, this thesis has nonetheless produced results that contribute significant insights to the evolving body of knowledge. The implications of these findings prompt us to consider not only the results themselves, but also the methodologies and approaches that have guided this research and those that lie ahead. As this thesis concludes, the ideas presented herein are expected to foster further exploration. These discoveries expand the current understanding of the field while simultaneously raising the question: what additional knowledge awaits discovery in the uncharted territories of the unknown?

Goldstone theorem at finite density

A

APPENDIX

The present appendix aims to expand more on Goldstone theorem [41, 93].

As observed, spontaneous symmetry breaking occurs in various areas of physics. Consequently, it becomes interesting to explore how Goldstone theorem is implemented in these different domains. In the context of particle physics, where quantum field theory formalism is utilized, the application of the theorem proves to be rather straightforward. However, extending this understanding to many-body systems at equilibrium presents a unique challenge.

To begin this exploration, attention is directed towards QFTs at zero temperature but with the inclusion of a chemical potential. This appendix aims to investigate this particular scenario.

In statistical systems, a chemical potential can be associated with each conserved charge. The microscopic dynamics of the system are typically dictated by either a Hamiltonian or a Lagrangian, both of which may possess symmetries, thereby defining conserved quantities. Introducing a chemical potential, denoted as μ, associated with the charge Q implies that external influences act upon the statistical system, allowing for variation in the "conserved" charge Q. Consequently, one operates within the grand canonical ensemble, where μ scales the energy cost associated with varying Q.

Considering the statistical system to be in equilibrium, its thermal state is determined by the grand canonical partition function $\mathcal{Z}$

$$\mathcal{Z} = \mathrm{Tr}\{e^{-\beta(H+\mu Q)}\} \ . \tag{A.1}$$

This trace represents a summation/integration over the phase space. Hence, in the limit of zero temperature, as the inverse temperature $\beta \to 0$, the saddle-point approximation can be applied. This implies that the thermal state is governed by minimizing the quantity $\bar{H} = H + \mu Q$ and accounting for small fluctuations around this minimum.

When dealing with relativistic theories, the spontaneous symmetry phenomena are described by the Goldstone theorem. The latter, as formulated so far, does no longer apply in non-relativistic theories and this leads to a much more variegated connection between the breaking of symmetries and the low-energy spectrum of the theory. QFTs at fixed charge lay between the relativistic and non-relativistic cases. In fact, the QFT is still relativistic but its fixed charge sector breaks both spacetime and internal symmetries.

The Goldstone theorem must be generalized to fit these cases: this new version is named charged Goldstone theorem [35].

Consider a relativistic theory with a global internal and continuous symmetry group G, generated by the set Q_a, with $a = 1, ..., \dim(G)$. Assume to fix a charge Q, this introduces the non-relativistic Hamiltonian $\bar{H} = H + \mu Q$; let us indicate $\bar{G}$ the invariant subgroup of G commuting with $\bar{H}$. Assuming also that:

- The number of spontaneously broken generators of G is n, then there exist n fields ϕ_i which satisfy
$$\det\langle 0|[\phi_i(0), Q_a(t)]|0\rangle \neq 0, \quad \bar{H}|0\rangle = 0 \, .$$
- The number of of spontaneously broken generators of $\bar{G}$ is h.
- Translational invariance is not completely broken.
- The currents j_a^μ evolve in time according to H as
$$j_a^\mu(t,x) = e^{i(Ht-P\cdot x)} j_a^\mu(0,0) e^{-i(Ht-P\cdot x)} \, .$$
- G is a direct product of simple compact Lie groups.

Then, in the spectrum of the theory, there are three types of "generalized" Goldstone bosons:

- Type I: "relativistic" GBs with low-energy dispersion relations characterized by odd powers in momenta $\omega_k \sim |k|^{2s+1}, (s \in \mathbb{Z})$ and they correspond to the usual GBs appearing in the relativistic Goldstone theorem at zero charge.
- Type II: "non-relativistic" GBs with low-energy dispersion relations characterized by even powers in momenta $\omega_k \sim |k|^{2s}, (s \in \mathbb{Z})$. They appear when two broken generators Q_a and Q_b satisfy $\langle 0|[Q_a, Q_b]|0\rangle \neq 0$. In this case the corresponding GBs become canonically conjugate variables reducing the number of d.o.f.
- Type III: "gapped" GBs with dispersion relations with a non-perturbatively fixed gap $\omega_{k\to 0} = q_a\mu$, where q_a is a group-theoretical calculable factor. They appear when the broken generators do not commute with the non-relativistic Hamiltonian $\bar{H}$. The chemical potential μ acts as an explicit symmetry breaking term that leads to a mass $\propto \mu$.

In this generalized version of the Goldstone Theorem the counting rule for GBs modifies. The sum of type I and type II modes equals the number of broken generators of $\bar{G}$:

$$n_I + 2n_{II} = h$$

where the type II count double for what have been said about the effective number of d.o.f.

Being $\{\bar{Q}_a\}$ the subset of $\{Q_a\}$ which generates $\bar{G}$, the numbers of type II and type III are given by:

$$n_{II} = \frac{1}{2}p, \qquad p = rank(\bar{\rho}), \qquad (\bar{\rho})_{ab} = \langle 0|[\bar{Q}_a, \bar{Q}_b]|0\rangle \, ,$$

$$n_{III} = \frac{1}{2}(rank(\rho) - p), \qquad\qquad (\rho)_{ab} = \langle 0|[Q_a, Q_b]|0\rangle \,.$$

H.B. Nielsen and S.Chadha provided the partial result $n_I + 2n_{II} \geq h$ in their paper [351]. The equality is a later improvement given by H. Watanabe and H. Murayama in [352], following Leutwylers works [353, 354].

Large charge expansion in perturbative theories

B

Appendix

The materials reviewed in this appendix are mainly based on [74, 75].

Let us start by an important distinction stressed by the authors. Generally, the classification of quantum systems is based on their corresponding path integrals, which depend on dynamics, boundary conditions, and operator insertions. One distinguishes in between weakly coupled and strongly coupled path integrals. Precisely, the former allow approximation via a loop expansion around a classical trajectory while the latter lack a saddle point approximation, making all observables inherently quantum mechanical.

Nevertheless, in weakly coupled QFTs, perturbation theory becomes inadequate as the number of process legs increases. Despite investigations in [355], progress was hindered by technical and conceptual challenges. However, when focusing on a simpler problem within $U(1)$-invariant scalar QFT, it was shown in [88] how to examine the scaling dimension of the charge-n operator at the Wilson-Fisher fixed point. Precisely, the EFT approach discussed in chapter 2 is well-suited for addressing strongly-coupled systems where small parameters other than $\frac{1}{\bar{Q}}$ are absent. Conversely, when a theory includes a perturbative parameter λ, one can bypass EFT construction and operate within the full theory. The large charge expansion resembles a *'t Hooft-like expansion*, where a 't Hooft coupling $\mathcal{A} = \lambda_* \bar{Q}$ is introduced, and the limit $\lambda \to 0$ and $\bar{Q} \to \infty$ with $\mathcal{A}$ fixed is considered. Therefore, in this appendix the focus is on the large charge expansion in perturbative theories.

Scaling dimensions can be computed in perturbation theory using the standard diagrammatic loop-expansion technique. Here, it is shown how this expansion can be reorganized when dealing with operators exhibiting large charges. Specifically, a significant conceptual finding is presented: the scaling dimension $\Delta_{\phi^{\bar{Q}}}$ of an operator can be determined through a systematic expansion around a non-trivial trajectory. This expansion yields

$$\Delta_{\phi^{\bar{Q}}} = \frac{1}{\lambda_*}\Delta_{-1}(\lambda_*\bar{Q}) + \Delta_0(\lambda_*\bar{Q}) + \lambda_*\Delta_1(\lambda_*\bar{Q}) + \dots \ . \tag{B.1}$$

To delve into the details of this result, the next section will unveil the games for the $U(1)$ theory with quartic interactions in $d = 4 - \epsilon$ dimensions.

§ B.1 Semiclassics for the U(1) model

Let us consider a $U(1)$ theory with quartic interactions in $d = 4 - \epsilon$ dimensions at the Wilson-Fisher fixed point to ensure the conformal invariance and show how it is possible to compute the scaling dimension Δ_{ϕ^n} for the large charge operator ϕ^n. The computation will be done in the double limit

$$\lambda_0 \to 0 \ ; \ \lambda_0 n = \text{const} \ . \tag{B.2}$$

Having the above hypothesis in mind, consider the theory

$$\mathcal{L} = \partial\bar{\phi}\partial\phi + \frac{\lambda_0}{4}(\bar{\phi}\phi)^2 \tag{B.3}$$

whose β-function, up to two-loops corrections, gets the form

$$\beta(\lambda) = -\epsilon\lambda + 5\frac{\lambda^2}{(4\pi)^2} - 15\frac{\lambda^3}{(4\pi)^4} + O\left(\lambda^4\right) \tag{B.4}$$

which means that the theory admits a fixed point in

$$\frac{\lambda_*}{(4\pi)^2} = \frac{\epsilon}{5} + \frac{3}{25}\epsilon^2 + O\left(\epsilon^3\right) , \tag{B.5}$$

where the fixed point depends on the dimensionality, so the theory is weakly coupled for $\epsilon \ll 1$. Let $[\phi^n]$ be the renormalised field and Z_ϕ the renormalisation factor of the field

$$\phi^n = Z_{\phi^n}[\phi^n] \quad \text{and} \quad \lambda_0 = \Lambda^\epsilon\ \lambda Z_\lambda \quad \text{with} \quad \Lambda \quad \text{the sliding scale} \tag{B.6}$$

the anomalous dimension γ_{ϕ^n} is then given by

$$\gamma_{\phi^n} = \frac{\partial \log\left(Z_{\phi^n}\right)}{\partial\lambda}\beta(\lambda) \ . \tag{B.7}$$

Solving the Callan-Symanzik equation, one can show that the operator's physical dimension at the fixed point is

$$\Delta_{\phi^n} = n\left(\frac{d}{2} - 1\right) + \gamma_{\phi^n}(\lambda_*) \ . \tag{B.8}$$

Clearly, the anomalous dimension is scheme-dependent but it becomes an observable at the Wilson-Fisher fixed point where there is scale invariance. A first attempt to calculate the scaling dimension could therefore involve the perturbations theory to obtain γ. Such calculation can be performed in two ways, both perturbative and divergent as n grows even when λ is small.

A way to compute it is to work directly on the correlation function and computing it via a semiclassical expansion on the path integral around a non-trivial trajectory. As mentioned before, perturbation theory breaks down at large n. Therefore, the next move is to search for and then implement a calculation scheme that naturally allows to perform the limit with large n, not only when λn is small, but even when λn grows. To this aim, let us focus directly on the correlation function

$$\langle \bar{\phi}^n(x_f)\phi^n(x_i)\rangle = \frac{\int \mathcal{D}\bar{\phi}\mathcal{D}\phi \; \bar{\phi}^n(x_f)\phi^n(x_i)\, e^{-\int \mathcal{L}}}{\int \mathcal{D}\bar{\phi}\mathcal{D}\phi \; e^{-\int \mathcal{L}}} \equiv Z^2_{\phi^n}\langle [\bar{\phi}^n](x_f)[\phi^n](x_i)\rangle \,. \tag{B.9}$$

The above integral can be re-cast as follows

$$\phi \to \frac{\phi}{\sqrt{\lambda_0}} \;\; ; \;\; -\int \mathcal{L} \to -\frac{1}{\lambda_0}\int \mathcal{L} \tag{B.10}$$

so that

$$Z^2_{\phi^n}\,\lambda_0^n\,\langle [\bar{\phi}^n](x_f)[\phi^n](x_i)\rangle = \frac{\int \mathcal{D}\bar{\phi}\mathcal{D}\phi \; e^{\left[-\frac{1}{\lambda_0}\int \partial\bar{\phi}\partial\phi + \frac{1}{4}(\bar{\phi}\phi)^2 - \lambda_0 n(\log\bar{\phi}(x_f) + \log\phi(x_i))\right]}}{\int \mathcal{D}\bar{\phi}\mathcal{D}\phi \; e^{\left[-\frac{1}{\lambda_0}\int \partial\bar{\phi}\partial\phi + \frac{1}{4}(\bar{\phi}\phi)^2\right]}} \,. \tag{B.11}$$

The path integral in the denominator can be computed by the saddle point expansion around the minima $\phi = \bar{\phi} = 0$, while the one in the numerator is stationary around non-trivial values of the fields $\phi, \bar{\phi} \neq 0$ due to the insertions (which spontaneously breaks the $U(1)$ symmetry so that the minimal value is no longer zero). The most general form for the whole path-integral is

$$Z^2_{\phi^n}\,\lambda_0^n\,\langle [\bar{\phi}^n](x_f)[\phi^n](x_i)\rangle = {\lambda_0}^n\; n!\; e^{\frac{1}{\lambda_0}\Gamma_{-1}(\lambda_0 n, x_{fi}) + \Gamma_0(\lambda_0 n, x_{fi}) + \lambda_0\Gamma_1(\lambda_0 n, x_{fi}) + \ldots} \tag{B.12}$$

The Γ coefficients will have a finite and a divergent part, namely Γ_K^{div} and Γ_K^{ren}

$$\lambda_0^k\;\Gamma_k(\lambda_0 n, x_{fi}) = \lambda^k\;\Gamma_k^{\text{div}}(\lambda n, \lambda) + \lambda^k\;\Gamma_k^{\text{ren}}(\lambda n, \lambda, x_{fi}, \Lambda) \quad \text{with} \quad \lambda \equiv \lambda(\Lambda) \tag{B.13}$$

then

$$Z^2_{\phi^n} = e^{\sum_{k=-1}\lambda^k\;\Gamma_k^{\text{div}}(\lambda n,\lambda)} \equiv e^{\sum_{k=-1}\lambda^k\;\bar{\Gamma}_k^{\text{div}}(\lambda n)} \tag{B.14}$$

so that

$$\langle [\bar{\phi}^n](x_f)[\phi^n](x_i)\rangle \equiv n! e^{\sum_{k=-1}\lambda^k\;\bar{\Gamma}_k^{\text{ren}}(\lambda n, x_{fi}, \Lambda)} \,. \tag{B.15}$$

The advantage to work on fixed point is that one can exploit the power of conformal invariance. First of all, following discussion in chapter 1, one shall map the theory from the plane to the cylinder in order to map the eigenvalues of the Dilation D into the eigenvalues of H_{cyl}, the energy spectrum on the cylinder.

Before moving on with the computation on the cylinder, let us conclude here with an intuitive discussion about the general form of the result that one can expect. The goal is to compute the scaling dimension of the simplest $U(1)$ operator, ϕ^n, by inspecting some peculiar Feynman diagrams appearing with it one can make useful realizations. Precisely, the Feynman diagrams can be classified according to their leading n-scaling and loop order l (see Figure B.1).

For example, the so-called *single petal diagram* scales as n^2 and all the other come out

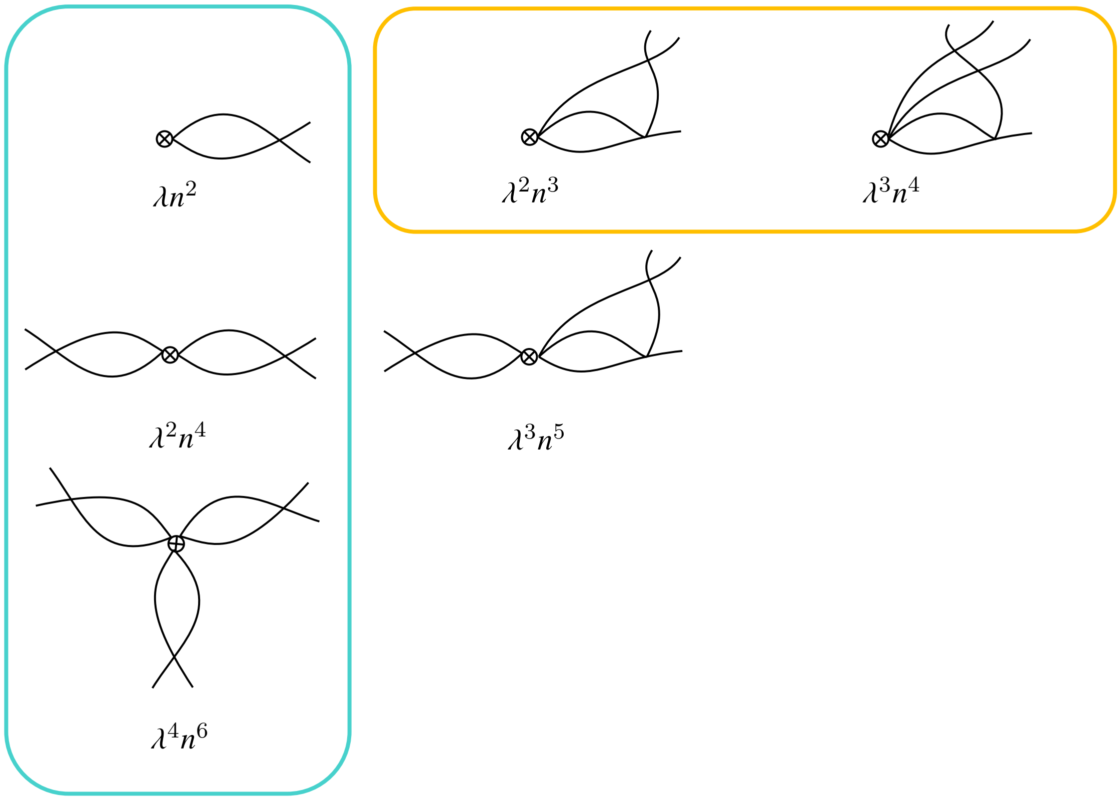

Figure B.1.: Some peculiar Feynman diagrams appearing in ϕ^n: in light blue the *daisy diagrams*, in dark yellow the *connected diagrams*. The first on top left is called *single petal diagram*.

just from a combinatorial count. In fact, the combinatorial factor is proportional to

$$\frac{n!}{(n-k)!} \tag{B.16}$$

with k being the number of external legs. Therefore at large n it is justified to use

$$\frac{n!}{(n-k)!} \sim n^k \tag{B.17}$$

which means that the leading n-scaling of a given diagram is indeed given by the number of external legs k and the loop order is clearly given by the number of vertices. Hence, at any $l \ll n$ the contributions to Z_{ϕ^n} scale like $\lambda^l n^{2l}$ (daisy diagrams) or like $\lambda^l n^{l+1}$ (connected diagrams). Additionally, one can observe that all the daisy diagrams for example are obtained from exponentiation of the single petal diagram. This can actually be generalised to all the diagrams: at any given loop, the terms having the highest powers of n are obtained from exponentiation from lower loops. As a result, the leading contribution appearing in (B.7) scales like $\lambda^l n^{l+1}$:

$$\gamma_{\phi^n} = n \sum_{l=1} \lambda^l P_l(n) = n \sum_{k=0} \lambda^k F_k(\lambda n) \,, \tag{B.18}$$

where P_l a polynomial of degree l, showing that when λn is highly enough the perturbation theory fails. Equation (B.18) is proven by (B.14) and (B.15). In this context, the terms $\bar{\Gamma}_{-1}^{\text{ren/div}}$ represent the $(k+1)$-loop correction to the saddle point approximation. Specifically, they denote the leading semiclassical contributions, corresponding to the exponent at the saddle point. By virtue of the previous arguments, these quantities completely determine the leading-n contribution $F_0(\lambda n)$, thereby summing the dominant powers of n across arbitrarily high loop orders in the standard diagrammatic approach.

B.1.1 **On the cylinder**

Throughout this subsection, the notation and conventions will be the same as those adopted in section 1.3. The action on the cylinder reads

$$S_{cyl} = \int d^d x \sqrt{g}\big[g^{\mu\nu}\partial_\mu\bar{\phi}\partial_\nu\phi + m^2\bar{\phi}\phi + \frac{\lambda_0}{4}(\bar{\phi}\phi)^2\big] \tag{B.19}$$

The mass term arises from the request of conformal invariance which can be gained just by coupling the field to the Ricci's scalar into a quadratic term as $\mathcal{R}(g)\bar{\phi}\phi$, therefore the m mass is just a rewriting of $m^2 = (\frac{d-2}{2R})^2$. As said before, the theory on the cylinder is fully equivalent to the one on flat space by the correspondence

$$\langle O^\dagger(x_f)O(x_i)\rangle_{cyl} = \left|x_f\right|^\Delta |x_i|^\Delta \langle O^\dagger(x_f)O(x_i)\rangle_{flat} \; . \tag{B.20}$$

Computing the limit for $x_i \to 0$ corresponding to $\tau_i \to -\infty$, one gets

$$\langle O^\dagger(x_f)O(x_i)\rangle_{cyl} \overset{\tau_i \to -\infty}{=} e^{-E_O(t_f - t_i)} \; , \tag{B.21}$$

where $E_O = \frac{\Delta_O}{R}$. Let us recall again that the previous equations can be read as follows making use of the state/operator correspondence: the action of O at $-\infty$ creates a state of energy E_O that carries all the quantum numbers of the operator. Consequently, the same expression can be obtained by replacing O with ϕ^n (let be $t_{f,i} = \pm T/2$)

$$\langle\bar{\phi}(x_f)\phi(x_i)\rangle = \mathcal{N} e^{-E_{\phi^n} T} \tag{B.22}$$

where the $\mathcal{N}$ coefficient is T-independent and divergent. The structure of the two-point function will have the form of the (B.12). Let us recall that the exponent of (B.12) has the form $\lambda_0^k \Gamma_k$, where each Γ_k has a finite and a divergent part. Hence, by comparison with (B.22) one can deduce that the divergent part of the Γ will be T-independent and will fix the $\mathcal{N}$ coefficient, while the finite part will necessary depend on T.

Similarly to the expression $\langle[\bar{\phi}^n(x_f)][\phi^n(x_i)]\rangle = n! e^{\sum \lambda_k \Gamma_k^{ren}}$, one can thus write

$$RE_{\phi^n} = \frac{1}{\lambda_0} e_{-1}(\lambda_0 n, d) + e_0(\lambda_0 n, d) + \lambda_0 e_1(\lambda_0 n, d) + \dots \tag{B.23}$$

$$= \frac{1}{\lambda}\bar{e}_{-1}(\lambda n, R\Lambda, d) + \bar{e}_0(\lambda n, R\Lambda, d) + \lambda \bar{e}_1(\lambda n, R\Lambda, d) + \dots \tag{B.24}$$

where the $\bar{e}_i$ coefficients are analogous with the e_i but renormalized and therefore they depend on a sliding scale, namely Λ. Thus, if the coupling is evaluated at the fixed point $\lambda = \lambda_*$, the dependence on such a scale must disappear by scale invariance giving a result of the form:

$$\Delta_{\phi^n} = \frac{1}{\lambda_*}\Delta_{-1}(\lambda_* n) + \Delta_0(\lambda_* n) + \lambda_* \Delta_1(\lambda_* n) \ldots \, . \tag{B.25}$$

The θ-angle and the Strong CP problem

C

Appendix

This appendix, mainly based on [28, 260, 266, 356, 357], serves as an introduction to the strong *CP* problem and for the both physical and mathematical contents used in chapter 4, chapter 6 and chapter 7.

§ C.1 The Vacuum structure for non-Abelian Gauge Theories

The perturbative approach typical of QFT has proved to be an essential tool for the explicit calculation of cross sections and decay rates in Particle Physics. However, there are non-perturbative aspects of QFT which can be investigated through semiclassical methods. These semiclassical approaches can be applied to the analysis of special configurations for fields which, providing a non-trivial topology to non-abelian gauge theories, require the existence of the so-called topological transitions, leading to the interesting branch of Topological Quantum Field Theory (TQFT). Among all the classes of special configurations for fields, it is worth mentioning that of solitons, instantons and sphalerons, which could imply important physical consequences. Despite the many common features of these classes, they are very different in their applications: while solitons are static objects like monopoles and vortices, instantons are dynamical events in the euclidean spacetime. Sphalerons are related to possible violations of fermionic quantum numbers as the baryon and lepton numbers, fundamental ingredients for the process of baryogenesis via leptogenesis [356].

Going into the details of all these topics would require an interesting but also too long dissertation. For what it is here concerned, it is sufficient to know that the vacuum structure for a non-abelian gauge theory consists of a countably infinite of homotopy classes of vacua. Each one is characterized by a winding number, also known as Chern-Simons number; a single representative of each class is called a Chern-Simons vacuum.

Vacua belonging to the same class are considered equivalent and are connected by a small gauge transformation; vacua belonging to different classes are connected by a large gauge transformation. It can be demonstrated that instantons constitute an example of large gauge transformations.

Considering the path integral formulation of a generic Yang-Mills theory $SU(N)$, one can perform a semiclassical expansion in $\hbar$ of the action: the leading term is the classical action $\mathcal{S}_E$, while the other terms are quantum corrections. Instantons correspond to the dominant solutions of the classical action. Their name is due to the fact that, as classical solutions, they must be localized event in the euclidean spacetime (obtained through a Wick rotation). They are topological transitions carrying a topological charge, corresponding to the difference between the Chern-Simons numbers of the connected classes.

The topological charge is defined trough the quantity:

$$Q = -\frac{g^2}{16\pi^2}\int d^4x \,\mathrm{Tr}\{F_{\mu\nu}\tilde{F}^{\mu\nu}\} = \frac{g^2}{32\pi^2}\int d^4x \, F^a_{\mu\nu}\tilde{F}^{\mu\nu}_a \tag{C.1}$$

where $F_{\mu\nu}$ is the usual strength tensor and $\tilde{F}^{\mu\nu} = \frac{1}{2}\epsilon_{\mu\nu\rho\sigma}F^{\rho\sigma}$ is its dual tensor [28]. The topological charge possesses a different nature respect to the usual Noether charges, because its existence is not a consequence of a symmetry in the Lagrangian. However, it exists a topological conservation law: it deals with the fact that the space of fields' configurations at finite $\mathcal{S}_E$ in which instantons live, is made up of disconnected components, each one characterized by a precise value for the topological charge.

To proceed, let us define the vacuum for such a theory. To this aim, indicate with $|n\rangle$ a certain vacuum state belonging to a certain homotopy class. Through an instanton is possible to move from this vacuum to another one characterized by a different winding number. In doing so, the initial vacuum would have an overlap with a different vacuum. The conclusion is that a single Chern-Simons vacuum would not be a well-defined vacuum configuration because it is not unique.

If one defines the true vacuum as the superposition of all possible Chern-Simons vacua, namely [356]

$$|\theta\rangle = \sum_{n=-\infty}^{+\infty} e^{-in\theta}|n\rangle\,, \tag{C.2}$$

the result is that any instantonic topological transition would transform the vacuum in the vacuum itself, satisfying the uniqueness requirement.

In fact, supposing to have another $|\theta'\rangle$ vacuum, it is possible show that

$$\langle\theta'|e^{-iHt}|\theta\rangle = \delta(\theta-\theta')I(\theta)\;. \tag{C.3}$$

Then, using the definition of vacuum, one has

$$\begin{aligned}
\langle\theta'|e^{-iHt}|\theta\rangle &= \sum_{m,n} e^{im\theta'}e^{-in\theta}\langle m|e^{-iHt}|n\rangle \\
&= \sum_{m,n} e^{-i(n-m)\theta}e^{im(\theta'-\theta)}\int [\mathcal{D}A]_{n-m}\, e^{-\frac{i}{\hbar}\int d^4x\mathcal{L}} \\
&= \delta(\theta'-\theta)\sum_{m,n} e^{-iQ\theta}\int [\mathcal{D}A]_{n-m}\, e^{-\frac{i}{\hbar}\int d^4x\mathcal{L}} = \delta(\theta-\theta')I(\theta)\,.
\end{aligned}$$

Remembering the definition of the topological charge and using the notation $\nu = n - m$ one obtains

$$I(\theta) = \sum_\nu \int [\mathcal{D}A]_\nu \, e^{-\frac{i}{\hbar}\int d^4x \mathcal{L}} e^{i\theta \frac{g^2}{16\pi^2}\int d^4x \, \mathrm{Tr}\{F_{\mu\nu}\tilde{F}^{\mu\nu}\}}$$

$$= \sum_\nu \int [\mathcal{D}A]_\nu \, e^{-\frac{i}{\hbar}\int d^4x \left[\mathcal{L} - \frac{\theta g^2}{16\pi^2}\mathrm{Tr}\{F_{\mu\nu}\tilde{F}^{\mu\nu}\}\right]} = \sum_\nu \int [\mathcal{D}A]_\nu \, e^{-\frac{i}{\hbar}\int d^4x \mathcal{L}_{\mathrm{eff}}}$$

where

$$\mathcal{L}_{\mathrm{eff}} = \mathcal{L} - \frac{\theta g^2}{16\pi^2}\mathrm{Tr}\{F_{\mu\nu}\tilde{F}^{\mu\nu}\} = -\frac{1}{4}F^a_{\mu\nu}F^{\mu\nu}_a - \theta q(x) \,. \tag{C.4}$$

being $q(x)$ the topological charge density. As a result, a topological term, whose coefficient is an angle, the θ-angle, appears as a direct consequence of the non triviality of vacuum topology. For this reason, when dealing with Yang-Mills theory one needs always to consider the topological sector represented by the topological charge multiplied by the θ angle.

From the mathematical point of view, this term is a renormalizable factor of dimension 4, it does not affect the dynamics being a volume term. As a building feature of the theory itself, there is no reason to neglect it. However, it is the cause of an unresolved issue related to CP invariance: it is a pseudoscalar CP odd. In QCD its presence presumes CP violations in processes driven by strong interactions. By the way, none of such violating interactions has never been observed. The topological term may be neglected only if $\theta = 0$ exactly, or better $\bar{\theta} = 0$ exactly, as will be specified soon. This conclusion has not been proved theoretically so far: there should be some physical reason, like a symmetry, for which one could affirm that. Experimentally, as observed from the measurements of the neutron electric dipole moment, the upper limit for its value is really small [266] (and references therein):

$$(\bar{\theta}_{QCD} < 10^{-10}) \,.$$

This fine tuning problem, known as strong CP problem, is still open. This brief review on the vacuum structure for non-abelian gauge theories can be deepened following [358–360].

A few basic concepts about the r-forms language [361], widely used in TQFT, are sufficient to understand the deep difference between the kinetic and the topological terms in the Yang-Mills Lagrangian. In fact, one can show that, in this intrinsic formalism:

$$\mathcal{L}^{vol}_{YM} = \mathcal{L}_{YM}\Omega = -\frac{1}{2}\mathrm{Tr}\{F \wedge \star F\} \tag{C.5}$$

where $\star$ is the Hodge operator and Ω is the invariant volume element. A differential form of order r or an r-form is a totally anti-symmetric tensor of type $(0, r)$. If $\Omega^r_p(M)$ defines the set of r-forms at $p \in M$, an element $\omega \in \Omega^r_p(M)$ is expanded as

$$\omega = \frac{1}{r!}\omega_{\mu_1\mu_2\ldots\mu_r} dx^{\mu_1} \wedge dx^{\mu_2} \wedge \ldots \wedge dx^{\mu_r} \tag{C.6}$$

where the wedge product $\wedge$ is a totally anti-symmetric tensor product.

The Hodge operator is a map

$$\star : \Omega^r(M) \to \Omega^{m-r}(M) \tag{C.7}$$

acting on a generic r-form ω in this way:

$$\star\omega = \frac{\sqrt{|g|}}{r!(m-r)!}\omega_{\mu_1\mu_2\ldots\mu_r}\epsilon^{\mu_1\mu_2\ldots\mu_r}_{\nu_{r+1}\ldots\nu_m}dx^{\nu_{r+1}} \wedge \ldots \wedge dx^{\nu_m} \ . \tag{C.8}$$

The gauge potential is a Lie algebra-valued connection 1-form

$$A = A^a_\mu dx^\mu \tau_a \quad \in \ \Omega^1(M) \otimes \mathfrak{g} \tag{C.9}$$

where τ_a are the $SU(N)$ generators that satisfy the Lie algebra $[\tau_a, \tau_b] = if_{abc}\tau^c$. The field strength tensor is a Lie algebra-valued curvature 2-form

$$F = \mathrm{D}A \quad \in \ \Omega^2(M) \otimes \mathfrak{g} \tag{C.10}$$

where D is the covariant derivative $\mathrm{D} = \mathrm{d} - igA$ with $d : \Omega^r(M) \to \Omega^{r+1}(M)$ is the external derivative.
In this language, it is possible to show that the standard kinetic term can be written as

$$F_{\mu\nu}F^{\mu\nu} \quad \propto \quad F \wedge \star F$$

while the topological term is

$$F_{\mu\nu}\tilde{F}^{\mu\nu} \quad \propto \quad F \wedge F$$

without the Hodge operator.

In fact, as one can naively affirm that "topology is geometry minus length and angle", is immediate to understand why the term $\propto F \wedge F$ is called "topological". While the kinetic term, constructed with the Hodge operator depends on the metric, the topological term, without "feeling" the metric at all gives only border contributions.

To end this section, let us demonstrate that the term $\mathrm{Tr}\{F_{\mu\nu}\tilde{F}^{\mu\nu}\}$ is indeed a volume term: it is the 4-divergence of the so-called Chern-Simons 4-current.

Since the trace implicitly takes into account the sum over the $SU(N)$ algebra indexes, one can dirgard them in the calculation below.

To begin with, let us derive the non-abelian expression for $F_{\mu\nu}$. Being A_μ the gauge field and τ_a the generators of the algebra:

$$[A_\mu, A_\nu] = [A^a_\mu\tau_a, A^b_\nu\tau_b] = A^a_\mu A^b_\nu[\tau_a, \tau_b] = if_{abc}A^a_\mu A^b_\nu\tau_c \tag{C.11}$$

$$\begin{aligned} F_{\mu\nu} = F^k_{\mu\nu}\tau_k &= (\partial_\mu A^k_\nu - \partial_\nu A^k_\mu + gf^k_{ij}A^i_\mu A^j_\nu)\tau_k = \\ &= \partial_\mu A_\nu - \partial_\nu A_\mu + gf^k_{ij}A^i_\mu A^j_\nu = \\ &= \partial_\mu A_\nu - \partial_\nu A_\mu - ig[A_\mu, A_\nu] \,. \end{aligned} \tag{C.12}$$

Thus, substituting in the topological term, one obtains

$$\begin{aligned}
\mathrm{Tr}\{F_{\mu\nu}\tilde{F}^{\mu\nu}\} &= \frac{1}{2}\epsilon^{\mu\nu\rho\sigma}\mathrm{Tr}\{F_{\mu\nu}F_{\rho\sigma}\} = \\
&= \frac{1}{2}\epsilon^{\mu\nu\rho\sigma}tr(\partial_\mu A_\nu - \partial_\nu A_\mu - ig[A_\mu, A_\nu])(\partial_\rho A_\sigma - \partial_\sigma A_\rho - ig[A_\rho, A_\sigma]) = \\
&= \frac{1}{2}\epsilon^{\mu\nu\rho\sigma}tr(\partial_\mu A_\nu\partial_\rho A_\sigma - \partial_\mu A_\nu\partial_\sigma A_\rho - ig\partial_\mu A_\nu[A_\rho, A_\sigma] - \partial_\nu A_\mu\partial_\rho A_\sigma + \\
&\quad \partial_\nu A_\mu\partial_\sigma A_\rho + ig\partial_\nu A_\mu[A_\rho, A_\sigma] - ig[A_\mu, A_\nu]\partial_\rho A_\sigma + ig[A_\mu, A_\nu]\partial_\sigma A_\rho + \\
&\quad - g^2[A_\mu, A_\nu][A_\rho, A_\sigma]) = \\
&= \frac{1}{2}\epsilon^{\mu\nu\rho\sigma}tr(4\partial_\mu A_\nu\partial_\rho A_\sigma - 4ig\partial_\mu A_\nu[A_\rho, A_\sigma] - g^2[A_\mu, A_\nu][A_\rho, A_\sigma]) = \\
&= 2\epsilon^{\mu\nu\rho\sigma}tr(\partial_\mu A_\nu\partial_\rho A_\sigma - ig\partial_\mu A_\nu[A_\rho, A_\sigma]) = \\
&= 2\epsilon^{\mu\nu\rho\sigma}tr(\partial_\mu(A_\nu\partial_\rho A_\sigma) - A_\nu\partial_\mu\partial_\rho A_\sigma - ig\partial_\mu A_\nu[A_\rho, A_\sigma]) = \\
&= 2\epsilon^{\mu\nu\rho\sigma}tr(\partial_\mu(A_\nu\partial_\rho A_\sigma) - ig\partial_\mu A_\nu[A_\rho, A_\sigma]) = \\
&= 2\epsilon^{\mu\nu\rho\sigma}tr(\partial_\mu(A_\nu\partial_\rho A_\sigma) - \frac{ig}{3}\partial_\mu(A_\nu[A_\rho, A_\sigma])) = \\
&= \partial_\mu(2\epsilon^{\mu\nu\rho\sigma}tr(A_\nu\partial_\rho A_\sigma - \frac{ig}{3}A_\nu[A_\rho, A_\sigma]) = \\
&= \partial_\mu(2\epsilon^{\mu\nu\rho\sigma}A^a_\nu(\partial_\rho A^a_\sigma - \frac{ig}{3}[A^a_\rho, A^a_\sigma]) = \\
&= \partial_\mu(2\epsilon^{\mu\nu\rho\sigma}A^a_\nu(\partial_\rho A^a_\sigma + \frac{g}{3}f_{abc}A^b_\rho A^c_\sigma))\,.
\end{aligned}$$

In conclusion

$$\mathrm{Tr}\{F_{\mu\nu}\tilde{F}^{\mu\nu}\} = \partial_\mu K^\mu \tag{C.13}$$

where one identifies (up to a factor) the Chern-Simons current as

$$K^\mu = 2\epsilon^{\mu\nu\rho\sigma}A^a_\nu(\partial_\rho A^a_\sigma + \frac{g}{3}f_{abc}A^b_\rho A^c_\sigma)\,. \tag{C.14}$$

§ C.2 The physics of the θ-angle

To study the physics of the QCD θ-term, it is convenient to use an effective approach at low energies. The QCD Lagrangian with N_f massless quark flavours possesses, at the classical level, a $U(N_f)_L \times U(N_f)_R$ chiral symmetry that spontaneously breaks to the diagonal vectorial subgroup $U(N_f)_V$. According to the Goldstone theorem, massless pseudoscalar Goldstone bosons appear. In the real world, however, even the light quarks are not actually massless, but they are considered light enough with respect to the intrinsic infrared QCD scale Λ_{QCD}. At low energy, these pseudoscalar bosons are described by the following phenomenological chiral Lagrangian [266, 357]

$$\mathcal{L}_{\text{eff}} = \frac{1}{2}Tr[\partial_\mu\Sigma\partial^\mu\Sigma^\dagger)] + \frac{F_\pi}{2\sqrt{2}}Tr[M(\Sigma + \Sigma^\dagger)] \tag{C.15}$$

whose mass matrix is diagonal and given by:

$$M_{ij} = m_i^2\delta_{ij}\,. \tag{C.16}$$

The chiral symmetry is spontaneously broken by imposing that the mesons' field satisfies the constrain

$$\Sigma\Sigma^\dagger = \frac{F_\pi^2}{2} \tag{C.17}$$

which implies

$$\Sigma(x) = \frac{F_\pi}{\sqrt{2}} e^{i\sqrt{2}\frac{\Phi(x)}{F_\pi}} , \qquad \Phi = \Pi^a T^a + \frac{S}{\sqrt{N_f}} . \tag{C.18}$$

The Π^a contains the GBs' fields, the T^a are the generators of $SU(N_f)$ and F_π is the pion decay constant $\sim$ 93MeV. The S-particle field derives from the SSB of the $U(1)_A$ symmetry and will be discussed in the next section.

Let us now discuss the possible consequences of a non-zero value for θ. The Lagrangian above is invariant under the symmetry $U(1)_A$, which is known to be anomalous. For taking care of this anomaly one can add, at this effective level, terms containing the topological charge density $q(x)$, considered as a background field (here, there is no care about its dynamics). It is possible to demonstrate [260, 266] that, when taking the limit of large number of colours N, it is sufficient to add only a quadratic term in $q(x)$, since higher powers are suppressed in this limit. Precisely, under the assumption that QCD exhibits, in the large N limit, both confinement and chiral symmetry breaking [260,261], one arrives at the following Lagrangian

$$\begin{aligned}\mathcal{L}_{\text{eff}} = \frac{1}{2}\mathrm{Tr}\{\partial_\mu\Sigma\partial^\mu\Sigma^\dagger)\} + \frac{F_\pi}{2\sqrt{2}}\mathrm{Tr}\{M(\Sigma+\Sigma^\dagger)\}+ \\ + \frac{i}{2}q(x)\mathrm{Tr}\left\{\log\frac{\Sigma}{\Sigma^\dagger}\right\} + \frac{q(x)^2}{aF_\pi^2} - \theta q(x)\end{aligned} \tag{C.19}$$

which is the simplest Lagrangian at the leading order in the number of colors, leading order in the quark masses and spacetime derivatives that reproduces the underlying axial anomaly; it moreover contains the topological sector.

To expand the theory around the correct vacuum state, one has to find the field configuration $\langle\Sigma\rangle$ which minimizes the energy. From the fact that $\Sigma\Sigma^\dagger = \frac{F_\pi^2}{2}$ then

$$\left\langle\Sigma_{ij}\right\rangle = e^{-i\alpha_i}\delta_{ij}\frac{F_\pi}{\sqrt{2}} \tag{C.20}$$

where the angles α_i related to every single GB are called Witten's angles and are determined by the equations of motion. To explicit the dependence on these angles, the entire theory can be rewritten in terms of a new matrix

$$\Sigma_{ij} = e^{-i\alpha_i}\mathcal{V}_{ij} , \quad \left\langle\mathcal{V}_{ij}\right\rangle = \frac{F_\pi}{\sqrt{2}}\delta_{ij} . \tag{C.21}$$

It is possible to directly verify that the condition of energy minimization is

$$m_i^2 \sin\alpha_i = a\Big(\theta - \sum_{i=1}^{N_f}\alpha_i\Big) . \tag{C.22}$$

Consequently:

- By expliciting the matrix Φ which contains the GB fields, one obtains a mass term for the S-particle: $M_S^2 = aN_f$ even if $M \to 0$.
- The conservation or violation of the CP symmetry depends on the quantity $\theta - \sum_{i=1}^{N_f} \alpha_i = \bar{\theta}$:

in the case $N_f = 3$, the conditions for the CP conservation are:

- $\alpha_i = 0 \quad \forall i \;\to\; \theta = 0$ (Mod 2π).
- One boson is massless $m_j^2 = 0\,,\; \alpha_j \neq 0\,,\; \alpha_{i\neq j} = 0 \quad \to \quad \theta = \alpha_j$ $\to \quad \theta$ can be "rotated away" due to the $U(1)$ invariance. In fact, the corresponding j-field can be exactly rotated of $e^{-i\alpha_j}$. This option is excluded experimentally.
- All GBs are massive and this implies that: $\sin\alpha_i = 0 \to \alpha_i = 0, \pm\pi \quad \forall i$ $\to \quad \theta = \sum \alpha_i = 0, \pm\pi$ (Mod 2π) .

§ C.3 The U(1) problem and the S-particle's mass

The classical global symmetry group in the chiral limit, previously mentioned, being

$$U_L(N_f) \times U_R(N_f) \sim SU_L(N_f) \times SU_R(N_f) \times U_L(1) \times U_R(1)$$

can also be written as

$$U_L(N_f) \times U_R(N_f) \sim SU_V(N_f) \times SU_A(N_f) \times U_V(1) \times U_A(1)\ .$$

Vector symmetries constitute the subset

$$SU(N_f)_V \times U(1)_V$$

while $SU(N_f)_A$ is defined as

$$SU(N_f)_A = SU(N_f)_L \times SU(N_f)_R / SU(N_f)_V$$

and it is conventionally called "axial symmetry group", though it is merely a coset. All of these classical symmetries, except $U(1)_V$, are explicitly broken by the quark masses. In fact

$$\partial_\mu J^\mu = 0 \tag{C.23}$$

$$\partial_\mu J_5^\mu = 2i \sum_f^{N_f} m_f \bar{\psi}_f \gamma_5 \psi_f \tag{C.24}$$

$$\partial_\mu V_a^\mu = i \sum_{i,j}^{N_f} (m_i - m_j) \bar{\psi}_i (T_a)_{ij} \psi_j \tag{C.25}$$

$$\partial_\mu A_a^\mu = i \sum_{i,j}^{N_f} (m_i + m_j) \bar{\psi}_i \gamma_5 (T_a)_{ij} \psi_j \tag{C.26}$$

The current associated to $SU(N_f)_V$ is conserved if there is degeneracy between the flavours (isospin or Gell-Mann symmetry), the current associated to $SU(N_f)_A$ is conserved if only all the masses are zero. The 4-current corresponding to the $U(1)_V$ symmetry is conserved at the classical level, it is associated to the conservation of the baryonic charge. However, at the quantum level, sphalerons destroy this symmetry for which, the quantum baryon number is not conserved. The same conclusion holds when discussing the conservation law for the quantum lepton number. Surprisingly, their anomalies have the same value, for which the quantum number $B-L$ is conserved as the anomalies cancel with each other. This is an important point when dealing with Grand Unification Theories(GUTs).

After the quantization process the quantity $\partial_\mu J_5^\mu$ has to be corrected adding the quantum corrections:

$$\partial_\mu J_5^\mu = 2i \sum_{f=1}^{N_f} m_f \bar{\psi}_f \gamma_5 \psi_f + 2N_f q(x) \tag{C.27}$$

this leads to the axial anomaly or Adler-Bell-Jackiw anomaly. In the case $N_f = 3$, the formation of the chiral condensate spontaneously breaks the symmetry to $SU(3)_V \times U(1)_V$, so one should have $8+1$ Goldstone bosons due to $SU(3)A$ and $U(1)_A$. The Goldstone boson relative to $U(1)_A$ is here indicated as the S-particle. The fact that there is no a GB corresponding to this particle, but the only candidate, the η', is much heavier of the other 8, is known as $U(1)$ *problem* or even *old strong problem*.

Witten [260] proposed that the S-particle acquires a mass in the chiral limit thanks to the anomaly. Moreover, this mass is even grater than that of the other pseudo-Goldstone and greater than the upper limit actually determined by Witten itself [261]. Thus, the resolution of the problem consists in recognising that, being anomalous, the axial symmetry is not a true symmetry of the quantum field theory. Since it is not a symmetry, it cannot be spontaneously broken.

This hypothesis has sense only if one can find some good parameters of the theory which, in some limits, leads to suppress at the same time both the anomaly and the mass of the S-particle, M_S. From the RGE one has

$$g_R^2(\mu) \sim \frac{1}{N} \; ; \tag{C.28}$$

for this reason 't Hooft proposed to expand the perturbative theory in $\frac{1}{N}$, in this way:

$$N \to \infty \,, \quad g_R \to 0 \quad \Rightarrow g_R^2 N = g^2 = \text{const} \,. \tag{C.29}$$

In this limit the anomalous contribution to the physical quantities is suppressed and in fact

$$q(x) = \frac{g_R^2}{32\pi^2} F^a_{\mu\nu} \tilde{F}^{\mu\nu}_a = \frac{g^2}{32\pi^2 N} F^a_{\mu\nu} \tilde{F}^{\mu\nu}_a \sim \frac{1}{N} \to 0 \,. \tag{C.30}$$

The problem now consists in determining the behaviour of the mass term respect to the parameter N. The solution to this problem is known as Witten-Veneziano mechanism and it is possible due to the presence of the θ-angle [266, 362].

Considering the $\mathcal{L}_{\text{eff}}$ written above, one can neglect the fermion contributions and add an external current J coupled to the topological charge density, to study the response of the system to variations of θ

$$\mathcal{L}_{\text{no ferm}} = \frac{q(x)^2}{aF_\pi^2} - \theta q(x) - iq(x)J \ . \tag{C.31}$$

this response is called topological susceptibility χ and can be determined by the partition function

$$\chi = \frac{1}{V_4}\frac{i}{Z(J,\theta)}\frac{d^2 Z(J,\theta)}{d\theta^2}\bigg|_{\theta=0} , \qquad Z(J,\theta) = e^{i\int d^4x \mathcal{L}_{\text{no ferm}}} \ . \tag{C.32}$$

Determining the field $q(x)$ thanks to its Euler-Lagrange equations

$$\partial_\mu \frac{\partial \mathcal{L}_{\text{no ferm}}}{\partial(\partial^\mu q(x))} - \frac{\partial \mathcal{L}_{\text{no ferm}}}{\partial q(x)} = 0 \quad \Rightarrow \quad q(x) = \frac{a}{2}F_\pi^2(\theta + iJ) \tag{C.33}$$

one obtains $\mathcal{L}_{\text{no ferm}} = -\frac{a}{4}F_\pi^2(\theta + iJ)^2$, that does not depend on x, from which it can be derived $Z(J,\theta)$. To calculate the topological susceptibility one sets $J = 0$ and then substitute: $\chi = \frac{a}{2}F_\pi^2$. Taking the value of M_S^2 and substituting the expression of the quantity a in function of the susceptibility one has

$$M_S^2 = \frac{2N_f}{F_\pi^2}\chi \sim \frac{1}{N} \tag{C.34}$$

from which it is understood that the quasi-Goldstone has a mass which goes to 0 in the limit $N \to \infty$. In conclusion, the Witten-Veneziano mechanism, together with the 't Hooft expansion, provides a quantitative relation between the axial anomaly and the S-particle's mass, ultimately confirming the Witten's solution to the $U(1)$ Problem.

§ C.4 Strong CP Problem: the Peccei-Quinn solution

The Peccei-Quinn's mechanism, proposed as solution of the Strong CP problem, is an extension of the Standard Model which consists in the introduction of a new degree of freedom $\mathcal{N}$ due to a new symmetry $U_{PQ}(1)$, which:

- Is classically exact.
- Is anomalous, with anomaly coefficient a_{PQ}.
- Spontaneously breaks at the scale F_α consequently leading to an extra Goldstone boson.

To extend the previous effective Lagrangian while satisfying all these requests, one can write

$$\mathcal{L}_{\text{eff}+PQ} = \mathcal{L}_{\text{eff}} + \frac{1}{2}\partial_\mu \mathcal{N} \partial^\mu \mathcal{N}^\dagger + \frac{i}{2}q(x)a_{PQ}(\log \mathcal{N} - \log \mathcal{N}^\dagger) \tag{C.35}$$

where $\mathcal{N}(x) = \frac{F_\alpha}{\sqrt{2}}e^{i\sqrt{2}\,\alpha(x)/F_\alpha}$ and α is the new Goldstone. Let us observe that the new terms are in pure analogy with the previous matrix notation for the mesons' fields and also with the additional term representing the anomaly through the coupling with the topological charge density. From the symmetry point of view:

$$U_A(1): \quad \Sigma \to e^{i\beta}\Sigma\,, \quad U_{PQ}(1): \quad \mathcal{N} \to e^{i\gamma}\mathcal{N}$$
$$\Rightarrow \delta\mathcal{L}_{\text{eff}+PQ} = -(N_f\beta + a_{PQ}\gamma)q(x)\ .$$

Imposing $N_f\beta + a_{PQ}\gamma = 0$ one has a full symmetry under the group $U(1)$ without anomalies, which spontaneously and explicitly breaks, implying the new pseudo-Goldstone α which is called axion.

To discuss the CP violation let us recall the same analysis done before, considering the effect of this additional d.o.f. whose expectation value is

$$\langle\mathcal{N}\rangle = \frac{F_\alpha}{\sqrt{2}}e^{-\frac{i\phi}{a_{PQ}}}\ ; \tag{C.36}$$

the configuration which minimized the energy is modified in:

$$a\Big(\theta - \sum_{i=1}^{N_f}\alpha_i - \phi\Big) = m_i^2\sin\alpha_i\ ; \quad \theta - \sum_{i=1}^{N_f}\alpha_i - \phi = 0\,. \tag{C.37}$$

In order to preserve CP, if all GBs are massive $m_i^2 \neq 0 \ \ \forall i \ \to \sin\alpha_i = 0 \to \alpha_i = 0, \pm\pi\,(\mathrm{Mod}\,2\pi) \Rightarrow \theta = \phi$. In this case, the outcome is the same result found in the case of a single massless GB: the dependence on θ disappears because this is rotated away. The masses for the quasi-Goldstones belonging to Φ and of the axion are obtained as eigenvalues of the mass matrix:

$$-\frac{1}{2}\Big[\sum_{i=1}^{N_f}m_i^2v_i^2 + a\Big(\sum_{i=1}^{N_f}v_i + b\alpha\Big)^2\Big] \quad \text{with} \quad b \equiv a_{PQ}\frac{F_\pi}{F_\alpha}\,. \tag{C.38}$$

In particular, the smallest eigenvalue corresponds to the following axion mass

$$m_\alpha^2 = \frac{b^2}{\frac{1}{a} + \sum_{i=1}^{N_f}\frac{1}{m_i^2}} \sim \frac{b^2}{\frac{1}{m_1^2} + \frac{1}{m_2^2}} = 2m_\pi^2 b^2\frac{m_1m_2}{(m_1+m_2)^2} < 0.01eV\,. \tag{C.39}$$

The results of this section can be summarised as follows: on the one hand, the introduction of the new anomalous $U(1)_{PQ}$ symmetry compensates the $U(1)_A$ anomaly, on the other hand the presence of the new d.o.f. solves the issue related to the θ-angle. The main consequence of this mechanism is the appearance of a new particle, the axion, which possesses very interesting features: it has a very small mass, it does not have electric charge and only weakly interact with ordinary matter. These properties make it invisible enough that it is considered a very strong candidate for Dark Matter.

§ C.5 Controversial viewpoint: is there CP violation at all?

Interestingly, a divergent line of thought was pointed out in [363], where it has been brought up that the effective decomposition (quantization) of gauge field configurations of finite action into topological sectors of integer winding number without imposing ad hoc boundary conditions can only be derived when taking the volume of Euclidean spacetime to infinity. In contrast, there is no physical motivation for fixed boundary conditions on a finite surface in Euclidean space. As a consequence, the limit of infinite spacetime volume must be taken before summing over topological sectors, and it turns out that CP remains conserved this way. Precisely, this order of limits corresponds to a well-defined integration contour in the path integral constructed from the steepest-descent flows. In contrast, the opposite conventional order of limits results in an integration that is inequivalent in the sense of the Cauchy theorem.

There, the focus of investigation regards whether a nonvanishing $\bar{\theta} = \theta - \sum_{i=1}^{N_f} \alpha_i$ is also a sufficient condition for CP violation in strong interactions. The crucial observations in these works stand in considering the partition function

$$\mathcal{Z}\left[\eta, \bar{\eta}\right] = \int \mathcal{D}\bar{\psi}\mathcal{D}\psi\mathcal{D}A\ e^{-\lim_{\Omega\to\infty} \int_\Omega d^4x\ \left(\mathcal{L} - \bar{\eta}\psi - \bar{\psi}\eta\right)} \tag{C.40}$$

that in infinite spacetime volume $\Omega \to \infty$ receives its non-vanishing contributions from saddle points of finite action and fluctuations about these. For these field configurations, the winding number Δn is an integer that labels the topological sector

$$\Delta n = \lim_{\Omega\to\infty} \int_\Omega d^4x\ \frac{1}{16\pi^2}\ \mathrm{Tr}\{F\tilde{F}\}\ \in \mathbb{Z}\,. \tag{C.41}$$

The value Δn is a consequence of $\Omega \to \infty$ and therefore the latter limit needs to be performed before the sum over all the topological sectors. Hence, all the contributions of the topological sectors are first evaluated in the limit $\Omega \to \infty$ and then added together. The other way around does not commute with it since

$$\lim_{\Delta n\to\pm\infty}\ \lim_{\Omega\to\infty} \frac{\Delta n}{\Omega} = 0 \tag{C.42}$$

leading to the consequence that there is no permanent electric dipole moment of the neutron [100, 101], independently from the value of $\bar{\theta}$.

The authors of [363] carry out all the reasoning by avoiding the use of a vacuum state to evaluate the path integral. In fact, they analogously compute the limit of infinite spacetime volume Ω by taking the limit of infinite Euclidean time.

Generally, (C.40) is shown to imply integration contour joining together the steepest-descent paths associated to each topological sector Δn. The integral appearing in (C.40) needs to be well-defined with opportune integration contours since when $\bar{\theta} \neq 0$ leads to a non-positive integrand. Hence, integration contours are essential to specify in which order the integration

$$\int \mathcal{D}A \tag{C.43}$$

is performed. Precisely, the question orbits around the correct order of integration: performing first the infinite volume limit or the sum over different topological sector. The Yang-Mills integral should be bounded from below on its domain meaning that it has minima that can in principle also exhibit degeneracies. If the volume Ω is infinite, the vector potential at these minima is just a pure gauge configuration at infinity. Consequently, these minima are thus topologically quantized: the result of the limit of the Yang-Mills integral corresponds to the winding number Δn as in (C.41).

The important detail here is that this reasoning does not need apposite boundary conditions since (C.40) admits the limit inside the path integral and it thus comes naturally for the ordering proposal of the authors [363]. Additionally, contours of steepest descent for various Δn do not intersect within finite S because within the boundless expanse of spacetime, solutions with distinct winding numbers are divided by barriers of infinite action. Consequently, integration paths across different sectors Δn can only link through configurations with infinite action S, which, however, yield no contribution to the partition function (C.40).

On the contrary, working in finite volume Ω, the boundary condition that is usually adopted for the gauge field $A_\mu = i\, \omega \partial_\mu \omega^{-1}$ on $\partial\Omega$ leads to field configurations in different topological sectors non continuously connected. Therefore, this implies that, without imposing arbitrary boundary conditions, according to the authors' opinion, one should not merge the distinct sectors prior to perform $\Omega \to \infty$. In fact, doing so would disrupt the integration contour in a discontinuous manner, typically resulting in an inequivalent outcome. This is because the integrand, particularly the sum across the topological sectors, lacks positive definiteness and absolute convergence [363].

The violation of *CP* symmetry is a consequence of the fact that in (C.40) one imposes ad hoc boundary conditions and perform the limit of infinite Ω as the last step. Moreover, not imposing immediately these boundary conditions leads to no conservation of topological charge within a certain finite Ω. Consequently, for what said above, the minima of the Yang-Mills integral do not exist. Therefore, the boundary conditions need to be imposed *but* they are a result of the infinite spacetime volume. The final outcome is an incongruity since imposing the boundary conditions would imply the commutation of the limits of infinite spacetime volume with the sum over infinitely many topological sectors [363].

Details of the second-order expansion

Appendix D

In this Appendix, there are the details on the derivation of the dispersion relations of the fluctuations that are parametrized as

$$\Sigma = e^{i\Omega}\Sigma_0 e^{i\Omega^t} \tag{D.1}$$

where Σ_0 corresponds to homogeneous ground state (7.5) while Ω has the form

$$\Omega = \begin{pmatrix} \pi & 0 \\ 0 & -\pi^t \end{pmatrix} + \tilde{\beta} S \begin{pmatrix} \mathbb{1}_{N_f} & 0 \\ 0 & \mathbb{1}_{N_f} \end{pmatrix} = \nu + \tilde{\beta} S \ \mathbb{1}_{2N_f}, \quad \tilde{\beta} = \frac{1}{\sqrt{2N_f}} \tag{D.2}$$

here $\pi = \sum_{a=0}^{\dim} \pi^a T_a$ belongs to the algebra of the coset space $\frac{U(N_f)}{Sp(N_f)}$. The normalization condition on the generators is $\langle T_a T_b \rangle = \frac{\delta_{ab}}{2}$. Writing $\Sigma = e^{2i\tilde{\beta}S} U(\alpha_i)\overline{\Sigma}$, one has that $\overline{\Sigma}$ can be written as

$$\begin{aligned}
\overline{\Sigma} = e^{i\nu}\Sigma_c e^{i\nu^t} &= \begin{pmatrix} e^{i\pi} & 0 \\ 0 & e^{-i\pi^t} \end{pmatrix} \left(\begin{pmatrix} 0 & \mathbb{1}_{N_f} \\ -\mathbb{1}_{N_f} & 0 \end{pmatrix} \cos\varphi + \begin{pmatrix} \sigma_2 \otimes \mathbb{1}_{N_f/2} & 0 \\ 0 & \sigma_2 \otimes \mathbb{1}_{N_f/2} \end{pmatrix} \sin\varphi \right) \begin{pmatrix} e^{i\pi} & 0 \\ 0 & e^{-i\pi^t} \end{pmatrix} \\
&= \begin{pmatrix} e^{i\pi} & 0 \\ 0 & e^{-i\pi^t} \end{pmatrix} \begin{pmatrix} 0 & \mathbb{1}_{N_f} \\ -\mathbb{1}_{N_f} & 0 \end{pmatrix} \begin{pmatrix} e^{i\pi^t} & 0 \\ 0 & e^{-i\pi} \end{pmatrix} \cos\varphi \\
&+ \begin{pmatrix} e^{i\pi} & 0 \\ 0 & e^{-i\pi^t} \end{pmatrix} \begin{pmatrix} \sigma_2 \otimes \mathbb{1}_{N_f/2} & 0 \\ 0 & \sigma_2 \otimes \mathbb{1}_{N_f/2} \end{pmatrix} \begin{pmatrix} e^{i\pi^t} & 0 \\ 0 & e^{-i\pi} \end{pmatrix} \sin\varphi \\
&= \begin{pmatrix} 0 & \mathbb{1}_{N_f} \\ -\mathbb{1}_{N_f} & 0 \end{pmatrix} \cos\varphi + e^{2i\nu} \mathbb{1}_2 \otimes \sigma_2 \otimes \mathbb{1}_{N_f/2} \sin\varphi.
\end{aligned} \tag{D.3}$$

Using this expression is easy to show that (for simplicity of notation, henceforth let us indicate the trace operation with the brackets)

$$\partial_\mu \overline{\Sigma} = 2ie^{2i\nu}\partial_\mu \nu \mathbb{1}_2 \otimes \sigma_2 \otimes \mathbb{1}_{N_f/2} \sin\varphi, \tag{D.4}$$

$$\partial_\mu \overline{\Sigma}^\dagger = -2i\mathbb{1}_2 \otimes \sigma_2 \otimes \mathbb{1}_{N_f/2} \partial_\mu \nu e^{-2i\nu} \sin\varphi, \tag{D.5}$$

$$\overline{\Sigma}\partial_0 \overline{\Sigma}^\dagger = \begin{pmatrix} 0 & -\sigma_2 \otimes \mathbb{1}_{N_f} \partial_0 \pi^t e^{-2i\pi^t} \\ -\sigma_2 \otimes \mathbb{1}_{N_f} \partial_0 \pi e^{-2i\pi} & 0 \end{pmatrix} \sin\varphi\cos\varphi - 2i\partial_0 \nu \sin^2\varphi \tag{D.6}$$

which implies $\left\langle \partial_\mu \overline{\Sigma} \partial^\mu \overline{\Sigma}^\dagger \right\rangle = 8\sin^2(\varphi) \left\langle \partial_\mu \pi \partial^\mu \pi \right\rangle$ and $\left\langle B \overline{\Sigma} \partial_0 \overline{\Sigma}^\dagger \right\rangle = -2i \sin^2(\varphi) \left\langle \partial_0 \pi \right\rangle$ where $B = \frac{1}{2}\sigma_3 \otimes \mathbb{1}_{N_f}$. Additionally:

$$\left\langle M\overline{\Sigma} + M^\dagger \overline{\Sigma}^\dagger \right\rangle = 4N_f \cos\varphi \tag{D.7}$$

$$\begin{aligned} \left\langle B\overline{\Sigma} B^t \overline{\Sigma}^\dagger \right\rangle &= \left\langle B e^{i\nu} \Sigma_0 e^{i\nu^t} B^t e^{-i\nu^t} \Sigma_0^\dagger e^{-i\nu} \right\rangle \\ &= \left\langle B \Sigma_0 B^t \Sigma_0^\dagger \right\rangle \end{aligned} \tag{D.8}$$

since $[B, \nu] = 0$.

Making use of the above results, one obtains that the matrix Σ satisfies

$$\partial_\mu \Sigma = e^{2i\tilde{\beta}S} U(\alpha_i) \left(2i\tilde{\beta} \partial_\mu S \overline{\Sigma} + \partial_\mu \overline{\Sigma} \right), \tag{D.9}$$

$$\partial_\mu \Sigma^\dagger = e^{-2i\tilde{\beta}S} U(\alpha_i) \left(-2i\tilde{\beta} \partial_\mu S \overline{\Sigma}^\dagger + \partial_\mu \overline{\Sigma}^\dagger \right) \tag{D.10}$$

$$\Sigma \partial_\mu \Sigma^\dagger = -2i\tilde{\beta} \partial_\mu S + \overline{\Sigma} \partial_\mu \overline{\Sigma}^\dagger \ . \tag{D.11}$$

From which it is easy to recognize that relevant traces are

$$\begin{aligned} \left\langle \partial_\mu \Sigma \partial^\mu \Sigma^\dagger \right\rangle &= \left\langle \partial_\mu \overline{\Sigma} \partial^\mu \overline{\Sigma}^\dagger \right\rangle + 4\tilde{\beta}^2 \left\langle \partial_\mu S \partial^\mu S \right\rangle + 2i\tilde{\beta} \partial^\mu S \left\langle \overline{\Sigma} \partial_\mu \overline{\Sigma}^\dagger \right\rangle \\ &= 8\sin^2\varphi \left\langle \partial_\mu \pi \partial^\mu \pi \right\rangle + 8N_f \tilde{\beta}^2 \partial_\mu S \partial^\mu S \\ &= 4\sin^2\varphi \ \partial_\mu \pi^a \partial^\mu \pi^a + 8N_f \tilde{\beta}^2 \partial_\mu S \partial^\mu S \end{aligned} \tag{D.12}$$

$$\begin{aligned} \left\langle B \Sigma \partial_0 \Sigma^\dagger \right\rangle &= \left\langle B \overline{\Sigma} \partial_0 \overline{\Sigma}^\dagger \right\rangle \\ &= -2i \sin^2\varphi \left\langle \partial_0 \pi \right\rangle \\ &= -2i\sqrt{2N_f} \sin^2\varphi \ \partial_0 \pi^0 \end{aligned} \tag{D.13}$$

$$\begin{aligned} \left\langle M\Sigma + M^\dagger \Sigma^\dagger \right\rangle &= \left\langle e^{2i\tilde{\beta}S} M U(\alpha_i) \overline{\Sigma} + e^{-2i\tilde{\beta}S} M^\dagger U(\alpha_i)^\dagger \overline{\Sigma}^\dagger \right\rangle \\ &= 2N_f \cos\varphi \left(X \cos\left(\sqrt{\frac{2}{N_f}} S \right) + Z \sin\left(\sqrt{\frac{2}{N_f}} S \right) \right) \end{aligned} \tag{D.14}$$

$$\left\langle \log\Sigma - \log\Sigma^\dagger \right\rangle = 8iN_f \tilde{\beta} S - \sum_i^{N_f} \alpha_i \ . \tag{D.15}$$

Finally, by plugging these results into the Lagrangian (7.22), the result reads

$$\begin{aligned} \mathcal{L} = &\ 4\nu^2 \sin^2\varphi \partial_\mu \pi^a \partial^\mu \pi^a e^{-2\sigma f} + 4\nu^2 \partial_\mu S \partial^\mu S e^{-2\sigma f} + 8\sqrt{2N}\mu \nu^2 \sin^2\varphi \partial_0 \pi^0 e^{-2\sigma f} \\ &+ 2\nu^2 \mu^2 N_f \sin^2\varphi e^{-2\sigma f} + 4N_f \nu^2 m_\pi^2 \cos\varphi \left[X \cos\left(\sqrt{2} \sqrt{\frac{1}{N_f}} S \right) + Z \sin\left(\sqrt{2} \sqrt{\frac{1}{N_f}} S \right) \right] e^{-y\sigma f} + \\ &- a\nu^2 (\bar{\theta} + \sqrt{2N_f} S)^2 e^{-2\sigma f} - \Lambda_0^4 e^{-4\sigma f} - \frac{R}{12 f^2} e^{-2\sigma f} + \frac{1}{2} (\partial_\mu \sigma \partial^\mu \sigma) e^{-2\sigma f} - V(\sigma) \ . \end{aligned} \tag{D.16}$$

By expanding the above to the quadratic order in the fluctuations of the dilaton field, one obtains the quadratic Lagrangian (6.61) considered in chapter 6.

Tables of the Skyrmion mass and the root mean square radius of the baryon charge

E

APPENDIX

In this appendix, there are a series of tables that list the results for the Skyrmion mass M_S and the root mean square radius of the baryon charge $\langle r^2 \rangle^{1/2}$ in the single spherical Skyrmion case studied in section 9.2. The estimated error is not larger than the 0.5% for all the entries. All the dimensionful quantities are measured in units of $\sqrt{K}$. $M_{\text{Skyrme}} = 15.67$ and $\langle r^2 \rangle^{1/2}_{\text{Skyrme}} = 0.215$ denote the Skyrmion mass and the root mean square radius in the absence of the dilaton, respectively.

E.0.1 General case

Skyrmion mass										
	$\mathbf{M_S}$					$\mathbf{M_S/M_{Skyrme}}$				
$\boldsymbol{\Delta}$	$m_\sigma = 1$	$m_\sigma = 2$	$m_\sigma = 3$	$m_\sigma = 4$	$m_\sigma = 5$	$m_\sigma = 1$	$m_\sigma = 2$	$m_\sigma = 3$	$m_\sigma = 4$	$m_\sigma = 5$
1	22.58	16.28	15.43	15.26	15.24	1.46	1.04	0.985	0.974	0.973
1.2	22.27	16.26	15.43	15.26	15.24	1.44	1.04	0.985	0.974	0.972
1.4	21.98	16.24	15.43	15.26	15.24	1.42	1.04	0.984	0.973	0.972
1.6	21.71	16.23	15.42	15.25	15.24	1.40	1.04	0.984	0.973	0.972
1.8	21.46	16.21	15.42	15.25	15.24	1.39	1.03	0.984	0.973	0.972
2	21.22	16.19	15.42	15.25	15.23	1.37	1.03	0.984	0.973	0.972
2.2	21.00	16.18	15.41	15.25	15.23	1.36	1.03	0.984	0.973	0.972
2.4	20.79	16.16	15.41	15.25	15.23	1.34	1.03	0.984	0.973	0.972
2.6	20.60	16.15	15.41	15.24	15.23	1.33	1.03	0.983	0.973	0.972
2.8	20.42	16.14	15.40	15.24	15.23	1.32	1.03	0.983	0.973	0.972
3	20.25	16.12	15.40	15.24	15.23	1.31	1.03	0.983	0.973	0.972
3.2	20.08	16.10	15.40	15.24	15.23	1.30	1.03	0.983	0.972	0.972
3.4	19.93	16.09	15.40	15.24	15.22	1.29	1.03	0.982	0.972	0.971
3.6	19.79	16.07	15.39	15.24	15.22	1.28	1.03	0.982	0.972	0.971
3.8	19.65	16.06	15.39	15.23	15.22	1.27	1.02	0.982	0.972	0.971
4	19.53	16.05	15.39	15.23	15.22	1.25	1.02	0.98	0.972	0.971

Table E.1.: *Numerical values of the Skyrmion mass for different values of the conformal dimension Δ and dilaton mass $m_\sigma = 1, 2, 3, 4, 5$. $M_{Skyrme} = 15.67$ denotes the Skyrmion mass in the absence of the dilaton.*

Root mean square radius of the baryon charge										
	$\langle r^2\rangle^{1/2}$ in units of 10^{-1}					$\langle r^2\rangle^{1/2}/\langle r^2\rangle^{1/2}_{\text{Skyrme}}$ in units of 10^{-1}				
Δ	$m_\sigma = 1$	$m_\sigma = 2$	$m_\sigma = 3$	$m_\sigma = 4$	$m_\sigma = 5$	$m_\sigma = 1$	$m_\sigma = 2$	$m_\sigma = 3$	$m_\sigma = 4$	$m_\sigma = 5$
1	1.50	2.04	2.14	2.158	2.161	6.99	9.47	9.94	10.03	10.04
1.2	1.52	2.04	2.14	2.158	2.161	7.08	9.48	9.94	10.03	10.04
1.4	1.54	2.04	2.14	2.158	2.161	7.17	9.49	9.94	10.03	10.04
1.6	1.56	2.04	2.14	2.158	2.161	7.25	9.50	9.94	10.03	10.04
1.8	1.58	2.05	2.14	2.158	2.161	7.33	9.51	9.94	10.03	10.04
2	1.60	2.05	2.14	2.159	2.161	7.43	9.52	9.95	10.03	10.04
2.2	1.61	2.05	2.14	2.159	2.161	7.50	9.53	9.95	10.03	10.04
2.4	1.63	2.05	2.14	2.159	2.161	7.57	9.54	9.95	10.03	10.05
2.6	1.64	2.05	2.14	2.159	2.161	7.64	9.54	9.95	10.03	10.05
2.8	1.66	2.06	2.14	2.159	2.162	7.70	9.55	9.95	10.04	10.05
3	1.67	2.06	2.14	2.159	2.162	7.76	9.56	9.95	10.04	10.05
3.2	1.68	2.06	2.14	2.160	2.162	7.82	9.57	9.96	10.04	10.05
3.4	1.70	2.06	2.14	2.160	2.162	7.88	9.57	9.96	10.04	10.05
3.6	1.71	2.06	2.14	2.160	2.162	7.93	9.58	9.96	10.04	10.05
3.8	1.72	2.06	2.14	2.160	2.162	7.98	9.59	9.96	10.04	10.05
4	1.73	2.07	2.14	2.160	2.162	8.05	9.61	9.96	10.04	10.05

Table E.2.: *Numerical values of the root mean square radius* $\langle r^2\rangle^{1/2}$ *of the baryon charge for different values of the conformal dimension* Δ *and dilaton mass* $m_\sigma = 1, 2, 3, 4, 5$. $\langle r^2\rangle^{1/2}_{Skyrme} = 0.215$ *denotes the root mean square radius of the baryon charge for the Skyrme model in the absence of the dilaton.*

Skyrmion mass										
	$\mathbf{M_S}$					$\mathbf{M_S/M_{\text{Skyrme}}}$				
$\boldsymbol{\Delta}$	$m_\sigma = 6$	$m_\sigma = 7$	$m_\sigma = 8$	$m_\sigma = 9$	$m_\sigma = 10$	$m_\sigma = 6$	$m_\sigma = 7$	$m_\sigma = 8$	$m_\sigma = 9$	$m_\sigma = 10$
1	15.27	15.31	15.35	15.38	15.41	0.974	0.977	0.979	0.982	0.984
1.2	15.27	15.31	15.35	15.38	15.41	0.974	0.977	0.979	0.981	0.984
1.4	15.27	15.30	15.34	15.38	15.41	0.974	0.977	0.979	0.981	0.984
1.6	15.26	15.30	15.34	15.38	15.41	0.974	0.976	0.974	0.981	0.983
1.8	15.26	15.30	15.34	15.38	15.41	0.974	0.976	0.979	0.981	0.983
2	15.26	15.30	15.34	15.38	15.41	0.974	0.976	0.979	0.981	0.983
2.2	15.26	15.30	15.34	15.38	15.41	0.974	0.976	0.979	0.981	0.983
2.4	15.26	15.30	15.34	15.38	15.41	0.974	0.976	0.979	0.981	0.983
2.6	15.26	15.30	15.34	15.38	15.41	0.974	0.976	0.979	0.981	0.983
2.8	15.26	15.30	15.34	15.37	15.41	0.974	0.976	0.979	0.981	0.983
3	15.26	15.30	15.34	15.37	15.41	0.973	0.976	0.979	0.981	0.983
3.2	15.25	15.29	15.34	15.37	15.41	0.973	0.976	0.979	0.981	0.983
3.4	15.25	15.29	15.33	15.37	15.41	0.973	0.976	0.978	0.981	0.983
3.6	15.25	15.29	15.33	15.37	15.41	0.973	0.976	0.978	0.981	0.983
3.8	15.25	15.29	15.33	15.37	15.40	0.973	0.976	0.978	0.981	0.983
4	15.25	15.29	15.33	15.37	15.40	0.973	0.976	0.978	0.981	0.983

Table E.3.: *Numerical values of the Skyrmion mass for different values of the conformal dimension Δ and dilaton mass $m_\sigma = 6, 7, 8, 9, 10$. $M_{Skyrme} = 15.67$ denotes the Skyrmion mass in the absence of the dilaton.*

Root mean square radius of the baryon charge										
	$\langle r^2\rangle^{1/2}$ in units of 10^{-1}					$\langle r^2\rangle^{1/2}/\langle r^2\rangle^{1/2}_{\mathrm{Skyrme}}$ in units of 10^{-1}				
Δ	$m_\sigma = 6$	$m_\sigma = 7$	$m_\sigma = 8$	$m_\sigma = 9$	$m_\sigma = 10$	$m_\sigma = 6$	$m_\sigma = 7$	$m_\sigma = 8$	$m_\sigma = 9$	$m_\sigma = 10$
1	2.160	2.159	2.159	2.159	2.159	1.004	1.004	1.003	1.003	1.003
1.2	2.160	2.159	2.159	2.159	2.159	1.004	1.004	1.003	1.003	1.003
1.4	2.160	2.159	2.159	2.159	2.159	1.004	1.004	1.003	1.003	1.003
1.6	2.160	2.159	2.159	2.158	2.159	1.004	1.004	1.003	1.003	1.003
1.8	2.160	2.159	2.159	2.158	2.159	1.004	1.003	1.003	1.003	1.003
2	2.160	2.159	2.158	2.158	2.159	1.004	1.003	1.003	1.003	1.003
2.2	2.160	2.159	2.158	2.158	2.159	1.004	1.003	1.003	1.003	1.003
2.4	2.160	2.159	2.158	2.158	2.159	1.004	1.003	1.003	1.003	1.003
2.6	2.160	2.159	2.158	2.158	2.159	1.004	1.003	1.003	1.003	1.003
2.8	2.160	2.159	2.158	2.158	2.159	1.004	1.003	1.003	1.003	1.003
3	2.160	2.159	2.158	2.158	2.158	1.004	1.003	1.003	1.003	1.003
3.2	2.160	2.159	2.158	2.158	2.158	1.004	1.003	1.003	1.003	1.003
3.4	2.160	2.159	2.158	2.158	2.147	1.004	1.003	1.003	1.003	1.003
3.6	2.160	2.159	1.003	2.158	2.158	1.004	1.003	1.003	1.003	1.003
3.8	2.160	2.159	2.158	2.158	2.158	1.004	1.003	1.003	1.003	1.003
4	2.160	2.159	2.158	2.158	2.158	1.004	1.003	1.003	1.003	1.003

Table E.4.: *Numerical values of the root mean square radius $\langle r^2\rangle^{1/2}$ of the baryon charge for different values of the conformal dimension Δ and dilaton mass $m_\sigma = 6, 7, 8, 9, 10$. $\langle r^2\rangle^{1/2}_{Skyrme} = 0.215$ denotes the root mean square radius of the baryon charge for the Skyrme model in the absence of the dilaton.*

E.0.2 M_S and $\langle r^2\rangle^{1/2}$ in the $\Delta \to 0$ limit

	Skyrmion mass	
	$\mathbf{M_S}$	$\mathbf{M_S/M_{Skyrme}}$
$m_\sigma = 1$	24.48	1.56
$m_\sigma = 2$	16.38	1.05
$m_\sigma = 3$	15.45	0.99
$m_\sigma = 4$	15.27	0.97
$m_\sigma = 5$	15.25	0.97
	Root mean square radius of the baryon charge	
	$\langle \mathbf{r^2} \rangle^{1/2}$	$\langle \mathbf{r^2} \rangle^{1/2} / \langle \mathbf{r^2} \rangle^{1/2}_{\mathbf{Skyrme}}$
$m_\sigma = 1$	0.140	0.65
$m_\sigma = 2$	0.203	0.94
$m_\sigma = 3$	0.214	0.99
$m_\sigma = 4$	0.216	1.00
$m_\sigma = 5$	0.216	1.00

Table E.5.: *Numerical values of the Skyrmion mass M_S and the root mean square radius of the baryon charge $\langle r^2 \rangle^{1/2}$ for $m_\sigma = 1, 2, 3, 4, 5$.*

	Skyrmion mass	
	$\mathbf{M_S}$	$\mathbf{M_S/M_{Skyrme}}$
$m_\sigma = 6$	15.27	0.974
$m_\sigma = 7$	15.31	0.977
$m_\sigma = 8$	15.35	0.980
$m_\sigma = 9$	15.39	0.982
$m_\sigma = 10$	15.42	0.984
	Root mean square radius of the baryon charge	
	$\langle \mathbf{r^2} \rangle^{1/2}$	$\langle \mathbf{r^2} \rangle^{1/2} / \langle \mathbf{r^2} \rangle^{1/2}_{\mathbf{Skyrme}}$
$m_\sigma = 6$	0.216	1.004
$m_\sigma = 7$	0.216	1.004
$m_\sigma = 8$	0.216	1.003
$m_\sigma = 9$	0.216	1.003
$m_\sigma = 10$	0.216	1.004

Table E.6.: *Numerical values of the Skyrmion mass and the root mean square radius $\langle r^2 \rangle^{1/2}$ of the baryon charge for different values of the dilaton mass measured in units of $\sqrt{K}$.*

Bibliography

[1] Jahmall Bersini, Alessandra D'Alise, Francesco Sannino, and Matías Torres. The θ-angle and axion physics of two-color QCD at fixed baryon charge. *JHEP*, 11:080, 2022.

[2] Jahmall Bersini, Alessandra D'Alise, Francesco Sannino, and Matías Torres. Charging the conformal window at nonzero θ angle. *Phys. Rev. D*, 107(12):125024, 2023.

[3] Jahmall Bersini, Alessandra D'Alise, Clelia Gambardella, and Francesco Sannino. Scaling results for charged sectors of near conformal QCD. *Phys. Rev. D*, 109(12):125015, 2024.

[4] Jahmall Bersini, Alessandra D'Alise, Francesco Sannino, and Matías Torres. Dilatonic dynamics of baryonic crystals, branes, and spheres. *Phys. Rev. D*, 110:094008, Nov 2024.

[5] Yu Nakayama. Scale invariance vs conformal invariance. *Phys. Rept.*, 569:1–93, 2015.

[6] Gabriel Francisco Cuomo. *Large charge, semiclassics and superfluids: from broken symmetries to conformal field theories*. PhD thesis, EPFL, 2020.

[7] John L Cardy. Operator content of two-dimensional conformally invariant theories. *Nuclear Physics B*, 270:186–204, 1986.

[8] John Cardy. *Scaling and Renormalization in Statistical Physics*. Cambridge Lecture Notes in Physics. Cambridge University Press, 1996.

[9] Hidetoshi Nishimori and Gerardo Ortiz. *Elements of Phase Transitions and Critical Phenomena*. Oxford University Press, 12 2010.

[10] Michele Della Morte, Domenico Orlando, and Francesco Sannino. Renormalization Group Approach to Pandemics: The COVID-19 Case. *Front. in Phys.*, 8:144, 2020.

[11] Bruno Buonomo, Alessandra D'Alise, Rossella Della Marca, and Francesco Sannino. Information index augmented erg to model vaccination behaviour: A case study of covid-19 in the us, 2024.

[12] Jean Zinn-Justin. *Phase Transitions and Renormalization Group*. Oxford University Press, 07 2007.

[13] Marc Gillioz. *Conformal field theory for particle physicists*. SpringerBriefs in Physics. Springer, 2023.

[14] Y. Itin and Y. Friedman. Backwards on minkowskis road. from 4d to 3d maxwellian electromagnetism. *Annalen der Physik*, 520(910):769786, September 2008.

[15] Harry Bateman. The conformal transformations of a space of four dimensions and their applications to geometrical optics. *Proceedings of the London Mathematical Society*, 2(1):70–89, 1909.

[16] Harry Bateman. The transformation of the electrodynamical equations. *Proceedings of the London Mathematical Society*, 2(1):223–264, 1910.

[17] Ebenezer Cunningham. The principle of relativity in electrodynamics and an extension thereof. *Proceedings of the London Mathematical Society*, 2(1):77–98, 1910.

[18] Hugh Osborn. Lectures on conformal field theories in more than two dimensions, 2019.

[19] P. Di Francesco, P. Mathieu, and D. Senechal. *Conformal Field Theory*. Graduate Texts in Contemporary Physics. Springer-Verlag, New York, 1997.

[20] Joshua D. Qualls. Lectures on Conformal Field Theory. 11 2015.

[21] Slava Rychkov. *EPFL Lectures on Conformal Field Theory in D>= 3 Dimensions*. SpringerBriefs in Physics. 1 2016.

[22] Abdus Salam and J Strathdee. Nonlinear realizations. i. the role of goldstone bosons. *Physical Review*, 184(5):1750, 1969.

[23] Abdus Salam and J Strathdee. Nonlinear realizations. ii. conformal symmetry. *Physical Review*, 184(5):1760, 1969.

[24] Chris J Isham, Abdus Salam, and J_ Strathdee. Spontaneous breakdown of conformal symmetry. *Physics Letters B*, 31(5):300–302, 1970.

[25] Victor I Ogievetsky. Nonlinear realizations of internal and space-time symmetries. *Proceedings of the Xth Winter School of Theoretical Physics in Karpacz*, 1:117, 1974.

[26] Joseph Polchinski. Scale and conformal invariance in quantum field theory. *Nuclear Physics B*, 303(2):226–236, 1988.

[27] Zhong-Zhi Xianyu. Nonlinear realization of global symmetries. *Notes*, pages 1–10, 2013.

[28] Mikio Nakahara. *Geometry, topology and physics*. CRC press, 2018.

[29] V. Riva and John L. Cardy. Scale and conformal invariance in field theory: A Physical counterexample. *Phys. Lett. B*, 622:339–342, 2005.

[30] Daniele Dorigoni and Vyacheslav S. Rychkov. Scale Invariance + Unitarity => Conformal Invariance? 10 2009.

[31] M. Hortacsu. Explicit examples on conformal invariance. *Int. J. Theor. Phys.*, 42:49, 2003.

[32] Steven Weinberg. Six-dimensional Methods for Four-dimensional Conformal Field Theories. *Phys. Rev. D*, 82:045031, 2010.

[33] G. Mack. All unitary ray representations of the conformal group SU(2,2) with positive energy. *Commun. Math. Phys.*, 55:1, 1977.

[34] Shiraz Minwalla. Restrictions imposed by superconformal invariance on quantum field theories. *Adv. Theor. Math. Phys.*, 2:783–851, 1998.

[35] Jahmall Matteo Bersini. *The charge expansion in quantum field theory*. PhD thesis, Zagreb U., Phys. Dept., Zagreb U., 2021.

[36] John L. Cardy. Conformal invariance and universality in finite-size scaling. *J. Phys. A*, 17:L385–L387, 1984.

[37] John L Cardy. Universal amplitudes in finite-size scaling: generalisation to arbitrary dimensionality. In *Current Physics–Sources and Comments*, volume 2, pages 370–373. Elsevier, 1988.

[38] Emmy Noether. Invariant Variation Problems. *Gott. Nachr.*, 1918:235–257, 1918.

[39] Frederik J Belinfante. On the current and the density of the electric charge, the energy, the linear momentum and the angular momentum of arbitrary fields. *Physica*, 7(5):449–474, 1940.

[40] Sidney R. Coleman and Roman Jackiw. Why dilatation generators do not generate dilatations? *Annals Phys.*, 67:552–598, 1971.

[41] Jeffrey Goldstone, Abdus Salam, and Steven Weinberg. Broken symmetries. *Physical Review*, 127(3):965, 1962.

[42] Gerald S Guralnik, C Richard Hagen, and Thomas WB Kibble. Broken symmetries and the goldstone theorem. *Advances in particle physics*, 2:567–708, 1968.

[43] Chris J Isham, Abdus Salam, and J Strathdee. Nonlinear realizations of space-time symmetries. scalar and tensor gravity. *Annals of Physics*, 62(1):98–119, 1971.

[44] Kiyoshi Higashijima. Nambu-goldstone theorem for conformal symmetry. *Proceedings of XX International Colloquium on Group Theoretical Methods in Physics*, 01 1994.

[45] OHS Delicaat. *The Goldstone theorem and spontaneous breaking of conformal symmetry*. PhD thesis, Faculty of Science and Engineering, 2016.

[46] Gerhard Mack and Abdus Salam. Finite-component field representations of the conformal group. *Annals of Physics*, 53(1):174–202, 1969.

[47] Oscar Delicaat. The goldstone theorem and spontaneous breaking of conformal symmetry. 2016.

[48] Michael E Peskin. *An introduction to quantum field theory*. CRC press, 2018.

[49] Joseph Polchinski. Effective field theory and the Fermi surface. In *Theoretical Advanced Study Institute (TASI 92): From Black Holes and Strings to Particles*, pages 0235–276, 6 1992.

[50] Ian Low and Aneesh V Manohar. Spontaneously broken spacetime symmetries and goldstones theorem. *Physical review letters*, 88(10):101602, 2002.

[51] John R. Ellis and Jozef Lanik. IS SCALAR GLUONIUM OBSERVABLE? *Phys. Lett. B*, 150:289–294, 1985.

[52] Walter D. Goldberger, Benjamin Grinstein, and Witold Skiba. Distinguishing the Higgs boson from the dilaton at the Large Hadron Collider. *Phys. Rev. Lett.*, 100:111802, 2008.

[53] Sidney Coleman. *Aspects of symmetry: selected Erice lectures*. Cambridge University Press, 1988.

[54] Alexander B Zamolodchikov. Irreversibility of the flux of the renormalization group in a 2d field theory. *JETP lett*, 43(12):730–732, 1986.

[55] Alexander A Belavin, Alexander M Polyakov, and Alexander B Zamolodchikov. Infinite conformal symmetry in two-dimensional quantum field theory. *Nuclear Physics B*, 241(2):333–380, 1984.

[56] Curtis G Callan Jr, Sidney Coleman, and Roman Jackiw. A new improved energy-momentum tensor. *Annals of physics*, 59(1):42–73, 1970.

[57] Helmut Reeh and Siegfried Schlieder. Bemerkungen zur unitäräquivalenz von lorentzinvarianten feldern. *Il Nuovo Cimento (1955-1965)*, 22:1051–1068, 1961.

[58] Vladimir Prochazka. *Aspects of trace anomaly in perturbation theory and beyond*. PhD thesis, Edinburgh U., 2017.

[59] MJ Duff. Observations on conformal anomalies. *Nuclear Physics B*, 125(2):334–348, 1977.

[60] Nicholas David Birrell and Paul Charles William Davies. Quantum fields in curved space. 1984.

[61] Damiano Anselmi, DZ Freedman, Marcus T Grisaru, and AA Johansen. Non-perturbative formulas for central functions of supersymmetric gauge theories. *Nuclear Physics B*, 526(1-3):543–571, 1998.

[62] Zohar Komargodski and Adam Schwimmer. On renormalization group flows in four dimensions. *Journal of High Energy Physics*, 2011(12):1–20, 2011.

[63] Zohar Komargodski. The constraints of conformal symmetry on rg flows. *Journal of High Energy Physics*, 2012(7):1–20, 2012.

[64] Ian Jack and Hugh Osborn. Analogs of the c-theorem for four-dimensional renormalisable field theories. *Nuclear Physics B*, 343(3):647–688, 1990.

[65] H Osborn. Weyl consistency conditions and a local renormalisation group equation for general renormalisable field theories. *Nuclear Physics B*, 363(2-3):486–526, 1991.

[66] Markus A Luty, Joseph Polchinski, and Riccardo Rattazzi. The a-theorem and the asymptotics of 4d quantum field theory. *Journal of High Energy Physics*, 2013(1):1–35, 2013.

[67] Ian Jack. The a-theorem. *Contemporary Physics*, 59(1):1–15, 2018.

[68] R. V. Lange. Goldstone theorem in nonrelativistic theories. *Phys. Rev. Lett.*, 14:3–6, Jan 1965.

[69] H.B. Nielsen and S. Chadha. On how to count goldstone bosons. *Nuclear Physics B*, 105(3):445–453, 1976.

[70] Tomá Brauner. Spontaneous symmetry breaking and nambugoldstone bosons in quantum many-body systems. *Symmetry*, 2(2):609–657, 2010.

[71] Haruki Watanabe and Hitoshi Murayama. Redundancies in nambu-goldstone bosons. *Phys. Rev. Lett.*, 110:181601, May 2013.

[72] D. T. Son. Low-energy quantum effective action for relativistic superfluids, 2002.

[73] Alberto Nicolis, Riccardo Penco, Federico Piazza, and Riccardo Rattazzi. Zoology of condensed matter: Framids, ordinary stuff, extra-ordinary stuff. *JHEP*, 06:155, 2015.

[74] A. Monin. Inconsistencies of higgsplosion. 8 2018.

[75] Gil Badel, Gabriel Cuomo, Alexander Monin, and Riccardo Rattazzi. The Epsilon Expansion Meets Semiclassics. *JHEP*, 11:110, 2019.

[76] Sidney Coleman, Julius Wess, and Bruno Zumino. Structure of phenomenological lagrangians. i. *Physical Review*, 177(5):2239, 1969.

[77] Curtis G Callan Jr, Sidney Coleman, Julius Wess, and Bruno Zumino. Structure of phenomenological lagrangians. ii. *Physical Review*, 177(5):2247, 1969.

[78] DB Kaplan and AE Nelson. Strange goings on in dense nucleonic matter. *Physics Letters B*, 175(1):57–63, 1986.

[79] GE Brown, Kuniharu Kubodera, Mannque Rho, and Vesteinn Thorsson. A novel mechanism for kaon condensation in neutron star matter. *Physics Letters B*, 291(4):355–362, 1992.

[80] D. T. Son and Misha A. Stephanov. QCD at finite isospin density. *Phys. Rev. Lett.*, 86:592–595, 2001.

[81] Thomas Schäfer, D. T. Son, Misha A. Stephanov, D. Toublan, and J. J. M. Verbaarschot. Kaon condensation and Goldstone's theorem. *Phys. Lett. B*, 522:67–75, 2001.

[82] Simeon Hellerman, Domenico Orlando, Susanne Reffert, and Masataka Watanabe. On the CFT Operator Spectrum at Large Global Charge. *JHEP*, 12:071, 2015.

[83] Gabriel Cuomo, Angelo Esposito, Emanuele Gendy, Andrei Khmelnitsky, Alexander Monin, and Riccardo Rattazzi. Gapped Goldstones at the cut-off scale: a non-relativistic EFT. *JHEP*, 02:068, 2021.

[84] Tomas Brauner. Spontaneous Symmetry Breaking and Nambu-Goldstone Bosons in Quantum Many-Body Systems. *Symmetry*, 2:609–657, 2010.

[85] Krishna Rajagopal and Frank Wilczek. *The Condensed matter physics of QCD*, pages 2061–2151. 11 2000.

[86] Yoichiro Nambu. Quasi-particles and gauge invariance in the theory of superconductivity. *Physical Review*, 117(3):648, 1960.

[87] Evgenii Mikhailovich Lifshitz and Lev Petrovich Pitaevskii. *Statistical physics: theory of the condensed state*, volume 9. Elsevier, 2013.

[88] Alexander Monin, David Pirtskhalava, Riccardo Rattazzi, and Fiona K. Seibold. Semiclassics, Goldstone Bosons and CFT data. *JHEP*, 06:011, 2017.

[89] S. Dubovsky, T. Gregoire, A. Nicolis, and R. Rattazzi. Null energy condition and superluminal propagation. *JHEP*, 03:025, 2006.

[90] Kara Farnsworth, Markus A. Luty, and Valentina Prilepina. Weyl versus Conformal Invariance in Quantum Field Theory. *JHEP*, 10:170, 2017.

[91] Humphrey J Maris. Phonon-phonon interactions in liquid helium. *Reviews of Modern Physics*, 49(2):341, 1977.

[92] Howard Georgi. Generalized dimensional analysis. *Phys. Lett. B*, 298:187–189, 1993.

[93] Luis Álvarez Gaumé, Domenico Orlando, and Susanne Reffert. Selected topics in the large quantum number expansion. *Phys. Rept.*, 933:1–66, 2021.

[94] Domenico Orlando, Susanne Reffert, and Francesco Sannino. Charging the Conformal Window. *Phys. Rev. D*, 103(10):105026, 2021.

[95] Gabriel Cuomo, Leonardo Rastelli, and Adar Sharon. Moduli spaces in CFT: large charge operators. *JHEP*, 09:185, 2024.

[96] S. Gandolfi, J. Lippuner, A. W. Steiner, I. Tews, X. Du, and M. Al-Mamun. From the microscopic to the macroscopic world: from nucleons to neutron stars. *J. Phys. G*, 46(10):103001, 2019.

[97] Tillmann Boeckel, Simon Schettler, and Jurgen Schaffner-Bielich. The Cosmological QCD Phase Transition Revisited. *Prog. Part. Nucl. Phys.*, 66:266–270, 2011.

[98] Francesco Sannino. Conformal Dynamics for TeV Physics and Cosmology. *Acta Phys. Polon. B*, 40:3533–3743, 2009.

[99] Giacomo Cacciapaglia, Claudio Pica, and Francesco Sannino. Fundamental Composite Dynamics: A Review. *Phys. Rept.*, 877:1–70, 2020.

[100] C. A. Baker et al. An Improved experimental limit on the electric dipole moment of the neutron. *Phys. Rev. Lett.*, 97:131801, 2006.

[101] C. Abel et al. Measurement of the Permanent Electric Dipole Moment of the Neutron. *Phys. Rev. Lett.*, 124(8):081803, 2020.

[102] Steven Weinberg. A New Light Boson? *Phys. Rev. Lett.*, 40:223–226, 1978.

[103] Frank Wilczek. Problem of Strong P and T Invariance in the Presence of Instantons. *Phys. Rev. Lett.*, 40:279–282, 1978.

[104] Jihn E. Kim. Weak Interaction Singlet and Strong CP Invariance. *Phys. Rev. Lett.*, 43:103, 1979.

[105] Mikhail A. Shifman, A. I. Vainshtein, and Valentin I. Zakharov. Can Confinement Ensure Natural CP Invariance of Strong Interactions? *Nucl. Phys. B*, 166:493–506, 1980.

[106] Michael Dine, Willy Fischler, and Mark Srednicki. A Simple Solution to the Strong CP Problem with a Harmless Axion. *Phys. Lett. B*, 104:199–202, 1981.

[107] Rabindra N. Mohapatra and G. Senjanovic. Natural Suppression of Strong p and t Noninvariance. *Phys. Lett. B*, 79:283–286, 1978.

[108] Ann E. Nelson. Naturally Weak CP Violation. *Phys. Lett. B*, 136:387–391, 1984.

[109] Stephen M. Barr. A Natural Class of Nonpeccei-quinn Models. *Phys. Rev. D*, 30:1805, 1984.

[110] Ann E. Nelson. Calculation of θ Barr. *Phys. Lett. B*, 143:165–170, 1984.

[111] S. D. H. Hsu and F. Sannino. New solutions to the strong CP problem. *Phys. Lett. B*, 605:369–375, 2005.

[112] Frank Wilczek and Guy Moore. Superheavy Light Quarks and the Strong P, T Problem. 1 2016.

[113] Randy Lewis, Claudio Pica, and Francesco Sannino. Light Asymmetric Dark Matter on the Lattice: SU(2) Technicolor with Two Fundamental Flavors. *Phys. Rev. D*, 85:014504, 2012.

[114] Ari Hietanen, Randy Lewis, Claudio Pica, and Francesco Sannino. Fundamental Composite Higgs Dynamics on the Lattice: SU(2) with Two Flavors. *JHEP*, 07:116, 2014.

[115] Thomas Appelquist, P. S. Rodrigues da Silva, and Francesco Sannino. Enhanced global symmetries and the chiral phase transition. *Phys. Rev. D*, 60:116007, 1999.

[116] Thomas A. Ryttov and Francesco Sannino. Ultra Minimal Technicolor and its Dark Matter TIMP. *Phys. Rev. D*, 78:115010, 2008.

[117] David B. Kaplan and Howard Georgi. SU(2) x U(1) Breaking by Vacuum Misalignment. *Phys. Lett. B*, 136:183–186, 1984.

[118] Eric D. Carlson, Marie E. Machacek, and Lawrence J. Hall. Self-interacting dark matter. *Astrophys. J.*, 398:43–52, 1992.

[119] Yonit Hochberg, Eric Kuflik, Tomer Volansky, and Jay G. Wacker. Mechanism for Thermal Relic Dark Matter of Strongly Interacting Massive Particles. *Phys. Rev. Lett.*, 113:171301, 2014.

[120] Yonit Hochberg, Eric Kuflik, Hitoshi Murayama, Tomer Volansky, and Jay G. Wacker. Model for Thermal Relic Dark Matter of Strongly Interacting Massive Particles. *Phys. Rev. Lett.*, 115(2):021301, 2015.

[121] Martin Hansen, Kasper Langæble, and Francesco Sannino. SIMP model at NNLO in chiral perturbation theory. *Phys. Rev. D*, 92(7):075036, 2015.

[122] Francesco Sannino and Kimmo Tuominen. Orientifold theory dynamics and symmetry breaking. *Phys. Rev. D*, 71:051901, 2005.

[123] Dennis D. Dietrich, Francesco Sannino, and Kimmo Tuominen. Light composite Higgs from higher representations versus electroweak precision measurements: Predictions for CERN LHC. *Phys. Rev. D*, 72:055001, 2005.

[124] Dennis D. Dietrich and Francesco Sannino. Conformal window of SU(N) gauge theories with fermions in higher dimensional representations. *Phys. Rev. D*, 75:085018, 2007.

[125] Francesco Sannino. Conformal Windows of SP(2N) and SO(N) Gauge Theories. *Phys. Rev. D*, 79:096007, 2009.

[126] Tuomas Karavirta, Jarno Rantaharju, Kari Rummukainen, and Kimmo Tuominen. Determining the conformal window: SU(2) gauge theory with N_f = 4, 6 and 10 fermion flavours. *JHEP*, 05:003, 2012.

[127] Hiroshi Ohki, Tatsumi Aoyama, Etsuko Itou, Masafumi Kurachi, C. J. David Lin, Hideo Matsufuru, Tetsuya Onogi, Eigo Shintani, and Takeshi Yamazaki. Study of the scaling properties in SU(2) gauge theory with eight flavors. *PoS*, LATTICE2010:066, 2010.

[128] Jarno Rantaharju, Tuomas Karavirta, Viljami Leino, Teemu Rantalaiho, Kari Rummukainen, and Kimmo Tuominen. The gradient flow running coupling in SU2 with 8 flavors. *PoS*, LATTICE2014:258, 2014.

[129] Ari Hietanen, Randy Lewis, Claudio Pica, and Francesco Sannino. Composite Goldstone Dark Matter: Experimental Predictions from the Lattice. *JHEP*, 12:130, 2014.

[130] Rudy Arthur, Vincent Drach, Martin Hansen, Ari Hietanen, Claudio Pica, and Francesco Sannino. SU(2) gauge theory with two fundamental flavors: A minimal template for model building. *Phys. Rev. D*, 94(9):094507, 2016.

[131] Viljami Leino, Kari Rummukainen, Joni M. Suorsa, Kimmo Tuominen, and Sara Tähtinen. Infrared Behaviour of SU(2) Gauge Theory with N_f fundamental flavours. *PoS*, Confinement2018:225, 2019.

[132] Francis Bursa, Luigi Del Debbio, Liam Keegan, Claudio Pica, and Thomas Pickup. Mass anomalous dimension in SU(2) with six fundamental fermions. *Phys. Lett. B*, 696:374–379, 2011.

[133] M. Hayakawa, K. I. Ishikawa, S. Takeda, and N. Yamada. Running coupling constant and mass anomalous dimension of six-flavor SU(2) gauge theory. *Phys. Rev. D*, 88(9):094504, 2013.

[134] T. Appelquist et al. Two-Color Gauge Theory with Novel Infrared Behavior. *Phys. Rev. Lett.*, 112(11):111601, 2014.

[135] Viljami Leino, Teemu Rantalaiho, Kari Rummukainen, Joni M. Suorsa, Kimmo Tuominen, and Sara Tähtinen. Gradient flow running coupling in SU(2) Nf=6 flavors. *PoS*, LATTICE2016:218, 2016.

[136] Joni M. Suorsa, Viljami Leino, Jarno Rantaharju, Teemu Rantalaiho, Kari Rummukainen, Kimmo Tuominen, and Sara Tähtinen. Mass anomalous dimension of SU(2) using the spectral density method. *PoS*, LATTICE2016:389, 2016.

[137] Atsushi Nakamura. Quarks and Gluons at Finite Temperature and Density. *Phys. Lett. B*, 149:391, 1984.

[138] Simon Hands, John B. Kogut, Maria-Paola Lombardo, and Susan E. Morrison. Symmetries and spectrum of SU(2) lattice gauge theory at finite chemical potential. *Nucl. Phys. B*, 558:327–346, 1999.

[139] John B. Kogut, Dominique Toublan, and D. K. Sinclair. Diquark condensation at nonzero chemical potential and temperature. *Phys. Lett. B*, 514:77–87, 2001.

[140] John B. Kogut, Dominique Toublan, and D. K. Sinclair. The Phase diagram of four flavor SU(2) lattice gauge theory at nonzero chemical potential and temperature. *Nucl. Phys. B*, 642:181–209, 2002.

[141] Shin Muroya, Atsushi Nakamura, and Chiho Nonaka. Behavior of hadrons at finite density: Lattice study of color SU(2) QCD. *Phys. Lett. B*, 551:305–310, 2003.

[142] Simon Hands, Seyong Kim, and Jon-Ivar Skullerud. Deconfinement in dense 2-color QCD. *Eur. Phys. J. C*, 48:193, 2006.

[143] Seamus Cotter, Pietro Giudice, Simon Hands, and Jon-Ivar Skullerud. Towards the phase diagram of dense two-color matter. *Phys. Rev. D*, 87(3):034507, 2013.

[144] Tamer Boz, Seamus Cotter, Leonard Fister, Dhagash Mehta, and Jon-Ivar Skullerud. Phase transitions and gluodynamics in 2-colour matter at high density. *Eur. Phys. J. A*, 49:87, 2013.

[145] V. V. Braguta, E. M. Ilgenfritz, A. Yu. Kotov, A. V. Molochkov, and A. A. Nikolaev. Study of the phase diagram of dense two-color QCD within lattice simulation. *Phys. Rev. D*, 94(11):114510, 2016.

[146] Lukas Holicki, Jonas Wilhelm, Dominik Smith, Björn Wellegehausen, and Lorenz von Smekal. Two-colour QCD at finite density with two flavours of staggered quarks. *PoS*, LATTICE2016:052, 2017.

[147] V. G. Bornyakov, V. V. Braguta, E. M. Ilgenfritz, A. Yu. Kotov, A. V. Molochkov, and A. A. Nikolaev. Observation of deconfinement in a cold dense quark medium. *JHEP*, 03:161, 2018.

[148] Tamer Boz, Ouraman Hajizadeh, Axel Maas, and Jon-Ivar Skullerud. Finite-density gauge correlation functions in QC2D. *Phys. Rev. D*, 99(7):074514, 2019.

[149] N. Yu. Astrakhantsev, V. G. Bornyakov, V. V. Braguta, E. M. Ilgenfritz, A. Yu. Kotov, A. A. Nikolaev, and A. Rothkopf. Lattice study of static quark-antiquark interactions in dense quark matter. *JHEP*, 05:171, 2019.

[150] Tamer Boz, Pietro Giudice, Simon Hands, and Jon-Ivar Skullerud. Dense two-color QCD towards continuum and chiral limits. *Phys. Rev. D*, 101(7):074506, 2020.

[151] Kei Iida, Etsuko Itou, and Tong-Gyu Lee. Two-colour QCD phases and the topology at low temperature and high density. *JHEP*, 01:181, 2020.

[152] Jonas Wilhelm, Lukas Holicki, Dominik Smith, Björn Wellegehausen, and Lorenz von Smekal. Continuum Goldstone spectrum of two-color QCD at finite density with staggered quarks. *Phys. Rev. D*, 100(11):114507, 2019.

[153] V. G. Bornyakov, V. V. Braguta, A. A. Nikolaev, and R. N. Rogalyov. Effects of Dense Quark Matter on Gluon Propagators in Lattice QC_2D. *Phys. Rev. D*, 102:114511, 2020.

[154] Kei Iida, Etsuko Itou, and Tong-Gyu Lee. Relative scale setting for two-color QCD with $N_f=2$ Wilson fermions. *PTEP*, 2021(1):013B05, 2021.

[155] N. Astrakhantsev, V. V. Braguta, E. M. Ilgenfritz, A. Yu. Kotov, and A. A. Nikolaev. Lattice study of thermodynamic properties of dense QC_2D. *Phys. Rev. D*, 102(7):074507, 2020.

[156] T. G. Khunjua, K. G. Klimenko, and R. N. Zhokhov. The dual properties of chiral and isospin asymmetric dense quark matter formed of two-color quarks. *JHEP*, 06:148, 2020.

[157] Toru Kojo and Daiki Suenaga. Thermal quarks and gluon propagators in two-color dense QCD. *Phys. Rev. D*, 103(9):094008, 2021.

[158] Daniel F. Litim and Francesco Sannino. Asymptotic safety guaranteed. *JHEP*, 12:178, 2014.

[159] Daniel F. Litim, Matin Mojaza, and Francesco Sannino. Vacuum stability of asymptotically safe gauge-Yukawa theories. *JHEP*, 01:081, 2016.

[160] Oleg Antipin and Francesco Sannino. Conformal Window 2.0: The large N_f safe story. *Phys. Rev. D*, 97(11):116007, 2018.

[161] Viljami Leino, Tobias Rindlisbacher, Kari Rummukainen, Francesco Sannino, and Kimmo Tuominen. Safety versus triviality on the lattice. *Phys. Rev. D*, 101(7):074508, 2020.

[162] Jarno Rantaharju, Tobias Rindlisbacher, Kari Rummukainen, Ahmed Salami, and Kimmo Tuominen. Spectrum of SU(2) gauge theory at large number of flavors. *Phys. Rev. D*, 104(11):114504, 2021.

[163] Max A. Metlitski and Ariel R. Zhitnitsky. Theta-parameter in 2 color QCD at finite baryon and isospin density. *Nucl. Phys. B*, 731:309–334, 2005.

[164] Julien Barrat. *Line defects in conformal field theory*. PhD thesis, Humboldt U., Berlin, Humboldt-Universität zu Berlin, 2024.

[165] Alberto García Martín-Caro. *Solitons and effective field theories in the Physics of strong interactions*. PhD thesis, Santiago de Compostela U., 2023.

[166] Geraint Wyn Evans. *Superconducting phases of strongly-interacting matter in large magnetic fields*. PhD thesis, University of Southampton, Southampton U., 2023.

[167] Victor V. Braguta. Phase Diagram of Dense Two-Color QCD at Low Temperatures. *Symmetry*, 15(7):1466, 2023.

[168] P. Achenbach et al. The present and future of QCD. *Nucl. Phys. A*, 1047:122874, 2024.

[169] WJ Marciano and H Pagels. Quantum chromodynamics: a review, phys. *Rept*, 36:137, 1978.

[170] N Brambilla, S Eidelman, P Foka, S Gardner, AS Kronfeld, MG Alford, R Alkofer, M Butenschoen, TD Cohen, J Erdmenger, et al. Qcd and strongly coupled gauge theories: challenges and perspectives. *The European Physical Journal C*, 74(10):2981, 2014.

[171] A Tawfik. Influence of strange quarks on the qcd phase diagram and chemical freeze-out. *Journal of Physics G: Nuclear and Particle Physics*, 31(6):S1105, 2005.

[172] A Tawfik. Qcd phase diagram: a comparison of lattice and hadron resonance gas model calculations. *Physical Review DParticles, Fields, Gravitation, and Cosmology*, 71(5):054502, 2005.

[173] TG Khunjua, KG Klimenko, and Roman N Zhokhov. Qcd phase diagram with chiral imbalance in njl model: Duality and lattice qcd results. In *Journal of Physics: Conference Series*, volume 1390, page 012015. IOP Publishing, 2019.

[174] Wenkai Fan, Xiaofeng Luo, and Hongshi Zong. Probing the qcd phase structure with higher order baryon number susceptibilities within the njl model. *Chinese Physics C*, 43(3):033103, 2019.

[175] Keitaro Nagata and Atsushi Nakamura. Qcd phase diagram with imaginary chemical potential. In *EPJ Web of Conferences*, volume 20, page 03006. EDP Sciences, 2012.

[176] Erhard Seiler. Status of complex langevin. In *EPJ Web of Conferences*, volume 175, page 01019. EDP Sciences, 2018.

[177] Luigi Scorzato. The lefschetz thimble and the sign problem. *arXiv preprint arXiv:1512.08039*, 2015.

[178] K Langfeld. Density-of-states. pos 2017. *LATTICE2016*, 256.

[179] D. T. Son and Misha A. Stephanov. QCD at finite isospin density: From pion to quark - anti-quark condensation. *Phys. Atom. Nucl.*, 64:834–842, 2001.

[180] J. B. Kogut, Misha A. Stephanov, D. Toublan, J. J. M. Verbaarschot, and A. Zhitnitsky. QCD - like theories at finite baryon density. *Nucl. Phys. B*, 582:477–513, 2000.

[181] Björn H Wellegehausen, Axel Maas, Andreas Wipf, and Lorenz von Smekal. Hadron masses and baryonic scales in g 2-qcd at finite density. *Physical Review D*, 89(5):056007, 2014.

[182] Gunnar Bali, Francis Bursa, Luca Castagnini, Sara Collins, Luigi Del Debbio, Biagio Lucini, and Marco Panero. Mesons in large-n qcd. *Journal of High Energy Physics*, 2013(6):1–52, 2013.

[183] DT Son. Superconductivity by long-range color magnetic interaction in high-density quark matter. *Physical Review D*, 59(9):094019, 1999.

[184] Martin Aria Mojahed. Two-flavor chiral perturbation theory at finite isospin density beyond leading order. Master's thesis, Norwegian U. Sci. Tech., 2020.

[185] T. H. R. Skyrme. A Nonlinear field theory. *Proc. Roy. Soc. Lond. A*, 260:127–138, 1961.

[186] David Scheffler. Two-color lattice qcd with staggered quarks. 2015.

[187] J. Kogut, M. Stone, H.W. Wyld, S.H. Shenker, J. Shigemitsu, and D.K. Sinclair. Studies of chiral symmetry breaking in su(2) lattice gauge theory. *Nuclear Physics B*, 225(3):326–370, 1983.

[188] JB Kogut, Misha A Stephanov, D Toublan, JJM Verbaarschot, and A Zhitnitsky. Qcd-like theories at finite baryon density. *Nuclear Physics B*, 582(1-3):477–513, 2000.

[189] Gerhard Ecker. Chiral perturbation theory. *Progress in Particle and Nuclear Physics*, 35:1–80, 1995.

[190] Antonio Pich. Chiral perturbation theory. *Reports on Progress in Physics*, 58(6):563, 1995.

[191] Stefan Scherer. Introduction to chiral perturbation theory. In *Advances in Nuclear Physics, Volume 27*, pages 277–538. Springer, 2003.

[192] Michael E Peskin. The alignment of the vacuum in theories of technicolor. *Nuclear Physics B*, 175(2):197–233, 1980.

[193] K. Splittorff, D. T. Son, and Misha A. Stephanov. QCD - like theories at finite baryon and isospin density. *Phys. Rev. D*, 64:016003, 2001.

[194] Michael E. Peskin. The Alignment of the Vacuum in Theories of Technicolor. *Nucl. Phys. B*, 175:197–233, 1980.

[195] Jonathan Thomas Lenaghan, Francesco Sannino, and Kim Splittorff. The superfluid and conformal phase transitions of two-color QCD. *Physical Review D*, 65(5), jan 2002.

[196] Massimo Mannarelli. Meson condensation. *Particles*, 2(3):411–443, 2019.

[197] Andrea Mammarella and Massimo Mannarelli. Intriguing aspects of meson condensation. *Phys. Rev. D*, 92(8):085025, 2015.

[198] Maarten Golterman and Yigal Shamir. Effective action for pions and a dilatonic meson. *PoS*, LATTICE2016:205, 2016.

[199] Tom Banks and A. Zaks. On the Phase Structure of Vector-Like Gauge Theories with Massless Fermions. *Nucl. Phys. B*, 196:189–204, 1982.

[200] Giacomo Cacciapaglia and Francesco Sannino. Evidence for complex fixed points in pandemic data. 8 2020.

[201] Alessandra D'Alise, Davide Iacobacci, and Francesco Sannino. A temporal playbook for multiple wave dengue pandemic from latin america and asia to italy, 2024.

[202] V. L. Berezinsky. Destruction of long range order in one-dimensional and two-dimensional systems having a continuous symmetry group. I. Classical systems. *Sov. Phys. JETP*, 32:493–500, 1971.

[203] J. M. Kosterlitz and D. J. Thouless. Ordering, metastability and phase transitions in two-dimensional systems. *J. Phys. C*, 6:1181–1203, 1973.

[204] J. M. Kosterlitz. The critical properties of the two-dimensional xy model. *J. Phys. C*, 7(6):1046, 1974.

[205] V. A. Miransky and Koichi Yamawaki. Conformal phase transition in gauge theories. *Phys. Rev. D*, 55:5051–5066, 1997. [Erratum: Phys.Rev.D 56, 3768 (1997)].

[206] V. A. Miransky. Dynamics of Spontaneous Chiral Symmetry Breaking and Continuum Limit in Quantum Electrodynamics. *Nuovo Cim. A*, 90:149–170, 1985.

[207] Thomas Appelquist, John Terning, and L. C. R. Wijewardhana. The Zero temperature chiral phase transition in SU(N) gauge theories. *Phys. Rev. Lett.*, 77:1214–1217, 1996.

[208] Holger Gies and Joerg Jaeckel. Chiral phase structure of QCD with many flavors. *Eur. Phys. J. C*, 46:433–438, 2006.

[209] Francesco Sannino. Jumping Dynamics. *Mod. Phys. Lett. A*, 28:1350127, 2013.

[210] Bob Holdom. Raising Condensates Beyond the Ladder. *Phys. Lett. B*, 213:365–369, 1988.

[211] Bob Holdom. Continuum Limit of Quenched Theories. *Phys. Rev. Lett.*, 62:997, 1989.

[212] Andrew G. Cohen and Howard Georgi. Walking Beyond the Rainbow. *Nucl. Phys. B*, 314:7–24, 1989.

[213] Chung Ngoc Leung, S. T. Love, and William A. Bardeen. Spontaneous Symmetry Breaking in Scale Invariant Quantum Electrodynamics. *Nucl. Phys. B*, 273:649–662, 1986.

[214] William A. Bardeen, Chung Ngoc Leung, and S. T. Love. The Dilaton and Chiral Symmetry Breaking. *Phys. Rev. Lett.*, 56:1230, 1986.

[215] Koichi Yamawaki, Masako Bando, and Ken-iti Matumoto. Scale Invariant Technicolor Model and a Technidilaton. *Phys. Rev. Lett.*, 56:1335, 1986.

[216] Francesco Sannino and Joseph Schechter. Chiral phase transition for SU(N) gauge theories via an effective Lagrangian approach. *Phys. Rev. D*, 60:056004, 1999.

[217] Deog Ki Hong, Stephen D. H. Hsu, and Francesco Sannino. Composite Higgs from higher representations. *Phys. Lett. B*, 597:89–93, 2004.

[218] Thomas Appelquist and Yang Bai. A Light Dilaton in Walking Gauge Theories. *Phys. Rev. D*, 82:071701, 2010.

[219] Zackaria Chacko and Rashmish K. Mishra. Effective Theory of a Light Dilaton. *Phys. Rev. D*, 87(11):115006, 2013.

[220] Shinya Matsuzaki and Koichi Yamawaki. Dilaton Chiral Perturbation Theory: Determining the Mass and Decay Constant of the Technidilaton on the Lattice. *Phys. Rev. Lett.*, 113(8):082002, 2014.

[221] Martin Hansen, Kasper Langæble, and Francesco Sannino. Extending Chiral Perturbation Theory with an Isosinglet Scalar. *Phys. Rev. D*, 95(3):036005, 2017.

[222] Maarten Golterman and Yigal Shamir. Low-energy effective action for pions and a dilatonic meson. *Phys. Rev. D*, 94(5):054502, 2016.

[223] Oscar Catà and Christoph Müller. Chiral effective theories with a light scalar at one loop. *Nucl. Phys. B*, 952:114938, 2020.

[224] Maarten Golterman, Ethan T. Neil, and Yigal Shamir. Application of dilaton chiral perturbation theory to $N_f = 8$, $\mathrm{SU}(3)$ spectral data. *Phys. Rev. D*, 102(3):034515, 2020.

[225] Thomas Appelquist, James Ingoldby, and Maurizio Piai. Nearly Conformal Composite Higgs Model. *Phys. Rev. Lett.*, 126(19):191804, 2021.

[226] Thomas Appelquist, James Ingoldby, and Maurizio Piai. Dilaton Effective Field Theory. *Universe*, 9(1):10, 2023.

[227] O. Catà, R. J. Crewther, and Lewis C. Tunstall. Crawling technicolor. *Phys. Rev. D*, 100(9):095007, 2019.

[228] Thomas Appelquist, James Ingoldby, and Maurizio Piai. Dilaton potential and lattice data. *Physical Review D*, 101(7):075025, 2020.

[229] Oleg Antipin, Matin Mojaza, and Francesco Sannino. Light Dilaton at Fixed Points and Ultra Light Scale Super Yang Mills. *Phys. Lett. B*, 712:119–125, 2012.

[230] Roman Marcarelli, Nicholas Miesch, and Ethan T. Neil. Mass-induced confinement near the sill of the conformal window. *Phys. Rev. D*, 107(7):076011, 2023.

[231] James Ingoldby. Hidden Conformal Symmetry from Eight Flavors. In *40th International Symposium on Lattice Field Theory*, 12 2023.

[232] Thomas Appelquist, James Ingoldby, and Maurizio Piai. Dilaton potential and lattice data. *Phys. Rev. D*, 101(7):075025, 2020.

[233] T. Appelquist et al. Nonperturbative investigations of SU(3) gauge theory with eight dynamical flavors. *Phys. Rev. D*, 99(1):014509, 2019.

[234] Thomas Appelquist, James Ingoldby, and Maurizio Piai. Analysis of a Dilaton EFT for Lattice Data. *JHEP*, 03:039, 2018.

[235] Yigal Shamir and Maarten Golterman. Dilaton chiral perturbation theory and application. *PoS*, LATTICE2021:372, 2022.

[236] Maarten Golterman and Yigal Shamir. Explorations beyond dilaton chiral perturbation theory in the eight-flavor SU(3) gauge theory. *Phys. Rev. D*, 102:114507, 2020.

[237] Andrew Freeman, Maarten Golterman, and Yigal Shamir. Dilaton chiral perturbation theory at next-to-leading order. *Phys. Rev. D*, 108(7):074506, 2023.

[238] Maarten Golterman and Yigal Shamir. Fits of $SU(3)$ $N_f = 8$ data to dilaton-pion effective field theory. *PoS*, LATTICE2019:130, 2019.

[239] Maarten Golterman and Yigal Shamir. Large-mass regime of the dilaton-pion low-energy effective theory. *Phys. Rev. D*, 98(5):056025, 2018.

[240] Debasish Banerjee, Shailesh Chandrasekharan, and Domenico Orlando. Conformal dimensions via large charge expansion. *Phys. Rev. Lett.*, 120(6):061603, 2018.

[241] Domenico Orlando, Susanne Reffert, and Francesco Sannino. Near-Conformal Dynamics at Large Charge. *Phys. Rev. D*, 101(6):065018, 2020.

[242] Simeon Hellerman, Daniil Krichevskiy, Domenico Orlando, Vito Pellizzani, Susanne Reffert, and Ian Swanson. The unitary Fermi gas at large charge and large N. 11 2023.

[243] Oleg Antipin, Jahmall Bersini, Francesco Sannino, Zhi-Wei Wang, and Chen Zhang. Charging the $O(N)$ model. *Phys. Rev. D*, 102(4):045011, 2020.

[244] Oleg Antipin, Jahmall Bersini, and Pantelis Panopoulos. Yukawa interactions at Large Charge. 8 2022.

[245] Oleg Antipin, Alexander Bednyakov, Jahmall Bersini, Pantelis Panopoulos, and Andrey Pikelner. Gauge Invariance at Large Charge. *Phys. Rev. Lett.*, 130(2):021602, 2023.

[246] Oleg Antipin, Jahmall Bersini, Pantelis Panopoulos, Francesco Sannino, and Zhi-Wei Wang. Infinite order results for charged sectors of the Standard Model. 12 2023.

[247] Gabriel Cuomo. A note on the large charge expansion in 4d CFT. *Phys. Lett. B*, 812:136014, 2021.

[248] G. Arias-Tamargo, D. Rodriguez-Gomez, and J. G. Russo. The large charge limit of scalar field theories and the Wilson-Fisher fixed point at $\epsilon = 0$. *JHEP*, 10:201, 2019.

[249] Debasish Banerjee, Shailesh Chandrasekharan, Domenico Orlando, and Susanne Reffert. Conformal dimensions in the large charge sectors at the O(4) Wilson-Fisher fixed point. *Phys. Rev. Lett.*, 123(5):051603, 2019.

[250] Debasish Banerjee and Shailesh Chandrasekharan. Subleading conformal dimensions at the O(4) Wilson-Fisher fixed point. *Phys. Rev. D*, 105(3):L031507, 2022.

[251] Hersh Singh. Large-charge conformal dimensions at the $O(N)$ Wilson-Fisher fixed point. 2 2022.

[252] Gabriel Cuomo, J. M. Viana Parente Lopes, José Matos, Júlio Oliveira, and Joao Penedones. Numerical tests of the large charge expansion. 4 2023.

[253] Simeon Hellerman and Shunsuke Maeda. On the Large R-charge Expansion in $\mathcal{N} = 2$ Superconformal Field Theories. *JHEP*, 12:135, 2017.

[254] Luis Alvarez-Gaume, Domenico Orlando, and Susanne Reffert. Large charge at large N. *JHEP*, 12:142, 2019.

[255] Domenico Orlando, Susanne Reffert, and Francesco Sannino. A safe CFT at large charge. *JHEP*, 08:164, 2019.

[256] Nicola Dondi, Ioannis Kalogerakis, Rafael Moser, Domenico Orlando, and Susanne Reffert. Spinning correlators in large-charge CFTs. 3 2022.

[257] RJ Crewther, P Di Vecchia, G Veneziano, and Edward Witten. Chiral estimate of the electric dipole moment of the neutron in quantum chromodynamics. *Physics Letters B*, 88(1-2):123–127, 1979.

[258] Roberto D Peccei and Helen R Quinn. Cp conservation in the presence of pseudoparticles. *Physical Review Letters*, 38(25):1440, 1977.

[259] Roberto D Peccei and Helen R Quinn. Constraints imposed by cp conservation in the presence of pseudoparticles. *Physical Review D*, 16(6):1791, 1977.

[260] Edward Witten. Large N Chiral Dynamics. *Annals Phys.*, 128:363, 1980.

[261] P. Di Vecchia and G. Veneziano. Chiral Dynamics in the Large n Limit. *Nucl. Phys. B*, 171:253–272, 1980.

[262] Davide Gaiotto, Zohar Komargodski, and Nathan Seiberg. Time-reversal breaking in QCD_4, walls, and dualities in 2 + 1 dimensions. *JHEP*, 01:110, 2018.

[263] Andrei V. Smilga. QCD at theta similar to pi. *Phys. Rev. D*, 59:114021, 1999.

[264] Michel H. G. Tytgat. QCD at theta similar to pi reexamined: Domain walls and spontaneous CP violation. *Phys. Rev. D*, 61:114009, 2000.

[265] Roger F. Dashen. Some features of chiral symmetry breaking. *Phys. Rev. D*, 3:1879–1889, 1971.

[266] Paolo Di Vecchia and Francesco Sannino. The Physics of the θ-angle for Composite Extensions of the Standard Model. *Eur. Phys. J. Plus*, 129:262, 2014.

[267] D. T. Son. Low-energy quantum effective action for relativistic superfluids. 4 2002.

[268] Edward Witten. Current Algebra Theorems for the U(1) Goldstone Boson. *Nucl. Phys. B*, 156:269–283, 1979.

[269] G. Veneziano. U(1) Without Instantons. *Nucl. Phys. B*, 159:213–224, 1979.

[270] Gregory S. Adkins, Chiara R. Nappi, and Edward Witten. Static Properties of Nucleons in the Skyrme Model. *Nucl. Phys. B*, 228:552, 1983.

[271] Gregory S. Adkins and Chiara R. Nappi. The Skyrme Model with Pion Masses. *Nucl. Phys. B*, 233:109–115, 1984.

[272] Gregory S. Adkins and Chiara R. Nappi. Stabilization of Chiral Solitons via Vector Mesons. *Phys. Lett. B*, 137:251–256, 1984.

[273] I. Zahed and G. E. Brown. The Skyrme Model. *Phys. Rept.*, 142:1–102, 1986.

[274] P. Jain, R. Johnson, Ulf G. Meissner, N. W. Park, and J. Schechter. Realistic Pseudoscalar Vector Chiral Lagrangian and Its Soliton Excitations. *Phys. Rev. D*, 37:3252, 1988.

[275] Ulf G. Meissner. Low-Energy Hadron Physics from Effective Chiral Lagrangians with Vector Mesons. *Phys. Rept.*, 161:213, 1988.

[276] William Detmold, Christoph Lehner, and Stefan Meinel. $\Lambda_b \to p\ell^-\bar{\nu}_\ell$ and $\Lambda_b \to \Lambda_c\ell^-\bar{\nu}_\ell$ form factors from lattice QCD with relativistic heavy quarks. *Phys. Rev. D*, 92(3):034503, 2015.

[277] Dante Bigi and Paolo Gambino. Revisiting $B \to D\ell\nu$. *Phys. Rev. D*, 94(9):094008, 2016.

[278] Yasmine Sara Amhis et al. Averages of b-hadron, c-hadron, and τ-lepton properties as of 2021. *Phys. Rev. D*, 107(5):052008, 2023.

[279] Curtis G. Callan, Jr. and Igor R. Klebanov. Bound State Approach to Strangeness in the Skyrme Model. *Nucl. Phys. B*, 262:365–382, 1985.

[280] Robert L. Jaffe. Perhaps a Stable Dihyperon. *Phys. Rev. Lett.*, 38:195–198, 1977. [Erratum: Phys.Rev.Lett. 38, 617 (1977)].

[281] N. N. Scoccola, H. Nadeau, Maciej A. Nowak, and Mannque Rho. The Hyperons as Skyrmions With Vector Mesons. *Phys. Lett. B*, 201:425, 1988. [Erratum: Phys.Lett.B 220, 658 (1989)].

[282] David B. Kaplan and Igor R. Klebanov. The Role of a Massive Strange Quark in the Large N Skyrme Model. *Nucl. Phys. B*, 335:45–66, 1990.

[283] Y. Kondo, S. Saito, and T. Otofuji. Semileptonic hyperon decays in the Skyrme model with bound kaon approach to strangeness. *Phys. Lett. B*, 256:316–320, 1991.

[284] H. Weigel, Reinhard Alkofer, and H. Reinhardt. Hyperons in the bound state approach to the Nambu-Jona-Lasinio chiral soliton. *Nucl. Phys. A*, 576:477–524, 1994.

[285] E. Eichten and F. Feinberg. Spin Dependent Forces in QCD. *Phys. Rev. D*, 23:2724, 1981.

[286] Zachary Guralnik, Michael E. Luke, and Aneesh V. Manohar. Properties of baryons containing a heavy quark in the Skyrme model. *Nucl. Phys. B*, 390:474–500, 1993.

[287] Elizabeth Ellen Jenkins and Aneesh V. Manohar. Hyperfine splittings of baryons containing a heavy quark in the Skyrme model. *Phys. Lett. B*, 294:273–280, 1992.

[288] Yong-seok Oh, Byung-Yoon Park, and Dong-Pil Min. Heavy baryons as Skyrmion with 1/m(Q) corrections. *Phys. Rev. D*, 49:4649–4658, 1994.

[289] Kumar S. Gupta, M. Arshad Momen, J. Schechter, and A. Subbaraman. Heavy quark solitons. *Phys. Rev. D*, 47:R4835–R4839, 1993.

[290] J. Schechter, A. Subbaraman, S. Vaidya, and H. Weigel. Heavy quark solitons: Towards realistic masses. *Nucl. Phys. A*, 590:655–679, 1995. [Erratum: Nucl.Phys.A 598, 583–583 (1996)].

[291] Masayasu Harada, Asif Qamar, Francesco Sannino, Joseph Schechter, and Herbert Weigel. Hyperfine splitting of low lying heavy baryons. *Nucl. Phys. A*, 625:789, 1997.

[292] Masayasu Harada, Francesco Sannino, Joseph Schechter, and Herbert Weigel. Generalization of the bound state model. *Phys. Rev. D*, 56:4098–4114, 1997.

[293] M. B. Voloshin and Mikhail A. Shifman. On the annihilation constants of mesons consisting of a heavy and a light quark, and $B^0 \leftrightarrow \overline{B}^{-0}$ oscillations. *Sov. J. Nucl. Phys.*, 45:292, 1987.

[294] Nathan Isgur and Mark B. Wise. Weak Decays of Heavy Mesons in the Static Quark Approximation. *Phys. Lett. B*, 232:113–117, 1989.

[295] Mark B. Wise. Combining chiral and heavy quark symmetry. In *CCAST Symposium on Particle Physics at the Fermi Scale*, pages 71–114, 5 1993.

[296] Matthias Neubert. Heavy quark symmetry. *Phys. Rept.*, 245:259–396, 1994.

[297] Michael E. Luke and Aneesh V. Manohar. Reparametrization invariance constraints on heavy particle effective field theories. *Phys. Lett. B*, 286:348–354, 1992.

[298] Adam F. Falk and Matthias Neubert. Second order power corrections in the heavy quark effective theory. 2. Baryon form-factors. *Phys. Rev. D*, 47:2982–2990, 1993.

[299] Adam F. Falk, Benjamin Grinstein, and Michael E. Luke. Leading mass corrections to the heavy quark effective theory. *Nucl. Phys. B*, 357:185–207, 1991.

[300] Aya Kasai, Ken-ichi Okumura, and Hiroshi Suzuki. A dilaton-pion mass relation. 9 2016.

[301] Maarten Golterman and Yigal Shamir. Effective pion mass term and the trace anomaly. *Phys. Rev. D*, 95(1):016003, 2017.

[302] Thomas Appelquist, James Ingoldby, and Maurizio Piai. Dilaton EFT Framework For Lattice Data. *JHEP*, 07:035, 2017.

[303] Maarten Golterman and Yigal Shamir. Dilaton chiral perturbation theory and applications. *PoS*, LATTICE2021:372, 2022.

[304] R. J. Crewther and Lewis C. Tunstall. $\Delta I = 1/2$ rule for kaon decays derived from QCD infrared fixed point. *Phys. Rev. D*, 91(3):034016, 2015.

[305] Roman Zwicky. QCD with an Infrared Fixed Point – Pion Sector. 6 2023.

[306] Fabrizio Canfora. Magnetized Baryonic layer and a novel BPS bound in the gauged-Non-Linear-Sigma-Model-Maxwell theory in (3+1)-dimensions through Hamilton-Jacobi equation. 9 2023.

[307] P. D. Alvarez, F. Canfora, N. Dimakis, and A. Paliathanasis. Integrability and chemical potential in the (3 + 1)-dimensional Skyrme model. *Phys. Lett. B*, 773:401–407, 2017.

[308] Eloy Ayon-Beato, Fabrizio Canfora, and Jorge Zanelli. Analytic self-gravitating Skyrmions, cosmological bounces and AdS wormholes. *Phys. Lett. B*, 752:201–205, 2016.

[309] Fabrizio Canfora, Diego Hidalgo, Marcela Lagos, Enzo Meneses, and Aldo Vera. Infinite conformal symmetry and emergent chiral fields of topologically nontrivial configurations: From Yang-Mills-Higgs theory to the Skyrme model. *Phys. Rev. D*, 106(10):105016, 2022.

[310] Fabrizio Canfora. Ordered arrays of Baryonic tubes in the Skyrme model in (3 + 1) dimensions at finite density. *Eur. Phys. J. C*, 78(11):929, 2018.

[311] Gonzalo Barriga, Fabrizio Canfora, Matías Torres, and Aldo Vera. Crystals of gauged solitons, force free plasma and resurgence. *Phys. Rev. D*, 103(9):096023, 2021.

[312] Gonzalo Barriga, Fabrizio Canfora, Marcela Lagos, Matías Torres, and Aldo Vera. On the robustness of solitons crystals in the Skyrme model. *Nucl. Phys. B*, 983:115913, 2022.

[313] Fabrizio Canfora and Scarlett C. Rebolledo-Caceres. Skyrmions at finite density. *Mod. Phys. Lett. A*, 38(12n13):2330002, 2023.

[314] Hee-Jung Lee, Byung-Yoon Park, Mannque Rho, and Vicente Vento. Sliding vacua in dense skyrmion matter. *Nucl. Phys. A*, 726:69–92, 2003.

[315] Byung-Yoon Park, Mannque Rho, and Vicente Vento. The Role of the Dilaton in Dense Skyrmion Matter. *Nucl. Phys. A*, 807:28–37, 2008.

[316] Yong-Liang Ma and Mannque Rho. Pseudoconformal structure in dense baryonic matter. *Phys. Rev. D*, 99(1):014034, 2019.

[317] Long-Qi Shao and Yong-Liang Ma. Scale symmetry and composition of compact star matter. *Phys. Rev. D*, 106(1):014014, 2022.

[318] Won-Gi Paeng, Thomas T. S. Kuo, Hyun Kyu Lee, Yong-Liang Ma, and Mannque Rho. Scale-invariant hidden local symmetry, topology change, and dense baryonic matter. II. *Phys. Rev. D*, 96(1):014031, 2017.

[319] G. E. Brown and Mannque Rho. On the manifestation of chiral symmetry in nuclei and dense nuclear matter. *Phys. Rept.*, 363:85–171, 2002.

[320] Jeremy W. Holt, Mannque Rho, and Wolfram Weise. Chiral symmetry and effective field theories for hadronic, nuclear and stellar matter. *Phys. Rept.*, 621:2–75, 2016.

[321] Yong-Liang Ma, Masayasu Harada, Hyun Kyu Lee, Yongseok Oh, Byung-Yoon Park, and Mannque Rho. Dense baryonic matter in the hidden local symmetry approach: Half-skyrmions and nucleon mass. *Phys. Rev. D*, 88(1):014016, 2013. [Erratum: Phys.Rev.D 88, 079904 (2013)].

[322] Won-Gi Paeng, Thomas T. S. Kuo, Hyun Kyu Lee, and Mannque Rho. Scale-Invariant Hidden Local Symmetry, Topology Change and Dense Baryonic Matter. *Phys. Rev. C*, 93(5):055203, 2016.

[323] GE Brown and Mannque Rho. Scaling effective lagrangians in a dense medium. *Physical review letters*, 66(21):2720, 1991.

[324] M. Harada, F. Sannino, J. Schechter, and H. Weigel. Scaling behavior in soliton models. *Phys. Lett. B*, 384:5–12, 1996.

[325] Yan-Ling Li, Yong-Liang Ma, and Mannque Rho. Chiral-scale effective theory including a dilatonic meson. *Phys. Rev. D*, 95(11):114011, 2017.

[326] Yong-Liang Ma and Wen-Cong Yang. Topology and Emergent Symmetries in Dense Compact Star Matter. *Symmetry*, 15(3):776, 2023.

[327] Yong-Liang Ma and Mannque Rho. Topology change, emergent symmetries and compact star matter. *AAPPS Bull.*, 31(1):16, 2021.

[328] Feng He, Yu-Zhu Jiang, Hai-Qing Lin, Randall G. Hulet, Han Pu, and Xi-Wen Guan. Emergence and disruption of spin-charge separation in one-dimensional repulsive fermions. *Phys. Rev. Lett.*, 125:190401, Nov 2020.

[329] Alberto Lerda. A Field theory approach to the t-J model and the spin charge separation. *Nucl. Phys. B*, 428:629–654, 1994.

[330] D. G. Ravenhall, C. J. Pethick, and J. R. Wilson. STRUCTURE OF MATTER BELOW NUCLEAR SATURATION DENSITY. *Phys. Rev. Lett.*, 50:2066–2069, 1983.

[331] Jorge A. Lopez, Claudio O. Dorso, and Guillermo A. Frank. Properties of nuclear pastas. *Front. Phys. (Beijing)*, 16(2):24301, 2021.

[332] Christoph Adam, Alberto Garcia Martin-Caro, Miguel Huidobro, and Andrzej Wereszczynski. Skyrme Crystals, Nuclear Matter and Compact Stars. *Symmetry*, 15(4):899, 2023.

[333] John Dirk Walecka. A theory of highly condensed matter. *Annals of Physics*, 83(2):491–529, 1974.

[334] Nicholas Manton and Paul Sutcliffe. *Topological solitons*. Cambridge University Press, 2004.

[335] Nicholas S Manton. *Skyrmions: A theory of nuclei*. World Scientific, 2022.

[336] Sergio L. Cacciatori, Fabrizio Canfora, Marcela Lagos, Federica Muscolino, and Aldo Vera. Analytic multi-Baryonic solutions in the SU(N)-Skyrme model at finite density. *JHEP*, 12:150, 2021.

[337] Gerard 't Hooft. A planar diagram theory for strong interactions. In *The Large N Expansion In Quantum Field Theory And Statistical Physics: From Spin Systems to 2-Dimensional Gravity*, pages 80–92. World Scientific, 1993.

[338] Edward Witten. Current algebra theorems for the u (1)goldstone boson. *Nuclear Physics B*, 156(2):269–283, 1979.

[339] Alexander A. Migdal and Mikhail A. Shifman. Dilaton Effective Lagrangian in Gluodynamics. *Phys. Lett. B*, 114:445–449, 1982.

[340] Masayasu Harada and Koichi Yamawaki. Hidden local symmetry at loop: A new perspective of composite gauge boson and chiral phase transition. *Physics Reports*, 381(1-3):1–233, 2003.

[341] G. Holzwarth and B. Schwesinger. Baryons in the Skyrme Model. *Rept. Prog. Phys.*, 49:825, 1986.

[342] Yong-Liang Ma and Masayasu Harada. Lecture notes on the Skyrme model. 4 2016.

[343] Mikhail Shifman and Alexei Yung. *Supersymmetric Solitons*. Cambridge Monographs on Mathematical Physics. Cambridge University Press, 7 2023.

[344] Mikhail Shifman. *Advanced topics in quantum field theory.: A lecture course*. Cambridge Univ. Press, Cambridge, UK, 2 2012.

[345] Stefan Bertini, S. L. Cacciatori, and Bianca L. Cerchiai. On the Euler angles for SU(N). *J. Math. Phys.*, 47:043510, 2006.

[346] S. L. Cacciatori, F. Dalla Piazza, and A. Scotti. Compact Lie groups: Euler constructions and generalized Dyson conjecture. *Trans. Am. Math. Soc.*, 369(7):4709–4724, 2017.

[347] James M. Cline, Matti Jarvinen, and Francesco Sannino. The Electroweak Phase Transition in Nearly Conformal Technicolor. *Phys. Rev. D*, 78:075027, 2008.

[348] Sebastian Bruggisser, Benedict Von Harling, Oleksii Matsedonskyi, and Géraldine Servant. Electroweak Phase Transition and Baryogenesis in Composite Higgs Models. *JHEP*, 12:099, 2018.

[349] Luigi Del Debbio, Leonardo Giusti, and Claudio Pica. Topological susceptibility in the SU(3) gauge theory. *Phys. Rev. Lett.*, 94:032003, 2005.

[350] B. Alles, Massimo D'Elia, A. Di Giacomo, and C. Pica. Analysis of systematic errors in the calculation of renormalization constants of the topological susceptibility on the lattice. *Phys. Rev. D*, 74:094503, 2006.

[351] Holger Bech Nielsen and S. Chadha. On How to Count Goldstone Bosons. *Nucl. Phys. B*, 105:445–453, 1976.

[352] Haruki Watanabe and Hitoshi Murayama. Unified Description of Nambu-Goldstone Bosons without Lorentz Invariance. *Phys. Rev. Lett.*, 108:251602, 2012.

[353] H. Leutwyler. Nonrelativistic effective Lagrangians. *Phys. Rev. D*, 49:3033–3043, 1994.

[354] H. Leutwyler. On the foundations of chiral perturbation theory. *Annals Phys.*, 235:165–203, 1994.

[355] D. T. Son. Semiclassical approach for multiparticle production in scalar theories. *Nucl. Phys. B*, 477:378–406, 1996.

[356] John F Donoghue, Eugene Golowich, and Barry R Holstein. *Dynamics of the standard model*. Cambridge university press, 2014.

[357] P. Di Vecchia, F. Nicodemi, Roberto Pettorino, and G. Veneziano. Large n, Chiral Approach to Pseudoscalar Masses, Mixings and Decays. *Nucl. Phys. B*, 181:318–334, 1981.

[358] Pavel Fileviez Pérez and Hiren H. Patel. The electroweak vacuum angle. *Physics Letters B*, 732:241–243, may 2014.

[359] Tomas Heldeweg. Sphaleron solutions and their phenomenology in the electroweak theory. Master's thesis, University of Groningen, 2018.

[360] Giovanni G. van Marion. Sphalerons and the vacuum structure of gauge theories. Master's thesis, Van Swinderen Institute, 2020.

[361] M. Nakahara. *Geometry, topology and physics*. 2003.

[362] Paolo Di Vecchia, Giancarlo Rossi, Gabriele Veneziano, and Shimon Yankielowicz. Spontaneous CP breaking in QCD and the axion potential: an effective Lagrangian approach. *JHEP*, 12:104, 2017.

[363] Wen-Yuan Ai, Bjorn Garbrecht, and Carlos Tamarit. CP Conservation in the Strong Interactions. *Universe*, 10(5):189, 2024.

[364] Brando Bellazzini, Csaba Csaki, Jay Hubisz, Javi Serra, and John Terning. A Naturally Light Dilaton and a Small Cosmological Constant. *Eur. Phys. J. C*, 74:2790, 2014.

[365] Roman Zwicky. QCD with an infrared fixed point and a dilaton. *Phys. Rev. D*, 110(1):014048, 2024.

[366] Francesco Coradeschi, Paolo Lodone, Duccio Pappadopulo, Riccardo Rattazzi, and Lorenzo Vitale. A naturally light dilaton. *JHEP*, 11:057, 2013.

[367] R. D. Peccei and Helen R. Quinn. Constraints Imposed by CP Conservation in the Presence of Instantons. *Phys. Rev. D*, 16:1791–1797, 1977.

[368] R. D. Peccei and Helen R. Quinn. CP Conservation in the Presence of Instantons. *Phys. Rev. Lett.*, 38:1440–1443, 1977.

[369] J. T. Lenaghan, F. Sannino, and K. Splittorff. The Superfluid and conformal phase transitions of two color QCD. *Phys. Rev. D*, 65:054002, 2002.

[370] Bob Holdom. Raising the Sideways Scale. *Phys. Rev. D*, 24:1441, 1981.

[371] Thomas Appelquist, Kenneth Lane, and Uma Mahanta. Ladder approximation for spontaneous chiral-symmetry breaking. *Phys. Rev. Lett.*, 61:1553–1556, Oct 1988.

[372] Tom Banks and Alexander Zaks. On the phase structure of vector-like gauge theories with massless fermions. *Nuclear Physics B*, 196(2):189–204, 1982.

[373] William E. Caswell. Asymptotic behavior of non-abelian gauge theories to two-loop order. *Phys. Rev. Lett.*, 33:244–246, Jul 1974.

[374] Dennis D. Dietrich and Francesco Sannino. Walking in the SU(N). *Physical Review D*, nov 2006.

[375] Mark Alford, Krishna Rajagopal, and Frank Wilczek. Qcd at finite baryon density: Nucleon droplets and color superconductivity. *Physics Letters B*, 422(1-4):247–256, 1998.

[376] Mark Alford, Krishna Rajagopal, and Frank Wilczek. Color-flavor locking and chiral symmetry breaking in high density qcd. *Nuclear Physics B*, 537(1-3):443–458, 1999.

[377] Thomas Schäfer. Patterns of symmetry breaking in qcd at high baryon density. *Nuclear Physics B*, 575(1-2):269–284, 2000.

[378] Francesco Sannino and Wolfgang Schäfer. Relativistic massive vector condensation. *Physics Letters B*, 527(1-2):142–148, 2002.

[379] Francesco Sannino. General structure of relativistic vector condensation. *Physical Review D*, 67(5):054006, 2003.

[380] J Kapusta, D Kharzeev, and L McLerran. Return of the prodigal goldstone boson. *Physical Review D*, 53(9):5028, 1996.

[381] Tomáš Brauner, Kenji Fukushima, and Yoshimasa Hidaka. Two-color quark matter: U (1) a restoration, superfluidity, and quarkyonic phase. *Physical Review DParticles, Fields, Gravitation, and Cosmology*, 80(7):074035, 2009.

[382] Alessandro Amato, Viljami Leino, Kari Rummukainen, Kimmo Tuominen, and Sara Tähtinen. From chiral symmetry breaking to conformality in SU(2) gauge theory. 6 2018.

[383] Byung Su Kim, Deog Ki Hong, and Jong-Wan Lee. Into the conformal window: Multirepresentation gauge theories. *Phys. Rev. D*, 101(5):056008, 2020.

[384] Thomas A. Ryttov and Robert Shrock. Higher-Loop Corrections to the Infrared Evolution of a Gauge Theory with Fermions. *Phys. Rev. D*, 83:056011, 2011.

[385] Francesco Sannino. Dynamical Stabilization of the Fermi Scale: Phase Diagram of Strongly Coupled Theories for (Minimal) Walking Technicolor and Unparticles. 4 2008.

[386] José R. Peláez. From controversy to precision on the sigma meson: A review on the status of the non-ordinary f0(500) resonance. *Physics Reports*, 658:1–111, 2016. From controversy to precision on the sigma meson: A review on the status of the non-ordinary f0(500) resonance.

[387] John C Collins, Anthony Duncan, and Satish D Joglekar. Trace and dilatation anomalies in gauge theories. *Physical Review D*, 16(2):438, 1977.

[388] Victor Gorbenko, Slava Rychkov, and Bernardo Zan. Walking, Weak first-order transitions, and Complex CFTs. *JHEP*, 10:108, 2018.

[389] Francesco Sannino. Phase Diagram of Strongly Interacting Theories. *Int. J. Mod. Phys. A*, 25:5145–5161, 2010.

[390] Thomas A. Ryttov. Consistent Perturbative Fixed Point Calculations in QCD and Supersymmetric QCD. *Phys. Rev. Lett.*, 117(7):071601, 2016.

[391] Thomas A. Ryttov and Francesco Sannino. Supersymmetry inspired QCD beta function. *Phys. Rev. D*, 78:065001, 2008.

[392] Heinz Pagels. Departures from Chiral Symmetry: A Review. *Phys. Rept.*, 16:219, 1975.

[393] Michael Creutz. Quark masses and chiral symmetry. *Phys. Rev. D*, 52:2951–2959, 1995.

[394] Edward Witten. An SU(2) Anomaly. *Phys. Lett. B*, 117:324–328, 1982.

[395] Valentin V. Khoze and Joey Reiness. Review of the semiclassical formalism for multiparticle production at high energies. *Phys. Rept.*, 822:1–52, 2019.

[396] Alexander Belyaev, Fedor Bezrukov, Chris Shepherd, and Douglas Ross. Problems with Higgsplosion. *Phys. Rev. D*, 98(11):113001, 2018.

[397] David J. Gross and Frank Wilczek. Asymptotically free gauge theories. i. *Phys. Rev. D*, 8:3633–3652, Nov 1973.

[398] Bob Holdom. Techniodor. *Phys. Lett. B*, 150:301–305, 1985.

[399] Thomas W. Appelquist, Dimitra Karabali, and L. C. R. Wijewardhana. Chiral Hierarchies and the Flavor Changing Neutral Current Problem in Technicolor. *Phys. Rev. Lett.*, 57:957, 1986.

[400] Raymond Frederick Streater and Arthur Strong Wightman. *PCT, spin and statistics, and all that*, volume 52. Princeton University Press, 2000.

[401] Irinel Caprini, Gilberto Colangelo, and Heinrich Leutwyler. Mass and width of the lowest resonance in QCD. *Phys. Rev. Lett.*, 96:132001, 2006.

[402] Ken Kawarabayashi and Nobuyoshi Ohta. The Problem of η in the Large N Limit: Effective Lagrangian Approach. *Nucl. Phys. B*, 175:477–492, 1980.

[403] Maxim Pospelov and Adam Ritz. Theta vacua, QCD sum rules, and the neutron electric dipole moment. *Nucl. Phys. B*, 573:177–200, 2000.

[404] Rouven Essig et al. Working Group Report: New Light Weakly Coupled Particles. In *Community Summer Study 2013: Snowmass on the Mississippi*, 10 2013.

[405] Cumrun Vafa and Edward Witten. Parity Conservation in QCD. *Phys. Rev. Lett.*, 53:535, 1984.

[406] Steven Weinberg. The u (1) problem. *Physical Review D*, 11(12):3583, 1975.

[407] Gerard t Hooft. How instantons solve the u (1) problem. *Physics Reports*, 142(6):357–387, 1986.

[408] George A Christos. Chiral symmetry and the u (1) problem. *Physics Reports*, 116(5):251–336, 1984.

[409] Pran Nath and R Arnowitt. U (1) problem: Current algebra and the θ vacuum. *Physical Review D*, 23(2):473, 1981.

[410] Savas Dimopoulos. Technicoloured signatures. *Nuclear Physics B*, 168(1):69–92, 1980.

[411] Jacobus Verbaarschot. Spectrum of the qcd dirac operator and chiral random matrix theory. *Physical Review Letters*, 72(16):2531, 1994.

[412] DI Diakonov and V Yu Petrov. Lecture notes in physics, 417, 1993.

[413] A Smilga and JJM Verbaarschot. Spectral sum rules and finite volume partition function in gauge theories with real and pseudoreal fermions. *Physical Review D*, 51(2):829, 1995.

[414] JJM Verbaarschot. Lectures given at apctp-rcnp joint international school on physics of hadrons and qcd, osaka, japan. In *1998 and the 1998 YITP Workshop on QCD and Hadron Physics, Kyoto, Japan*, 1998.

[415] Makoto Oka, Hiroyuki Yabu, T Matsui, and Kazunori Itakura. *Physics Of Hadrons And Qcd-Proceedings Of The Apctp-rcnp Joint International School And 1998 Yitp Workshop*. World Scientific, 1999.

[416] JT Lenaghan, F Sannino, and K Splittorff. Superfluid and conformal phase transitions of two-color qcd. *Physical Review D*, 65(5):054002, 2002.

[417] Paolo Di Vecchia and Francesco Sannino. The physics of the θ-angle for composite extensions of the standard model. *The European Physical Journal Plus*, 129(12):1–19, 2014.

[418] Igor G. Irastorza and Javier Redondo. New experimental approaches in the search for axion-like particles. *Prog. Part. Nucl. Phys.*, 102:89–159, 2018.

[419] M. K. Gaillard, M. B. Gavela, R. Houtz, P. Quilez, and R. Del Rey. Color unified dynamical axion. *Eur. Phys. J. C*, 78(11):972, 2018.

[420] M. B. Gavela, M. Ibe, P. Quilez, and T. T. Yanagida. Automatic Peccei–Quinn symmetry. *Eur. Phys. J. C*, 79(6):542, 2019.

[421] Luca Di Luzio, Belen Gavela, Pablo Quilez, and Andreas Ringwald. An even lighter QCD axion. *JHEP*, 05:184, 2021.

[422] Ryuichiro Kitano, Ryutaro Matsudo, Norikazu Yamada, and Masahito Yamazaki. Peeking into the θ vacuum. *Phys. Lett. B*, 822:136657, 2021.

[423] Gabriele Veneziano. U (1) without instantons. *Nuclear Physics B*, 159(1-2):213–224, 1979.

[424] Holger Bech Nielsen and S. Chadha. On How to Count Goldstone Bosons. *Nucl. Phys. B*, 105:445–453, 1976.

[425] Michael Creutz. Anomalies and chiral symmetry in QCD. *Annals Phys.*, 324:1573–1584, 2009.

[426] Nils Strodthoff and Lorenz Von Smekal. Polyakov-quark–meson–diquark model for two-color qcd. *Physics Letters B*, 731:350–357, 2014.

[427] C. Rosenzweig, J. Schechter, and C. G. Trahern. Is the Effective Lagrangian for QCD a Sigma Model? *Phys. Rev. D*, 21:3388, 1980.

[428] J. M. Cornwall and A. Soni. COUPLINGS OF LOW LYING GLUEBALLS TO LIGHT QUARKS, GLUONS, AND HADRONS. *Phys. Rev. D*, 29:1424, 1984.

[429] A. Salomone, J. Schechter, and T. Tudron. Properties of Scalar Gluonium. *Phys. Rev. D*, 23:1143, 1981.

[430] Francesco Sannino. Polyakov loops versus hadronic states. *Phys. Rev. D*, 66:034013, 2002.

[431] Roland Kaiser and H. Leutwyler. Large N(c) in chiral perturbation theory. *Eur. Phys. J. C*, 17:623–649, 2000.

[432] David B. Kaplan, Jong-Wan Lee, Dam T. Son, and Mikhail A. Stephanov. Conformality Lost. *Phys. Rev. D*, 80:125005, 2009.

[433] Hidenori S. Fukano and Francesco Sannino. Conformal Window of Gauge Theories with Four-Fermion Interactions and Ideal Walking. *Phys. Rev. D*, 82:035021, 2010.

[434] Taro V. Brown, Maarten Golterman, Svend Krøjer, Yigal Shamir, and K. Splittorff. The ϵ-regime of dilaton chiral perturbation theory. *Phys. Rev. D*, 100(11):114515, 2019.

[435] Stephen D. H. Hsu, Francesco Sannino, and Joseph Schechter. Anomaly induced QCD potential and quark decoupling. *Phys. Lett. B*, 427:300–306, 1998.

[436] G. Veneziano and S. Yankielowicz. An Effective Lagrangian for the Pure N=1 Supersymmetric Yang-Mills Theory. *Phys. Lett. B*, 113:231, 1982.

[437] R. Gomm, P. Jain, R. Johnson, and J. Schechter. Scale Anomaly and the Scalars. *Phys. Rev. D*, 33:801, 1986.

[438] Chung Ngoc Leung, ST Love, and William A Bardeen. Spontaneous symmetry breaking in scale invariant quantum electrodynamics. *Nuclear Physics B*, 273(3-4):649–662, 1986.

[439] William A Bardeen, Chung Ngoc Leung, and ST Love. Dilaton and chiral-symmetry breaking. *Physical Review Letters*, 56(12):1230, 1986.

[440] Koichi Yamawaki, Masako Bando, and Ken-iti Matumoto. Scale-invariant hypercolor model and a dilaton. *Physical Review Letters*, 56(13):1335, 1986.

[441]

[442] John B Kogut, Dominique Toublan, and DK Sinclair. Diquark condensation at nonzero chemical potential and temperature. *Physics Letters B*, 514(1-2):77–87, 2001.

[443] Riccardo Rattazzi and Alberto Zaffaroni. Comments on the holographic picture of the randall-sundrum model. *Journal of High Energy Physics*, 2001(04):021, 2001.

[444] Zackaria Chacko and Rashmish K Mishra. Effective theory of a light dilaton. *Physical Review D*, 87(11):115006, 2013.

[445] Maarten Golterman and Yigal Shamir. Low-energy effective action for pions and a dilatonic meson. *Physical Review D*, 94(5):054502, 2016.

[446] Thomas Appelquist, James Ingoldby, and Maurizio Piai. Dilaton effective field theory. *Universe*, 9(1):10, 2023.

[447] J. Schechter. Effective Lagrangian with Two Color Singlet Gluon Fields. *Phys. Rev. D*, 21:3393–3400, 1980.

[448] Bruno Zumino. Effective lagrangians and broken symmetries. *Lectures on elementary particles and quantum field theory*, 2(70):437, 1970.

[449] Haruki Watanabe, Tomáš Brauner, and Hitoshi Murayama. Massive Nambu-Goldstone Bosons. *Phys. Rev. Lett.*, 111(2):021601, 2013.

[450] Alberto Nicolis, Riccardo Penco, Federico Piazza, and Rachel A. Rosen. More on gapped Goldstones at finite density: More gapped Goldstones. *JHEP*, 11:055, 2013.

[451] Alberto Nicolis and Federico Piazza. Implications of Relativity on Nonrelativistic Goldstone Theorems: Gapped Excitations at Finite Charge Density. *Phys. Rev. Lett.*, 110(1):011602, 2013. [Addendum: Phys.Rev.Lett. 110, 039901 (2013)].

[452] Ting-Wai Chiu. Improved study of the β-function of $SU(3)$ gauge theory with $N_f = 10$ massless domain-wall fermions. *Phys. Rev. D*, 99(1):014507, 2019.

[453] T. Appelquist, G. T. Fleming, M. F. Lin, E. T. Neil, and D. A. Schaich. Lattice Simulations and Infrared Conformality. *Phys. Rev. D*, 84:054501, 2011.

[454] Thomas Appelquist, George T. Fleming, and Ethan T. Neil. Lattice study of the conformal window in QCD-like theories. *Phys. Rev. Lett.*, 100:171607, 2008. [Erratum: Phys.Rev.Lett. 102, 149902 (2009)].

[455] Thomas Appelquist, George T. Fleming, and Ethan T. Neil. Lattice Study of Conformal Behavior in SU(3) Yang-Mills Theories. *Phys. Rev. D*, 79:076010, 2009.

[456] Anna Hasenfratz, Claudio Rebbi, and Oliver Witzel. Gradient flow step-scaling function for SU(3) with twelve flavors. *Phys. Rev. D*, 100(11):114508, 2019.

[457] Claudio Pica and Francesco Sannino. UV and IR Zeros of Gauge Theories at The Four Loop Order and Beyond. *Phys. Rev. D*, 83:035013, 2011.

[458] Giacomo Cacciapaglia, Corentin Cot, and Francesco Sannino. Second wave COVID-19 pandemics in Europe: a temporal playbook. *Sci.Rep.*, 10, 15514, 2020.

[459] Anna Hasenfratz, Ethan T. Neil, Yigal Shamir, Benjamin Svetitsky, and Oliver Witzel. Infrared fixed point of the SU(3) gauge theory with Nf=10 flavors. *Phys. Rev. D*, 108(7):L071503, 2023.

[460] Maarten Golterman and Yigal Shamir. Power counting of the pion-dilaton effective field theory. 7 2024.

[461] Gerard 't Hooft. Naturalness, chiral symmetry, and spontaneous chiral symmetry breaking. *NATO Sci. Ser. B*, 59:135–157, 1980.

[462] Gerard 't Hooft. A Planar Diagram Theory for Strong Interactions. *Nucl. Phys. B*, 72:461, 1974.

[463] Gerard 't Hooft. A Two-Dimensional Model for Mesons. *Nucl. Phys. B*, 75:461–470, 1974.

[464] Hee-Jung Lee, Byung-Yoon Park, Dong-Pil Min, Mannque Rho, and Vicente Vento. A unified approach to high density: Pion fluctuations in skyrmion matter. *Nuclear Physics A*, 723(3-4):427–446, 2003.

[465] Francesco Sannino, Alessandro Strumia, Andrea Tesi, and Elena Vigiani. Fundamental partial compositeness. *JHEP*, 11:029, 2016.

[466] Luigi Del Debbio and Roman Zwicky. Dilaton and massive hadrons in a conformal phase. *JHEP*, 08:007, 2022.

[467] Steven Weinberg. Implications of Dynamical Symmetry Breaking. *Phys. Rev. D*, 13:974–996, 1976. [Addendum: Phys.Rev.D 19, 1277–1280 (1979)].

[468] Zhi-yong Duan, P. S. Rodrigues da Silva, and Francesco Sannino. Enhanced global symmetry constraints on epsilon terms. *Nucl. Phys. B*, 592:371–390, 2001.

[469] David B. Kaplan, Howard Georgi, and Savas Dimopoulos. Composite Higgs Scalars. *Phys. Lett. B*, 136:187–190, 1984.

[470] Giacomo Cacciapaglia and Francesco Sannino. Fundamental Composite (Goldstone) Higgs Dynamics. *JHEP*, 04:111, 2014.

[471] Ben Gripaios, Alex Pomarol, Francesco Riva, and Javi Serra. Beyond the Minimal Composite Higgs Model. *JHEP*, 04:070, 2009.

[472] Jamison Galloway, Jared A. Evans, Markus A. Luty, and Ruggero Altair Tacchi. Minimal Conformal Technicolor and Precision Electroweak Tests. *JHEP*, 10:086, 2010.

[473] James Barnard, Tony Gherghetta, and Tirtha Sankar Ray. UV descriptions of composite Higgs models without elementary scalars. *JHEP*, 02:002, 2014.

[474] Serge Droz, Markus Heusler, and Norbert Straumann. New black hole solutions with hair. *Phys. Lett. B*, 268:371–376, 1991.

[475] Anna Hasenfratz. Emergent strongly coupled ultraviolet fixed point in four dimensions with eight Kähler-Dirac fermions. *Phys. Rev. D*, 106(1):014513, 2022.

[476] Zoltan Fodor, Kieran Holland, Julius Kuti, Daniel Nogradi, Chris Schroeder, and Chik Him Wong. Can the nearly conformal sextet gauge model hide the Higgs impostor? *Phys. Lett. B*, 718:657–666, 2012.

[477] Thomas Appelquist, James Ingoldby, and Maurizio Piai. Composite two-Higgs doublet model from dilaton effective field theory. *Nucl. Phys. B*, 983:115930, 2022.